Low Density Lipoprotein Induction of Intracellular Oxidants Production

A thesis submitted in partial fulfilment
of the requirements for the Degree of

Doctor of Philosophy
in Biochemistry

School of Biological Sciences
University of Canterbury
New Zealand

Mohd Izani Othman

May 2015

TABLE OF CONTENTS

LIST OF FIGURES

LIST OF TABLES

ABBREVIATIONS

ΔΨm	Mitochondrial membrane potential
7-KC	7-Keto-cholesterol
7,8- NP	7,8-dihydroneopterin
acLDL	Acetylated LDL
ADP	Adenosine diphosphate
AMP	Adenine monophosphate
ANOVA	Analysis of variance
Apocynin	4'-hydroxy-3'-methoxyacetophenone
ATP	Adenosine triphosphate
BCA	Bicinchoninic acid
BSA	Bovine serum albumin
BrA	Calcium ionophore A23187
$CaCl_2$	Calcium chloride
$C_2H_3NaO_2$	Sodium acetate
CD36	Cluster of differentiation 36 scavenger receptor
Cl^-	Chloride ion
CO_2	Carbon dioxide
CPDA-1	Citrate-phosphate-dextrose-adenine
$CuCl_2$	Copper chloride
Cyto b558	Flavocytochrome b558
DHE	Dihydroethidium
DIC	Differential interference contrast
DMSO	Dimethyl sulphoxide
DNA	Deoxyribonucleic acid
DPI	Diphenyleneiodonium
ECM	Extracellular matrix
ECs	Endothelial cells
EDTA	Ethylenediaminetetraacetic acid

EGTA	Ethylene glycol-bis(2-aminoethylether)-N,N,N’,N’- tetracetic acid
ER	Endoplasmic reticulum
ETC	Electron transport chain
EtOH	Ethanol
FAD	Flavin adenine dinucleotide
FBS	Foetal bovine serum
GAPDH	Glyceraldehyde-3-phosphate dehydrogenase
GM-CSF	Granulocyte-macrophage colony – stimulating factor
GSH	Glutathione
GSSG	Glutathione disulfides
GTP	Guanosine triphosphate
GR	Glutathione reductase
H^+	Protons
H_2O_2	Hydrogen peroxide
HCl	Hydrochloric acid
HDL	High density lipoprotein
HIHS	Heat-inactivated human serum
HOCl	Hypochlorous acid
HPLC	High performance liquid chromatography
HUVECs	Human umbilical vein endothelial cells
IFN-γ	Interferon-γ
IMM	Inner mitochondrial membrane
IMS	Inter-membrane space
KOH	Potassium hydroxide
KBr	Potassium bromide
L-	Lipid
$L^{\bullet}$	Lipid radical
LDL	Low density lipoprotein
LC_{50}	Median lethal concentration
LH	Polyunsaturated fatty acyl group

$LOO^{\bullet}$	Lipid peroxyl radical
LOOH	Lipid hydroperoxide
mmLDL	Minimally modified LDL
$MnCl_2$	Manganese chloride
MOMP	Mitochondrial outer membrane permeabilization
MPO	Myeloperoxidase
MPT	Mitochondrial permeability transition
MPTP	Mitochondrial permeability transition pore
MTT	3-[4,5- Dimetylthiazol -2 - yl]-2,5-diphenyl-tetrazolium bromide
$NADP^{+}$	Nicotinamide adenine dinucleotide phosphate
NaCl	Sodium chloride
$NaH_2PO_4 .H_2O$	Sodium dihydrogen phosphate monohydrate
NaOH	Sodium hydroxide
NADPH	Reduced nicotinamide adenine dinucleotide phosphate
NC	Nitrocellulose
NO	Nitric acid
$NO_2^{\bullet}$	Nitrogen dioxide
NOX	NADPH oxidase
O_2	Molecular oxygen
O_2^{-}	Superoxide anion
$OH^{\bullet}$	Hydroxyl radical
OMM	Outer mitochondrial membrane
$ONOO^{-}$	Peroxynitrite
oxLDL	Oxidized LDL
PBS	Phosphate buffered saline
phox	Phagocytic oxidase
PI	Propidium iodide
PMA	Phorbol 12-myristate 13-acetate
PS	Phosphatidylserine
PUFA	Polyunsaturated fatty acid

$R^{\bullet}$	Free radical
$RO^{\bullet}$	Alkoxyl radical
$RO_2^{\bullet}$	Peroxyl radical
ROOH	Protein hydroperoxide
ROS	Reactive oxygen species
rpm	Revolutions/minute
RPMI-1640	Roswell Park Memorial Institute 1640 complete medium
SD	Standard deviation
SDS	Sodium dodecyl sulphate
SEM	Standard error of the mean
SH3	Src homology 3
SMCs	Smooth muscle cells
SOD	Superoxide dismutase
SR-A	Scavenger receptor type A
TBARS	Thiobarbituric acid reactive substances
TBS	Tris-buffered saline
TCA	Trichloroacetic acid
TMRM	Tetramethylrhodamine methyl ester
TNF-α	Tumour necrosis factor-α
U937	U937 monocyte-like cell line
VLDL	Very low density lipoprotein
$^{v}/_{v}$	volume/volume
$^{w}/_{v}$	weight/volume

ACKNOWLEDGMENTS

First and foremost, my utmost grateful to the Almighty God for His blessings and guidance, making this journey a dream come true.

My utmost thanks and gratitude go to my senior supervisor – Associate Professor Steven Gieseg for replying to an email from Malaysia, keeping me updated and inviting me to Christchurch (just after the devastating earthquakes!) to be part of his research team. I would like extend my thanks to my co-supervisors – Dr. Ashley Garrill (University of Canterbury) and Dr. Barry Hock (University of Otago, Christchurch). To all lab mates past and present: Anastasia, Ela, Alpha, Hannah, Hanadi, Raj, Sian, Shane, Angus, Joe, Ed, Billy, Helen, Sean and Olivia – a lot to say actually, thank you for everything, these years are full of memories. To the technician/lab manager: Craig and Maggie – thank you heaps for all the help, support and making things easy from the beginning.

A million thanks to all the blood donors at New Zealand Blood Service (NZBS) – this research would not have been possible without the steady supply of blood from the haemochromatosis patients and also to the staff of NZBS for collecting the blood. I would like to extend my thanks to all the plasma donors – for LDL supply and the nurse from University of Canterbury Health Centre, Wendy, for collecting the blood. Special thanks to Associate Professor Sally McCormick and Biochemistry Department of Otago University in Dunedin for their help and allowing me to use their unltracentrifuge and facilities after the Canterbury earthquakes. Big thanks to Professor Matthew Whiteman from University of Exeter Medical School in the UK for the generous gifts of H_2S donors.

Special thanks to my sponsors - Ministry of Education, Malaysia and Universiti Teknologi MARA (UiTM) for granting me the scholarship to pursue this study. Much appreciation goes to Professor Aishah Adam, Dean of the Faculty of Pharmacy, UiTM for the support all this while. My thanks are also extended to the dedicated staff of UiTM's Human Resources Department and Scholarship Division (SLAB/SLAI), Ministry of Education, Malaysia for their time and assistance.

Most of all, all my love and eternal thanks to my wonderful wife – Asma Kholilah Mohaiyuddin for her patience, affection and understanding; for supporting and encouraging

me and always be there for me especially through tough times. To my sweethearts – Alya, Danish and Nadira, blessed to have all of you here to go through this journey together. To my mum, dad and families back home, heartiest thanks for the prayers and wishes. Special thanks to my brother, Idrus Othman and sister in-law, Sharimah Jaafar for taking care of the emerging problems back home since we are thousands of miles away. I would also like to thank my dear friends, Azlan Othman and Salwa Damanhuri for their help and kind hospitality especially during the first month of our stay in Christchurch. Heaps of thanks to all friends and individuals which I've not mentioned their names here for their help and contributions throughout this journey. Last but not least, thanks to Nathan Wain for helping me with the formatting of my thesis.

This journey is long and it has been a while now, I know. Coming home now…

ABSTRACT

Atherosclerosis is a complex cardiovascular disease characterized by chronic progressive inflammation of the arteries. The progression of atherosclerosis from fatty streak to advance atherosclerotic plaque involves the development of a necrotic core region consists of cholesterol, lipids, calcium (Ca^{2+}), dead cells and other cellular debris. Macrophage infiltrations occurred in all stages of atherosclerotic progression and they are abundantly found in atherosclerotic plaques. Oxidised low density lipoprotein (oxLDL) plays a vital role in the initiation and development of atherosclerosis. OxLDL is present within atherosclerotic plaque and has been shown to be cytotoxic to various types of cells including macrophages.

This research initially examined the cytotoxic effects of copper oxidised LDL on U937, human monocytes and HMDM cells. As expected oxLDL was cytotoxic; causing rapid, concentration and time dependent cell viability loss in all types of cells examined. Examination of the cell morphology showed that oxLDL caused a necrotic like cell death characterised by cell swelling and lysis. Flow cytometric assay coupled with propidium iodide (PI) staining of necrotic cells was compared to MTT reduction assays of cell viability. The flow cytometric technique had the advantage over the MTT reduction assay of being rapid and showing both the live and dead cell levels at an individual cell level.

The progression of oxLDL-induced cell death correlated with the rapid increased in intracellular ROS production in the cytosol and the mitochondria. Immunoblotting results showed that oxLDL induced NADPH oxidase (NOX) activation and increased $p47^{phox}$ expression. This suggests NOX as the generator of reactive oxygen species (ROS) induced by oxLDL in these cells. However, apocynin and VAS2870, the two NOX inhibitors used in this study, were unable to inhibit the ROS generation caused by the oxLDL. This suggests that either these inhibitors are unable to inhibit the targeted NOX or other sources of ROS might exist and contributed to the overall increase in oxidative flux.

OxLDL caused a rapid increase in cytosolic Ca^{2+} level. This was contributed by the extracellular Ca^{2+} source as well as Ca^{2+} mobilisation from the intracellular stores such as endoplasmic reticulum (ER). OxLDL-induced intracellular Ca^{2+} increase also correlated with the increase in intracellular ROS. Nevertheless, blocking of oxLDL-induced intracellular Ca^{2+} elevation by Ca^{2+} chelator, EGTA, did not reduce intracellular ROS generation.

Accordingly, this suggests that oxLDL-induced intracellular Ca^{2+} increase is not the cause for oxLDL-induced cell death. Additionally, oxLDL may also initiate a Ca^{2+}-independent cell death pathway.

The excess cytosolic Ca^{2+} taken up by the mitochondria may be detrimental and could result in mitochondrial Ca^{2+} overload. This will increase mitochondrial ROS production and initiate mitochondrial permeability transition (MPT) pores opening. Consequently, this could collapse the mitochondrial membrane potential ($\Delta\Psi m$) due to the rupture of outer mitochondrial membrane (OMM) and resulted in cell death. Blocking of Ca^{2+} uptake into the mitochondria by ruthenium red protected cells from oxLDL-mediated cell death, possibly by reducing ROS production and preventing MPT activation.

This study also demonstrated the protective effect of 7,8-dihydroneopterin (7,8-NP) on oxLDL-induced oxidative stress. 7,8-NP protected cells from oxLDL-induced intracellular ROS generation and cell viability loss. Intracellular Ca^{2+} increase was also reduced by 7,8-NP in particular after 3 hours incubation with oxLDL. The action of 7,8-NP was better than that of apocynin in protecting U937 cells from oxLDL suggests its potential ability to scavenge ROS from various sources.

Studies have implicated the involvement of H_2S in various biological processes including atherosclerosis. Thus, the disruption of H_2S homeostasis may contribute to the progression of atherosclerosis. Slow releasing H_2S molecules (H_2S donors) have been developed for a controlled and stable delivery of H_2S to cells. In this study, specific H_2S donors, including one which targets the mitochondria, were found to be protective against oxLDL-induced cell death in U937, human monocytes and HMDM cells. Although the exact mechanism is yet to be elucidated, these H_2S donors were shown to block the elevation of intracellular Ca^{2+} and ROS production mediated by oxLDL. Therefore, these H_2S donors could be the potential candidates for future development of therapeutics in treating atherosclerosis.

CHAPTER ONE

1. Introduction

Atherosclerosis and cardiovascular disease

Atherosclerosis is a chronic inflammatory disease (Ross, 1999) that involves local thickening of the arterial vessel wall which is characterised by endothelial dysfunction, vascular inflammation and build-up of lipids, cholesterol, calcium and cellular debris within the intima layer (Libby, 2006). This will results in plaque formation, vascular remodelling, acute and chronic luminal obstruction, abnormalities of blood flow and diminished oxygen supply to target organs (Anderson, 1999). Most of the cardiovascular diseases developed are secondary to atherosclerosis (Bahorun *et al.*, 2006).

Accumulation of oxLDL within the plaques is a typical attribute of atherosclerosis (Yla-Herttuala *et al.*, 1989) which plays a vital role in the pathogenesis and contributes to the inflammatory state of atherosclerosis (Ross, 1999; Steinberg *et al.*, 1989). Epidemiological studies have revealed a number of risk factors linked to atherosclerosis which could be divided into two categories i.e. modifiable and non-modifiable. Non-modifiable risk factors include age, gender and family history of heart disease whereas; cigarette smoking, obesity, physical inactivity, hypertension, diabetes and hyperlipidemia are amongst the modifiable risk factors (Frohlich & Al-Sarraf, 2013; Stocker & Keaney, 2004).

Pathogenesis of atherosclerosis

Atherosclerosis is rather asymptomatic and atherosclerotic plaque development is a progressive process that usually takes years, yet early changes in vessel walls which lead to atherosclerotic lesions are found even in healthy young people (Itabe, 2003). Three types of arteries are well known as the major sites of atherosclerosis i.e. coronary arteries, cerebral arteries and the aorta. Extensive atherosclerotic development narrows the lumen of the arteries, reduces blood flow and leads to heart attack.

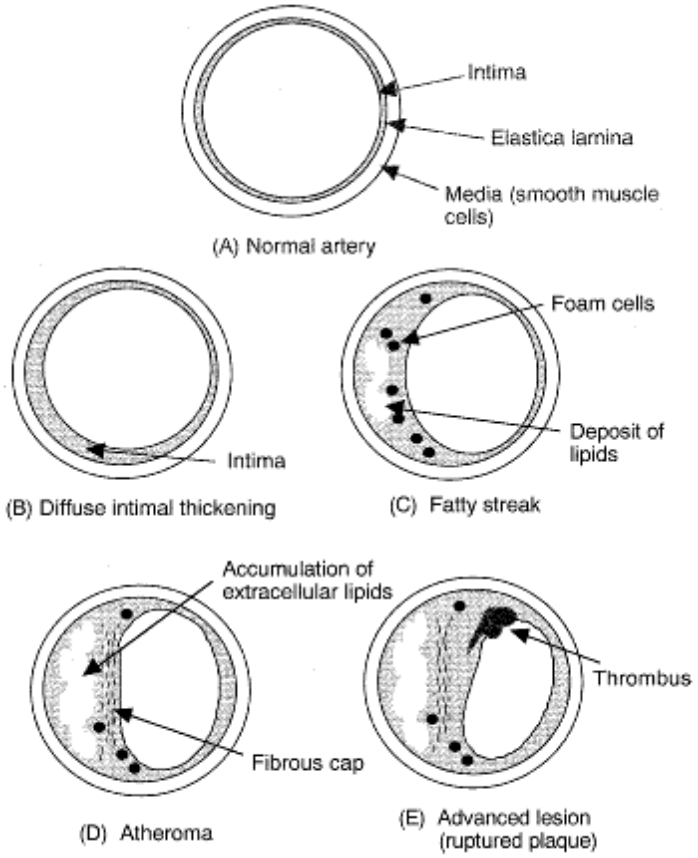

Figure 1.1: Atherosclerosis development in the arterial wall

The progression of atherosclerosis at different stages depicted from the earliest intimal thickening, fatty streak, atheroma until advanced lesion associated with plaque rupture and thrombosis (Itabe, 2003).

The typical anatomy of normal arteries and atherosclerotic lesions are illustrated by **Figure 1.1**. In normal arteries (A), the innermost layer of the artery i.e. intima is bounded by a monolayer of endothelial cells on the luminal side and a sheet of elastic fibres (the internal elastic lamina) on the peripheral side. The normal intima consists of extracellular connective tissue matrix made up primarily of proteoglycans and collagen. The middle layer i.e. media, consists of smooth mucle cells (SMCs) while the outer layer i.e. adventitia, consists of connective tissues with interspersed fibroblasts and SMCs. In the earliest stages of atherosclerotic lesions, there is accumulation of collagen fibers and lipids and invasion of various cells including macrophages between the endothelial cells and the elastic lamina (B).

This is followed by the formation of lumps on the vessel walls which unite to form lesions which are called fatty streaks (Ross, 1986; Steinberg *et al.*, 1989). Massive accumulation of lipids in the intimal areas and large numbers of macrophage-derived foam cells are found in

this stage (C). The next is the atheroma formation, characterised by the fibrous caps which contain smooth muscle cells and fibrous proteins such as collagens. Large accumulations of macrophages, smooth muscle cells and extracellular matrix proteins are found in the atheroma (D) (Ross, 1986; Steinberg *et al.*, 1989). A thrombus is formed when the luminal surface of the atherosclerotic lesion is damaged, attracting platelets to adhere and aggregate at the damaged site (E). Thrombus formation can lead to complete occlusion of the blood vessel which is the primary cause of myocardial and cerebral infarction.

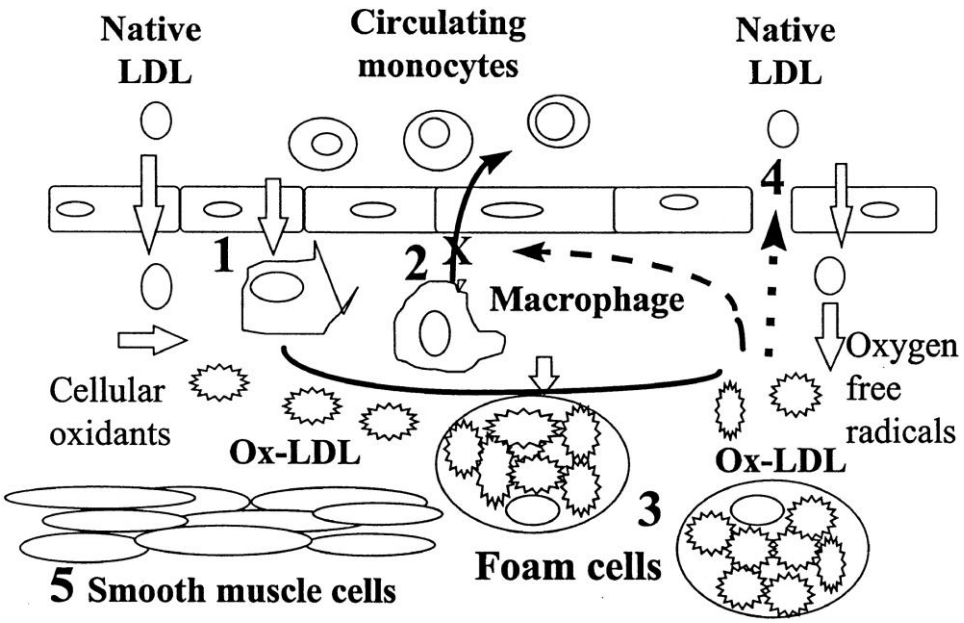

Figure 1.2: Initiating events of early atherosclerosis development

Native LDL entered into subendothelial space and subsequently oxidized by endothelial cells, macrophages or smooth muscle cells. OxLDL aids in recruiting circulating monocytes into the intima where they are differentiated into macrophages (1). OxLDL inhibits macrophage movement from the intima (2). OxLDL is then taken up by macrophages via scavenger receptors CD36 and SR-A to become lipid laden foam cells or fatty streak which is the early sign of atherosclerosis (3). This will cause injury and dysfunction of the endothelial (4) and enhances the proliferation of smooth muscle cells and other cells. Adapted from Lau (2001).

Many hypotheses have emerged in order to explain the complex events associated with the development of atherosclerosis. At least three distinct hypotheses have been postulated, namely ‘response-to-injury’, ‘response-to-retention’ and ‘oxidative modification’ (reviewed in Stocker and Keaney (2004)).

According to the ‘response to injury’ hypothesis, endothelial injury is a key event which initiates the inflammatory mechanisms associated with atherosclerosis (Ross, 1999). The endothelial damage precedes smooth muscle cell migration and proliferation, deposition of

the intracellular and extracellular lipid and accumulation of extracellular matrix. The 'response to retention' hypothesis postulated that the central atherogenic process is the sub-endothelial retention and accumulation of lipoproteins by extracellular matrix molecules such as proteoglycans (Williams & Tabas, 1995). The 'oxidation modification' hypothesis on the other hand suggested that the central component of the atherogenic process is the oxidative modification of LDL that acts as an immunogenic stimulus for monocyte recruitment to the vessel wall and phagocytic uptake of oxidized LDL by macrophages (Witztum, 1994).

Much evidence has implicated the changes to the endothelial cells as the primary event in the complex atherosclerosis development which is progressively derived by inflammation (Libby *et al.*, 2010). Ross (1993) hypothesised that when endothelial cells are injured or stressed, they will generate cytokines in response to the injury. These cytokines then, activate other cells in the vasculature such as macrophages, SMCs and neutrophils. Stimulated endothelial cells express surface molecules and chemokines which attract monocytes in the blood to attach to the endothelial cells. Subsequently, the monocytes transmigrate into vessel walls and differentiate into macrophages. LDL enters the intima soon after monocytes recruitment and undergoes modifications such as oxidation, proteolysis and aggregation, which may be partially caused by exposure to oxidants released by vascular wall (Lusis, 2000). OxLDL is then taken up by macrophages resulting in the formation of foam cells which is an early sign of atherosclerosis (Ross, 1993). Nevertheless, the details of these processes remain controversial especially on the exact initial events during the early stage of lesion formation.

Oxidative modification hypothesis of atherosclerosis development suggests that LDL may accumulate within the intima. The increased permeability of LDL at the arterial branch points allows the entry and accumulation of LDL in the intima (Lusis, 2000). Trapped LDL is susceptible to modification, particularly by oxidation resulting in the formation of oxLDL. OxLDL activates endothelial cells and up-regulates adhesion molecule expression and chemotactic chemokine secretion such as monocyte chemoattractant ptotein 1 (MCP-1), which will contribute to the recruitment of circulating monocytes into the intima. Brandes *et al.* (2001) has identified oxygen radicals as messengers for the expression of MCP-1 that attracts the migration of monocytes into the intima. The migrated monocytes will then proliferate and differentiate into macrophages. OxLDL and other forms of modified LDL are taken up rapidly by these macrophages via scavenger receptors, such as SR-A and CD36 (Glass & Witztum, 2001; Steinberg *et al.*, 1989). Internalization of oxLDL by macrophages

potentiates the inflammatory response, thus leads to the formation of foam cells which is a feature of the early stage atherosclerotic lesion (**Figure 1.2**). Continued formation and death of foam cells lead to the development of fatty streak followed by necrotic lipid core within the intima (Douglas & Channon, 2010).

Role of monocytes/macrophages in atherosclerosis

Monocytes are a heterogenous group of cells from the myeloid lineage constituting about 5 to 10% of the total white blood cells that play important roles in health and diseases. Monocytes originate from the bone marrow and enter the circulation where they remain for up to 72 hours after which they either enter the tissues or die (Martinez, 2009). In their study, Auffray *et al.* (2007) have found a group of resident monocytes patrolling for sites of inflammation in healthy arteries. In the tissues, they become activated and differentiate into tissue macrophages under the influence of macrophage- or granulocyte/macrophage colony stimulating factor (M-CSF or GM-CSF).

Macrophages are also the most abundant cell type found in atherosclerotic plaques. Macrophage infiltration happened in all stages of atherosclerotic lesion development, from diffused intimal thickening (Nakashima *et al.,* 2008) to the advanced plaque (Shaikh *et al.*, 2012). Macrophages play an important role in the early phase of atherosclerotic plaque development by ingesting oxLDL particles recognised via scavenger receptors on their cell surface (Peiser *et al.,* 2002) whereby the inability to process these particles results in lipid-filled foam cells formation (Libby, 2002). Macrophages in atherosclerotic lesions have been shown to comprise cellular features of both apoptosis and necrosis (Hegyi *et al.,* 1996). The death of macrophages is believed to be one of the main events in the development of atherosclerosis that could be initiated *in vitro* by oxLDL (Marchant *et al.*, 1995; Tertov *et al.*, 1989). Nevertheless, the mechanism of how oxLDL induced macrophages death is not fully understood.

Oxidised low density lipoprotein (oxLDL) and atherogenesis

OxLDL cytotoxicity

Atherosclerosis is an inflammatory disease whereby oxLDL plays a vital role in the initiation and progression of the disease (Ross, 1999). OxLDL has been found in atherosclerotic lesions

of experimental animals and humans (Yla-Herttuala *et al.*, 1989). An increased level of circulating oxLDL is associated with metabolic syndrome that may contribute to atherogenesis and heart disease (Holvoet *et al.*, 2008).

LDL can be oxidised by various substances including metal ions such as Cu^{2+}, Fe^{2+}, radical products (e.g. H_2O_2), radiation or prolonged incubation with cells (endothelial cells, smooth muscle cells and monocyte-macrophages) (Gieseg *et al.*, 2008; Steinbrecher *et al.*, 1984). OxLDL consists of various lipid peroxidation products including thiobarbituric reactive substances, conjugated dienes, lipid hydroperoxides and aldehydes (Steinberg, 1997).

OxLDL induces various cellular activities and the production of pro-inflammatory cytokines and growth factors by almost all cell types of the arterial wall (Kume & Gimbrone, 1994) including up-regulation of monocyte chemoattractant protein-1 (MCP-1) and increased expression of vascular cell adhesion molecule-1 (VCAM-1) (Steinberg, 2009). OxLDL contributes to endothelial dysfunction and inflammation in vasculature by up-regulating the expression of inflammatory mediators (Maziere & Maziere, 2009). OxLDL was also capable in altering the balance of pro-coagulant and anti-coagulant activities in the vascular cell surface (Ishii *et al.*, 1996). Studies in cultured endothelial cells suggest that oxLDL may enhance thrombogenecity through increased expression of plasminogen activator inhibitor-1 (PAI-1) (Drake *et al.*, 1991).

OxLDL has been considered as a key risk factor in foam cell formation, endothelial dysfunction and inflammation whereby it manifests many deleterious effects including the transformation of macrophages and smooth muscle cells to foam cells (Rosenfeld & Ross, 1990). Small dense LDL particles are taken up by macrophage scavenger receptor leading to foam cell formation (Chapman *et al.*, 1998). Studies have shown that exposure to oxLDL for a prolonged period may cause cytotoxicity to the vascular cells (Cathcart *et al.*, 1991; Steinberg, 1997).

OxLDL-induced cell death

OxLDL has been shown to be causing death in various types of cells involved in atherogenesis including endothelial cells (Hessler *et al.*, 1979), lymphocytes (Alcouffe *et al.*, 1999), smooth muscle cells, macrophages, monocytes and monocyte-like U937 and THP-1 cell lines (Baird *et al.*, 2005; Gieseg *et al.*, 2010; Marchant *et al.*, 1995). The exact

mechanisms on how oxLDL causes cell death *in vitro* still remain unclear. Previous studies suggested that oxysterols, particularly 7-ketocholesterol (7-KC) as the main component of oxLDL that contributes to cell death. However, recent study from this laboratory has clearly indicated that 7-KC is not the one (Rutherford & Gieseg, 2012). Thus, it is more likely that oxidative stress induced by oxLDL is the main initiator of the death cascade.

Depending on the cell type and extent of damaged, oxLDL-mediated cell death may occur via caspase-dependent or caspase–independent apoptosis or via necrosis (Asmis & Begley, 2003; Baird *et al.*, 2004; Vicca *et al.*, 2000). Previous studies done in this lab revealed that THP-1 cells underwent a caspase-mediated apoptosis characterised by a relatively slow depletion of GSH compared to U937 cells which manifested necrotic cell death due to lack of caspase activation with rapid GSH loss and no phosphatidyl serine (PS) exposure (Baird *et al.*, 2004). The difference in response to oxLDL between the two types of cell may be related to varying uptake mechanism of oxLDL (Baird *et al.*, 2004) whereby U937 cells has been shown to express a 4-folds higher levels of CD36 scavenger receptors compared to THP-1 (Nguyen-Khoa *et al.*, 1999). Both caspase-dependent (Wintergerst *et al.*, 2000) and -independent (Asmis & Begley, 2003; Yang *et al.*, 2012b) cell death have been observed with HMDM cells. In our current setting, HMDM cells were observed to undergo a caspase-3 independent necrosis with a rapid GSH loss (Gieseg *et al.*, 2010; Shchepetkina, 2013). Nevertheless, the exact cell death mechanism initiated by oxLDL may vary in the atherosclerotic plaque depending on the types of cells as well as the local environment (Baird *et al.*, 2004)

Types of cell death

Necrosis and apoptosis

Necrosis and apoptosis are the classical types of cellular death associated with oxLDL-induced cell death which could be differentiated by their distinct morphological and biochemical changes (Salvayre *et al.*, 2002). Necrosis is characterised by a complete loss of ion homeostasis resulting in cell swelling, degradation of internal organelle structure, nuclear membrane disruption and eventual rupture of plasma membrane (Syntichaki & Tavernarakis, 2003). Mitochondrial integrity disruption prevents ATP production while loss of plasma membrane integrity caused the release of cellular contents including denatured proteins, DNA fragments and other debris into the extracellular compartment. Antioxidants such as GSH, pro-oxidants such as metal ions and damaging molecules such as activated calpains

(Halliwell, 2003) may also present in the discharged cellular contents that may affect neighbouring cells. Activated calpains or cathepsins could cause irreversible damage to the skeletal proteins that will eventually result in necrosis (Yang *et al.*, 2012a). Additionally, abrupt loss of ATP could also lead to necrosis (Yang, 2009).

Apoptosis is a highly regulated process (Kerr *et al.*, 1972) that involves a series of intracellular signalling pathways for controlled shutdown of cells. Morphologically, apoptotic cells are characterised by cell shrinkage, plasma membrane blebbing and chromatin condensation while maintaining ion homeostasis and internal organelle integrity (Yuan & Yankner, 2000). Eventually, cells are broken down into apoptotic bodies without rupture of organelle membranes. Subsequently, the apoptotic bodies are recognised and engulfed by surrounding cells and phagocytes (Duprez *et al.*, 2009) without causing an inflammatory response. Typical biochemical changes accompanying apoptosis include cytochrome *c* release from the mitochondria and redistribution of phosphatidylserine (PS) to the outer surface of plasma membrane which enables recognition of apoptotic bodies by phagocytes (van Engeland *et al.*, 1998). A secondary necrosis causing the apoptotic bodies to lyse and release their contents will occur if they are not phagocytosed (Tabas, 2005)

Endoplasmic reticulum (ER) stress-induced cell death

The endoplasmic reticulum (ER) has emerged as a key player in various cellular responses including a variety of apoptotic signaling pathways (Heath-Engel *et al.*, 2008) and cell stress. Studies have implicated a crucial role of ER stress in atherosclerosis and plaque rupture due to the presence of oxidized lipids, inflammation and metabolic stress (Muller *et al.*, 2011a). Moreover, Yao *et al.* (2013) have showed that oxLDL was able to induce ER stress. ER is the primary site for intracellular Ca^{2+} storage and is the location for the folding and some post-translational modification of transmembrane and secreted proteins. Disruption of ER functions could result in protein misfolding and activation of an adaptive stress response termed the unfolded protein response (UPR). The UPR attempts to increase the folding capacity of the ER through the induction of key proteins involved in chaperoning, protein folding and degradation pathways.

Transduction of the UPR pathway occurs through three ER resident chaperone proteins that function as primary sensors of endoplasmic reticulum stress i.e. PKR-like endoplasmic reticulum kinase (PERK) (Harding *et al.*, 1999), inositol requiring enzyme 1 (IRE1) (Shen *et*

al., 2001) and activating transcription factor 6 (ATF6) (Haze *et al.*, 1999) that sense the accumulation of unfolded proteins within the ER lumen. Glucose-regulated protein 78 (GRP78) is bound to these proteins, maintaining the sensors in an inactive configuration in the absence of stress induction (Bertolotti *et al.*, 2000). Accumulation of unfolded proteins and the altered redox status within the ER lumen up-regulate the expression of GRP78 and trigger its dissociation leading to the initiation of UPR signal transduction pathways. OxLDL have also been shown to induce translocation of ATF6 from cytoplasm to the nucleus as well as up-regulating GRP78 (Yao *et al.*, 2013). Sustained and unresolved ER stress can lead to apoptotic cell death via the induction of the proapoptotic transcriptional factor C/EBP homologous protein (CHOP), activation of c-jun amino-terminal kinase (JNK) and the Bcl-2 proteins (Muller *et al.*, 2011a).

Autophagy

Autophagy is another cellular response mainly regulated at the ER (Heath-Engel *et al.*, 2008). It has been associated with oxLDL-induced ER and lysosomal oxLDL degradation (Muller *et al.*, 2011b). During autophagy, cells form autophagosomes that sequester organelles, proteins or portions of the cytoplasm for delivery to the lysosome (He & Klionsky, 2009). The sequestered contents are degraded in the lysosome, allowing cells to eliminate damaged or harmful components through catabolism and recycling them to maintain nutrient and energy homeostasis. However, induction of autophagy may also lead to cell death (Kundu & Thompson, 2005). Unlike apoptosis, autophagic cell death is a caspase independent process characterized by the accumulation of autophagic vacuoles in the cytoplasm with extensive degradation of the Golgi complex and ER preceding destruction of the nucleus (Klionsky & Emr, 2000). This followed by the fusion of the autophagosome with lysosomes for catabolism by intralysosomal enzymes (Maiuri *et al.*, 2007).

Moreover, studies have suggested that there have been cross-talks between these cell death mechanisms which indicate that individual components of the cell death machinery do not operate in isolation whereby the activation of one cell death mechanism alone might not be sufficient to eliminate all damaged cells (Zhivotovsky & Orrenius, 2010).

Calcium and atherosclerosis

General calcium homeostasis

The balance between the influx of calcium (Ca^{2+}) into the cytoplasm from extracellular compartment or intracellular organelles (sarco/endoplasmic reticulum) and the efflux of calcium from the cytoplasm regulates intracellular free Ca^{2+} concentration. The cytosolic concentration of Ca^{2+} is tightly controlled by complex interactions between pumps, channels, exchangers and binding proteins. In resting condition, cytoplasmic Ca^{2+} is approximately 10,000 times (100-200 nM) lower than extracellular Ca^{2+} (1-2 mM).

This condition is maintained by the low permeability of the plasma membrane to ions and by the activity of the plasma membrane Ca^{2+}-ATPase (PMCA) and of the Na^{+}/ Ca^{2+} exchanger (NCX) (**Figure 1.3**). The PMCA pumps Ca^{2+} out of the cytosol by actively transporting Ca^{2+} against a large transmembrane Ca^{2+} electrochemical gradient whereby one molecule of ATP is hydrolysed for every Ca^{2+} ion that is expulsed. On the other hand, NCX is expressed only in excitable cells (e.g. muscle and neurons) that extensively use Ca^{2+} signals (Strehler, 1990). The energy stored in the Na^{+} electrochemical gradient drives the removal of Ca^{2+} whereby one Ca^{2+} ion is expelled in exchange of three Na^{+} ions. The net effect of these plasma membrane mechanisms is to maintain of low cytosolic Ca^{2+} environment relative to the extracellular space (Putney, 1997).

The increase in intracellular Ca^{2+} can be induced through Ca^{2+} mobilisation from intracellular stores (mainly the sarco/endoplasmic reticulum (SR/ER)) and through the entry from the extracellular compartment. The main route inducing Ca^{2+} release from intracellular stores involves the IP3 receptor (IP3R). When extracellular soluble agonists binds a G-coupled protein receptor, different isoforms of phospholipase C (PLC) are activated producing inositol-1,4,5-trisphosphate (IP3) and diacyl glycerol (DAG) (Berridge & Irvine, 1989) from the hydrolysis of phosphatidylinositol 4,5 bisphosphate (PIP2). DAG remained bound to the membrane while IP3 is released into the cytosol and binds to the IP3 receptor (IP3R) (Lemasters *et al.*, 2009). The binding of IP3 to IP3R induces its opening and the release of Ca^{2+} from SR/ER into the cytosol.

Ryanodine receptor (RyR) which is also located on the ER membrane is another mechanism for ER Ca^{2+} efflux whereby it is activated by Ca^{2+} itself (Zucchi & Ronca-Testoni, 1997).

Thus, a small amount of cytosolic Ca^{2+} near the receptor can stimulate the release of even more Ca^{2+} creating a positive feedback loop. RyR is considered as a calcium-induced calcium release (CICR) Ca^{2+} channel (Fabiato, 1983). IP3R are the predominant Ca^{2+} release channels in non-excitable (non-muscle) cells while RyR are predominant in excitable (muscle) cells (Iino, 1999).

Intracellular store depletion of Ca^{2+} due to the opening of the IP3R and RyR triggers the activation of an inward rectifying Ca^{2+} current from the extracellular space termed as capacitative Ca^{2+} entry (CCE). Mechanism inducing intracellular Ca^{2+} increases involves the opening of the plasma membrane Ca^{2+} channels which include: Voltage Operated Ca^{2+} channels (VOCCs), Receptor Operated Ca^{2+} channels (ROCCs) and Second Messenger Operated Channels (SMOCs). VOCCs open following a decrease of membrane potential (Bertolino & Llinas, 1992), ROCCs (also called ligand gated channels) open due to the binding of an external ligand (McFadzean & Gibson, 2002) and SMOCs open following the binding of a second messenger on the inner surface of the membrane (Meldolesi & Pozzan, 1987). VOCCs are classified into high-voltage activated channels including the L, N, P/Q and R-type channels and low-voltage activated channels represented by T-type channels. VOCCs can be inhibitid by calcium channel blockers (CCBs).

The mechanisms of Ca^{2+} clearance from the cytosol is of equal importance to the regulation of Ca^{2+} release from the ER/SR. The sarco/endoplasmic reticulum Ca^{2+} ATPase (SERCA) is a Ca^{2+} pump located in the membrane of the SR and ER whose function is to transport Ca^{2+} from the cytosol to be stored into SR/ER using ATP as an energy source (MacLennan *et al.*, 1997). SERCA functions are regulated by both cytosolic and ER/SR conditions. Under resting conditions SERCA is relatively inactive but following an increase in cytosolic Ca^{2+}, the activity of the pump is increased, resulting in re-sequestration of Ca^{2+} into the ER (Lytton *et al.*, 1992). From the other side, the Ca^{2+} pumping activity of SERCA is regulated by the Ca^{2+} content of the ER. SERCA activity is maximal when the stored Ca^{2+} is depleted and decreases as the store approaches its maximal capacity (Mogami *et al.*, 1998).

The role of mitochondria in Ca^{2+} signalling pathways will be further elaborated in **Mitochondria – an overview** section.

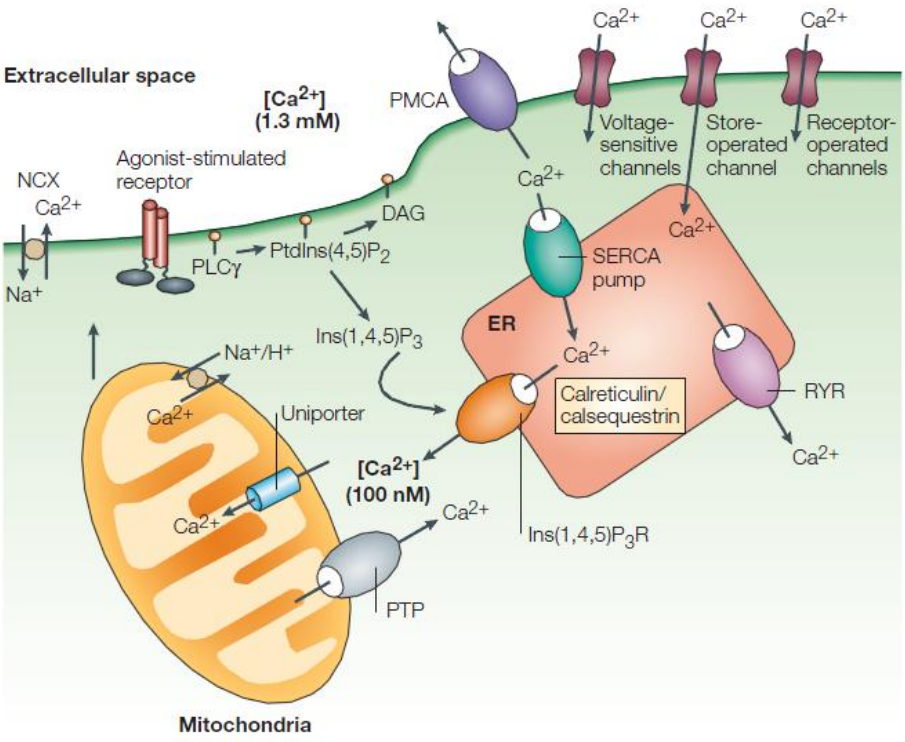

Figure 1.3: Regulation of intracellular calcium
(Orrenius et al., 2003)

Calcium and oxidative stress association in cell death and atherosclerosis

Dysregulation of Ca^{2+} homeostasis has been implicated to play a vital role in cell injury. Studies using various types of cells have showed that increased cytosolic Ca^{2+} levels after ROS or toxin treatment led to either caspase-3-dependent or –independent apoptosis (Escargueil-Blanc *et al.*, 1994; Vindis *et al.*, 2005; Yap *et al.*, 2006) or necrosis (Aguilar *et al.*, 1996; Escargueil-Blanc *et al.*, 1994).

Ca^{2+} may play an important role in the initiation and progression of the atherosclerotic lesion whereby many cellular processes that are involved in lesion formation being regulated by changes in intracellular Ca^{2+}. These include the migration and proliferation of smooth muscle cells, release of growth factors, secretion of extracellular matrix protein, activation of platelets, cholesterol esterification, recruitment of monocytes and endothelial permeation (Orimo & Ouchi, 1990; Phair, 1988; Ross, 1986). Nicotera *et al.* (1992) has stated in their review the relation between oxidative stress and intracellular Ca^{2+} in cell injury leading to cell death. Geeraerts *et al.* (1991) have shown that in human endothelial cells challenged with oxidative stress, Ca^{2+} overload occurred and caused plasma membrane blebbing.

The deleterious effects of ROS are mainly due to the ability of ROS to produce changes in subcellular organelles and induce intracellular Ca^{2+} overload. Evidence shows that ROS can induce an increase in intracellular Ca^{2+} levels by releasing Ca^{2+} from internal stores and disturb Ca^{2+} clearance systems whereby intracellular Ca^{2+} increased is a hallmark of pathological states associated with oxidative stress (Camello-Almaraz *et al.*, 2006). In addition, increased formation of ROS indicating the presence of oxidative stress has been observed in a wide variety of experimental and clinical conditions associated with cardiovascular disease including atherosclerosis (Dhalla *et al.*, 2000).

Oxidative stress and reactive oxygen species (ROS)

Oxidative stress and atherosclerosis

Oxidative stress is defined as an imbalance between ROS formation and antioxidant defense mechanisms in cell or tissue (Forbes *et al.*, 2008) that leads to an altered redox status which can result in cell dysfunction and/or cell death (Madamanchi & Runge, 2007). Oxidative stress has been identified throughout the process of atherogenesis (Warnholtz *et al.*, 1999) and as the process of atherogenesis proceeds, inflammatory cells and other constituents of the atherosclerotic plaque release large amounts of ROS, which further enhance this process. In general, increased production of ROS may affect fundamental mechanisms that contribute to atherogenesis i.e. oxidation of LDL, endothelial cell dysfunction, vascular smooth muscle growth and monocytes migration (Berliner & Heinecke, 1996).

Reactive oxygen species (ROS)

Reactive oxygen species (ROS) are molecules or ions formed by the incomplete one-electron reduction of oxygen. ROS can be classified into two groups: 1) radicals – groups that contain an unpaired electron and are highly chemically reactive; 2) non-radicals – do not possess an unpaired electron but are prone to exchanging electrons with other molecules (Guzik & Harrison, 2006). **Table 1.1** illustrates the common radicals and non-radicals of ROS.

Table 1.1: Various types of radicals and non-radical reactive oxygen species (ROS)

Radicals		Non-Radicals	
$O_2^{\cdot -}$	Superoxide	H_2O_2	Hydrogen peroxide
$OH^{\cdot}$	Hydroxyl	$HOCl^{-}$	Hypochlorous acid
$RO_2^{\cdot}$	Peroxyl	O_3	Ozone
$RO^{\cdot}$	Alkoxyl	$^1O_2$	Singlet oxygen
$HO_2^{\cdot}$	Hydroperoxyl	$ONOO^{-}$	Peroxynitrite

Sources of ROS in the vasculature

Various potential enzymatic sources of vascular ROS have been identified including NADPH oxidases (NOX), xanthine oxidase, lipoxygenase, cycloygenase, P450 monoxygenase, uncoupling of nitric oxide synthase (NOS) and mitochondrial respiration as illustrated in **Figure 1.4** (Kyaw *et al.*, 2004). However, NOX are thought to be the predominant source of ROS in the vasculature (Griendling *et al.*, 2000). As opposed to the other sources of ROS, NOX seem to be the only dedicated ROS producing enzyme. Since the sole purpose of NOX is the formation of ROS, this makes them as potential therapeutic targets for oxidative stress. Detail information on NOX is further elaborated in **NADPH oxidase (NOX)** section.

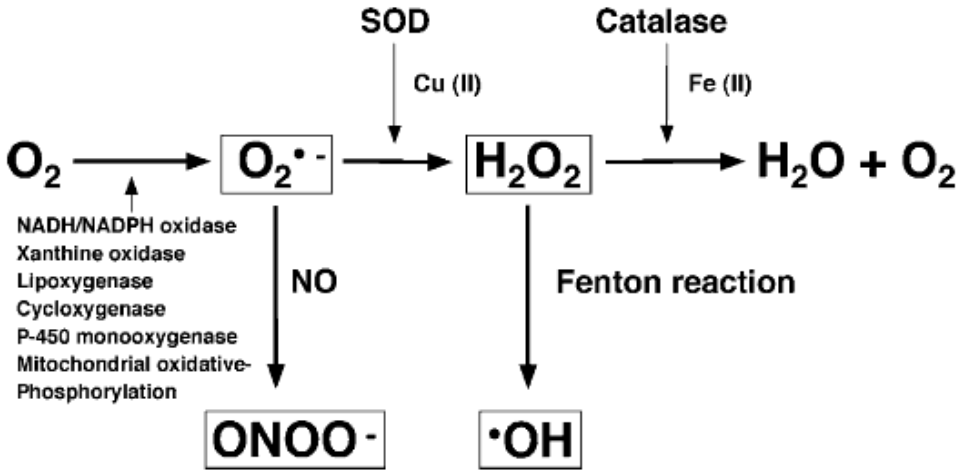

Figure 1.4: Sources of reactive oxygen species in the vasculature

Potential sources for $O_2^{\cdot -}$ generation in the vasculature include NADPH oxidase (NOX), xanthine oxidase, lipooxygenases, cyclooxygenases and mitochondria. $O_2^{\bullet -}$ can be rapidly dismutated to H_2O_2 by superoxide dismutases (SODs) followed by $OH^{\cdot}$ formation via Fenton reaction. $O_2^{\bullet -}$ may also react with NO to form $ONOO^{-}$, a much more potent oxidant. H_2O_2 can be broken down by catalase to form H_2O and O_2. (Kyaw et al., 2004)

Mitochondria – an overview

The mitochondrion is defined by two structurally and functionally different membranes i.e. the plain outer membrane (OMM) and the highly selective inner membrane (IMM) with an intermembrane space (IMS) in between. Mitochondria are the major source of ATP via oxidative phosphorylation. The process of oxidative phosphorylation takes place in the IMM (Madamanchi *et al.*, 2005) which consists of the electron transport chain (ETC) complex. ETC is composed of 5 multiple subunit complexes namely, Complex I (NADH-ubiquinone dehydrogenase), Complex II (succinate cytochrome *c* reductase), Complex III (ubiquinone cytochrome *c* reductase), Complex IV (cytochrome *c* oxidase) and Complex V (ATP synthase).

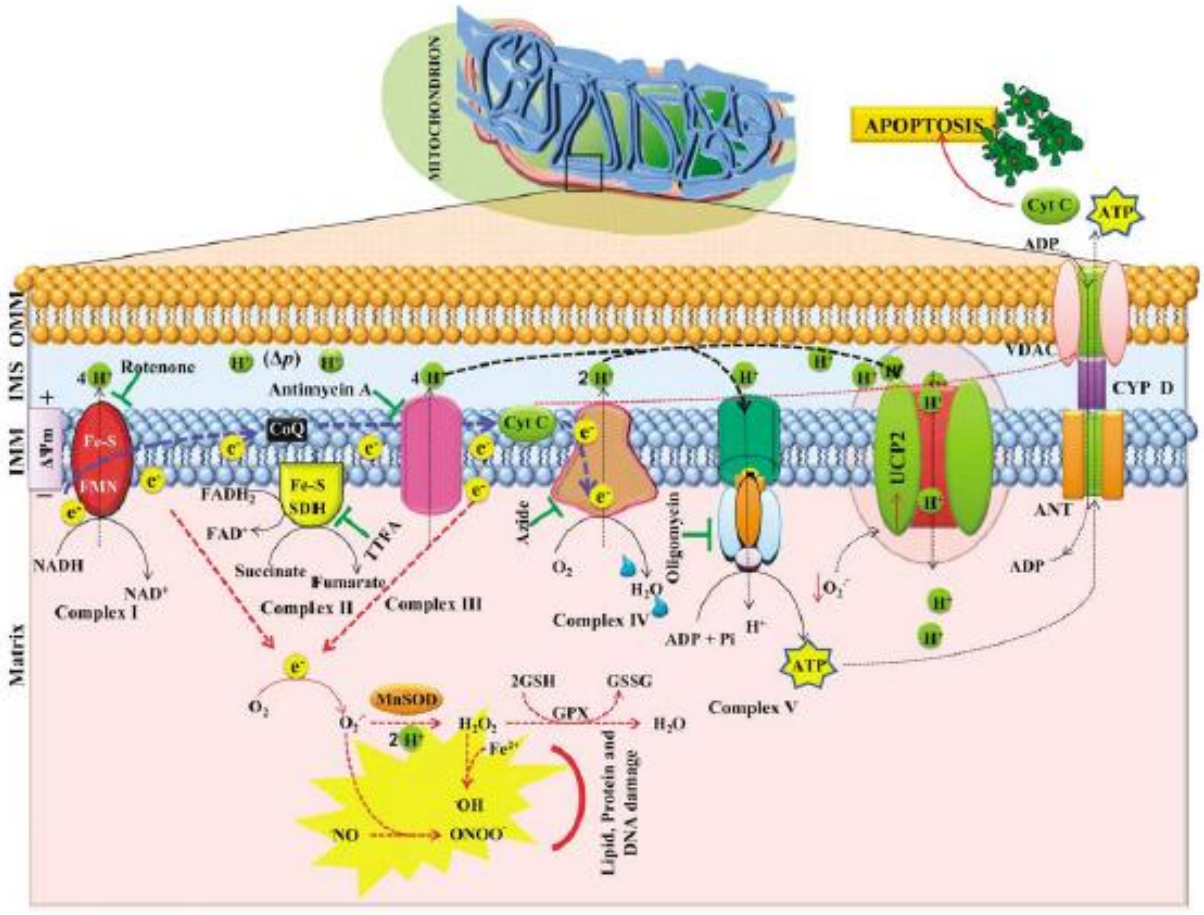

Figure 1.5: A schematic illustration of mitochondria showing mitochondrial electron transport chain (ETC) complexes.
(Mehta & Li, 2009)

NADH and $FADH_2$ are final products generated by the citric acid cycle from multiple chains of reactions. Electrons are transferred from NADH to Complex I or $FADH_2$ to Complex II and passed on to ubiquinol via coenzyme Q which will then get transferred to Complex III. Cytochrome *c* transfers electrons from Complex III to Complex IV and in this process water is formed from reduced molecular oxygen. The transfer of electrons in ETC creates trans-membrane electrochemical gradient through constant pumping of electrons across IMM at Complexes I, III and IV. The proton-motive force (Δp) initiates protons re-entry into the matrix which is then used by Complex V to synthesise ATP from inorganic phosphate and ADP. Additionally, Δp also mediates ATP-ADP exchange by the adenine nucleotide translocase (ANT). Approximately 0.2 – 2.0% of the molecular oxygen leaks through ETC to form ROS (Madamanchi & Runge, 2007)(**Figure 1.5**).

Mitochondria play an important role in the development of atherosclerosis. As the key intracellular organelles determining the survival and death of the cells, mitochondria are the key source and primary target for intracellular detrimental ROS production (Murphy, 2009). Complex I and III are considered as the primary sites for ROS production (Turrens, 2003). In the absence of ATP, reverse electron transport could occur whereby electrons derived from $FADH_2$ via Complex II are transferred into Complex I, (D. Han *et al.*, 2003; Y. Liu *et al.*, 2002) thus generating more ROS. Thereby, Complex I is considered as a pathophysiologically relevant source of ROS production in the ETC.

Moreover, various factors are involved in the regulation of ROS in mitochondria such as ETC, oxygen concentration, availability of NADH and $FADH_2$, uncoupling proteins, antioxidant defences and the modulation of nuclear factors (Ballinger, 2005). Superoxide formed in the matrix is rapidly converted to H_2O_2 by superoxide dismutase (SOD) which is then converted to water by glutathione peroxidase (GPx). Nevertheless, transition metals may also reduce H_2O_2 into hydroxyl radical (Madamanchi & Runge, 2007). Superoxide can also reacts with NO to generate peroxynitrite, which is capable in causing the inactivation of enzymes, DNA damage and mitochondrial dysfunction (Ballinger *et al.*, 2000). Studies also indicate that cellular ROS generated by NOX might act as a positive feedback, leading to increased production of ROS from mitochondria, which is termed as ROS-induced ROS release (Brandes, 2005). In addition, increased superoxide generation by NOX also induces mitochondrial oxidative damage via structural changes to the IMM and disturbs flow in the ETC which enhances ROS production (Doughan *et al.*, 2008; Ray & Shah, 2005).

Calcium and mitochondria

Mitochondria are closely involved in many Ca^{2+} signalling roles (Rizzuto *et al.*, 2000). Mitochondria sequester Ca^{2+} through the mitochondrial uniporter (MCU) which uses the mitochondrial membrane potential (MMP) to trigger the uptake of positively charged Ca^{2+} (Kirichok *et al.*, 2004). When cytoplasmic Ca^{2+} level rises, Ca^{2+} can diffuse through the OMM into the IMS via the voltage-dependent anion channel (VDAC), which will then get transported into the mitochondria via MCU located in the IMM (Gunter *et al.*, 2000; Rizzuto *et al.*, 2000) (**Figure 1.6**). While resting cytoplasmic Ca^{2+} levels are below the MCU affinity values for Ca^{2+}, there are a number of mitochondria which are strategically located near Ca^{2+} release site of the ER (Rizzuto *et al.*, 1998). This will then cause local Ca^{2+} concentration to exceed MCU affinity values and are above the threshold for uptake (Rizzuto *et al.*, 1992). In addition, MCU appears to be gated by local adenine nucleotide concentrations (ATP>ADP>AMP) located at the outer surface of the IMM (Bianchi *et al.*, 2004).

Mitochondrial Ca^{2+} efflux normally occurs via the mitochondrial Na^{+}/Ca^{2+} exchanger (mNCX) (Palty *et al.*, 2010) and the mitochondrial H^{+}/Ca^{2+} exchanger (mHCX) located on the IMM whereby Ca^{2+} gradient across the IMM provides energy for the counter-transport. The mNCX imports 3 Na^{+} ions for every Ca^{2+} ion exported (Baysal *et al.*, 1994) whereas the mHCX imports 2 H^{+} for each Ca^{2+} ion (Gunter *et al.*, 2000). However, rapid mitochondrial Ca^{2+} influx can saturate these efflux pathways (Bernardi, 1999), thus increasing mitochondrial Ca^{2+} levels resulting in Ca^{2+} overload.

Ca^{2+} overload which has been taken up by mitochondria can subsequently stimulate the opening of the mitochondrial permeability transition pore (MPTP) connecting the cytosol with the mitochondrial matrix (Bianchi *et al.*, 2004; Crompton, 1999; Kroemer *et al.*, 2007)) thus causes mitochondrial permeability transition (MPT). MPT is followed by IMM depolarization, uncoupling of oxidative phosphorylation, matrix swelling and OMM rupture (Kroemer *et al.*, 2007). Therefore, if majority of mitochondria in the cell are disrupted, it may lead to inadequate glycolytic sources of ATP. These ATP-depleted cells may then undergo subsequent events of cell death.

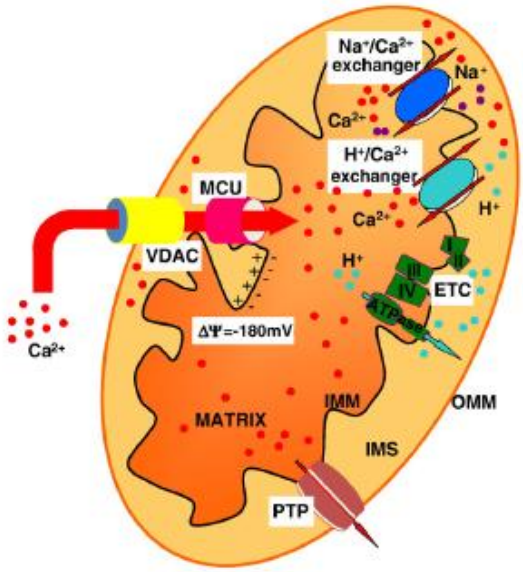

Figure 1.6: Mitochondrial Ca^{2+} transporters
(Celsi et al., 2009)

NADPH oxidases (NOX)

NOX structure, homologs and distribution

NOX are a group of membrane associated enzymes expressed in vascular cells. The structure and functions of NOX are well characterized in phagocytic cells such as neutrophils and macrophages. Under pathological conditions, NOX is one of the enzymes that can be activated in many cell systems to generate large amounts of superoxide (Griendling *et al.*, 2000). In the majority of vascular disease models, NOX have been shown to be the main source of superoxide (Guzik & Harrison, 2006).

NOX family consists of several homologs (or isoforms) which differ in their expression, structure and function. Seven homologs of NOX are NOX1, NOX2, NOX3, NOX4, NOX5, DUOX1 and DUOX2 (**Figure 1.8**). NOX homologs contain an FAD and NADPH binding site, two heme molecules and six transmembrane domains (**Figure 1.7**). DUOX1 and DUOX2 are very similar to NOX5 but they possessed an additional peroxidase domain. NOX1 and NOX4 share approximately 60% and 39% amino acid identity with NOX2 respectively (Bedard & Krause, 2007). With regards to NOX4, Poldip2 has been identified by Lyle *et al.* (2009) as a likely component with the capacity to directly regulate its activity.

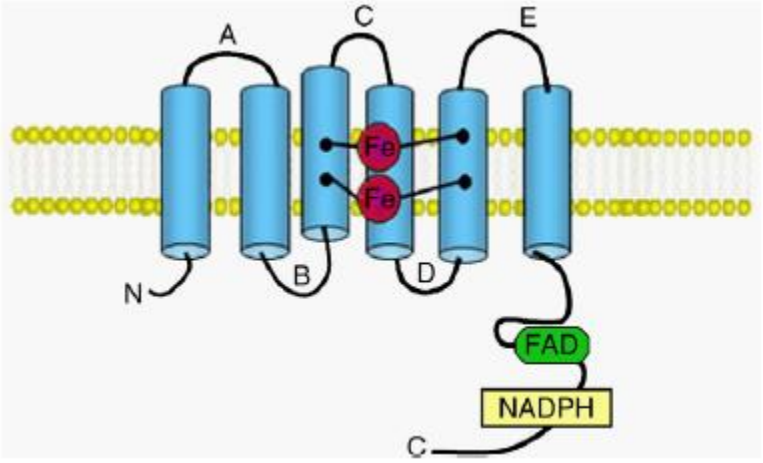

Figure 1.7: Common gp91phox/NOX2 structure

Each NOX family members contain this common components which consits of six transmembrane domains (A-E), two heme molecules and an FAD and NADPH binding site (Al Ghouleh *et al.*, 2011).

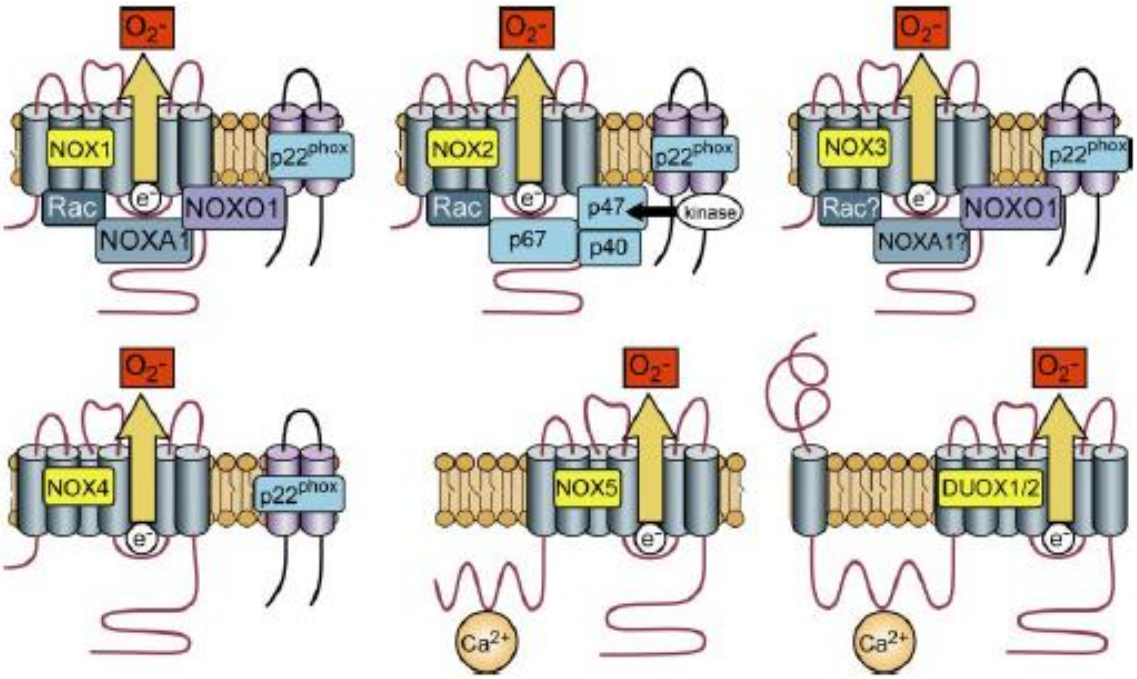

Figure 1.8: Models of NOX homologs

Each of the seven members of the NOX family requires a different set of conditions and protein association. Upper lane from left to right: NOX1, NOX2, NOX3; lower lane from left to right: NOX4, NOX5 and DUOX1/2 (Bedard & Krause, 2007).

NOX complex consists of two membrane components, $p22^{phox}$ (a small α-subunit) and $gp91^{phox}$ (a larger β-subunit which is termed as NOX2). NOX2 associates with $p22^{phox}$ in a 1:1 complex that contributes to its stabilization. NOX2 and $p22^{phox}$ formed the cytochrome b_{558} complex (Groemping & Rittinger, 2005). In addition, NOX complex contains four cytoplasmic subunits i.e. $p47^{phox}$, $p67^{phox}$, $p40^{phox}$ and guanine nucleotide binding protein Rac1 or Rac2. Upon stimulation, these cytoplasmic subunits translocate to cytochrome b_{558} whereby this assembly is mandatory for NOX activation and facilitates electron transfer from NADPH to oxygen (**Figure 1.9).**

SH3 binding domain on $p22^{phox}$ is a docking site for the soluble cytoplasmic subunits $p47^{phox}$, $p67^{phox}$ and $p40^{phox}$ (Groemping & Rittinger, 2005). NOX1-4 are associated with $p22^{phox}$ as a docking subunit (Guzik & Harrison, 2006), which is important for their activity whereas NOX5, DUOX1 and DUOX2 do not require $p22^{phox}$ (Al Ghouleh *et al.*, 2011). NOX4 is constitutively active and do not need any regulatory subunits (Dworakowski *et al.*, 2008).

Expression and distribution of NOX in various types of cells/tissues/organs is summarized by **Table 1.2**. Cellular distributions and localization of NOX homologs play a vital role as to how individual NOX regulate signaling (Al Ghouleh *et al.*, 2011). Nevertheless, it should be noted that different species may have different profiles of NOX protein expression. For example, NOX5 is not expressed in the vasculature of rodents (Maru *et al.*, 2005) whereas DUOX1/2 are not expressed in mouse airway epithelial cells.

Table 1.2: Distribution and localization of NOX

(adapted from Al Ghouleh et al. (2011))

Nox isoform	Cellular distribution	Subcellular localization
Nox1	Colon epithelium, vascular smooth muscle cells, endothelial cells, osteoclasts, reproductive organs	Intracellular membranes close to ER, endosomes, signalosomes, caveolae
Nox2	Neutrophils, macrophages, endothelial cells, vascular smooth muscle cells, fibroblasts, skeletal muscle cells, cardiomyocytes, and hepatocytes	Cell membrane, phagosomes, perinuclear
Nox3	Inner ear (vestibular system, cochlea), skull, brain, fetal tissues	Plasma membrane
Nox4	Kidney, vascular smooth muscle cells, fibroblasts, hematopoietic stem cells, osteoclasts, neurons, endothelial cells	Focal adhesions, ER, nucleus, mitochondria
Nox5	Vascular smooth muscle cells, endothelial cells, bone marrow, lymph nodes, spleen, reproductive tissues, stomach, pancreas, fetal tissues	Plasma membrane, ER
Duox1/2	Thyroid, airway epithelia, prostate, digestive system (Duox2)	Apical membrane

Mechanism of NOX activation

NOX activation process has been well characterized in leukocytes. In resting state, cytoplasmic subunits interact with each other in a trimeric (1:1:1) complex (Vignais, 2002). At this stage, $p47^{phox}$ is in an auto-inhibited form where two SH3 domains bind to a polybasic region (Groemping *et al.*, 2003) and upon activation, $p47^{phox}$ becomes highly phosphorylated. This is mandatory to abolish the auto-inhibited state and thereby enables its translocation to cytochrome b_{558} (Ago *et al.*, 2003). Subsequently, this results in the assembly of p47-p67-$p40^{phox}$ to the membrane and docks via its SH3 domain to $p22^{phox}$ (Groemping *et al.*, 2003). In addition, docking of $p47^{phox}$ to cytochrome b_{558} also facilitates the interaction between $p67^{phox}$ and NOX2 which is needed for the activation of catalytic subunit (Han *et al.*, 1998). DeLeo *et al.* (1995) have reported three interaction sites between $p47^{phox}$ and NOX2 whereas more than a dozen sites of $p47^{phox}$ have been shown to undergo phosphorylation when cells are activated (Huang & Kleinberg, 1999). Next critical step is the translocation of the activated GTPase Rac to cytochrome b_{558} that occurs independent of $p47^{phox}$ since Rac-GTP anchors itself in the membrane through its prenylated tail (Brandes & Kreuzer, 2005). NOX activation is illustrated in **Figure 1.9**.

However, the exact composition and assemble of vascular (non-phogocytes) NOX is not fully understood. Vascular cells demonstrate a constitutively active NOX that generates significantly low levels of ROS compared to leukocytes (Lassègue & Clempus, 2003). Additionally, Li and Shah (2002) have found a pre-assembled NOX in endothelial cells consisting of NOX2, $p22^{phox}$, $p47^{phox}$ and $p67^{phox}$. Moreover, NOX4 was shown to generate ROS if co-expressed with $p22^{phox}$ but $p47^{phox}$ and $p67^{phox}$ cytosolic subunits and also novel subunits NOXO1 and NOXA1 provide no further increase in its activity (Ago *et al.*, 2004; Kawahara *et al.*, 2005). The difference between phagocytic and non-phagocytic NOX is showed in **Figure 1.10**.

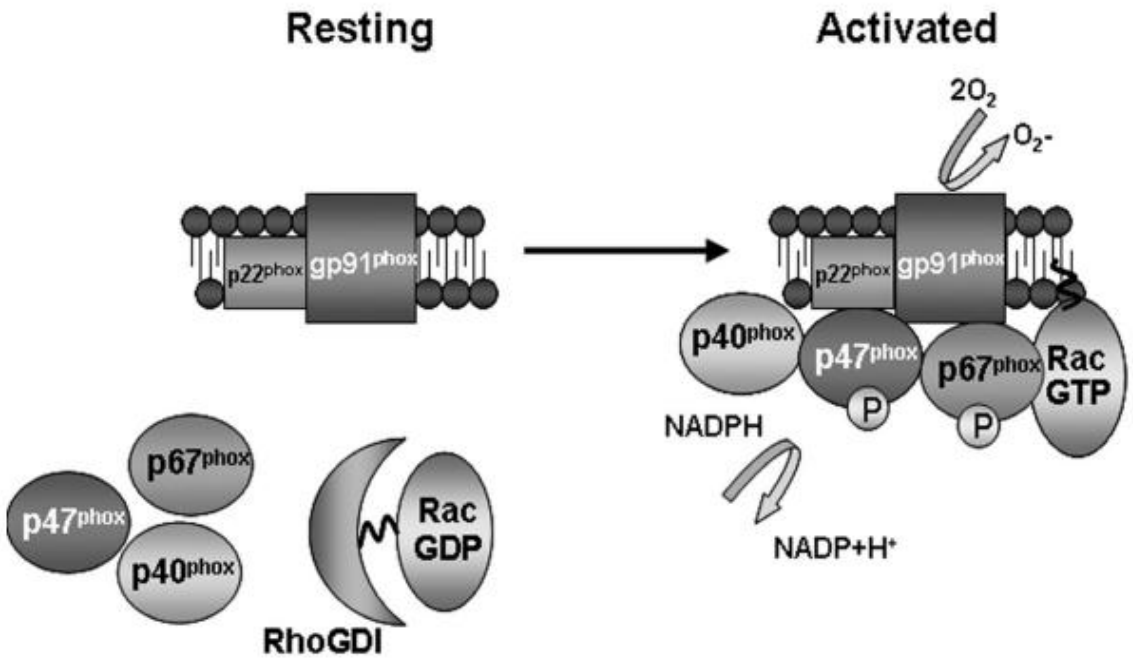

Figure 1.9: Activation of the NADPH oxidase (NOX) complex

NADPH oxidase (NOX) consists of two integral membrane proteins, $p22^{phox}$ and $gp91^{phox}$ (NOX2), which form a heterodimeric flavoprotein known as cytochrome b_{558}. Cytosolic components consist of $p47^{phox}$, $p67^{phox}$, $p40^{phox}$ and the small G-protein Rac. Upon activation (by various inflammatory stimuli), cytoplasmic signalling events stimulate the phosphorylation of $p47^{phox}$ and $p67^{phox}$ and the GDP/GTP exchange on Rac. The cytosolic components then translocate to the membrane where they form a complex with cytochrome b_{558}. The oxidase complex then initiates electron flow and generation of O_2^- through the NADPH-derived electron reduction by the flavocytochrome (adapted from (Wilkinson & Landreth, 2006)).

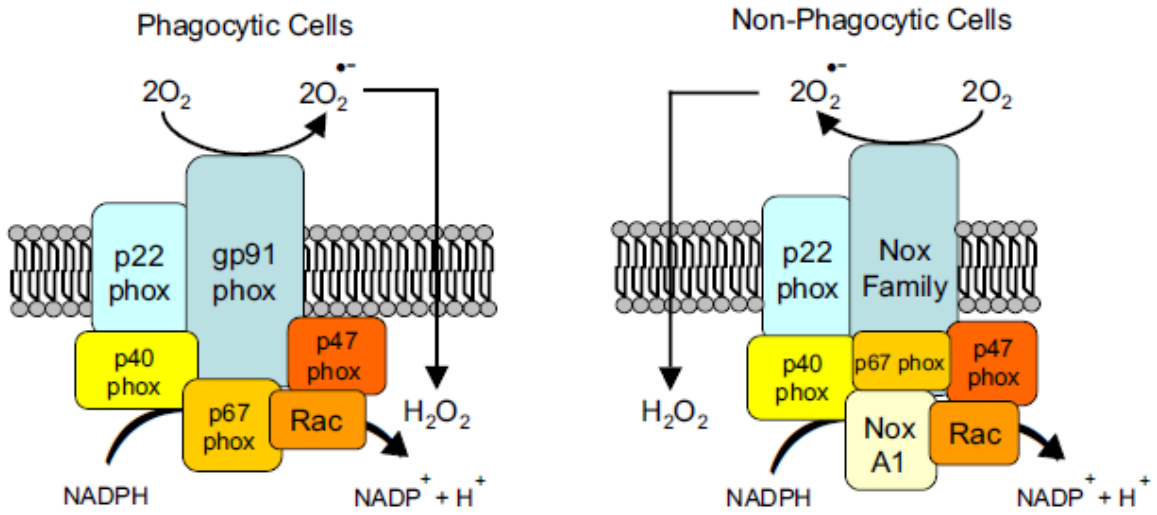

Figure 1.10: Differences of NADPH oxidase components between phagocytic and non-phagocytic cells

(Novo & Parola, 2008)

Studies have revealed that various stimuli may lead to the activation of NOX and ROS production. OxLDL has been suggested to activate NOX through CD36 binding in smooth muscle cells (Sukhanov *et al.*, 2006) whereby ROS production after oxLDL treatment caused the loss of the glycolytic enzyme, GAPDH. Subsequently, this halted cellular ATP stores and led to necrosis. The loss of GAPDH can be prevented by NOX inhibitors and various antioxidants (Sukhanov *et al.*, 2006). Additionally, in smooth muscle cells, ROS production and GAPDH loss was also prevented by anti-CD36 antibodies, suggesting that NOX activation could be triggered by oxLDL binding to CD36 (Sukhanov *et al.*, 2006).

NOX-derived ROS and atherosclerosis

The importance and involvement of NOX in inflammatory diseases including atherosclerosis has been extensively studied (Aviram *et al.*, 1996; Harrison *et al.*, 2003; Singh & Jialal, 2006). Generally, all processes related to the development of atherosclerotic plaque are associated with NOX (Amanso & Griendling, 2012). As an example, NOX-derived superoxide from macrophages might contribute to the oxidation of lipids in atherosclerosis (Cathcart, 2004). In human atherosclerotic plaque, Sorescu *et al.* (2002) has demonstrated the increase of NOX2 parallel with the atherosclerotic plaque development whereas NOX4 mRNA remained unchanged throughout the stages of atherosclerosis. However, NOX4 expression was much lower in advanced lesions. Another study by Barry-Lane *et al.* (2001) have demonstrated the role of NOX in apolipoprotein E and $p47^{phox}$ ($ApoE^{-/-}/p47^{phox-/-}$) double-knock out mice where a marked reduction of atherosclerotic lesions was observed.

NOX inhibitors

Currently, there are a number of NOX inhibitors being used mostly in experimental works, classified as peptide and non-peptide based inhibitors. Among the peptide based inhibitors are PR-39 antibiotic peptide (Shi *et al.*, 1996) and gp91-ds-tat (Rey *et al.*, 2001) while the non-peptide inhibitors include DPI (diphenyl iodonium) (Majander *et al.*, 1994), phenylarsine oxide (PAO) (Vignais, 2002), gliotoxin (Nishida *et al.*, 2005), 4-(2-aminoethyl)-benzenesulfonyl fluoride (AEBSF) (Diatchuk *et al.*, 1997), neopterin (Kojima *et al.*, 1993), plumbagin (Ding *et al.*, 2005), S17834 (Cayatte *et al.*, 2001), apocynin (Basu *et al.*, 1971) and VAS2870 (ten Freyhaus *et al.*, 2006). GKT is another compound emerging as a promising and clinically relevant NOX inhibitor (Altenhofer *et al.*, 2014). Although there are

many possible NOX inhibitors available, most of them are either non-specific (Bedard & Krause, 2007) or are having unclear mechanism of action.

Apocynin

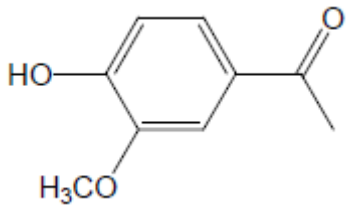

Figure 1.11: Chemical structure of apocynin
(Petronio *et al.*, 2013)

Apocynin (4-hydroxy-3-methoxy-acetophenone) (**Figure 1.11**), isolated from the roots of a *Picrorizha kurroa* plant (Basu *et al.*, 1971) is a naturally occurring NOX inhibitor used in Ayurvedic medicine for the treatment of asthma. Apocynin has been studied as a possible remedy for many inflammation related diseases including cardiovascular disease (Williams & Griendling, 2007). It inhibits NOX activity in neutrophils (Simons *et al.*, 1990) and non-phagocytic cells (Meyer *et al.*, 1999). Even though its exact mechanism of action is unknown, it is proposed that apocynin prevents the translocation of $p47^{phox}$ and $p67^{phox}$ to the membrane thus blocking NOX assembly (Meyer *et al.*, 1999; Stolk *et al.*, 1994a). Its inhibitory action is believed not to be NOX specific but also involves myeloperoxidase (MPO) (Van den Worm *et al.*, 2001). Nevertheless, it has been suggested that apocynin requires H_2O_2 and peroxidases (e.g. MPO) to be activated into an active dimer of diapocynin (Stolk *et al.*, 1994a; Vejrazka *et al.*, 2005) that reacts with thiol groups in the NOX subunit which prevents NOX assembly upon activation.

Apocynin has been described as a promising candidate for therapeutic and research uses because of good oral bioavailability and not toxic *in vivo*. Apocynin is known to be a potent intracellular inhibitor of superoxide generation by activated neutrophils and eosinophils (Stolk *et al.*, 1994a; Stolk *et al.*, 1994b). However, studies have shown that apocynin can also stimulate ROS generation in non-phagocytic cells (Riganti *et al.*, 2006; Vejrazka *et al.*, 2005) thus raised the issue of specificity of this compound in exerting its effects. Moreover, apocynin has been shown to act more as an antioxidant by increasing GSH synthesis and activates the AP-1 transcription factor (Lapperre *et al.*, 1999). Apocynin also affects cell

processes in the vasculature other than NOX activity including arachidonic acid metabolism (Engels *et al.*, 1992), nitric oxide synthesis and cyclooxygenase pathway (Aldieri *et al.*, 2008; Heumuller *et al.*, 2008). Besides, apocynin has also been shown to be a direct ROS scavenger in certain experimental conditions (Heumuller *et al.*, 2008).

VAS2870

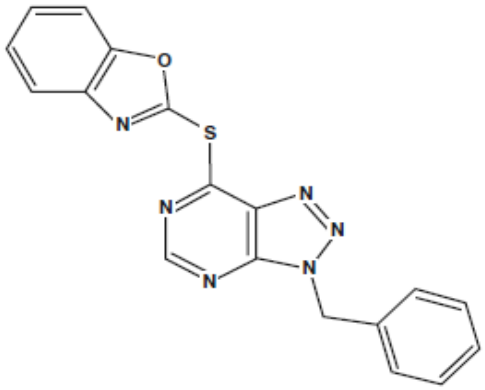

Figure 1.12: Chemical structure of VAS2870
(Stielow *et al.*, 2006)

VAS2870 (3-benzyl-7-(2-benzoxazolyl)thio-1,2,3-triazolo(4,5-d)pyrimidine) (**Figure 1.12**) is the prototype of the triazolo pyrimidine compounds reported to act as a rapid and reversible inhibitor of NOX activity (Schramm *et al.*, 2012). VAS2870 has been shown to inhibit NOX activity in oxLDL-exposed human umbilical vein endothelial cells (HUVEC), which mainly expressed NOX4 (Stielow *et al.*, 2006) and platelet-derived growth factor (PDGF)-stimulated rat smooth muscle cells (ten Freyhaus *et al.*, 2006). In addition, VAS2870 does not have direct ROS scavenging properties and does not interfere with xanthine oxidase-mediated ROS generation (ten Freyhaus *et al.*, 2006). Despite its ability to inhibit NOX, its mechanism of action remains elusive. In human leukocytes, ten Freyhaus *et al.* (2006) have shown that VAS2870 does not block the translocation of $p47^{phox}$ to the membrane, instead it may interfere with NOX assembly once the translocation occurred. This is supported by experiments in a cell free system that showed inhibition of VAS2870 on NOX2 activity when added before but not after NOX has been stimulated (Wingler *et al.*, 2011).

VAS2870 has been regarded as not selective for any NOX isoforms since it also inhibited NOX2-induced oxidative stress in HL-60 cells and in a cell free system of human neutrophils (ten Freyhaus *et al.*, 2006). Therefore, studies are required to determine the characteristics of

VAS2870 and its derivatives in terms of their specific mechanism of action, pharmacokinetics and efficacy (Wingler *et al.*, 2011). In addition, VAS2870 has been shown to modify T regulatory cell function (Efimova *et al.*, 2011) and increases TGF-β-induced apoptosis of liver tumour cells (Sancho & Fabregat, 2011). VAS2870 also inhibits the stimulation of vasculogenesis of mouse embryonic stem cells upon treatment with PDGF-BB (Lange *et al*., 2009).

7,8-dihydroneopterin (7,8-NP)

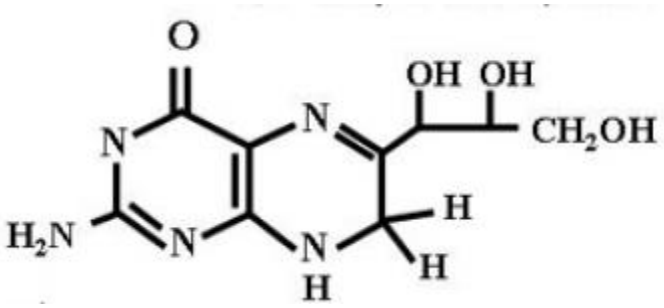

Figure 13: Chemical structure of 7,8-NP

In macrophages, γ-interferon (IFN-γ) which is released by activated T cells stimulates the synthesis and secretion of 7,8-NP (**Figure 1.13**). Gieseg *et al.* (2009a) suggests that in atherosclerotic plaque, 7,8-NP may exert its effects within inflammatory sites to protect macrophages from the possible oxidants. *In vitro* studies have shown that 7,8-NP is a potent antioxidant that can prevent oxidative damage on cells, cellular membranes, cellular proteins and protein thiols (Duggan *et al.*, 2002; Gieseg *et al.*, 2000; Gieseg *et al.*, 2001b).

The protective effects of 7,8-NP appears to be attributed to its radical scavenging capability. 7,8-NP has been shown to scavenge oxidants, including superoxide and hydrogen peroxide (Shen, 1994), hydroxyl radicals (Heales *et al.*, 1988), peroxyl radicals (Oettl *et al.*, 2004), lipid peroxyl radicals (Gieseg *et al.*, 1993) and HOCl (Yang, 2009). 7,8-NP can also prevent copper-, peroxyl radical- and cell-mediated LDL oxidation by scavenging the lipid-derived radicals which promote the protein peroxidation (Gieseg *et al.*, 2003; Gieseg *et al.*, 1995).

Moreover, 7,8-NP has also been shown to prevent oxLDL-induced intracellular GSH loss in U937 cells by scavenging oxLDL-mediated ROS, which in turn maintained the intracellular redox environment, thus prevented cell death (Baird, 2003). 7,8-NP may also protect

HMDMs from oxLDL-mediated cell death via down-regulation of scavenger receptor CD36, therefore decreasing CD36-mediated uptake of oxLDL (Gieseg *et al.*, 2010). Much evidence in the literature have also recorded the anti-inflammatory and antioxidant properties of 7,8-NP. Thus, with known antioxidant capacity and the ability of protecting cells from oxLDL-induced cell death from previous investigations, 7,8-NP is of relevant to this research.

Hydrogen sulfide (H_2S)

Hydrogen sulfide (H_2S) is a colourless, flammable and poisonous gas with a characteristic rotten egg odour. It is present in the effluent of hydrothermal vents and sulphur springs (di Masi & Ascenzi, 2013; Smith & Gosselin, 1979) and has long been known as a toxic pollutant (Mancardi *et al.*, 2009). Interestingly, H_2S has been recognized as an important signalling molecule of the cardiovascular, inflammatory and immune systems (Wagner *et al.*, 2009). It plays a vital role as a novel biologically active gas alongside with nitric oxide (NO) and carbon monoxide (CO) which involves in intracellular signalling processes (Song *et al.*, 2014).

Biosynthesis and metabolism

H_2S is enzymatically synthesised from amino acid cysteine, homocysteine and cystathionine by pyridoxal-5'-phosphate (PLP)-dependent enzymes such as cystathionine-β-synthase (CBS; E.C. 4.2.1.22) and cystathionine-γ-lyase (CSE; E.C. 4.4.1.1) (Vandiver & Snyder, 2012; Wang, 2002; Whiteman *et al.*, 2011a). CBS and CSE are expressed in various locations including the brain, peripheral nervous system, liver, joint cells, intrauterine tissue, placenta and kidney (Whiteman *et al.*, 2011a). However, CBS is predominantly expressed in the brain and nervous system (Abe & Kimura, 1996; Kimura, 2000) while CSE is mainly observed in vascular smooth muscle cells and in the heart (Geng *et al.*, 2004; Zhao *et al.*, 2001). It has also been proposed that 3-mercaptopyruvate sulfurtransferase (3-MST) which is an α-ketoglutarate and cysteine-dependent enzyme located in mitochondria (Shibuya *et al.*, 2009) generates H_2S within the mitochondria (Modis *et al.*, 2013a). 3-MST is also expressed in the brain and most of the H_2S produced by this enzyme is bound to the form of sulfane sulphur.

In vivo, H_2S is metabolised by oxidation in mitochondria or by methylation in cytosol and can be scavenged by methemoglobin or by metallo- or disulfide-containing molecules such as oxidised glutathione (Beauchamp *et al.*, 1984; Wang, 2003). H_2S is mainly excreted in the

kidney as free or conjugated sulfate and as thiosulfate (Wang, 2003) and is also exhaled from the lungs. Biosynthesis and metabolism of H_2S are simplified in **Figure 1.14**.

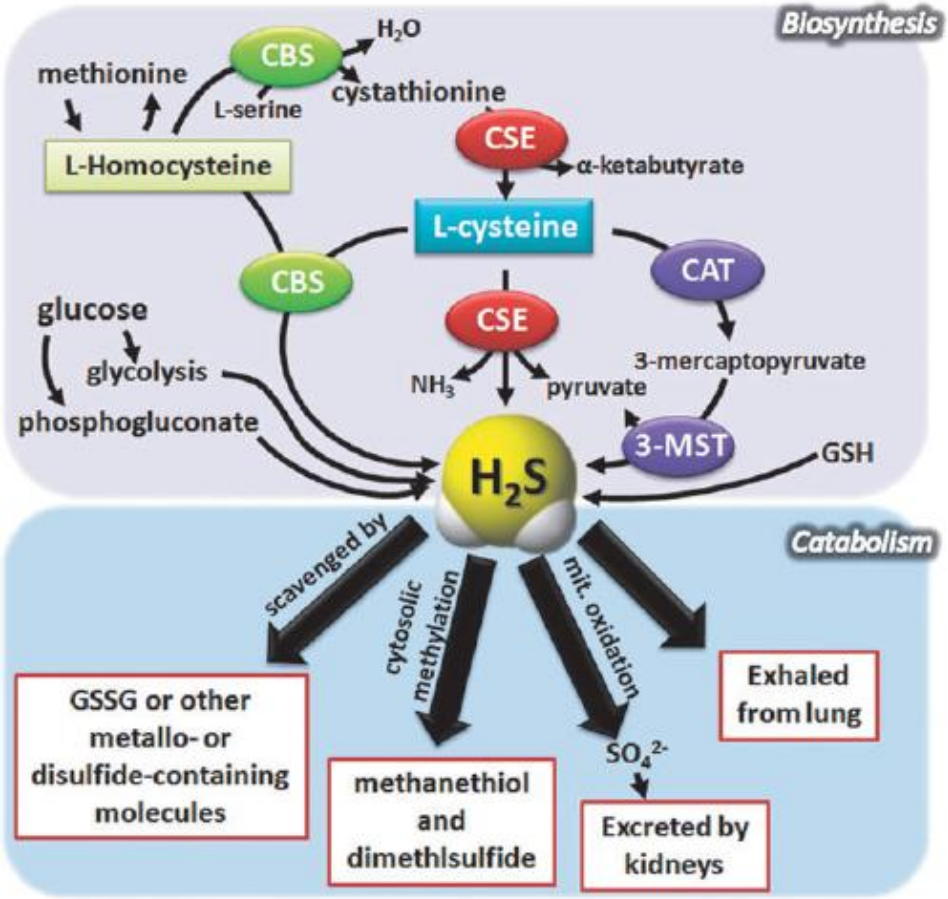

Figure 1.14: H_2S metabolism pathways
(Mani *et al.*, 2014)

Physiological and pathophysiological roles of H_2S

Various physiological effects of H_2S include as a major endothelium-derived hyperpolarizing factor (EDHF) which causes hyperpolarization and vasorelaxation of vascular endothelium and smooth muscle cells (Mustafa *et al.*, 2011; Yang *et al.*, 2008). As an antioxidant, H_2S can also prevent cytokine or oxidant-induced oxidative damage (Taniguchi *et al.*, 2011). Moreover, H_2S can also down-regulate NF-κB activation or up-regulate heme oxygenase 1 expression, thus inhibiting the expression of pro-inflammatory factors (Hu *et al.*, 2007; Oh *et al.*, 2006; Pan *et al.*, 2011). Additionally, H_2S may help in regulating various bodily functions with its cytoprotective (Calvert *et al.*, 2010), antifibrotic (Tan *et al.*, 2011) and antiapoptotic properties (Sen *et al.*, 2012).

Pathophysiological role of H_2S has been implicated in many inflammatory and cardiovascular diseases (Bhatia, 2012). H_2S has been demonstrated to protect against oxidative injury in *in vivo* and *in vitro* models of myocardial ischemia-reperfusion models (Chen *et al.*, 2007; Chen *et al.*, 2006). Moreover, the inhibition of H_2S synthesis has been shown to accelerate the recovery of mean arterial pressure in a haemorrhagic shock model (Mok *et al.*, 2004). Other beneficial effects of lowering H_2S levels was demonstrated in carrageenan-induced hindpaw edema (Bhatia *et al.*, 2005b), acute pancreatitis (Bhatia *et al.*, 2005a) and septic shock (Li *et al.*, 2005). **Table 1.3** summarizes various H_2S roles in physiological and pathological conditions.

Table 1.3: H_2S roles in physiological and pathophysiological conditions

(adapted from di Masi & Ascenzi (2013))

	Physiological roles	**Pathophysiological roles**
Cardiovascular system	Homeostatic regulation of blood pressure	Cardiovascular diseases (atherosclerosis, hypertension, myocardial injury)
Central nervous system	Neuroprotective effect	Neuroinflammation and neurodegenerative diseases
Respiratory system	Lung remodelling Inhibition of collagen accumulation	Respiratory distress
Endocrine system	Regulation of pancreatic structure and function	Diabetes
Gastrointestinal system	Motility of jejunum and colon Regulation of secretion	Inflammation

Research programme

During atherosclerotic lesion formation, oxLDL has been shown to play a vital role in causing cell death to the macrophages. Since the pathogenesis of atherosclerosis is complex, extensive studies have been done by researchers around the world to develop understanding of this disease. The major aim of this PhD project is to investigate the mechanism of cell death induced by oxLDL focusing on intracellular oxidants (ROS) production, particularly superoxide. The current research will study and compare these effects in three different types

of cells i.e. U937 cells, human monocytes and human monocytes derived macrophages (HMDM cells). U937 cell line has been used extensively in various health and disease studies whereas human monocytes and HMDM cells are the best type of cells for *in vitro* study since those cells are involve in the development of atherosclerosis *in vivo*. Although the exact mechanism and the real processes that occurred *in vivo* are never known, these cells will be the best to mimic the actual phenomena happening in the human body.

The initial part of **Chapter Three** will examine the cytotoxic effects of oxLDL on cell viability of U937, human monocytes and HMDM cells. Effects of oxLDL on cell morphology and cell viability will be determined to establish the LC_{50} concentration for each batch of oxLDL prepared for further experimentation throughout the research programme. The analysis was to confirm and extend the studies done by previous researchers in this group. Comparison between MTT and PI-flow cytometry assays for the determination of cell viability will also be studied to validate the agreement between the two methods and to determine the benefits and drawbacks of one assay over another.

Previous studies have shown that oxLDL had caused oxidative stress by inducing intracellular production of ROS through the activation of NADPH oxidase (NOX) enzymes on the plasma membrane of the cells. Accordingly, **Chapter Four** will study the effects of oxLDL-induced oxidative stress, ROS generation and NOX activation mechanism. The effects of NOX inhibitors i.e. apocynin and VAS2870 as well as 7,8-dihydroneopterin on intracellular ROS production and cell viability will also be studied.

Study by our previous researcher in this laboratory has showed the importance of calcium (Ca^{2+}) in HOCl-mediated cell death in HMDM cells. Our hypothesis is that Ca^{2+} is essential and is the main cause of oxLDL-mediated cell death. Hence, **Chapter Five** will investigate the role of Ca^{2+} in oxLDL-mediated cell death. The study will examine the effects of intracellular and extracellular Ca^{2+} on cell death induced by oxLDL. Different types of Ca^{2+} channel inhibitors and Ca^{2+} chelators will be tested to determine their ability in preventing intracellular Ca^{2+} rise when induced with oxLDL as well as preserving cell viability from the toxicity of oxLDL.

Hydrogen sulfide (H_2S) involvement in biological processes has proved to be promising, particularly with atherosclerosis. Therefore, **Chapter Six** will study for the first time the

effects of different types of slow releasing H_2S donor compounds on oxLDL-mediated cell death. If these compounds are able to protect cell death caused by oxLDL, their mechanism of action will also be investigated with regards to Ca^{2+} and ROS generation.

CHAPTER TWO

2. Materials and methods

Materials

Reagents

Throughout this research, experiments were carried out using reagents of analytical grade or better. Water was deionized and ultrafiltered using a Milli-Q filtration water system and, unless otherwise stated, all solutions were prepared using this nanopure water.

β-mercaptoethanol	Sigma Chemical Co., Missouri, USA
2-aminoethoxydiphenyl borate (2-APB)	Sigma Chemical Co., Missouri, USA
3-[4,5-Dimethylthiazol-2-yl]-2,5-diphenyl-tetrazolium bromide (MTT)	Sigma-Aldrich Co., LLC, New Zealand
4-bromo-calcium ionophore A23187 (Br-A)	Sigma Chemical Co., Missouri, USA
4-Morpholine-propanesulfonic acid (MOPS)	Sigma Chemical Co., Missouri, USA
7,8-Dihydroneopterin (7,8-NP)	Schirck Laboratories, Switzerland
Acetic acid (glacial)	Scharlau Chemie S.A., Barcelona, Spain
Acetone	Merck Ltd, Poole, England
Anchor non fat milk powder	Fonterra New Zealand, Ltd, New Zealand
4'-hydroxy-3-methoxyacetophenone (apocynin)	Sigma Chemical Co., Missouri, USA
Argon gas	BOC Gases, Auckland, New Zealand
BAPTA-AM	Invitrogen, Life Technologies, New Zealand
Bicinchoninic acid (BCA) protein determination kit	Pierce, Illinois, USA
Bovine serum albumin (BSA)	Gibco Invitrogen Corporation, Auckland, New Zealand
Bromophenol blue	Sigma Chemical Co., Missouri, USA
Calcium ionophore A23187	Sigma Chemical Co., Missouri, USA
Chelex 100 resin	Bio-Rad Laboratories, California, USA
Cholesterol reagent	Roche Diagnostics, USA
Copper chloride ($CuCl_2$)	Sigma Chemical Co., Missouri, USA
Coumassie blue	Bio-Rad Laboratories, California, USA
Cyclosporin	Sigma Chemical Co., Missouri, USA

2′,7′-dichlorodihydrofluorescein diacetate (H_2DCF-DA)	Invitrogen,, Oregon, USA
Dantrolene	Sigma Chemical Co., Missouri, USA
Dihydroethidium (DHE)	Invitrogen,, Oregon, USA
Dimethyl sulphoxide (DMSO)	BDH Laboratory Supplies Ltd., Poole, England
Dipotassium phosphate (K_2HPO_4)	Scharlau Chemie, Italy
Ethanol	Merck, Darmstadt, Germany
Ethylenediaminetetraacetic acid (EDTA)	Sigma Chemical Co., Missouri, USA
Ethyleneglycoltetraacetic acid (EGTA)	Sigma Chemical Co., Missouri, USA
Ferrous ammonium sulphate	Sigma Chemical Co., Missouri, USA
Flunarizine	Sigma Chemical Co., Missouri, USA
Fluo 3 AM	Invitrogen,, Oregon, USA
Glycerol	Sigma Chemical Co., Missouri, USA
Glycine	Bio-Rad Laboratories, California, USA
Granulocytes-macrophage colony-stimulating factor (GM-CSF) as Leukine® sargamostim	Seattle, USA
Hydrochloric acid, fuming 37 % (HCl)	Merck, Darmstadt, Germany
Isopropanol	Mallinckrodt Chemicals, New Jersey, USA
Methanol	Merck, Darmstadt, Germany
MitoSox red	Invitrogen,, Oregon, USA
Molecular Weight Marker	Bio-Rad
Nifedipine	Sigma Chemical Co., Missouri, USA
Nitrogen gas	BOC Gases, Auckland, New Zealand
NuPAGE 4-12% Bis-Tris Gel, 1.0 mm x 10 well	Invitrogen, California, USA
Phorbol 12-myristate 13-acetate (PMA)	Sigma Chemical Co., Missouri, USA
Ponceau S	Sigma Chemical Co., Missouri, USA
Potassium bromide (KBr)	Merck, Darmstadt, Germany
Potassium chloride (KCl)	Merck Darmstadt, Germany
Potassium dihydrogen phosphate (KH_2PO_4)	Scharlau Chemie, Italy
Potassium hydroxide (KOH)	Merck, Darmstadt, Germany
Ruthenium Red	Sigma Chemical Co., Missouri, USA
Sodium chloride (NaCl)	Merck, Darmstadt, Germany
Sodium dihydrogen orthophosphate monohydrate ($NaH_2PO_4.H_20$)	Merck, Darmstadt, Germany
Sodium dodecyl sulphate (SDS)	Sigma-Aldrich Co., LLC, New Zealand
Sodium hydrogen carbonate ($NaHCO_3$)	Merck, Darmstadt, Germany
Sodium hydroxide (NaOH)	Scharlau Chemie, Italy
Supersignal West Dura chemiluminescence	Pierce Biotechnology Inc., Illinois, USA
Thapsigargin	Sigma-Aldrich Co., LLC, New Zealand
Thimerosal	Sigma Chemical Co., Missouri, USA

Trichloroacetic acid (TCA)	Sigma Chemical Co., Missouri, USA
Tris buffer	Roche Diagnostics GmbH, Mannheim, Germany
Trypan blue solution (0.4%)	Sigma Chemical Co., Missouri, USA
Tween-20	Sigma Chemical Co., Missouri, USA
VAS2870	Sigma Chemical Co., Missouri, USA
Verapamil hydrochloride	Sigma Chemical Co., Missouri, USA

Media

Foetal bovine serum (FBS)	Invitrogen, Life Technologies, New Zealand
Penicillin/Streptomycin (10000 units/ml penicillin G and 10000 µg/ml streptomycin)	Invitrogen, Life Technologies, New Zealand
Roswell Park Memorial Institute (RPMI) -1640 media, with phenol red	Sigma-Aldrich Co., LLC, New Zealand
Roswell Park Memorial Institute (RPMI) -1640 media, without phenol red	Sigma-Aldrich Co., LLC, New Zealand
Earle's Balanced Salt Solution (EBSS)	Gibco® , Life Technologies, New Zealand

Antibodies

Mouse monoclonal against β-Actin	Sigma-Aldrich Chemical Co., USA
Mouse monoclonal IgG_1 p47-phox	Santa Cruz Biotechnology Inc., USA
Goat Anti-mouse IgG HRP-conjugated	Santa Cruz Biotechnology Inc., USA

General solutions and buffers

Phosphate buffered saline (PBS)

Phosphate buffered saline (PBS) contained 150 mM sodium chloride (NaCl, MW= 58.44 g/mol) to 10 mM sodium dihydrogen orthophosphate (pH 7.4) ($NaH_2PO_4.H_2O$, MW= 137.99g/mol). A litre of PBS was prepared by adding 50 mL of 3M NaCl, 40 mL of $NaH_2PO_4.H_2O$ (pH 7.4) and 910 mL of nano-pure water. PBS solution for cell culture work was vacuum filtered using a 0.45um membrane (Phenomenex) and sterilized by autoclaving (15 minutes, 121ºC and 15 psi). Prior to use with cells, it was warmed up to 37ºC in a water bath.

7,8-dihydroneopterin (7,8-NP) solution

A 2 mM stock of 7,8-dihydroneopterin (7,8-NP) (MW= 255.2 g/mol) was prepared fresh every time, immediately before each experiment. 7,8-NP powder (Schircks Laboratories, Switzerland) was dissolved in the appropriate medium (depending on experiment to be done) followed by 10-15 minutes ultrasonication. The 7,8-NP solution was then filter-sterilised using a 0.22 µm MS® PES syringe filter (Membrane Solutions, USA) and diluted to working concentrations before added to cells. The solution was kept on ice at all times.

Apocynin solution

A 2 mM stock solution of apocynin (MW= 166.17 g/mol) was prepared by dissolving apocynin powder (Sigma-Aldrich) in PBS or RPMI-1640 media. After being filter-sterilised through a 0.22 µm MS® PES syringe filter, the solution was stored at -4^{o}C and used within a month.

Phorbol 12-myristate 13-acetate (PMA)

A 5 mM stock solution of PMA (MW= 616.83 g/mol) was made by dissolving PMA in DMSO, stored at -20 ºC and diluted to 5 µM in PBS or RPMI1640 with no phenol red before addition to the cells.

MTT assay solution

MTT (3-[4,5-Dimethylthiazol-2-yl]-2,5-diphenyl-tetrazolium bromide) stock solution was prepared by dissolving MTT powder (Sigma-Aldrich Co., St. Louis, USA) in RPMI 1640 without phenol red to give a final concentration of 5 mg/mL. This solution was filter-sterilised using a 0.22 μm MS® PES syringe filter and stored at -20 ºC in the dark until use. For viability assay, the stock solution was diluted in pre-warmed RPMI-1640 without phenol red to give a final concentration 0.5 mg/mL MTT.

A 0.01 M HCl solution was made up from 11.44 M HCl and nano pure water. Sodium dodecyl sulphate (SDS) powder was added to this solution and stirred up slowly to give a final concentration of 10% ($^{w}/_{v}$) SDS.

Methods

Cell culture

All cell culture work and experiments were conducted under aseptic conditions in a class II biological safety cabinet (Clyde-Apex BH 200). All equipment and plastic wares were supplied sterile, ready to use and disposable (Falcon, Terumo, Unomedical, Greiner Bio-one) or had been sterilised by autoclaving (15 min, 121^{o}C, 15 psi). All media and solutions were sterilised either by autoclaving or by filtration through a sterile 0.22 μm membrane filter (Membrane Solutions, USA). All equipment and tissue culture items were sprayed thoroughly with 70% ($^{v}/_{v}$) ethanol (diluted in distilled water) before being placed into the class II biological safety cabinet. Cells were incubated in an incubator at 37ºC in a humidified atmosphere containing 5% CO_2 (Sanyo Electric Co. Ltd., Japan).

Cell culture media

Cell culture media with different chemical compositions were used for cell culture depending on the suitability of the cells and experimental conditions. In the present study, Roswell Park Memorial Institute 1640 medium (RPMI-1640) was used in the culture of U937 cell line, human monocytes and human monocyte derived macrophages (HMDM).

Roswell Park Memorial Institute (RPMI)-1640 media (with or without phenol red)

The media was prepared according to the manufacturer's instructions. Powdered RPMI (with or without phenol red) was first dissolved in nano-pure water. Whenever necessary, 11.4 M hydrochloric acid (HCl) was added to completely dissolve the powder. It was then followed by the addition of sodium bicarbonate ($NaHCO_3$) and pH adjustment to 7.4 with 1 M NaOH. The media was filter-sterilised through a 0.22 um MillexR-GP filter/a 0.20 µm Sartolab®-P20 filter (Sartorius AG, Goettingen, Germany) using a peristaltic pump (CP-600, Life Technologies) into sterile 500 mL bottles. The prepared media was stored at 4ºC and warmed to 37ºC in a water bath before use.

Earle's Balanced Salt Solution (EBSS) (without calcium, magnesium and phenol red)

EBSS (Gibco®, Life Technologies) was used for experiments that involved determination of intracellular and extracellular calcium. This solution was supplied as ready to use. $CaCl_2$ was added to the solution to give a concentration of 0.423 nM of calcium when needed for experiments.

Standard RPMI-1640 media

RPMI-1640 medium (with phenol red) supplemented with 100 U/mL penicillin G, 100 µg/mL streptomycin and 5% (v/v) foetal bovine serum (FBS) was used for normal U937 cell maintenance. As for human monocytes and HMDM, 10% (v/v) human serum was used to substitute FBS for normal cell maintenance.

Cell culture experimental conditions and procedures

Experiments were performed using 24-well suspension culture plates (Cellstar®, Greiner Bio-one) for both U937 cells and human monocytes. For experiments with U937 cells, wells of the plates were coated with 8 µL of 50 mg/mL bovine serum albumin (Sigma-Aldrich) whereas 5% human serum was added for human monocytes. Total experimental volume was 1 mL for each well. Cells were counted using a haemocytometer and a light microscope after staining with trypan blue at a ratio of 1:1 for U937 cells whereas for human monocytes a ten times dilution with trypan blue was normally perform prior to cell counting. The required quantity of cells for the experiment was centrifuged at 500 g for 5 minutes at room temperature and re-suspended in the appropriate experimental medium at 37ºC. The cell

suspension was then aliquoted into wells containing the medium at a final concentration of 0.5 x 10^6 cells/mL for U937 cells and 1 x 10^6 cells/mL for human monocytes.

Unless stated otherwise, experiments for HMDM were performed in the original plates where they were seeded into at a concentration of 1 x 10^6 cells/mL in a 48 well plates. The total volume of incubation medium during experiments was 500 µL and 5% human serum was also added into each well during treatment.

Preparation of human serum for cell culture

Human serum used for cell culture of human monocytes and HMDM in the present study was from haemochromatosis blood donors obtained under ethics approval CTY/98/07/069 approved by the Upper South (B) Regional Ethics Committee. Unlinked blood from consenting donors was collected into 450 mL dry blood bags (no anticoagulant added, Fresenius Kabi, Homburg, Germany) by the New Zealand Blood Service (Riccarton branch, Christchurch). The blood bags were left in a vertical position in the poplypropylene container at room temperature for 2 hours to allow blood clot. Subsequently, the blood bags were transferred to 4^{o}C fridge and stored overnight to grant adequate time for the separation of serum from the clot.

Next, the blood bags were cut opened under aseptic conditions in the CII cabinet and the serum was collected into 50 mL centrifuge tubes using a 25 mL sterile plastic pipette. The tubes were centrifuged for 15 minutes at 1000 g (Heraeus Multifuge-SR, BioStrategy,New Zealand) to pellet the remaining red blood cells. If the resulting serum appeared to contain any red blood cells, the centrifugation was repeated. The clear serum obtained after centrifugation was transferred to new 50 mL tubes and stored in a – 20^{o}C freezer until frozen followed by a – 80^{o}C freezer for long term storage of up to 6 months.

Preparation and culture of U937 cell line

The U937 cell line is a type of immortal cell line and was originally isolated from the pleural fluid of a 37 year old male patient with histiocytic lymphoma (Sundstrom & Nilsson, 1976). U937 cells resemble many monocyte/macrophage-like morphology and characteristics and they are widely used as an *in vitro* model for various biomedical research. U937 cells used in

this laboratory were a gift from the Haematology Research Laboratory at the Christchurch School of Medicine, University of Otago and stored in 1 mL vials in liquid nitrogen storage.

Before the cells are being used for experiments, a frozen 1 ml vial containing 20 x 10^6 cells/mL in DMSO was removed from liquid nitrogen storage and defrosted in a water bath at 37ºC until almost completely thawed. The concentrated cell suspension was poured into 30 ml of RPMI-1640 medium in a 50 ml centrifuge tube and centrifuged at 500 g for 5 minutes to separate the DMSO freezing medium and the cells. The cell pellet was resuspended in 10 ml of RPMI-1640 medium in a 25 cm^2 tissue culture flask (Falcon, BD, USA).

Once the cells achieved an appropriate density i.e. approximately 1.0 x 10^6 cells/mL and are having a normalised division rate followed by 20-48 hours in the subsequent subculturing, they were considered fit for experimental purpose. Microscopically, U937 cells are round in shape with short microvilli (Pagliara *et al.*, 2005). Cell density was maintained at 0.3-1.5 x 10^6 cells/mL by subculturing in Cellstar® 150 cm^2 tissue culture flasks (Greiner Bio-one, Germany) every 2-4 days. A new stock of the concentrated U937 cells was brought up after six month of usage of the existing cells in order to avoid any contaminations or possible problems associated with prolonged cell culture.

Preparation and culture of human monocytes and human monocytes derived macrophages (HMDM)

Isolation of monocytes from whole blood

Blood with no donor identification (unlinked) from healthy consenting haemochromatosis individuals were collected into 500 mL autologous blood bag containing citrate phosphate dextrose adenine anticoagulant (CPDA-1, Compoflex®) by the New Zealand Blood Service (NZBS). The cells were normally prepared immediately after blood collection or kept for up to 18 hours at 4ºC if processing cannot be carried out on the same day.

The technique described by Amit (2008) and Yang (2009) has been used to separate the monocytes from other types of blood cells. Firstly, a bag of whole blood was inverted gently for 10-12 times to ensure even distribution of the cells before placing it into the CII cabinet aseptically. Next, one of the blood bag tube was cut opened and the blood was transferred into sterile 50 mL centrifuge tubes and centrifuged at 1000 g (slow deceleration) for 30

minutes at room temperature. After centrifugation, the cells were separated into a few layers consisting of erythrocytes at the bottom, topped with white layer of leukocytes (buffy coat) and overlaid with plasma layer. The plasma layer was aspirated leaving the leukocytes layer (approximately 17.5 mL) which was removed using a mixing cannula attached to a 10 mL plastic syringe, pooled and mixed with equal volume of PBS by inverting thoroughly. The mixture was then under laid with 15 mL of Lymphoprep® (lymphoprep) using a mixing cannula attached to a 20 mL plastic syringe before being centrifuged again at 1000 g (slow acceleration/deceleration) for 30 minutes at room temperature. The resulting white layer of monocytes/lymphocytes was visible about halfway down the 50 mL tube encircled by clear plasma and lymphoprep layers. The top layer solution was aspirated leaving approximately 2 cm above the leukocytes layer.

The cells in solution were transferred into a new 50 mL centrifuge tubes using a mixing cannula attached to plastic syringe and thoroughly resuspended and evenly divided between a designated numbers of tubes with each containing 15 mL of solution. A volume of 30 mL of PBS was topped up into each tube and mixed by inverting before being centrifuged at 500 g for 15 minutes. Once centrifuged, the supernatant was aspirated, cell pellets were resuspended with 45mL of PBS and tubes were inverted to mix and centrifuged at 500 g for another 10 minutes. This washing step was repeated once more before the cells were resuspended in the RPMI-1640 media containing Pen/Strep but no serum. The cells were then plated into 6 well suspension plates (Cellstar) and incubated in the CO_2 incubator for 40 hours (37^oC, 5% CO_2).

Seeding, culture and monitoring of HMDM cells

After approximately 40 hours of incubation in the absence of serum, the T-cells died due to lack of serum, the platelets attached to the bottom surface of the plate while the monocytes stayed viable in the suspension (Yang, 2009). At this stage, experiments with human monocytes were able to commence and the cells were acceptable for experimental purpose for another 3 to 4 days. The cell suspension was aspirated, pooled into 50 mL tubes and centrifuged at 500 g for 15 minutes at room temperature and the supernatant was removed. The cells were resuspended in RPMI-1640 media supplemented with 10% (v/v) human serum. Granulocytes macrophage colony stimulating factor (GM-CSF) administered as Leukine® (Bayer, USA) was added to the cell suspension to enhance the differentiation of

monocytes into macrophages. The final concentration of GM-CSF was 50 ng/mL of cell suspension.

The cells were seeded (plated) into 48 well plates (adherent, Cellstar) at a concentration of $1x10^6$ cells/mL. Media change using RPMI-1640 with 10% human serum was carried out every 3 to 4 days. Experiments using HMDM were conducted once the majority of the monocytes had matured into macrophages, normally between days 11 and 16 after seeding of the monocytes. Every 3 to 4 days, HMDM differentiation and morphology were monitored and examined using Leica DM IL (Leica Microsystems, Wetzlar, Germany) inverted microscope equipped with a camera and connected to the computer with Leica Application Suite Version 2.8.1 software which enabled images of the cells to be taken and recorded. Approximately 7 days after seeding, a good or satisfactory cell preparation will end up with majority of the well surface dominated by round poached-egg like cells.

Blood collection from donors and plasma preparation for LDL purification

Blood collection was done under ethics approval granted from Upper South (B) Regional Ethics Committee - CTY/98/07/069. All healthy blood donors (male and female) were required to fast overnight plus a written consent was obtained from each donor before blood collection. Blood was collected by venipuncture using a 21G x $^3/_4$ inch or 19 G needle attached to a 30 mL syringe (Terumo, USA). The blood was then collected directly into 50 mL centrifuge tubes (Greiner Bio-one) containing 500 µL of 100 mg/mL EDTA (pH 7.4), to give a final concentration of 0.1% EDTA. A total of 200 mL of blood was collected from each donor.

The blood was then centrifuged for 20 minutes at 4ºC in a swing-out rotor at 4,100 g with the brake off to separate red blood cells and plasma. The plasma was subsequently transferred to 50 mL round bottomed centrifuge tubes and centrifuged at 11,000 g for 30 minutes at 4ºC, with slow acceleration/deceleration in a fixed angle rotor to remove any remaining cellular debris. Plasma from all donors was then pooled together into a single measuring cylinder to minimise inter-individual variation (Gieseg & Esterbauer, 1994). The plasma was stored at -80ºC in 30 mL aliquots for up to 6 months.

LDL purification from pooled plasma

Isolation of LDL from plasma using gradient centrifugation

The method of Chung *et al.* (1980) with modifications of a single vertical spin described by Gieseg and Esterbauer (1994) was used for LDL isolation in the present study. This method involves preparing one step gradient that redistributes to form a continuous gradient that separates the lipoproteins during ultracentrifugation.

Frozen human plasma in a 30 mL tube was thawed under cold running water and centrifuged at 4,700 rpm for 10 minutes at 4ºC to remove any precipitated fibrinogen. The supernatant was decanted into a glass beaker and placed on ice. The plasma density was adjusted to 1.24 g/mL by gradually adding 11.4 g of solid potassium bromide (KBr). The solution was capped with parafilm and gentle stirring was applied while dissolving KBr in order to prevent the formation of foam.

Approximately, 8 mL of 1 mg/mL EDTA (pH 7.4) was added to each of the 8 polyallomer ultracentrifugation tubes (OptiSeal™, Beckman Coulter, USA). This was followed by under-layering with around 4 mL of KBr-plasma using a long luer-fitting needle attached to a 5 ml syringe. The tubes were transferred to the Beckman Near Vertical (NVTi-65) rotor (**Figure 2.1**) and centrifuged at 60,000 rpm for 2 hours at 10ºC using slow acceleration/deceleration in Optima™ L-90K Preparative Ultracentrifuge (Beckman Coulter Inc., Fullerton, California) (**Figure 2.1**). After centrifugation, a yellow/orange coloured band of LDL (**Figure 2.2**) in the density range of 1.019 to 1.063 g/mL was collected into a 15 mL centrifuge tube using a 90^{o}-bent needle attached to a 10 mL syringe. Freshly prepared LDL was then flushed with argon and kept at 4ºC until use.

Figure 2.1: Beckman Optima™ L-90K Preparative Ultracentrifuge and Beckman Near Vertical (NVTi65) rotor

The plasma was centrifuged at 60,000 rpm for 2 hours at 10^{o}C using slow acceleration/deceleration for LDL isolation.

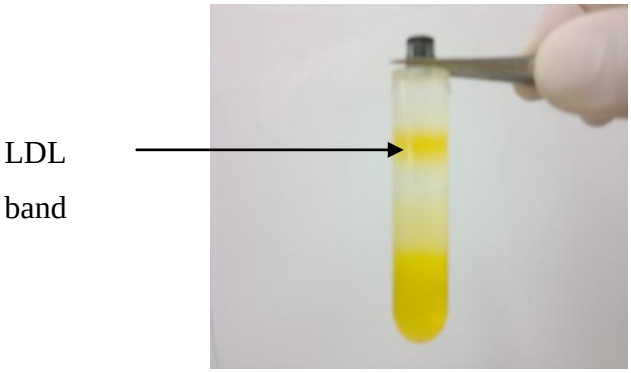

Figure 2.2: LDL purification

LDL isolated from pooled plasma using density centrifugation. LDL band as indicated by the arrow.

LDL concentration determination

LDL concentration was determined as a function of total cholesterol content by an enzymatic reaction using a cholesterol kit supplied by Roche Diagnostic. The assay involves incubating 10 µL of LDL with 1 mL of cholesterol reagent at room temperature for 10 minutes. Absorbance was then read at 500 nm against a blank containing only cholesterol reagent.

LDL concentration was then calculated from this absorbance, based on the estimate of cholesterol accounting for 31.69% of the whole LDL particle by weight and LDL having a molecular weight of 2500 kDa (Gieseg & Esterbauer, 1994). The value used for LDL concentration in the present study is in total mass with the value of total LDL mass relates to

the mass of apolipoprotein B (protein component of the LDL molecule) as 5:1 (Gieseg & Esterbauer, 1994)

Calculation of LDL concentration:

Absorbance x 14.9 = [cholesterol] (mM)

[cholesterol] (M) x 386.64 g/mol = [cholesterol] (g/L)

[cholesterol] (g/L) x 100/31.69 = [LDL] (g/L or mg/mL)

LDL washing and concentration

LDL was concentrated using Amicon® Ultra-15 filter tubes (Millipore, USA). Before usage, the filter tubes were rinse with nano pure water followed by centrifugation with PBS for 2 minutes to wash. LDL was placed into the filter tubes, topped up with PBS and centrifuged at 3,000 g for 30 minutes at 4ºC (fast acceleration/deceleration). This step was then repeated thrice to ensure elimination of EDTA from the LDL. The duration of the last centrifugation varied depending on the desired final volume/concentration of LDL. The final concentration of the concentrated LDL was adjusted to approximately 10 mg of LDL per mL of solution (total mass) (see **LDL concentration determination**). After use, the filter tubes were rinsed with nano pure water. It was then followed by 2 minutes centrifugation with nano pure water and 1 minute centrifugation with 95% ethanol before storage in a fridge at 4^{o}C with 5 mL of 50% ethanol at the bottom of the tubes.

LDL oxidation

Preparation of dialysis tubing

The dry dialysis membrane tubes (Medicell International Ltd., London, England) with 14.4 mm flat width and 14,000 Daltons molecular weight cut off were pre-treated before use. The dialysis tube was cut into approximately 25 cm length sections and boiled in a glass beaker containing solution of 5% $^{w}/_{v}$ $NaHCO_3$ and 1 mM EDTA for 20 minutes on a heating block. The tubes were then washed with distilled water and re-boiled in a glass beaker containing nano pure water for 20 minutes. Finally, the tubes were washed thoroughly with nano pure water and stored in 50% ethanol at 4ºC. The tubes were rinsed thoroughly with nano pure water followed by PBS before being used for LDL oxidation.

Copper oxidation of LDL

LDL oxidation method used in this study was adapted from (Gerry *et al.*, 2008). Concentrated LDL at approximately 10 mg/mL (total mass) was mixed with 0.5 mM copper chloride ($CuCl_2$) and placed into a double-knotted dialysis tube secured at both ends with 1.7 mL micro tubes. The LDL-containing dialysis tubing was placed in a large glass bottle containing 1 L of PBS per 10 mg of LDL protein and $CuCl_2$ at a final concentration of 0.5 mM $CuCl_2$. LDL in the dialysis tube was dialysed for 24 hours at 37ºC in an orbital shaker (Bioline, Edwards Instrument Company, Australia). Complete oxidation of LDL occurred when the yellow LDL colour turned colourless with a tinge of cloudy white (**Figure 2.3**).

The dialysis tube containing oxLDL was then transferred to a fresh bottle containing 1 L of PBS, a quarter teaspoon of washed Chelex-100 and a magnetic flea and stirred at 4ºC for two hours in order to remove the excessive copper ion. This step was repeated twice with the third change of PBS-Chelex taking place overnight. OxLDL was then taken out from the dialysis tube, filter-sterilised through a 0.22 µm MS® PES syringe filter in the CII cabinet and stored at 4ºC. The oxLDL was used within a month after oxidation.

Figure 2.3:LDL in dialysis tube after oxidation
LDL turned colourless which indicates complete oxidation.

Cell viability analysis

MTT reduction assay

The MTT reduction assay is a widely used and accepted method for measuring cell viability. It has been shown previously in this laboratory that results obtained by this method correlate with the results produced by the trypan blue exclusion assay (Baird, 2003). Viable cells with active metabolism reduce the yellow tetrazolium MTT compound via the action of NADH and NADPH dehydrogenase enzymes into an insoluble purple formazan product with a maximum absorbance near 570 nm (**Figure 2.4**). The resulting formazan crystals can be solubilised and quantified spectrophotometrically (Mosmann, 1983) so that the colour intensity indicates both the number of cells and their metabolic activity..

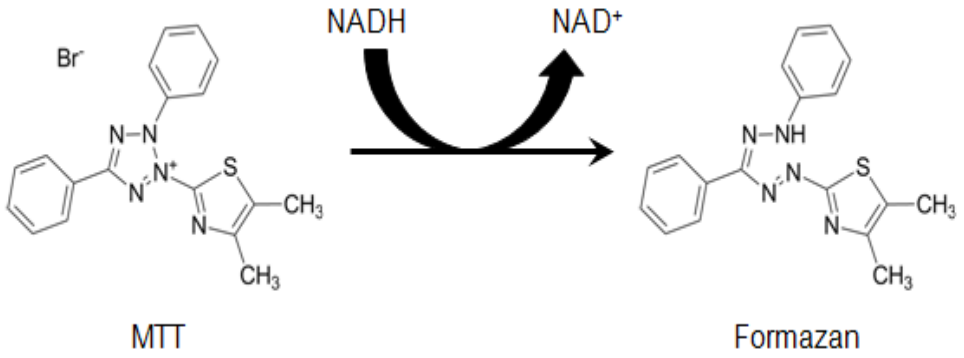

Figure 2.4: The structures of MTT and coloured formazan product
The dehydrogenase enzymes of metabolising cells generate reducing agents, NADH and NADPH which reduce yellow tetrazolium salt to purple formazan.

HMDM cells were washed with warm PBS and incubated with 600 µL of MTT solution at 37^{o}C in the dark for 30 minutes to 1 hour. The incubation time with MTT varied depending on the cell density and overall metabolic activity of the control cells. For experiment with U937 cells or human monocytes, the cells (in culture plates) were incubated in RPMI-1640 without phenol red and the MTT reagent of 5 mg/mL was added directly to the wells to give a final concentration of 0.5 mg/ml MTT for 2 hours. The cells were incubated in the dark at 37^{o}C for 1 to 2 hours to allow sufficient formazan crystals to develop. The purple formazan crystals were then dissolved by the addition of an equal volume of 10% ($^{w}/_{v}$) SDS in 0.01 M

HCl into each well with thorough mixing. Absorbance was read at 570 nm against a blank that contained the reagents only.

Trypan Blue Exclusion Staining

The number of viable cells in the culture can be measured using trypan blue exclusion staining method. This is done by mixing the dye with the suspension cells at the appropriate ratio (normally 1:1 for U937 cells and 1:10 for human monocytes) prior to counting the number of live cells in the defined regions of a haemocytometer (Marienfeld, Germany). Viable cells have intact membranes that are impermeable to the dye rendering them to appear opaque when viewed under the light microscope. In contrast, dead cells which have compromised membrane integrity developed a deep blue stained due to trypan blue uptake. However, this stain is unable to distinguish between healthy cells and cells that are still alive but losing cell function.

Propidium Iodide (PI) Staining

Another method used in this research for the determination of cell viability is propidium iodide (PI) stain done via flow cytometer (see **Flow cytometry analysis – Propidium Iodide**). Since this technique is rapid with more advantages compared to MTT and trypan blue, it has been used as the major method in assessing cell viability throughout the whole course of this study.

Determination of protein concentration

Protein concentration was determined using the bicinchoninic acid (BCA) protein determination kit (Pierce™, Rockford, USA). This method combines the reduction of Cu^{2+} to Cu^{+} by protein in an alkaline medium with the colorimetric detection Cu^{+} using a unique reagent containing bicinchoninic acid (Smith *et al.*, 1985). This reaction product of this assay exhibits a strong absorbance at 562 nm with increasing protein concentrations ranging from 20 to 2000 µg/mL (Pierce™ Instruction Manual).

The working reagent was freshly prepared by mixing Reagent A (sodium carbonate, sodium bicarbonate, BCA and sodium tartrate in 0.1 M sodium hydroxide) and Reagent B (4% $CuSO_4.5H_2O$) at a 50:1 ratio (1 mL Reagent A to 20 µL Reagent B).

The assay was done by mixing 50 µL of sample with 1 mL of working reagent and incubated at 60°C for 30 minutes with gentle shaking in a heated shaking block. The reaction was stopped by placing samples on ice before absorbance reading was performed at 562 nm against water blank.

Protein concentration was determined from a standard curve prepared by the incubation of known concentrations of BSA (0-250 µg/mL) in 1 mL of working reagent (**Figure 2.5**).

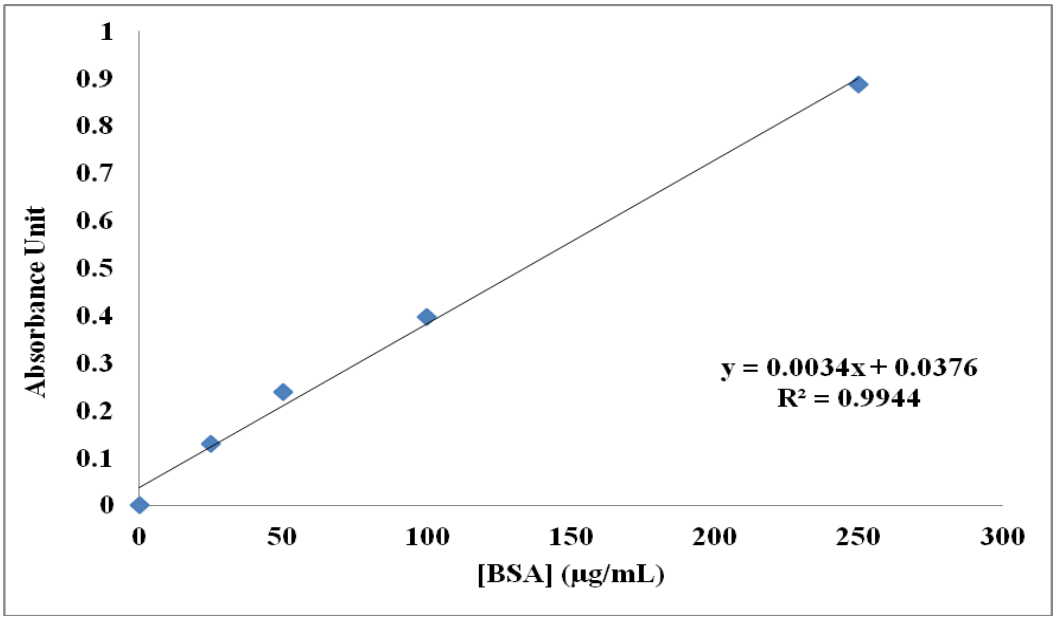

Figure 2.5: Example of standard curve for protein concentration determination using BCA reagent kit

SDS-PAGE and Western blot analysis

Solutions for SDS-PAGE and Western blot analysis

Cracker buffer was prepared by dissolving 1% ($^{w}/_{v}$) SDS (MW= 288.38 g/mol), 20% ($^{w}/_{v}$) glycerol (MW= 92.10 g/mol), 0.1% ($^{w}/_{v}$) bromophenol blue (MW= 670.02 g/mol) and 125 mM Tris-HCl, pH 6.8 (adjusted with concentrated HCl) in nano pure water. Prior to use, 1 mL of the above solution was mixed with 2% ($^{v}/_{v}$) of β-mercaptoethanol and 0.5 mM EDTA.

Lysis buffer consisted of 40 mM of HEPES (MW= 238.31 g/mol), 50 mM of NaCl (MW= 58.44 g/mol) and 1 mM EGTA (MW = 380.4 g/mol) in nano pure water, pH adjusted to 7.4

using 10 M NaOH and stored at 4°C. Prior to use, Complete Mini (Roche Diagnostics, Germany)) protease inhibitor stock (7x) was added to lysis buffer.. One Complete Mini protease inhibitor cocktail tablet was dissolved in 1.5 mL of nanopure water to give a 7× stock solution. The complete lysis buffer was stored on ice until use.

A 10x stock solution of MOPS (4-morpholine-propanesulfonic acid) buffer was prepared with 500 mM MOPS, 500 mM Tris base, 1% ($^{w}/_{v}$) SDS and 10 mM EDTA in nano pure water with the pH adjusted to 7.7 by adding concentrated HCl. The stock solution was diluted to 1x concentration before use.

Transfer buffer for Western blot analysis contained 25 mM Tris, 200 mM glycine (MW= 75.07 g/mol) and 20% ($^{v}/_{v}$) methanol in nano pure water, stored at 4°C.

Ponceau S stain for staining of nitrocellulose membrane contained 0.01% ($^{w}/_{v}$) Ponceau S and 5% ($^{v}/_{v}$) acetic acid.

Tris-buffered saline (TBS) for washing of nitrocellulose membrane consisted of 40 mM Tris-HCl (pH 7.5), 150 mM NaCl, 0.05% ($^{w}/_{v}$) Tween-20, and 0.01% ($^{w}/_{v}$) thimerosal (contains Hg) in nano pure water.

The 5% ($^{w}/_{v}$) blocking solution (TBS-milk, TBSM) was prepared by dissolving 10 g of non-fat milk powder (Anchor, New Zealand) in 200 mL of TBS and was stored at 4°C while the 2% TBSM were made up by diluting the 5% TBSM with TBS accordingly.

Sample preparation for U937cells, human monocytes and HMDM cells – Western Blot analysis

Cell samples for U937 were collected and washed twice with cold PBS by centrifuging at 500 g for 5 minutes at room temperature whilst for HMDM cells, the attached cells were washed twice with cold PBS. A volume of 150 µL of ice cold complete lysis buffer was used to lyse U937 cell pellets and HMDM cell in the culture plates. The cell lysate was then transferred into a 1.7 mL eppendorf tube and incubated on ice for 30 minutes to lyse the cells fully. The cell lysate was then vortexed briefly and was stored at -80°C until use. Protein assay was done to ascertain the amount of protein in the cell lysate (see **Determination of protein concentration**).

Sodium dodecyl sulfate polyacrylamide gel electrophoresis (SDS-PAGE) protein electrophoresis

A required amount of cell lysate (based on the protein concentration) was aliqouted into 1.7 mL micro tubes. Ice cold acetone was added to each tube (the volume of acetone was 10x of cell lysate) and centrifuged at 15,000 g for 10 minutes at 0^{o}C to precipitate the proteins. The supernatant was discarded and the protein pellets in the tubes were left in the fume cabinet to dry off the remaining acetone. The pellets were dissolved in the cracker buffer with 2% β-mercaptoethanol to the final protein concentration of 0.5 – 2 µg protein per µL. The samples were then heated in a heating block at 95ºC for 3 minutes to denature the protein followed by centrifugation for 5 minutes at 20,800 g at room temperature to remove cell debris.

Gel electrophoresis was performed on the samples using a gradient polyacrylamide gel, 4-12% (Bis-Tris Gel, Invitrogen, Carslband, CA, USA) which was run in the XCell SureLock™ Mini-Cell system (Invitrogen, US) containing 1x MOPS running buffer. Five microliters of pre-stained molecular weight marker mix (BioRad, USA) and 5-25 µL of samples (depending on required protein content) were loaded into the wells of the gel. The gel was run at 200 V until the dye front reached the bottom of the gel.

Western blot – membrane transfer and immunoblotting

The proteins on the SDS-PAGE gel were transferred onto a nitrocellulose membrane (NC) (0.45 µm pore size, Invitrogen, USA) using a tank transfer electrophoresis unit (Hoefer™ TE22, USA) filled with cold transfer buffer. The transfer duration was 10 hours with voltage set at 70 V using the PowerPac 300 (BioRad, USA) power supply. After completion of the transfer, the NC was rinsed with nano pure water and stained with Ponceau S stain for 1 minute to check the result of the transfer.

The washing and incubation of the NC membrane were performed on a rocking platform mixer (Ratex Instruments, Australia). After brief rinsing with nano pure water, the membrane was blocked using 5% TBSM for 1.5 hours (changed at each 30 minutes during incubation). This was followed by three times of 5-minute wash in TBS. The membrane was then probed with the primary mouse monoclonal IgG_1 antibodies against $p47^{phox}$ (Santa Cruz Biotechnology Inc, USA) in 1:250 dilution using 2% TBSM for 1.5 hours. The NC membrane was then washed for 5 times with TBS (5 minutes each). An incubation of the NC

membrane with the secondary antibody goat anti-mouse IgG-HRP (Santa Cruz Biotechnology Inc, USA) diluted to 1:750 with 2% TBSM was then performed. The membrane was then washed as mentioned above and was followed by quick rinsing in nano pure water twice to remove any residual TBS. Tween-20 in TBS inhibits peroxidase from reacting with the chemiluminescence substrates and this may interfere with the detection (see **Detection**).

Detection

The secondary HRP-coupled antibody chemiluminescene signal on the NC membrane was detected using Supersignal West Dura Chemiluminescence (TerumoScientific, USA) kit which consists of the luminal/enhancer solution and the substrate peroxide solution. The working solution was made up of the two solutions at 1:1 ratio immediately before being applied onto the NC membrane. The luminal/enhancer reacts with the horseradish peroxidase (HRP) of the secondary antibody on the NC membrane and hydrogen peroxide in the solution to generate 3- aminophthalate plus the emission of light at 425 nm.

The working solution was applied evenly onto the NC membrane and incubated in the dark for 10 minutes. The images on the NC were obtained on high resolution, without filter and in the absence of light using time-lapse auto-exposure setting on Syngene Chemigenius-2 bioimaging system (Syngene, USA). The images were analysed for band intensity using GeneSnap software (Syngene, USA). The NC membrane was then stored in TBS at 4ºC for β-actin detection (see **β-actin detection**).

β-actin detection

The NC membrane was re-probed for β-actin as control for checking equal loading of proteins. The membrane was incubated for 1.5 hours with the primary mouse monoclonal antibodies against β-actin (Sigma-Aldrich Chemical Co., USA) diluted to 1:10,000 in 1% TBSM. The procedures and detection were the same as those mentioned in the two sections above**.** The only two exceptions in the procedure were that the secondary antibody goat anti-mouse IgG-HRP (Santa Cruz Biotechnology Inc, USA) was diluted to 1:1,000 in 2 % TBSM and the exposure time for chemiluminescence signal detection was 2 minutes.

Flow cytometry analysis

Flow cytometry is powerful method that is used for huge number of quantitative biomedical applications and it provides rapid, reliable and accurate quantitative analysis of cells of interest. Flow cytometry also gives high-throughput automated quantification of fluorescence compared to fluorescent microscopy. It allows the analysis of various properties of single cells suspended in a fluid and can be used for the analysis of cell cycle, viability, apoptosis, calcium influx, membrane potential or amounts of surface receptors or intracellular proteins and many more.

Principles of flow cytometry

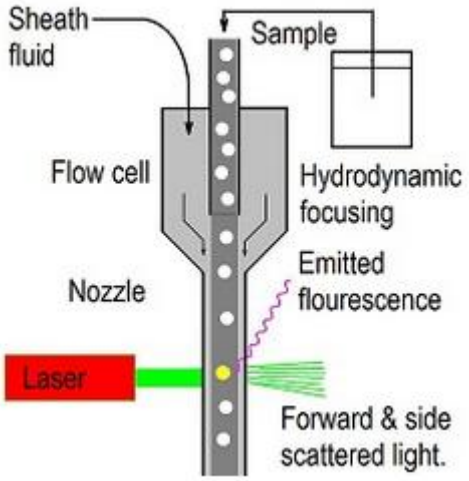

Figure 2.6: A cross section showing the flow chamber.

The principle called hydrodynamic focusing is used in flow cytometry. In the flow chamber (**Figure 2.6**), sample containing single cells suspension emerges from the sample needle into a surrounding sheath fluid which is moving at a greater speed. Consequently, acceleration resulting at the orifice forces the cells to travel separately in the central part of the fluid jet that emerges from the flow chamber. The cells are illuminated by a focused laser beam when they flow past the detector point and the illuminating light gets scattered. The relative size and granularity of a cell influenced the way in which light is scattered. Low angle scattered light depends on cell size and is detected as forward scatter (FSC). On the other hand, cell granularity and surface convolutions scatter light at higher angles and the signal is measured orthogonal to the stream as side scatter (SSC). At the same time, fluorescence emission will also occur if the cells have been previously probed with a fluorescent dye capable of

absorbing the illuminating light. Both the scattered light and emitted fluorescence are collected and sent to different detectors using optical filters. Fluorescence (FL) measurements are also made in the orthogonal direction with detectors appropriate to the specific emission spectrum of the fluorescent probes used.

All of the research work involving intracellular processes in this study was carried out using Accuri C6 flow cytometer® (BD Biosciences, USA) (**Figure 2.7**). Cytosolic calcium ion (Ca^{2+}) level, intracellular superoxide (ROS) production, mitochondrial membrane potential and cell viability in U937 cells, human monocytes and HMDMs were studied by probing the cells with the appropriate fluorescent dyes followed by flow cytometry analysis. Depending on the purpose of the experiments, different sets of settings including flow rate, core size and number of events were applied. The laser settings used were 488 nm excitation wavelength plus a range of emission fluorescence detectors/filters including FL1 for Fluo-3AM, FL2 for DHE and TMRM and FL3 for PI (shown in **Figure 2.8**). Data were recorded and analysed using the cFlow Plus software (BD Biosciences).

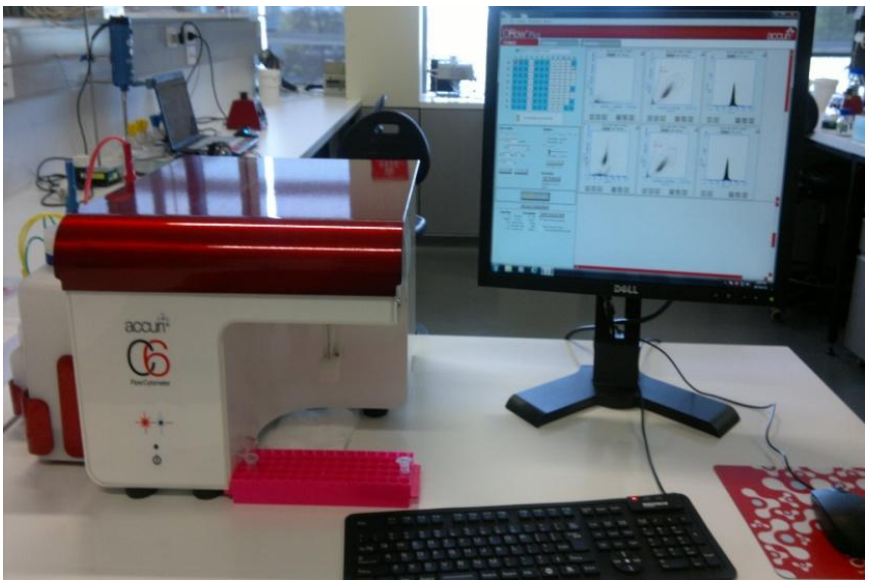

Figure 2.7: Accuri C6 flow cytometer – a complete unit.

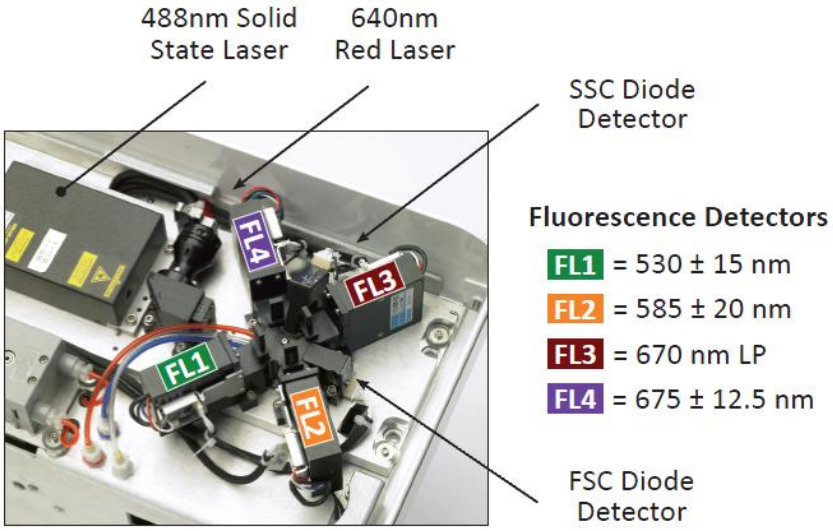

Figure 2.8: Lasers and detectors of Accuri C6 flow cytometer® (BD Biosciences, USA).

The Accuri C6® flow cytometer is calibrated weekly using 8 peak beads and 6 peak beads solutions before running samples for analysis. Examples of the calibration histograms are shown in **Figure 2.9**.

A) 8 peak beads

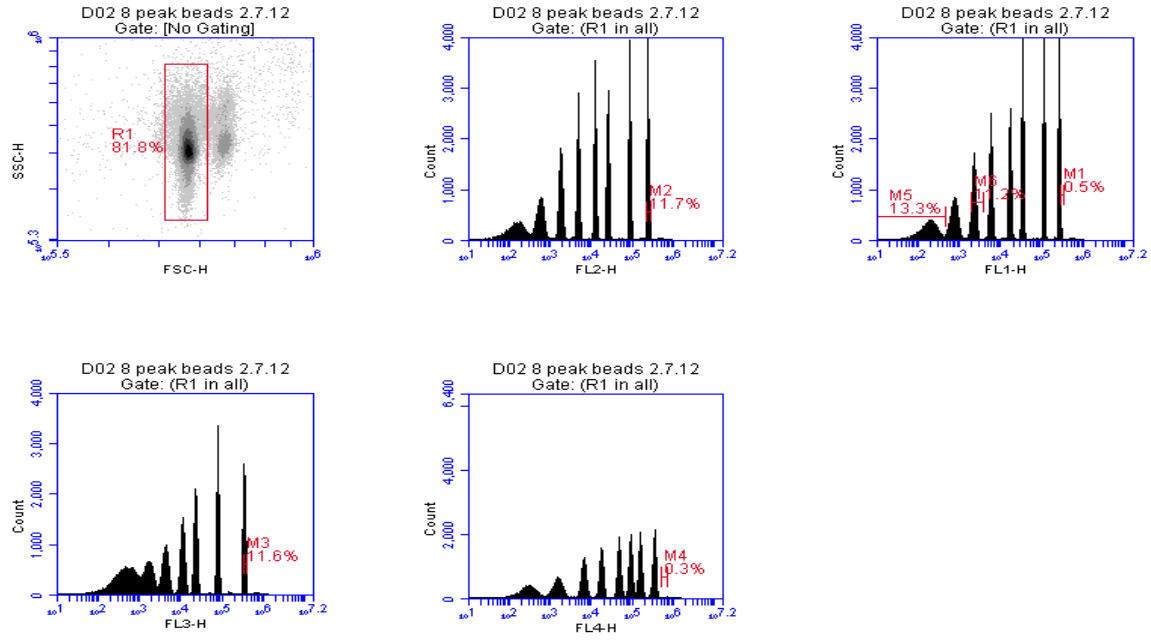

B) 6 peak beads

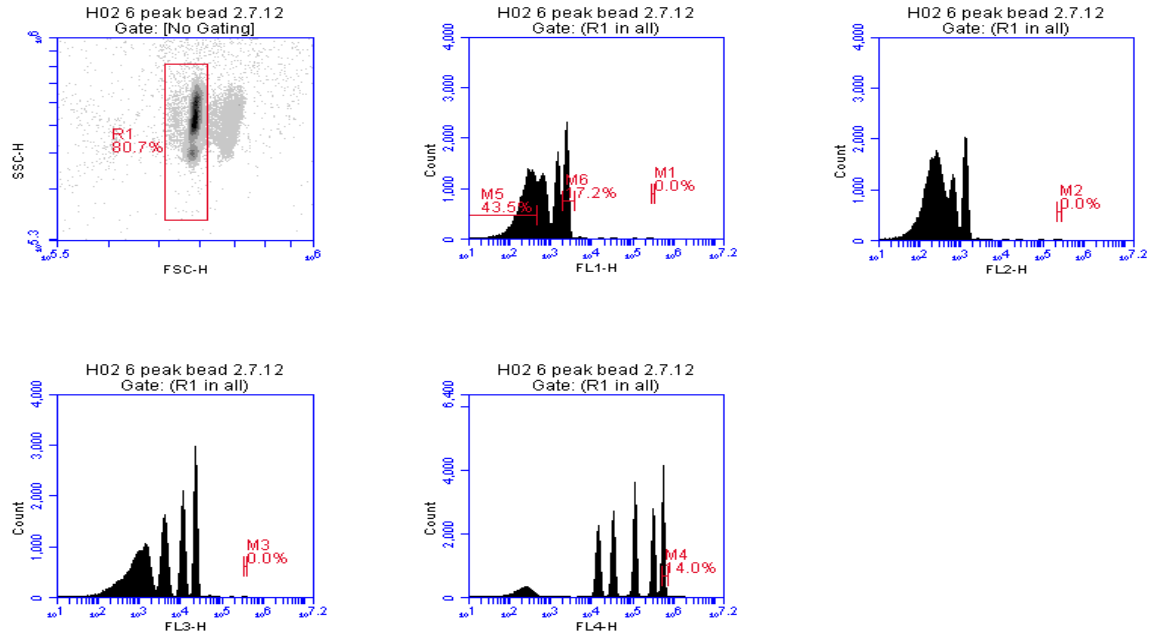

Figure 2.9: Calibration histrograms of Accuri C6® flow cytometer

Example of histograms showing the A) 8 peak beads and B) 6 peak beads calibration of SSC/FSC and each filter channels.

Fluo-3-acetoxymethyl ester (Fluo-3 AM)

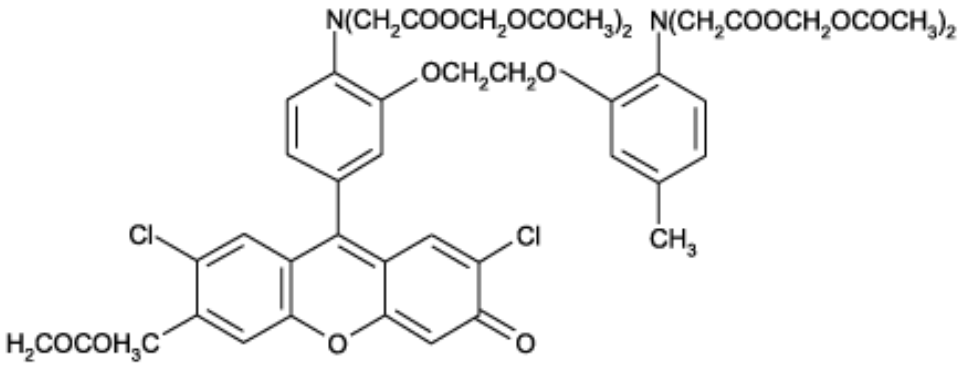

Figure 2.10: Chemical structure of Fluo-3 AM.

Fluo-3-acetoxymethyl (AM) ester (**Figure 2.10**) is a fluorochrome used to measure intracellular (cytosolic) free calcium. This AM form can easily penetrate the plasma membrane and is entrapped within the cells after cleavage of the ester group by intracellular (cytoplasmic) esterase enzymes to form Fluo-3 and AM. Upon excitation at 488 nm, Fluo-3 emits a green fluorescence at 530 nm wavelength when bound to free calcium ions in the cytosol (Minta *et al.*, 1989).

Fluo-3AM (1 mM in DMSO; MW = 1129.9 g/mol) (Life Technologies, NZ) was purchased as ready to be used and stored at -20ºC. Final concentration of the dye used was 1.5 uM. Cells were incubated with Fluo-3AM for 30 to 40 minutes in the dark before treatment with various calcium channel blockers and oxLDL. Levels of intracellular free calcium were measured from 10,000 live cells gated area via flow cytometer (FL1 filter).

Propidium iodide (PI)

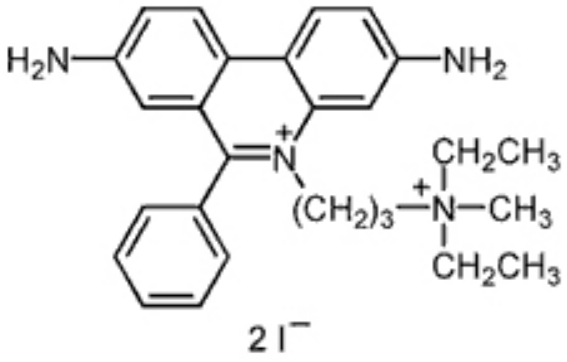

Figure 2.11: Chemical structure of PI

Propidium iodide (PI) (**Figure 2.11**) is a highly fluorescent red dye which is generally impermeable to viable cells. It binds to double stranded DNA of the cells by intercalating between base pairs. The cell membrane integrity excludes PI in viable and apoptotic cells whereas necrotic cells are permeable to PI (Moller *et al.*, 2005) resulting in non-viable cells having bright red fluorescent while viable cells are non-fluorescent (Ross *et al.*, 1989). PI is excited at 488 nm and emits at a maximum wavelength of 617 nm. PI can be used in combination with other dyes such as fluorescein isothiocyanate (FITC) and phycoerythrin (PE) that are also exited at 488 nm due to its spectral properties.

Stock solution of 1 mg/mL PI was prepared by dissolving 10 mg PI in 10 mL nano pure water and stored at 4^{o}C, final concentration used was 1.5 µg/mL. U937 cells and human monocytes were incubated with PI (in RPMI-1640 or PBS) for 10 to 15 minutes in the dark before measurement using flow cytometer. As for HMDM cells, PI was added directly to Accutase™ and incubated for 15 minutes to allow detachment of the adherent cells before subjected to flow cytometry analysis (FL3 filter).

A same volume of cell samples (10 to 15 µL) were run through the flow cytometer. On the FSC vs FL3 (PI) plot, a rectangle was drawn from 0 to approximately 1,000,000 on the FSC scale and from 0 to approximately 10^6 on the FL3 scale (**Figure 2.12 A**). This is the area where cellular debris usually located and will be excluded from the analysis. Next, on the Count vs FL3 (PI) plot, two horizontal bars (sections) were drawn i.e. one from approximately 10^6 to the far left of the plot (percentage of PI negative cells) and one from approximately 10^6 to the far right of the plot (percentage of PI positive cells) (**Figure 2.12 B**).

The total number of cells from each bar (section) will be automatically calculated and displayed by the Accuri C6® flow cytometer. Result is reported as a percentage of total number of cells in the control samples excluding the debris (assuming that same volume of samples should contain similar number of cells). PI positive cells are cells that stained with PI (dead cells) whilst PI negative cells represent viable cells.

A) **B)**

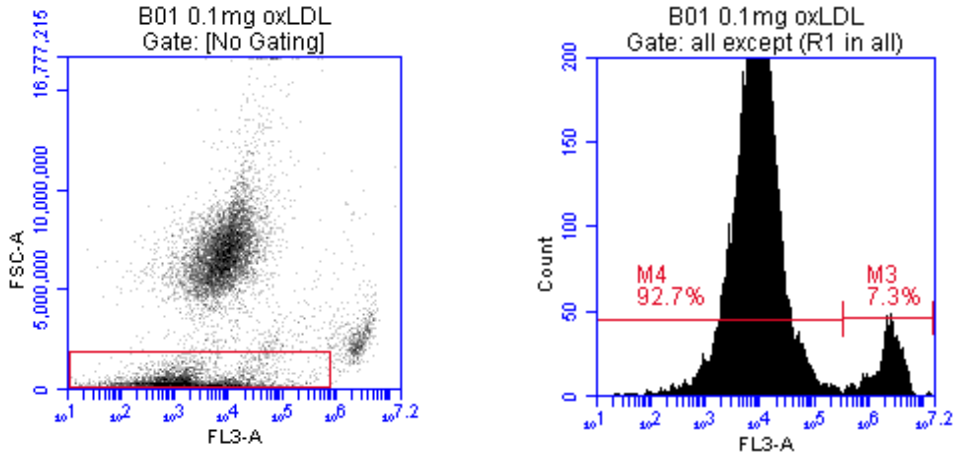

Figure 2.12: Flow cytometry measurement and analysis of cell viability

Example of dot plot/histogram of U937 cells. A) shows FSC vs FL3: a rectangle drawn to exclude cellular debris; B) shows Count vs FL3: M3 is the percentage of PI positive cells and M4 is the percentage of PI negative cells (M3 + M4 = 100%).

Dihydroethidium (DHE)

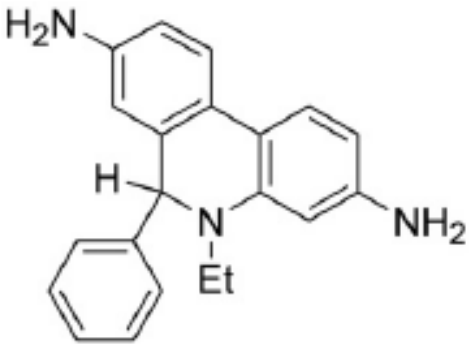

Figure 2.13: Chemical structure of DHE

Dihydroethidium (DHE) (**Figure 2.13**) is a fluorescent probe widely used for detecting intracellular superoxide anions (Zhao *et al.*, 2005). This dye reacts with superoxide resulting in the formation of a two-electron oxidised product, ethidium (E^+), which binds to DNA and leads to enhancement of red fluorescence (Zhao *et al.*, 2003).

Stock solution of 1 mM DHE (MW = 315.4 g/mol) was prepared in DMSO and stored at -20^{o}C. Final concentration of DHE used was 10 µM in cell preparation. After an experimental treatment and PBS washing, U937 cells and human monocytes were incubated with 200 µL of 10 µM DHE in sterile PBS for 20 minutes in the dark before measurement using flow cytometer. For HMDM cells, DHE was added directly to Accutase™ and incubated for 20 minutes to allow detachment of the adherent cells before subjected to flow cytometry analysis. Intracellular superoxide was measured by flow cytometer using FL2 filter from 10,000 viable cells gated area.

Tetramethylrhodamine methyl ester (TMRM)

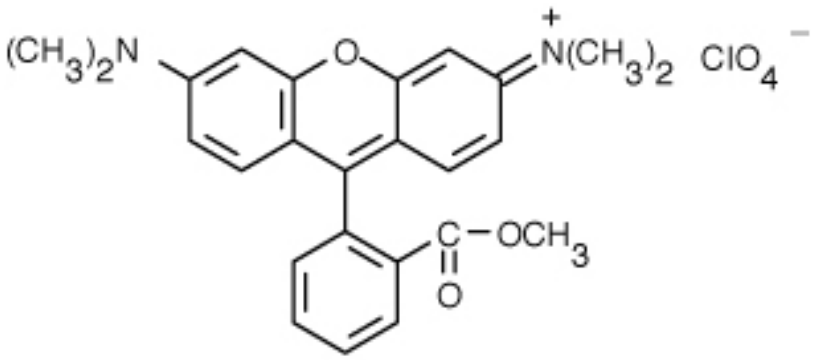

Figure 2.14: Chemical structure of TMRM

Tetramethylrhodamine methyl ester (TMRM) (**Figure 2.14**) is a fluorescent probe used to monitor mitochondrial membrane potential. It is a lipophilic cation, which accumulates in mitochondria proportionate to the mitochondrial membrane potential. The cationic nature of TMRM will cause intense fluorescence at more negative membrane potentials and losing its fluorescence as the membrane potential becomes more positive (Scaduto & Grotyohann, 1999).

TMRM (MW 500.9) stock was prepared in methanol and stored at -20ºC. Final concentration of TMRM used was 10 nM. After experimental treatments and PBS washing, U937 cells and

human monocytes were incubated with 150 µL of 10 nM TMRM in sterile PBS for 20 minutes in the dark before measurement using flow cytometer. For HMDM cells, TMRM was added directly to Accutase™ and incubated for 20 minutes to allow detachment of the adherent cells before subjected to flow cytometry analysis (FL2 filter).

MitoSOX Red (MitoSOX) - mitochondrial superoxide probe

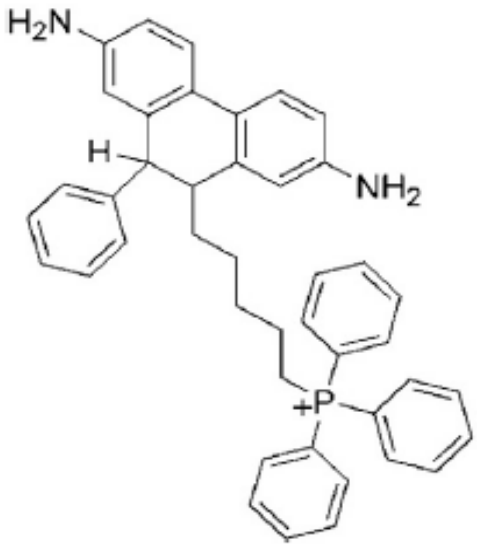

Figure 2.15: Chemical structure of MitoSOX

MitoSOX Red (MitoSOX) (**Figure 2.15**) is a novel fluorochrome for highly selective detection of superoxide in the mitochondria of live cells (Robinson *et al.*, 2006). The probing principle of this cell permeable probe is very similar to that of DHE but it is more selectively targeted to the mitochondria. It uses the steep electrochemical gradient across the mitochondrial inner membrane to enrich the triphenylphosphonium cation (TPP+)-tag fluorescence over a 100-fold within the mitochondria compared with the cytosol (Smith *et al.*, 2011). Once in the mitochondria, MitoSOX is readily oxidized by superoxide but not other ROS and exhibits red fluorescence (excitation/emission = 510/580 nm) (Janes *et al.*, 2004). The oxidation product becomes highly fluorescent upon binding to nucleic acid. MitoSOX (MW = 759 g/mol) of 5 mM stock solution was prepared by dissolving one vial (50 µg) of MitoSOX in 13 µL DMSO immediately before use.

After an experimental treatment and PBS washing, HMDM cells were incubated with 130 µL of Accutase™ plus 5 µM MitoSOX for 15 minutes at 37 °C in the dark. After detachment of

the cells, flow cytometry analysis was carried out to measure the level of mitochondrial superoxide from 10,000 live cells gated area (FL2 filter).

Special methods

Preparation of hydrogen sulfide (H_2S) donors for experiments

Hydrogen sulfide (H_2S) donors in powder form were prepared fresh before experiments were carried out. Stock solutions were prepared by reconstituting H_2S donors in PBS except for AP39 which was reconstituted in DMSO. H_2S stock solutions were further diluted to the final concentrations when added to the cells (**Table 2.1)**.

Table 2.1: Preparation of H_2S donors solutions.

H_2S donors	Molecular weight (g/mol)	Physical appearance	Stock concentration	Final concentration
GYY4137	376.4	White powder	2 mM (in PBS)	200 µM
AP39	721.7	Orange-brownish powder	100 µM (in DMSO)	100 nM
AP67	273.3	Whitish powder	2 mM (in PBS)	200 µM
AP72	287.3	Whitish powder	2 mM (in PBS)	200 µM
AP105	372.5	Yellowish powder	2 mM (in PBS)	200 µM
AP106	402.5	Yellowish powder	2 mM (in PBS)	200 µM

Statistical analysis

Statistical analysis was performed on all graphed data using GraphPad Prism version 6.0 for Windows (GraphPad Software, San Diego, California, USA). Significance was confirmed via analysis of variance (ANOVA) followed by multiple comparison post tests (Dunnet, Sidak, Bonferroni or Tukey) where appropriate for the quantitative indication of significance between treatments and/or time points. Significant levels are indicated in the following manner: (*) $p \leq 0.05$, (**) $p \leq 0.01$ and (***) $p \leq 0.001$.

The results revealed in this thesis were obtained from triplicates of one experiment which is representative of at least three separate experiments unless stated otherwise. The mean and standard errors of the mean (SEM) shown within each experiment were calculated from triplicate samples in the representative experiment.

CHAPTER THREE

3. OxLDL cytotoxicity and flow cytometry analysis of cell viability

Introduction

This chapter aims to examine the toxic effects of oxLDL on U937 cells, human monocytes and HMDM cells which includes cell viability analysis and cell morphology determination. LC_{50} for each batch of oxLDL preparations will be determined for further experiments. Comparison of MTT and PI-flow cytometry assays for cell viability determination will also be done to establish a major technique to be used in subsequent studies.

OxLDL is associated with the initiation and development of atherosclerosis (Ross, 1999; Smook *et al.*, 2008). One of the characteristics that might mediate this process is its cytotoxic effect. Studies have shown that oxLDL is toxic and caused death in variety of cells including macrophages (Hardwick *et al.*, 1996), endothelial cells (Porn-Ares *et al.*, 2003; Quinn *et al.*, 1985), smooth muscle cells (Guyton *et al.*, 1995; Hessler *et al.*, 1979; Nishio *et al.*, 1996) and lymphocytes (Meilhac *et al.*, 1999). This laboratory has previously shown oxLDL cytotoxicity on U937 and THP-1 cell lines (Baird *et al.*, 2004; Chen, 2012) and HMDM cells (Gieseg *et al.*, 2010; Katouah, 2012; Shchepetkina, 2013). *In vitro*, oxLDL has also been shown to cause both apoptotic and necrotic cell death (Asmis & Wintergest, 1998; Gieseg *et al.*, 2010; Hardwick *et al.*, 1996) depending on the dose and duration of exposure to oxLDL (Han & Pak, 1999).

The research describe in this thesis is focused on the mechanisms of oxLDL-mediated cell death in U937 cells, human monocytes and HMDM cells. Therefore, cytotoxicity of oxLDL to these cells needed to be characterised before further studies on the mechanism of oxLDL-mediated cell death were carried out in chapter 4, 5 and 6. This analysis also allowed previous findings by this laboratory on the effects of oxLDL toxicity on cell viability to be verified. In this study, cells were exposed to the acute toxicity of oxLDL by treating with oxLDL for 24 hours whereby previous studies in this laboratory normally measured cell viability after a standard 24 hours incubation with oxLDL (Amit, 2008; Baird, 2003).

Experiments were carried out with different concentrations of oxLDL for 24 hours that enabled the determination of LC_{50} concentration of a particular batch of oxLDL. This LC_{50} concentration will then be used as a guide for subsequent experiments using a same oxLDL batch. LC_{50} is the concentration of oxLDL that caused 50% cell death within 24 hours (Zhang *et al.*, 2006). Additionally, time-course studies were also performed to investigate the kinetics of oxLDL toxicity in all three types of cells by incubating with LC_{50} concentration of oxLDL for up to 24 hours.

Cell viability assays: MTT versus PI

In this chapter, cell viability measurements using MTT reduction and PI-flow cytometry assays were compared. MTT (3-[4,5-dimethylthiazol-2-yl]-2,5-diphenyl tetrazolinum bromide) reduction assay is a widely used method in analysing cell activities such as cell viability and proliferation rates in cell cultures (Denizot & Lang, 1986; Mosmann, 1983). It is one of the metabolic assays that based on the reduction of MTT to water-insoluble purple formazan complex inside the viable cells through mitochondrial dehydrogenases as well as non mitochondrial, cytosolic and microsomal enzymes (Gonzalez & Tarloff, 2001; Liu *et al.*, 1997). Nevertheless, intracellular MTT reduction rate is assumed to be closely related to the number of actively metabolising cells in the cell culture (Gonzalez & Tarloff, 2001; Mosmann, 1983).

In contrast, propidium iodide (PI) assay is based on the ability of this highly fluorescent dye to penetrate cells that lack membrane integrity. Early apoptotic cells exclude PI but not necrotic and late apoptotic cells. Integrating PI and flow cytometry analysis therefore, enables the detection of viable cells from dead cells whereby the latter emitted bright red fluorescence compared to the former which do not fluoresced (Ross *et al.*, 1989). The most prominent working principle of flow cytometry assay is that is allows direct counting of cells without being influenced by the metabolic state of the cells (Wang & Zheng, 2002).

Results

OxLDL-induced cytotoxicity in U937 cells, human monocytes and HMDM cells: effects of different oxLDL concentrations

The acute toxicity of oxLDL to U937 cells, human monocytes and HMDM cells was investigated by exposing cells to the increasing concentrations of oxLDL for 24 hours. Cell viability was measured using PI via flow cytometry assay (data analysis using PI stain and flow cytometry is detailed in **Chapter Two**). A concentration-dependent decrease in the cell viability (PI negative cells) with the increasing amount of oxLDL was observed for all types of cells (**Figure 3.1 B, 3.2 B** and **3.3 B**). Morphological changes of the cells occurred after oxLDL treatment were also examined under the inverted light microscope (**Figure 3.1 A, 3.2 A** and **3.3 A**). Flow cytometry histograms also illustrate the loss of viable cells with increasing oxLDL concentrations whereby more cells being stained with PI (PI positive cells) which shifted to right of the histograms (increased in fluorescence) and a decrease in viable cells (PI negative cells) (**Figure 3.1 C, 3.2 C** and **3.3 C**).

Final oxLDL concentrations of 0.10, 0.25, 0.50 and 0.75 mg/mL reduced U937 cell viability (PI negative cells) by 10%, 30%, 50% and 75% respectively (compared to control) (**Figure 3.1 B**). Approximately 15% and less viable cells were seen with the treatment of 1.00, 1.25 and 1.50 mg/mL oxLDL. Therefore, LC_{50} concentration obtained was between 0.25 to 0.50 mg/mL oxLDL. On the other hand, percentage of cell death was also increased with increasing concentrations of oxLDL (PI positive cells). However, the sum of PI negative cells and PI positive cells was always lower than 100% due to a number of cells which had completely lysed and became debris, thus not counted either as PI negative or PI positive cells (**Figure 3.1 B**). Morphologically, control cells (no oxLDL added) were round in shape, which is the classic feature of U937 cells. Cells treated with 0.10 and 0.25 mg/mL oxLDL showed swelling appearance whilst cells treated with 0.50 mg/mL oxLDL had more distorted cell membranes and cell debris. OxLDL at 0.75 mg/mL and above had caused significant cell damages with disruption of cell membranes and loss of cellular contents (**Figure 3.1 A).** These are characteristics of necrotic cell death. This finding is in-line with Chen (2012) who obtained the LC_{50} concentrations of oxLDL between 0.2 to 0.5 mg/mL with U937 cells throughout her studies.

Histograms of PI-flow cytometry for U937 cells showed that with increasing concentrations of oxLDL, the number of cells shifted to the right of the histograms also increased (M3 - PI positive cells) while there were lesser cells with low PI stained (M4 – PI negative) . This indicates that more cells were taking up PI stain (PI positive) which reflects higher percentage of cell death with higher concentrations of oxLDL (**Figure 3.1 C)**.

A)

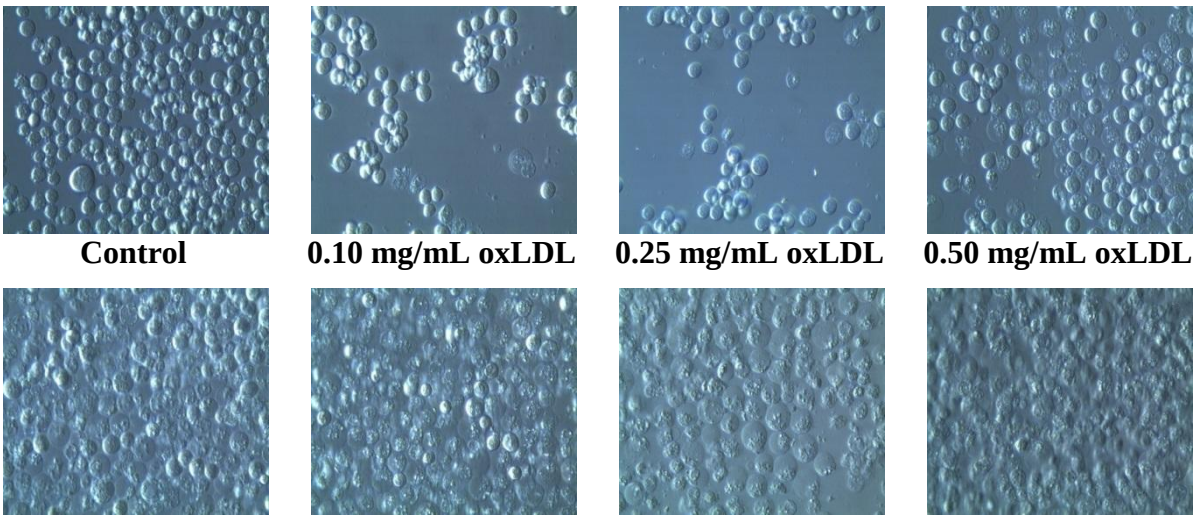

B)

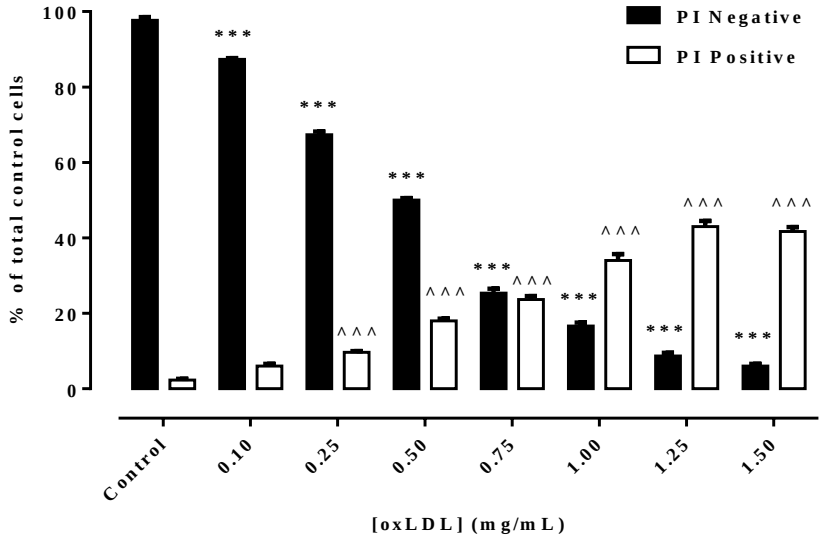

C)

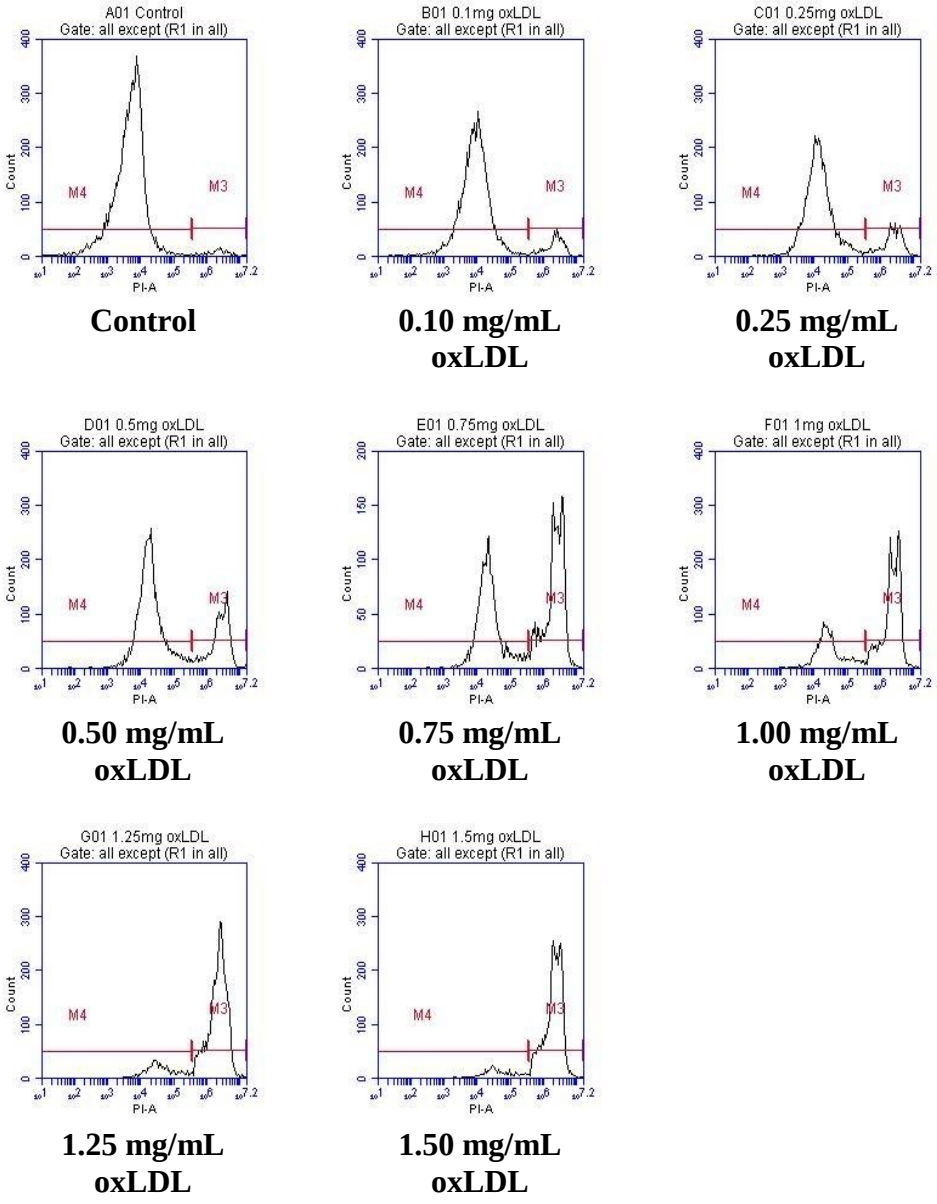

Control | **0.10 mg/mL oxLDL** | **0.25 mg/mL oxLDL**

0.50 mg/mL oxLDL | **0.75 mg/mL oxLDL** | **1.00 mg/mL oxLDL**

1.25 mg/mL oxLDL | **1.50 mg/mL oxLDL**

Figure 3.1: Effect of oxLDL on U937 cell viability.

U937 cells (0.5×10^6 cells/mL) were incubated at 37^{o}C in non-phenol red RPMI-1640 with increasing concentrations of oxLDL for 24 hours. A) Cells were viewed *in situ* in tissue culture wells using an inverted microscope (400x magnification) after 24 hours incubation with oxLDL. Images were taken using a Leica C-Mount camera and processed using Leica Application Suite software. B) Cell viability was determined using PI-flow cytometry assay. Data are expressed as percentage of the total cells in cell only control samples. Results shown are mean ± SEM of triplicates from a representative experiment. Statistical significance (two-way ANOVA, Sidak's multiple test) is indicated from: PI negative cell only control vs PI negative oxLDL treatments, ***, $p<0.001$; PI positive cell only control vs PI negative oxLDL treatments, ^^^,$p<0.001$. C) Flow cytometry histograms of U937 cells treated with different concentrations of oxLDL (counts vs PI), M3 indicates PI positive stained cells and M4 indicates PI negative stained cells.

Human monocytes are relatively smaller compared to U937 cells with average cell size ranging from 7 to 10 µm. Average cell viability reduction of 10 and 30% compared to control (PI negative) has been observed with final oxLDL concentrations of 0.25 and 0.50 mg/mL, respectively. Approximately 50%, 35% and 25% of cells were still viable (PI negative) after 24 hours treatment with 0.75, 1.00 and 1.50 mg/mL oxLDL, respectively. Thus, for human monocytes, LC_{50} concentration of oxLDL was determined between 0.75 to 1.00 mg/mL. Likewise, concentration-dependent cell death (PI positive) occurred with increasing concentrations of oxLDL (**Figure 3.2 B**). Moreover, some of the cells might have undergone cell lysis and became debris.

Morphologically, control cells (no oxLDL added) were small, round in shape and appeared bright yellow under light microscope. Cells treated with 0.25 mg/mL oxLDL showed swelling appearance whilst cells treated with 0.50 mg/mL oxLDL had more distorted cell membranes and cell debris. OxLDL at 0.75 mg/mL and above had caused cell damages with disruption of cell membranes and loss of cellular contents (**Figure 3.2 A)**. The morphological changes in human monocytes caused by oxLDL also suggest the necrotic type of cell death.

Additionally, flow cytometry histograms (**Figure 3.2 C**) showed a small population of cells have shifted to the right of the histogram with 0.25 mg/mL oxLDL treatment (PI positive) while more obvious shifting of the cells to the right (taking up more PI stain) when treated with 0.5 mg/mL oxLDL, indicating more dead cells in the population. Live cells (M8 - PI negative) were greatly reduced while dead cells (M7 - PI positive) were significantly increased with 0.75, 1.00 and 1.50 mg/mL oxLDL treatments.

A)

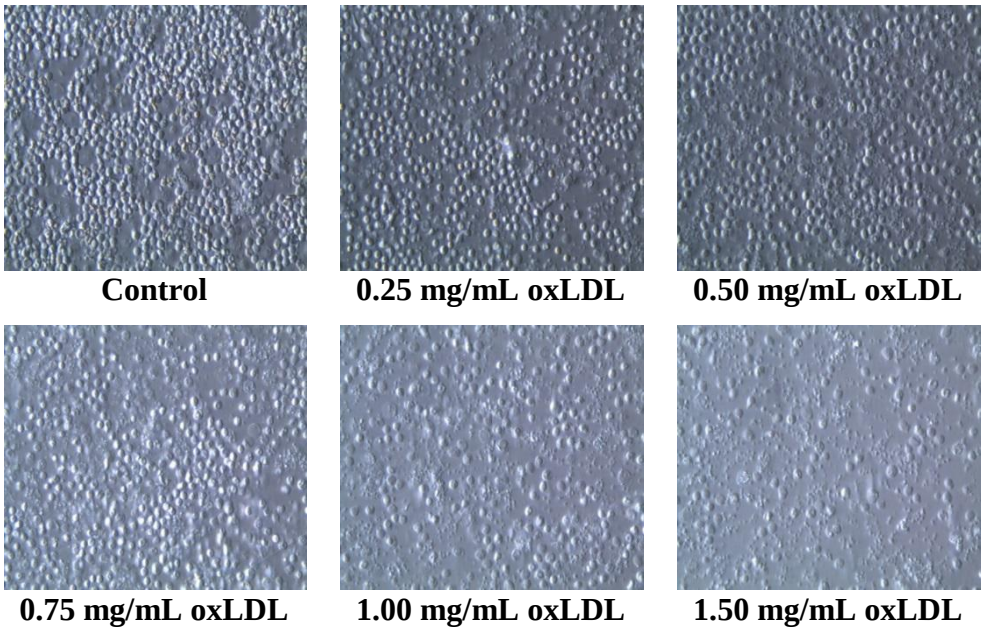
Control
0.25 mg/mL oxLDL
0.50 mg/mL oxLDL
0.75 mg/mL oxLDL
1.00 mg/mL oxLDL
1.50 mg/mL oxLDL

B)

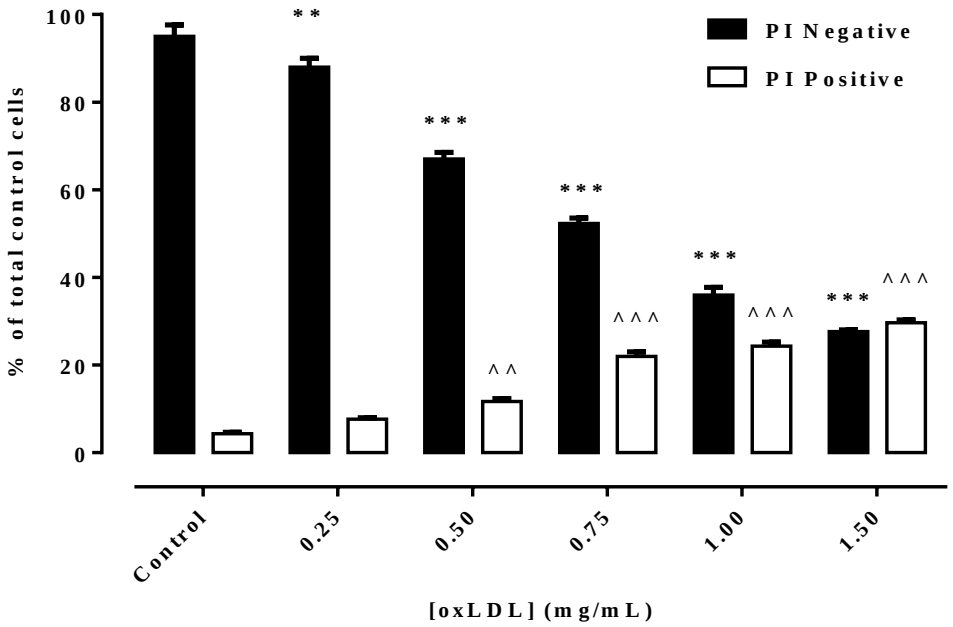
PI Negative
PI Positive
% of total control cells
100
80
60
40
20
0
**
***
***
***
***
^^
^^^
^^^
^^^
Control
0.25
0.50
0.75
1.00
1.50
[oxLDL] (mg/mL)

C)

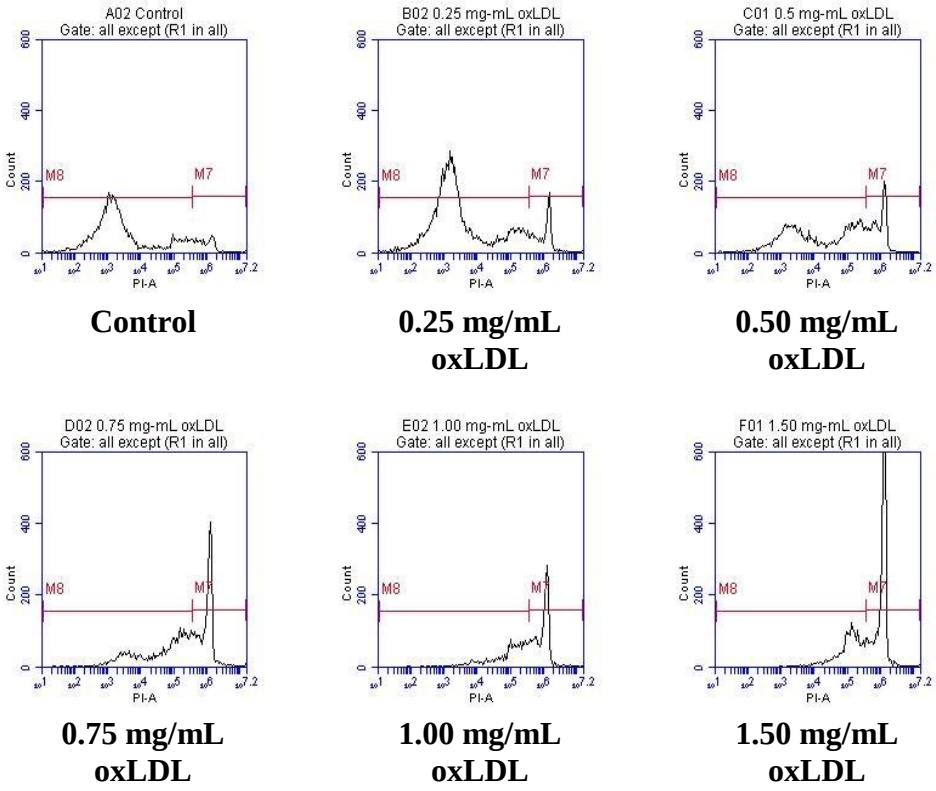

Figure 3.2: Effect of oxLDL on human monocytes cell viability.

Human monocytes (1×10^6 cells/mL) were incubated at 37^{o}C in non-phenol red RPMI-1640 with increasing concentration of oxLDL for 24 hours. A) Cells were viewed *in situ* in tissue culture wells using an inverted microscope (400x magnification) after 24 hours incubation with oxLDL. Images were taken using a Leica C-Mount camera and processed using Leica Application Suite software. B) Cell viability was determined using PI-flow cytometry assay. Data are expressed as percentage of the total cells in cell only control samples. Results shown are mean ± SEM of triplicates from a representative experiment. Statistical significance (two-way ANOVA, Sidak's multiple test) is indicated from: PI negative cell only control vs PI negative oxLDL treatments, **, $p<0.01$, ***, $p<0.001$; PI positive cell only control vs PI negative oxLDL treatments, ^^, $p< 0.01$, ^^^, $p<0.001$. C) Flow cytometry histograms of U937 cells treated with different concentrations of oxLDL (counts vs PI), M7 indicates PI positive stained cells and M8 indicates PI negative stained cells.

HMDM cells were cultured and differentiated from human monocytes using GM-CSF. HMDM cells are relatively large compared to human monocytes with an average cell diameter of 20 µm. At oxLDL concentration of 0.75 mg/mL, cell viability (PI negative) was reduced by 15% (compared to control). Treatment with 1.00, 1.50 and 2.00 mg/mL oxLDL had resulted in decreased viable cells (PI negative) by approximately 40, 50 and 70% respectively compared to control cells. Thus, LC_{50} concentration achieved was between 1.0 to 1.5 mg/mL oxLDL (**Figure 3.3 B**). This finding agreed with Amit (2008) whereby 1.0 mg/mL oxLDL was able to cause approximately 50% of cell viability loss (determined using MTT reduction assay) but a lower oxLDL concentration was reported by Gieseg *et al.* (2010). Increased in cell death (PI positive cells) was also been observed with increasing oxLDL concentrations.

Control cells (with no oxLDL added) resembled poached egg-like appearance which is the classic morphology of HMDM cells. Cells treated with oxLDL appeared swollen, enlarged and distorted compared to control cells especially with higher oxLDL concentrations. Loss of cellular contents resulted in the presence of cell debris while a number of cells were also seen detached and were floating in the culture media (**Figure 3.3 A)**. These characteristics of cell death were similar to those observed with U937 cells and human monocytes, thus suggesting that oxLDL had caused necrotic cell death for all three types of cells.

Flow cytometry histograms (**Figure 3.3 C**) indicated shifting of HMDM cell population to the right when treated with increasing oxLDL concentrations. This clearly showed that oxLDL is toxic to HMDM cells, thus causing a decrease in viable cells (M6 - PI negative cells) and an increased in dead cells (M5 - PI positive cells).

A)

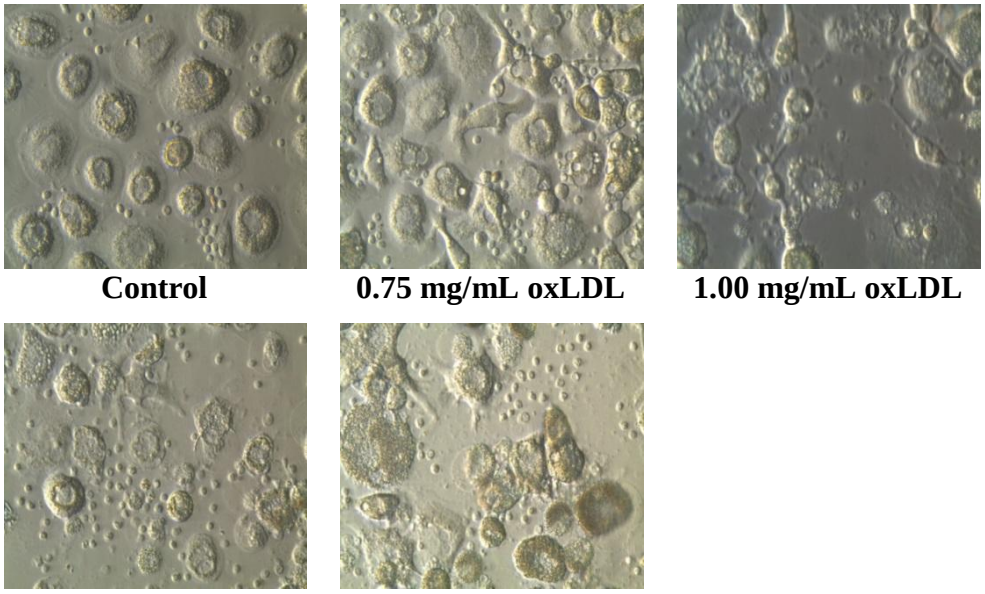
Control
0.75 mg/mL oxLDL
1.00 mg/mL oxLDL
1.50 mg/mL oxLDL
2.00 mg/mL oxLDL

B)

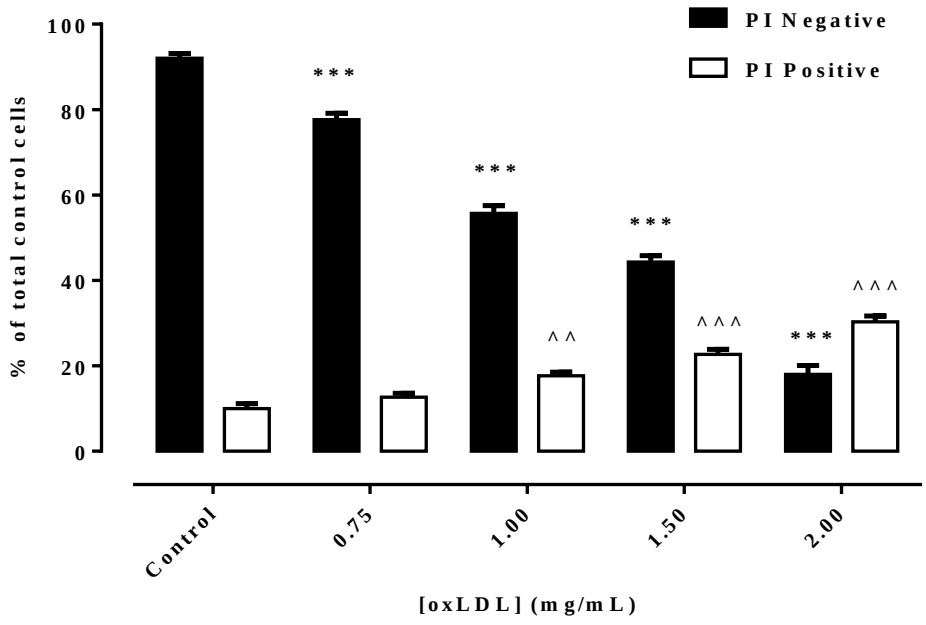
PI Negative
PI Positive
% of total control cells
100
80
60
40
20
0
***
***
***
***
^^
^^^
^^^
Control
0.75
1.00
1.50
2.00
[oxLDL] (mg/mL)

C)

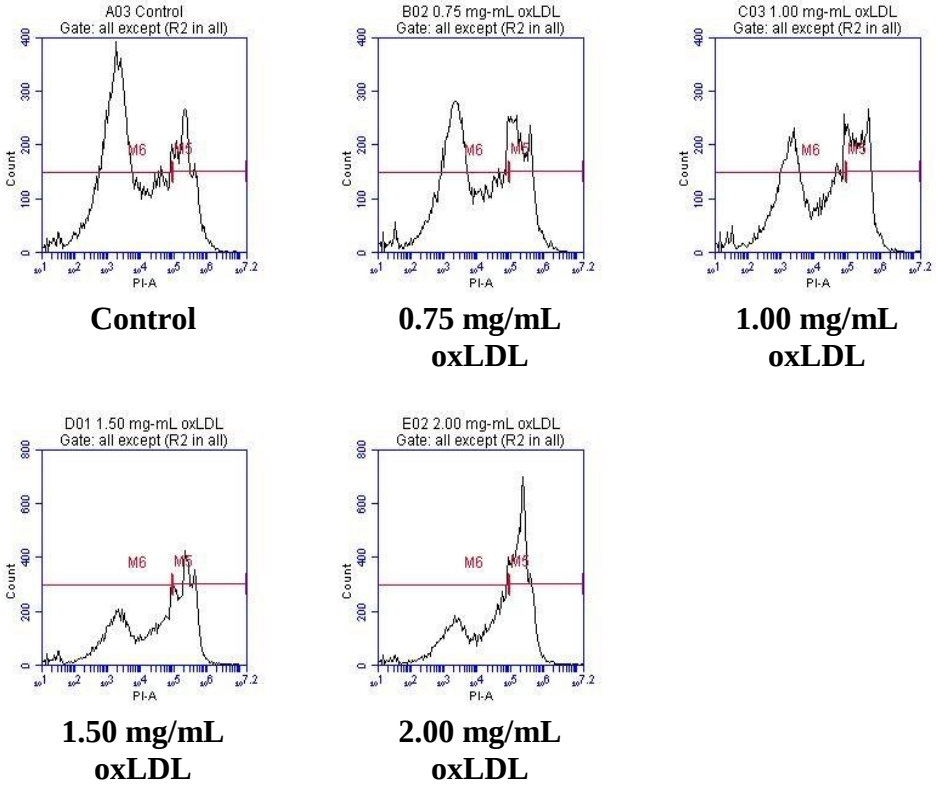

Control | **0.75 mg/mL oxLDL** | **1.00 mg/mL oxLDL**

1.50 mg/mL oxLDL | **2.00 mg/mL oxLDL**

Figure 3.3: Effect of oxLDL on HMDM cell viability.

HMDM cells ($1x10^6$ cells/mL) were incubated at 37^oC in non-phenol red RPMI-1640 with increasing concentration of oxLDL for 24 hours. A) Cells were viewed *in situ* in tissue culture wells using an inverted microscope (400x magnification) after 24 hours incubation with oxLDL. Images were taken using a Leica C-Mount camera and processed using Leica Application Suite software. B) Cell viability was determined using PI-flow cytometry assay. Data are expressed as percentage of the total cells in cell only control samples. Results shown are mean ± SEM of triplicates from a representative experiment. Statistical significance (two-way ANOVA, Sidak's multiple test) is indicated from: PI negative cell only control vs PI negative oxLDL treatments, ***, $p<0.001$; PI positive cell only control vs PI negative oxLDL treatments, ^^, $p< 0.01$, ^^^, $p<0.001$. C) Flow cytometry histograms of U937 cells treated with different concentrations of oxLDL (counts vs PI), M5 indicates PI positive stained cells and M6 indicates PI negative stained cells.

OxLDL-induced cytotoxicity in U937 cells, human monocytes and HMDM cells: examination over time

A time course study was performed to observe the progression of oxLDL-mediated cell death in all three types of cells by incubating with LC_{50} concentration of oxLDL for up to 24 hours (incubated with oxLDL for 0, 3, 6, 9, 12 and 24 hours). **Figures 3.4 A, 3.5 A** and **3.6 A** illustrated the morphological changes in U937, human monocytes and HMDM cells observed under the inverted microscope during their incubation with oxLDL respectively. At the end of the respective incubation time, samples were collected and cell viability (PI negative/PI positive) was determined using PI-flow cytometry assay (**Figure 3.4 B, 3.5 B** and **3.6 B**).

For U937 cells, there were no clear changes in cell appearance after 3 hours incubation with oxLDL. After 6 hours of incubation with oxLDL, cells had swelling appearance with distorted cell membranes and bleb formation. Obvious changes of cell morphology were seen at 9 and 12 hours incubation whereby large number of cells had undergone severe cell damage with cell membrane disruption and loss of cellular contents. After 24 hours, majority of cells appeared lysed and cellular debris was release into the culture media (**Figure 3.4 A**). Likewise, morphological changes manifested by these cells resembled the characteristics of necrotic cell death.

Viable cells (PI negative cells) were about 10%, 15% and 20% less compared to control after incubation of 3, 6, and 9 hours with oxLDL, respectively. Further drop to 60% of viable cells (PI negative) was observed after 12 hours incubation with oxLDL and this was significantly reduced to about 30% at the end of 24 hours incubation (**Figure 3.4 B**). Similarly, the decreased in viable cells (PI negative) resulted in the increased of dead cells (PI positive) but cells have also lysed, became debris (especially at longer incubation time) and not measured as PI positive cells. This is the reason accounting for only 25% of cells were measured as PI positive (dead cells) after 24 hours incubation with oxLDL.

Flow cytometry histograms showed the cell dynamics over the incubation period with oxLDL (**Figure 3.4 C**). Number of viable cells (M1 – PI negative) has reduced while the dead cells were increased in number (M2 – PI positive) with the increasing time of incubation with oxLDL.

A)

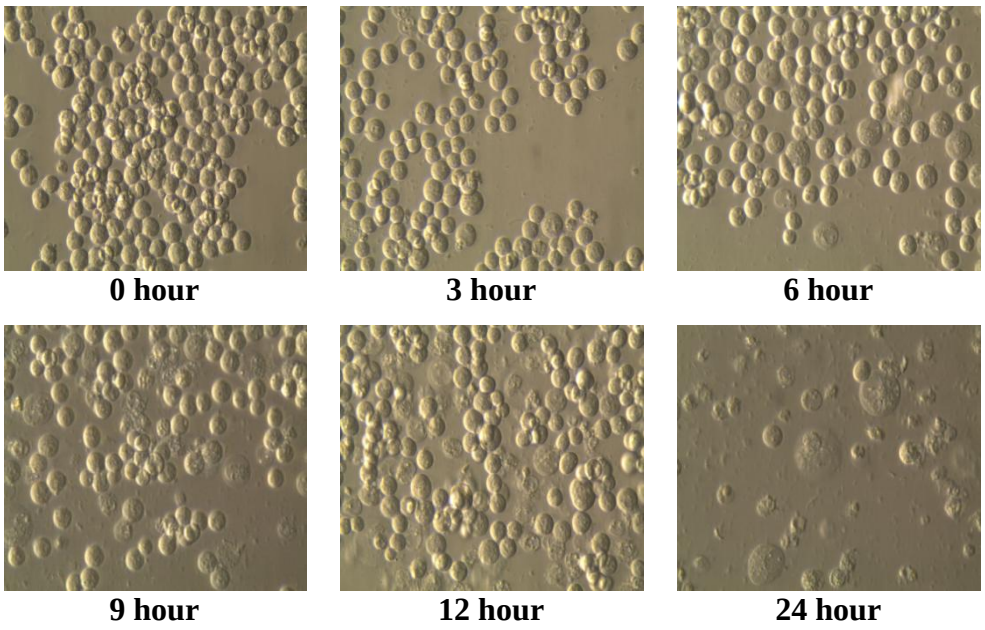
0 hour
3 hour
6 hour
9 hour
12 hour
24 hour

B)

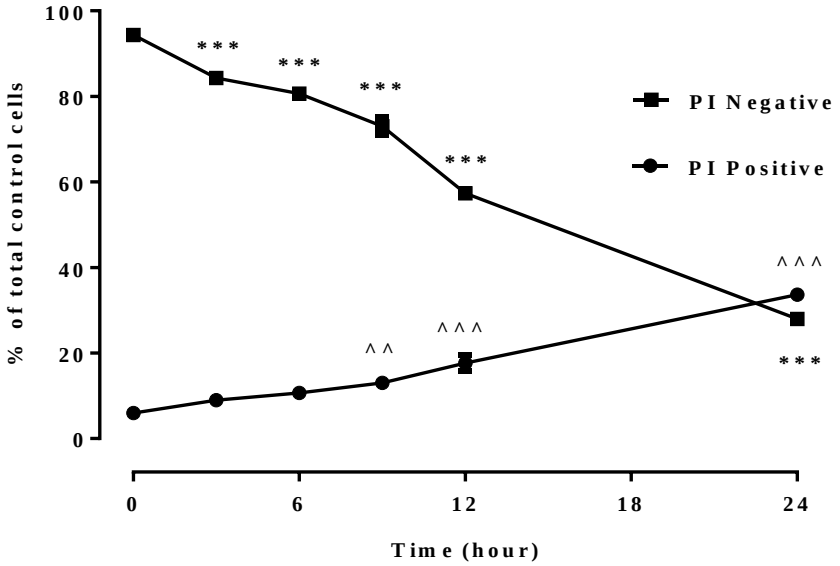
100
80
60
40
20
0
% of total control cells
0
6
12
18
24
Time (hour)
PI Negative
PI Positive
***
***
***
***
***
^^
^^^
^^^

C)

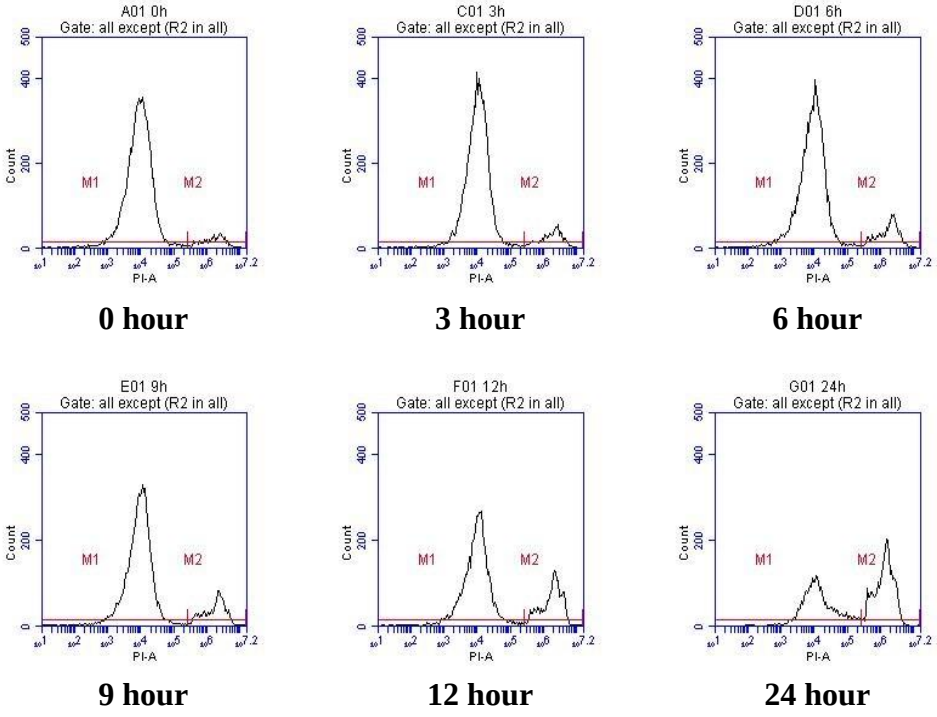

Figure 3.4: Time course effects of oxLDL-induced cell viability loss in U937 cells

U937 cells (0.5×10^6 cells/mL) were incubated at 37°C in non-phenol red RPMI-1640 with the LC_{50} concentration of oxLDL for the indicated time. A) Cells were viewed *in situ* in tissue culture wells using an inverted microscope (400x magnification) after 0, 3, 6, 9, 12 and 24 hours incubation with oxLDL. Images were taken using a Leica C-Mount camera and processed using Leica Application Suite software. B) Cell viability was determined using PI-flow cytometry assay. Data are expressed as percentage of the total cells in 0 hour control samples. Results shown are mean ± SEM of triplicates from a representative experiment. Statistical significance (two-way ANOVA, Sidak's multiple test) is indicated from: PI negative 0 hour control vs PI negative oxLDL treatments, ***, $p<0.001$; PI positive 0 hour control vs PI negative oxLDL treatments, ^^, $p< 0.01$, ^^^, $p<0.001$. C) Flow cytometry histograms of U937 cells treated with different concentrations of oxLDL (counts vs PI), M2 indicates PI positive stained cells and M1 indicates PI negative stained cells.

With human monocytes, there were no obvious morphological changes after 3 hours incubation with oxLDL. Cells started to swell and became distorted after 6 hours incubation with more noticeable damage happened after 9 and 12 hours. After 24 hours, there were massive dead cells with cellular debris present **(Figure 3.5 A)**. Proved by the morphological characteristics, necrotic cell death also occurred in human monocytes caused by acute oxLDL toxicity.

Cell viability loss (decreased in PI negative cells) was approximately 10, 20 and 25% after 3, 6, and 9 hours of incubation with oxLDL, compared to 0 hour control. After 12 and 24 hours incubation with oxLDL, viable cells (PI negative) were about 60 and 45% compared to 0 hour control cells. In addition, cell death has also increased over the incubation period with oxLDL whereby 25% of the cells were dead (PI positive) after 24 hours (**Figure 3.5 B**).

Flow cytometry histograms showed the shifting of the cells to the right with longer incubation time with oxLDL. Number of viable cells (M4 - PI negative) has reduced significantly while the number of dead cells (M3 – PI positive) has gained (**Figure 3.5 C**).

At 24 hours, the rise in PI positive cells was not significant compared to the 12 hour time measurement. But the number of PI negative cells had significantly reduced suggesting significant cell lysis of the monocytes had occurred by 24 hours.

A)

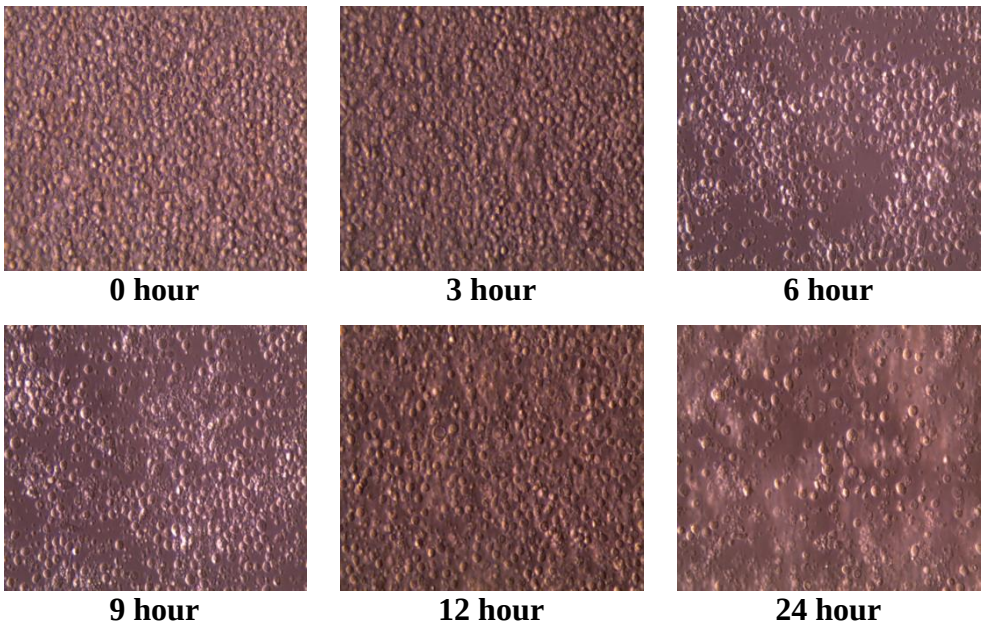
0 hour
3 hour
6 hour
9 hour
12 hour
24 hour

B)

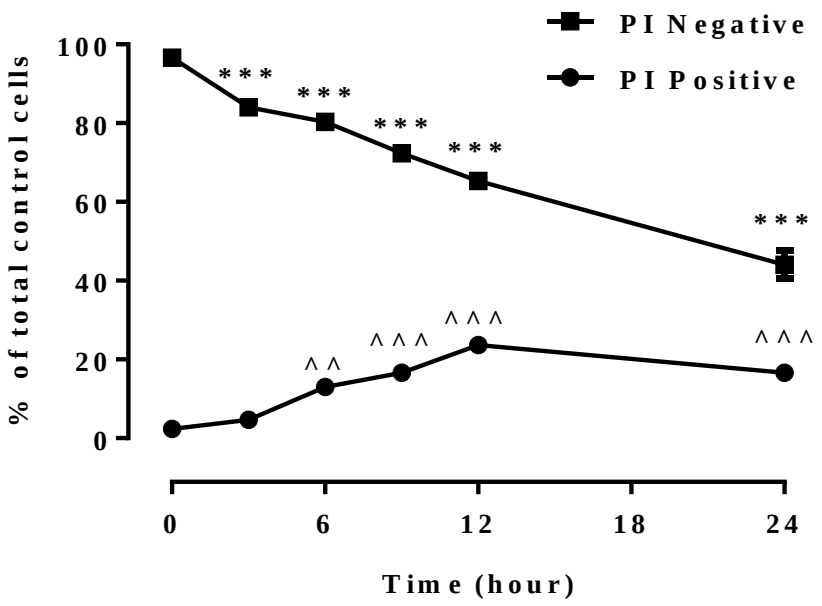
PI Negative
PI Positive
% of total control cells
100
80
60
40
20
0
***
***
***
***
***
^^
^^^
^^^
^^^
0
6
12
18
24
Time (hour)

C)

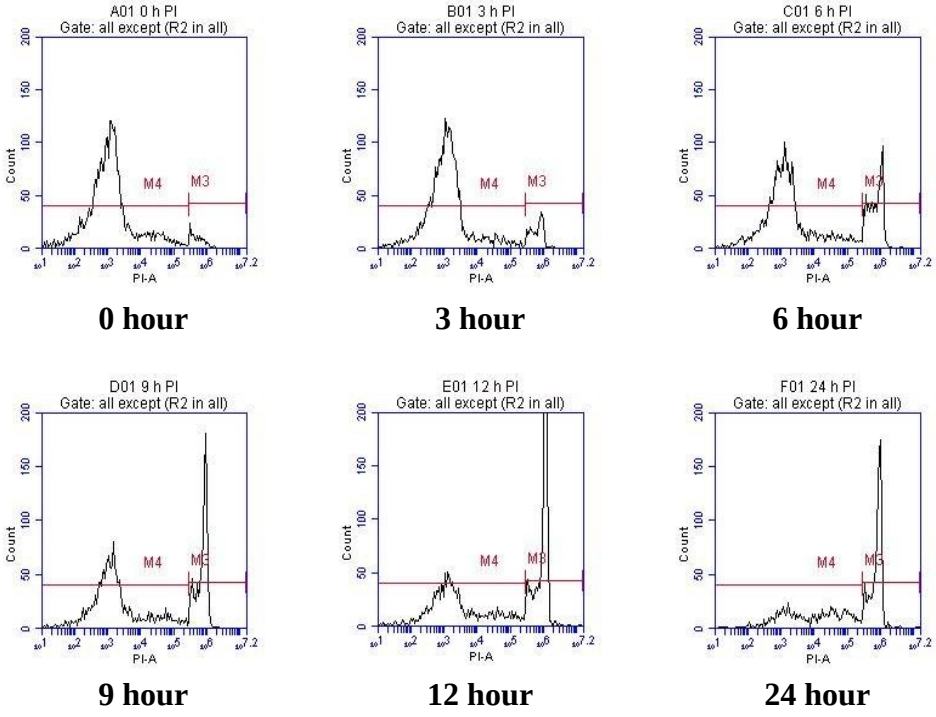

Figure 3.5: Time course effects of oxLDL-induced cell viability loss in human monocytes.

Human monocytes (1×10^6 cells/mL) were incubated at 37^{o}C in non-phenol red RPMI-1640 with the LC_{50} concentration of oxLDL for the indicated time. A) Cells were viewed *in situ* in tissue culture wells using an inverted microscope (400x magnification) after 0, 3, 6, 9, 12 and 24 hours incubation with oxLDL. Images were taken using a Leica C-Mount camera and processed using Leica Application Suite software. B) Cell viability was determined using PI-flow cytometry assay. Data are expressed as percentage of the total cells in 0 hour control samples. Results shown are mean ± SEM of triplicates from a representative experiment. Statistical significance (two-way ANOVA, Sidak's multiple test) is indicated from: PI negative 0 hour control vs PI negative oxLDL treatments, ***, $p<0.001$; PI positive 0 hour control vs PI negative oxLDL treatments, ^^, $p< 0.01$, ^^^, $p<0.001$. C) Flow cytometry histograms of U937 cells treated with different concentrations of oxLDL (counts vs PI), M3 indicates PI positive stained cells and M4 indicates PI negative stained cells.

HMDM cells incubated with LC_{50} concentration of oxLDL did not show significant morphological changes in the first 3 hours of incubation. After 6 hours, the cells appeared to be enlarged and swollen compared to the 0 hour control cells. Cell membranes became distorted and disrupted with the presence of cellular debris after 9, 12 and 24 hours incubation with oxLDL. A number of cells were also detached from the bottom of the culture plate and were floating in the culture media (**Figure 3.6 A**). These morphological changes showed that oxLDL-induced HMDM cell death also resulted in necrotic type of cell death as been observed in U937 cells and human monocytes.

Figure 3.6 B showed that after 12 hours incubation with oxLDL, viable cells (PI negative) left were approximately 60%. A further reduction of 20% of viable cells occurred within 12 to 24 hours of incubation and this finding agreed with the previous work of Katouah (2012) and Shchepetkina (2013). Nevertheless, percentage of dead cells (PI positive) at 12 hours and 24 hours treatment with oxLDL remained approximately the same, suggesting that most of the cells have also lysed and became debris, thus was not counted as PI positive stained cells.

Flow cytometry histograms illustrated the shifting of cells from viable cells (M1 – PI negative) to become dead cells (M2 – PI positive) over the designated incubation time with oxLDL (**Figure 3.6 C**).

A)

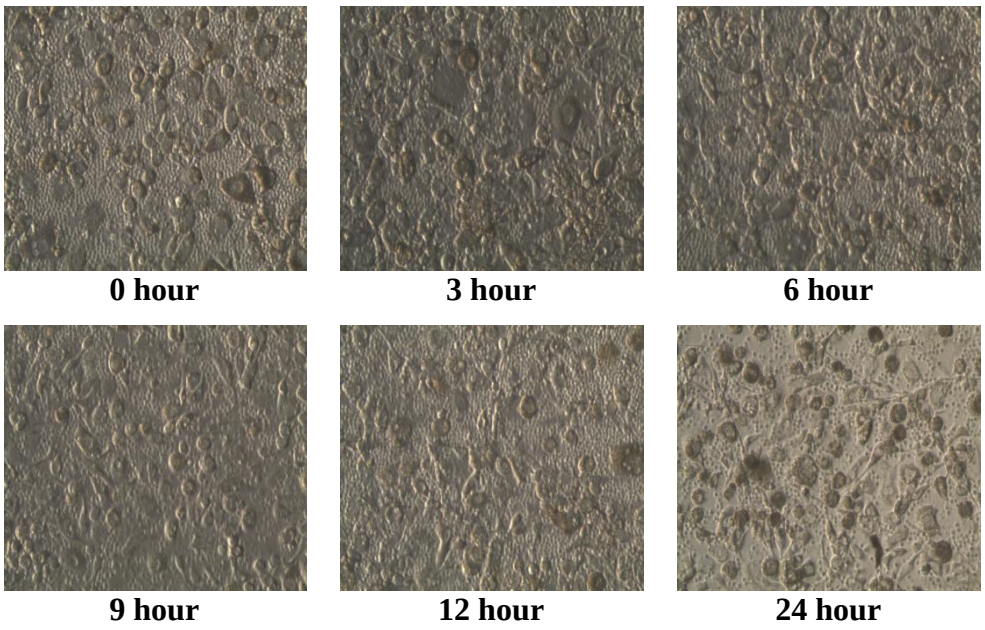
0 hour
3 hour
6 hour
9 hour
12 hour
24 hour

B)

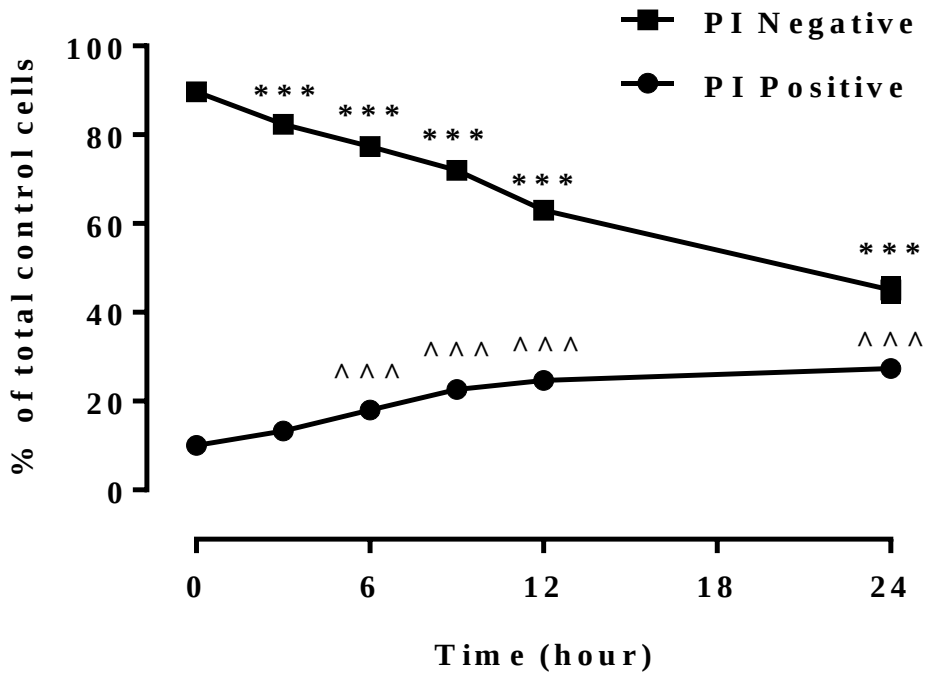
PI Negative
PI Positive
% of total control cells
100
80
60
40
20
0
***
***
***
***
***
^^^
^^^
^^^
^^^
0
6
12
18
24
Time (hour)

C)

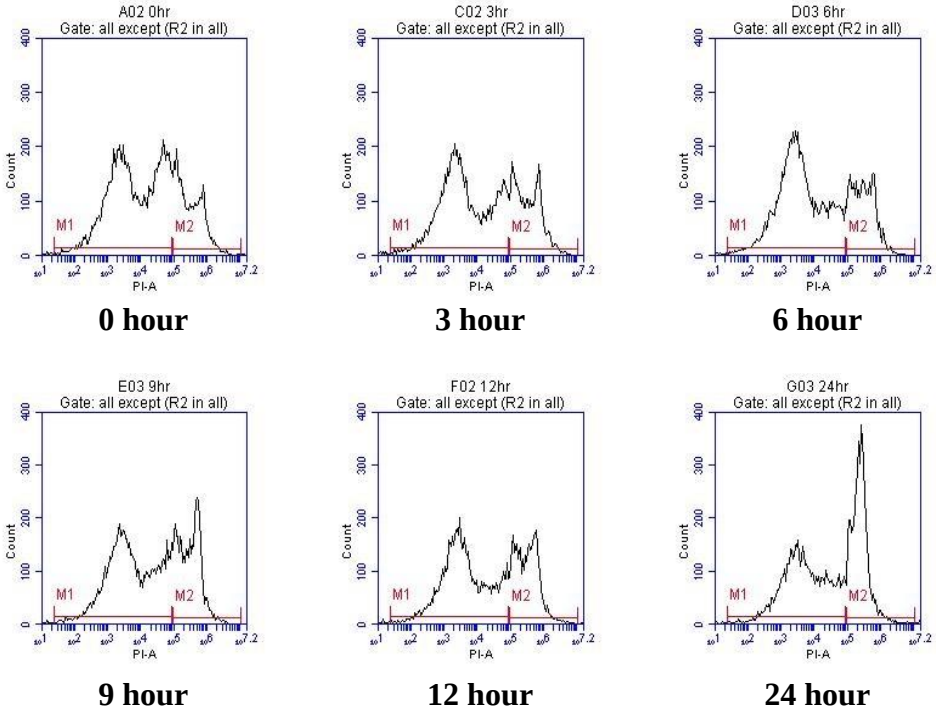

Figure 3.6: Time course effects of oxLDL-induced cell viability loss in HMDM cells.

HMDM cells (1×10^6 cells/mL) were incubated at 37°C in non-phenol red RPMI-1640 with the LC_{50} concentration of oxLDL for the indicated time. A) Cells were viewed *in situ* in tissue culture wells using an inverted microscope (400x magnification) after 0, 3, 6, 9, 12 and 24 hours incubation with oxLDL. Images were taken using a Leica C-Mount camera and processed using Leica Application Suite software. B) Cell viability was determined using PI-flow cytometry assay. Data are expressed as percentage of the total cells in 0 hour control samples. Results shown are mean ± SEM of triplicates from a representative experiment. Statistical significance (two-way ANOVA, Sidak's multiple test) is indicated from: PI negative 0 hour control vs PI negative oxLDL treatments, ***, $p<0.001$; PI positive 0 hour control vs PI negative oxLDL treatments, ^^^, $p<0.001$. C) Flow cytometry histograms of U937 cells treated with different concentrations of oxLDL (counts vs PI), M2 indicates PI positive stained cells and M1 indicates PI negative stained cells.

Comparison of cell viability measurements: MTT and PI-flow cytometry assays

Cell viability assays can be classified into assays that measure metabolic activity, metabolic markers or loss of membrane integrity. Previous work for cell viability determination in our laboratory has been carried out using MTT reduction assay which measures intracellular metabolic activity. Cell viability assay using PI exploits the loss of membrane integrity in dead cells whereby DNA of the compromised cells will be stained by PI as opposed to the viable cells. Integrating PI with flow cytometry method creates a new dimension for the analysis of cell viability in this laboratory. Therefore, another focus of this chapter is to study and compare both types of assay in various aspects.

Example of an experiment and the results obtained from MTT reduction assay and PI-flow cytometry assay are shown in **Figure 3.7**. The end result of MTT reaction with U937 cells after solubilisation of MTT formazan with 10% SDS in a cell culture plate is showed in **Figure 3.7 A**. Depending on the reaction between MTT reagent and the cells, this then resulted in different colour (intensities) being formed which is the basis of measuring cell viability using MTT reduction assay.

Flow cytometry histograms (count vs PI) for U937 cells treated with different concentrations of oxLDL after 24 hours that has been stained with PI are showed in **Figure 3.7 B**. With increasing concentrations of oxLDL, more cells have shifted from viable cells region (M1 – PI negative) to the right of the histogram. This shifting showed that more cells are being stained with PI (M2 – PI positive) which depicts decreasing cell viability with increasing oxLDL concentrations. From the histograms, almost none of the cells were viable when treated with higher oxLDL concentrations of 0.8 and 1.2 mg/mL. Although both assays (MTT and PI) are not in the same of category for cell viability measurements, results obtained by each method were comparable (R^2= 0.9721) (**Figure 3.7 C** and **3.7 D**). This will be explained further in the discussion section of this chapter.

A)

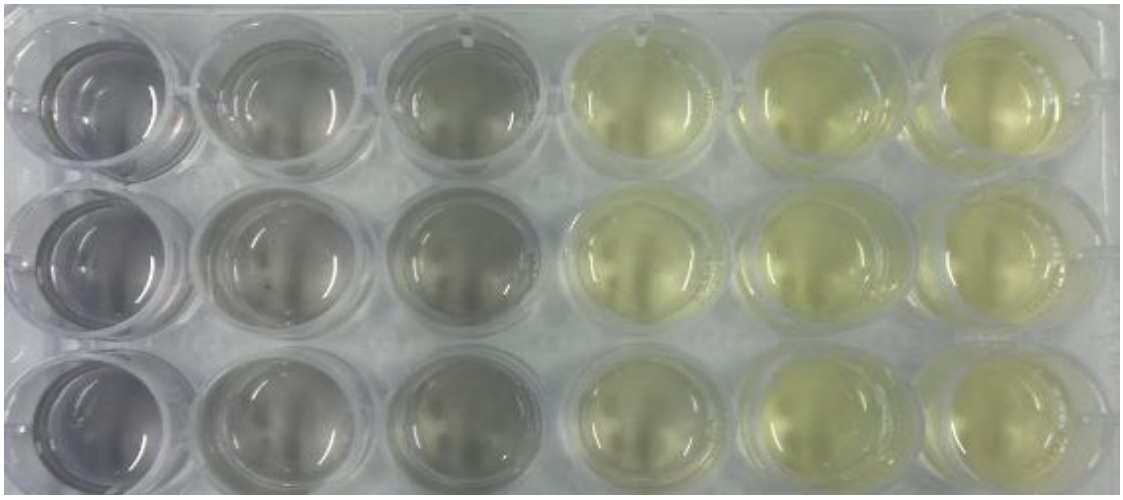

Control | **0.2 mg/mL oxLDL** | **0.4 mg/mL oxLDL** | **0.6 mg/mL oxLDL** | **0.8 mg/mL oxLDL** | **1.2 mg/mL oxLDL**

B)

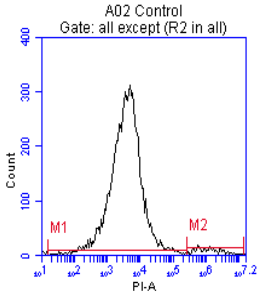

Control

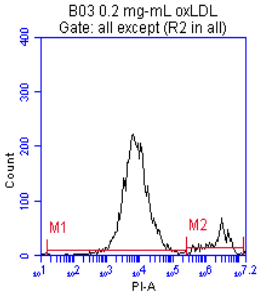

0.2 mg/mL oxLDL

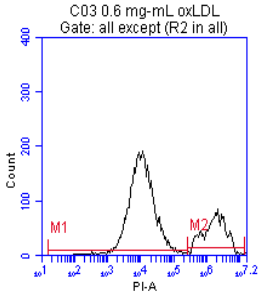

0.4 mg/mL oxLDL

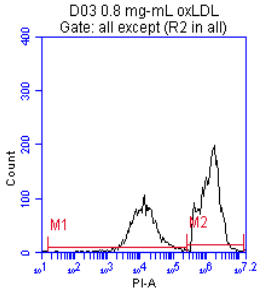

0.6 mg/mL oxLDL

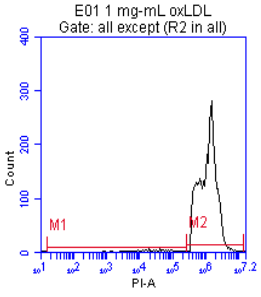

0.8 mg/mL oxLDL

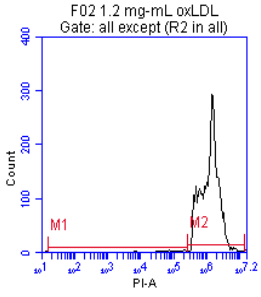

1.2 mg/mL oxLDL

C)

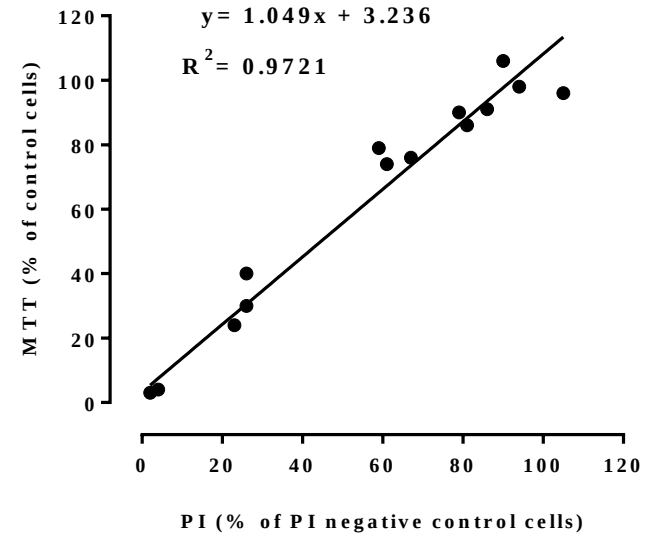

D)

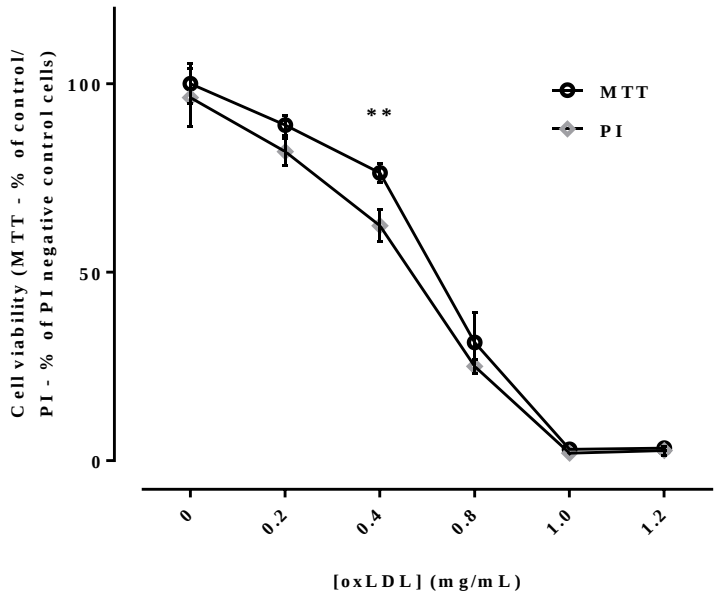

Figure 3.7: Example of cell viability determination experiment using MTT reduction and PI-flow cytometry assays and results obtained for U937 cells.

U937 cells (0.5×10^6 cells/mL) were incubated with increasing concentrations of oxLDL at 37^{o}C in non-phenol red RPMI-1640 for 24 hours. A) Cell viability was measured using MTT reduction assay and B) PI-flow cytometry assay (M1 – PI negative stained cells; M2 – PI positive stained cells). The results are analysed as percentage of the cell only control for MTT reduction assay and percentage of PI negative cells compared to total number of cells in cell only control for PI-flow cytometry assay Results are displayed as mean ± SEM of triplicates and data from both assays were compared for C) correlation between percentages of viable cells and D) effects of different oxLDL concentrations, significance is indicated between both methods at LDL concentration of 0.4 mg/mL, **, $p<0.01$ (two-way ANOVA, Sidak's multiple test).

A) U937 cells

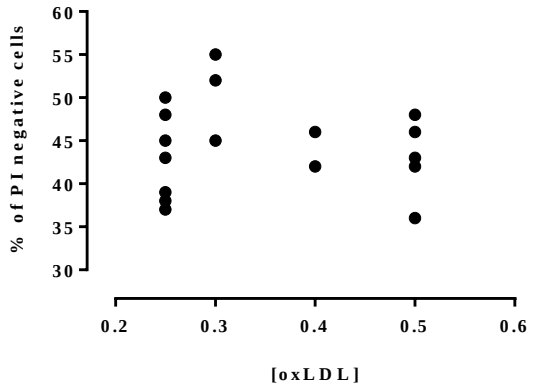

B) Human monocytes

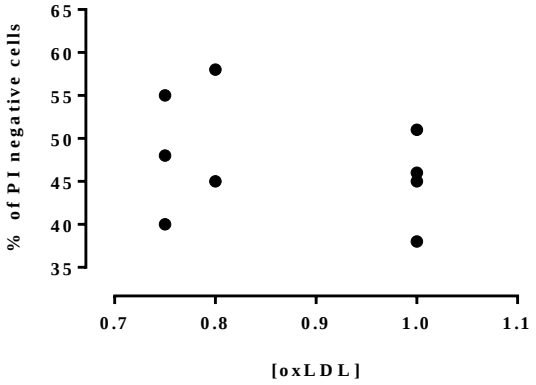

C) HMDM cells

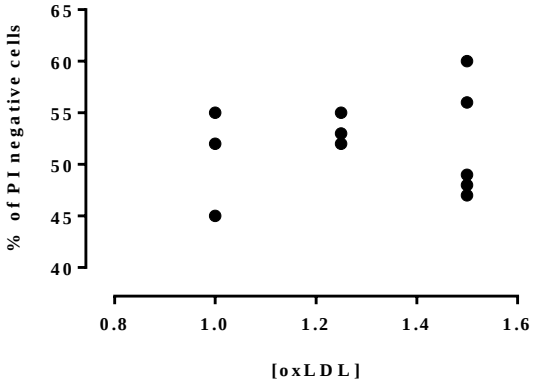

Figure 3.8: LC_{50} of oxLDL of different batches to U937, human monocytes and HMDM cells.

Dot plots presenting a range of LC_{50} determined for oxLDL from various oxLDL batches (LC_{50} of oxLDL vs percentage of PI negative cells compared to control) for A) U937 cells, B) Human monocytes and C) HMDM cells, respectively. Different toxicities with different percentages of PI negative cells were observed with various batches of oxLDL.

Discussion

Effects of oxLDL on cell viability and morphology

Results in this chapter confirmed previous data that low mg/mL concentrations of oxLDL levels are toxic to U937 cells, human monocytes and HMDM cells. OxLDL toxicity was concentration- and time-dependent where higher cell viability loss was observed with increased oxLDL concentrations and this is in agreement with the previous findings from our laboratory (Baird, 2003; Rutherford & Gieseg, 2012). It is noticeable from this study that the toxicity of oxLDL to the cells appeared to be variable between different oxLDL batches (**Figure 3.8**). LC_{50} concentrations of between 0.25 and 0.50 mg/mL oxLDL was observed for U937 cells while LC_{50} for human monocytes and HMDM cells appeared to be higher i.e. between 0.75 and 1.00 mg/mL and between 1.00 to 1.50 mg/mL, respectively. This finding is in-line with the previous studies (Gieseg *et al.*, 2009b; Katouah, 2012) in this laboratory even though the exact cause of cytotoxicity difference is still unknown (Gieseg *et al.*, 2009b). The differences in oxLDL cytotoxicity between U937 cells, human monocytes and HMDM cells could be due to differences in cell type, cell size, mechanism of oxLDL uptake and cell metabolism. Therefore, the toxicity of each batch of oxLDL was tested to determine the LC_{50} concentration before the particular oxLDL was used in subsequent experiments.

Glutathione (GSH) is the main component of intracellular antioxidant defence mechanism whereby its loss is an excellent biomarker of oxidative damage (Valko *et al.*, 2007). Various levels of GSH within the cells have been found to change the LC_{50} for HOCl toxicity towards HMDM cells. Previous studies from this lab have demonstrated that prior to cell death, rapid loss in intracellular GSH was one of the earliest cellular events in U937 and HMDM cells in response to oxLDL or HOCl insult (Baird *et al.*, 2004; Chen, 2012; Rutherford & Gieseg, 2012; Yang, 2009). GSH loss was faster than cell viability loss at each time point, with a 20% and 60% reduction after 3 and 6 hours, respectively (Amit, 2008). This might indicate that the gradual loss of GSH mediated by oxLDL preceded HMDM cell death and might also suggest that the depletion of GSH was required for oxLDL-mediated macrophage toxicity (Amit, 2008; Gieseg *et al.*, 2009b). These findings are in-line with various researchers who have showed that depletion in reduced GSH levels enhances oxLDL toxicity in human monocytes and macrophages (Darley-Usmar *et al.*, 1991; Gotoh *et al.*, 1993; Wang *et al.*, 2006). Shchepetkina (2013) also showed that oxLDL caused a concentration-dependent GSH loss in HMDM cells. Additionally, the timing of initial ROS generation and the drop in GSH level

was parallel, suggesting a connection between them (Gieseg *et al.*, 2010; Shchepetkina, 2013).

OxLDL-induced toxicity could either be of necrosis or apoptosis type of death depending on the types of cells (Baird *et al.*, 2004; Gieseg *et al.*, 2009b). Biochemical assays are normally used to determine cell viability e.g. MTT, PI and trypan blue. However, in order to support cell viability results, changes in cell morphology had also been captured using inverted light microscope parallel to the incubation period with oxLDL. Results from this study clearly showed that acute toxicity of oxLDL had caused the necrotic type of cell death in U937 cells, human monocytes and HMDM cells. Morphological appearance of these cells showed features of cell swelling, cell membrane disruption and loss of cellular contents which corresponded with necrotic cell death.

Previous studies in our lab showed that oxLDL caused necrotic death in U937 and HMDM cells with a rapid loss of intracellular GSH without caspase-3 activation (Gieseg *et al.*, 2009b). In U937 cells, this resulted in the oxidation of essential free thiol groups in the active site with no phosphatidylserine (PS) exposure on the cell membrane (Baird *et al.*, 2004). Nonetheless, it has been shown that oxLDL caused caspase-3 dependant apoptosis (Baird *et al.*, 2004; Vicca *et al.*, 2000) in THP-1 cells with a small reduction in cellular GSH level, cell shrinkage and PS exposure to the outer space of the cell membrane which stained Annexin V positive. This phenomenon could be the result of varying mechanism of oxLDL intake by the different types of cells whereby one of the possibilities could be due to the scavenger receptors presence on the cell surface. Scavenger receptors (SR) are highly implicated as the key players in the initiation and development of atherosclerosis (Goldstein *et al.*, 1979). Of these SR, scavenger receptor A (SR-A) and CD36 are known to be involved in oxLDL-induced cell death as well as foam cell formation (Gieseg *et al.*, 2009b). CD36 expression levels in U937 cells has been shown to be significantly higher compared to THP-1 which may result in an initial burst of oxLDL uptake during oxidative stress (Nguyen-Khoa *et al.*, 1999).

In this study, a delay in oxLDL causing damage to the cells have been observed as there were no significant difference in cell morphology and viability decrease within 3 hours incubation of oxLDL. Different oxLDL preparations have contributed to this observation by previous researchers in this lab. This delay suggests that oxLDL does not cause instant damage to the

cells but triggers cellular events such as GSH loss and metabolic dysfunction (Baird *et al.*, 2005; Shchepetkina, 2013) that will initiate cell death cascade. It has also been shown by Shchepetkina (2013) that HMDM cells committed to death after 6 hours of incubation with oxLDL whereby removing oxLDL from the media at this time did not help to recover cell viability.

Results obtained in this chapter confirmed that oxLDL is toxic to cells in the culture but the exact molecular mechanisms involved in oxLDL-induced cell death remain unclear. Previous findings in our laboratory strongly suggested that oxidative damage could be triggering the rapid cell viability loss (Chen, 2012; Gieseg *et al.*, 2010; Shchepetkina, 2013). This was further explored in the following chapters of this thesis.

Cell viability assays: comparison between PI-flow cytometry and MTT assays

The study of cell death mechanism is the main objective of this whole research. Therefore, it is essential to determine and choose the appropriate type of analysis or assay with the best features for the determination of cell viability throughout the study. MTT reduction and PI-flow cytometry are among the cell-based viability assays used to distinguish viable cells from dead cells. The percentage of viable cells measured using MTT assay is proportional to the amount of purple formazan being generated by cellular NADPH-converting enzymes, thus depending on the intracellular metabolism that reflects the mitochondrial activity of the cells (Mosmann, 1983). Since the measurement of formazan is based on the optical density value (absorbance) measured by spectrophotometer, therefore, MTT assay can represent the cell number and can be compared among the samples, only when cells in the particular sample are in the same metabolic rate. In contrast, flow cytomety assay directly counts the number of cells that flow through the laser beam of the flow cytometer (detailed in **Chapter 2 – Principles of flow cytometry**). Hence, the number of cells counted is proportional to the cell concentration and not the metabolic state of the cells (Wang & Zheng, 2002).

In this study, there was agreement between MTT and PI-flow cytometry assays for cell viability (**Figure 3.7 C)**. The reasons are that the cells used for the two assays were of the same type, being treated with the same concentrations of oxLDL and were in the same metabolic state (Wang & Zheng, 2002) when measurements were done. The percentage of cytotoxicity obtained using both MTT and PI-flow cytometry assays also showed an

increasing trend with increasing oxLDL concentrations (**Figure 3.7 D**). Nevertheless, cell viability measurement using MTT assay yielded higher percentage of viable cells compared to PI-flow cytometry. The contributing factor might be due to the specificity of the assays i.e. MTT assay is measuring the metabolic activity of the cells. This means that some cells that are dying might still be able to metabolise MTT and contribute to the higher percentage of live cells as compared to PI which only binds to the DNA of the dead cells. Since the plasma membrane is the first to be exposed to oxLDL, it may be more readily and easily affected compared to the mitochondria thus explains why PI-flow cytometry assay is more sensitive (Liao *et al.,* 2011). Cell viability data obtained by MTT assay is therefore impacted by the changes in intracellular metabolic activity that indirectly reflect overall cell viability (Wang & Zheng, 2002).

Since the MTT assay only depends on colour reactions, colour intensities of the controls would affect the interpretation of results. Additionally, the percentage of cells in control samples measured by MTT will always be regarded as 100% but in real condition there will always be some dead cells in the control samples. Thus, this could contribute to the higher percentage of the control cells measured by MTT reduction assay compared to PI-flow cytometry analysis.

However, there are distinct characteristics of PI-flow cytometry assay that may provide added advantages over MTT reduction assay. First, it requires only a few treatment steps (Wang & Zheng, 2002) before measurement of cell viability is carried out. A required volume of cells need to be transferred into a vial before PI is added and incubated in the dark before analysis. It requires only a short incubation time period of 15 minutes compared to MTT assay which needs approximately 1 to 2 hours incubation time with MTT reagent. MTT assay requires an extra step of dissolving the purple formazan complex with SDS before absorbance can be measured using a spectrophotometer. PI-flow cytometry assay also has added advantage of quantitative analysis of the cells whereby it allows the counting of the cells.

In addition, PI-flow cytometry assay has fast turnaround time with only few seconds to less than a minute to run a sample. Notably, a relatively small volume of sample is required for analysis (approximately 150-200 µL) compared to MTT assay. Another feature exclusive to PI-flow cytometry assay is that the cell profile as well as dynamic changes of the cells can be obtained and distinguished through dot plots and histograms. This is useful as we are able to

see the changing in the size of the cells (forward scatter) and fluorescence intensities when the cells move from 'live phase' (PI negative) to 'dead phase' (PI positive) as shown in **Figure 3.1 C, 3.2 C, 3.3 C, 3.4 C, 3.5 C, 3.6 C** and **3.7 B**. The number of viable cells (PI negative) and dead cells (PI positive) in each sample are able to be quantitated as opposed to MTT assay. Another advantage of using PI-flow cytometry is that it allows repeated measurements of the same sample. For MTT assay, this is a limitation because the cells become non-viable with the chemical treatment used in the assay, thus repeating or complementary assays cannot be carried out on the same plate of cells.

Flow cytometry assay also enable more than one dye (dyes that are not using the same filter for measurement) to stain the cells at the same time and measurement can be carried out simultaneously (e.g. PI and Annexin V for the measurement of necrotic and apoptotic cells). Another advantage of PI-flow cytometry is the use of very small volume of reagent compared to MTT assay. In this study, approximately 4 uL of 100 µg/mL PI was added to a 250 µL sample and this volume is significantly less than the volume needed for MTT assay.

Summary

Results in this chapter have clearly demonstrated that oxLDL is toxic to U937 cells, human monocytes and HMDM cells. The toxicity caused by oxLDL is concentration and time dependent i.e. increased toxicity with higher oxLDL concentrations and longer incubation time. These findings were in agreement with the previous studies done by other researchers in this lab and also in other labs using oxLDL. LC_{50} concentrations of oxLDL varied for different types of cells and falls within certain ranges of concentrations. Morphological changes of the cells viewed under the light microscope serve as an additional tool in confirming the results obtained by biochemical analysis (MTT, PI and trypan blue). Flow cytometry assay of cell viability using PI dye has more advantages over the conventional MTT reduction assay. PI-flow cytometry assay is rapid, reliable, accurate, easy and cheap to run, thus making it favourable for usage throughout the study. In this study, MTT reduction assay was used mainly to compare and to check the results obtained by PI-flow cytometry whenever needed or required.

CHAPTER FOUR

4. OxLDL induces oxidative stress and NADPH oxidase (NOX) activation

Introduction

This chapter aims to investigate whether oxLDL caused toxicity through oxidative stress. Effects of oxLDL on intracellular ROS production and NOX activation will be studied. Two NOX inhibitors namely, apocynin and VAS2870 as well as 7,8-dihydroneopterin will be used to determine their effects on ROS generation, NOX activation and cell viability.

Results from **Chapter Three** have revealed that oxLDL caused toxicity to different types of cells but the exact mechanism on how oxLDL exerts its toxicity is still unclear. Thus, the aim of this chapter is to investigate the most prominent mechanism proposed to govern oxLDL cytotoxicity which is oxidative stress. Atherosclerosis is one of the diseases associated with oxidative stress whereby it is highly related with the mechanism of action of oxLDL cytotoxicity (Galle *et al.*, 2006; Gieseg *et al.*, 2009b; Salvayre *et al.*, 2002).

OxLDL-induced oxidative stress

OxLDL-induced ROS generation has been studied in various types of vascular cells including neutrophils (Maeba *et al.*, 1995), endothelial cells (Zmijewski *et al.*, 2005), smooth muscle cells (Higashi *et al.*, 2005; Hsieh *et al.*, 2001; Jimenez-Corona *et al.*, 2012) and macrophages (Asmis & Begley, 2003; Lee *et al.*, 2010). Our laboratory has previously showed that oxLDL caused a significant increase in ROS (superoxide) levels in U937 cells (Chen, 2012) and HMDM cells (Shchepetkina, 2013).

Increased intracellular ROS generation plays a vital role in oxLDL-mediated macrophage cell death (Asmis & Begley, 2003; Ball *et al.*, 1995; Seimon & Tabas, 2009). Moreover, studies have addressed the involvement of oxidative stress in the development of atherosclerosis via over-production of ROS or failure of antioxidant defence system (Harrison *et al.*, 2003; Stocker & Keaney, 2004). Previous findings showed that oxLDL triggered an increased

oxidative stress in HMDM, resulting in the excessive production of intracellular superoxide, rapid loss of cellular GSH and eventual loss of cell viability (Gieseg *et al.*, 2010). Superoxide has been proposed as the primary ROS generated after exposure to oxLDL (Gieseg *et al.*, 2010), yet it is the precursor of other ROS that are more active and toxic such as H_2O_2, peroxyl, peroxynitrite and HOCl (**Chapter One - Figure 1.4**) (Stocker & Keaney, 2004). It has been shown that the main contributors of macrophage lysis were peroxide and the resulting peroxyl radical rather than superoxide (Asmis & Begley, 2003) but the particular oxidant(s) triggered by oxLDL signalling is/are difficult to distinguish due to lack of specificity of the existing molecular probes (Mukhopadhyay *et al*., 2007).

In this section, oxLDL-induced oxidative stress in U937 cells, human monocytes and HMDM cells was investigated by studying the effect of oxLDL on intracellular ROS (superoxide) and mitochondrial ROS (superoxide) production using the fluorogenic dyes, dihydroethidium (DHE) and MitoSOX Red, respectively.

NADPH oxidase (NOX)

NADPH oxidases (NOXs) potentially play a major role in the development and progression of cardiovascular diseases (Williams & Griendling, 2007) whereby the only known function of NOX is to generate ROS. This feature makes NOX different from other sources of ROS such as xanthine oxidase (XOD) or uncoupled NOS since these enzymes generate ROS only when they are in a dysfunctional state. Therefore, it might be beneficial to target NOXs and develop therapeutics against them. To date, a handful of compounds (mentioned in **Chapter One – NOX inhibitors**) have been developed and tested against NOX inhibition but data are still lacking, particularly on their mechanism of action.

NOX inhibitors – apocynin and VAS2870

The ability of apocynin to inhibit NOX has been studied extensively in *in vivo* and *in vitro* experimental models. In human cellular studies using neutrophils, Van den Worm *et al.* (2001) has determined an IC_{50} (half maximal inhibitory concentration) of 10 µM for apocynin when stimulated with opsonised zymosan A (OPZ) or PMA. Moreover, apocynin does not interfere with the killing capacity of polymorphonuclear cells (PMNs) and it exhibits a very low toxicity with a LD_{50} of 9 g/kg when orally given to mice (Van den Worm *et al.*, 2001). Although its exact mechanism of action is unknown, many studies have proposed that

apocynin prevents the translocation of $p47^{phox}$ cytosolic subunit of NOX, therefore preventing NOX activation. Ximenes *et al.* (2007) have suggested that MPO catalyses apocynin oxidation into an active dimer radical form. This radical form of apocynin is thought to react with the essential thiol groups of $p47^{phox}$, thus inhibits the activation of NOX (**Figure 4.1**).

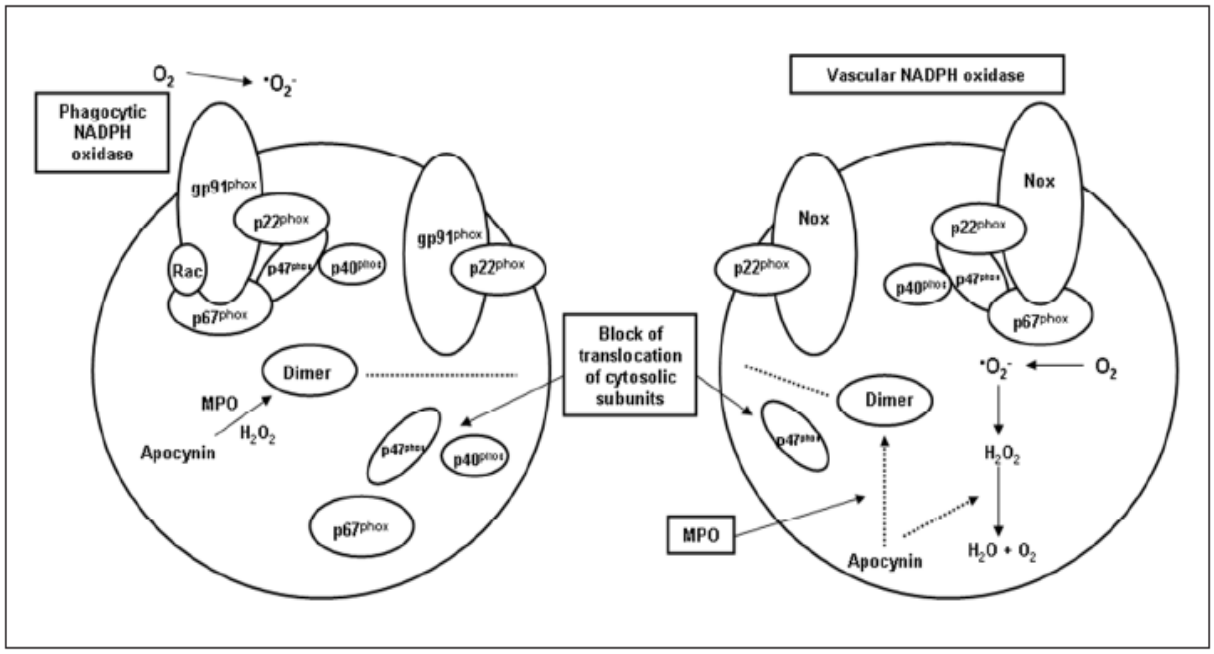

Figure 4.1: NADPH oxidase inhibition mechanism by apocynin in phagocytic and non-phagocytic cells

The inhibition by apocynin is effective only in the presence of apocynin dimers which is catalyses by MPO (Rabelo *et al.*, 2010).

With regards to atherosclerosis, Aviram *et al.* (1996) have showed that inhibition of J-774 A.1 murine macrophage NOX with 600 µM apocynin inhibited macrophage-induced oxidation of LDL by 89% compared to control cells. Additionally, Holland *et al.* (1998) have demonstrated that when stimulated with thrombin (phospholipase A_2 activator), endothelial cells incubated 600 µM apocynin inhibited NOX resulting in reduced ROS generation. Likewise, apocynin was also seen to significantly reduce cellular H_2O_2 levels mediated by high LDL in endothelial cells (Holland *et al.*, 1997).

However, the use of apocynin has been controversial and may have potential downsides. Studies in various types of cells have shown that apocynin may caused oxidative stress and could be pro-oxidant because of MPO-mediated apocynin radical generation. Apocynin was found to stimulated ROS production in rat vascular fibroblast and inhibited respiratory burst

in rat monocytes induced by zymosan. This indicated that it might act as an NOX inhibitor in phagocytes and as a stimulator in non-phagocytes (Vejrazka *et al.*, 2005). Apocynin has been shown to induce an increase in H_2O_2 formation and a reduction in GSH/GSSG ratio, followed by an enhanced efflux of GSH in N11 glial cells (Riganti *et al.*, 2006). Riganti *et al.* (2006) have also observed reduced GSH levels in alveolar epithelial cells treated with apocynin. Meanwhile, Castor *et al.* (2010) proposed that GSH oxidation was due to the pro-oxidant activity of apocynin radicals. Thus, apocynin itself could be inducing oxidative stress followed by cytotoxic effects depending on cell types and conditions.

The compound, VAS2870 was discovered via a high-throughput screening assay specific for NOX activity and further characterised by NMR and spectrometry. VAS2870 has been shown to inhibit superoxide generation with an IC_{50} of 10.6 µM in cell free system containing membranes and cytosolic fractions of human neutrophil and 2 µM in whole-cell assay of HL-60 cells, respectively (ten Freyhaus *et al.*, 2006). At 10 µM, VAS2870 inhibits NOX activity in oxLDL-treated human umbilical vein endothelial cells (HUVEC) (Stielow *et al.*, 2006) and platelet-derived growth factor (PDGF)-induced primary rat aortic vascular smooth muscle cells (VSMC) (ten Freyhaus *et al.*, 2006). At 50 µM, upon exposure to PDGF-BB, VAS2870 inhibits the stimulation of vasculogenesis of mouse embryonic stem cells (Lange *et al.*, 2009). In zebrafish larvae, VAS2870 inhibits wound margin H_2O_2 production without obvious toxicity (Niethammer *et al.*, 2009).

VAS3947, which is a derivative of VAS2870 has been shown to inhibit NOX activity in various types of cells (Wind *et al.*, 2010). Comparative analysis of VAS3947 and other common molecules used to inhibit NOX activity such as apocynin, AEBSF and DPI demonstrate a more effective and specific inhibition of this compound. However, the IC_{50} values of VAS3947 varied depending on the cell models. Established IC_{50} of 12 µM for CaCo-2 cells (mainly NOX1 and NOX2 and some NOX4 and NOX5), 2 µM for HL-60 cells (NOX2 and NOX5) and 13 µM for A7r5 cells (mainly NOX4 and some NOX1 and NOX3) indicates that this compound is not an isoform-specific NOX inhibitor although it is specific for NOX class of enzymes (Cifuentes-Pagano *et al.*, 2012).

In this study, the ability of oxLDL to activate NOX will be investigated by examining $p47^{phox}$ phosphorylation via western blotting. Despite not knowing their exact mechanism of action, apocynin and VAS2870 have been shown by many studies to inhibit ROS flux in various

types of cells. However, there was no information on how these NOX inhibitors affect cell survival of oxLDL-exposed cells (particularly on U937, human monocytes and HMDM cells). Since ROS-mediated oxidative stress is reported to play a vital role in oxLDL-induced cell death, the effect of NOX on cell death triggered by oxLDL will also be examined on those cells.

Results

OxLDL induces intracellular ROS production in U937 cells, human monocytes and HMDM cells.

OxLDL-induced intracellular ROS generation was studied in U937 cells, human monocytes and HMDM cells. The intracellular ROS were detected using fluorescence detection of dihydroethidium (DHE) measured using flow cytometry (see **Chapter Two – Dihydroethidium (DHE)**). DHE is a widely used probe for detecting intracellular superoxide (Zhao *et al.*, 2005).

The initial experiments were to confirm that oxLDL induces the generation of intracellular ROS (superoxide) in the cells. U937 cells were incubated with increasing concentrations of oxLDL for 3 hours, followed by DHE fluorescence measurement using flow cytometer. Results showed that the intracellular fluorescence intensity was significantly increased in cells treated with oxLDL compared to control. An increase of 30%, 100% and 130% in DHE fluorescence (compared to control) were observed when the cells were treated with 0.25, 0.50 and 1.00 mg/mL oxLDL respectively (**Figure 4.2**). This clearly shows that oxLDL induced intracellular ROS production, in particular – superoxide which then may contribute to oxidative stress.

Effects of oxLDL on ROS production induced by oxLDL between different cell lines were also compared between U937 and THP-1. Results showed that with increasing oxLDL concentrations, DHE levels also increase in both types of cells. Though, the increased in DHE fluorescence was relatively low for THP-1 cells compared to U937 cells. This might indicate different responses of the cells to oxLDL (**Figure 4.3**). Previous studies had shown that only a small loss in GSH was observed in oxLDL treated THP-1 cells while almost all of the GSH was lost in U937 cells.

A)

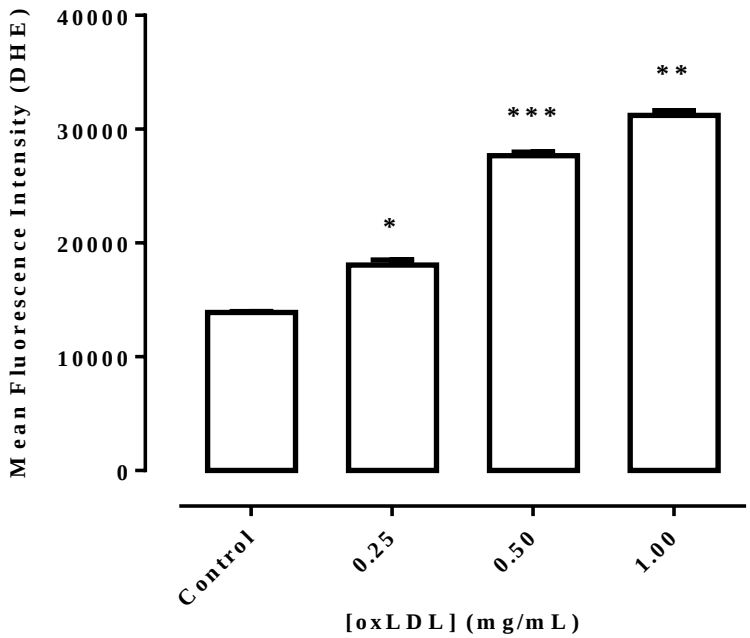

B)

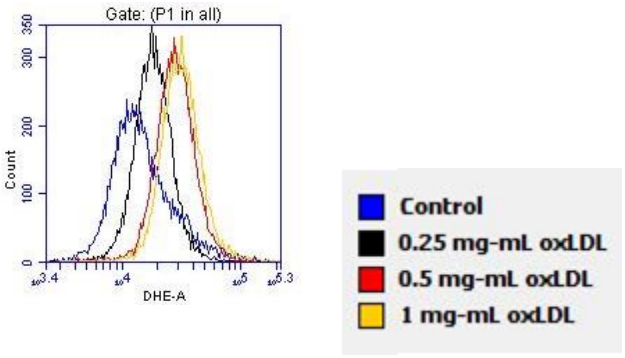

Figure 4.2: Effect of different concentrations of oxLDL on intracellular ROS production in U937 cells.

U937 cells (0.5×10^6 cells/mL) were incubated in RPMI-1640 containing the increasing concentrations of oxLDL for 3 hours at 37°C. A cell only control with 0 mg/mL oxLDL added was included. At the end of treatment, the cells were washed with PBS and probed with 10 μM DHE for 20 minutes in the dark before measuring the DHE fluorescence by flow cytometry for intracellular ROS. Results are presented as mean fluorescence intensity (MFI) ± SEM of triplicates from a representative experiment. Significance is indicated from the cell only control (one-factor ANOVA, Sidak's post test): *, $p<0.05$; **, $p<0.01$; ***, $p<0.001$.

A)

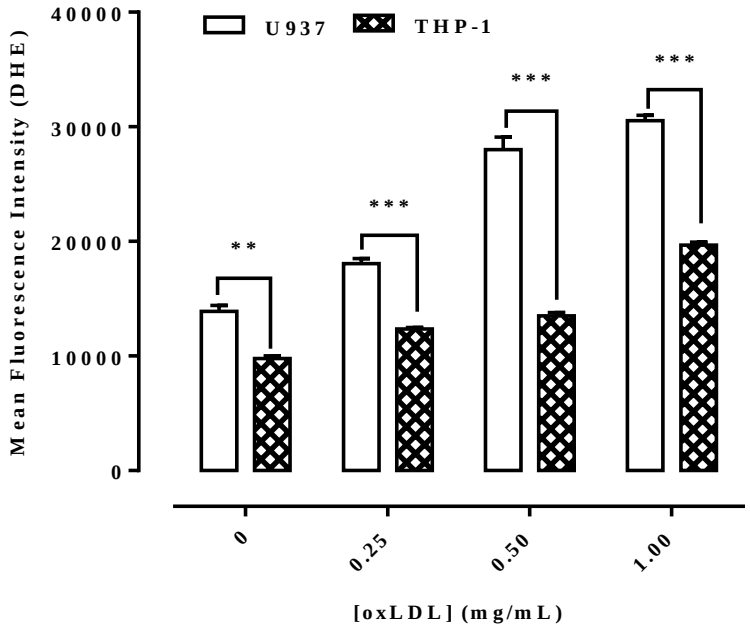

B)

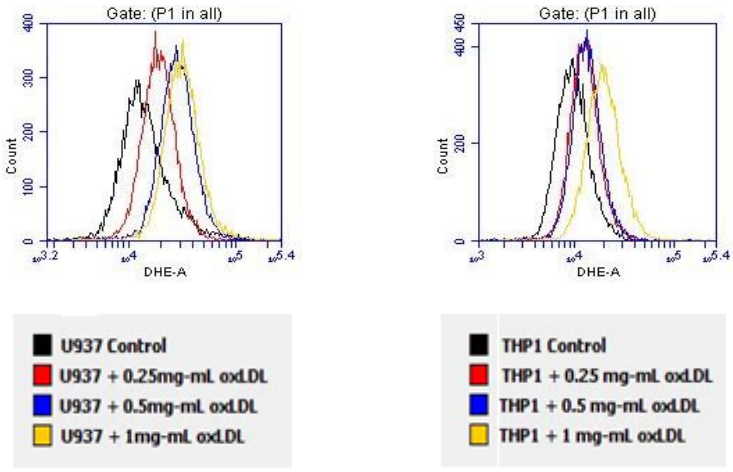

Figure 4.3: Effects of different concentrations of oxLDL on intracellular ROS production in U937 and THP-1 cells.

U937 and THP-1 cells (0.5×10^6 cells/mL) were incubated in RPMI-1640 containing the increasing concentrations of oxLDL for 3 hours at 37°C. A cell only control with 0 mg/mL oxLDL added was included. At the end of treatment, the cells were washed with PBS and probed with 10 μM DHE for 20 minutes in the dark before measuring the DHE fluorescence by flow cytometry for intracellular ROS. Results are presented as mean fluorescence intensity (MFI) ± SEM of triplicates from a representative experiment. Significance is indicated between U937 and THP-1 cells for each oxLDL concentration (two-factor ANOVA, Sidak's post test): **, $p<0.01$; ***, $p<0.001$.

A time course study was also performed to examine the kinetics of the oxLDL induction. Cells were incubated with LC_{50} concentration of oxLDL (0.5, 1.0 and 1.5 mg/mL for U937, human monocytes and HMDM cells, respectively) for a designated period of time followed by probing with DHE. Flow cytometer was used to measure the DHE fluorescence levels at various times which reflect the production of superoxide anion (Rodrigues *et al.*, 2013) over time. A time-dependent increased in the DHE levels occurred in U937 cells, human monocytes and HMDM cells treated with oxLDL. For U937 cells, an average increased in DHE fluorescence of 30%, 50%, 85% and 130% compared to 0 hour control was observed after 1, 3, 6 and 9 hour incubation with oxLDL respectively. The DHE level dropped after 9 hours with a decreased of 15% fluorescence intensity after 12 hours incubation with oxLDL (**Figure 4.4 A**). This is supported by the flow cytometry histogram which showed a shift to the right of the histogram over time which indicates increased fluorescence levels (**Figure 4.4 B**).

This was different to the trend observed by Chen (2012) whereby marked increased in DHE fluorescence reached maximum at 3 hours and dropped severely to the 0 hour control level after 6 hours. The abrupt decrease in fluorescence may be due to cell lysis occurred after 3 hours incubation with oxLDL which caused the leakage of oxidants from the cells. In addition, the measurement of DHE fluorescence was then performed using fluorescent microscopy. Fluorescent microscopy technique has a few disadvantages including only allowing a semi-quantitative measurement of a relatively limited numbers of cells at the same time. Furthermore, cells loaded with fluorescent dyes tend to increase ROS generation by itself due to the exposure of lasers or uv compared to flow cytometry (Mukhopadhyay *et al.*, 2007).

A)

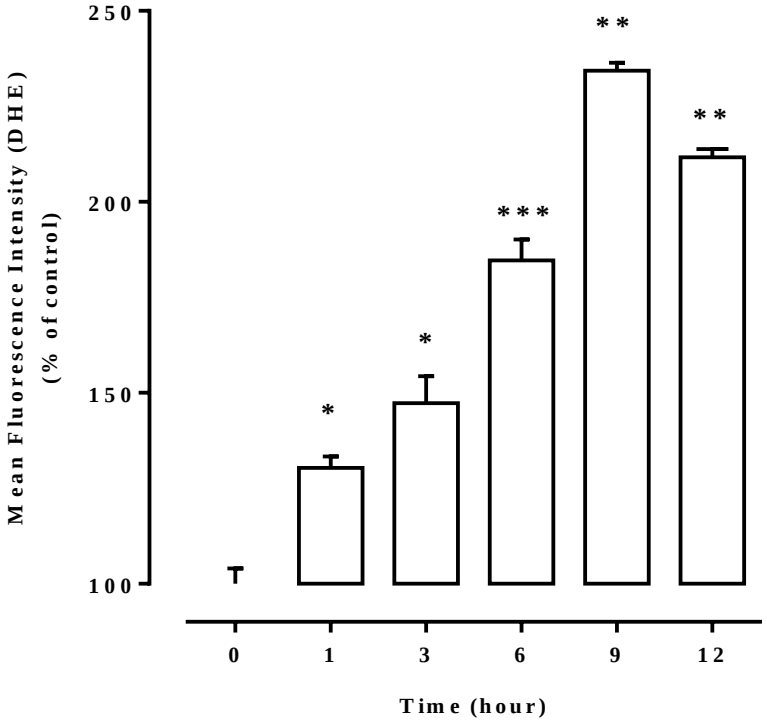

B)

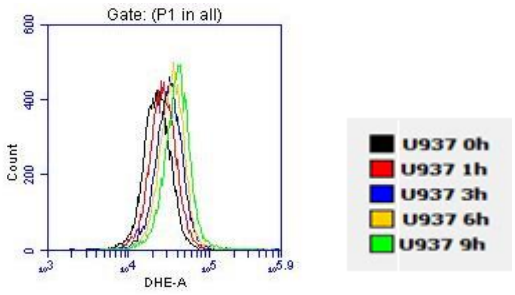

Figure 4.4: Time course effect of oxLDL-induced intracellular ROS production in U937 cells.

U937 cells (0.5×10^6 cells/mL) were incubated in RPMI-1640 containing the LC_{50} concentration (0.5 mg/mL) of oxLDL at 37°C. At various times, cells were collected, washed with PBS and probed with 10 μM DHE for 20 minutes in the dark before measuring the DHE fluorescence by flow cytometry for intracellular ROS. A) shows the mean fluorescence intensities presented as a percentage of 0 hour control. Results are presented as mean fluorescence intensity (MFI) ± SEM of triplicates from a representative experiment. B) shows the flow cytometry histogram plot of cell count against DHE fluorescence. Significance is indicated from the 0 hour control. (one-factor ANOVA, Dunnett's post test): *, $p<0.05$; **, $p<0.01$; ***, $p<0.001$.

A time course effects of oxLDL-induced ROS production were also studied in human monocytes and HMDM cells. For human monocytes, an increase of 10% (compared to 0 hour control) in DHE fluorescence was seen as fast as 1 hour incubation with oxLDL. A further increase of 20% occurred at 3 hours (compared to 1 hour) while greater increase of fluorescence were measured after 6 and 9 hours of oxLDL incubation (70 % increase compared to 0 hour control). The DHE fluorescence increase peaked at 9 hour before declining by 30% after 12 hours (**Figure 4.5**). Similarly, this shows that oxLDL was able to cause ROS generation in human monocytes and the similar pattern of increasing intracellular oxidative flux occurred over time, reached maximum level before gradual declined from peak value.

Time-course effect of oxLDL on intracellular ROS production in HMDM cells is showed in **Figure 4.6**. An early increase in DHE fluorescence occurred after 1 hour and continuously increased after 3 and 6 hours incubation with oxLDL. Mean fluorescence intensity reached maximum after 9 hour with 40% increased above 0 hour control before a sharp decline after 12 hours to almost the same level obtained at 6 hour. This finding confirmed the ability of oxLDL to initiate oxidative stress in HMDM cells that caused intracellular ROS generation. In this study, the trend of increasing ROS generation overtime and gradual decline after reaching maximum activity agrees with Shchepetkina (2013).

A)

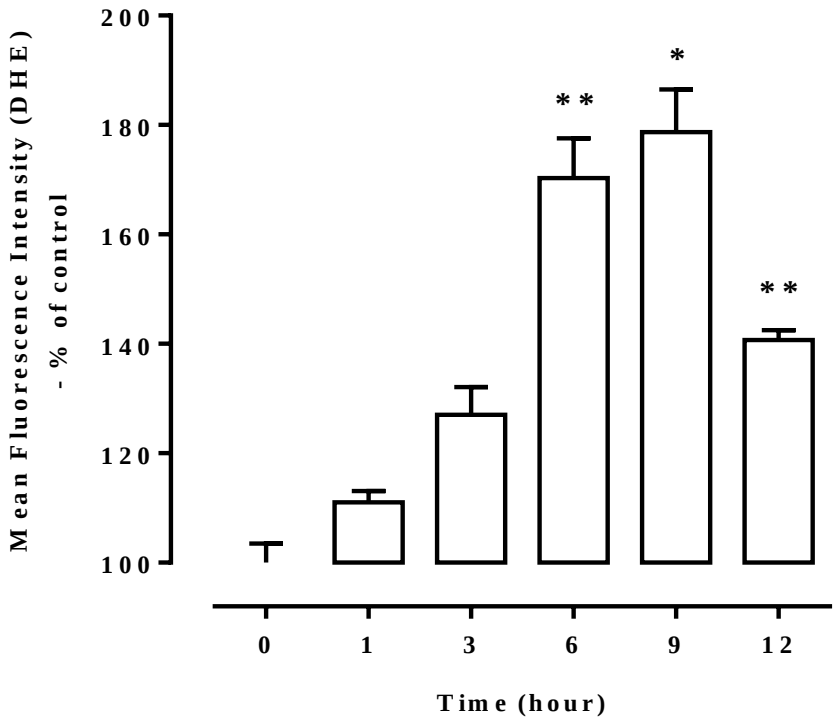

B)

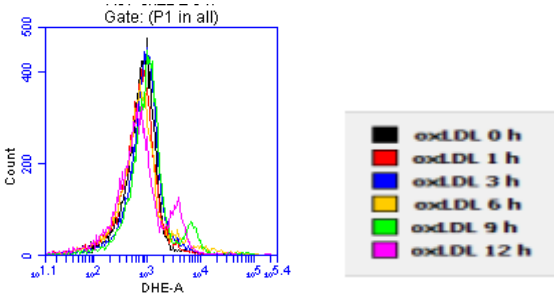

Figure 4.5: Time course effect of oxLDL-induced intracellular ROS production in human monocytes.

Human monocytes (1×10^6 cells/mL) were incubated in RPMI-1640 containing the LC_{50} concentration (1 mg/mL) of oxLDL at 37°C. At various times, cells were collected, washed with PBS and probed with 10 µM DHE for 20 minutes in the dark before measuring the DHE fluorescence by flow cytometry for intracellular ROS. A) shows the mean fluorescence intensities presented as a percentage of 0 hour control. Results are presented as mean fluorescence intensity (MFI) ± SEM of triplicates from a representative experiment. B) shows the flow cytometry histogram plot of cell count against DHE fluorescence. Significance is indicated from the 0 hour control (one-factor ANOVA, Dunnett's post test): *, $p<0.05$, **, $p<0.01$.

A)

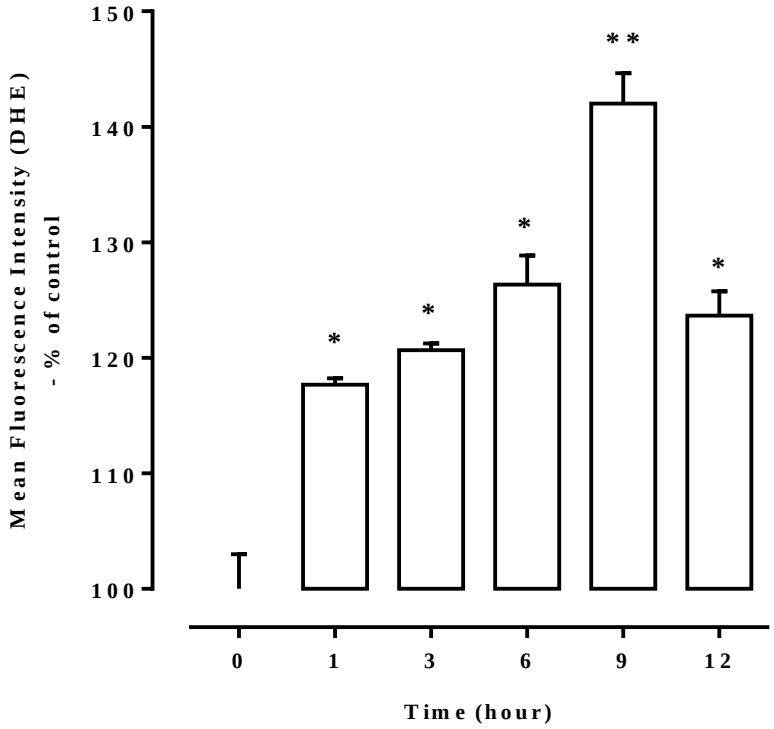

B)

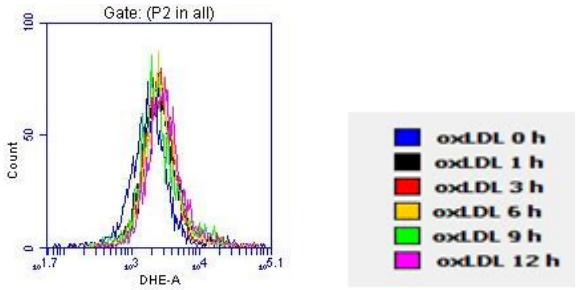

Figure 4.6: Time course effect of oxLDL-induced intracellular ROS production in HMDM cells.

HMDM cells (1×10^6 cells/mL) were incubated in RPMI-1640 containing the LC_{50} concentration (1.5 mg/mL) of oxLDL at 37°C. At various times, cells were collected, washed with PBS and probed with 10 μM DHE for 20 minutes in the dark before measuring the DHE fluorescence by flow cytometry for intracellular ROS. A) shows the mean fluorescence intensities presented as a percentage of 0 hour control. Results are presented as mean fluorescence intensity (MFI) ± SEM of triplicates from a representative experiment. B) shows the flow cytometry histogram plot of cell count against DHE fluorescence. Significance is indicated from the 0 hour control. (one-factor ANOVA, Dunnett's post test): *, $p<0.05$; **, $p<0.01$.

Mitochondrial ROS detection

Mitochondria have been known as the potential source of superoxide production and undergo oxidative damage upon exposure to oxLDL (Zmijewski *et al.*, 2005). MitoSOX, which contains a triphenylphosphonium cation (TPP+) conjugated to DHE via a linker carbon-carbon alkyl chain has been used effectively to directly measure mitochondrial superoxide (Robinson *et al.*, 2006; Mukhopadhyay *et al.*, 2007). The effect of oxLDL on mitochondrial superoxide production in HMDM cells was studied by treating cells with LC_{50} concentration of oxLDL, followed by probing with MitoSOX Red (MitoSOX) which is specifically targeted to mitochondrial ROS (see **Chapter 2 – MitoSOX Red**) before detection via flow cytometry. Data collected at FSC/SSC of 585/542 nm in the FL2 channel. In this part of the study, a time course experiment has been performed to detect and quantify the production of mitochondrial ROS in HMDM cells. Mitochondrial ROS detection using MitoSOX in U937 cells has been done by Chen (2012) in this lab.

Results obtained from this experiment showed that oxLDL caused an increase in mitochondrial ROS production over time. Approximately 20% increase in fluorescence was observed after 1 hour incubation with oxLDL followed by an increase of 30%, 50% and 70% after 3, 6 and 9 hours respectively compared to 0 hour control. After12 hours of incubation with oxLDL, more than 15% reduction in MitoSOX fluorescence was observed (**Figure 4.7**).

Previous study in this laboratory has utilised MitoSOX for the detection of mitochondrial ROS in U937 cells after stimulation by increasing concentrations of oxLDL using fluorescent microscope (Chen, 2012). It has been shown by Chen (2012) that the increase in mitochondrial ROS production in U937 cells was concentration dependent and appeared to be more linear compared to the increase in overall oxLDL-induced intracellular ROS production. Chen (2012) suggested that the oxidative damage caused by oxLDL on mitochondria could be a later event whereby the increased in oxidative stress was primarily from an extra-mitochondrial origin in U937 cells. This may also imply that mitochondrial dysfunction could be a secondary event initiated by oxLDL-induced ROS overproduction and other cellular oxidative damages in the cytosol.

A)

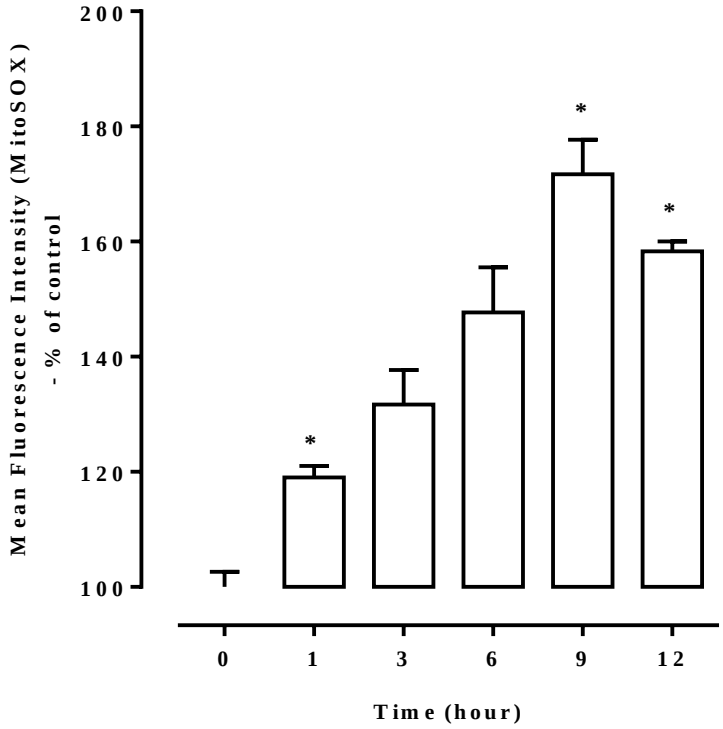

B)

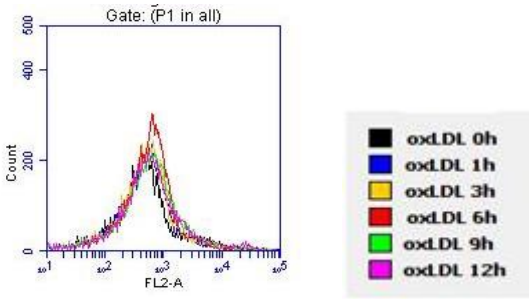

Figure 4.7: Time course effect of oxLDL-induced ROS production in the mitochondria of HMDM cells.

HMDM cells (1×10^6 cells/mL) were incubated in RPMI-1640 containing the LC_{50} concentration (1.5 mg/mL) of oxLDL at 37°C. At various times, cells were collected, washed with PBS and probed with 5 μM MitoSOX red for 10 minutes in the dark before measuring the fluorescence by flow cytometry for mitochondrial superoxide. Results are presented as mean fluorescence intensity (MFI) ± SEM of triplicates from a representative of experiment. Significance is indicated from the 0 hour control. (one-factor ANOVA, Dunnett's post test): *, $p<0.05$; **, $p<0.01$.

NADPH oxidases (NOX) involvement in oxLDL-induced oxidative stress: effects of NOX inhibitors – apocynin and VAS2870 on cell death

It has been shown that oxLDL had caused the increase in ROS production that resulted in oxidative stress in all three types of cells in the earlier experiments. Studies suggest that excessive generation of ROS is a key player that contributes to the progression of atherosclerosis. This is supported by the presence of oxidation products of lipids and proteins in atherosclerotic plaques (Stocker & Keaney, 2004). However, the source of the ROS and the mechanism of oxLDL triggering ROS production are still unclear. NOX has been implicated as the major superoxide generating enzyme complex and thus it was hypothesised that NOX may be the predominant source of ROS leading to oxidative stress in the progression of atherosclerotic plaque (Aviram *et al.*, 1996; Singh & Jialal, 2006).

The following studies were aimed to examine the ability of oxLDL to activate NOX and the role of NOX in oxLDL-induced oxidative stress. The effects of NOX inhibitors, apocynin and VAS2870 on oxLDL-induced cell death and superoxide production will be studied. Initial experiments in this section were performed to examine the effects of apocynin and VAS2870 on U937 cells, human monocytes and HMDM cells. This is important to ensure that the resulting cell death was caused by oxLDL but not by apocynin or VAS2870 being toxic to the cells.

Cells were incubated with different concentrations of apocynin for 3 hours before addition of oxLDL and cell viability (PI positive and PI negative stained cells) was measured using PI-flow cytometry assay. The same experiments in the absence of oxLDL were also carried out to examine the effects of apocynin alone on U937 cells, human monocytes and HMDM cells. For U937 cells, there was no cell viability loss compared to the cell only control after treatment with 10, 20, 50, 100 and 200 µM apocynin for 27 hours (**Figure 4.8**) implicating that apocynin had no cytotoxic effect in these range of doses. With the presence of oxLDL for 24 hours, cell viability (PI negative cells) has been reduced by 65% compared to cell only control. Pre-treatment with of apocynin of different concentrations has seen significant protection from oxLDL-induced cell death by 15-20% (PI negative cells) (**Figure 4.9**). In the previous study by Chen (2012), significant protection of 10-20% from oxLDL-induced cell loss has been observed with pre-incubation of 10 – 100 µM of apocynin (using MTT reduction assay for cell viability determination).

For human monocytes, there was also no cell viability loss in cells incubated with different ranges of apocynin as compared to cell only control (**Figure 4.10**) indicating that apocynin itself is not cytotoxic. However, following a 24-hour incubation with LC_{50} concentration of oxLDL, no significant protection of apocynin was seen as there was no difference in cell viability loss (PI negative cells) compared to oxLDL treated cells (**Figure 4.11**). This shows that, despite not being toxic, apocynin was not able to provide protection to human monocytes against oxLDL-induced cytotoxicity.

Likewise, apocynin of different concentrations were not toxic to HMDM cells as no significant cell viability loss (PI negative cells) was observed compared to cell only control (**Figure 4.12**). However, there was also no significant protection of apocynin on oxLDL-induced cell loss (PI negative cells) was observed with pre-incubation of apocynin ranging from 10 to 200 µM (**Figure 4.13**). This finding agrees with Shchepetkina (2013) who had also showed no protection of apocynin (50, 100 and 200 µM) to oxLDL-induced toxicity on HMDM cells despite its ability to reduce 7,8-NP oxidation. Extended study by Shchepetkina (2013) had the incubation period with apocynin shortened to 15 hours and found that the distribution of apoptotic, necrotic and live cells after oxLDL treatment was unaffected by the presence of apocynin.

A)

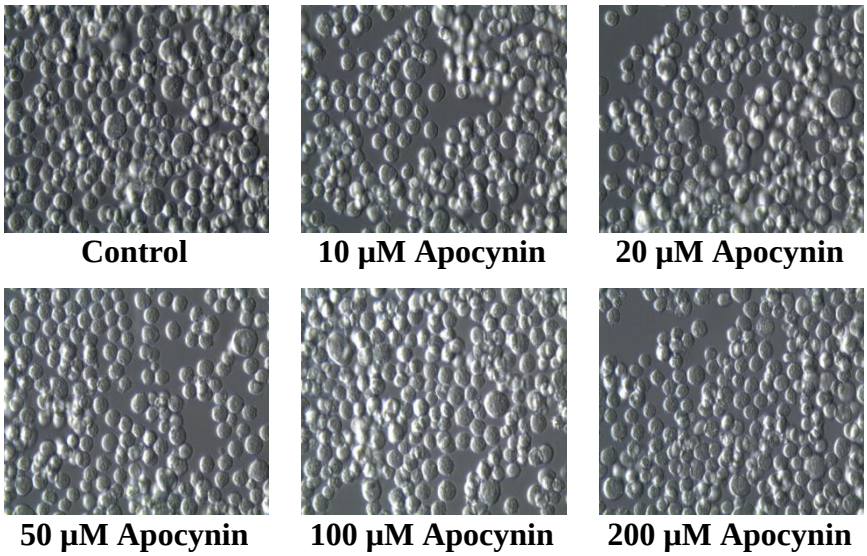

B)

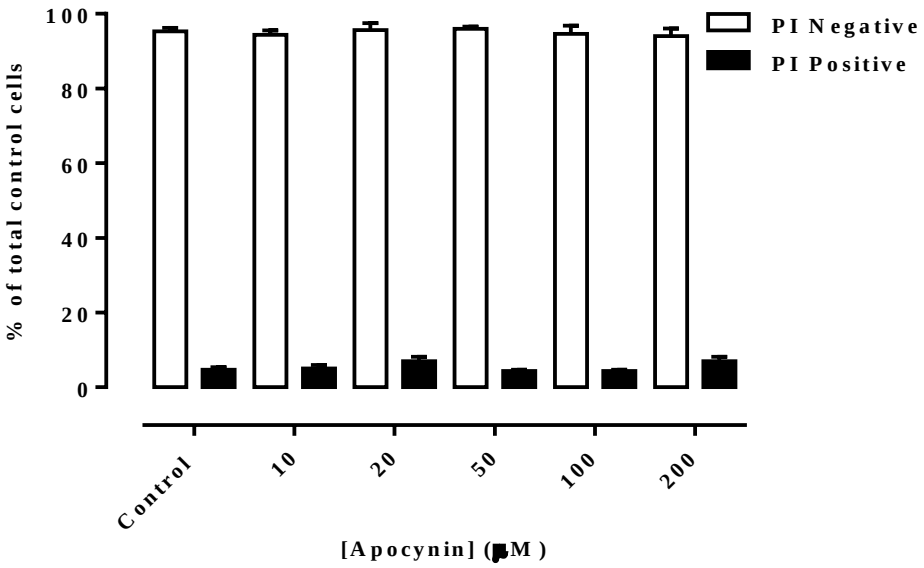

Figure 4.8: Effect of different concentrations of apocynin on U937 cells.

U937 cells (0.5×10^6 cells/mL) were incubated at 37°C in non-phenol red RPMI-1640 with increasing concentrations of apocynin for 27 hours. A cell only control was added. A) Cells were viewed *in situ* in tissue culture wells using an inverted microscope (400x magnification) after 27 hours incubation with oxLDL. Images were taken using a Leica C-Mount camera and processed using Leica Application Suite software. B) Cell viability was determined using PI-flow cytometry. Data are expressed as percentage of the total number of cells in control samples. Results shown are mean ± SEM of triplicates from a representative experiment.

A)

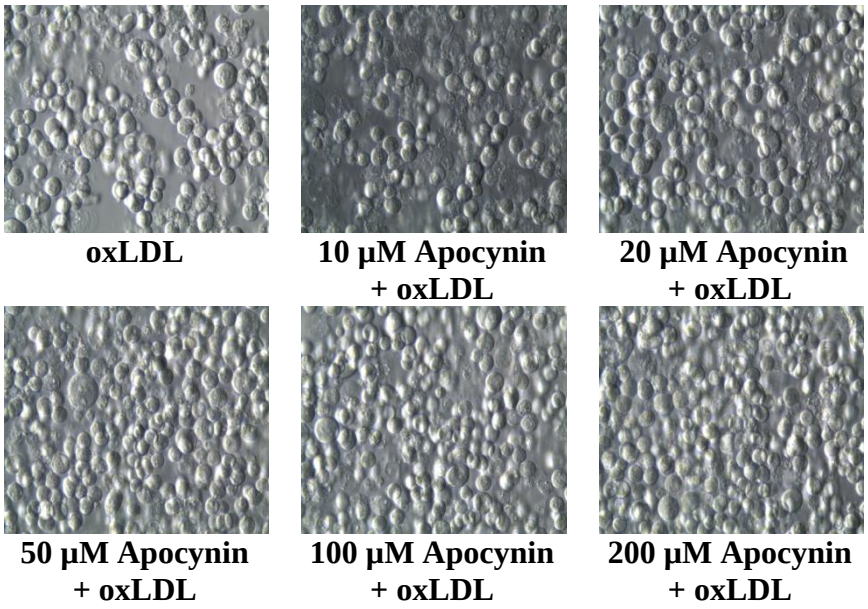

B)

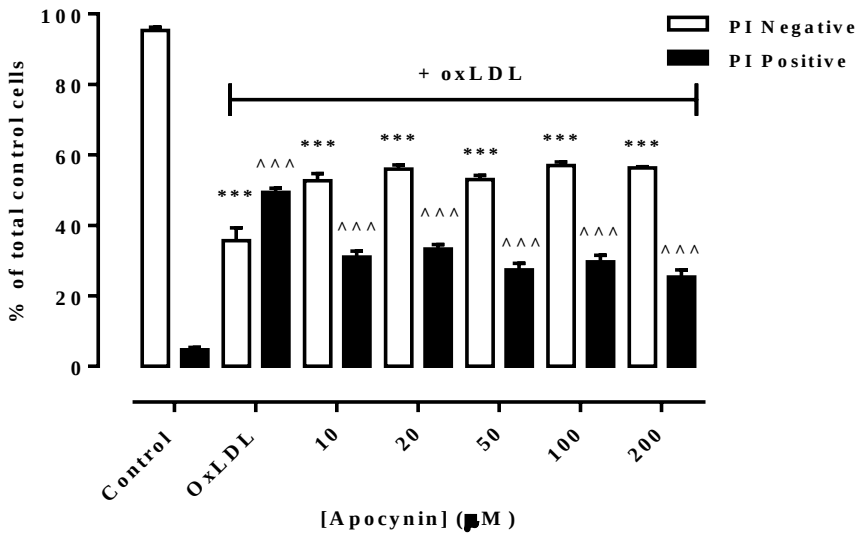

Figure 4.9: Effect of different concentrations of apocynin and oxLDL on U937 cells.

U937 cells (0.5×10^6 cells/mL) were incubated at 37°C in non-phenol red RPMI-1640 with increasing concentrations of apocynin for 3 hours followed by treatment of LC_{50} concentration (0.4 mg/mL) of oxLDL for 24 hours. A cell only control was included. A) Cells were viewed *in situ* in tissue culture wells using an inverted microscope (400x magnification) after 27 hours incubation with oxLDL. Images were taken using a Leica C-Mount camera and processed using Leica Application Suite software. B) Cell viability was determined using PI-flow cytometry. Data are expressed as percentage of the total number of cells in control samples. Results shown are mean ± SEM of triplicates from a representative experiment. Statistical significance (two-factor ANOVA, Sidak's post test) is indicated from: PI negative cells - control vs oxLDL and oxLDL vs apocynin + oxLDL, ***, $p<0.001$; PI positive cells – control vs oxLDL and oxLDL vs apocynin + oxLDL, ^^^, $p<0.001$.

A)

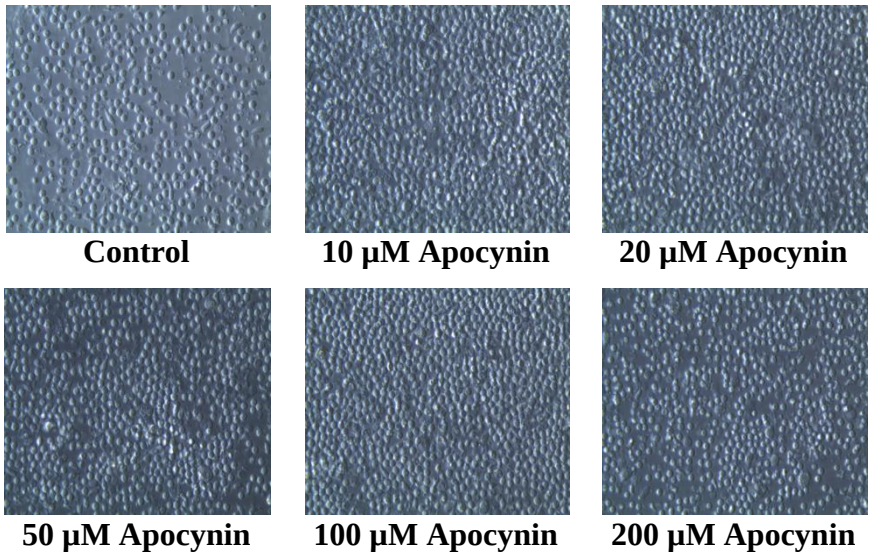

B)

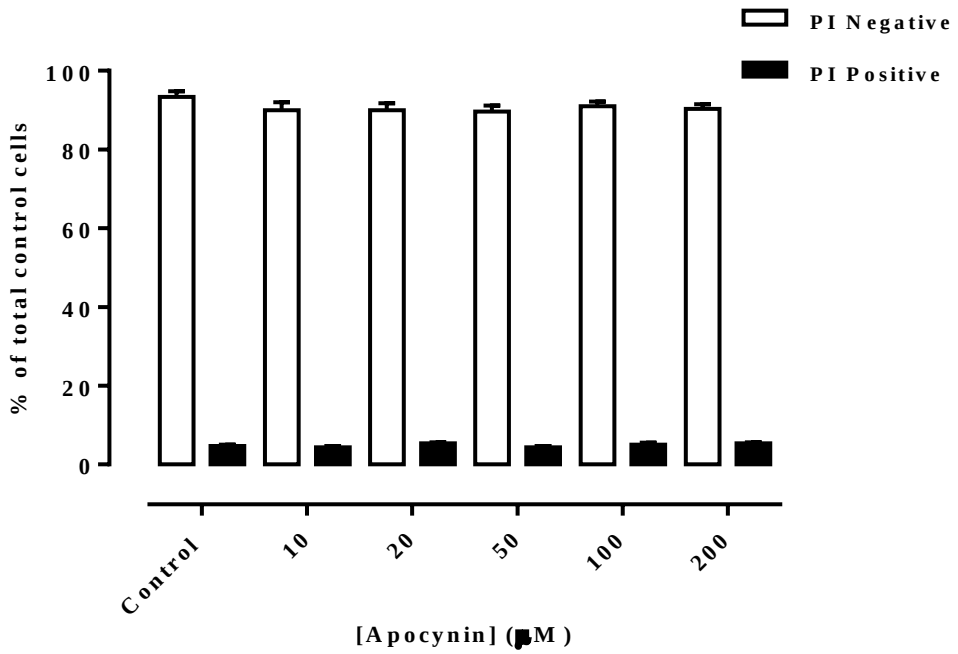

Figure 4.10: Effect of different concentrations of apocynin on human monocytes.

Human monocytes (1×10^6 cells/mL) were incubated at 37°C in non-phenol red RPMI-1640 with increasing concentrations of apocynin for 27 hours. A cell only control was added. A) Cells were viewed *in situ* in tissue culture wells using an inverted microscope (400x magnification) after 27 hours incubation with oxLDL. Images were taken using a Leica C-Mount camera and processed using Leica Application Suite software. B) Cell viability was determined using PI-flow cytometry. Data are expressed as percentage of the total number of cells in control samples. Results shown are mean ± SEM of triplicates from a representative experiment.

A)

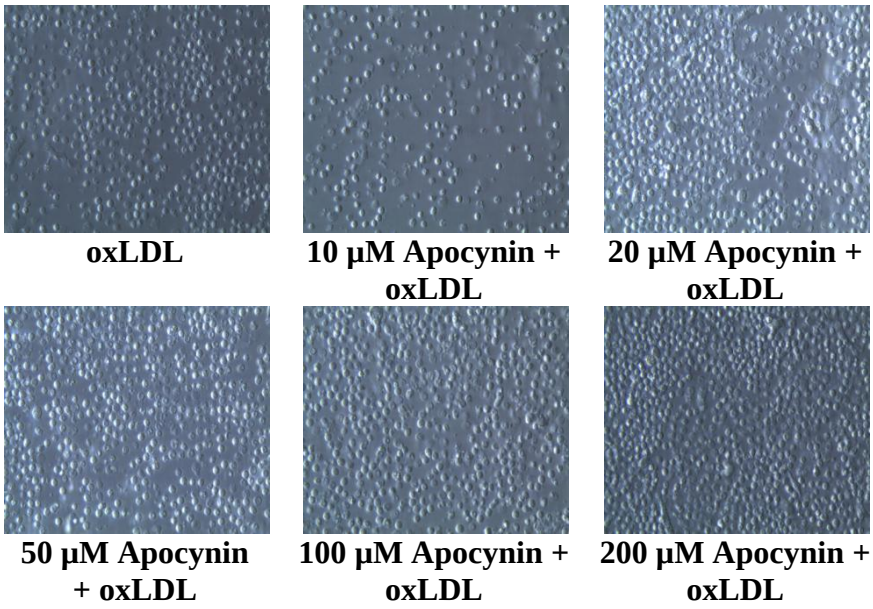

B)

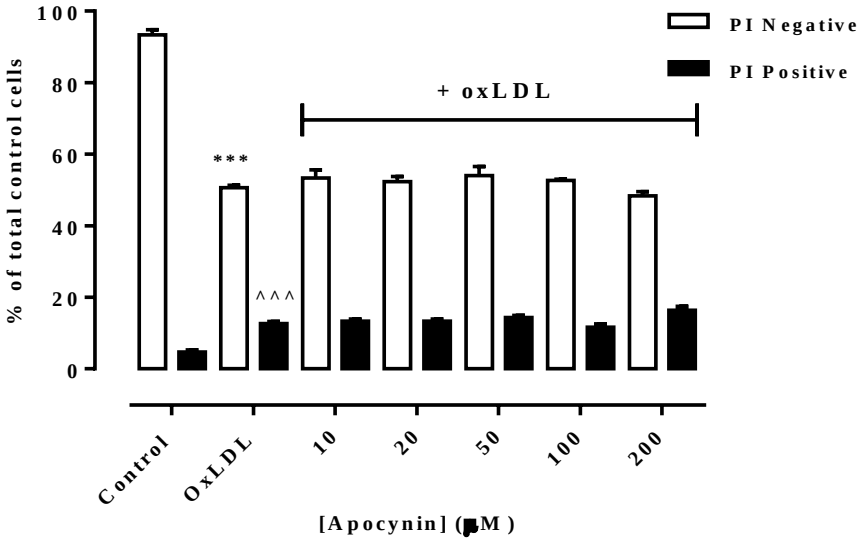

Figure 4.11: Effect of different concentrations of apocynin and oxLDL on human monocytes.

Human monocytes (1×10^6 cells/mL) were incubated at 37°C in non-phenol red RPMI-1640 with increasing concentrations of apocynin for 3 hours followed by treatment of LC_{50} concentration (0.8 mg/mL) of oxLDL for 24 hours. A cell only control was included. A) Cells were viewed *in situ* in tissue culture wells using an inverted microscope (400x magnification) after 27 hours incubation. Images were taken using a Leica C-Mount camera and processed using Leica Application Suite software. B) Cell viability was determined using PI-flow cytometry. Data are expressed as percentage of the total number of cells in control samples. Results shown are mean ± SEM of triplicates from a representative experiment. Statistical significance (two-factor ANOVA, Sidak's post test) is indicated from: PI negative cells - control vs oxLDL, ***, $p<0.001$; PI positive cells – control vs oxLDL, ^^^, $p<0.001$.

A)

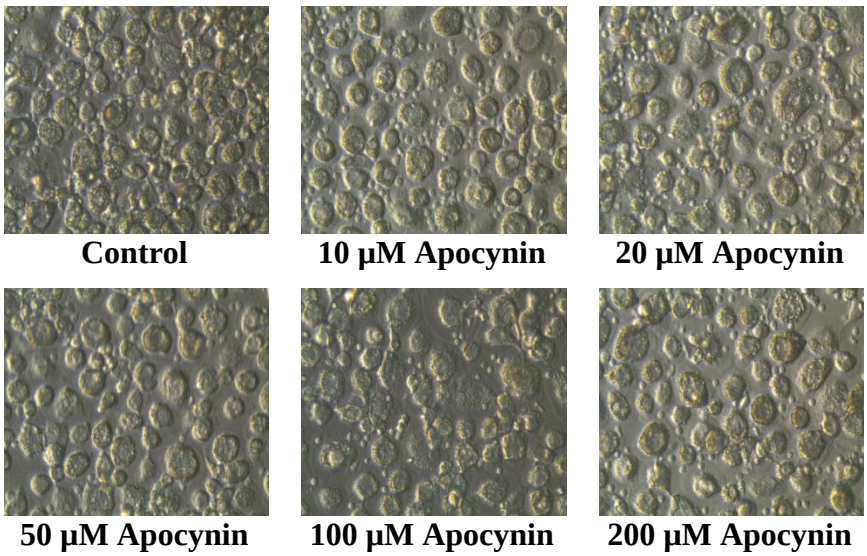

B)

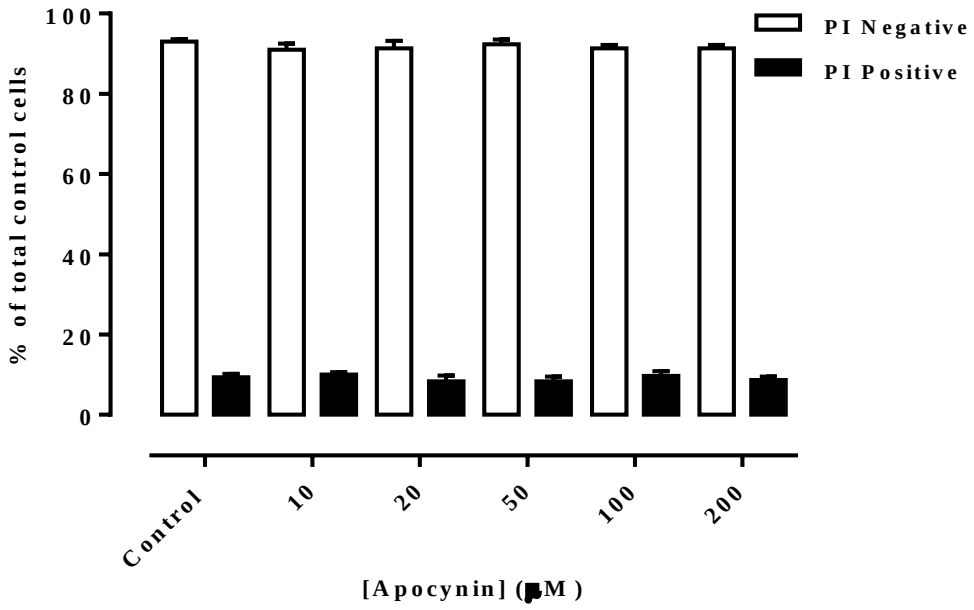

Figure 4.12: Effect of different concentrations of apocynin on HMDM cells.

HMDM cells (1×10^6 cells/mL) were incubated at 37°C in non-phenol red RPMI-1640 with increasing concentrations of apocynin for 27 hours. A cell only control was added. A) Cells were viewed *in situ* in tissue culture wells using an inverted microscope (400x magnification) after 27 hours incubation. Images were taken using a Leica C-Mount camera and processed using Leica Application Suite software. B) Cell viability was determined using PI-flow cytometry. Data are expressed as percentage of the total number of cells in control samples. Results shown are mean ± SEM of triplicates from a representative experiment.

A)

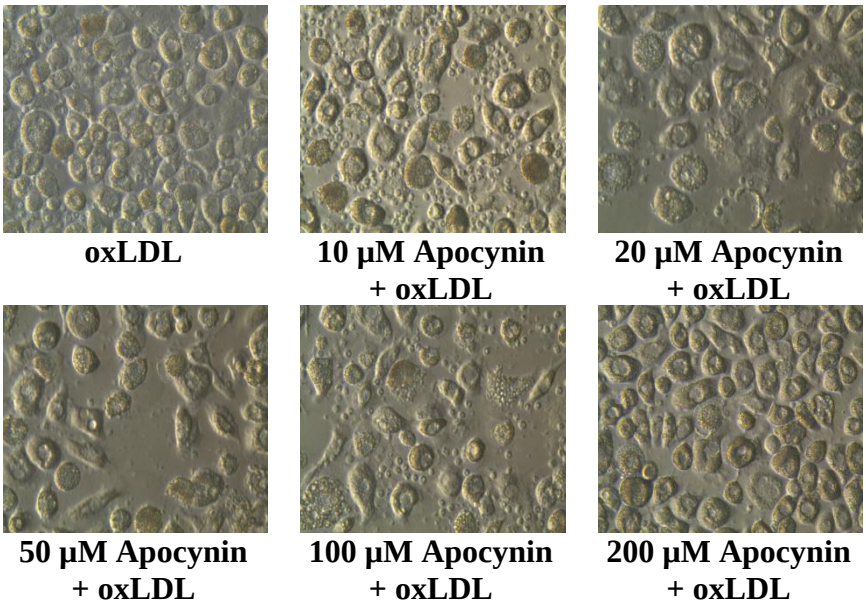

B)

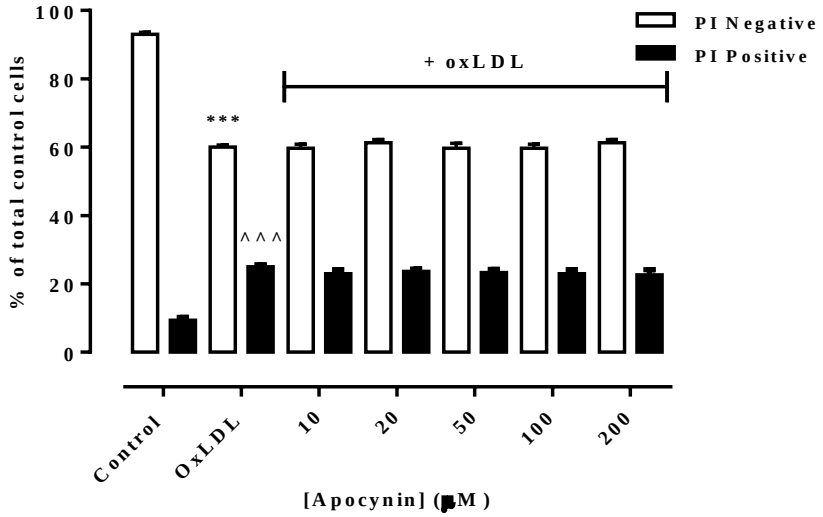

Figure 4.13: Effect of different concentrations of apocynin and oxLDL on HMDM cells.

HMDM cells (1×10^6 cells/mL) were incubated at 37°C in non-phenol red RPMI-1640 with increasing concentrations of apocynin for 3 hours followed by treatment of LC_{50} concentration (1.5 mg/mL) of oxLDL for 24 hours. A cell only control was included. A) Cells were viewed *in situ* in tissue culture wells using an inverted microscope (400x magnification) after 27 hours incubation. Images were taken using a Leica C-Mount camera and processed using Leica Application Suite software. B) Cell viability was determined using PI-flow cytometry. Data are expressed as percentage of the total number of cells in control samples. Results shown are mean ± SEM of triplicates from a representative experiment. Statistical significance (two-factor ANOVA, Sidak's post test) is indicated from: PI negative cells - control vs oxLDL, ***, $p<0.001$; PI positive cells – control vs oxLDL, ^^^, $p<0.001$.

Cells were incubated with different concentrations of VAS2870 for 30 minutes before addition of oxLDL and cell viability (PI negative and PI positive stained cells) was measured using PI-flow cytometry assay. The same experiments in the absence of oxLDL were also carried out to examine the effects of VAS2870 itself on U937 cells, human monocytes and HMDM cells.

From this study, VAS2870 of 5 µM and above was toxic to U937 cells. Cell viability loss of 10 to 15%% (PI negative cells) was observed with 1 µM and 2 µM VAS2870 but was statistically insignificant compared to cell only control. Statistically significant cell viability loss (PI negative cells) of about 20, 60 and 80% were recorded in U937 cells incubated with 5, 10 and 15 µM VAS2870 respectively (**Figure 4.14)**. An increase in cell death (PI positive cells) was also significant in cells incubated with 5, 10 and 15 µM VAS2870. In the presence of oxLDL, VAS2870 has shown no protection against oxLDL-induced cell death in U937 cells. After 24 hours, U937 cells incubated with LC_{50} oxLDL only had cell viability loss (PI negative) of about 70%. As expected, prior treatment with VAS2870 before addition of oxLDL did not help in preserving cell viability against oxLDL insult. With the presence of oxLDL, cell viability loss (PI negative) was about 70% for cells treated with both 1 and 2 µM VAS2870 while 80 to 95% of cell viability loss was observed in cells incubated with 5 to 15 µM VAS2870 (**Figure 4.15**).

VAS2870 itself was also found to be cytotoxic to human monocytes. Cells incubated with 5, 10 and 15 µM VAS2870 had significantly reduced cell viability (PI negative cells) by 15, 40 and 50% respectively compared to cell only control (**Figure 4.16**). With the presence of oxLDL, cell viability loss was further increased with increasing concentrations of VAS2870. OxLDL had caused loss of human monocytes viability (PI negative cells) by 35%. In the presence of oxLDL, cell viability loss (PI negative cells) was significantly reduced to approximately 30 to 20% in cells treated with 1 to 15 µM of VAS2870 (**Figure 4.17**).

Surprisingly, VAS2870 alone had only caused a smaller percentage of cell loss to HMDM cells compared to U937 cells and human monocytes. Incubation of HMDM cells with 10 and 15 µM VAS2870 for 24 hours had significantly reduced cell viability (PI negative cells) by 10 and 20% respectively (**Figure 4.18)**. However, in the presence of oxLDL, VAS2870 at different concentrations was unable to protect HMDM cells from oxLDL-induced cell death (**Figure 4.19**).

A)

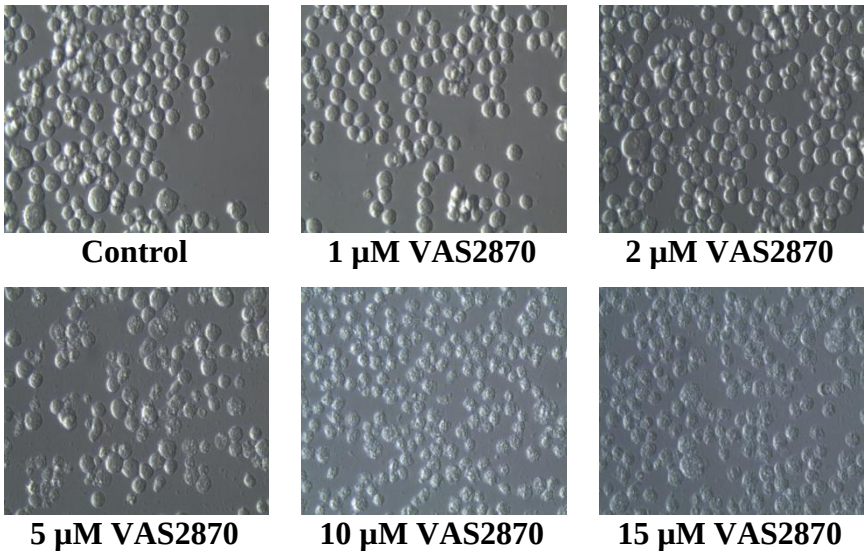

B)

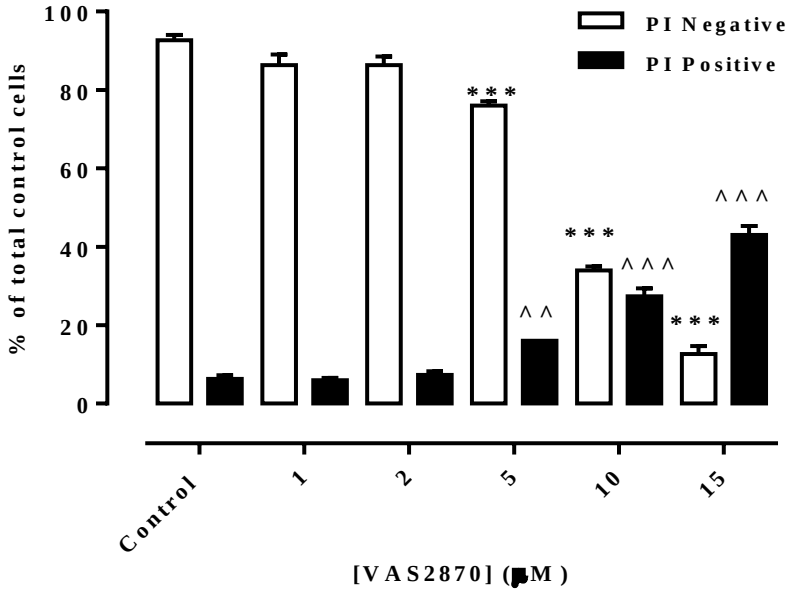

Figure 4.14: Effect of different concentrations of VAS2870 on U937cells.

U937 cells (0.5×10^6 cells/mL) were incubated at 37°C in non-phenol red RPMI-1640 with increasing concentrations of VAS2870 for 24 hours. A cell only control was included. A) Cells were viewed *in situ* in tissue culture wells using an inverted microscope (400x magnification) after 24 hours incubation. Images were taken using a Leica C-Mount camera and processed using Leica Application Suite software. B) Cell viability was determined using PI-flow cytometry. Data are expressed as percentage of the total number of cells in control samples. Results shown are mean ± SEM of triplicates from a representative experiment. Statistical significance (two-factor ANOVA, Sidak's post test) is indicated from: PI negative cells - control vs VAS2870, ***, $p<0.001$; PI positive cells – control vs VAS2870, ^^, $p<0.01$, ^^^, $p<0.001$.

A)

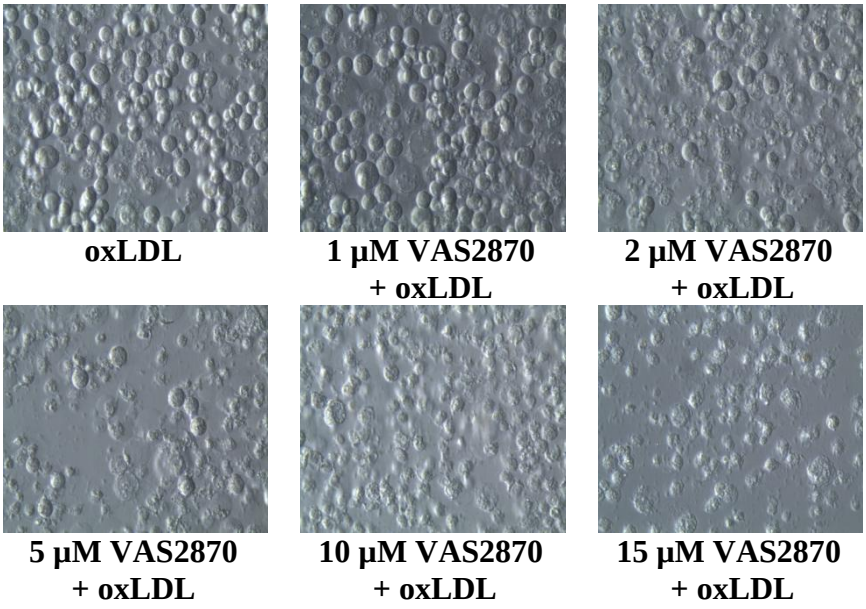

B)

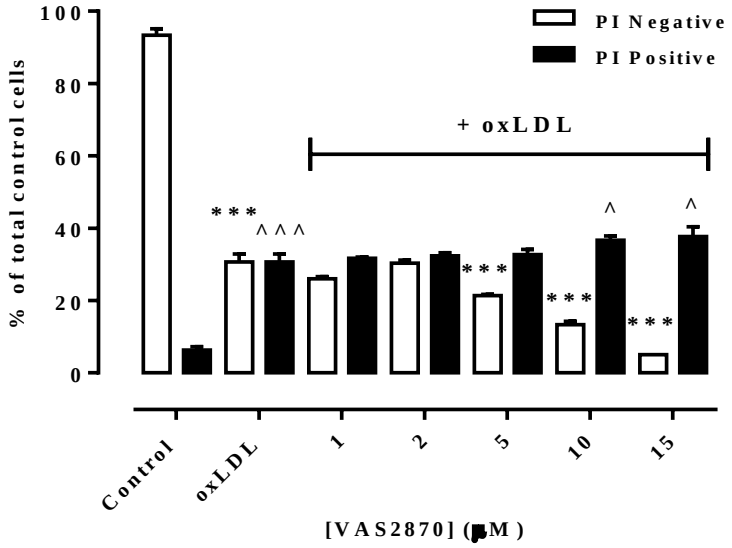

Figure 4.15: Effect of different concentrations of VAS2870 and oxLDL on U937cells.

U937 cells (0.5×10^6 cells/mL) were incubated at 37°C in non-phenol red RPMI-1640 with increasing concentrations of VAS2870 for 30 minutes before addition of LC_{50} concentration of oxLDL (0.4 mg/mL) and incubated for 24 hours. A cell only control was included A) Cells were viewed *in situ* in tissue culture wells using an inverted microscope (400x magnification) after 24 hours incubation with oxLDL. Images were taken using a Leica C-Mount camera and processed using Leica Application Suite software. B) Cell viability was determined using PI-flow cytometry. Data are expressed as percentage of the total number of cells in control samples. Results shown are mean ± SEM of triplicates from a representative experiment. Statistical significance (two-factor ANOVA, Sidak's post test) is indicated from: PI negative cells - control vs oxLDL and oxLDL vs VAS2870 + oxLDL, ***, $p<0.001$; PI positive cells – control vs oxLDL and oxLDL vs VAS2870 + oxLDL, ^, $p<0.05$, ^^^, $p<0.001$.

A)

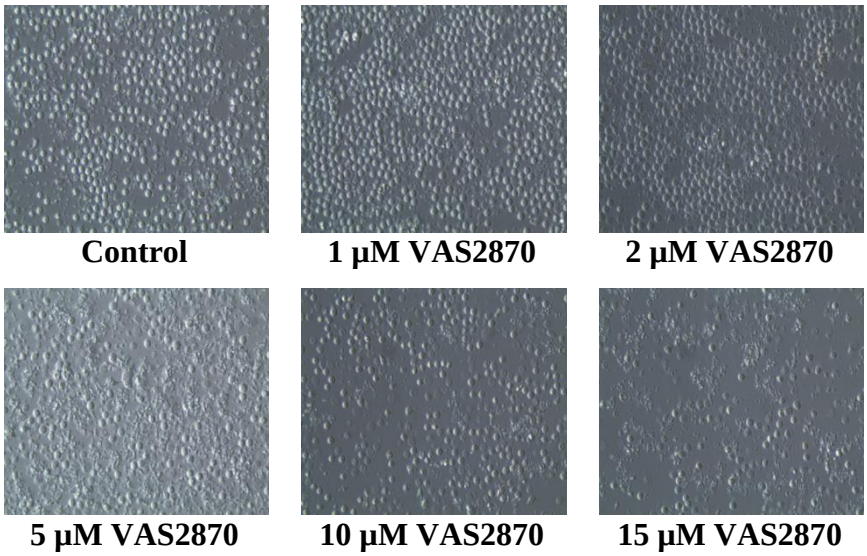

B)

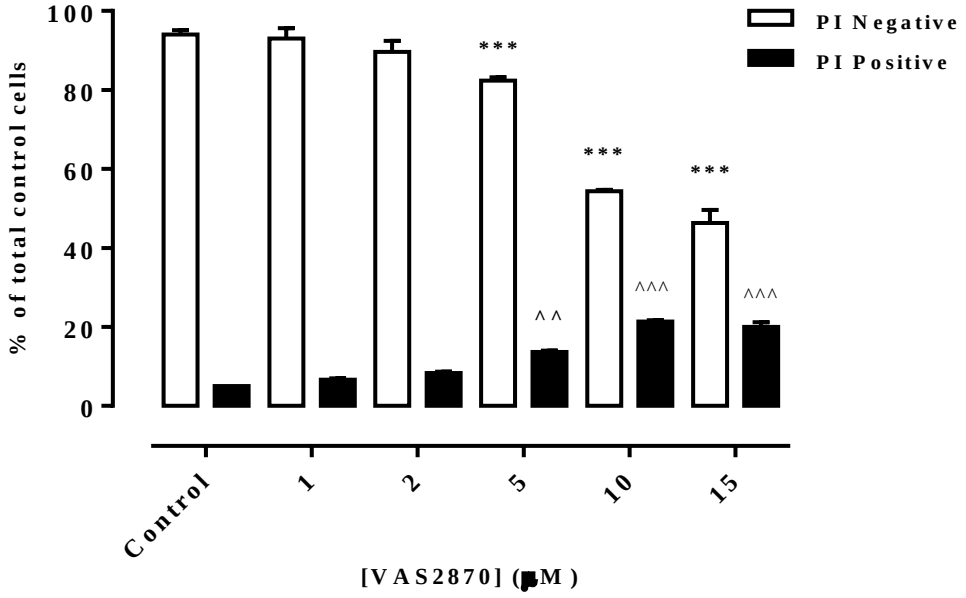

Figure 4.16: Effect of different concentrations of VAS2870 on human monocytes.

Human monocytes (1×10^6 cells/mL) were incubated at 37°C in non-phenol red RPMI-1640 with increasing concentrations of VAS2870 for 24 hours. A cell only control was included A) Cells were viewed *in situ* in tissue culture wells using an inverted microscope (400x magnification) after 24 hours incubation with oxLDL. Images were taken using a Leica C-Mount camera and processed using Leica Application Suite software. B) Cell viability was determined using PI-flow cytometry. Data are expressed as percentage of the total number of cells in control samples. Results shown are mean ± SEM of triplicates from a representative experiment. Statistical significance (two-factor ANOVA, Sidak's post test) is indicated from: PI negative cells - control vs VAS2870, ***, $p<0.001$; PI positive cells – control vs VAS2870, ^^, $p<0.01$, ^^^, $p<0.001$.

A)

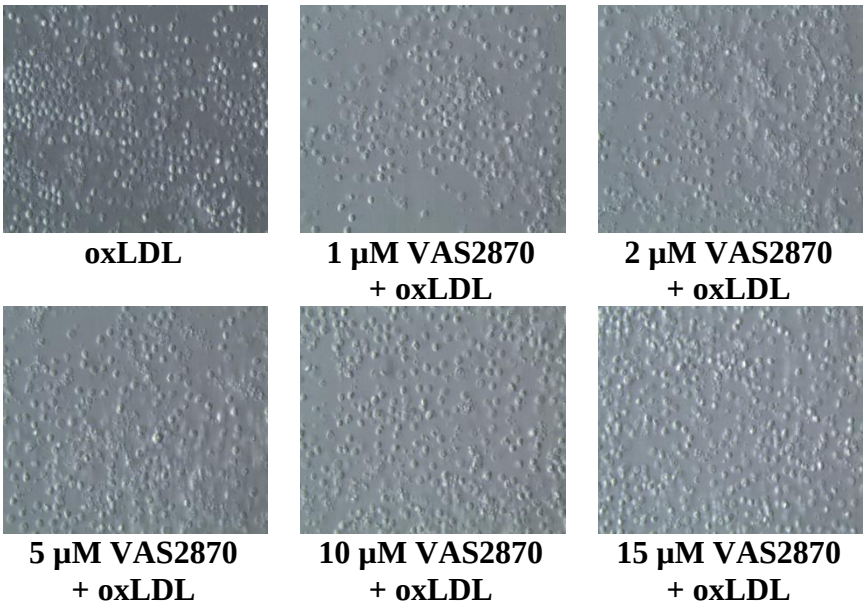

B)

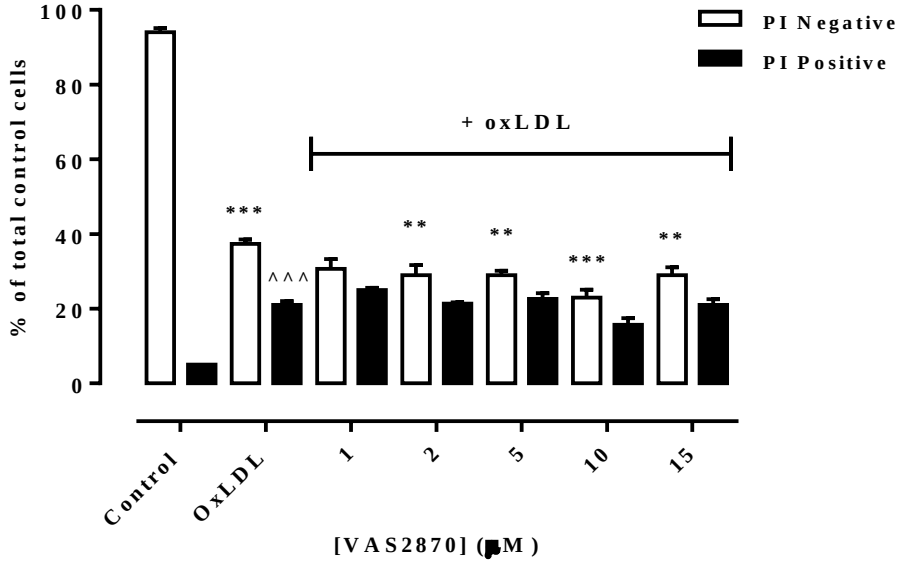

Figure 4.17: Effect of different concentrations of VAS2870 and oxLDL on human monocytes.

Human monocytes (1×10^6 cells/mL) were incubated at 37°C in non-phenol red RPMI-1640 with increasing concentrations of VAS2870 for 30 minutes before addition of LC_{50} concentration (0.8 mg/mL) of oxLDL and incubated for 24 hours. A cell only control was included. A) Cells were viewed *in situ* in tissue culture wells using an inverted microscope (400x magnification) after 24 hours incubation with oxLDL. Images were taken using a Leica C-Mount camera and processed using Leica Application Suite software. B) Cell viability was determined using PI-flow cytometry. Data are expressed as percentage of the total number of cells in control samples. Results shown are mean ± SEM of triplicates from a representative experiment. Statistical significance (two-factor ANOVA, Sidak's post test) is indicated from: PI negative cells - control vs oxLDL and oxLDL vs VAS2870, **, $p<0.01$, ***, $p<0.001$; PI positive cells – control vs oxLDL, ^^^, $p<0.001$.

A)

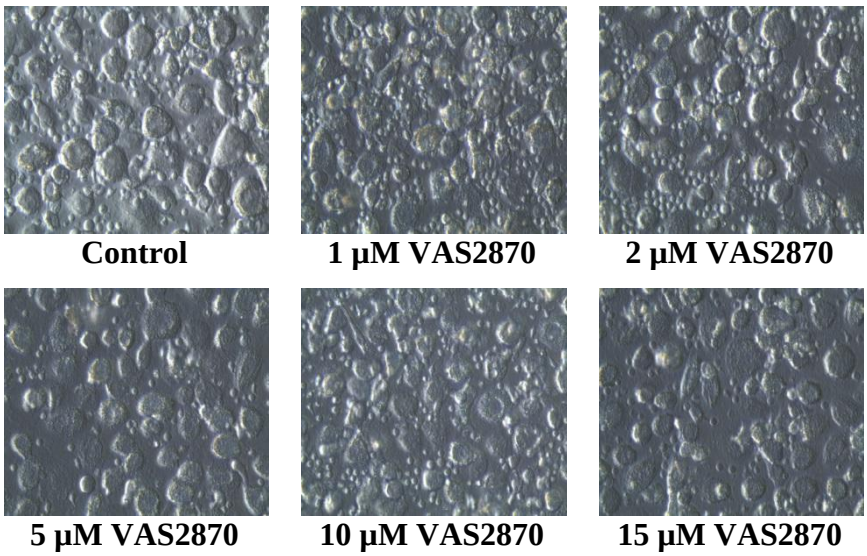

B)

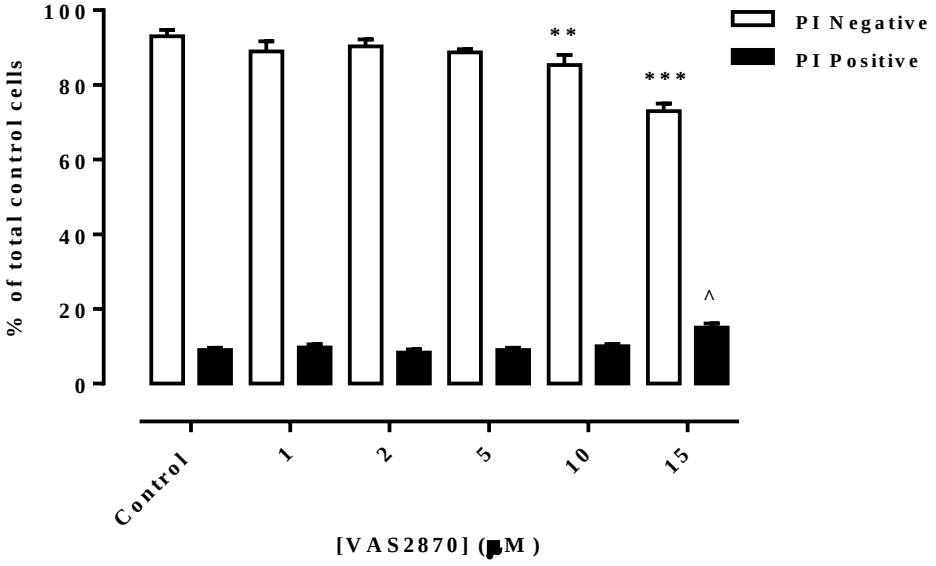

Figure 4.18: Effect of different concentrations of VAS2870 on HMDM cells.

HMDM cells (1×10^6 cells/mL) were incubated at 37°C in non-phenol red RPMI-1640 with increasing concentrations of VAS2870 for 24 hours. A cell only control was included. A positive control of cell only treatment and a negative control of cells treated with oxLDL were included A) Cells were viewed *in situ* in tissue culture wells using an inverted microscope (400x magnification) after 24 hours incubation with oxLDL. Images were taken using a Leica C-Mount camera and processed using Leica Application Suite software. B) Cell viability was determined using PI-flow cytometry. Data are expressed as percentage of the total number of cells in control samples. Results shown are mean ± SEM of triplicates from a representative experiment. Statistical significance (two-factor ANOVA, Sidak's post test) is indicated from: PI negative cells - control vs VAS2870, **, $p<0.01$, ***, $p<0.001$; PI positive cells – control vs VAS2870, ^, $p<0.05$.

A)

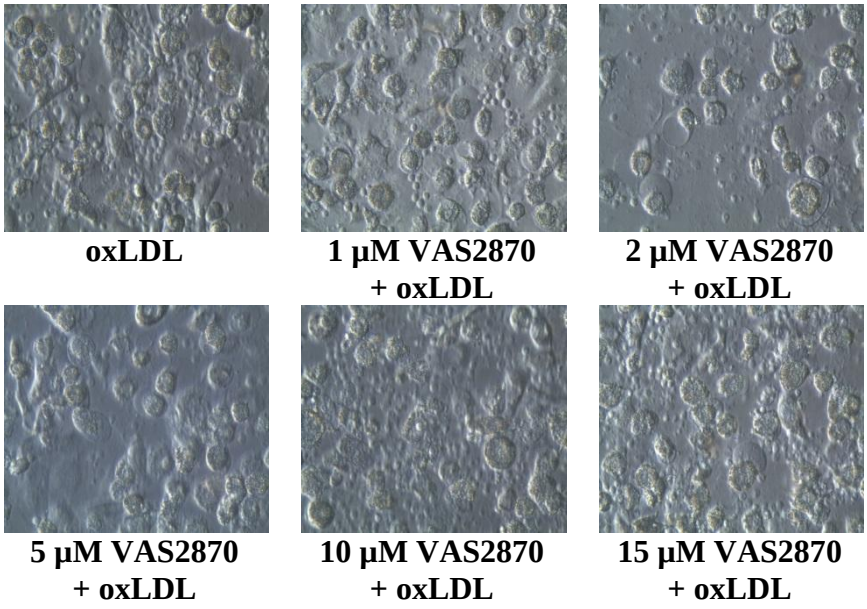

B)

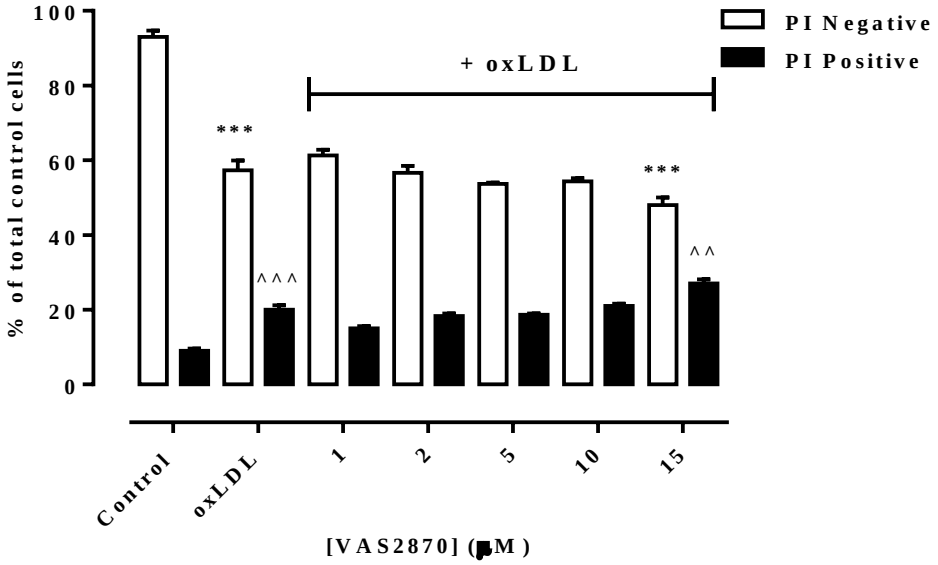

Figure 4.19: Effect of different concentrations of VAS2870 and oxLDL on HMDM cells.

HMDM cells (1×10^6 cells/mL) were incubated at 37°C in non-phenol red RPMI-1640 with increasing concentrations of VAS2870 for 30 minutes before addition of LC_{50} concentration (1.5 mg/mL) of oxLDL and incubated for 24 hours. A cell only control was included. A) Cells were viewed *in situ* in tissue culture wells using an inverted microscope (400x magnification) after 24 hours incubation with oxLDL. Images were taken using a Leica C-Mount camera and processed using Leica Application Suite software. B) Cell viability was determined using PI-flow cytometry. Data are expressed as percentage of the total number of cells in control samples. Results shown are mean ± SEM of triplicates from a representative experiment. Statistical significance (two-factor ANOVA, Sidak's post test) is indicated from: PI negative cells - control vs oxLDL and oxLDL vs VAS2870, ***, $p<0.001$; PI positive cells – control vs oxLDL and oxLDL vs VAS2870, ^^, $p<0.0$, ^^^, $p<0.001$.

7,8-dihydroneopterin (7,8-NP) protection against oxLDL-induced oxidative stress and cell death

Previous researchers in this lab have shown that 7,8-dihydroneopterin (7,8-NP) protects cells from oxLDL-induced cell death. 7,8-NP has been shown to prevent oxLDL-induced cell viability loss by scavenging radical flux and reducing oxidative stress (Baird *et al.*, 2005; Gieseg *et al.*, 2009b). In order to ascertain the contribution of NOX-derived oxidative stress to oxLDL-induced cell death, another experiment using HMDM cells which included 7,8-NP together with apocynin and VAS2870 was carried out (**Figure 4.20**).

Results showed that 200 µM apocynin, 2 µM VAS2870 as well as 200 µM 7,8-NP alone were not toxic to HMDM cells. Cell viability experiments using different concentrations of 7,8-NP was done earlier during this study whereby 200 µM 7,8-NP was found to be the optimum concentration of 7,8-NP. Cell viability loss (PI negative cells) was about 40% in cells incubated with oxLDL only. Likewise, pre-incubation of cells with apocynin and VAS2870 did not restore cell viability in the presence of oxLDL. Cells pre-incubated with 7,8-NP had a significant increased in cell viability (PI negative cells) of about 77% compared to oxLDL only treated cells. The number of PI positive were also decreased compared to oxLDL treated cells but was not statistically significant.

In the presence of oxLDL, the increased in cell viability in cells pre-incubated with 7,8-NP might be due to the ability of 7,8-NP to scavenge intracellular oxidants generated by oxLDL. Therefore, in the next section, experiments were carried out to investigate the effects of 7,8-NP as well as the NOX inhibitors (apocynin and VAS2870) on intracellular ROS production.

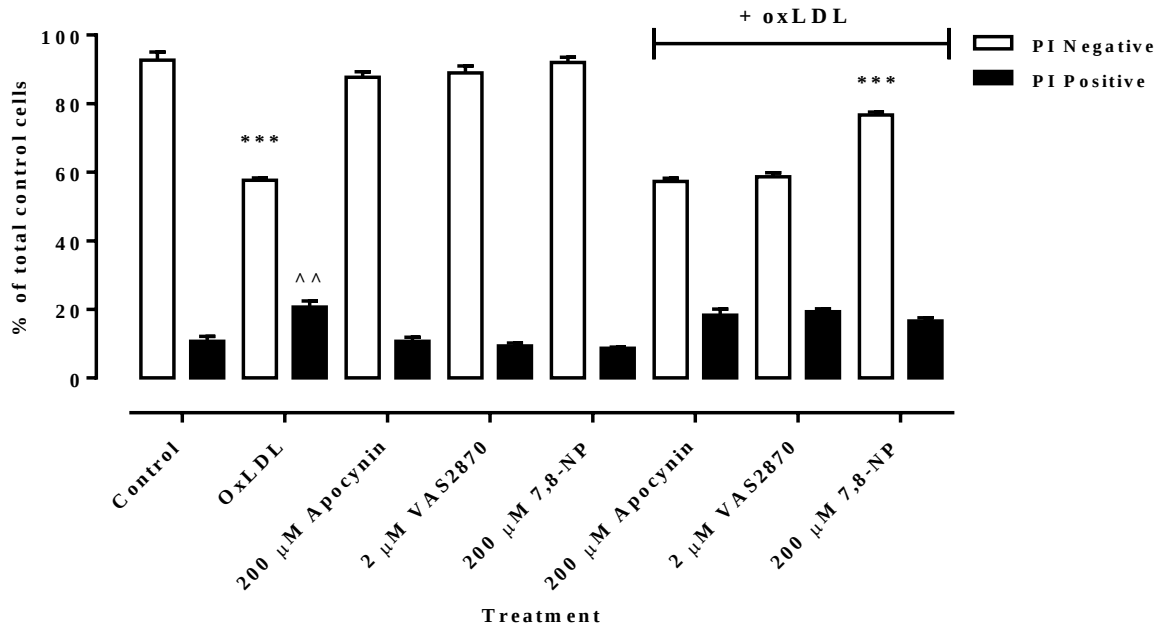

Figure 4.20: Effect of apocynin, VAS2870 and 7,8-NP on oxLDL-mediated cell death on HMDM cells.

HMDM cells (1×10^6 cells/mL) were treated with LC_{50} concentration oxLDL (1.25 mg/mL) after pre-incubation at 37°C in non-phenol red RPMI-1640 with either 200 µM 7,8-NP for 10 minutes, 5 µM VAS2870 for 30 minutes or 200 µM apocynin for 3 hours. A positive control of cell only treatment, a negative control with oxLDL only and cells incubated with the same concentration of 7,8-NP, VAS2870 and apocynin without oxLDL were also included as controls. After 24 hours of incubation with oxLDL, cell viability was determined using PI-flow cytometry. Data are expressed as percentage of the total number of cells in control samples. Results shown are mean ± SEM of triplicates from a representative experiment. Statistical significance (two-factor ANOVA, Sidak's post test) is indicated from: PI negative cells - control vs oxLDL and oxLDL vs 7,8-NP, ***, $p<0.001$; PI positive cells – control vs oxLDL, ^^, $p<0.01$.

Effects of apocynin, VAS2870 and 7,8-NP on oxLDL-mediated intracellular ROS production

Further investigations were carried out to ascertain the effects of apocynin, VAS2870 and 7,8-NP on intracellular ROS levels. There was no significant difference between the control and cell treated with various concentrations of apocynin, VAS2870 and 7,8-NP only (**Figure 4.21 A, B** and **C**) in all types of cells. This suggests that apocynin, VAS2870 and 7,8-NP do not induce ROS production in these cells. In the presence of oxLDL, cells pre-treated with apocynin and 7,8-NP showed a significant decrease in DHE fluorescence intensities for U937 cells. There was no protection against increased DHE fluorescence observed in cell pre-treated with VAS2870 (**Figure 4.21 A**). In contrary, in the presence of oxLDL, the increase in DHE fluorescence intensities was not blocked in human monocytes and HMDM cells pre-treated with apocynin. However, when incubated with oxLDL, a reduction in DHE fluorescence was observed in cells pre-treated with 7,8-NP. Likewise, VAS2870 did not convey any reduction to DHE fluorescence intensities when challenged with oxLDL (**Figure 4.21 B** and **C**).

These results clearly showed that 7,8-NP was able to scavenge ROS in all types of cells and oxLDL-induced DHE fluorescence was largely suppressed. In the presence of oxLDL, apocynin was able to reduce DHE fluorescence only in U937 cells but not human monocytes and HMDM cells. This is in agreement with the work of Chen (2012) in this lab, who showed a significant reduction in oxLDL-induced fluorescence increase in U937 cells treated with 10 to 100 µM apocynin using fluorescence microscopy. This may indicate the involvement of NOX for the intracellular ROS generation in response to oxLDL activation but this appeared to be specific to U937 cells.

A) U937 cells

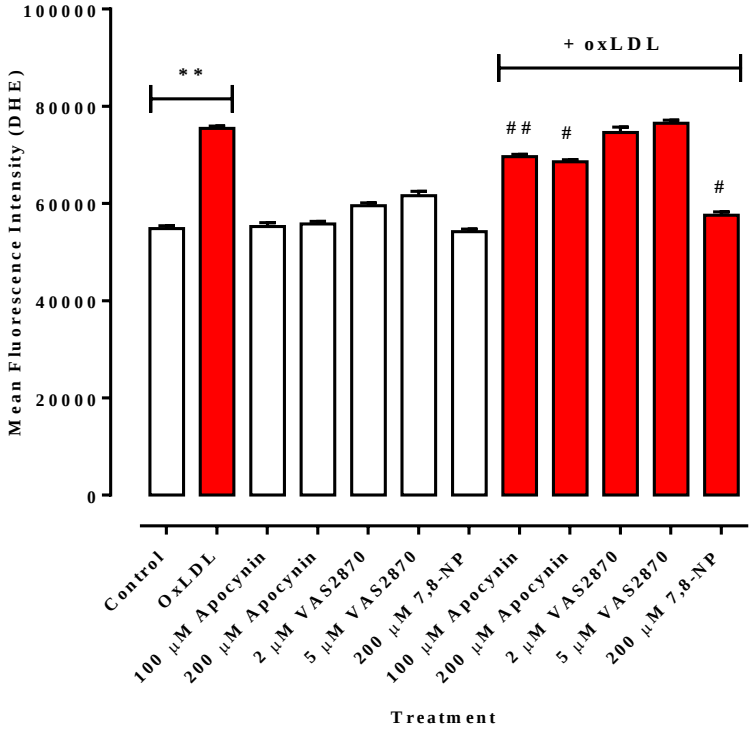

B) Human monocytes

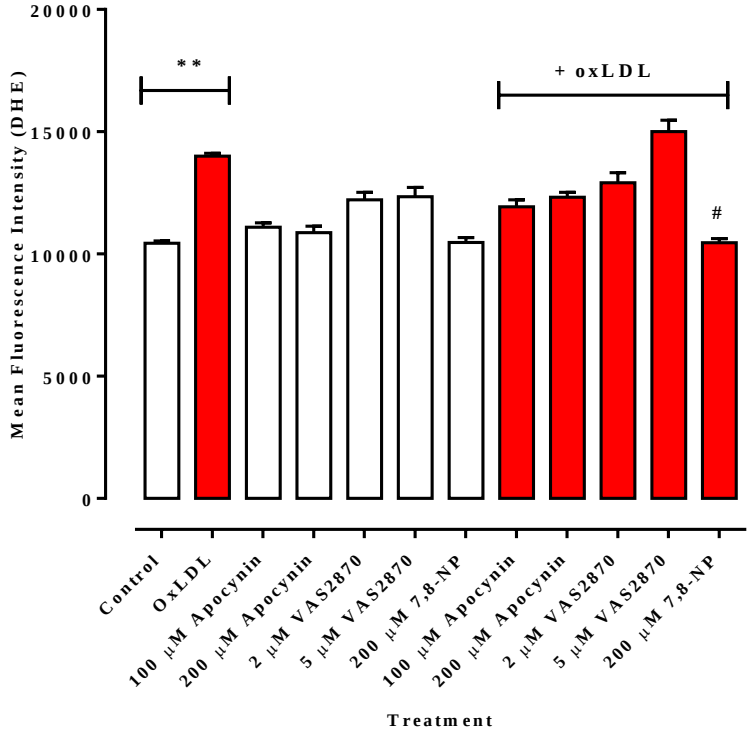

C) HMDM cells

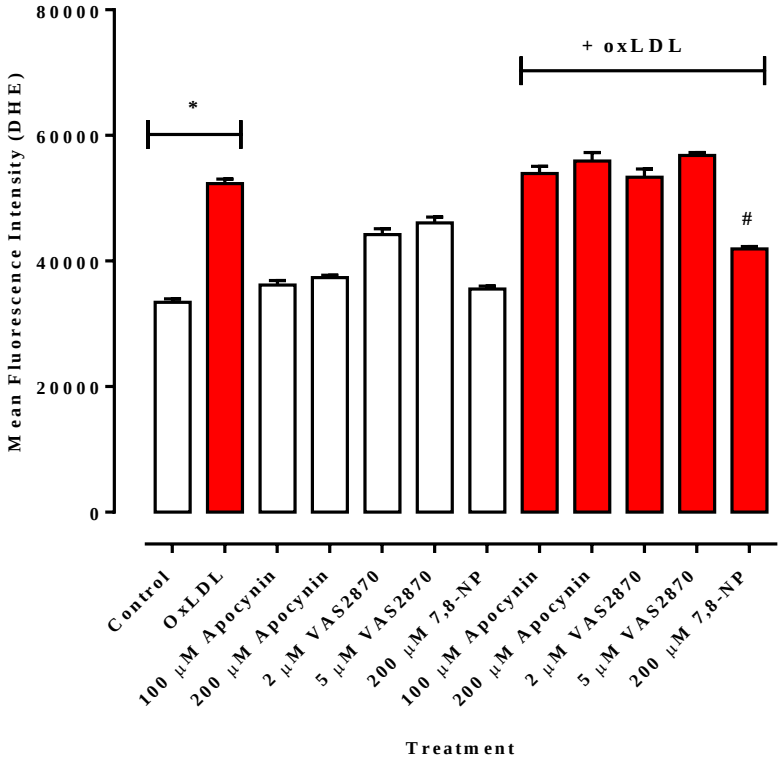

Figure 4.21: Effect of apocynin, VAS2870 and 7,8-NP on intracellular ROS production in U937, human monocytes and HMDM cells.

U937 cells (0.5×10^6 cells/mL), human monocytes (1×10^6 cells/mL) and HMDM cells (1×10^6 cells/mL) were treated with LC_{50} concentration oxLDL (0.5, 1 and 1.5 mg/mL oxLDL for U937, human monocytes and HMDM cells, respectively) after pre-incubation at 37°C in non-phenol red RPMI-1640 with either 200 µM 7,8-NP for 10 minutes, 5 µM VAS2870 for 30 minutes or 200 µM apocynin for 3 hours. A cell only control was included. After 6 hours of incubation with oxLDL (3 hours for U937), cells were washed and stained with 10 µM DHE for 20 minutes in the dark before analysis using PI-flow cytometry. Results shown are mean ± SEM of triplicates from a representative experiment. Statistical significance (two-factor ANOVA, Sidak's multiple test) is indicated from: Control vs oxLDL, *, $p<0.05$, **, $p<0.01$; oxLDL vs apocynin/7,8-NP + oxLDL, #, $p<0.05$, ##, $p<0.001$.

Mechanism of NOX activation

It is believed that NOX is the major producer of ROS leading to oxidative stress. In the previous study done in this laboratory, oxLDL has been shown to activate NOX in U937 cells (Chen, 2012). A time course experiments were performed to study $p47^{phox}$ protein expression upon stimulation with oxLDL to prove that oxLDL directly activates NOX. Thus, it is clearly showed in this study that oxLDL activates NOX in U937, human monocytes and HMDM cells (**Figure 4.22, 4.23** and **4.24**) in a time-dependent manner. Phosphorylated $p47^{phox}$ had generally increased after 1 hour incubation with oxLDL and peaked at 3 hour. This was followed by gradual decrease in $p47^{phox}$ protein. The protein band intensities were quantified and corrected with β-actin. The maximum increase of $p47^{phox}$ protein was found to be around 30% (average) compared to 0 hour control for both U937 and HMDM cells whereas for human monocytes the increase was 70% (average).

Studies have implicated that apocynin inhibits the translocation of $p47^{phox}$ in different types of cells including human monocytes (Barbieri *et al.*, 2004) and vascular cells (Kinkade *et al.*, 2013) leading to inactivation of NOX. Previous studies in this lab by Chen (2012) showed that apocynin was able to inhibit oxLDL-induced NOX in U937 cells by suppressing $p47^{phox}$ phosphorylation that consequently protected against oxLDL-induced oxidative stress. The ability of oxLDL to activate NOX and apocynin to inhibit NOX was examined through $p47^{phox}$ protein expression by western blot in HMDM cells. PMA, an agonist which activates protein kinase C (PKC) that phosphorylates $p47^{phox}$ in phagocytic cells (Li *et al.*, 2002) was included as a positive control. HMDM cells were incubated with apocynin for 3 hours followed by treatment with oxLDL for another 6 hours before cells were collected and processed for western blot to analyse $p47^{phox}$ protein expression. Western blot results (**Figure 4.25**) revealed that apocynin was not able to inhibit NOX in HMDM cells. This is further explained in the discussion section of this chapter.

A)

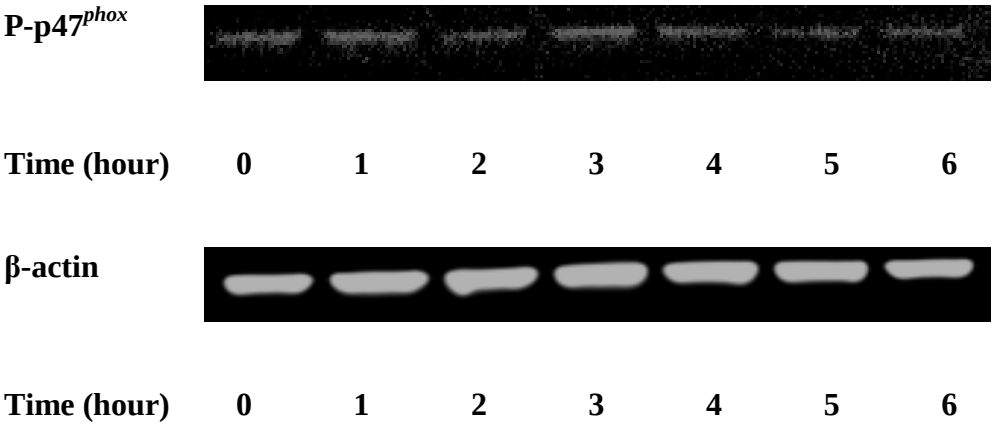

B)

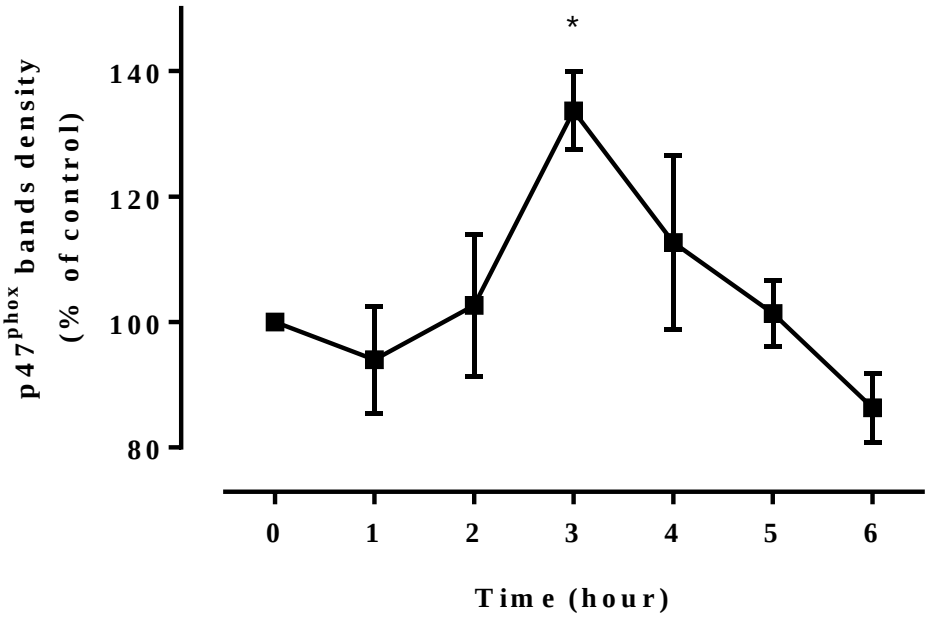

Figure 4.22: Time course study of p47^{phox} activation by oxLDL in U937 cells.

U937 cells (0.5×10^6 cells/mL) were treated with LC_{50} concentration (0.25 – 0.40 mg/mL) of oxLDL in RPMI-1640. A) After the designated incubation time, whole cell lysate was prepared and the presence of activated p47^{phox} was examined by western blotting. B) The protein band intensities were quantified using Image J software and corrected for β-actin. Data are expressed as percentage of the 0 hour control and significance is indicated from this control. Results are displayed as mean ± SEM of three separate experiments (one-way ANOVA, Dunnett's multiple comparison): *, $p<0.05$; ***, $p<0.001$. (P-p47^{phox} = phosphorylated p47^{phox}).

A)

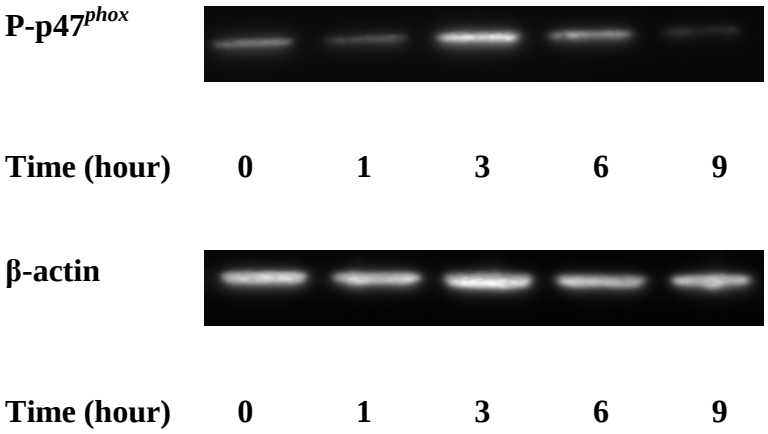

B)

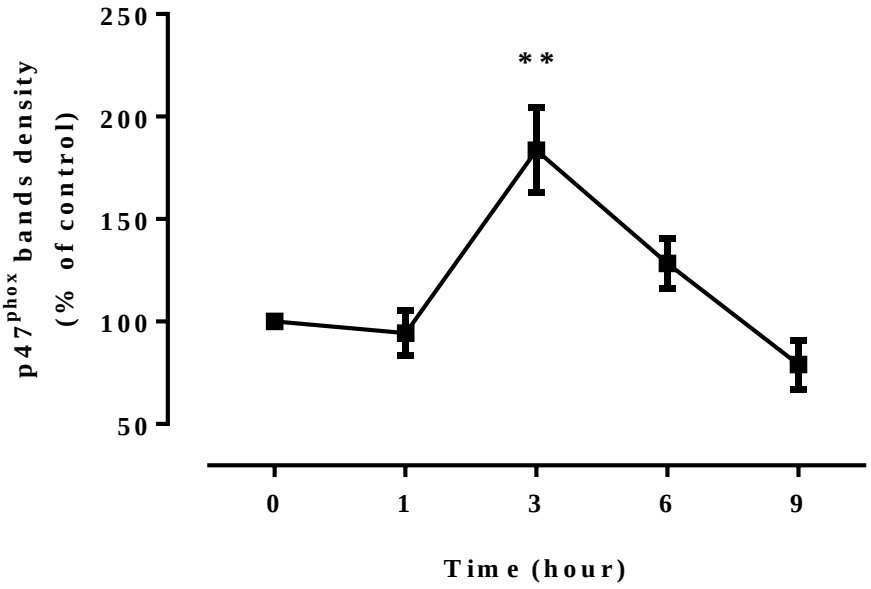

Figure 4.23: Time course study of p47^{phox} activation by oxLDL in human monocytes.

Human monocytes (1×10^6 cells/mL) were treated with LC_{50} concentration (0.75 – 1 mg/mL) of oxLDL in RPMI-1640. A) After the designated incubation time, whole cell lysate was prepared and the presence of activated p47^{phox} was examined by western blotting. B) The protein band intensities were quantified using Image J software and corrected for β-actin. Data are expressed as percentage of the 0 hour control and significance is indicated from this control. Results are displayed as mean ± SEM of three separate experiments (one-way ANOVA, Dunnett's multiple comparison): **, $p<0.01$. (P-p47^{phox} = phosphorylated p47^{phox}).

A)

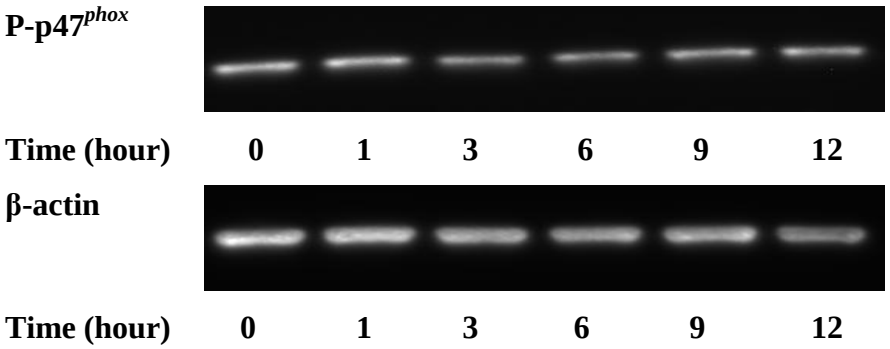

B)

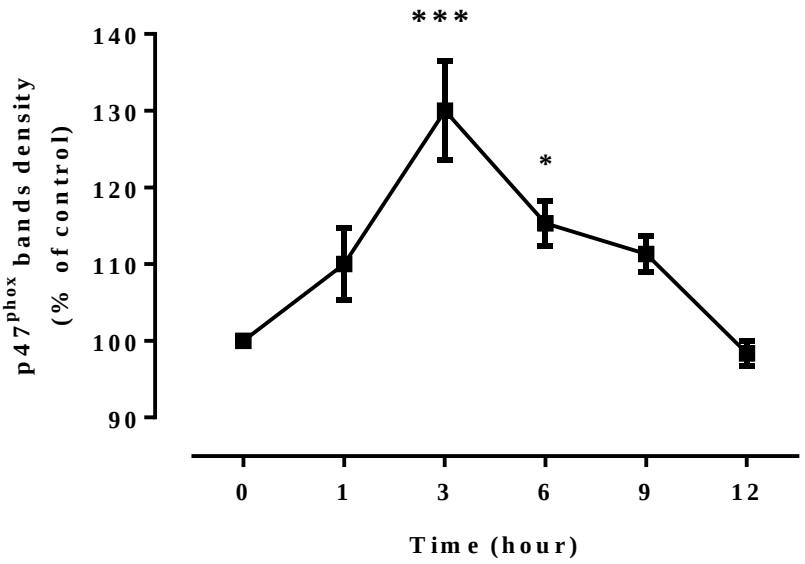

Figure 4.24: Time course study of p47*phox* activation by oxLDL in HMDM cells.

HMDM cells (1×10^6 cells/mL) were treated with LC_{50} concentration (1.25 – 1.50 mg/mL) of oxLDL in RPMI-1640. A) After the designated incubation time, whole cell lysate was prepared and the presence of activated p47*phox* was examined by western blotting. B) The protein band intensities were quantified using Image J software and corrected for β-actin. Data are expressed as percentage of the 0 hour control and significance is indicated from this control. Results are displayed as mean ± SEM of three separate experiments (one-way ANOVA, Dunnett's multiple comparison): *, $p<0.05$; ***, $p<0.001$. (P-p47*phox* = phosphorylated p47*phox*).

A)

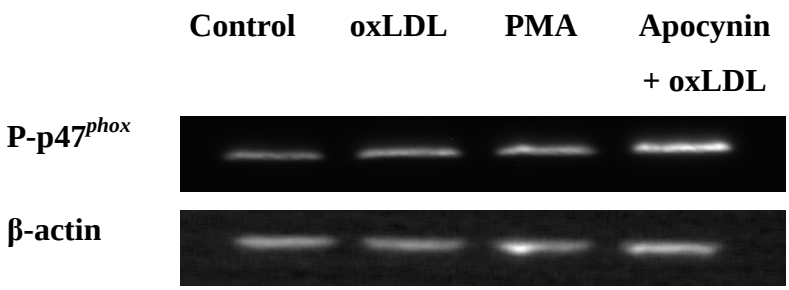

B)

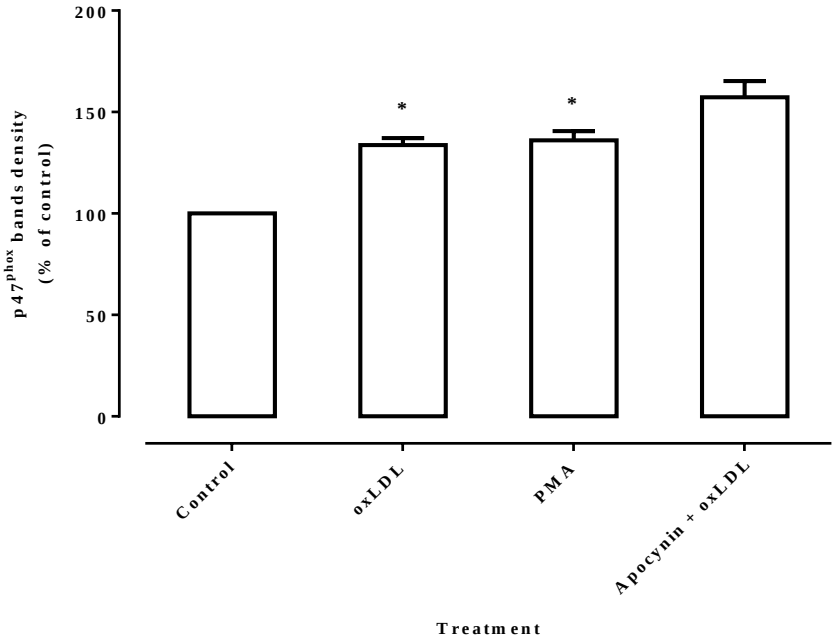

Figure 4.25: Effect of apocynin on NADPH oxidase subunit p47^{phox} protein expression in HMDM cells.

HMDM cells (1×10^6 cells/ml) were pre-treated with 200 μM apocynin in RPMI-1640 at 37^{o}C for 3 hours, followed by incubation with LC_{50} concentration of oxLDL (1.25 - 1.5 mg/mL) for 6 hours. A positive control with 5 μM PMA treatment and a negative control with oxLDL only treatment were also included. A) At the end of treatment, the presence of activated p47^{phox} in the whole cell lysate was examined by western blotting. A representative western blot of p47^{phox} is shown. B) The protein band intensities were quantified using Image J software and corrected with β-actin. Data are expressed as percentage of the positive cell only control data. Results are displayed as mean ± SEM of three separate experiments. Significance (one-way ANOVA, Dunnett's multiple comparison) is indicated from the cell only control: *, $p<0.05$. (P-p47^{phox} = phosphorylated p47^{phox}).

Effects of apocynin, VAS2870 and 7,8-NP on oxLDL-induced intracellular Ca^{2+} levels

Pathological increase in cytosolic Ca^{2+} could also trigger a cascade of cellular events. Elevated cytosolic Ca^{2+} could promote NOX activation by inducing PKC and PLA2 which could also trigger the phosphorylation of NOX subunit, $p47^{phox}$ (Cathcart, 2004). Both ROS generation and intracellular Ca^{2+} increase (**Chapter Five – Role of calcium in oxLDL-induced cell death**) have been shown to be the early events of oxLDL-induced toxicity. Thus, the following experiments were carried out to investigate the involvement of ROS in oxLDL-induced intracellular Ca^{2+} rise.

A time-course study to investigate the effect of apocynin, VAS2870 and 7,8-NP on oxLDL-induced Ca^{2+} increase was carried out using flow cytometry over a period of 6 hours in U937, human monocytes and HMDM cells (**Figure 4.26 A, B** and **C**). In the absence of oxLDL, cells treated with 200 µM apocynin, 2 µM VAS2870 or 200 µM 7,8-NP displayed similar mean fluorescence intensities as the cell only control. OxLDL triggered a rapid fluorescence increase in the first 3 to 4 hours in all types of cells. U937 cells pre-treated with apocynin demonstrated a slightly lower oxLDL-induced fluorescence intensity increase compared to oxLDL only treated cells (**Figure 4.26 A**). However, the same decreasing trend was not observed in apocynin pre-treated human monocytes and HMDM cells in the presence of oxLDL (**Figure 4.26 B** and **C**).

The oxLDL-induced fluorescence intensities increase was significantly reduced in the presence of 7,8-NP especially after the first 3 hours incubation with oxLDL. The similar pattern of oxLDL-induced fluorescence intensities decrease occurred U937, human monocytes and HMDM cells. These results indicate that 7,8-NP inhibited oxLDL-induced intracellular Ca^{2+} influx but this protection seemed to occur after 3 hours. The role of Ca^{2+} in oxLDL-induced cell death is further examined and discussed in the next chapter.

A) U937 cells

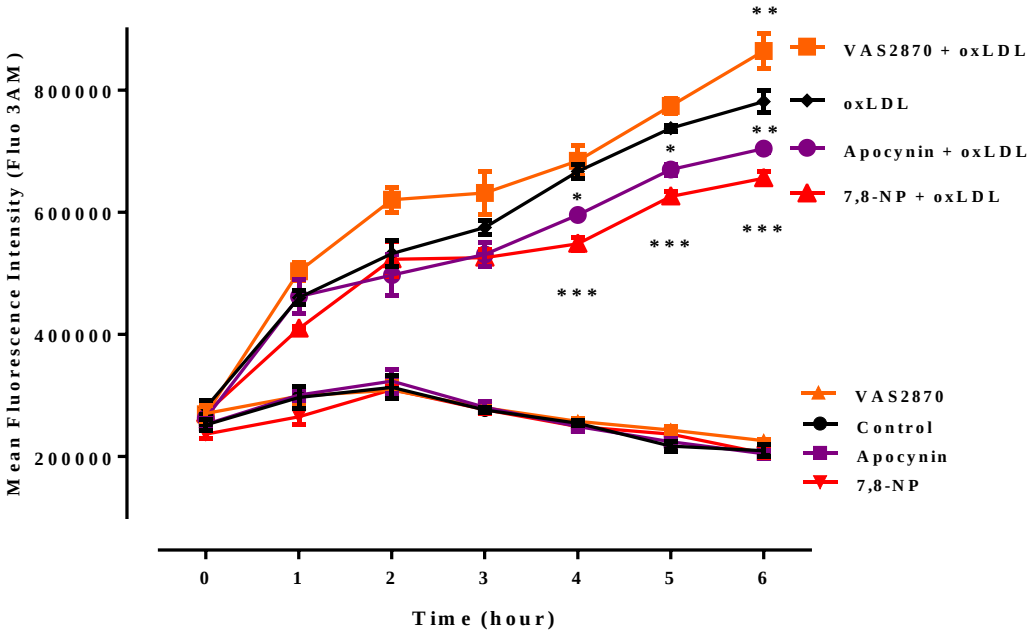

B) Human monocytes

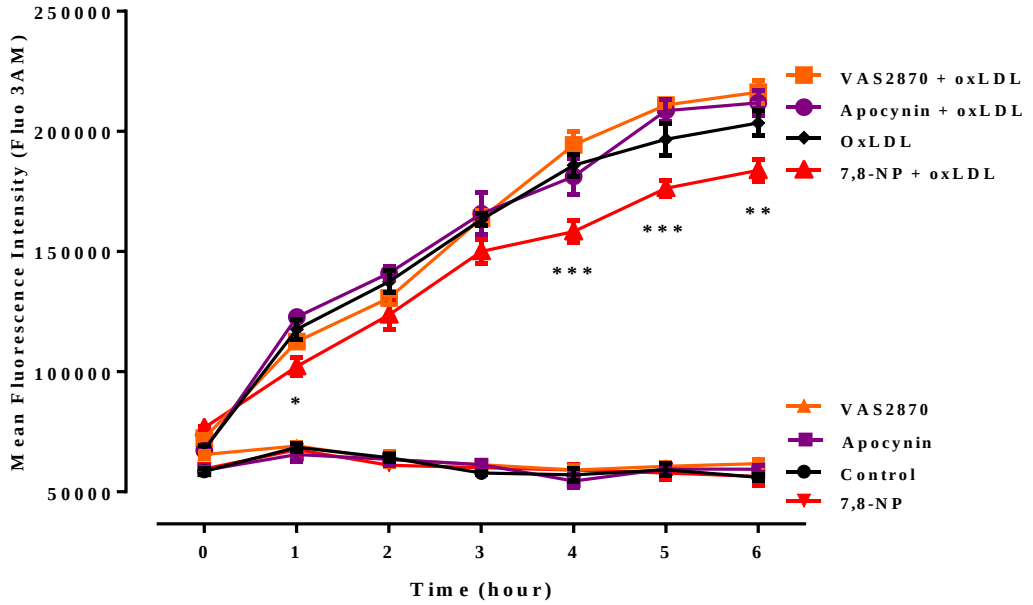

C) HMDM cells

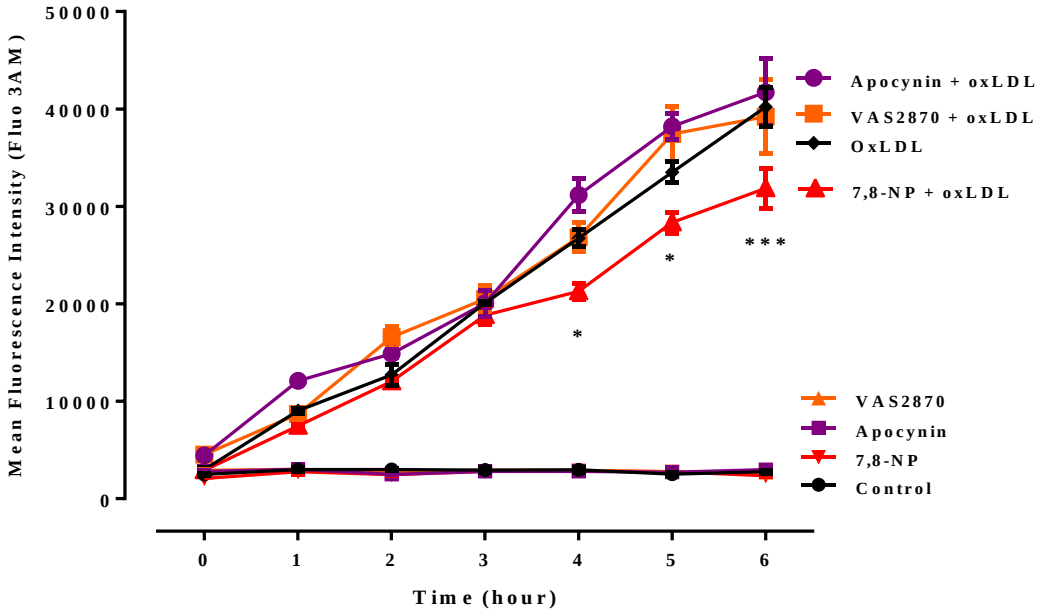

Figure 4.26: Effects of apocynin, VAS2870 and 7,8-NP on oxLDL-induced intracellular Ca^{2+} in U937, human monocytes and HMDM cells

U937 cells (0.5×10^6 cells/mL), human monocytes (1×10^6 cells/mL), HMDM cells (1×10^6 cells/mL) were pre-incubated with 1.5 µM of Fluro-3AM with or without 200 µM apocynin/5 µM VAS2870/200 µM 7,8-NP for 40 minutes, followed by treatment with LC_{50} concentration (0.25, 0.75, 1.25 mg/mL oxLDL for U937, human monocytes and HMDM cells, respectively)of oxLDL in non-phenol red RPMI-1640 at 37°C. At various times, cell samples were removed and analyzed by flow cytometry. Mean fluorescence intensities are measured by flow cytometry over 6 hours. Results shown are mean fluorescence intensities (MFI) ± SEM of triplicates of a representative experiment. At each time point, intracellular Ca^{2+} levels were significantly elevated with the addition of oxLDL ($p<0.05$). Significance indicated in the graph was detected from the oxLDL treated cells and cells pre-treated with apocynin/VAS2870/7,8-NP with the presence of oxLDL at each time point.

Discussion

Oxidative stress: effects of oxLDL on ROS production

Results from the experiments in this chapter clearly showed that oxLDL was able to induced ROS generation, most likely as superoxide. Investigations of intracellular ROS productions using DHE and MitoSOX demonstrated that oxLDL caused a time-dependent increased level of intracellular and intra-mitochondrial superoxide generations as early as 1 hour after incubation with oxLDL (**Figure 4.4, 4.5, 4.6** and **4.7**). The increase in intracellular ROS generation also depends on oxLDL concentration as well as the type of cells (**Figure 4.2** and **4.3**). These results showed that abnormal increase in intracellular ROS production (oxidative flux) is an early event and one of the key features in oxLDL toxicity. Nevertheless, the exact mechanism of how oxLDL initiates ROS generation within the cells is not fully understood. OxLDL treated with different antioxidants before incubation with the cells did not reduce its toxicity or ROS generations (Gieseg *et al.*, 2009b). This suggests that oxLDL might be activating or stimulating the oxidant generating system in the cells such as NOX and mitochondrial electron transport chain (mETC) by initiating a shift in redox balance and subsequent induction of downstream signalling cascades (Gieseg *et al.*, 2009b; Gieseg *et al.*, 2009a). Studies have also showed that H_2O_2 and MitoSOX levels were elevated in U937 cells after 5 and 4 hours treatment with copper oxLDL (Al Gadban *et al.*, 2010; Ermak *et al.*, 2010). In our lab, Gieseg *et al.* (2010) have demonstrated that oxLDL induced a DHE detected oxidative stress over the first six hours which was also supported by the work of Shchepetkina (2013) in HMDM cells.

The increase in mitochondrial ROS (MitoSOX levels) could lead to mitochondrial dysfunction which eventually causes cell death. This could be a secondary event due to oxLDL-induced excessive ROS production and other cellular oxidative damage happened in the cytosol. Possibly, this could also be due to the oxidants generated by the mETC. Additionally, Cadenas and Davies (2000) have reported that the production of mitochondrial superoxide is estimated to be 5 to 10-fold higher than that of cytosol and nucleus.

In this study, DHE and MitoSOX have been used to detect intracellular production of ROS. To date, there are many fluorescent probes and assays available for ROS detection but choosing the appropriate probes for detection of specific ROS is often difficult. DHE is suitable for the detection of intracellular superoxide and oxidants even though is not

exclusively specific (Kalyanaraman *et al.*, 2012; Tarpey *et al.*, 2004). Thus, DHE as a probe of superoxide is sufficient for this study since no identification of specific source of ROS is required. Moreover, there is no perfect assay for ROS detection and almost all have some limitations over the other (Maghzal *et al.*, 2012).

One obvious observation from this study was that U937 cells always demonstrate higher fluorescence value compared to human monocytes and HMDM cells. This could be due to higher cell surface volume due to greater cell size compared to human monocytes and HMDM cells or the U937 cells are easily penetrable by the dye.

NOX activation by oxLDL - effect of apocynin

Since NOX plays a vital role in ROS generation, studies have suggested that inhibition of NOX and ROS reduction could compensate oxidative stress, thus improved cell survival (Aviram *et al.*, 1996; Sukhanov *et al.*, 2006). Apocynin has been widely known and used as NOX inhibitor (Bedard & Krause, 2007) in many studies involving various types of cells (phagocytes and non-phagocytes).

Apocynin is activated by cellular peroxidases including myeloperoxidase (MPO) (Stolk *et al.*, 1994a) into an activated dimer form. In our setting, HMDM cells are cultured with GM-CSF (Sugiyama *et al.*, 2001), thus MPO should be present in the cells. Moreover, the presence of NOX2 is common in macrophages whereby apocynin is believed to act by inhibiting the translocation of the cytosolic subunits to the plasma membrane (Bedard & Krause, 2007; Meyer *et al.*, 1999; Stolk *et al.*, 1994a).

In our lab, Chen (2012) has demonstrated that apocynin protected U937 cells from oxLDL-mediated cell death. However, the protection from cell loss was only about 10 to 15% compared to oxLDL treated cells despite an increase of 60% of GSH levels compared to control cells. Additionally, western blot analysis for the activation of $p47^{phox}$ in U937 cells in response to oxLDL stimulation revealed the involvement of NOX with maximum activity peaked at 3 hours after incubation with oxLDL. Chen (2012) also showed that apocynin was able to block the translocation of $p47^{phox}$ subunit of NOX resulting in NOX inactivation in U937 cell system. Taken together, this finding suggests that oxLDL was able to activate NOX and give rise to ROS generation in U937 cells. Inhibiting NOX activation by apocynin may result in preventing cell death to certain extend but there might be other sources of ROS

in U937 cell system other than NOX that could cause death to the remaining of the cells. Possibly, an excessive increase in GSH level might impose adverse effects on cell survival. Meanwhile, apocynin has also been reported to increase GSH synthesis in alveolar epithelial cells (Lapperre *et al.*, 1999).

The current study showed that apocynin has no protection against oxLDL-induced cell death in human monocytes and HMDM cells (**Figure 4.11** and **4.13**). OxLDL is shown to induce NOX activation in U937, human monocytes and HMDM cells as indicated by western blot results (**Figure 4.22, 4.23** and **Figure 4.24**). However, the percentage of NOX activation increased was only about 30% in HMDM cells after 3 hours incubation with oxLDL (**Figure 4.24 B**). These results showed the involvement of NOX2 in oxLDL-induced ROS generation because NOX2 is dependent on $p47^{phox}$ activation. Nevertheless, western blot analysis revealed that apocynin was unable to inhibit $p47^{phox}$ phosphorylation induced by oxLDL in HMDM cells (**Figure 4.25)**. Based on the proposed mechanism of action, apocynin targets NOX homolog with the presence of $p47^{phox}$ (which is NOX2), thus it should not interfere with other NOX types that are independent of $p47^{phox}$ like NOX4. In their recent studies, Lee *et al.* (2010) have discovered the existence of NOX4 in human monocytes and macrophages which was inducible by oxLDL. They have also showed that NOX4 localised in intracellular compartment (ER and nucleus) and colocalises with $p22^{phox}$ which formed a functional ROS-producing enzyme complex (Bedard & Krause, 2007). Lee *et al.* (2010) also suggested that NOX4 in HMDM cells is present as NOX4/$p22^{phox}$ dimers and constitutively active. Therefore, this might affect the action of apocynin due to the existence of both NOX isoforms (NOX2 and NOX4).

Another possibility that could cause apocynin not to be functioning is that it needs to be activated by peroxidases (**Figure 4.1**) and these enzymes might not be present in all types of cells. However, this is unlikely since MPO has known to be present in HMDM cells cultured with GM-CSF (Sugiyama *et al.*, 2001). Additionally, Riganti *et al.* (2006) and Vejrazka *et al.* (2005) have shown that apocynin increases ROS generation in neuronal cells and vascular fibroblasts instead of decreasing it. For those reasons, results obtained with apocynin should always be treated and interpreted with caution.

In this study, apocynin was able to provide a small percentage of protection to U937 cells against oxLDL-mediated cell death (**Figure 4.9**). This finding is in line with the work of

Chen (2012) in this lab, who also showed that apocynin inhibited NOX activation by preventing $p47^{phox}$ translocation. However, apocynin at various concentrations did not offer any protection against oxLDL-induced toxicity to human monocytes and HMDM cells (**Figure 4.11** and **4.13**). This is in line with Shchepetkina (2013) who demonstrated that apocynin partially prevented 7,8-NP oxidation to neopterin by oxLDL in HMDM cells but did not convey protection against oxLDL-induced cell death. This may correspond to the inability of apocynin to inhibit $p47^{phox}$ phosphorylation in HMDM cells which was demonstrated in this study. Although there are much evidence on ROS-generating effect of NOX in macrophages and other cells (Bedard & Krause, 2007; Brandes *et al.*, 2010), data showing direct effects of NOX on cell viability with oxLDL treatment in macrophages is still lacking. This could possibly be due to the specificity problems associated with NOX inhibitors (Altenhofer *et al.*, 2012). Apocynin has also been proven to lacking NOX specificity (Aldieri *et al.*, 2008) which suggested that apocynin is not a NOX specific inhibitor. Moreover, Shchepetkina (2013) had showed that the increase in intracellular 7,8-NP oxidation to neopterin was prevented by half when apocynin pre-treated HMDM cells were incubated with 7,8-NP in the presence of oxLDL. This suggested that NOX is one of the key sources of ROS that lead to 7,8-NP oxidation though the inhibition was incomplete. Shchepetkina (2013) also proposed that in HMDM cells, NOX-generated superoxide reacted with chloride ion (Cl^-) via myeloperoxidase (MPO) to produce HOCl that oxidises 7,8-NP to neopterin. Therefore, since NOX inhibition by apocynin did not prevent 7,8-NP oxidation completely, the remaining HOCl could have been generated form a different source such as the mitochondria. Moreover, it has been shown in this study that mitochondrial superoxide level was increased in HMDM cells upon exposure to oxLDL (**Figure 4.7**). Furthermore, apocynin and AEBSF have been shown by Sukhanov *et al.* (2006) to offer only partial prevention of GAPDH down regulation by oxLDL.

Non-NOX sources of ROS could also be generated by the cells and are sufficient to induce cell death. Mitochondrial ROS generation could be the most possible source of ROS in HMDM cells since Complex III of the mETC was identified as the superoxide source in compromised cells (Turrens, 2003). This study and previous work by Chen (2012) have showed that mitochondrial superoxide level was elevated upon oxLDL treatment of HMDM (**Figure 4.7**) and U937 cells, respectively. In addition, it has been demonstrated that oxLDL-induced mitochondrial depolarisation and dysfunction contribute to macrophage cell death (Asmis & Begley, 2003). In addition, Hampton *et al.* (1998) suggested in their review that

ROS generated by NOX2 are either directed to extracellular space or to the phagosomes, thus making it not a likely source of the intracellular ROS observed in macrophages when stimulated with oxLDL (Lee *et al.*, 2010).

With regards to intracellular ROS production, a decrease in oxLDL-induced DHE fluorescence which was only seen in U937 cells but not in human monocytes or HMDM cells (**Figure 4.21**) also suggest the unspecific effects of apocynin.

NOX activation by oxLDL - effect of VAS2870

VAS2870 is a new class of NOX inhibitor developed with improved specificity (Wingler *et al.*, 2011) and was chosen as an alternative to apocynin. It has been shown in this study that VAS2870 does not protect U937 cells, human monocytes and HMDM cells from oxLDL-mediated cell death (**Figure 4.15, 4.17, 4.19** and **4.20**). In fact, VAS2870 itself was toxic to the cells at high concentrations (10 µM and above) (**Figure 4.14, 4.16** and **4.18**). Moreover, it was found that VAS2870 did not prevent oxidative stress mediated by oxLDL. The DHE levels measured showed no difference in cells pre-incubated with VAS2870 in the presence of oxLDL compared to oxLDL treated cells (**Figure 4.21 A, B** and **C**). In addition, VAS2870 was also unable to inhibit intracellular Ca^{2+} rise when challenged with oxLDL in all types of cells used in this study (**Figure 4.26 A, B** and **C**).

In other studies using VAS2870, Stielow *et al.* (2006) showed the suppression of superoxide in HUVEC (non-phagocytic cells) which expressed NOX4 as the major isoform before stimulation with oxLDL but no indication of VAS2870 protection from cell viability loss was mentioned from his observations. In addition, ten Freyhaus *et al.* (2006) have shown that VAS2870 does not affect PMA stimulated $p47^{phox}$ translocation in human PMN cells which indicates that VAS2870 is not inhibiting NOX2. VAS2870 and its derivative, VAS3947 have been shown to inhibit NOX activity in cells that are predominantly express NOX4 since NOX4 was found to be active independently of $p47^{phox}$ and $p67^{phox}$ (Ago *et al.*, 2004; Shiose *et al.*, 2001). Since NOX2 is mainly associated with macrophages (phagocytic cells), this may be the main reason why VAS2870 was not working in inhibiting oxLDL-induced NOX and protecting the cells. Nevertheless, the exact mechanism of action of VAS2870 is still not well developed. On the other hand, there is a possibility that ROS were also generated by other sources such the mETC or xanthine oxidase which was not reduced by VAS2870.

Results gained through this study have showed that intracellular ROS production in U937, human monocytes and HMDM cells was not inhibited by VAS2870 (**Figure 4.21**). Therefore, it is suggested that a more specific NOX inhibitor, for example gp91-ds-tat (Rey *et al.*, 2001) which is specific to NOX2 to be used in future studies investigating the involvement of NOX in oxLDL related studies.

7,8-NP protection against oxLDL-induced intracellular ROS production and cell death

Studies from our lab have showed that 7,8-NP protects cells of myelocytic origin from oxLDL cytotoxicity (Baird *et al.*, 2005; Gieseg *et al.*, 2010; Gieseg *et al.*, 2001b), which is one of the main events in atherosclerotic plaque development. Studies in this lab has demonstrated a maximum protection against oxLDL-induced cell death in U937 and HMDM cells at 200 µM 7,8-NP (Baird, 2003). Although the exact mechanism of 7,8-NP protection against oxLDL-induced cell death is not exactly clear, available data suggest that this protection could be attributed to the antioxidant capacity of 7,8-NP as well as 7,8-NP-mediated reduction of oxLDL uptake by macrophages (Gieseg *et al.*, 2010).

Results from this study clearly demonstrated that 7,8-NP reduced oxLDL-induced DHE-reactive intracellular ROS levels in all three types of cells (**Figure 4.21 A, B** and **C**), proposed to be primarily superoxide and H_2O_2 (Rothe & Valet, 1990; Tarpey *et al.*, 2004) . These results suggest that oxLDL triggered oxidative stress in the cells and 7,8-NP itself as an antioxidant could be scavenging the intracellular oxidants generated. Moreover, in the presence of oxLDL, intracellular Ca^{2+} increase induced by oxLDL was also reduced by 7,8-NP compared to the oxLDL only treated cells (**Figure 4.26 A, B** and **C**). This also suggests that 7,8-NP scavenges intracellular ROS, which in turn reduces the intracellular Ca^{2+} increase. Taken together, this may eventually leads to the protection of the cells from oxLDL insult.

Monocyte-like U937 cells have been used as an excellent model for human macrophages due to the similar characteristics in manifesting oxLDL-induced cytotoxicity such as rapid oxidative stress, absence of caspase activation and necrotic type of cell death (Baird *et al.*, 2004; Katouah, 2012). The inability of 7,8-NP to inhibit oxLDL-induced NOX activation of $p47^{phox}$ protein demonstrated by Chen (2012) in U937 cells through western blot, strongly indicates that the mechanism of action of 7,8-NP is by scavenging NOX-derived ROS and

not directly inhibits NOX activation. Since 7,8-NP has also been shown to protect both U937 and HMDM cells (Baird *et al.*, 2005; Gieseg *et al.*, 2010), it is therefore suggests that 7.8-NP might act similarly in HMDM cells. For these reasons, 7,8-NP was not included in the western blot done to determine the effect of NOX inhibitors on the activation of $p47^{phox}$ protein (**Figure 4.25**).

These findings are in-line with other studies which showed that 7,8-NP might protect cells from oxLDL-mediated oxidative damage through scavenging various types of radicals including superoxide, peroxyl and hydroxyl as well as hypochlorite (Duggan *et al.*, 2002; Gieseg *et al.*, 2001a; Oettl *et al.*, 1997). This radical scavenging property of 7,8-NP may provide explanation to the inhibition of radical-induced damages to cells and cellular substrates where this compound is presence (Duggan *et al.*, 2001; Duggan *et al.*, 2002). Moreover, 7.8-NP has been shown to prevent oxLDL-mediated GSH loss in U937 and HMDM cells by scavenging oxLDL induced intracellular oxidants, which eventually balanced the redox environment and maintained cell survival (Baird *et al.*, 2004; Baird *et al.*, 2005; Gieseg *et al.*, 2010).

The ability of 7,8-NP to down-regulate the scavenger receptor, CD36 might also protects cells against oxLDL-induced toxicity. Studies have shown that the inhibition of CD36 by anti-CD36 antibody has significantly reduced ROS production level, caspase activation and cell death (Sukhanov *et al.*, 2006; Wintergerst *et al.*, 2000). Gieseg *et al.* (2010) have demonstrated that 7,8-NP induced a down-regulation of plasma membrane glycoform of CD36 (100 kDa) in HMDM cells. Recent studies by Shchepetkina (2013) have also showed the reduction of CD36 scavenger receptor and mRNA levels by 7,8-NP in HMDM cells.

Nonetheless, protective effects of 7,8-NP may be cell specific whereby it depends on the type and nature of the cells. Baird *et al.* (2005) have shown that 7,8-NP protects U937 and HMDM cells from oxLDL-mediated cell death and prevents loss of intracellular GSH but no protection against oxLDL toxicity as well as cellular thiol restoration were noticed with THP-1 cells. Moreover, CD36 expression on THP-1 surface is significantly lower compared to U937 cells (Alessio *et al.*, 1996) which may explain why 7,8-NP failed to protect THP-1 cells against oxLDL toxicity. Additionally, low expression of CD36 may also reduce oxLDL uptake by THP-1 cells resulting in lower ROS production as seen in **Figure 4.3**.

Mechanism of NOX activation by oxLDL

Immunoblotting results from this study revealed that oxLDL activated NOX and increased the protein levels of $p47^{phox}$ subunit of NOX (**Figure 4.22, 4.23** and **4.24**). This shows that NOX may contribute to the generation of ROS mediated by oxLDL. However, the increased in NOX activity that peaked at 3 hours was only about 30% compared the 0 hour control. It is not known how much $p47^{phox}$ is needed for NOX activation to occur but an increased in NOX subunit protein levels may further increase NOX activity (Cifuentes *et al.*, 2000). Likewise, how oxLDL stimulates NOX activation is not precisely known. For future studies, it is recommended that both phosphorylated and total $p47^{phox}$ to be included for western blotting. This could provide a better understanding regarding NOX activation by oxLDL.

Studies have found that lysophosphatidylcholine (lysoPC) present in oxLDL could activate protein kinase C (PKC) upon oxLDL uptake (Kugiyama *et al.*, 1992; Ohgushi *et al.*, 1993) whereby PKC activation could stimulate $p47^{phox}$ phosphorylation and subsequent NOX activation. Other studies have proposed scavenger receptor CD36 to be a key activator of NOX which involved the binding of lipid and protein components of oxLDL (Nguyen-Khoa *et al.*, 1999). It has been shown that oxLDL-induced NOX activation level in U937 cells was significantly higher than that in THP-1 cells, which corresponded to the higher CD36 expression levels in U937 cells (Nguyen-Khoa *et al.*, 1999). Nevertheless, Gieseg *et al.* (2010) have shown that CD36 is down regulated by 7,8-NP and study by Chen (2012) demonstrated the failure of 7,8-NP to prevent oxLDL-mediated activation of NOX. Taken together, this may imply the involvement of receptors other than CD36 in the mechanism of oxLDL-induced NOX activation.

Effects of apocynin, VAS2870 and 7,8-NP on oxLDL-induced intracellular Ca^{2+} levels

Time course studies of oxLDL-induced Ca^{2+} influx showed that intracellular Ca^{2+} increase was reduced by 7,8-NP after 3 hours incubation with oxLDL (**Figure 4.26**). The ability of 7,8-NP to scavenge oxLDL-induced ROS shown in the earlier experiments may contribute to the reduced intracellular Ca^{2+} rise. However, the failure of 7,8-NP inhibition of oxLDL-stimulated NOX activation showed by (Chen, 2012) indicates that 7,8-NP did not protect cells by inhibiting NOX activity, but by scavenging NOX-derived ROS.

Summary

Oxidative stress is one of the key features associated with oxLDL-mediated cell death. Results from this study clearly showed that oxLDL caused intracellular generation of ROS (possibly superoxide) in the cytosol and mitochondria. Further investigation in this chapter by measuring $p47^{phox}$ activation indicates that oxLDL induced NOX activation which suggests that NOX might be the possible generator of ROS. However, the amount of $p47^{phox}$ required for NOX activation was not quantified. In addition, the inability of both apocynin and VAS2870 to inhibit NOX may also suggest that either these NOX inhibitors are not specific for the targeted NOX or other sources of ROS might exist and contributed to the oxidative flux. 7,8-NP is shown is this study to scavenge oxLDL-induced ROS that could in turn reduce Ca^{2+} influx and protects cells from oxLDL insult.

CHAPTER FIVE

5. Role of calcium in oxLDL-induced cell death

Introduction

This chapter will study the position and function of calcium (Ca^{2+}) in oxLDL-mediated cell death. This will include investigating the effects of oxLDL on Ca^{2+} levels (intracellular and extracellular), ROS production and cell viability. Effects of different types of Ca^{2+} channel blockers and Ca^{2+} chelators will also be examined related to intracellular Ca^{2+} and ROS generation as well as cell viability in oxLDL-induced cells.

Ca^{2+} is an important signalling molecule or secondary messenger involved and responsible in numerous cellular processes including proliferation, gene transcription, post-translational protein modifications and metabolism (Clapham, 2007). Therefore, it is mandatory for cell to maintain a very low cytosolic Ca^{2+} concentration in order to exquisitely control and coordinate these processes (Rasola & Bernardi, 2011).

In general, regulation of Ca^{2+} homeostasis is common in all eukaryotic cells. However, each cell type expresses a unique complement of molecules which enables it to specifically modulate amplitude, kinetics and subcellular distribution of Ca^{2+} signals (Rasola & Bernardi, 2011). Extracellular Ca^{2+} can cross the plasma membrane via two different channels i.e. voltage-gated Ca^{2+} channels (VOCCs) and receptor-operated Ca^{2+} channels (ROCCs) (Pinilla *et al.*, 2005). On the other hand, Ca^{2+} can be mobilised from intracellular organelles through the stimulation of ryanodine receptors (RyRs) and IP3 receptors (IP3Rs) on the ER (Alberdi *et al.*, 2005; Duchen *et al.*, 2008). Both conditions resulted in increased level of intracellular Ca^{2+}. Buffering of Ca^{2+} in the cytosol occurred through sequestering of Ca^{2+} into the ER/SR by SERCA or pump out of the plasma membrane by PMCA (Clapham, 2007). Besides, mitochondria have been implicated to actively taking part in regulating intracellular Ca^{2+} due to their capacity to rapidly accumulate Ca^{2+} (Carafoli, 2010). **Figure 5.1** illustrates the

position of mitochondria in Ca^{2+} signalling. General Ca^{2+} homeostasis has been described in detail in **Chapter One**.

Studies have implicated the importance of Ca^{2+} signalling in atherosclerosis (Berthier *et al.*, 2004; Meilhac *et al.*, 1999). OxLDL-induced increase in cytosolic Ca^{2+} appears to be the common event in triggering necrosis or apoptosis in various types of cells (Berthier *et al.*, 2004; Deng *et al.*, 2009; Porn-Ares *et al.*, 1998). OxLDL has been found to cause a Ca^{2+} rise in variety of cells including vascular smooth muscle cells (Augé *et al.*, 1996; Massaeli *et al.*, 2001; Weisser *et al.*, 1992), endothelial cells (Negre-Salvayre *et al.*, 1992; Zhao *et al.*, 1997), leukocytes (van Tits *et al.*, 2000), lymphocytes (Maziere *et al.*, 2005), lymphoblastoid cultured cells (Escargueil-Blanc *et al.*, 1994) and U937 cells (Deng *et al.*, 2005). Studies have also demonstrated that increased intracellular Ca^{2+} has been associated with enhance ROS generation in intact cultured cells including cardiomyocytes (Przygodzki *et al.*, 2005), striatal neurons (Peterson *et al.*, 2000), astrocytes (Jou *et al.*, 2010) and human keratinocytes (Goldman *et al.*, 1998).

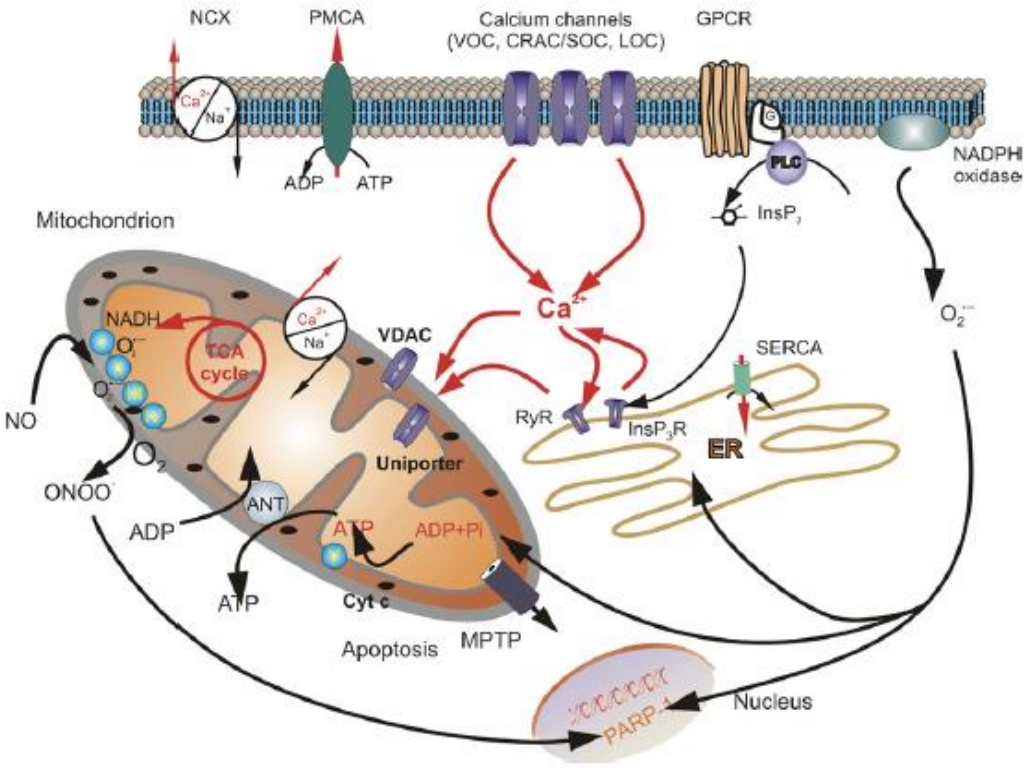

Figure 5.1: Calcium signalling and and its involvement in the mitochondria
(Duchen *et al.*, 2008)

Abnormal rise in cytosolic Ca^{2+} might activate phopholipase A_2, which could then, cleaves membrane phospholipids and cause the disruption of membrane organization, activation of Ca^{2+}-dependent endonucleases triggering DNA disruption and activation of transglutaminases catalysing the cross-linking of proteins to produce insoluble aggregates (Kowaltowski *et al.*, 2001). Additionally, excessive increase in cytosolic Ca^{2+} could also activate Ca^{2+}-dependent calpains which subsequently resulted in the cleavage of cytoskeletal proteins including spectrin, talin, and α-actin. This will eventually cause the elimination of plasma membrane anchorage to the cytoskeleton and contribute to plasma membrane blebbing (Miyoshi *et al.*, 1996; Weber *et al.*, 2005). Membrane blebbing is also facilitated by oxidation of thiol groups on cytoskeletal proteins by ROS and loss of intracellular ATP, which is required for the maintenance of cytoskeletal integrity. If the blebbing extends to a point where rupture occurs without immediate resealing, cell loses its ion gradient thus causing necrotic type of cell death whereby the cellular contents will be released into the surrounding area.

Research in this chapter was carried out to investigate the effect of oxLDL on intracellular Ca^{2+} level in three different types of cells (U937, human monocytes and HMDM cells) followed by experiments using various types of calcium channel blockers and calcium chelators. This chapter also examined the intracellular ROS production induced by oxLDL and the effect of various calcium channels blockers and calcium chelators on intracellular ROS levels. Additionally, the effect of calcium channel blockers and calcium chelators on cell viability in the absence and presence of oxLDL was also examined.

Mitochondrial permeability transition (MPT) and mitochondrial membrane potential (ΔΨm) – association between ROS and Ca^{2+}

Mitochondria play key role in vital cellular functions such as ATP production, regulation of cellular metabolism and cell death. Thus, mitochondrial dysfunction may contribute to a lot of diseases and at cellular level which leads to cell death (Lemasters *et al.*, 2009). Cytosolic Ca^{2+} overload can be taken up by the mitochondria, causing the mitochondrial permeability transition pore (MPTP) opening. This will then cause an increase of the inner mitochondrial membrane (IMM) to ions and solutes up to 1500 daltons (Bernardi, 1999; Crompton, 1999) due to the loss of mitochondrial membrane potential (ΔΨm), which eventually starts the cell death cascade that leads to necrotic or apoptotic cell death (Deng *et al.*, 2009; Madamanchi & Runge, 2007; Whiteman, *et al.*, 2004).

Mitochondrion consists of two membranes, inner membrane (IMM) and outer membrane (OMM) and the electron transport chain (ETC) located at IMM. ΔΨm is created as a result of H^+ pumping from the matrix to the intermembrane space (IMS) through complex I to IV of the ETC. At complex IV, ATP synthase uses these H^+ ions to produce ATP. Thus, the ΔΨm decreases as the protons are used to produce energy. Studies have also showed that during Ca^{2+} uptake, ΔΨm decreases and the decrease is proportional to the amount of Ca^{2+} uptake by the mitochondria (Nicotera *et al.,* 1992). However, the membrane potential is maintained by pumping more protons across the membrane (from matrix to the IMS). In order to maintain this critical gradient, transport across the IMM is tightly regulated by many specific transporters for various metabolites across the IMM. These transporters include Na^+/H^+ exchanger, H^+/K^+ antiporter, $Cl^-/HCO3^-$ antiporter, and uncoupling proteins. Additionally, the IMM also contains protein channels and the adenine translocator (ANT) that exchanges ADP and ATP between the matrix and IMS. Moreover, many of the apoptosis-inducing proteins reside in the IMS, including cytochrome *c*, apoptosis inducing factor (AIF) and few pro-caspases (Giorgi *et al.,* 2012). Thus, a change in ΔΨm is a signal for mitochondrial dysfunction which also reflects the metabolic state of the mitochondria.

Stimulation of the Krebs/TCA cycle and oxidative phosphorylation by Ca^{2+} can accelerate ROS generation by increasing mitochondrial metabolism and oxygen consumption which trigger more superoxide leakage from the mitochondrial respiratory chain (Brookes *et al.*, 2004; Nicotera & Orrenius, 1998). In addition, mitochondrial ROS can serve as the oxidising agent for MPTP via the activation of essential thiol groups of the membrane proteins (Inoue *et al.*, 2008; Kowaltowski *et al.,* 1997). MPTP opening causes ΔΨm loss and the subsequent rupture of OMM and mitochondrial dysfunctions (Deng *et al.,* 2009; Yang *et al.,* 2012a). MPTP opening could also resulted in the released of apoptotic factors such as cytochrome *c*, leading to caspase-3 activation followed by apoptotic cell death (Nicotera & Orrenius, 1998) but MPTP opening has always been associated with necrotic cell death (Zhivotovsky & Orrenius, 2011). Having stated the importance and association of Ca^{2+} and MPT, cell death could be prevented by inhibitors of mitochondrial Ca^{2+} uptake and MPTP formation such as ruthenium red and cyclosporin A, respectively (Zhivotovsky & Orrenius, 2011). This will also be investigated in this study.

Results

Effects of oxLDL on intracellular Ca^{2+} levels in U937 cells, human monocytes and HMDM cells

Previous study in our laboratory showed that HOCl-induced oxidative stress had caused the opening of Ca^{2+} channels leading to intracellular Ca^{2+} influx which is important in HOCl-mediated cell death (Yang *et al.*, 2012a). In the current study, the association between intracellular Ca^{2+} changes and the increased in oxidative stress was further explored with oxLDL. In the first part of this chapter, experiments were carried out to examine the effect of oxLDL on intracellular Ca^{2+} levels in U937 cells, human monocytes and HMDM cells over a period of time.

Cells were pre-incubated with a fluorescent dye, Fluo-3AM, to detect intracellular (cytosolic) free Ca^{2+} (see **Chapter 2 - Fluo-3-acetoxymethyl ester (Fluo-3 AM)**). The AM form of the dye can easily penetrate through the plasma membrane whereby upon cleavage of the ester group by cytoplasmic esterases, it is entrapped within the cells. Cells were then treated with oxLDL followed by flow cytometry measurements at different time points. Results have showed a similar time-dependent shifts in the fluorescence intensities over time in all types of cells (**Figure 5.2 A, 5.3 A** and **5.4 A**). This finding is in agreement with the work of Chen (2012) in this lab using U937 cells, who showed that the fluorescence intensity increase was observed as early as 5 minutes after incubation with oxLDL compared to the starting point (0 hour). This suggests that oxLDL caused a rapid intracellular Ca^{2+} influx which is the primary event upon the exposure of the cells to oxLDL.

In U937 cells, there was a 3-fold increase in fluorescence intensity after 1 hour incubation with oxLDL compared to the 0 hour. The fluorescence intensity increased by 4- and 6-fold after 2 hours and 3 hours incubation with oxLDL, respectively. The increased in fluorescence intensities has been observed up till 6 hours (**Figure 5.2**). As for human monocytes, a sharp increase in fluorescence intensity has been observed from the starting point (0 hour) until 3 hours incubation with oxLDL indicating the continuous rise in the intracellular Ca^{2+} levels in the first 3 hours.. After the 3 hour point, the increase in fluorescence intensity was minimal compared to the increase in the first 3 hours (**Figure 5.3**). Incubation of HMDM cells with oxLDL had also resulted in the increase in fluorescence intensities indicating increasing intracellular Ca^{2+} levels. The increase was about 2.5-fold after 1 hour incubation with oxLDL

compared to the 0 hour which then continued to rise until the next 2 hour. The fluorescence intensities seemed to stay stable over the next 3 hour treatment with oxLDL (**Figure 5.4**). These results suggest that the increase in cytosolic free Ca^{2+} occurred rapidly and it appears to be the primary event when cells are being exposed to oxLDL which may be responsible for the subsequent cellular oxidative events.

Experiment was also performed to examine the effect of different concentrations of oxLDL on intracellular Ca^{2+} levels over time. A time course study over a period of 6 hours was carried out using oxLDL concentrations of 0.25, 0.50, 0.75 and 1.00 mg/mL on U937 cells. Results showed that the mean fluorescence intensity increases with higher concentration of oxLDL (**Figure 5.5**) which indicates increased influx with increasing concentration of oxLDL. This finding is in agreement with Maziere *et al.* (2005) who showed that oxLDL-mediated increase in intracellular Ca^{2+} was dose-dependent.

A)

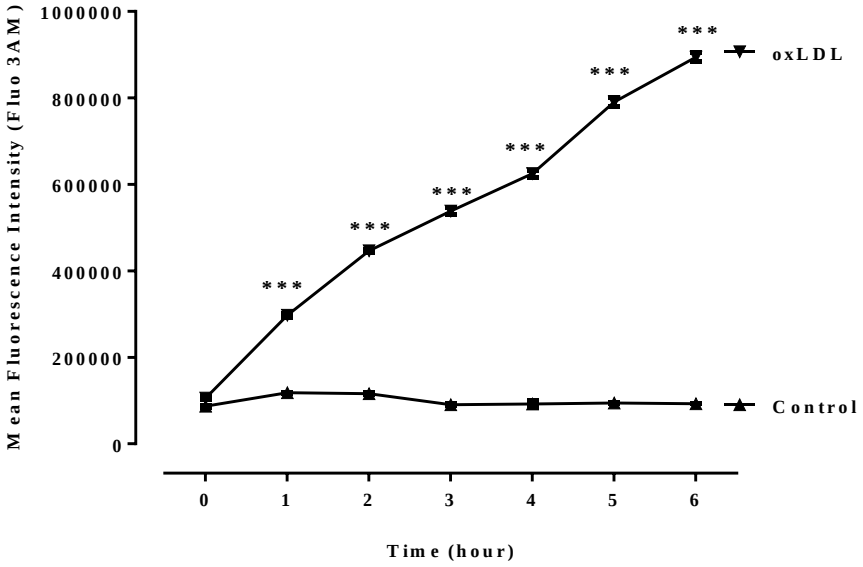

B)

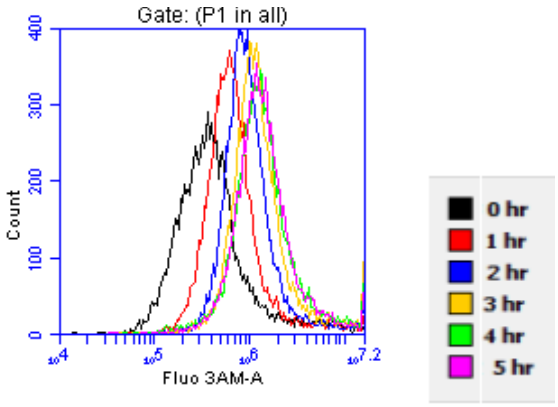

Figure 5.2: Effect of oxLDL on intracellular calcium levels in U937 cells.

U937 (0.5×10^6 cells/mL) were pre-incubated with 1.5 µM Fluo-3 AM for 40 minutes, followed by treatment with 0.5 mg/mL oxLDL in non-phenol red RPMI1640 at 37°C. At various times, cells were removed and analysed by flow cytometer. A) shows the median cellular fluorescence measured by flow cytometer over 6 hours (10,000 events were collected in the gated area for analysis). B) shows the representative cytometry histogram plot of cell counts against Fluo-3 AM over 4 hours Significance is indicated from the 0 hour data. Results displayed as mean fluorescence intensity (MFI) ± SEM of triplicate measurements from a representative experiment. Significance (two-way ANOVA, Sidak's post test) is indicated from the 0 hour control, ***, $p<0.001$.

A)

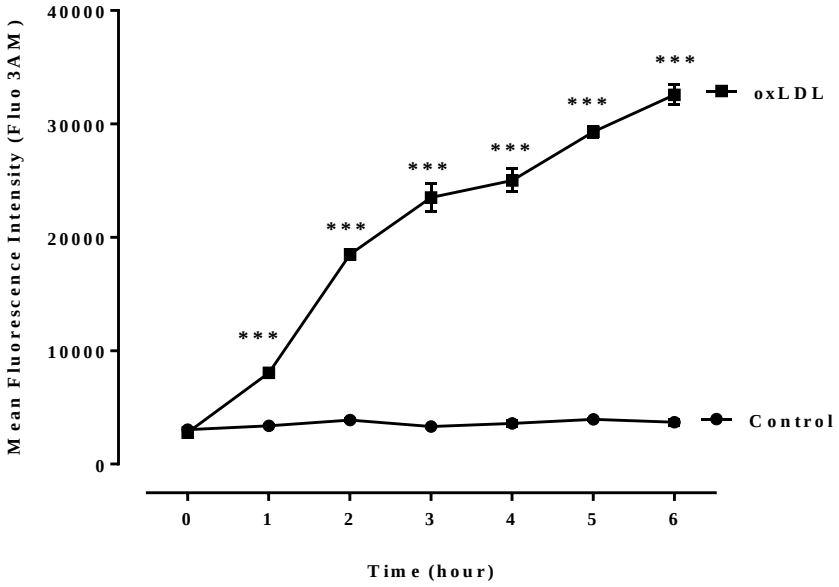

B)

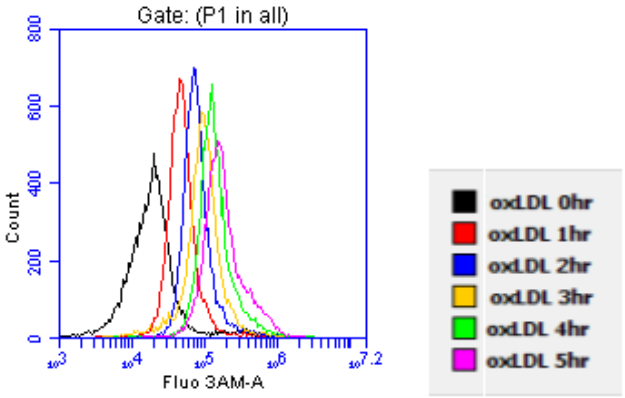

Figure 5.3: Effect of oxLDL on intracellular calcium levels in human monocytes.

Human monocytes (1×10^6 cells/mL) were pre-incubated with 1.5 µM Fluo-3 AM for 40 minutes, followed by treatment with 1 mg/mL oxLDL in non-phenol red RPMI1640 at 37°C. At various times, cells were removed and analysed by flow cytometer. A) shows the median cellular fluorescence measured by flow cytometer over 6 hours (10,000 events were collected in the gated area for analysis). B) shows the representative cytometry histogram plot of cell counts against Fluo-3 AM over 4 hours Significance is indicated from the 0 hour data. Results displayed as mean fluorescence intensity (MFI) ± SEM of triplicate measurements from a representative experiment. Significance (two-way ANOVA, Sidak's post test) is indicated from the 0 hour data, ***, $p<0.001$.

A)

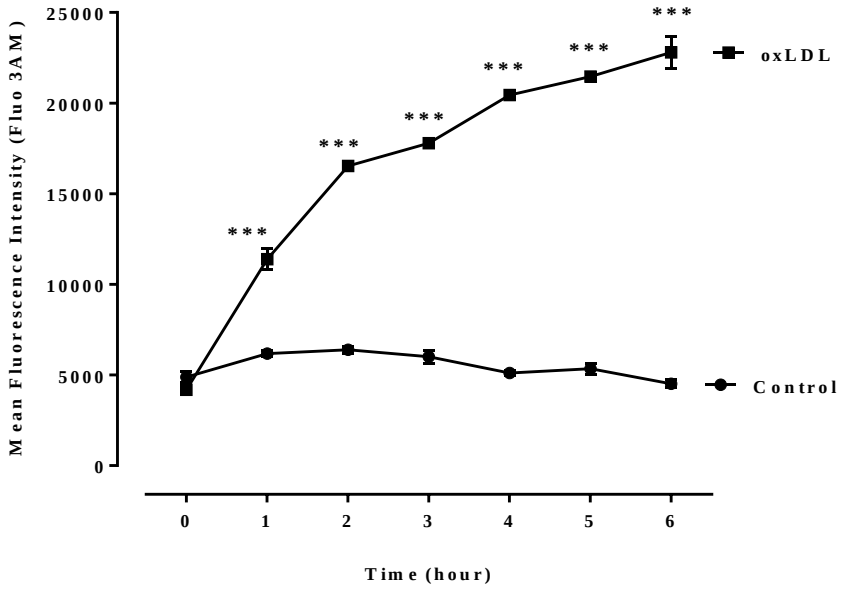

B)

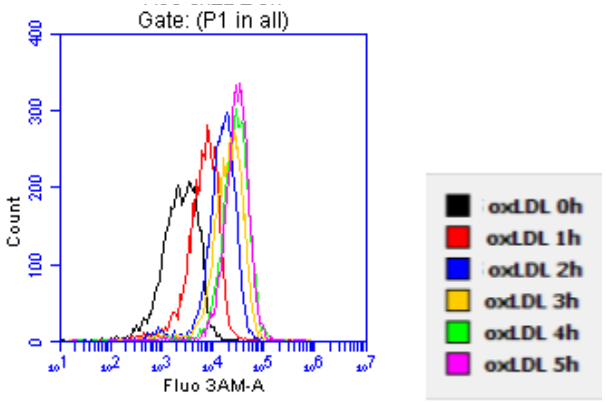

Figure 5.4: Effect of oxLDL on intracellular calcium levels in HMDM cells.

HMDM cells (1×10^6 cells/mL) were pre-incubated with 1.5 µM Fluo-3 AM for 40 minutes, followed by treatment with 1.5 mg/mL oxLDL in non-phenol red RPMI1640 at 37°C. At various times, cells were removed and analysed by flow cytometer. A) shows the median cellular fluorescence measured by flow cytometer over 6 hours, 10,000 events were collected in the gated area for analysis. B) shows the representative cytometry histogram plot of cell counts against Fluo-3 AM over 4 hours Significance is indicated from the 0 hour data. Results displayed as mean fluorescence intensity (MFI) ± SEM of triplicate measurements from a representative experiment. Significance (two-way ANOVA, Sidak's post test) is indicated from the 0 hour data, ***, $p<0.001$.

A)

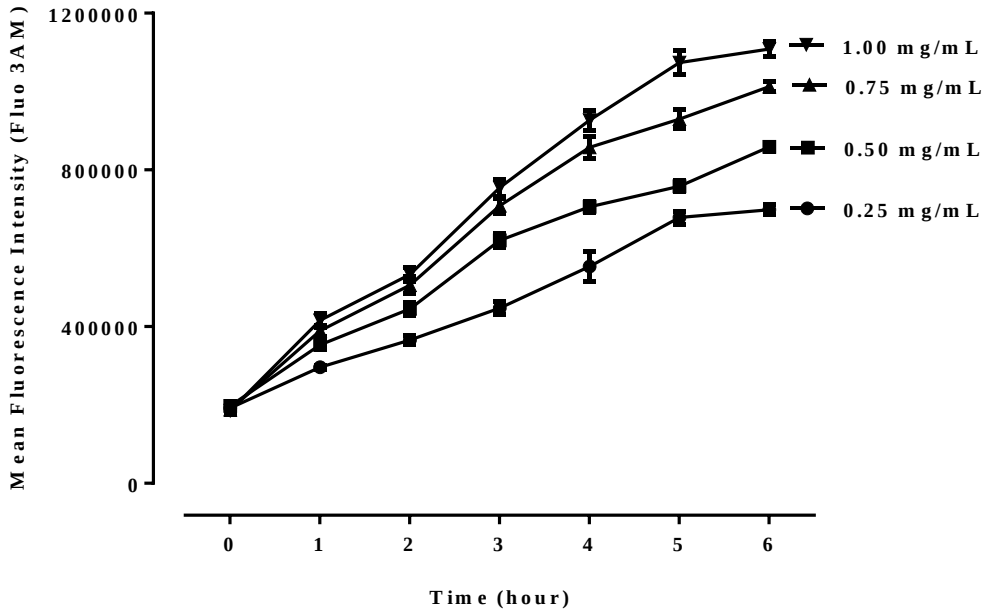

B)

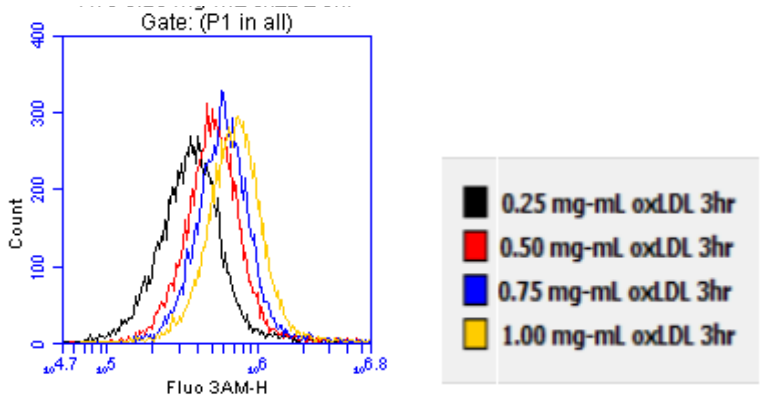

Figure 5.5: Effect of different concentrations of oxLDL on intracellular calcium levels in U937 cells.

U937 (0.5×10^6 cells/mL) were pre-incubated with 1.5 µM Fluo-3 AM for 40 minutes, followed by treatment with different concentrations of oxLDL in non-phenol red RPMI1640 at 37°C. After 3 hours of incubation, cells were removed and analysed by flow cytometry. A) shows the mean fluorescence intensity (MFI) measured by flow cytometry (10,000 events were collected in the gated area for analysis). B) shows the representative cytometry histogram plot of cell counts against Fluo-3 AM. Results displayed as median fluorescence ± SEM of triplicate measurements from a representative experiment.

Effects of oxLDL on intracellular Ca^{2+} in different types of media – RPMI1640, EBSS with Ca^{2+} (EBSS+Ca^{2+}) and EBSS without Ca^{2+} (EBSS-Ca^{2+})

Experiments were also carried out to examine the effect of oxLDL on intracellular Ca^{2+} levels in different type media i.e. RMPI1640, EBSS+Ca^{2+} and EBSS-Ca^{2+}. EBSS-Ca^{2+} (EBSS no Ca^{2+}) contains potassium chloride (KCl), sodium bicarbonate ($NaHCO_3$), sodium chloride (NaCl) and sodium phosphate monobasic and dextrose. EBSS+Ca^{2+} (EBSS with Ca^{2+}) contains the same ingredients but Ca^{2+} was added to resemble the Ca^{2+} concentration in RMPI1640. Subsequent experiments studying the effect and source (intracellular/extracellular) of Ca^{2+} were done using EBSS+Ca^{2+} and EBSS-Ca^{2+}. It has also been noted through morphological observations throughout the study that condition of the cells incubated in these media were not as good as they were in RMPI1640 which is the best media for cell culture. Nevertheless, most experiments conducted using EBSS required only short incubation time (e.g. 3 and 6 hours).

Results illustrated a consistent similar pattern of Ca^{2+} levels in all three types of cells (**Figure 5.6**). Highest fluorescence level depicting highest intracellular Ca^{2+} influx was obtained from cells in EBSS+Ca^{2+} followed by RPMI1640 and EBSS-Ca^{2+} (with or without the presence of oxLDL). These results also implicated the effect of extracellular Ca^{2+} influx to the increase in intracellular Ca^{2+}. With the presence of oxLDL, intracellular Ca^{2+} increase has also been observed from cells incubated in EBSS-Ca^{2+}. Since there was no extracellular Ca^{2+} presence in EBSS-Ca^{2+}, the rise in intracellular Ca^{2+} suggests that the source of Ca^{2+} was from intracellular organelles particularly ER. This finding will be further studied using specific Ca^{2+} blocker and inhibitors to determine the source and effects Ca^{2+}.

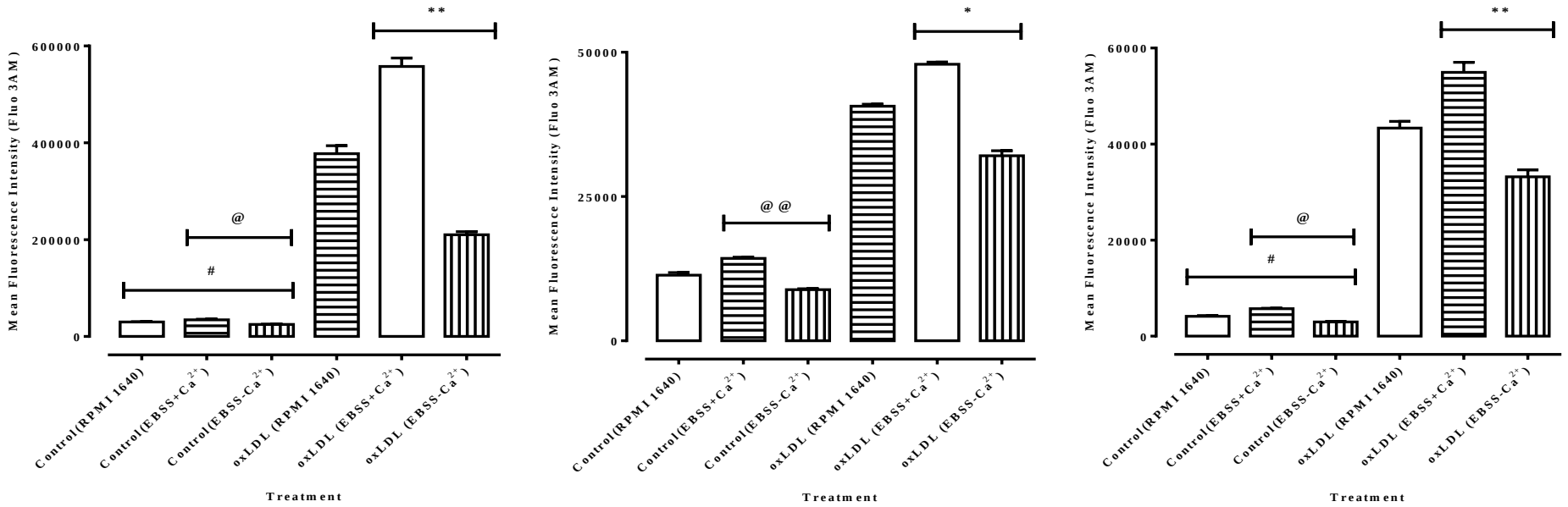

Figure 5.6: Effect of oxLDL on intracellular calcium levels in U937 cells, human monocytes and HMDM cells using different types of media.

U937 cells (0.5×10^6 cells/mL), human monocytes (1×10^6 cells/mL) and HMDM cells (1×10^6 cells/mL) were pre-incubated with 1.5 µM Fluo-3 AM for 40 minutes, followed by treatment with LC_{50} concentration of oxLDL (0.5 mg/mL, 1 mg/mL, 1.75 mg/mL for U937, human monocytes and HMDM cells, respectively) in non-phenol red RPMI1640, EBSS+Ca^{2+} or EBSS+Ca^{2+} at 37^{o}C. Cells were removed after 3 hours incubation with oxLDL and analysed by flow cytometry. A), B) and C) show the mean cellular fluorescence measured by flow cytometry over 3 hours (10,000 events were collected in the gated area for analysis) for U937 cells, human monocytes and HMDM cells, respectively. Results displayed as mean fluorescence ± SEM of triplicate measurements from a representative experiment. Significance (two-way ANOVA, Sidak's post test) is indicated from: Control (RPMI1640) vs Control (EBSS-Ca^{2+}), #, $p<0.05$; Control (EBSS+Ca^{2+}) vs Control (EBSS-Ca^{2+}), @, $p<0.05$, @@, $p<0.01$ and oxLDL (EBSS+Ca^{2+}) vs oxLDL (EBSS-Ca^{2+}), *, $p<0.05$, **, $p<0.01$, ***.

Calcium ionophore A23187 (BrA) was used as a positive control to confirm that the increase in fluorescence detected by flow cytometer resulted from Ca^{2+} reacting with the Fluo 3AM dye and not oxLDL reacting with the dye. BrA is a lipid soluble molecule that has been widely used to study calcium dynamics. It is highly selective for Ca^{2+} and enhances the ability of Ca^{2+} to cross the cell membrane and increases cytoplasmic Ca^{2+}. The fluorescence pattern showed that U937 cells (**Figure 5.7 A**) exhibited a concentration dependent increase in fluorescence intensity by 25% to 40% when treated with 5 and 7 μM of BrA respectively. The same pattern occurred for human monocytes and HMDM cells as shown in **Figure 5.7 B** and **5.7 C**.

Experiments were performed to further confirm that the cytosolic Ca^{2+} increase was able to cause cell viability loss in U937 cells, human monocytes and HMDM cells. Cells were exposed to different concentrations of Ca^{2+} ionophore A23187 (BrA) and cell viability was analysed after 24 hours. BrA at 3 μM did not cause any significant cell viability loss after 24 hour post-treatment but 5 and 7 μM BrA caused approximately 40 to 80% cell viability loss (**Figure 5.8 A, B** and **C**). These results suggest that the cytosolic Ca^{2+} increase induced by BrA treatment did cause loss of cell viability. No significant loss of cell viability was observed in cells incubated with 3 μM BrA indicates that a certain intracellular concentration of cytosolic Ca^{2+} is needed to cause decrease in cell viability. This finding is in agreement with Yang (2009) who also observed a rapid cell viability loss in HMDM cells after 5 minutes treatment with BrA of 5 μM and above in concentration. In the current study, 5 μM BrA was found to cause cell viability loss of 40 to 50% compared to the cell only control. This specific BrA concentration was used in the subsequent experiments involving BrA throughout the study.

A) U937 cells **B) Human monocytes** **C) HMDM cells**

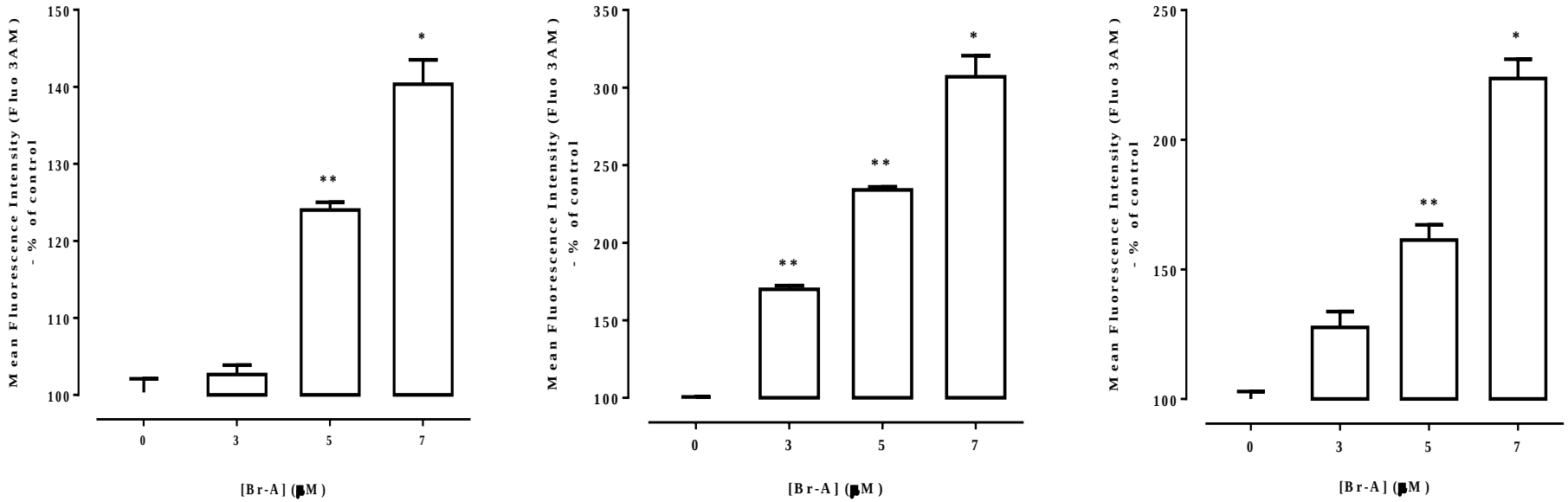

Figure 5.7: Calcium ionophore A23187 (Br-A) induced an increase in intracellular calcium levels in U937, human monocytes and HMDM cells.

HMDMs (1×10^6 cells/mL) were pre-incubated with 1.5 µM Fluo 3AM for 40 minutes, followed by treatment with increasing concentrations of calcium ionophore A23187 (BrA) in non-phenol red RPMI1640 at 37^{o}C for 3 hours. A cell only control (0 µM BrA) was included. Mean fluorescence intensity (MFI) was measured by flow cytometry (10,000 events were collected in the gated area for analysis) Significance is indicated from the cell only control. Results shown are mean fluorescence ± SEM of triplicate measurements from a representative experiment. Significance (two-way ANOVA, Sidak's post test) is indicated from the cell only control, *, $p<0.05$, **, $p<0.01$.

A) U937 cells **B) Human monocytes** **C) HMDM cells**

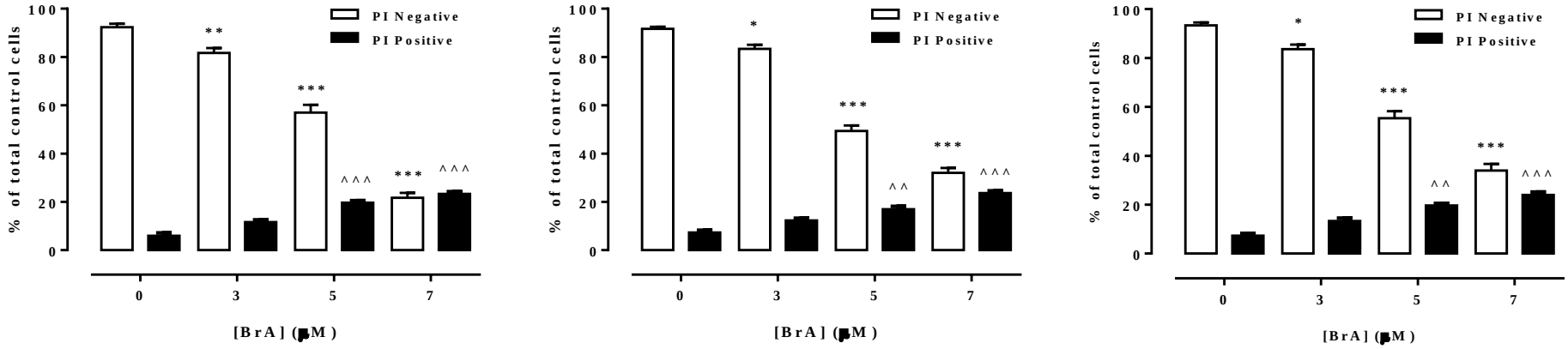

Figure 5.8: Calcium ionophore A23187 (Br-A) caused cell viability loss in U937, human monocytes and HMDM cells.

U937 (0.5×10^6 cells/mL), human monocytes (1×10^6 cells/mL) or HMDM cells (1×10^6 cells/mL) were incubated with increasing concentrations of calcium ionophore A23187 (BrA) in non-phenol red RPMI1640 at 37°C for 24 hours. A cell only control (0 μM BrA) was included. **A, B** and **C** show cell viability measured via PI-flow cytometry after 24 hours for U937 cells, human monocytes and HMDM cells, respectively. Data are expressed as percentage of the cell only control ± SEM of triplicate measurements from a representative experiment. Significance is indicated from the cell only control (two-way ANOVA, Sidak's post test): PI negative, *, $p<0.05$, **, $p<0.01$, ***, $p<0.001$; PI positive, ^^, $p<0.01$, ^^^, $p<0.001$.

Effects of media with Ca^{2+} (EBSS+Ca^{2+}) and without Ca^{2+} (EBSS+Ca^{2+}) and removal of oxLDL on intracellular Ca^{2+} level and cell viability

Experiments were also conducted to ascertain the effect of Ca^{2+} and removal of oxLDL on intracellular Ca^{2+} level and cell death. U937 cells, human monocytes and HMDM cells were incubated with oxLDL in EBSS with Ca^{2+} (EBSS+Ca^{2+}) and without Ca^{2+} (EBSS-Ca^{2+}) for 6 hours. At 6 hours, intracellular Ca^{2+} levels were measured. Cells were then washed to remove oxLDL and were further incubated in RPMI1640 for 18 hours. At the end of experiment, cell viability was determined.

The same patterns of results were seen for all types of cells. After 6 hours incubation with oxLDL, intracellular Ca^{2+} levels were increased. The increase was relatively higher in EBSS+Ca^{2+} compared to EBSS-Ca^{2+} which indicates the influx of extracellular Ca^{2+} into intracellular compartment. Intracellular Ca^{2+} increase in cells incubated in EBSS-Ca^{2+} was most likely due to Ca^{2+} mobilisation from intracellular organelles (**Figure 5.9 A, 5.10 A** and **5.11 A**). Removal of oxLDL (which is the toxic agent causing Ca^{2+} rise) from the media at 6 hours followed by incubation in fresh culture media for 18 hours did not restore cell viability despite lesser increase in intracellular Ca^{2+} level in cells incubated in EBSS-Ca^{2+} (**Figure 5.9 B, 5.10 B** and **5.11 B**). This effect will be further explained in the discussion section of this chapter.

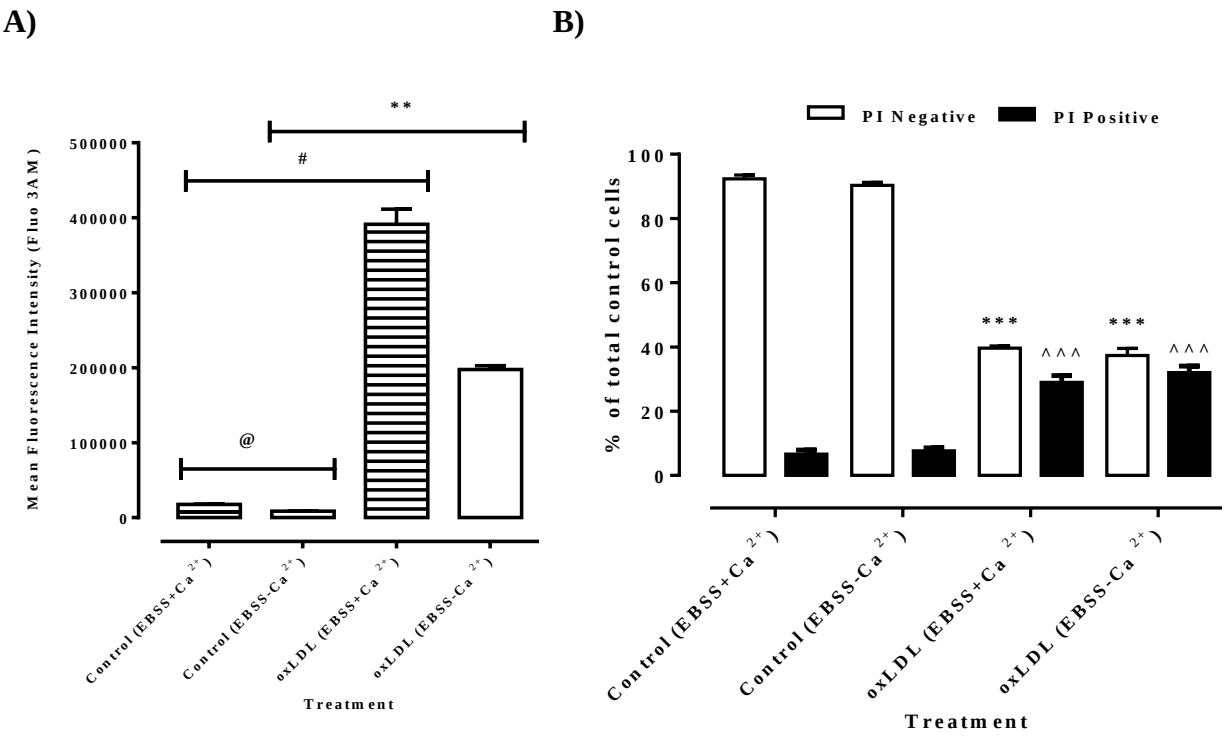

Figure 5.9: Effect of different media and removal of oxLDL on intracellular calcium and cell viability in U937 cells.

U937 (0.5×10^6 cells/mL) were incubated with LC_{50} concentration of oxLDL (0.4 mg/mL) in EBSS+Ca^{2+} and EBSS-Ca^{2+} at 37^{o}C for 6 hours. OxLDL was removed and cells were incubated in fresh RPMI1640 media for 18 hours. A) shows the mean fluorescence intensity (MFI) (Fluo-3AM) measured by flow cytometry after 6 hours (10,000 events were collected in the gated area for analysis). B) shows cell viability measured via PI-flow cytometry after 18 hours. Data are expressed as MFI and percentage of the respective control (EBSS+Ca^{2+}/EBSS-Ca^{2+}) ± SEM of triplicate measurements from a representative experiment, respectively. A) Significance (two-way ANOVA, Sidak's multiple test) is indicated from: EBSS+Ca^{2+} Control vs EBSS-Ca^{2+} Control, @, $p<0.05$; EBSS+Ca^{2+} Control vs EBSS+Ca^{2+} oxLDL, #, $p<0.05$ and EBSS-Ca^{2+} Control vs EBSS-Ca^{2+} oxLDL, **, $p<0.01$. B) Significance is indicated from the respective control (EBSS+Ca^{2+}/EBSS+Ca^{2+}) (two-way ANOVA, Sidak's multiple test), ***, $p<0.001$ (PI negative cells), ^^^, $p<0.001$ (PI positive cells).

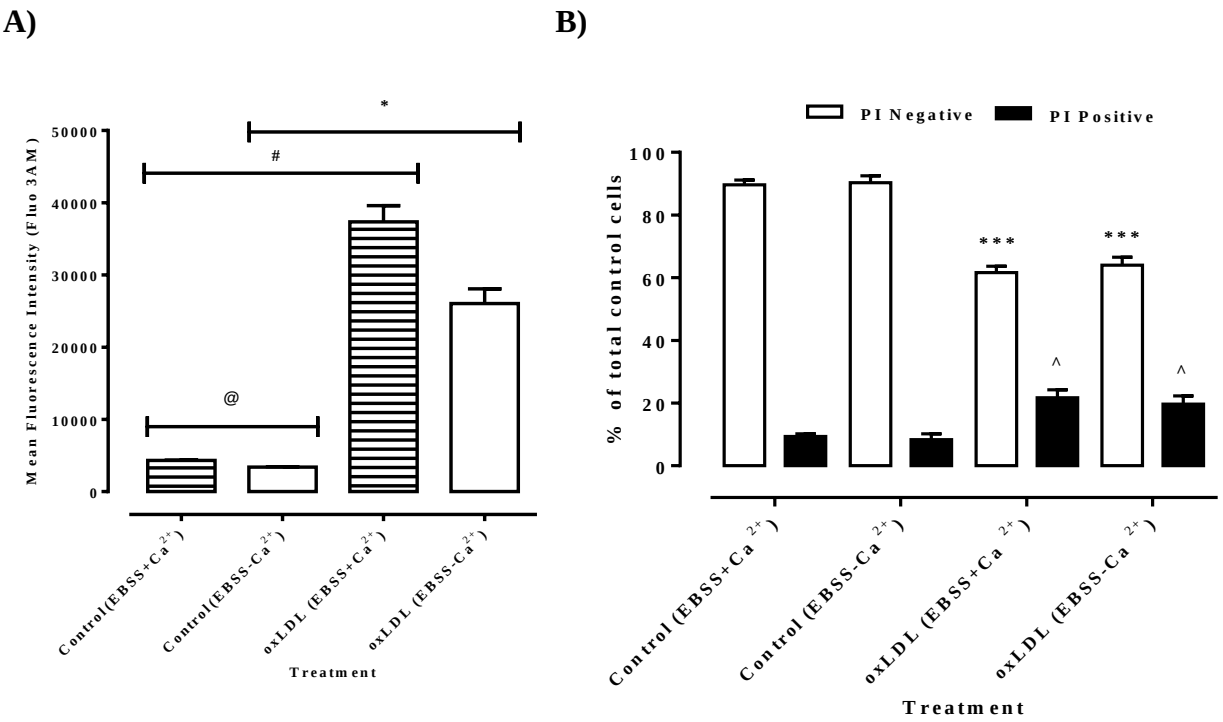

Figure 5.10: Effect of different media and removal of oxLDL on intracellular calcium and cell viability in human monocytes.

Human monocytes (1×10^6 cells/mL) were incubated with LC_{50} concentration of oxLDL (1 mg/mL) in EBSS+Ca^{2+} and EBSS-Ca^{2+} at 37°C for 6 hours. OxLDL was removed and cells were incubated in fresh RPMI1640 media for 18 hours. A) shows the mean fluorescence intensity (MFI) (Fluo-3AM) measured by flow cytometry after 6 hours (10,000 events were collected in the gated area for analysis). B) shows cell viability measured via PI-flow cytometry after 18 hours. Data are expressed as MFI and percentage of the respective control (EBSS+Ca^{2+}/EBSS+Ca^{2+}) ± SEM of triplicate measurements from a representative experiment, respectively. A) Significance (two-way ANOVA, Sidak's multiple test) is indicated from: EBSS+Ca^{2+} Control vs EBSS-Ca^{2+} Control, @, $p<0.05$; EBSS+Ca^{2+} Control vs EBSS+Ca^{2+} oxLDL, #, $p<0.05$ and EBSS-Ca^{2+} Control vs EBSS-Ca^{2+} oxLDL, *, $p<0.05$. B) Significance is indicated from the respective control (EBSS+Ca^{2+}/EBSS+Ca^{2+}) (two-way ANOVA, Sidak's multiple test), ***, $p<0.001$ (PI negative cells), ^, $p<0.05$ (PI positive cells).

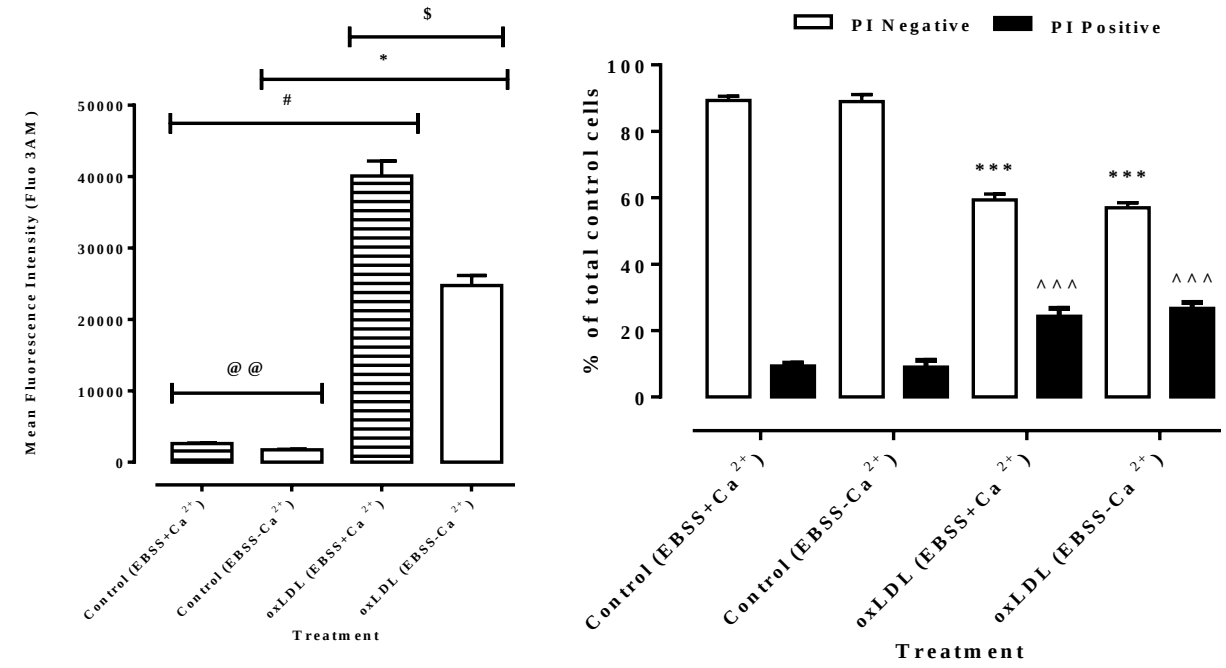

Figure 5.11: Effect of different media and removal of oxLDL on intracellular calcium and cell viability in HMDM cells.

HMDM cells (1×10^6 cells/mL) were incubated with LC_{50} concentration of oxLDL (1.5 mg/mL) in EBSS+Ca^{2+} and EBSS-Ca^{2+} at 37°C for 6 hours. OxLDL was removed and cells were incubated in fresh RPMI1640 media for 18 hours. A) shows the mean fluorescence intensity (MFI) (Fluo-3AM) measured by flow cytometry after 6 hours (10,000 events were collected in the gated area for analysis). B) shows cell viability measured via PI-flow cytometry after 18 hours. Data are expressed as MFI and percentage of the respective control (EBSS+Ca^{2+}/EBSS+Ca^{2+}) ± SEM of triplicate measurements from a representative experiment, respectively. A) Significance (two-way ANOVA, Sidak's multiple test) is indicated from: EBSS+Ca^{2+} Control vs EBSS-Ca^{2+} Control, @@, $p<0.01$; EBSS+Ca^{2+} Control vs EBSS+Ca^{2+} oxLDL, #, $p<0.05$; EBSS-Ca^{2+} Control vs EBSS-Ca^{2+} oxLDL, *, $p<0.05$ and EBSS+Ca^{2+} oxLDL vs EBSS-Ca^{2+} oxLDL, $, $p<0.05$. B) Significance is indicated from the respective control (EBSS+Ca^{2+}/EBSS+Ca^{2+}) (two-way ANOVA, Sidak's multiple test), ***, $p<0.001$ (PI negative cells), ^^^, $p<0.001$ (PI positive cells).

Effects of calcium channels blockers and calcium chelators on oxLDL-induced intracellular Ca^{2+}, ROS generation and cell viability

Results in the earlier part of this chapter have clearly demonstrated the ability of oxLDL to initiate an increase in intracellular Ca^{2+}. In Chapter Four, it has been shown that oxLDL caused intracellular ROS production including in the mitochondria. It has also been shown in the same chapter that oxLDL activated NOX and increased NOX subunit $p47^{phox}$ protein levels which may indicate NOX as a key source of intracellular oxidants (superoxide) mediated by oxLDL. Thus, it is suspected that these oxidants induced plasma membrane Ca^{2+} channels, ryanodine receptors (RyRs) and inositol triphosphate receptors (IP3Rs) on the ER membrane to open via thiol alterations on the protein complex. This will then lead to Ca^{2+} influx from the extracellular space and ER Ca^{2+} release. The accumulation of Ca^{2+} in the cytosol mediates the mitochondrial Ca^{2+} uptake through Ca^{2+} uniporter that will cause oxidative stress in the mitochondria. This results in series of events including calpain activation, opening of MPTP and loss of $\Delta\Psi m$ which will eventually lead to cell death. Studies have demonstrated the relation between Ca^{2+} levels and oxidative stress. It has been suggested that an increase in intracellular Ca^{2+} caused an elevation in oxidative stress and vice versa (Sun *et al.*, 2013).

Therefore, further investigation will examine the effects of L-type and T-type Ca^{2+} channel blockers, RyR blockers, sarcoplasmic/endoplasmic reticulum Ca^{2+} ATPase (SERCA) blocker, and Ca^{2+} chelators on intracellular Ca^{2+}, ROS production and cell viability in U937 cells, human monocytes and HMDM cells. Various Ca^{2+} channel blockers and Ca^{2+} chelators are used in this study including: flunarizine and nifedipine (L-type Ca^{2+} channel blockers); verapamil (T-type Ca^{2+} channel blockers); dantrolene (RyR blocker); thapsigargin (SERCA blocker) as well as EGTA and BAPTA-AM (Ca^{2+} chelators).

Flunarizine and nifedipine are Ca^{2+} channel blockers that block L-type VOCC. In U937 cells, with the addition of oxLDL, cells pre-treated with flunarizine appeared to be having less fluorescence compared to oxLDL only treated cells (**Figure 5.12 A**) which may indicate blockage of extracellular Ca^{2+} influx into the intracellular compartment. With the presence of oxLDL, fluorescence levels were also lower compared to oxLDL only treated cells. This suggests that flunarizine might be blocking the L-type channel but the blocking was not complete. Results of the similar trend as found with U937 cells were observed with human monocytes but with a lower concentration of flunarizine (10 µM) (**Figure 5.12 B**). As for

HMDM cells, there was no protection against increased level of intracellular Ca^{2+} observed (**Figure 5.12 C**).

Compared to oxLDL treated cells, addition of oxLDL to 10 µM nifedipine pre-treated U937 cells resulted in a slightly lower fluorescence. Lower fluorescence intensity was also seen in cells treated with 10 µM nifedipine only compared to control cells (**Figure 5.13 A**). Slight protection against oxLDL-induced intracellular Ca^{2+} increase was observed in human monocytes at nifedipine concentration of 10 µM but not 50 µM (**Figure 5.13 B**). In addition, there was also a slight decrease in fluorescence level in HMDM cells pre-treated with 10 µM nifedipine with the presence of oxLDL (**Figure 5.13 C**). Nifedipine alone, at 50 µM caused an increase in intracellular Ca^{2+} level in both human monocytes and HMDM cells.

Another Ca^{2+} channel blocker used in this study was verapamil which is the T-type VOCC blocker. In U937 cells, 10 µM verapamil demonstrated a significant protection against oxLDL-induced intracellular Ca^{2+} level increase (**Figure 5.14 A**). In human monocytes, pre-treatment with 50 µM verapamil only resulted in a significant increase in cellular fluorescence compared to cell only control. With the presence of oxLDL, cells treated with both concentrations of verapamil exhibited higher fluorescence levels compared oxLDL only treated cells indicating increased intracellular Ca^{2+} influx (**Figure 5.14 B**). HMDM cells pre-treated with verapamil had an increased in fluorescence intensity compared to cell only control. Likewise, with the presence of oxLDL, fluorescence intensity was greater in cells incubated with 50 µM verapamil compared to cells treated with oxLDL only (**Figure 5.14 C**).

These results showed the involvement of extracellular Ca^{2+} influx and that all plasma membrane Ca^{2+} channel blockers (flunarizine, nifedipine, verapamil) were unable to fully block Ca^{2+} influx triggered by oxLDL into the cytosol. Another possibility could be that Ca^{2+} diffused through the different type of VOCC i.e when T-type of VOCC is blocked, Ca^{2+} influx through the L-type of VOCC could occur. Although a multiple blockade (combination of flunarizine, nifedipine and verapamil) was thought during this study, this was not done for several reasons. Firstly, there might be adverse reactions between them that could cause toxicity to the cells. For example, flunarizine alone caused an increase in intracellular ROS and was toxic to U937 cells (**Figure 5.15** and **5.18**). Additionally, previous study in this lab by Yang (2009) on HOCl-induced cytosolic Ca2+ increase had also tested the effects of these Ca^{2+} blockers separately. The inability of flunarizine, nifedipine and verapamil to inhibit Ca^{2+}

rise could possibly be due to the involvement of Ca^{2+} sources which are insensitive to these inhibitors (Berthier *et al.*, 2004). Deng *et al.* (2005) have suggested that cytosolic Ca^{2+} increase could also occur via other non-specific pathway. It may also indicate that the insult caused by oxLDL is upstream to the blocking of Ca^{2+} channels that it could have damaged to the Ca^{2+} channels. This will be further detailed in the discussion section.

Moreover, the protective effect of these Ca^{2+} channel blockers might be cell specific that protection against oxLDL toxicity is offered in certain types of cells but not others. In this study, flunarizine alone was found to be cytotoxic to U937 cells but non-toxic to human monocytes and HMDM cells. Earlier studies by Negre-Salvayre and Salvayre (1992) have showed that nifedipine but not verapamil exhibited direct cytoprotective effect against oxLDL toxicity in culture lymphoid cells.

A) U937 cells **B) Human monocytes** **C) HMDM cells**

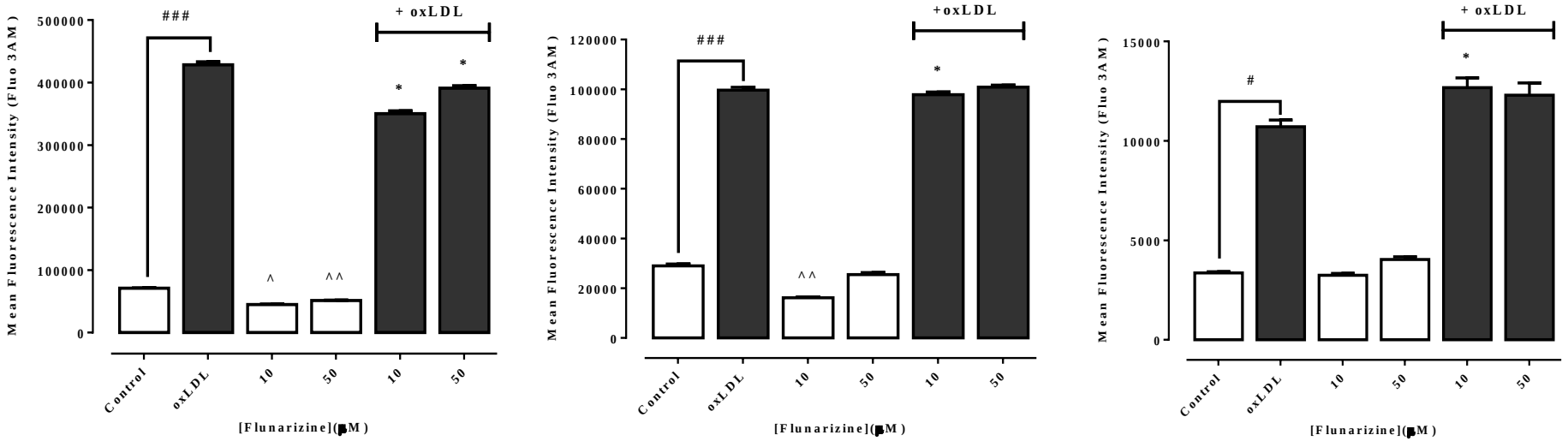

Figure 5.12: Effect of flunarizine (Flu) and oxLDL on intracellular calcium levels in U937, human monocytes and HMDM cells.

U937 cells (0.5×10^6 cells/mL), human monocytes (1×10^6 cells/mL) or HMDM cells (1×10^6 cells/mL) were pre-incubated with 1.5 µM Fluo 3AM for 40 minutes, followed by treatment with 10 µM and 50 µM Flu for 30 minutes before incubation with LC_{50} concentration of oxLDL (0.5, 1.0, 1.5 mg/mL for U937, human monocytes and HMDM cells, respectively) at 37°C in RPMI1640 with no phenol red for 3 hours. A), B) and C) show the mean fluorescence intensity measured by flow cytometry in U937 cells, human monocytes and HMDM cells, respectively (10,000 events were collected in the gated area for analysis). Results are displayed as mean fluorescence ± SEM of triplicates from a representative experiment. Significance (two-way ANOVA, Sidak's multiple test) is indicated from: control vs oxLDL, #, $p<0.05$, ###, $p<0.01$; control vs Flu, ^, $p<0.05$, ^^, $p<0.01$; oxLDL vs Flu with oxLDL, *, $p<0.05$.

A) U937 cells **B) Human monocytes** **C) HMDM cells**

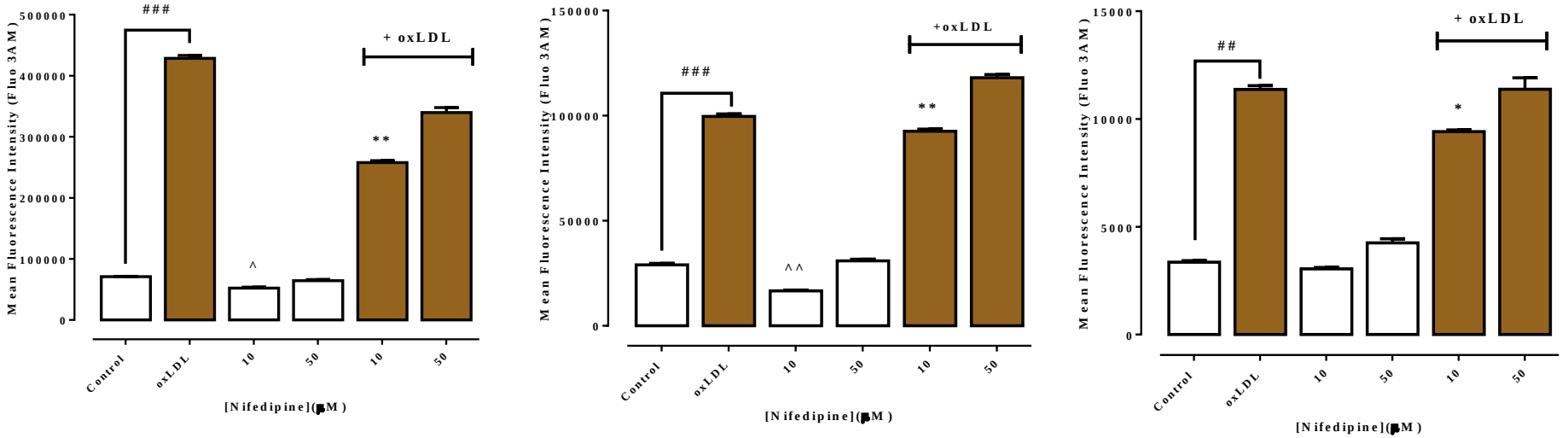

Figure 5.13: Effect of nifedipine (Nif) and oxLDL on intracellular calcium levels in U937, human monocytes and HMDM cells.

U937 cells (0.5×10^6 cells/mL), human monocytes (1×10^6 cells/mL) or HMDM cells (1×10^6 cells/mL) were pre-incubated with 1.5 µM Fluo-3 AM for 40 minutes, followed by treatment with 10 µM and 50 µM Nif for 30 minutes before incubation with LC_{50} concentration of oxLDL (0.5, 1.0, 1.5 mg/mL for U937, human monocytes and HMDM cells, respectively) at 37°C in RPMI1640 with no phenol red for 3 hours. A), B) and C) show the mean fluorescence intensity measured by flow cytometry in U937 cells, human monocytes and HMDM cells, respectively (10,000 events were collected in the gated area for analysis). Results are displayed as mean fluorescence ± SEM of triplicates from a representative experiment. Significance (two-way ANOVA, Sidak's multiple test) is indicated from: control vs oxLDL, ##, $p<0.01$, ###, $p<0.01$; control vs Nif, ^, $p<0.05$, ^^, $p<0.01$; oxLDL vs Nif with oxLDL, *, $p<0.05$, **, $p<0.01$.

A) U937 cells **B) Human monocytes** **C) HMDM cells**

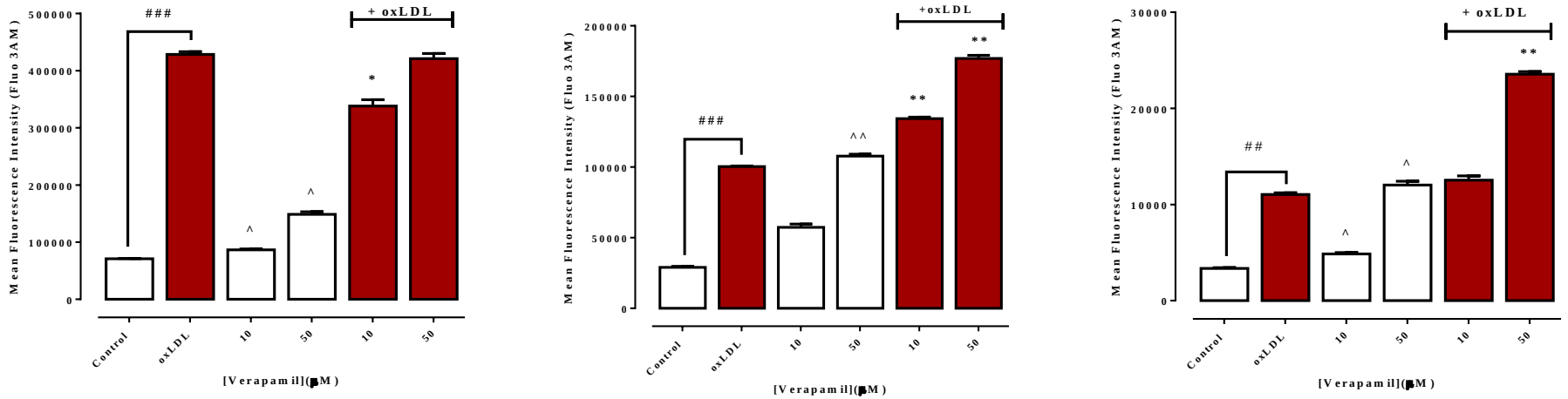

Figure 5.14: Effect of verapamil (Ver) and oxLDL on intracellular calcium levels in U937, human monocytes and HMDM cells.

U937 cells (0.5×10^6 cells/mL), human monocytes (1×10^6 cells/mL) or HMDM cells (1×10^6 cells/mL) were pre-incubated with 1.5 µM Fluo-3 AM for 40 minutes, followed by treatment with 10 µM and 50 µM Ver for 30 minutes before incubation with LC_{50} concentration of oxLDL (0.5, 1.0, 1.5 mg/mL for U937, human monocytes and HMDM cells, respectively) at 37°C in RPMI1640 with no phenol red for 3 hours. A), B) and C) show the mean fluorescence intensity measured by flow cytometry in U937 cells, human monocytes and HMDM cells, respectively (10,000 events were collected in the gated area for analysis). Results are displayed as mean fluorescence ± SEM of triplicates from a representative experiment. Significance (two-way ANOVA, Sidak's multiple test) is indicated from: control vs oxLDL, ##, $p<0.01$, ###, $p<0.01$; control vs Ver, ^, $p<0.05$, ^^, $p<0.01$; oxLDL vs Ver with oxLDL, *, $p<0.05$, **, $p<0.01$.

Experiments were then carried out to examine the effects of flunarizine, nifedipine and verapamil on intracellular ROS production in U937, human monocytes and HMDM cells. Incubation with flunarizine only in U937 cells resulted in increased production of ROS compared to control and oxLDL treated cells. With the presence of oxLDL, intracellular ROS production was even greater than that observed in oxLDL only treated cells (**Figure 5.15 A**). As for human monocytes and HMDM cells, no protection against oxLDL-induced intracellular ROS production was observed with different concentrations of flunarizine (**Figure 5.15 B** and **C**).

Increased in DHE fluorescence was observed in U937 cells pre-treated with nifedipine only compared to untreated cells (control). In the presence oxLDL, the fluorescence intensities were greater in nifedipine pre-treated cells compared to oxLDL treated cells especially at 50 µM nifedipine (**Figure 5.16 A**). Similar reaction trend with nifedipine was seen in human monocytes (**Figure 5.16 B**) while no protection against oxLDL-induced intracellular ROS production was observed in HMDM cells (**Figure 5.16 C**).

U937 cells pre-treated with verapamil exhibited higher DHE fluorescence compared to control cells. In the presence of oxLDL, no protection against oxLDL-induced ROS production was seen in cells pre-treated with verapamil (**Figure 5.17 A**). Likewise, similar trend of results were observed with human monocytes **(Figure 5.17 B**) whereas no protection against oxLDL-induced ROS generation was seen in HMDM cells. Moreover, 50 µM verapamil generated a greater DHE fluorescence in the presence of oxLDL compared to oxLDL only treated cells (**Figure 5.17 C**).

A) U937 cells **B) Human monocytes** **C) HMDM cells**

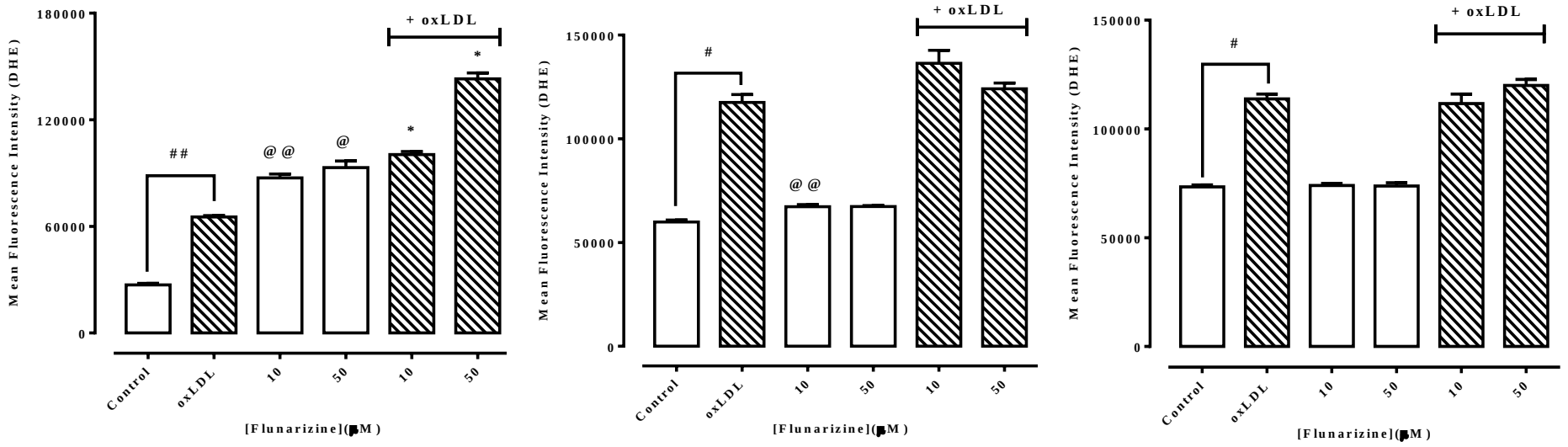

Figure 5.15: Effect of flunarizine (Flu) and oxLDL on intracellular ROS levels in U937, human monocytes and HMDM cells.

U937 cells (0.5×10^6 cells/mL), human monocytes (1×10^6 cells/mL) or HMDM cells (1×10^6 cells/mL) were incubated with 10 µM and 50 µM flunarizine for 30 minutes before incubation with LC_{50} concentration of oxLDL (0.5, 1.0, 1.5 mg/mL for U937, human monocytes and HMDM cells, respectively) at 37°C in RPMI1640 no phenol red for 6 hours. A), B) and C) show the mean fluorescence intensity measured by flow cytometry in U937 cells, human monocytes and HMDM cells, respectively. 10,000 events were collected in the gated area for analysis. Results are displayed as mean fluorescence ± SEM of triplicates from a representative experiment. Significance (two-way ANOVA, Sidak's test) is indicated from the cell only control, *, $p<0.05$, **, $p<0.01$, ***, $p<0.001$.

A) U937 cells **B) Human monocytes** **C) HMDM cells**

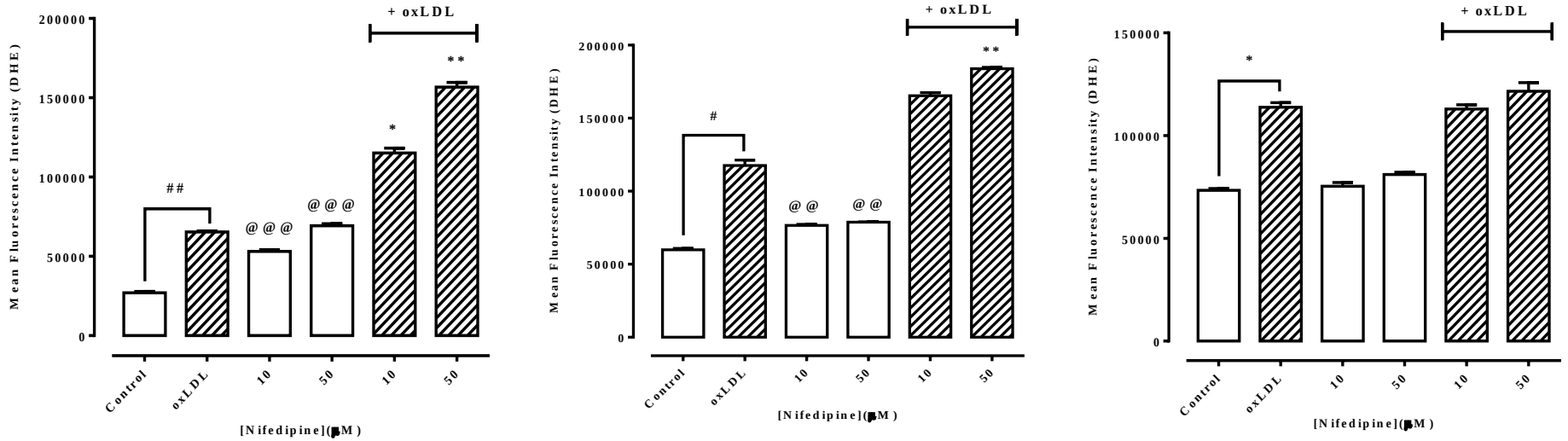

Figure 5.16: Effect of nifedipine (Nif) and oxLDL on intracellular ROS levels in U937, human monocytes and HMDM cells.

U937 cells (0.5×10^6 cells/mL), human monocytes (1×10^6 cells/mL) or HMDM cells (1×10^6 cells/mL) were incubated with 10 µM and 50 µM nifedipine for 30 minutes before incubation with LC_{50} concentration of oxLDL (0.5, 1.0, 1.5 mg/mL for U937, human monocytes and HMDM cells, respectively) at 37°C in RPMI1640 no phenol red for 6 hours. A), B) and C) show the mean fluorescence intensity measured by flow cytometry in U937 cells, human monocytes and HMDM cells, respectively. 10,000 events were collected in the gated area for analysis. Results are displayed as mean fluorescence ± SEM of triplicates from a representative experiment. Significance (two-way ANOVA, Sidak's test) is indicated from the cell only control, *, $p<0.05$, **, $p<0.01$, ***, $p<0.001$.

A) U937 cells **B) Human monocytes** **C) HMDM cells**

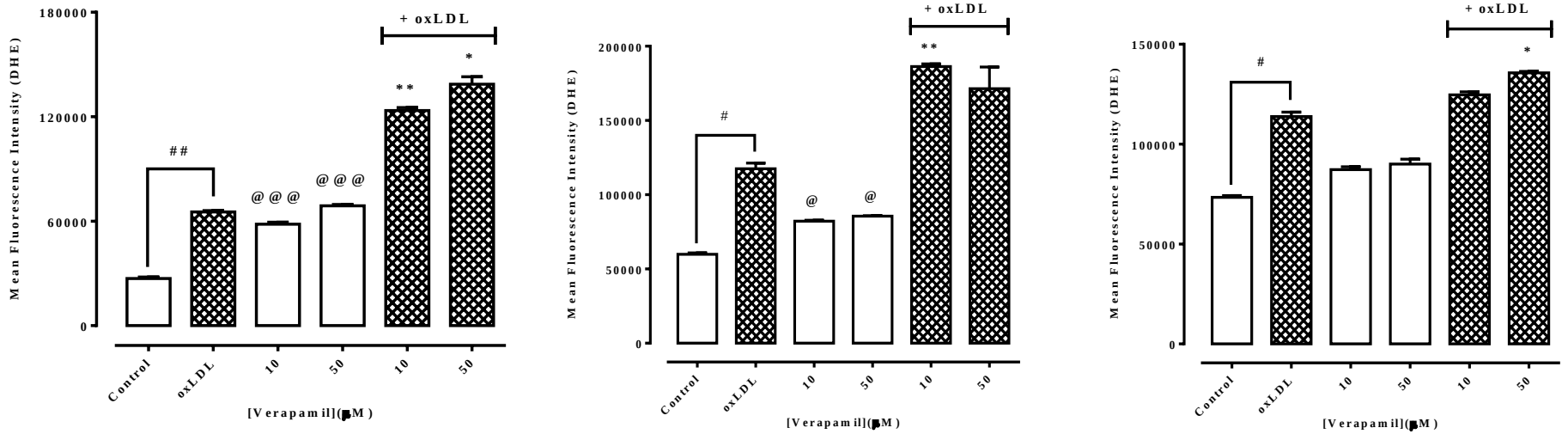

Figure 5.17: Effect of verapamil (Ver) and oxLDL on intracellular ROS levels in U937, human monocytes and HMDM cells.

U937 cells (0.5×10^6 cells/mL), human monocytes (1×10^6 cells/mL) or HMDM cells (1×10^6 cells/mL) were incubated with 10 μM and 50 μM verapamil for 30 minutes before incubation with LC_{50} concentration of oxLDL (0.5, 1.0, 1.5 mg/mL for U937, human monocytes and HMDM cells, respectively) at 37°C in RPMI1640 no phenol red for 6 hours. A), B) and C) show the mean fluorescence intensity measured by flow cytometry in U937 cells, human monocytes and HMDM cells, respectively. 10,000 events were collected in the gated area for analysis. Results are displayed as mean fluorescence ± SEM of triplicates from a representative experiment. Significance (two-way ANOVA, Sidak's test) is indicated from the cell only control, *, $p<0.05$, **, $p<0.01$, ***, $p<0.001$.

The effect of flunarizine, nifedipine and verapamil on oxLDL-mediated cell death was examined. Flunarizine (L-type Ca^{2+} channel blocker) alone was found to be cytotoxic to U937 cells and resulted in loss of cell viability (PI negative cells) of approximatlely 45% at high concentration (50 µM) (**Figure 5.18**). OxLDL itself caused cell viability loss (PI negative cells) by half compared to the control cells. Addition of oxLDL to 10 µM and 50 µM flunarizine pre-treated cells has reduced cell viability (PI negative cells) to an average of 44% and 34%, respectively while PI positive cells have also increased. On the other hand, flunarizine alone was not toxic to both human monocytes (**Figure 5.19**) and HMDM cells (**Figure 5.20**). However, flunarizine was also not protective against oxLDL-induced cell death for both types of cells.

Another L-type Ca^{2+} channel blocker used in this study was nifedipine. Contrary to flunarizine, nifedipine alone was not cytotoxic to U937 cells (**Figure 5.21)**, human monocytes (**Figure 5.22**) and HMDM cells (**Figure 5.23**). When oxLDL was added to the nifedipine pre-treated cells, cell viability loss was observed in all cell types (decreased in PI negative cells and increased in PI positive cells). OxLDL has caused about 45% to 50% cell loss (PI negative cells) in all types of cells. In the presence of oxLDL, cell viability loss was also increased (decreased in PI negative cells) in cells pre-treated with nifedipine. This shows that nifedipine is not protecting the cells against oxLDL toxicity.

Verapamil (T-type channel blocker) was also found not protective against oxLDL-induced cell death whereby the same trend of cell viability loss occurred in all types of cells. There was a significant cell loss of 40% to 50% in oxLDL only treated cells. Likewise, there was no protection against oxLDL-induced cytotoxicity seen in cells pre-treated with verapamil (**Figure 5.24** and **5.25**). In addition, oxLDL has further reduced cell viability (decrease in PI negative) of HMDM cells pre-treated with 50 µM verapamil (**Figure 5.26**).

A)

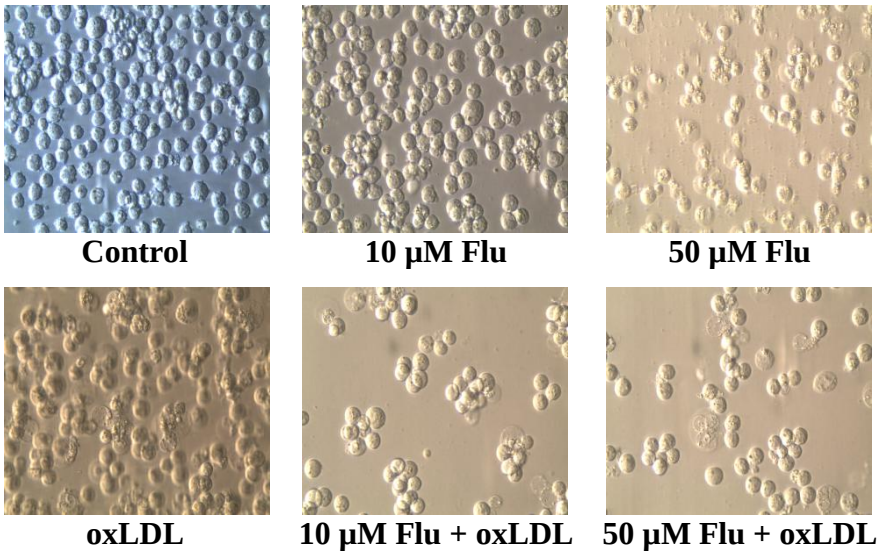

B)

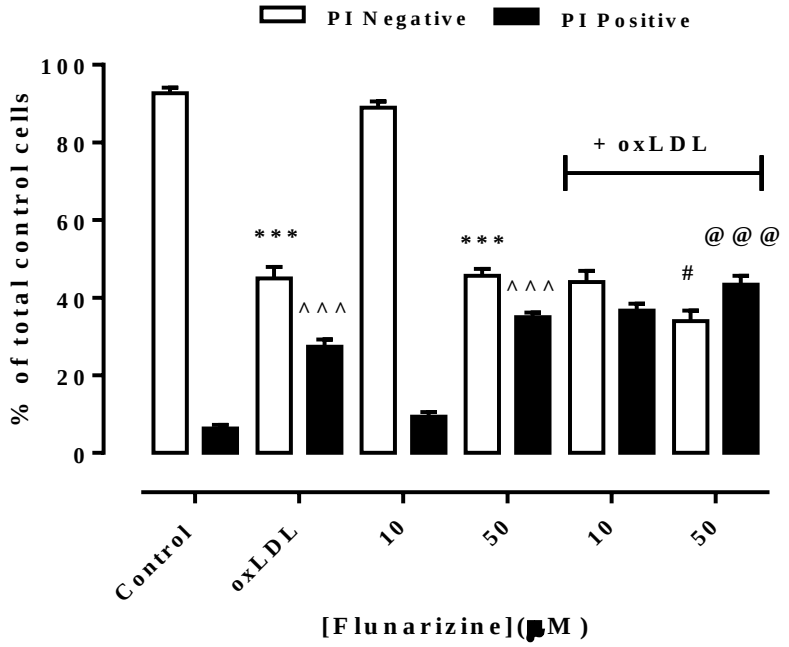

Figure 5.18: Effect of flunarizine (Flu) and oxLDL on U937 cell viability.

U937 cells (0.5×10^6 cells/mL) were treated with different concentrations of flunarizine for 30 minutes followed by addition of LC_{50} concentration (0.5 mg/mL) of oxLDL and incubated at 37°C in non-phenol red RPMI-1640 for 24 hours. A) Cells were viewed *in situ* in tissue culture wells using an inverted microscope (400x magnification) after 24 hours. Images were taken using a Leica C-Mount camera and processed using Leica Application Suite software. B) Cell viability was measured using PI-flow cytometry assay after 24 hours. Data are expressed as a percentage of the cell only control. Results are displayed as mean ± SEM of triplicates from a representative experiment. Significance (two-way ANOVA, Sidak's multiple test) is indicated from: cell only control vs oxLDL and cell only control vs 50 µM Flu, ***, $p<0.001$ (PI negative cells), ^^^, $p<0.001$ (PI positive cells); oxLDL vs 50 µM with oxLDL, #, $p<0.05$ (PI negative cells), @@@, $p<0.001$ (PI positive cells).

A)

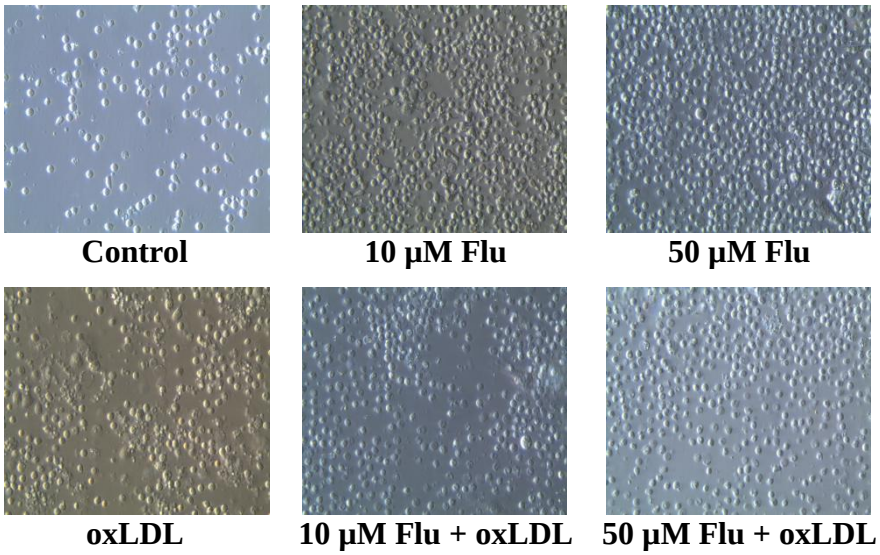

B)

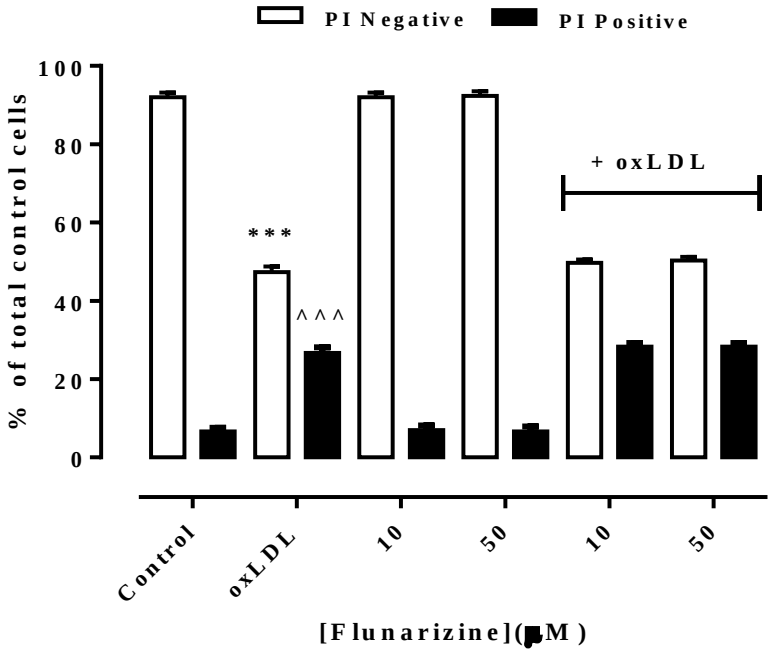

Figure 5.19: Effect of flunarizine (Flu) and oxLDL on human monocytes viability.

Human monocytes (1×10^6 cells/mL) were treated with different concentrations of flunarizine for 30 minutes followed by addition of LC_{50} concentration (1 mg/mL) of oxLDL and incubated at 37°C in non-phenol red RPMI-1640 for 24 hours. A) Cells were viewed *in situ* in tissue culture wells using an inverted microscope (400x magnification) after 24 hours. Images were taken using a Leica C-Mount camera and processed using Leica Application Suite software. B) Cell viability was measured using PI-flow cytometry assay after 24 hours. Data are expressed as a percentage of the cell only control. Results are displayed as mean ± SEM of triplicates from a representative experiment. Significance (two-way ANOVA, Sidak's multiple test) is indicated from: cell only control vs oxLDL, ***, $p<0.001$ (PI negative cells), ^^^, $p<0.001$ (PI positive cells).

A)

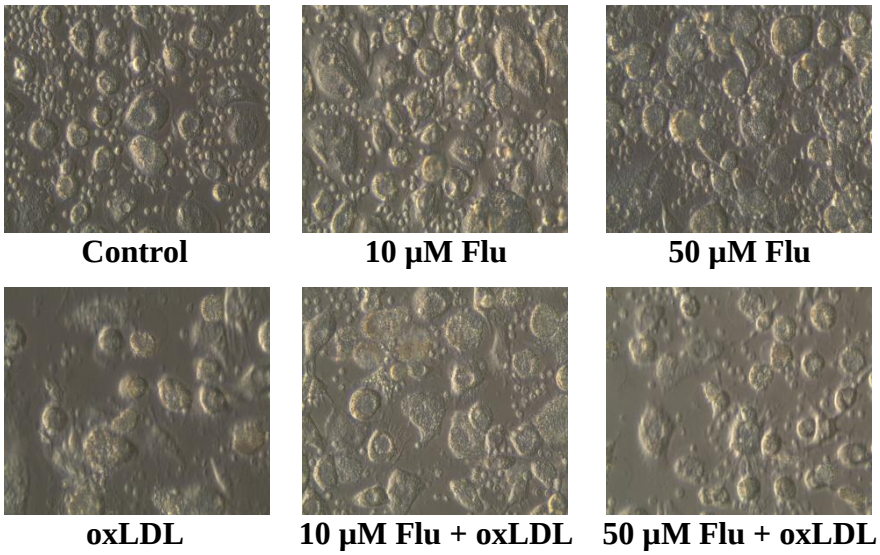

B)

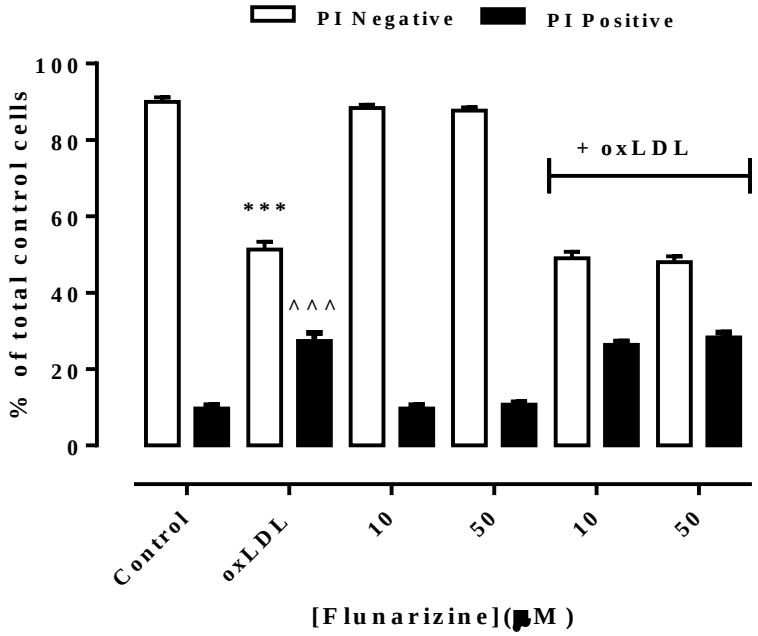

Figure 5.20: Effect of flunarizine (Flu) and oxLDL on HMDMs cell viability.

HMDM cells (1×10^6 cells/mL) were treated with different concentrations of flunarizine for 30 minutes followed by addition of LC_{50} concentration (1.5 mg/mL) of oxLDL and incubated at 37°C in non-phenol red RPMI-1640 for 24 hours. A) Cells were viewed *in situ* in tissue culture wells using an inverted microscope (400x magnification) after 24 hours. Images were taken using a Leica C-Mount camera and processed using Leica Application Suite software. B) Cell viability was measured using PI-flow cytometry assay after 24 hours. Data are expressed as a percentage of the cell only control. Results are displayed as mean ± SEM of triplicates from a representative experiment. Significance (two-way ANOVA, Sidak's multiple test) is indicated from: cell only control vs oxLDL, ***, $p<0.001$ (PI negative cells), ^^^, $p<0.001$ (PI positive cells).

A)

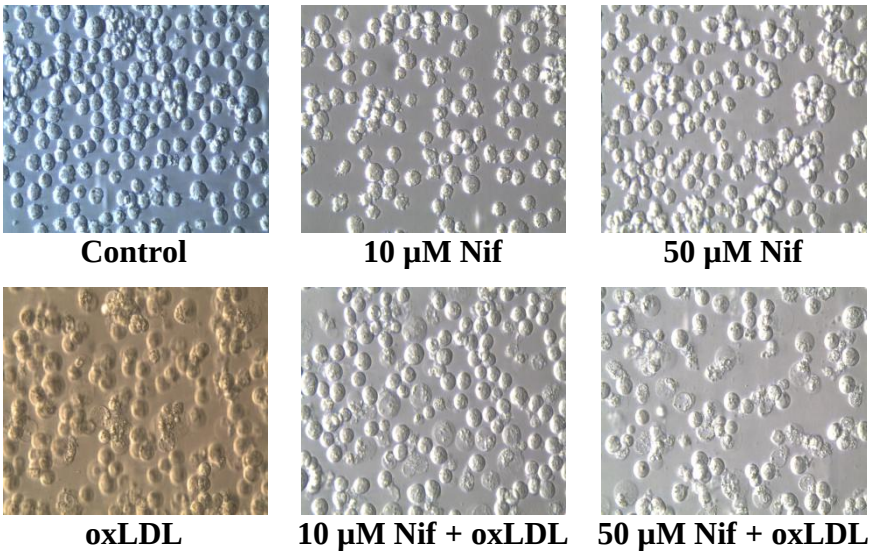

B)

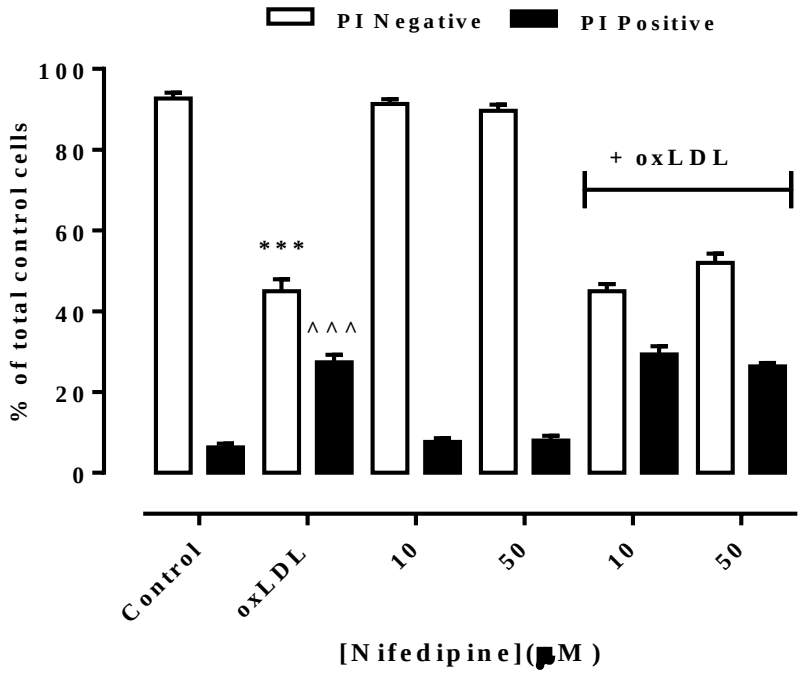

Figure 5.21: Effect of nifedipine (Nif) and oxLDL on U937 cell viability.

U937 cells (0.5×10^6 cells/mL) were treated with different concentrations of nifedipine for 30 minutes followed by addition of LC_{50} concentration (0.5 mg/mL) of oxLDL and incubated at 37°C in non-phenol red RPMI-1640 for 24 hours. A) Cells were viewed *in situ* in tissue culture wells using an inverted microscope (400x magnification) after 24 hours. Images were taken using a Leica C-Mount camera and processed using Leica Application Suite software. B) Cell viability was measured using PI-flow cytometry assay after 24 hours. Data are expressed as a percentage of the cell only control. Results are displayed as mean ± SEM of triplicates from a representative experiment. Significance (two-way ANOVA, Sidak's multiple test) is indicated from: cell only control vs oxLDL, ***, $p<0.001$ (PI negative cells), ^^^, $p<0.001$ (PI positive cells).

A)

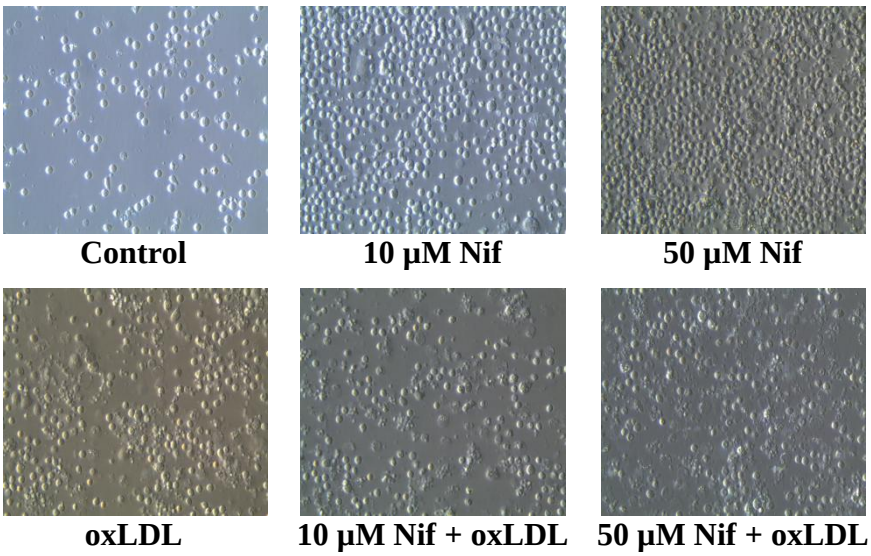

B)

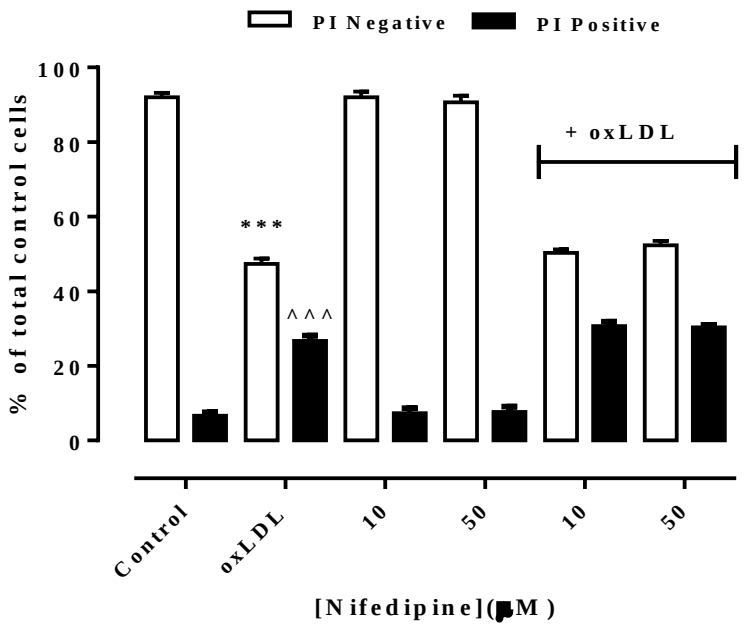

Figure 5.22: Effect of nifedipine (Nif) and oxLDL on human monocytes viability.

Human monocytes (1×10^6 cells/mL) were treated with different concentrations of nifedipine for 30 minutes followed by addition of LC_{50} concentration (1 mg/mL) of oxLDL and incubated at 37^{o}C in non-phenol red RPMI-1640 for 24 hours. A) Cells were viewed *in situ* in tissue culture wells using an inverted microscope (400x magnification) after 24 hours. Images were taken using a Leica C-Mount camera and processed using Leica Application Suite software. B) Cell viability was measured using PI-flow cytometry assay after 24 hours. Data are expressed as a percentage of the cell only control. Results are displayed as mean ± SEM of triplicates from representative experiment. Significance (two-way ANOVA, Sidak's multiple test) is indicated from: cell only control vs oxLDL, ***, $p<0.001$ (PI negative cells), ^^^, $p<0.001$ (PI positive cells).

A)

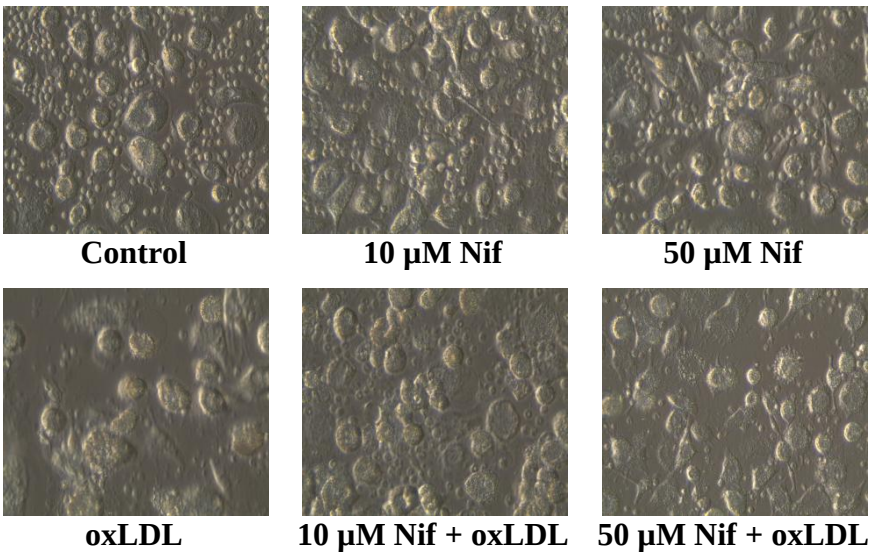

B)

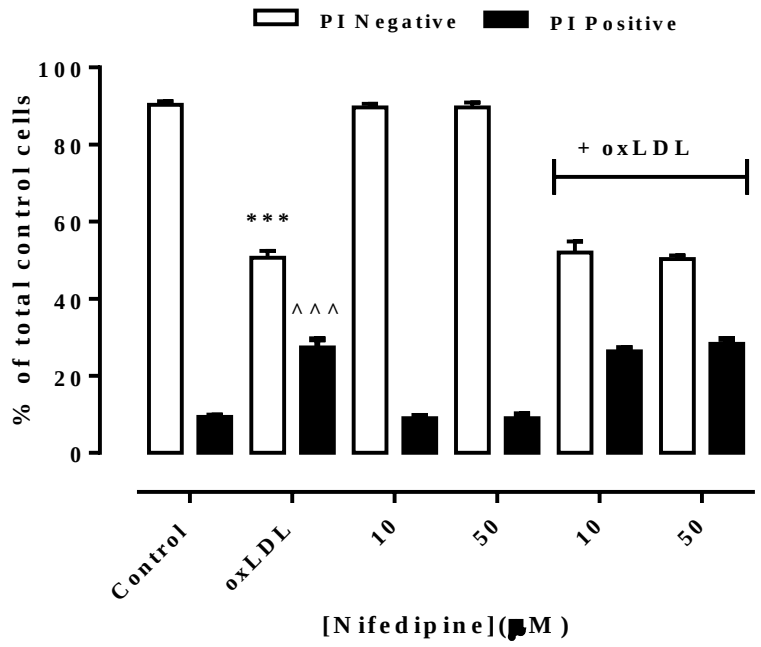

Figure 5.23: Effect of nifedipine (Nif) and oxLDL on HMDMs cell viability.

HMDM cells (1×10^6 cells/mL) were treated with different concentrations of nifedipine for 30 minutes followed by addition of LC_{50} concentration (1.5 mg/mL) of oxLDL and incubated at 37^{o}C in non-phenol red RPMI-1640 for 24 hours. A) Cells were viewed *in situ* in tissue culture wells using an inverted microscope (400x magnification) after 24 hours. Images were taken using a Leica C-Mount camera and processed using Leica Application Suite software. B) Cell viability was measured using PI-flow cytometry assay after 24 hours. Data are expressed as a percentage of the cell only control. Results are displayed as mean ± SEM of triplicates from a representative experiment. Significance (two-way ANOVA, Sidak's multiple test) is indicated from: cell only control vs oxLDL, ***, $p<0.001$ (PI negative cells), ^^^, $p<0.001$ (PI positive cells).

A)

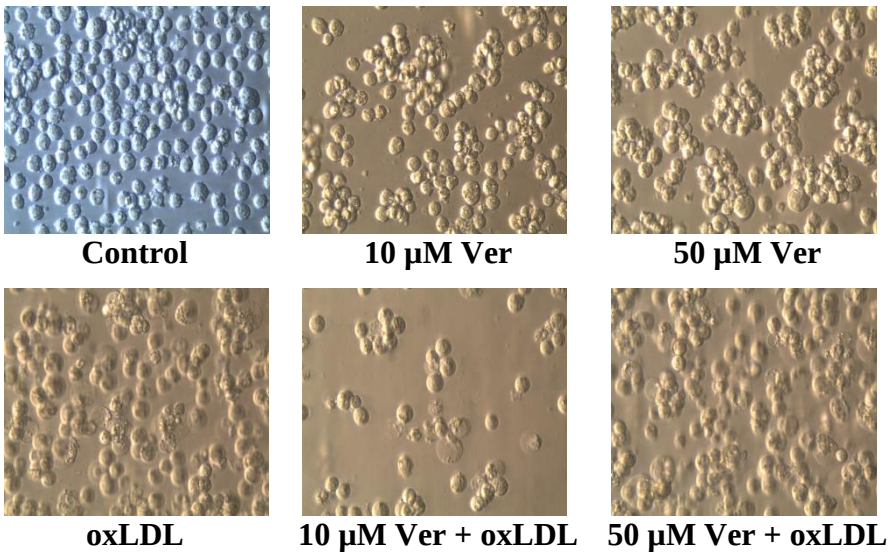

B)

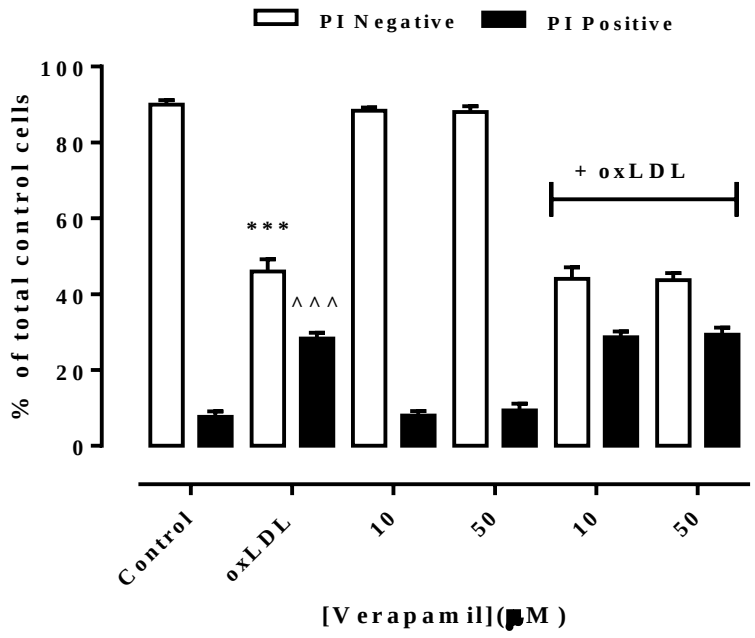

Figure 5.24: Effect of verapamil (Ver) and oxLDL on U937 cell viability.

U937 cells (0.5×10^6 cells/mL) were treated with different concentrations of verapamil for 30 minutes followed by addition of LC_{50} concentration (0.5 mg/mL) of oxLDL and incubated at 37°C in non-phenol red RPMI-1640 for 24 hours. A) Cells were viewed *in situ* in tissue culture wells using an inverted microscope (400x magnification) after 24 hours. Images were taken using a Leica C-Mount camera and processed using Leica Application Suite software. B) Cell viability was measured using PI-flow cytometry assay after 24 hours. Data are expressed as a percentage of the cell only control. Results are displayed as mean ± SEM of triplicates from representative experiment. Significance (two-way ANOVA, Sidak's multiple test) is indicated from: cell only control vs oxLDL, ***, $p<0.001$ (PI negative cells), ^^^, $p<0.001$ (PI positive cells).

A)

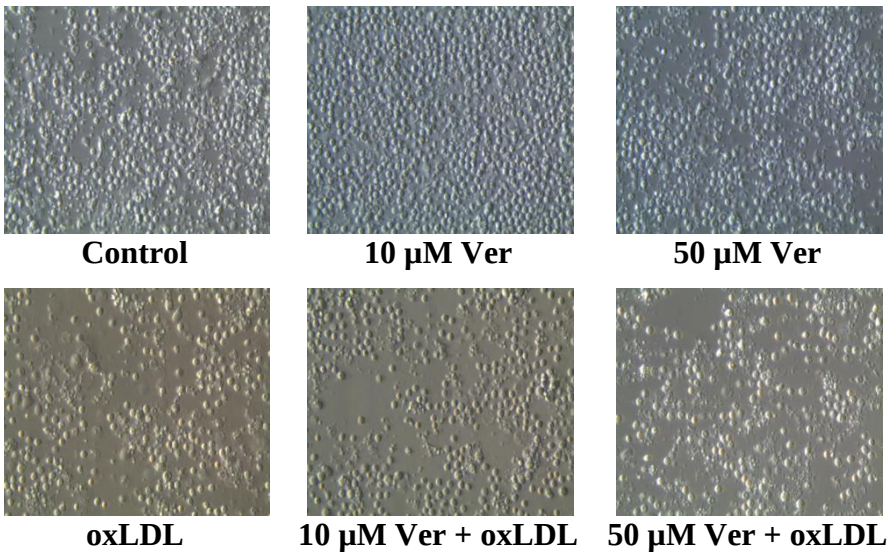

B)

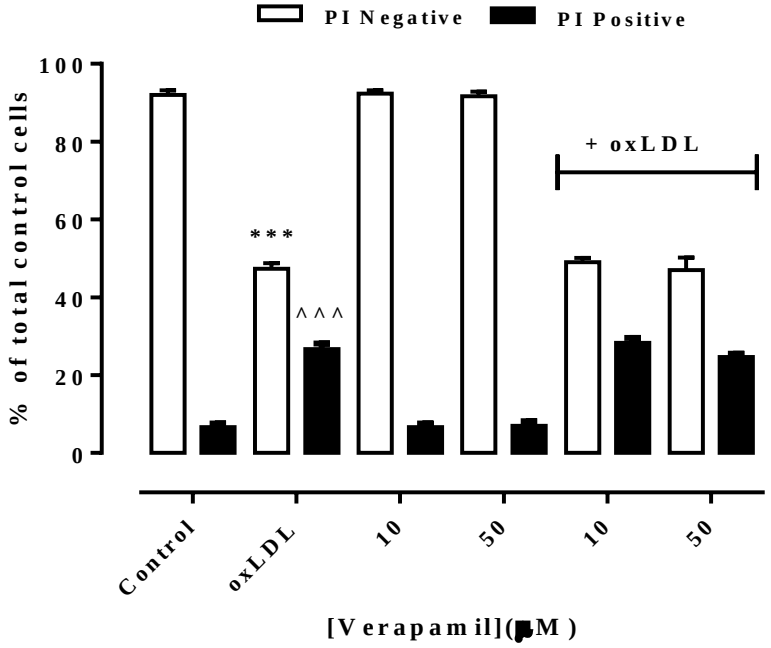

Figure 5.25: Effects of verapamil (Ver) and oxLDL on human monocytes viability.

Human monocytes (1×10^6 cells/mL) were treated with different concentrations of verapamil for 30 minutes followed by addition of LC_{50} concentration (1 mg/mL) of oxLDL and incubated at 37°C in non-phenol red RPMI-1640 for 24 hours. A) Cells were viewed *in situ* in tissue culture wells using an inverted microscope (400x magnification) after 24 hours. Images were taken using a Leica C-Mount camera and processed using Leica Application Suite software. B) Cell viability was measured using PI-flow cytometry assay after 24 hours. Data are expressed as a percentage of the cell only control. Results are displayed as mean ± SEM of triplicates from a representative experiment. Significance (two-way ANOVA, Sidak's multiple test) is indicated from: cell only control vs oxLDL, ***, $p<0.001$ (PI negative cells), ^^^, $p<0.001$ (PI positive cells).

A)

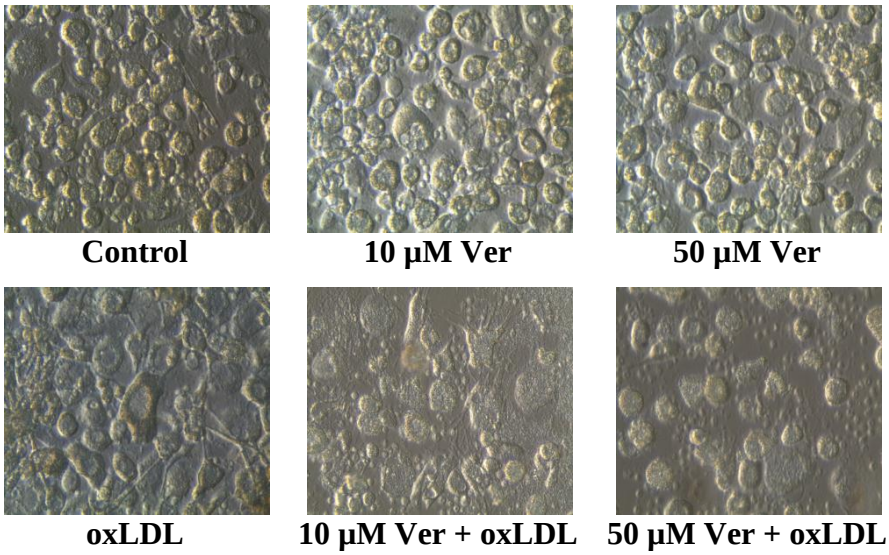

B)

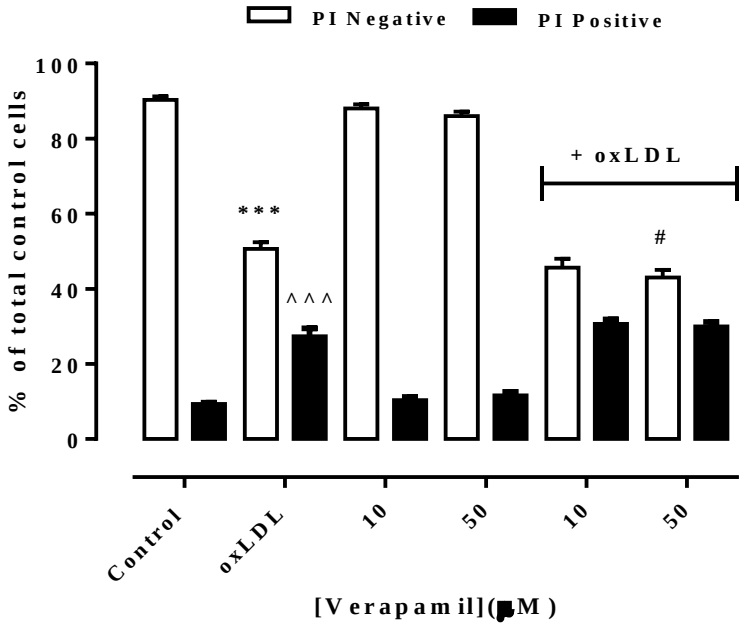

Figure 5.26: Effect of verapamil (Ver) and oxLDL on HMDMs cell viability.

HMDM cells (1×10^6 cells/mL) were treated with different concentrations of verapamil for 30 minutes followed by addition of LC_{50} concentration (1.5 mg/mL) of oxLDL and incubated at 37°C in non-phenol red RPMI-1640 for 24 hours.A) Cells were viewed *in situ* in tissue culture wells using an inverted microscope (400x magnification) after 24 hours. Images were taken using a Leica C-Mount camera and processed using Leica Application Suite software. B) Cell viability was measured using PI-flow cytometry assay after 24 hours. Data are expressed as a percentage of the cell only control. Results are displayed as mean ± SEM of triplicates from a representative experiment. Significance (two-way ANOVA, Sidak's multiple test) is indicated from: cell only control vs oxLDL, ***, $p<0.001$ (PI negative cells), ^^^, $p<0.001$ (PI positive cells); oxLDL vs 50 µM Ver + oxLDL, #, $p<0.05$ (PI negative cells).

Dantrolene blocks ryanodine receptors (RyR) on ER, thus blocking Ca^{2+} release into the cytoplasm from RyR channels (Zhao *et al.*, 2001). In U937 cells, there was no significant difference in intracellular Ca^{2+} levels between control cells and dantrolene pre-treated cells. With the addition of oxLDL, intracellular Ca^{2+} level was raised in cells pre-treated with 10 µM dantrolene (**Figure 5.27 A**). However, in human monocytes, intracellular Ca^{2+} increase mediated by oxLDL was significantly lowered in dantrolene pre-treated cells. Fluorescence intensity was also lower in cells pre-treated with dantrolene compared to control (**Figure 5.27 B**). No protection against oxLDL-induced intracellular Ca^{2+} increase was observed in HMDM cells pre-treated with dantrolene. Greater fluorescence level compared to oxLDL was also seen in cells treated with 10 µM dantrolene compared with oxLDL only (**Figure 5.27 C**). Results showed that the influx of extracellular Ca^{2+} into the cytoplasm and Ca^{2+} could be released from the other channel on the ER i.e. IP3R that caused the overall increase in intracellular Ca^{2+} level in response to oxLDL.

The contribution of intracellular Ca^{2+} to oxLDL-induced Ca^{2+} rise was determined by depleting intracellular Ca^{2+} ER store with thapsigargin. Sarco-endoplasmic reticulum calcium ATPase (SERCA) is a pump that returns Ca^{2+} from the cytoplasm to the ER. Thapsigargin selectively prevents Ca^{2+} binding to SERCA (Sagara *et al.*, 1992) thus increases intracellular Ca^{2+} by inhibiting the sequestration of Ca^{2+} into ER. **Figure 5.28 A, B** and **C** show that stimulation with oxLDL caused a further increase in intracellular Ca^{2+} above that induced by thapsigargin. This suggests that extracellular Ca^{2+} influx into the cells caused by oxLDL would otherwise be distributed into the ER (if no blockade by thapsigargin) and potentially overloads ER Ca^{2+} stores. Therefore, blockade by thapsigargin causes a massive increase in the cytosolic Ca^{2+} level.

A) U937 cells **B) Human monocytes** **C) HMDM cells**

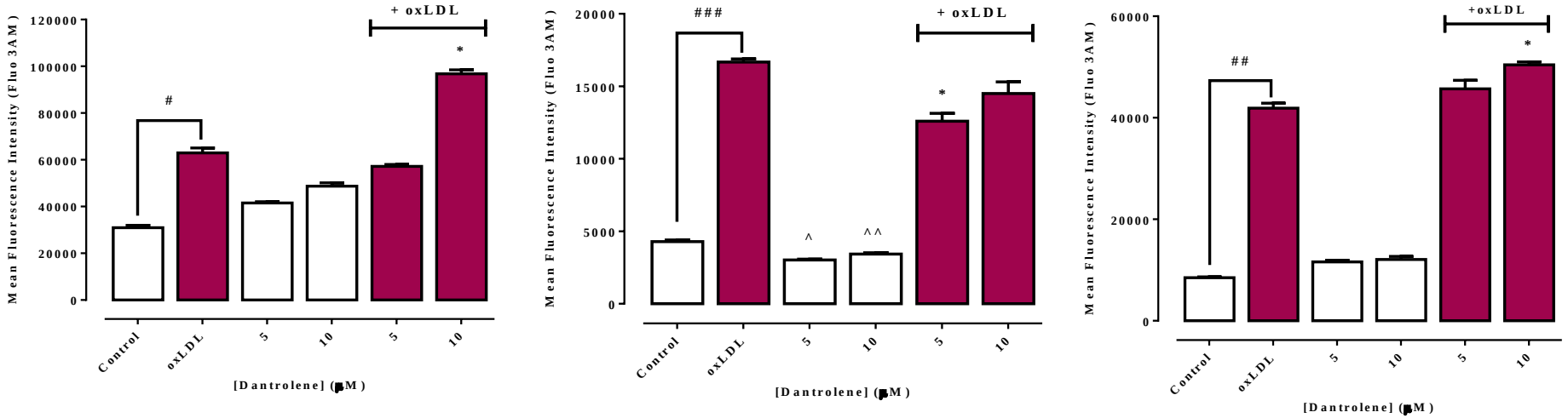

Figure 5.27: Effect of dantrolene (Dan) and oxLDL on intracellular calcium levels in U937, human monocytes and HMDM cells.

U937 cells (0.5×10^6 cells/mL), human monocytes (1×10^6 cells/mL) or HMDM cells (1×10^6 cells/mL) were pre-incubated with 1.5 µM Fluo-3 AM for 40 minutes, followed by treatment with 5 µM and 10 µM Dan for 30 minutes before incubation with LC_{50} concentration of oxLDL (0.5, 1.0, 1.5 mg/mL for U937, human monocytes and HMDM cells, respectively) at 37°C in RPMI1640 with no phenol red for 3 hours. A), B) and C) show the mean fluorescence intensity measured by flow cytometry in U937 cells, human monocytes and HMDM cells, respectively (10,000 events were collected in the gated area for analysis). Results are displayed as mean fluorescence ± SEM of triplicates from a representative experiment. Significance (two-way ANOVA, Sidak's multiple test) is indicated from: control vs oxLDL, #, $p<0.05$, ##, $p<0.01$, ###, $p<0.01$; control vs Dan, ^, $p<0.05$, ^^, $p<0.01$; oxLDL vs Dan with oxLDL, *, $p<0.05$.

A) U937 cells **B) Human monocytes** **C) HMDM cells**

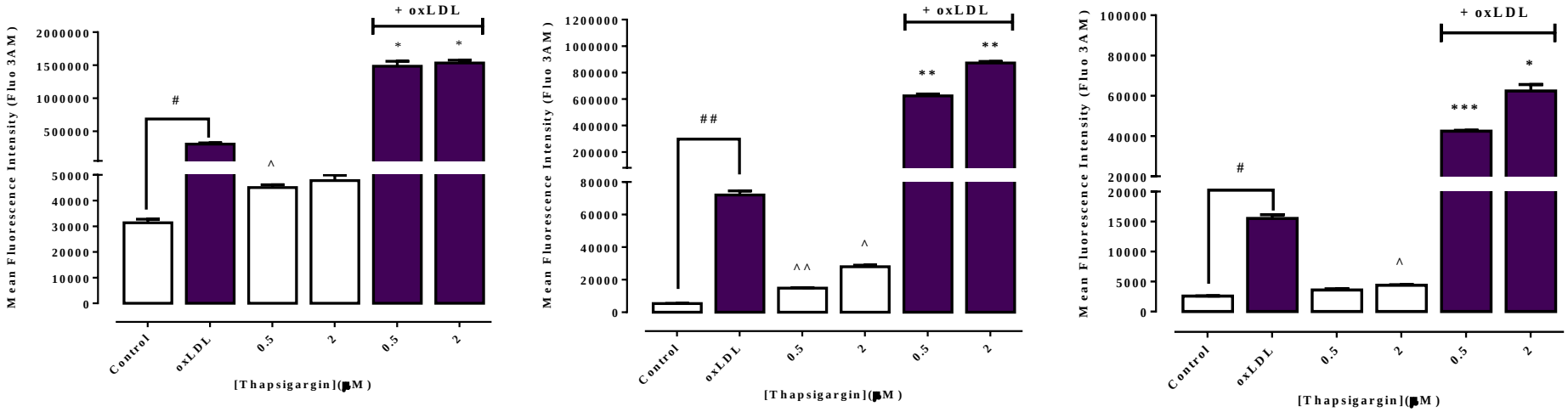

Figure 5.28: Effect of thapsigargin (Tg) and oxLDL on intracellular calcium levels in U937, human monocytes and HMDM cells.

U937 cells (0.5×10^6 cells/mL), human monocytes (1×10^6 cells/mL) or HMDM cells (1×10^6 cells/mL) were pre-incubated with 1.5 µM Fluo-3 AM for 40 minutes, followed by treatment with 0.5 µM and 2 µM Tg for 30 minutes before incubation with LC_{50} concentration of oxLDL (0.5, 1.0, 1.5 mg/mL for U937, human monocytes and HMDM cells, respectively) at 37°C in RPMI1640 with no phenol red for 3 hours. A), B) and C) show the mean fluorescence intensity measured by flow cytometry in U937 cells, human monocytes and HMDM cells, respectively (10,000 events were collected in the gated area for analysis). Results are displayed as mean fluorescence ± SEM of triplicates from a representative experiment. Significance (two-way ANOVA, Sidak's multiple test) is indicated from: control vs oxLDL, #, $p<0.05$, ##, $p<0.01$; control vs Tg, ^, $p<0.05$, ^^, $p<0.01$; oxLDL vs Tg with oxLDL, *, $p<0.05$, **, $p<0.01$, ***, $p<0.001$.

Intracellular ROS was determined in cells incubated with dantrolene. U937 cells incubated with dantrolene alone had a higher ROS level compared to cell only control. In response to oxLDL, a higher ROS level was also observed in cells incubated with dantrolene (**Figure 5.29 A**). Almost similar trend of results were seen in human monocytes treated with dantrolene alone and with the presence of oxLDL (**Figure 5.29 B**). There was also no protection against oxLDL-induced ROS generation observed in HMDM cells pre-treated with dantrolene (**Figure 5.29 C**).

The similar pattern of in DHE fluorescence increase was observed in thapsigargin treated U937, human monocytes and HMDM cells (**Figure 5.30 A, B** and **C**). Cells treated with thapsigargin exhibited greater DHE fluorescence compared to cell only control. Likewise, in response to oxLDL, thapsigargin treated cells also generated higher DHE fluorescence compared to oxLDL only treated cells. These results showed the relation between Ca^{2+} and ROS whereby the increase in intracellular Ca^{2+} levels correlates with the increase in intracellular ROS production but this is not universal to all types of cells.

A) U937 cells **B) Human monocytes** **C) HMDM cells**

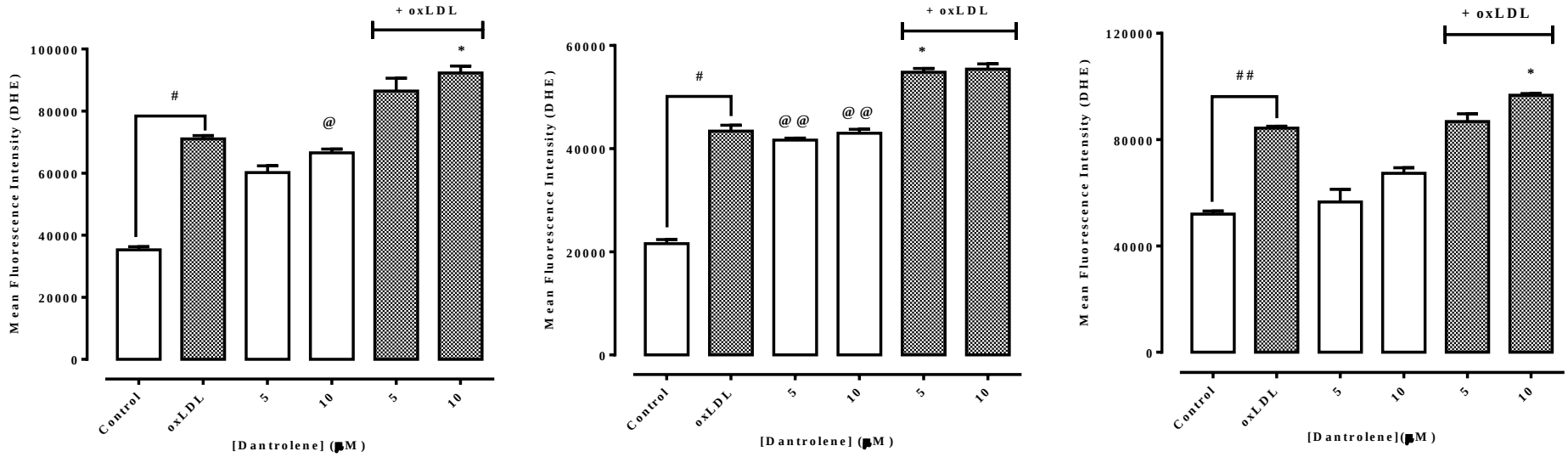

Figure 5.29: Effect of dantrolene (Dan) and oxLDL on intracellular ROS levels in U937, human monocytes and HMDM cells.

U937 cells (0.5×10^6 cells/mL), human monocytes (1×10^6 cells/mL) or HMDM cells (1×10^6 cells/mL) were incubated with 5 µM and 10 µM Dan for 30 minutes before incubation with LC_{50} concentration of oxLDL (0.5, 1.0, 1.5 mg/mL for U937, human monocytes and HMDM cells, respectively) at 37°C in RPMI1640 no phenol red for 6 hours. A), B) and C) show the mean fluorescence intensity measured by flow cytometry in U937 cells, human monocytes and HMDM cells, respectively. 10,000 events were collected in the gated area for analysis. Results are displayed as mean fluorescence ± SEM of triplicates from a representative experiment. Significance (two-way ANOVA, Sidak's test) is indicated from the cell only control, *, $p<0.05$, **, $p<0.01$, ***, $p<0.001$.

A) U937 cells **B) Human monocytes** **C) HMDM cells**

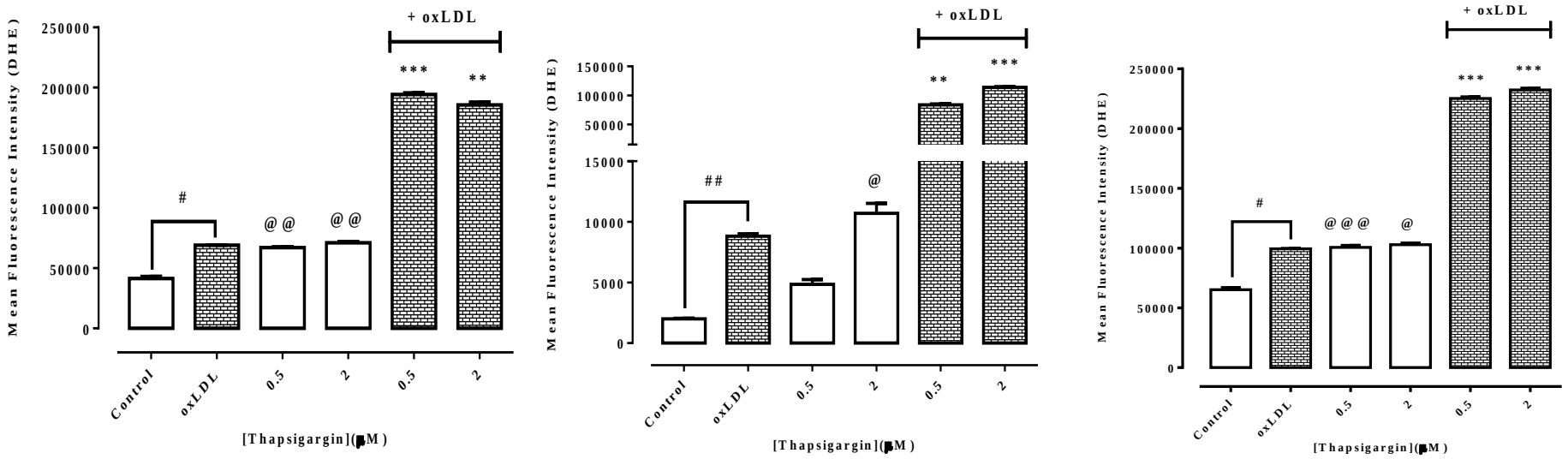

Figure 5.30: Effect of thapsigargin (Tg) and oxLDL on intracellular ROS levels in U937, human monocytes and HMDM cells.

U937 cells (0.5×10^6 cells/mL), human monocytes (1×10^6 cells/mL) or HMDM cells (1×10^6 cells/mL) were incubated with 0.5 µM and 2 µM Tg for 30 minutes before incubation with LC_{50} concentration of oxLDL (0.5, 1.0, 1.5 mg/mL for U937, human monocytes and HMDM cells, respectively) at 37°C in RPMI1640 no phenol red for 6 hours. A), B) and C) show the mean fluorescence intensity measured by flow cytometry in U937 cells, human monocytes and HMDM cells, respectively. 10,000 events were collected in the gated area for analysis. Results are displayed as mean fluorescence ± SEM of triplicates from a representative experiment. Significance (two-way ANOVA, Sidak's test) is indicated from the cell only control, *, $p<0.05$, **, $p<0.01$, ***, $p<0.001$.

With regards to cell viability, oxLDL caused approximately 50% of cell viability loss (PI negative) in U937 cells. In the presence of oxLDL, approximately the same percentage of cell viability loss (PI negative) has been observed in cells pre-treated with dantrolene (**Figure 5.31**). OxLDL caused cell viability loss by 45% in human monocytes yet dantrolene has no protective effect on oxLDL-induced cell death (**Figure 5.32**). Likewise, dantrolene was also not protective to HMDM cells against oxLDL-mediated cytotoxicity (**Figure 5.33**).

Additionally, results showed that cell viability loss caused by oxLDL toxicity was not restored by thapsigargin. For U937 cells, an average of 48% of cell viability loss (PI negative cells) was observed in oxLDL treated cells. In the presence of oxLDL, there was a significant drop in cell viability percentage (PI negative cells) of cells pre-treated with thapsigargin. Similarly, this trend was also observed in human monocytes pre-treated with thapsigargin. Moreover, in thapsigargin treated cells, oxLDL had caused a further decrease in cell viability compared to control cells for both U937 cells and human monocytes (**Figure 5.34** and **5.35**). It was also noted that 2 µM thapsigargin alone had caused a significant loss in cell viability for human monocytes. In HMDM cells, thapsigargin was also not protective against oxLDL-induced cell death. The percentage of cell viability loss in oxLDL-treated cells was similar to thapsigargin pre-treated cells in the presence of oxLDL (**Figure 5.36**).

A)

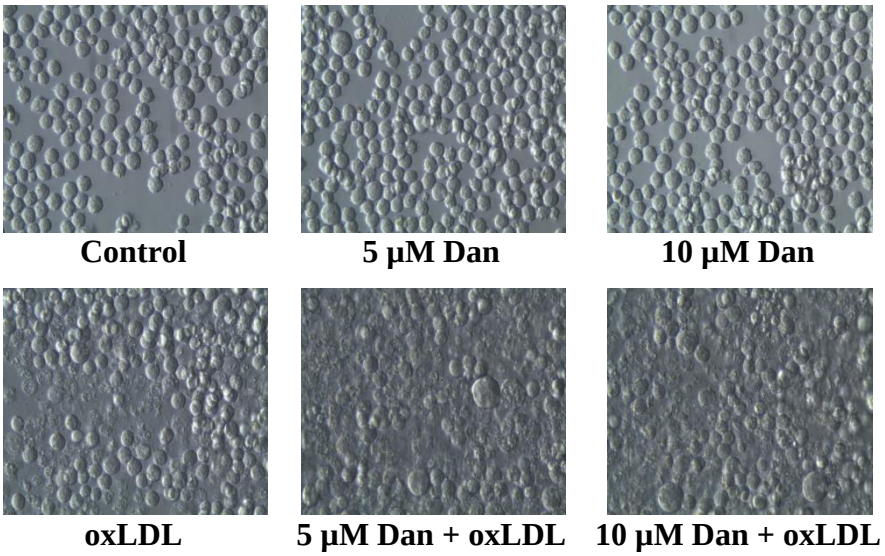

B)

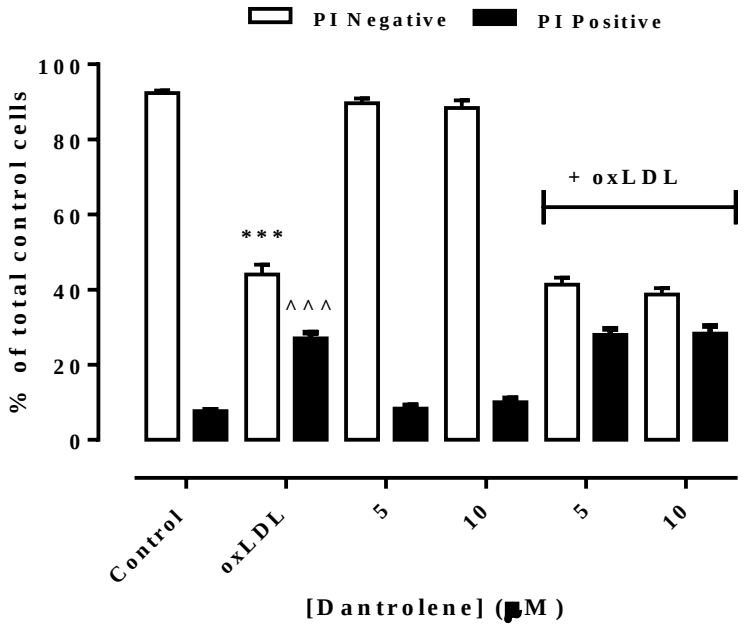

Figure 5.31: Effects of dantrolene (Dan) and oxLDL on U937 cell viability.

U937 cells (0.5×10^6 cells/mL) were treated different concentrations of dantrolene for 30 minutes followed by addition of LC_{50} concentration (0.5 mg/mL) of oxLDL and incubated at 37°C in non-phenol red RPMI-1640 for 24 hours. A) Cells were viewed *in situ* in tissue culture wells using an inverted microscope (400x magnification) after 24 hours. Images were taken using a Leica C-Mount camera and processed using Leica Application Suite software. B) Cell viability was measured using PI-flow cytometry assay after 24 hours. Data are expressed as a percentage of the cell only control. Results are displayed as mean ± SEM of triplicates from a representative experiment. Significance (two-way ANOVA, Sidak's multiple test) is indicated from: cell only control vs oxLDL, ***, $p<0.001$ (PI negative cells), ^^^, $p<0.001$ (PI positive cells).

A)

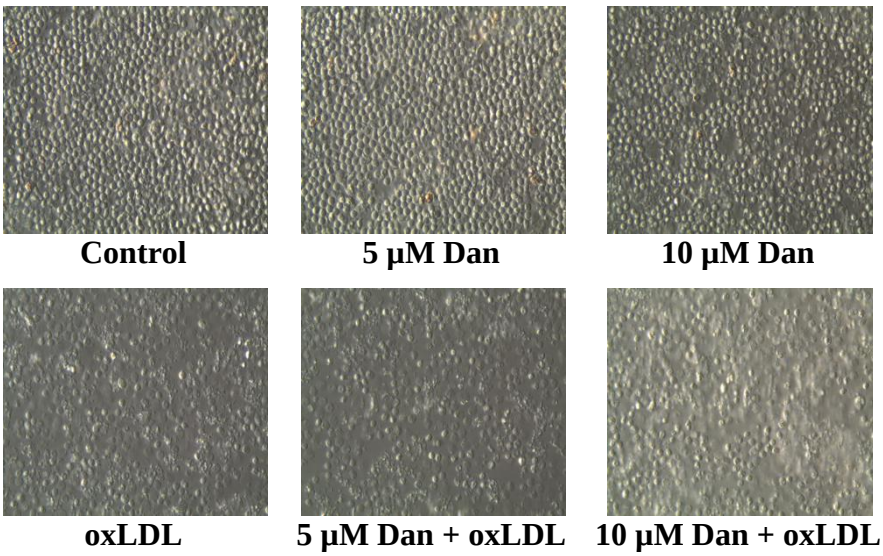

B)

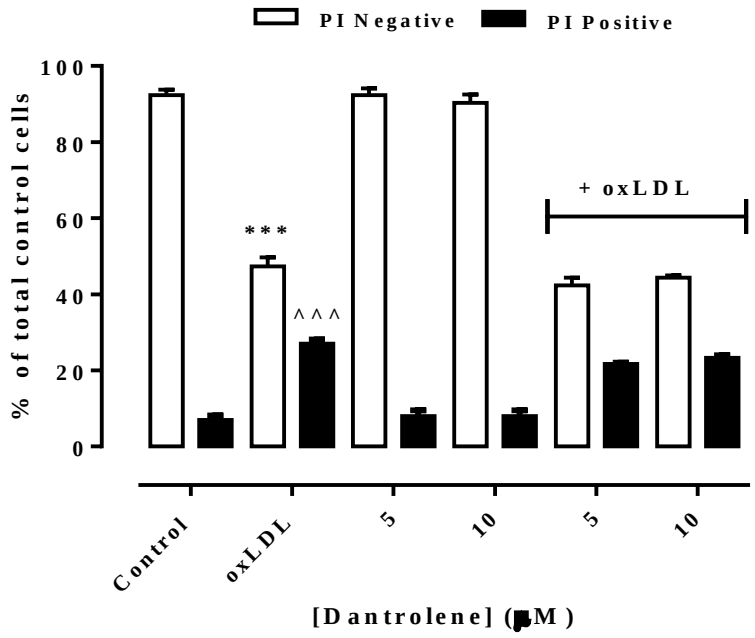

Figure 5.32: Effect of dantrolene (Dan) and oxLDL on human monocytes viability.

Human monocytes (1×10^6 cells/mL) were treated with different concentrations of dantrolene for 30 minutes followed by addition of LC_{50} concentration (1 mg/mL) of oxLDL and incubated at 37°C in non-phenol red RPMI-1640 for 24 hours.A) Cells were viewed *in situ* in tissue culture wells using an inverted microscope (400x magnification) after 24 hours. Images were taken using a Leica C-Mount camera and processed using Leica Application Suite software. B) Cell viability was measured using PI-flow cytometry assay after 24 hours. Data are expressed as a percentage of the cell only control. Results are displayed as mean ± SEM of triplicates from a representative experiment. Significance (two-way ANOVA, Sidak's multiple test) is indicated from: cell only control vs oxLDL, ***, $p<0.001$ (PI negative cells), ^^^, $p<0.001$ (PI positive cells).

A)

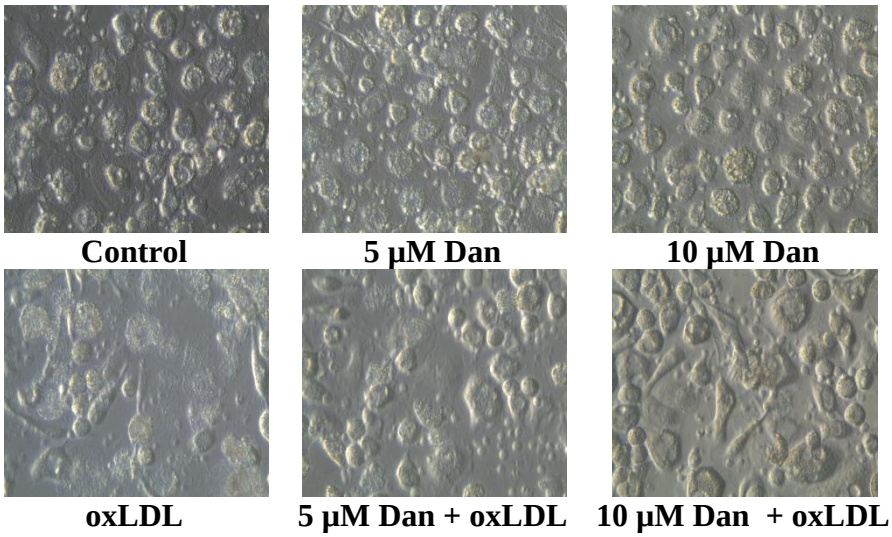

B)

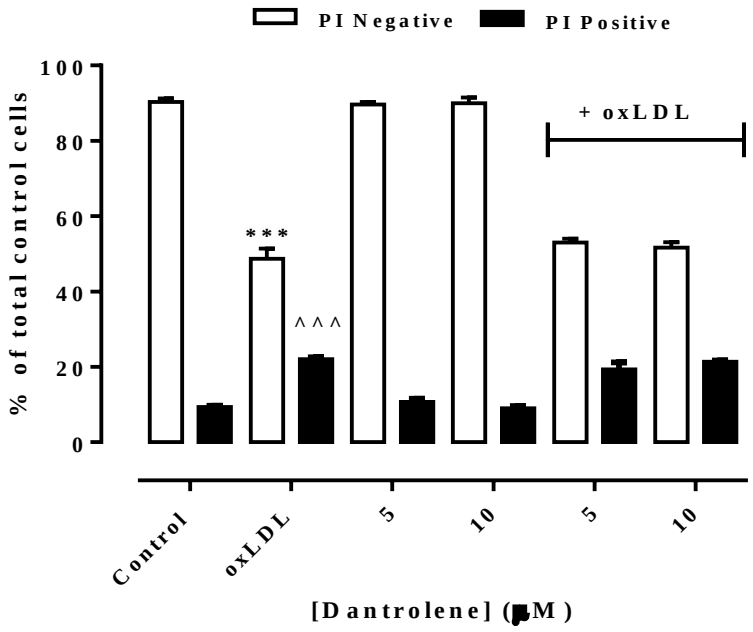

Figure 5.33: Effect of dantrolene (Dan) and oxLDL on HMDM cell viability.

HMDM cells (1×10^6 cells/mL) were treated with different concentrations of dantrolene for 30 minutes followed by addition of LC_{50} concentration (1.5 mg/mL) of oxLDL and incubated at 37°C in non-phenol red RPMI-1640 for 24 hours.A) Cells were viewed *in situ* in tissue culture wells using an inverted microscope (400x magnification) after 24 hours. Images were taken using a Leica C-Mount camera and processed using Leica Application Suite software. B) Cell viability was measured using PI-flow cytometry assay after 24 hours. Data are expressed as a percentage of the cell only control. Results are displayed as mean ± SEM of triplicates from a representative experiment. Significance (two-way ANOVA, Sidak's multiple test) is indicated from: cell only control vs oxLDL, ***, $p<0.001$ (PI negative cells), ^^^, $p<0.001$ (PI positive cells).

A)

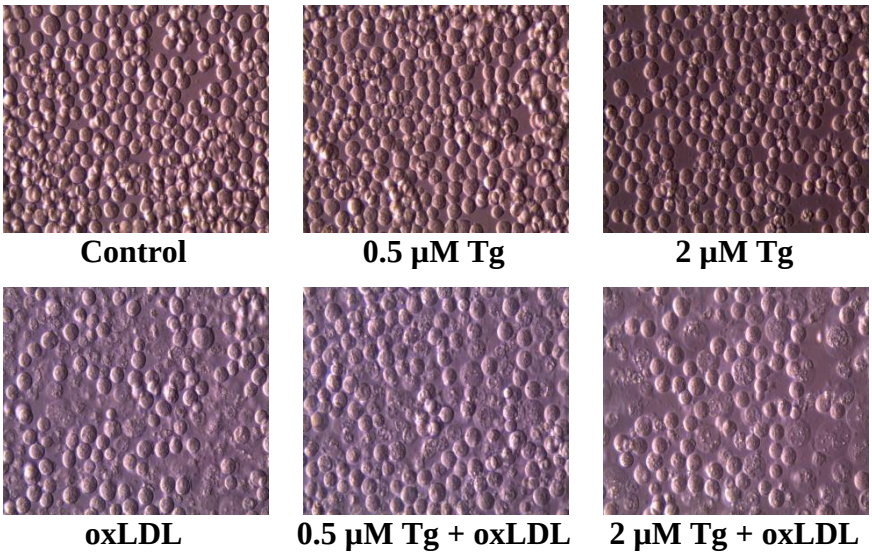

B)

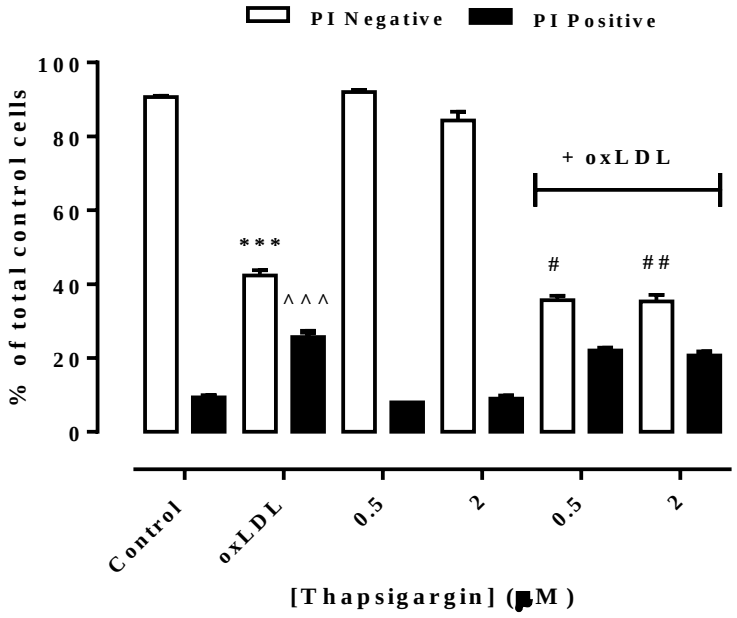

Figure 5.34: Effect of thapsigargin (Tg) and oxLDL on U937 cell viability.

U937 cells (0.5×10^6 cells/mL) were treated with different concentrations of thapsigargin for 30 minutes followed by addition of LC_{50} concentration (0.5 mg/mL) of oxLDL and incubated at 37°C in non-phenol red RPMI-1640 for 24 hours. A) Cells were viewed *in situ* in tissue culture wells using an inverted microscope (400x magnification) after 24 hours. Images were taken using a Leica C-Mount camera and processed using Leica Application Suite software. B) Cell viability was measured using PI-flow cytometry assay after 24 hours. Data are expressed as a percentage of the cell only control. Results are displayed as mean ± SEM of triplicates from a representative experiment. Significance (two-way ANOVA, Sidak's multiple test) is indicated from: cell only control vs oxLDL, ***, $p<0.001$ (PI negative cells), ^^^, $p<0.001$ (PI positive cells); oxLDL vs 0.5 µM Tg + oxLDL, #, $p<0.05$ (PI negative cells) and oxLDL vs 2 µM Tg + oxLDL, ##, $p<0.01$ (PI negative cells).

A)

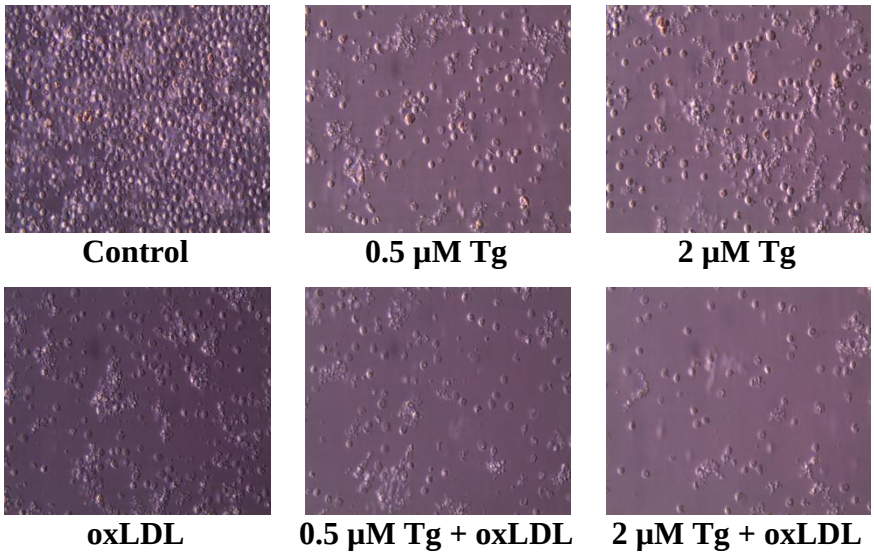

B)

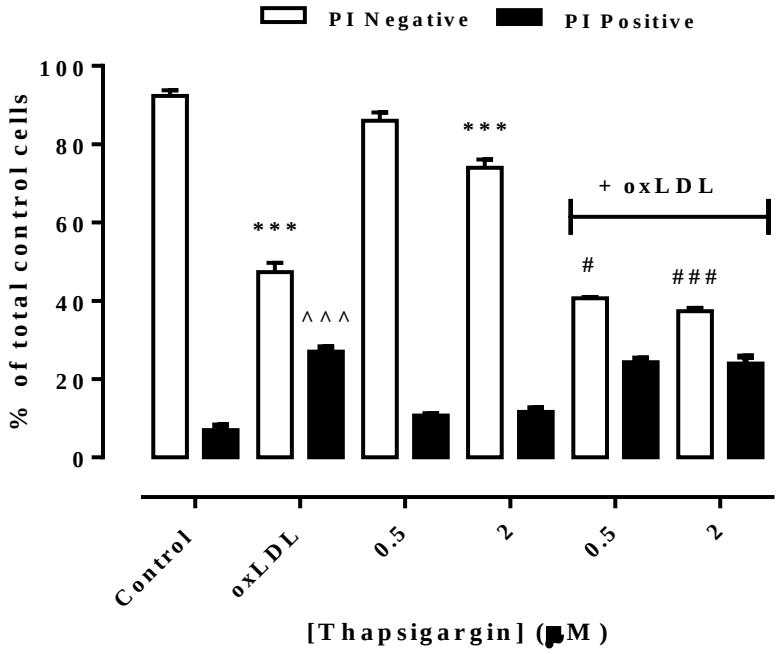

Figure 5.35: Effect of thapsigargin (Tg) and oxLDL on human monocytes viability.

Human monocytes (1×10^6 cells/mL) were treated with different concentrations of thapsigargin for 30 minutes followed by addition of LC_{50} concentration (1 mg/mL) of oxLDL and incubated at 37°C in non-phenol red RPMI-1640 for 24 hours. A) Cells were viewed *in situ* in tissue culture wells using an inverted microscope (400x magnification) after 24 hours. Images were taken using a Leica C-Mount camera and processed using Leica Application Suite software. B) Cell viability was measured using PI-flow cytometry assay after 24 hours. Data are expressed as a percentage of the cell only control. Results are displayed as mean ± SEM of triplicates from a representative experiment. Significance (two-way ANOVA, Sidak's multiple test) is indicated from: cell only control vs oxLDL, ***, $p<0.001$ (PI negative cells), ^^^, $p<0.001$ (PI positive cells); oxLDL vs 0.5 µM Tg + oxLDL, #, $p<0.05$ (PI negative cells) and oxLDL vs 2 µM Tg + oxLDL, ##, $p<0.01$ (PI negative cells).

A)

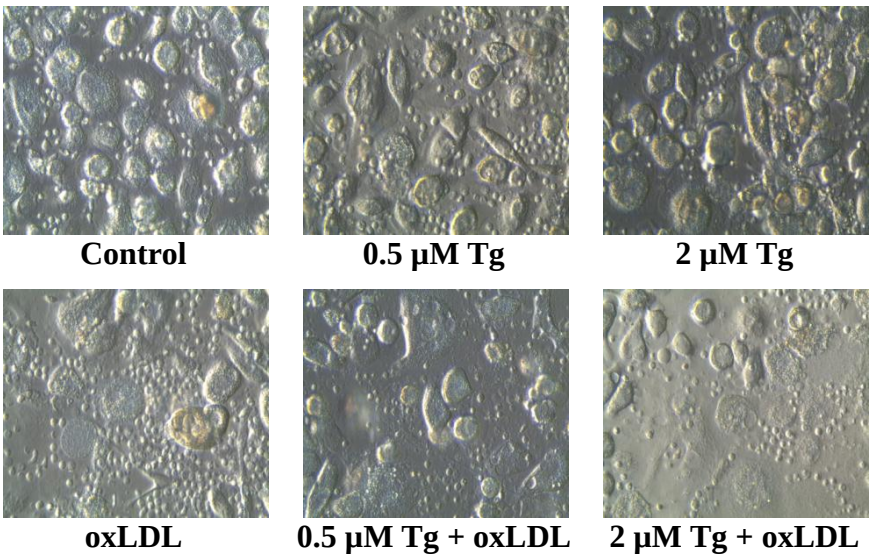

B)

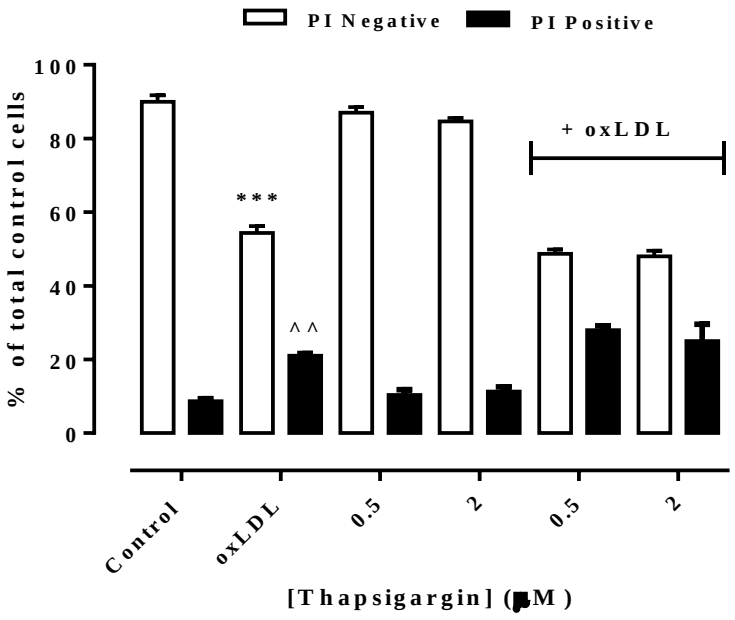

Figure 5.36: Effects of thapsigargin (Tg) and oxLDL on HMDM cell viability.

HMDM cells (1×10^6 cells/mL) were treated with different concentrations of thapsigargin for 30 minutes followed by addition of LC_{50} concentration (1.5 mg/mL) of oxLDL and incubated at 37°C in non-phenol red RPMI-1640 for 24 hours.A) Cells were viewed *in situ* in tissue culture wells using an inverted microscope (400x magnification) after 24 hours. Images were taken using a Leica C-Mount camera and processed using Leica Application Suite software. B) Cell viability was measured using PI-flow cytometry assay after 24 hours. Data are expressed as a percentage of the cell only control. Results are displayed as mean ± SEM of triplicates from a representative experiment. Significance (two-way ANOVA, Sidak's multiple test) is indicated from: cell only control vs oxLDL, ***, $p<0.001$ (PI negative cells), ^^^, $p<0.001$ (PI positive cells).

Next, the effect of Ca^{2+} chelators i.e. BAPTA-AM and EGTA were also examined. BAPTA-AM is a cell permeable Ca^{2+} chelator which is widely used as the intracellular Ca^{2+} 'sponge'. In U937 cells, pre-incubation with BAPTA-AM reduced intracellular Ca^{2+} level by 50% in the presence of oxLDL compared to oxLDL treated cells (**Figure 5.37 A**). Likewise, in response to oxLDL, human monocytes and HMDM cells pre-treated with BAPTA-AM had a decrease in intracellular Ca^{2+} by almost $^{2}/_{3}$ of that induced by oxLDL (**Figure 5.37 B** and **C**). This indicates that while BAPTA-AM has chelated the intracellular Ca^{2+} yet extracellular Ca^{2+} influx still occur in response to oxLDL.

Incubation with EGTA resulted in the decrease of intracellular Ca^{2+} in all cell types. Intracellular Ca^{2+} levels in cells treated with EGTA was lower compared to control only cells. With the presence of oxLDL, lower intracellular Ca^{2+} levels were observed in EGTA treated cells compared to oxLDL treated cells (**Figure 5.38 A, B** and **C**). This shows that Ca^{2+} chelation with EGTA has completely blocked intracellular Ca^{2+} rise induced by oxLDL.

Intracellular ROS was measured to examine the effect of Ca^{2+} chelation with EGTA. Results showed a significant reduction of DHE fluorescence which indicates a decrease in intracellular ROS. However, intracellular ROS generation was not prevented or reduced to the same degree as intracellular Ca^{2+}. EGTA could not suppress intracellular ROS production to the basal level compared to control cells (**Figure 5.39 A, B** and **C**). Therefore, these results suggest that other Ca^{2+}-independent signalling pathway/mechanism might be involved in generating ROS in response to oxLDL insult. This observation is in agreement with the finding of Sun *et al.* (2013) in their research using geldanamycin-treated 9L rat brain tumour cells.

A) U937 cells **B) Human monocytes** **C) HMDM cells**

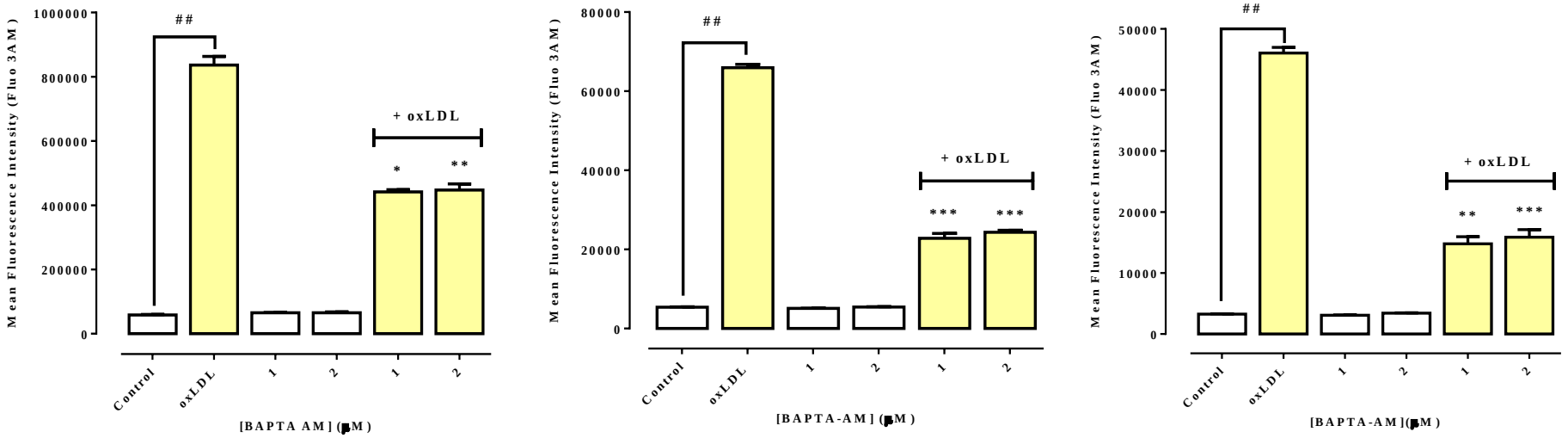

Figure 5.37: Effect of BAPTA-AM and oxLDL on intracellular calcium levels in U937, human monocytes and HMDM cells.

U937 cells (0.5×10^6 cells/mL), human monocytes (1×10^6 cells/mL) or HMDM cells (1×10^6 cells/mL) were pre-incubated with 1.5 µM Fluo-3 AM for 40 minutes, followed by treatment with 5 µM and 10 µM BAPTA-AM for 30 minutes before incubation with LC_{50} concentration of oxLDL (0.5, 1.0, 1.5 mg/mL for U937, human monocytes and HMDM cells, respectively) at 37°C in RPMI1640 with no phenol red for 3 hours. A), B) and C) show the mean fluorescence intensity measured by flow cytometry in U937 cells, human monocytes and HMDM cells, respectively (10,000 events were collected in the gated area for analysis). Results are displayed as mean fluorescence ± SEM of triplicates from a representative experiment. Significance (two-way ANOVA, Sidak's multiple test) is indicated from: control vs oxLDL, ##, $p<0.01$; oxLDL vs BAPTA AM with oxLDL, *, $p<0.05$, **, $p<0.01$, ***, $p<0.001$.

A) U937 cells **B) Human monocytes** **C) HMDM cells**

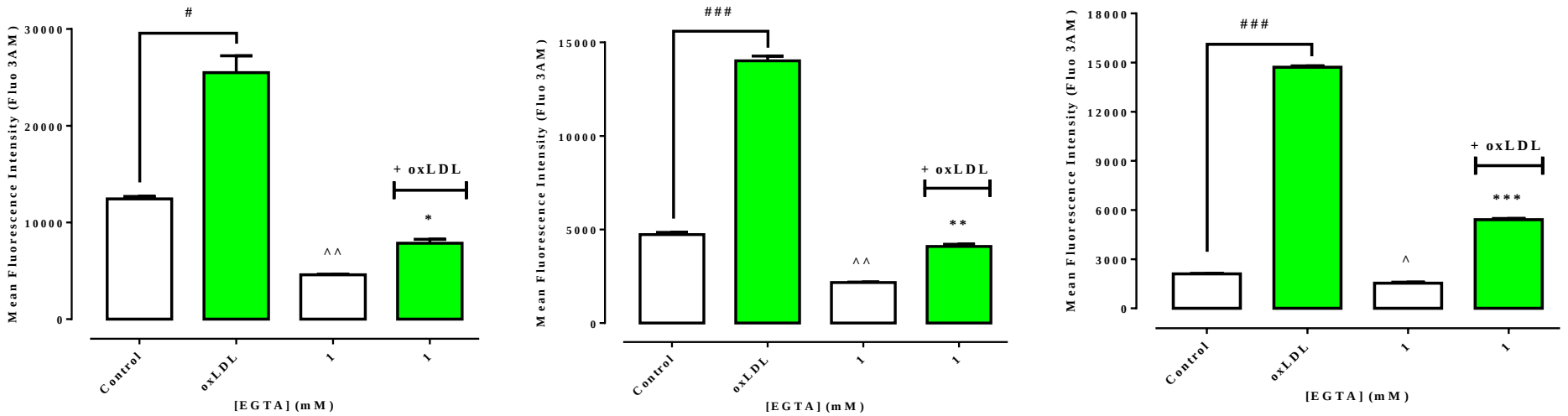

Figure 5.38: Effect of EGTA and oxLDL on intracellular calcium levels in U937, human monocytes and HMDM cells.

U937 cells (0.5×10^6 cells/mL), human monocytes (1×10^6 cells/mL) or HMDM cells (1×10^6 cells/mL) were pre-incubated with 1.5 µM Fluo-3 AM for 40 minutes, followed by treatment with 1 mM EGTA for 30 minutes before incubation with LC_{50} concentration of oxLDL (0.5, 1.0, 1.5 mg/mL for U937, human monocytes and HMDM cells, respectively) at 37°C in RPMI1640 with no phenol red for 3 hours. A), B) and C) show the mean fluorescence intensity measured by flow cytometry in U937 cells, human monocytes and HMDM cells, respectively (10,000 events were collected in the gated area for analysis). Results are displayed as mean fluorescence ± SEM of triplicates from a representative experiment. Significance (two-way ANOVA, Sidak's multiple test) is indicated from: control vs oxLDL, #, $p<0.05$, ###, $p<0.01$; control vs EGTA, ^, $p<0.05$, ^^, $p<0.01$; oxLDL vs EGTA with oxLDL, *, $p<0.05$, **, $p<0.01$, ***, $p<0.001$.

A) U937 cells **B) Human monocytes** **C) HMDM cells**

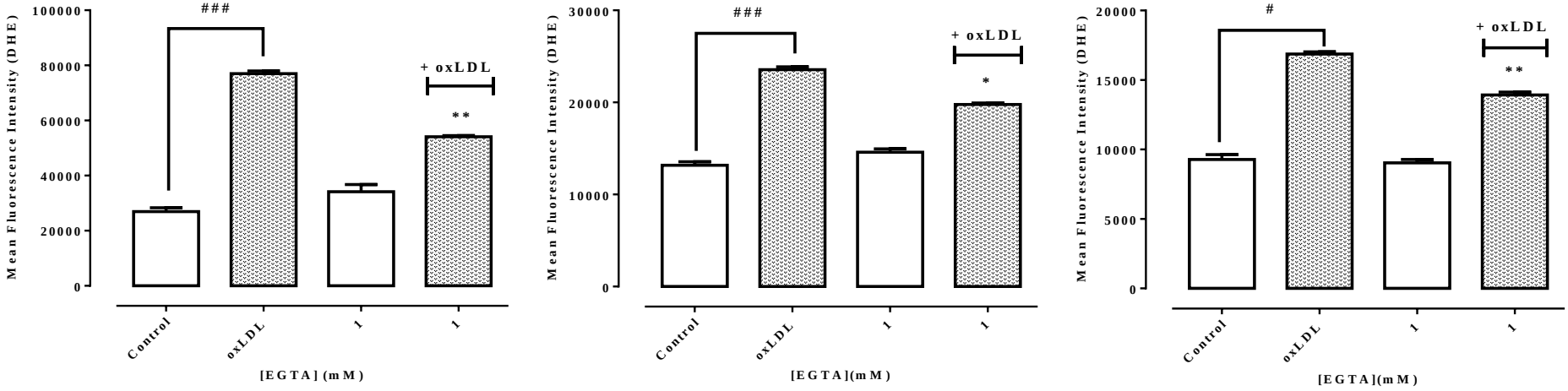

Figure 5.39: Effect of EGTA and oxLDL on intracellular ROS levels in U937, human monocytes and HMDM cells.

U937 cells (0.5×10^6 cells/mL), human monocytes (1×10^6 cells/mL) or HMDM cells (1×10^6 cells/mL) were incubated with 1 mM EGTA for 30 minutes before incubation with LC_{50} concentration of oxLDL (0.5, 1.0, 1.5 mg/mL for U937, human monocytes and HMDM cells, respectively) at 37°C in RPMI1640 no phenol red for 6 hours. A), B) and C) show the mean fluorescence intensity measured by flow cytometry in U937 cells, human monocytes and HMDM cells, respectively. 10,000 events were collected in the gated area for analysis. Results are displayed as mean fluorescence ± SEM of triplicates from a single experiment. Significance (two-way ANOVA, Sidak's test) is indicated from the cell only control, *, $p<0.05$, **, $p<0.01$, ***, $p<0.001$.

Preliminary experiments carried out by incubating BAPTA-AM alone with all three types of cells showed an increase in cell viability loss at high concentrations (5 to 20 µM). Cell viability loss was worsened with the addition of oxLDL. For U937 cells, oxLDL caused cell viability loss (PI negative cells) of close to 50% compared to control. With the addition of oxLDL, the percentage of cell viability loss for BAPTA-AM pre-treated cells was similar to the oxLDL only treated cells (**Figure 5.40**). For human monocytes, oxLDL cytotoxicity resulted in 45% of cell viability loss (PI negative cells) in oxLDL only treated cells compared to control. The percentage of cell viability loss (PI negative cells) was slightly higher but not significant when oxLDL was added to the BAPTA-AM pre-treated cells (**Figure 5.41**). Cell viability loss mediated by oxLDL in HMDM cells was approximately 35% compared to control cells (PI negative cells). Likewise, there was no difference in cell viability loss observed with BAPTA-AM pre-treated cells in the presence of oxLDL compared to oxLDL only treated cells (**Figure 5.42**). These result showed that BAPTA-AM was not protective against oxLDL-induced cell death despite its ability to reduce intracellular Ca^{2+} levels.

EGTA is a general Ca^{2+} chelator used in this study. In the previous study by Yang (2009), 1 mM EGTA has been shown to preserve cell viability of HMDM cells exposed to 150 µM HOCl (by MTT reduction assay). Results from the present study showed that oxLDL cytotoxicity was not prevented with the chelation of Ca^{2+}. Approximately, 40 to 50% of cell viability loss (PI negative cells) has been measured in cells treated with oxLDL compared to control cells (**Figure 5.43, 5.44** and **5.45**). Chelation of Ca^{2+} by EGTA did not convey any protection against oxLDL toxicity as the percentage of cell viability loss remained approximately similar when oxLDL was added to cells pre-treated with EGTA compared to oxLDL only treated cells.

A)

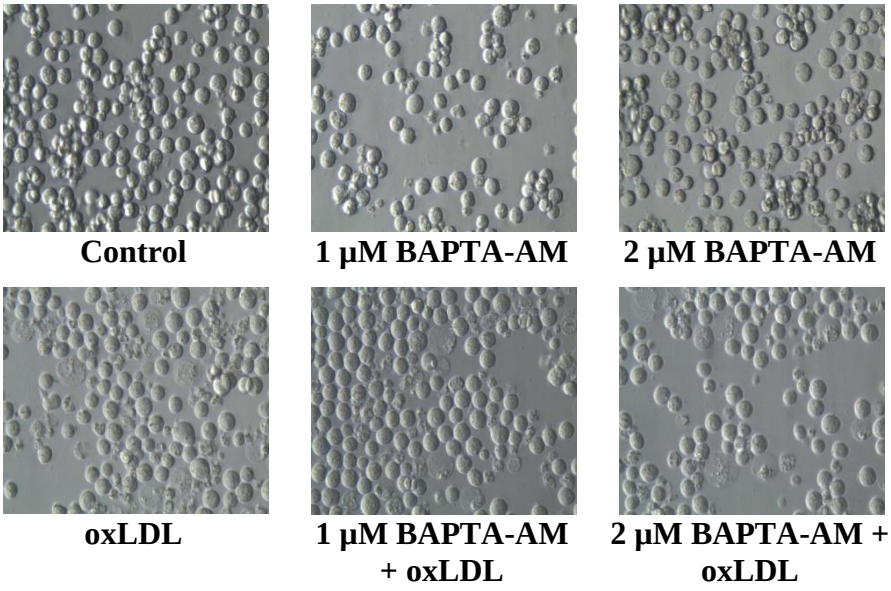

B)

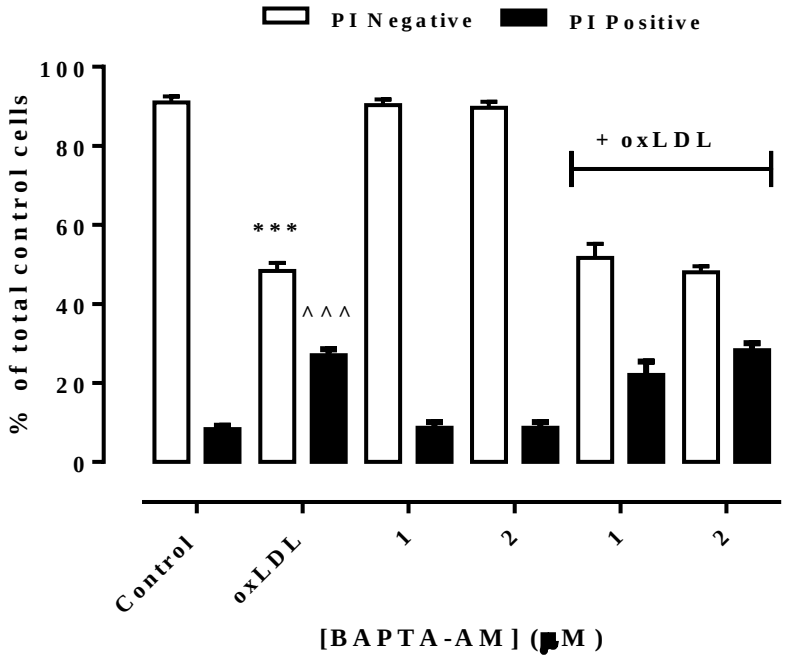

Figure 5.40: Effect of BAPTA-AM and oxLDL on U937 cell viability.

U937 cells (0.5×10^6 cells/mL) were treated with different concentrations of BAPTA-AM for 30 minutes followed by addition of LC_{50} concentration (0.5 mg/mL) of oxLDL and incubated at 37°C in non-phenol red RPMI-1640 for 24 hours. A) Cells were viewed *in situ* in tissue culture wells using an inverted microscope (400x magnification) after 24 hours. Images were taken using a Leica C-Mount camera and processed using Leica Application Suite software. B) Cell viability was measured using PI-flow cytometry assay after 24 hours. Data are expressed as a percentage of the cell only control. Results are displayed as mean ± SEM of triplicates from a representative experiment. Significance (two-way ANOVA, Sidak's multiple test) is indicated from: cell only control vs oxLDL, ***, $p<0.001$ (PI negative cells), ^^^, $p<0.001$ (PI positive cells).

A)

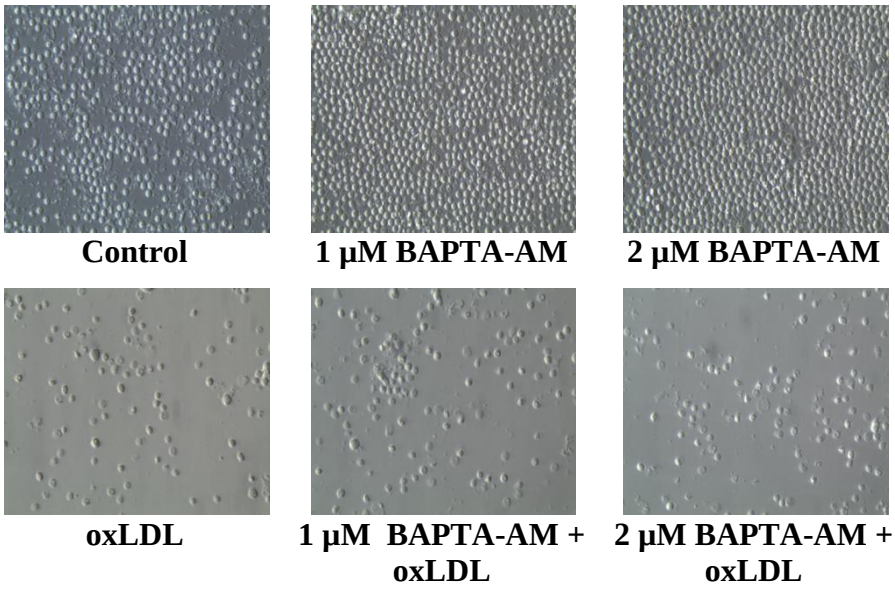

B)

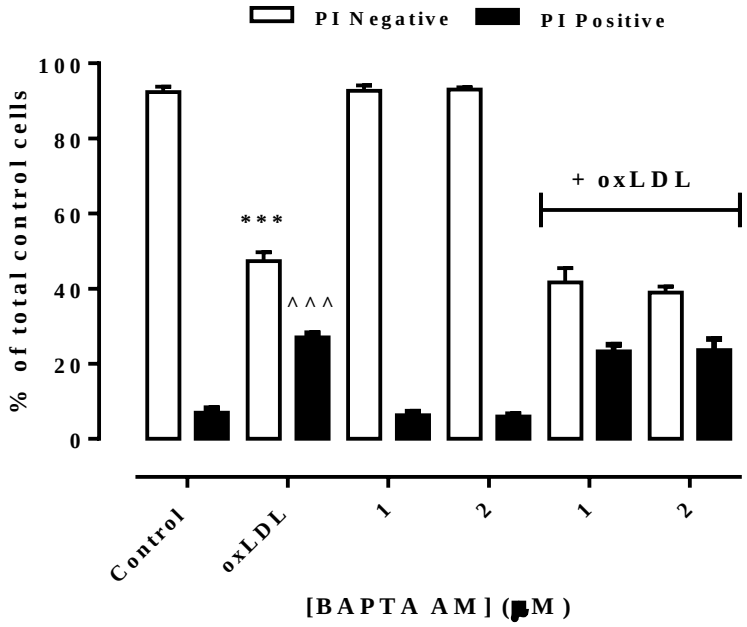

Figure 5.41: Effect of BAPTA-AM and oxLDL on human monocytes viability.

Human monocytes (1×10^6 cells/mL) were treated with different concentrations of BAPTA-AM for 30 minutes followed by addition of LC_{50} concentration (1 mg/mL) of oxLDL and incubated at 37°C in non-phenol red RPMI-1640 for 24 hours. A) Cells were viewed *in situ* in tissue culture wells using an inverted microscope (400x magnification) after 24 hours. Images were taken using a Leica C-Mount camera and processed using Leica Application Suite software. B) Cell viability was measured using PI-flow cytometry assay after 24 hours. Data are expressed as a percentage of the cell only control. Results are displayed as mean ± SEM of triplicates from a representative experiment. Significance (two-way ANOVA, Sidak's multiple test) is indicated from: cell only control vs oxLDL, ***, $p<0.001$ (PI negative cells), ^^^, $p<0.001$ (PI positive cells).

A)

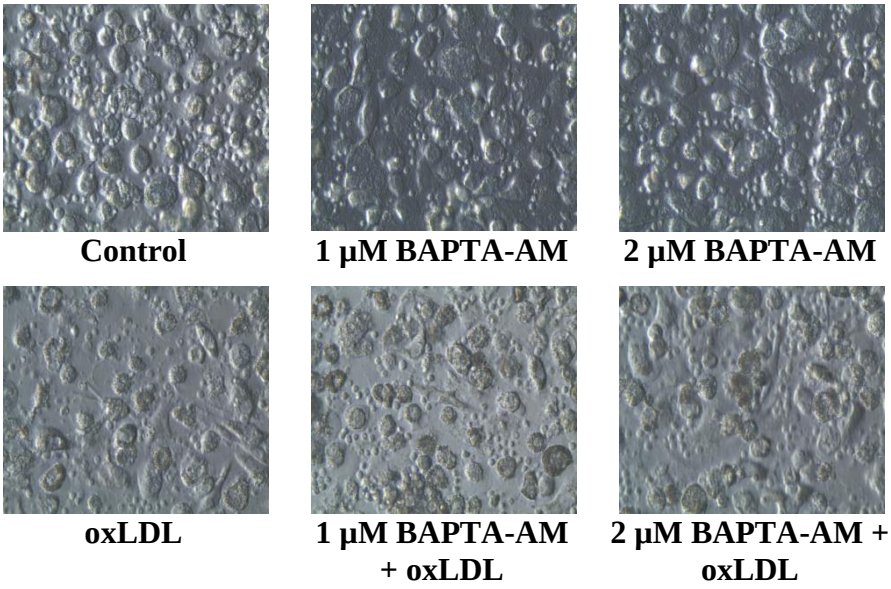

B)

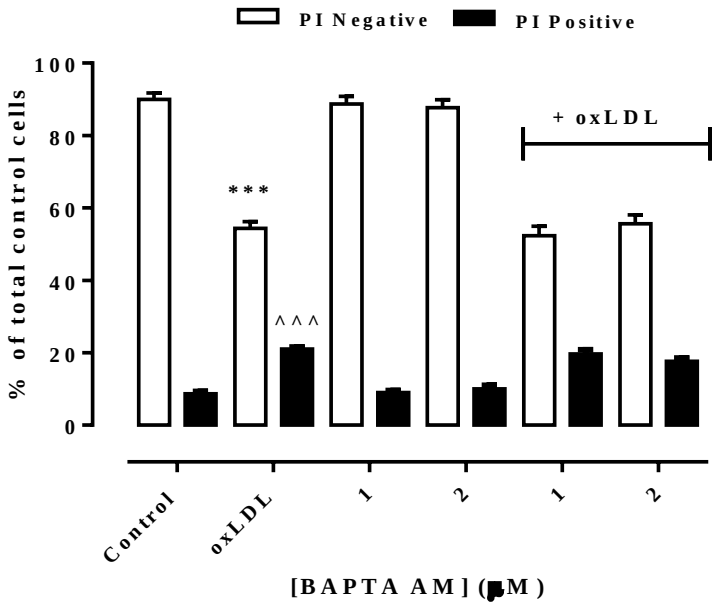

Figure 5.42: Effect of BAPTA-AM and oxLDL on HMDM cell viability.

HMDM cells (1×10^6 cells/mL) were treated with different concentrations of BAPTA-AM for 30 minutes followed by addition of LC_{50} concentration (1.5 mg/mL) of oxLDL and incubated at 37°C in non-phenol red RPMI-1640 for 24 hours. A) Cells were viewed *in situ* in tissue culture wells using an inverted microscope (400x magnification) after 24 hours. Images were taken using a Leica C-Mount camera and processed using Leica Application Suite software. B) Cell viability was measured using PI-flow cytometry assay after 24 hours. Data are expressed as a percentage of the cell only control. Results are displayed as mean ± SEM of triplicates from a representative experiment. Significance (two-way ANOVA, Sidak's multiple test) is indicated from: cell only control vs oxLDL, ***, $p<0.001$ (PI negative cells), ^^^, $p<0.001$ (PI positive cells).

A)

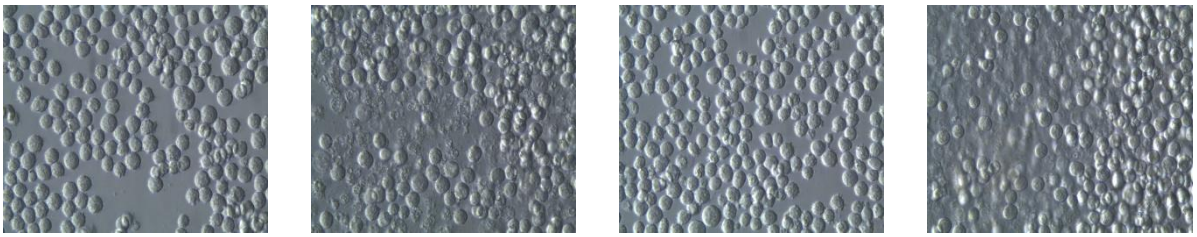

Control | **oxLDL** | **1 mM EGTA** | **1 mM EGTA + oxLDL**

B)

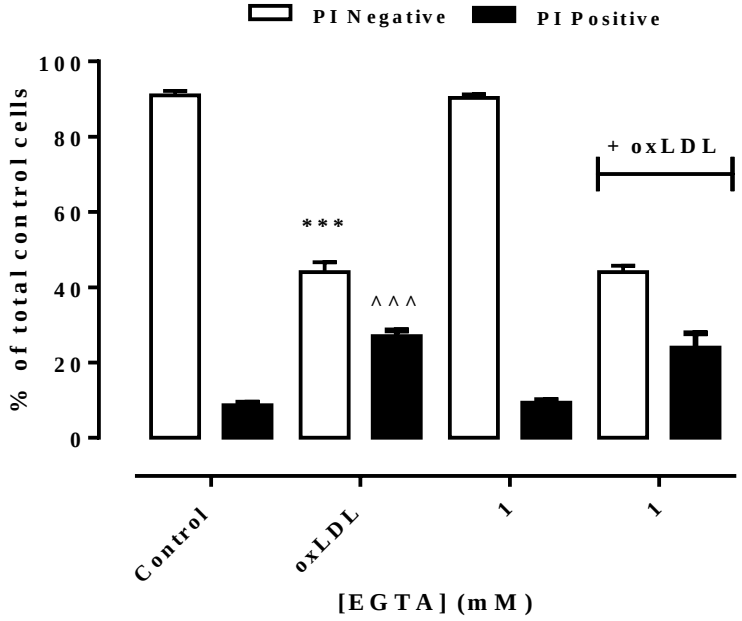

Figure 5.43: Effect of EGTA and oxLDL on U937 cell viability.

U937 cells (0.5×10^6 cells/mL) were treated with 1 mM EGTA for 30 minutes followed by addition of LC_{50} concentration (0.5 mg/mL) of oxLDL and incubated at 37°C in non-phenol red RPMI-1640 for 24 hours. A) Cells were viewed *in situ* in tissue culture wells using an inverted microscope (400x magnification) after 24 hours. Images were taken using a Leica C-Mount camera and processed using Leica Application Suite software. B) Cell viability was measured using PI-flow cytometry assay after 24 hours. Data are expressed as a percentage of the cell only control. Results are displayed as mean ± SEM of triplicates from a representative experiment. Significance (two-way ANOVA, Sidak's multiple test) is indicated from: cell only control vs oxLDL, ***, $p<0.001$ (PI negative cells), ^^^, $p<0.001$ (PI positive cells).

A)

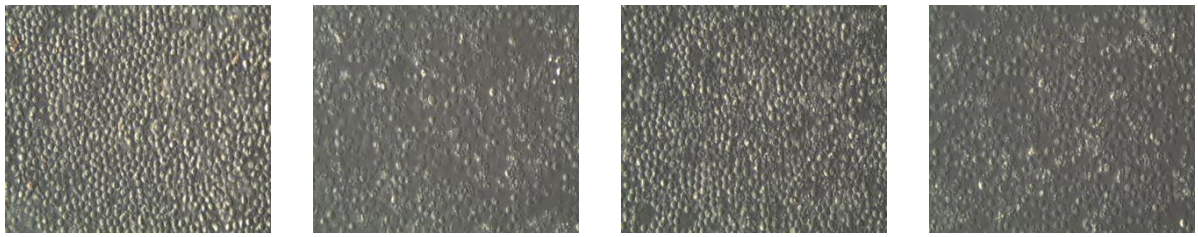

Control **oxLDL** **1 mM EGTA** **1 mM EGTA + oxLDL**

B)

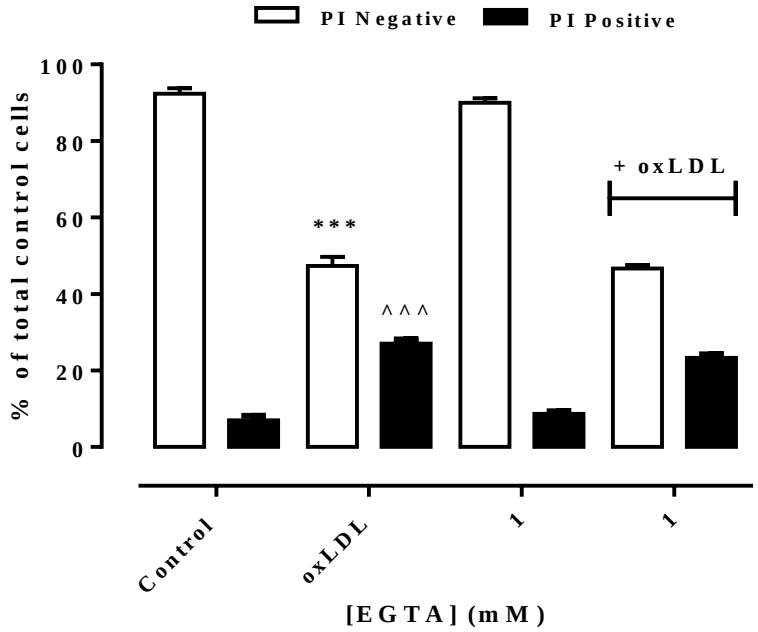

Figure 5.44: Effect of EGTA and oxLDL on human monocytes viability.

Human monocytes (1×106 cells/mL) were treated with 1 mM EGTA for 30 minutes followed by addition of LC50 concentration (1 mg/mL) of oxLDL and incubated at 37oC in non-phenol red RPMI-1640 for 24 hours. A) Cells were viewed in situ in tissue culture wells using an inverted microscope (400x magnification) after 24 hours. Images were taken using a Leica C-Mount camera and processed using Leica Application Suite software. B) Cell viability was measured using PI-flow cytometry assay after 24 hours. Data are expressed as a percentage of the cell only control. Results are displayed as mean ± SEM of triplicates from representative experiment. Significance (two-way ANOVA, Sidak's multiple test) is indicated from: cell only control vs oxLDL, ***, $p<0.001$ (PI negative cells), ^^^, $p<0.001$ (PI positive cells).

A)

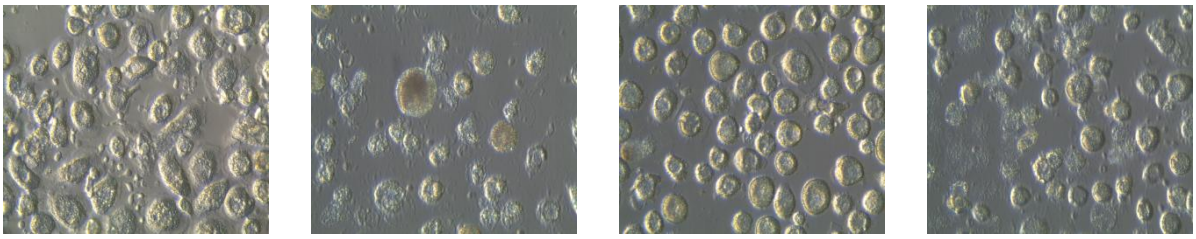

Control **oxLDL** **1 mM EGTA** **1 mM EGTA + oxLDL**

B)

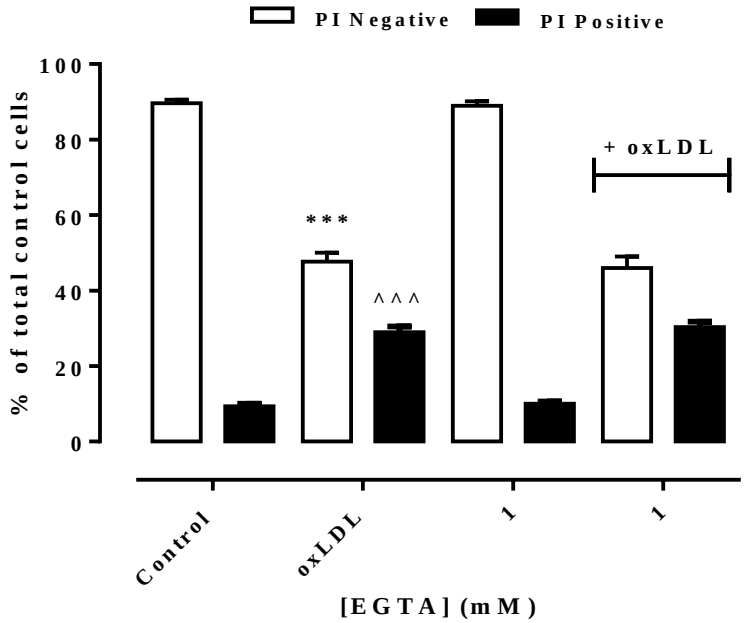

Figure 5.45: Effect of EGTA and oxLDL on HMDMs cell viability.

HMDM cells (1×10^6 cells/mL) were treated with 1 mM EGTA for 30 minutes followed by addition of LC_{50} concentration (1.5 mg/mL) of oxLDL and incubated at 37°C in non-phenol red RPMI-1640 for 24 hours.A) Cells were viewed *in situ* in tissue culture wells using an inverted microscope (400x magnification) after 24 hours. Images were taken using a Leica C-Mount camera and processed using Leica Application Suite software. B) Cell viability was measured using PI-flow cytometry assay after 24 hours. Data are expressed as a percentage of the cell only control. Results are displayed as mean ± SEM of triplicates from a representative experiment. Significance (two-way ANOVA, Sidak's multiple test) is indicated from: cell only control vs oxLDL, ***, $p<0.001$ (PI negative cells), ^^^, $p<0.001$ (PI positive cells).

Effect of oxLDL on MPT activation and mitochondrial membrane potential (ΔΨm)

Studies by Yang (2009) in this lab have showed that HOCl caused the polarisation of mitochondrial membrane potential (ΔΨm) in HMDM cells. The effect is concentration dependent and ΔΨm loss was followed by cell viability loss. To study the effect of oxLDL on mitochondria, cells were tested for ΔΨm loss using tetramethyrhodamine methyl ester (TMRM). TMRM is a potentiometric, cell-permeable fluorescent indicator that accumulates in the highly negatively charged interior of mitochondria. In order to avoid auto-quenching of mitochondrial TMRM, low concentration of TMRM should be used. The fluorescence signal of TMRM can be directly correlated to ΔΨm across the inner mitochondrial membrane (IMM) whereby a loss of ΔΨm causes TMRM to leak from mitochondria resulting in a loss of fluorescence intensity (Joshi & Bakowska, 2011). Results showed that oxLDL caused a time-dependent ΔΨm loss in U937, human monocytes and HMDM cells (**Figure 5.46 A, B** and **C**). This suggests that there may be an interaction between Ca^{2+} and mitochondrial stability.

A) U937 cells **B) Human monocytes** **C) HMDM cells**

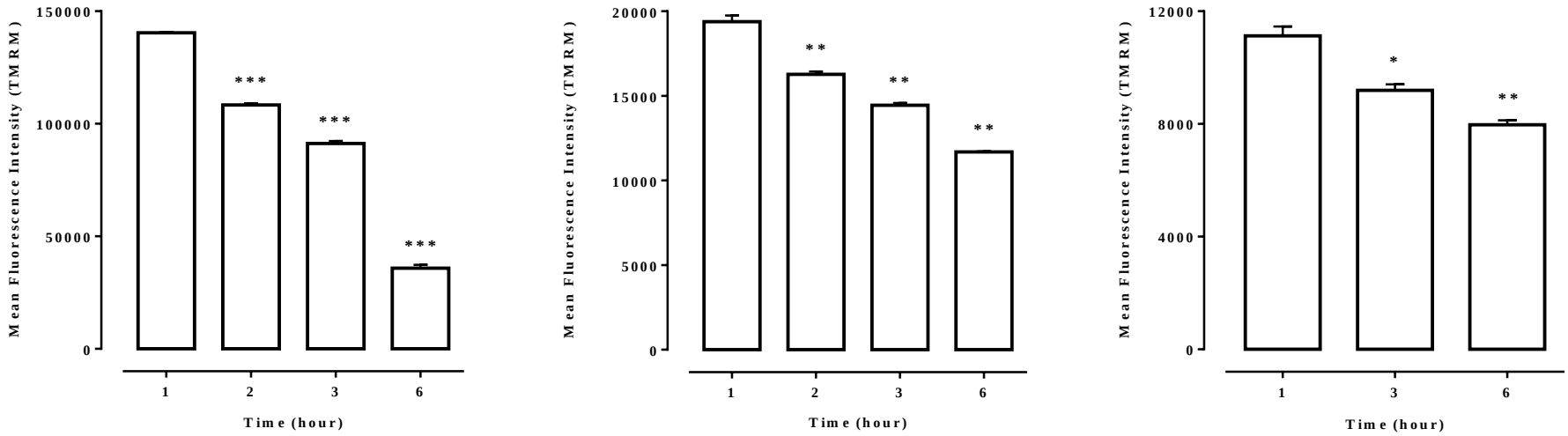

Figure 5.46: Effect of oxLDL on mitochondrial membrane potential in U937, human monocytes and HMDM cells.

U937 cells (0.5×10^6 cells/mL), human monocytes (1×10^6 cells/mL) or HMDM cells (1×10^6 cells/mL) were incubated with 100 nM TMRM for 30 minutes and washed before incubation with LC_{50} concentration of oxLDL (0.5, 1.0, 1.5 mg/mL for U937, human monocytes and HMDM cells, respectively) at 37°C in RPMI1640 no phenol red. Cell samples were taken at the designated time and TMRM fluorescence was measured using flow cytometry. A), B) and C) show the mean fluorescence intensity measured by flow cytometry in U937 cells, human monocytes and HMDM cells, respectively (10,000 events were collected in the gated area for analysis). Results are displayed as mean fluorescence ± SEM of triplicates from a representative experiment. Significance (two-way ANOVA, Sidak's multiple test) is indicated from the 1 hour sample, *, $p<0.05$, **, $p<0.01$, ***, $p<0.001$.

Ruthenium red is a mitochondrial uniporter (MCU) inhibitor. It was used in this study to examine the effects of blocking Ca^{2+} from being taken up into the mitochondria. Results showed statistically significant protection by ruthenium red against oxLDL cytotoxicity in all type of cells (increased in PI negative cells) whereby treatment with oxLDL has resulted in a reduction of cell viability (PI negative cells) of 40 to 50% compared to control cells. Cell viability increased in ruthenium red pre-treated cells was about 20% compared to oxLDL treated cells (**Figure 5.47, 5.48** and **5.49**).

In addition, ruthenium red was able to reduce DHE levels in oxLDL treated cells which indicates a reduction in intracellular ROS generation (**Figure 5.50**). Taken together, these results suggest that blocking Ca^{2+} uptake into the mitochondria could reduce intracellular ROS production which in turn protected cells from oxLDL-induced cell death.

A)

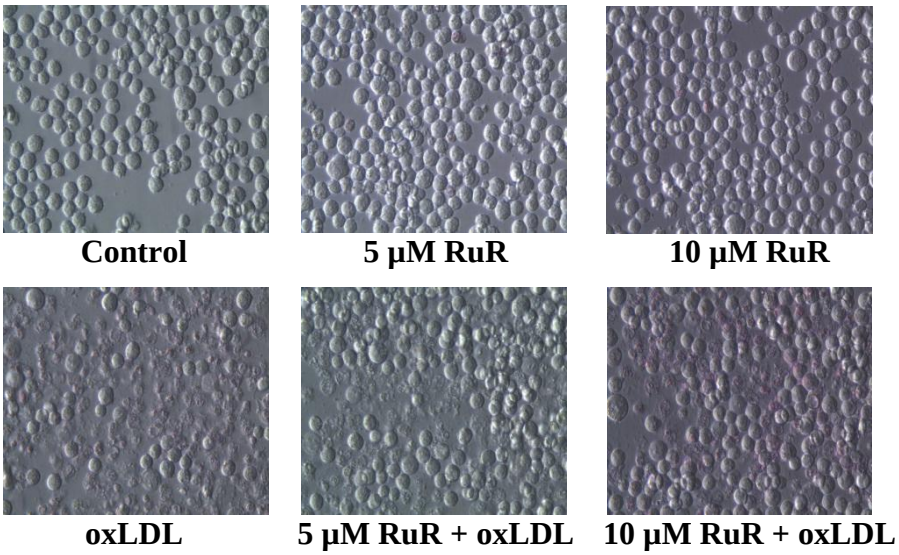

B)

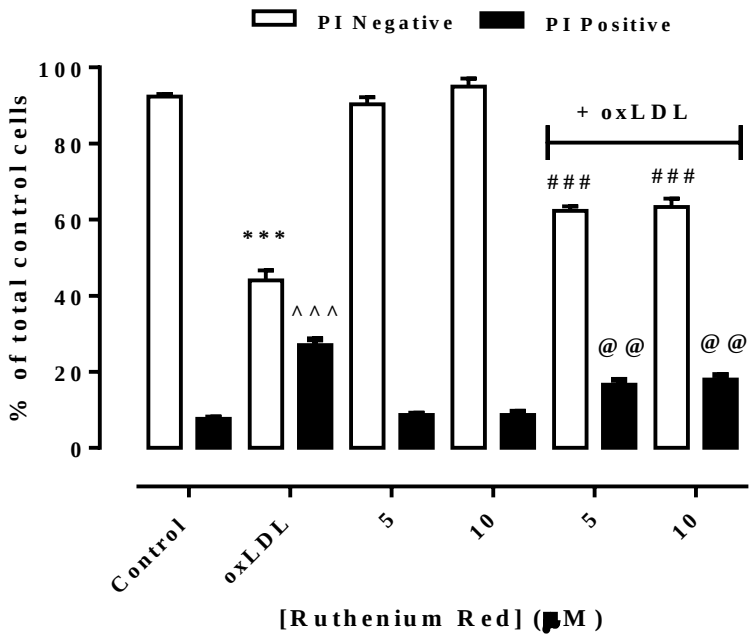

Figure 5.47: Effect of ruthenium red (RuR) and oxLDL on U937 cell viability.

U937 cells (0.5×10^6 cells/mL) were treated with different concentrations of ruthenium red for 30 minutes followed by addition of LC_{50} concentration (0.5 mg/mL) of oxLDL and incubated at 37°C in non-phenol red RPMI-1640 for 24 hours. A) Cells were viewed *in situ* in tissue culture wells using an inverted microscope (400x magnification) after 24 hours. Images were taken using a Leica C-Mount camera and processed using Leica Application Suite software. B) Cell viability was measured using PI-flow cytometry assay after 24 hours. Results are displayed as mean ± SEM of triplicates from a representative experiment. Significance (two-way ANOVA, Sidak's post test) is indicated from: cell only control vs oxLDL, ***, $p<0.001$ (PI negative cells), ^^^, $p<0.001$ (PI positive cells); oxLDL vs 5 µM + oxLDL and oxLDL vs 10 µM RuR + oxLDL, ###, $p<0.001$ (PI negative cells), @@, $p<0.01$ (PI positive cells).

A)

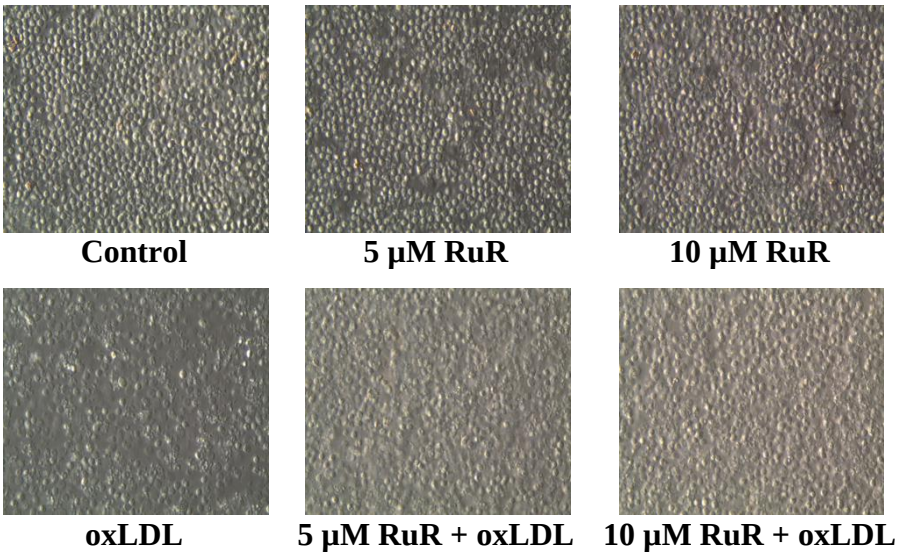

B)

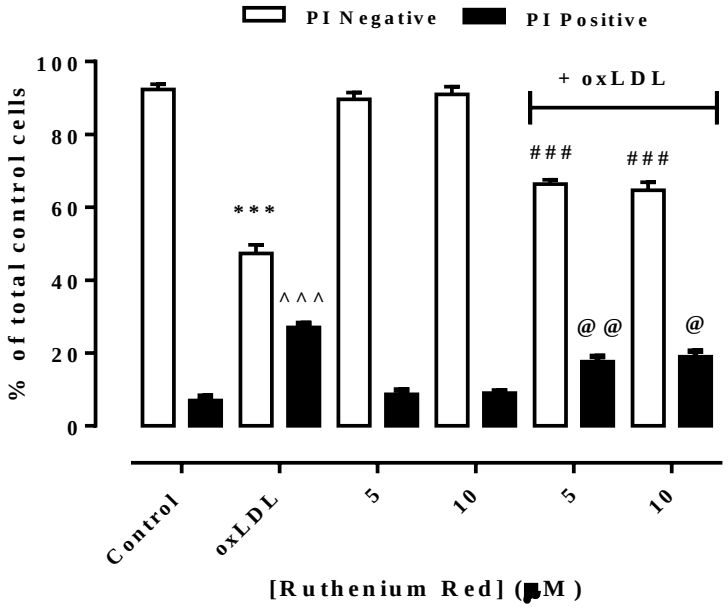

Figure 5.48: Effect of ruthenium red (RuR) and oxLDL on human monocytes viability.

Human monocytes (1×10^6 cells/mL) were treated with different concentrations of ruthenium red for 30 minutes followed by addition of LC_{50} concentration (1 mg/mL) of oxLDL and incubated at 37°C in non-phenol red RPMI-1640 for 24 hours. A) Cells were viewed *in situ* in tissue culture wells using an inverted microscope (400x magnification) after 24 hours. Images were taken using a Leica C-Mount camera and processed using Leica Application Suite software. B) Cell viability was measured using PI-flow cytometry assay after 24 hours. Data are expressed as a percentage of the cell only control. Results are displayed as mean ± SEM of triplicates from a representative experiment. Significance (two-way ANOVA, Sidak's post test) is indicated from: cell only control vs oxLDL, ***, $p<0.001$ (PI negative cells), ^^^, $p<0.001$ (PI positive cells); oxLDL vs 5 µM + oxLDL and oxLDL vs 10 µM RuR + oxLDL, ###, $p<0.001$ (PI negative cells), @, $p<0.05$, @@, $p<0.01$ (PI positive cells).

A)

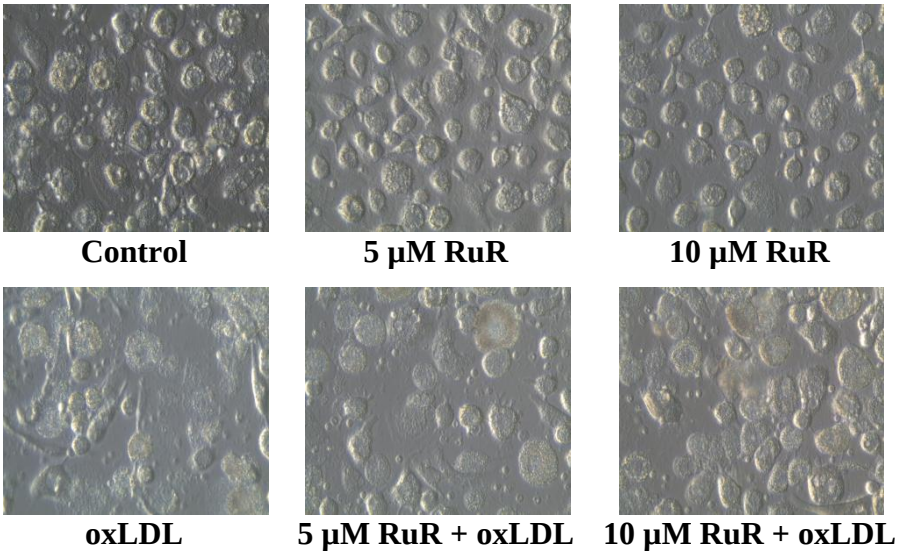

B)

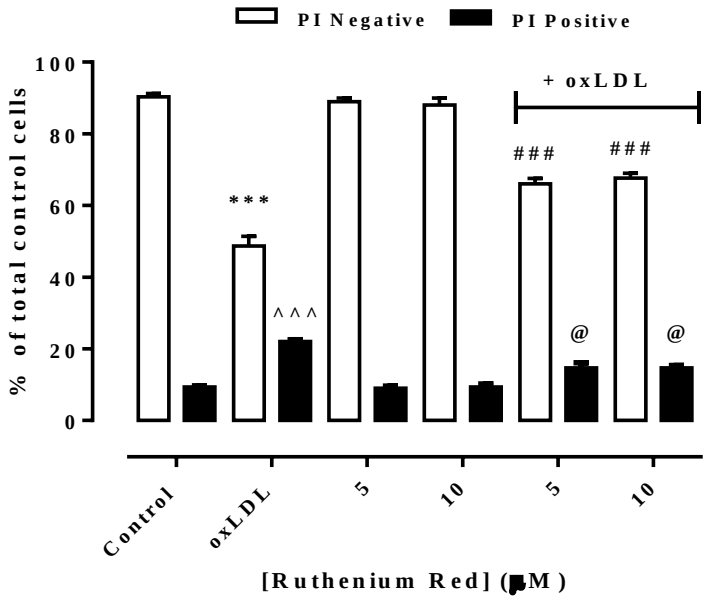

Figure 5.49: Effect of ruthenium red (RuR) and oxLDL on HMDM cell viability.

HMDM cells (1×10^6 cells/mL) were treated with different concentrations of ruthenium red for 30 minutes followed by addition of LC_{50} concentration (1.5 mg/mL) of oxLDL and incubated at 37°C in non-phenol red RPMI-1640 for 24 hours. A) Cells were viewed *in situ* in tissue culture wells using an inverted microscope (400x magnification) after 24 hours. Images were taken using a Leica C-Mount camera and processed using Leica Application Suite software. B) Cell viability was measured using PI-flow cytometry assay after 24 hours. Data are expressed as a percentage of the cell only control. Results are displayed as mean ± SEM of triplicates from a representative experiment. Significance (two-way ANOVA, Sidak's post test) is indicated from: cell only control vs oxLDL, ***, $p<0.001$ (PI negative cells), ^^^, $p<0.001$ (PI positive cells); oxLDL vs 5 µM + oxLDL and oxLDL vs 10 µM RuR + oxLDL, ###, $p<0.001$ (PI negative cells), @, $p<0.05$ (PI positive cells).

A) U937 cells **B) Human monocytes** **C) HMDM cells**

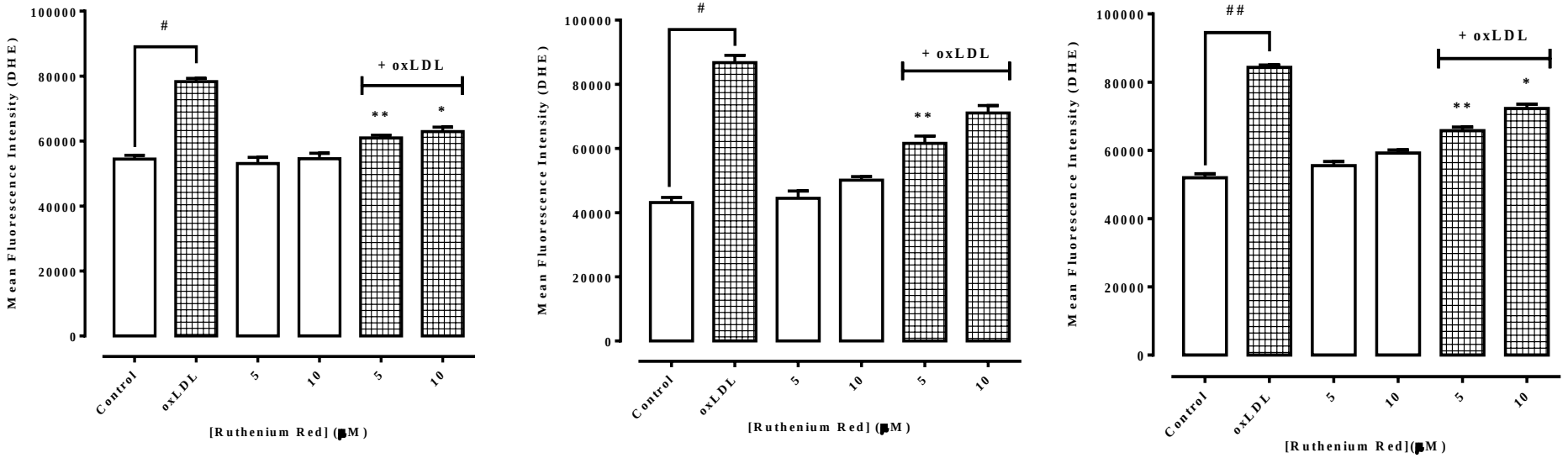

Figure 5.50: Effect of ruthenium red (RuR) and oxLDL on intracellular ROS levels in U937, human monocytes and HMDM cells.

U937 cells (0.5×10^6 cells/mL), human monocytes (1×10^6 cells/mL) or HMDM cells (1×10^6 cells/mL) were incubated with 5 µM and 10 µM ruthenium red for 30 minutes before incubation with LC_{50} concentration of oxLDL (0.5, 1 and 1.5 mg/mL for U937, human monocytes and HMDM cells, respectively) at 37°C in RPMI1640 no phenol red for 6 hours. A), B) and C) show the mean fluorescence intensity measured by flow cytometry in U937 cells, human monocytes and HMDM cells, respectively. 10,000 events were collected in the gated area for analysis. Results are displayed as mean fluorescence ± SEM of triplicates from a representative experiment. Significance (two-way ANOVA, Sidak's post test) is indicated from: cell only control vs oxLDL, #, $p<0.05$, ##, $p<0.01$; oxLDL vs RuR + oxLDL, *, $p<0.05$, **, $p<0.01$.

Cyclosporin A (CsA) has been shown by Yang (2009) to inhibit HOCl-induced ΔΨm and cell viability loss of HMDM cells by inhibiting MPTP formation. Additionally, CsA also protected HMDM cells againts lysosomal destabilization mediated by HOCl. Experiments were carried out to investigate the effect of CsA with and without oxLDL on cell viability. Results showed an increase in cell viability loss (decreased PI negative cells) in U937 cells pre-treated with CsA compared to control cells whereby 20% cell loss happened in cells pre-treated with 10 µM CsA (**Figure 5.51**). With the presence of oxLDL, further reduction in cell viability of 8 to 10% compared to oxLDL treated cells was observed in cells pre-treated with 5 µM and 10 µM CsA, respectively. For human monocytes, CsA was also found not protective against oxLDL toxicity (**Figure 5.52**). Pre-treatment of cells with CsA did not help in preserving cell viability as the percentage of cell viability loss (PI negative cells) obtained from oxLDL only treated cells was approximately similar with CsA treated cells in the presence of oxLDL. Moreover, incubation with CsA alone caused a slight reduction in cell viability but was not statistically significant. Surprisingly, CsA showed some protection to HMDM cells against oxLDL insult. OxLDL caused cell viability loss (PI negative cells) of approximately 40%, whilst 20-25% of cell viability loss (PI negative cells) was recovered in cells treated with CsA in the presence of oxLDL (**Figure 5.53**).

Experiments were also conducted to examine the effects of CsA on intracellular ROS production and to find out why CsA was not protecting U937 cells and human monocytes form oxLDL cytotoxicity. Results showed that CsA alone caused an increase in DHE fluorescence levels in both U937 cells and human monocytes (**Figure 5.54 A** and **Figure 5.54 B**) but not in HMDM cells (**Figure 5.54 C**), thus indicating an elevated production of ROS in U937 cells and human monocytes. This finding is in agreement with de Hornedo *et al.* (2007) who found that CsA induced oxidative stress and mitochondrial dysfunction in renal tubular cells. In conjunction, CsA had also caused endothelial dysfunction by elevating superoxide generation (Diederich *et al.*, 1994). In this study, CsA protects HMDM cells from oxLDL-induced cell viability loss. This therefore may indicate the importance of mitochondria in cell death as CsA is an agent known to prevent MPT activation but it is specific to HMDM cells only.

A)

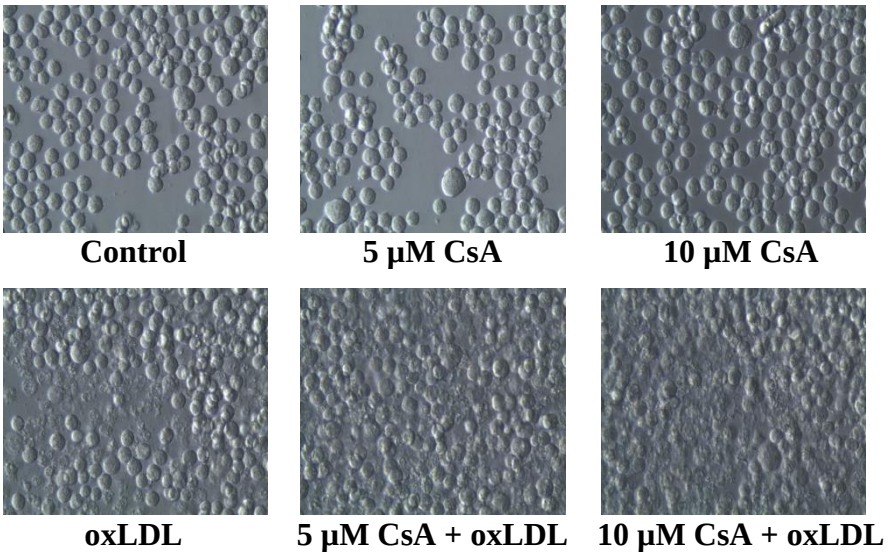

B)

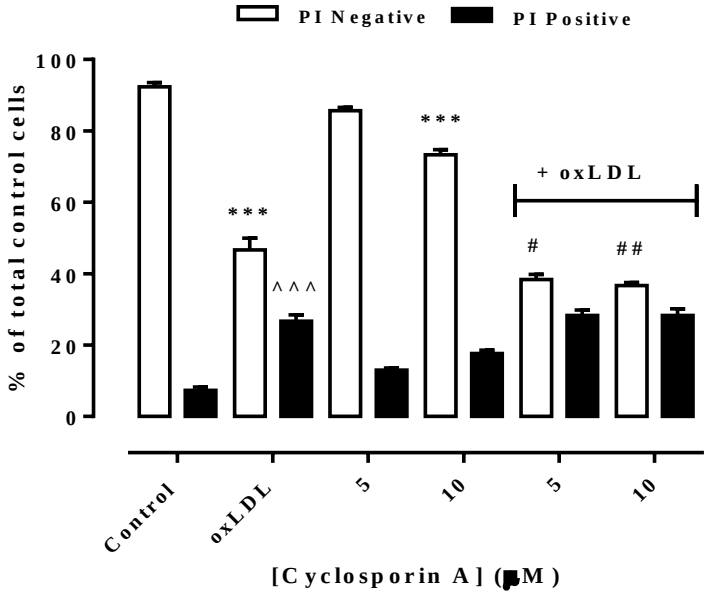

Figure 5.51: Effect cyclosporin A (CsA) and oxLDL on U937 cell viability.

U937 cells (0.5×10^6 cells/mL) were treated with different concentrations of cyclosporin A for 30 minutes followed by addition of LC_{50} concentration (0.5 mg/mL) of oxLDL and incubated at 37°C in non-phenol red RPMI-1640 for 24 hours. A) Cells were viewed *in situ* in tissue culture wells using an inverted microscope (400x magnification) after 24 hours. Images were taken using a Leica C-Mount camera and processed using Leica Application Suite software. B) Cell viability was measured using PI-flow cytometry assay after 24 hours. Data are expressed as a percentage of the cell only control. Results are displayed as mean ± SEM of triplicates from a representative experiment. Significance (two-way ANOVA, Sidak's post test) is indicated from: cell only control vs oxLDL, ***, $p<0.001$ (PI negative cells), ^^^, $p<0.001$ (PI positive cells); cell only control vs 5 µM CsA, ***, $p<0.001$ (PI negative cells); oxLDL vs 5 µM CsA + oxLDL and oxLDL vs 10 µM RuR + oxLDL, #, $p<0.05$, ##, $p<0.01$ (PI negative cells), respectively.

A)

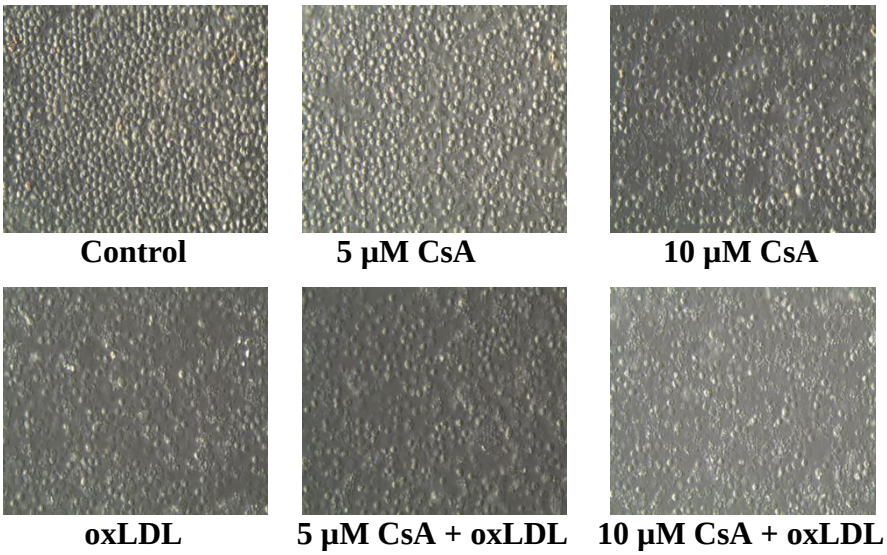

B)

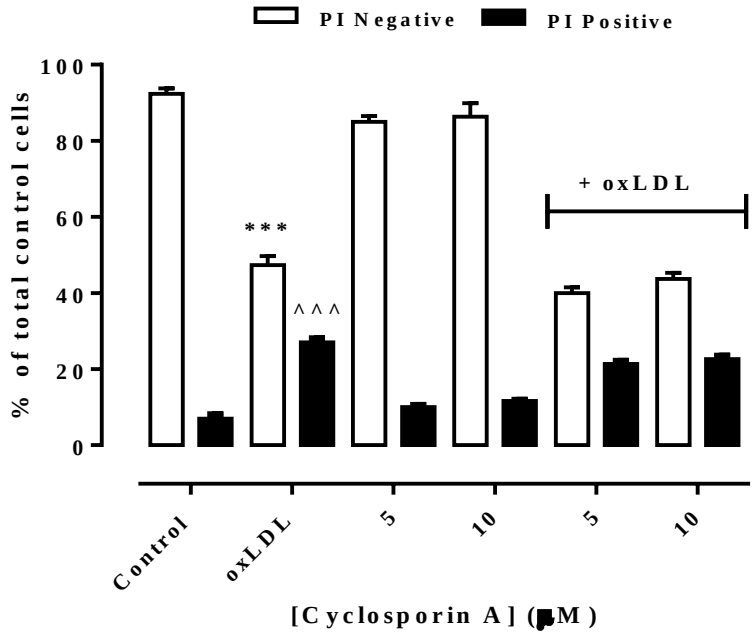

Figure 5.52: Effect cyclosporin A (CsA) and oxLDL on human monocytes cell viability.

Human monocytes (1×10^6 cells/mL) were treated with different concentrations of cyclosporin A for 30 minutes followed by addition of LC_{50} concentration (1 mg/mL) of oxLDL and incubated at 37°C in non-phenol red RPMI-1640 for 24 hours. A) Cells were viewed *in situ* in tissue culture wells using an inverted microscope (400x magnification) after 24 hours. Images were taken using a Leica C-Mount camera and processed using Leica Application Suite software. B) Cell viability was measured using PI-flow cytometry assay after 24 hours. Data are expressed as a percentage of the cell only control. Results are displayed as mean ± SEM of triplicates from a representative experiment. Significance (two-way ANOVA, Sidak's post test) is indicated from: cell only control vs oxLDL, ***, $p<0.001$ (PI negative cells), ^^^, $p<0.001$ (PI positive cells).

A)

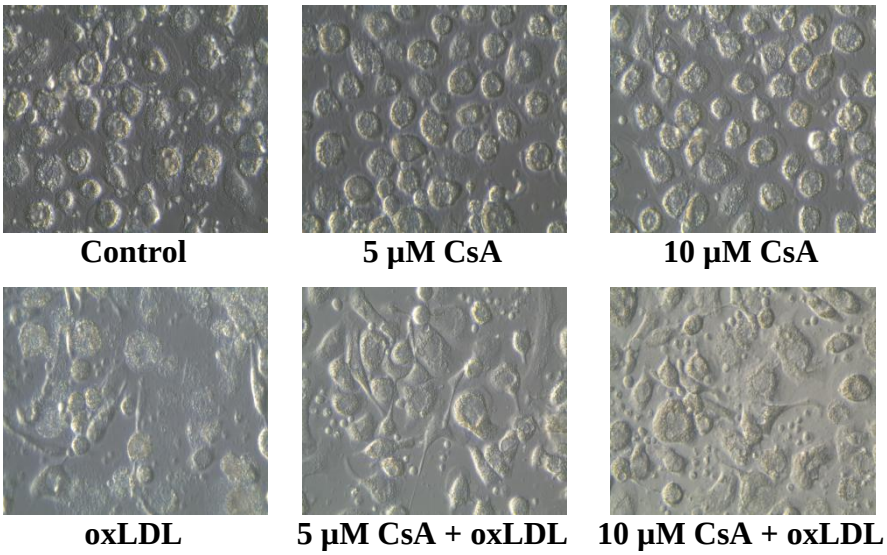

B)

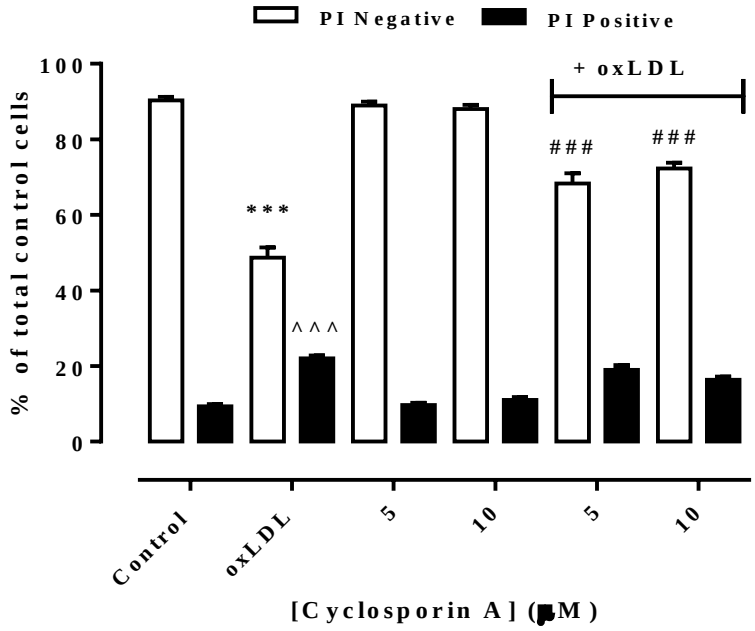

Figure 5.53: Effect of cyclosporin A (CsA) and oxLDL on HMDM cell viability.

HMDM cells (1×10^6 cells/mL) were treated with different concentrations of cyclosporin A for 30 minutes followed by addition of LC_{50} concentration (1.5 mg/mL) of oxLDL and incubated at 37°C in non-phenol red RPMI-1640 for 24 hours. A) Cells were viewed *in situ* in tissue culture wells using an inverted microscope (400x magnification) after 24 hours. Images were taken using a Leica C-Mount camera and processed using Leica Application Suite software. B) Cell viability was measured using PI-flow cytometry assay after 24 hours. Data are expressed as a percentage of the cell only control. Results are displayed as mean ± SEM of triplicates from a representative experiment. Significance (two-way ANOVA, Sidak's post test) is indicated from: cell only control vs oxLDL, ***, $p<0.001$ (PI negative cells), ^^^, $p<0.001$ (PI positive cells); oxLDL vs 5 µM CsA + oxLDL and oxLDL vs 10 µM RuR + oxLDL, ###, $p<0.001$ (PI negative cells).

A) U937 cells **B) Human monocytes** **C) HMDM cells**

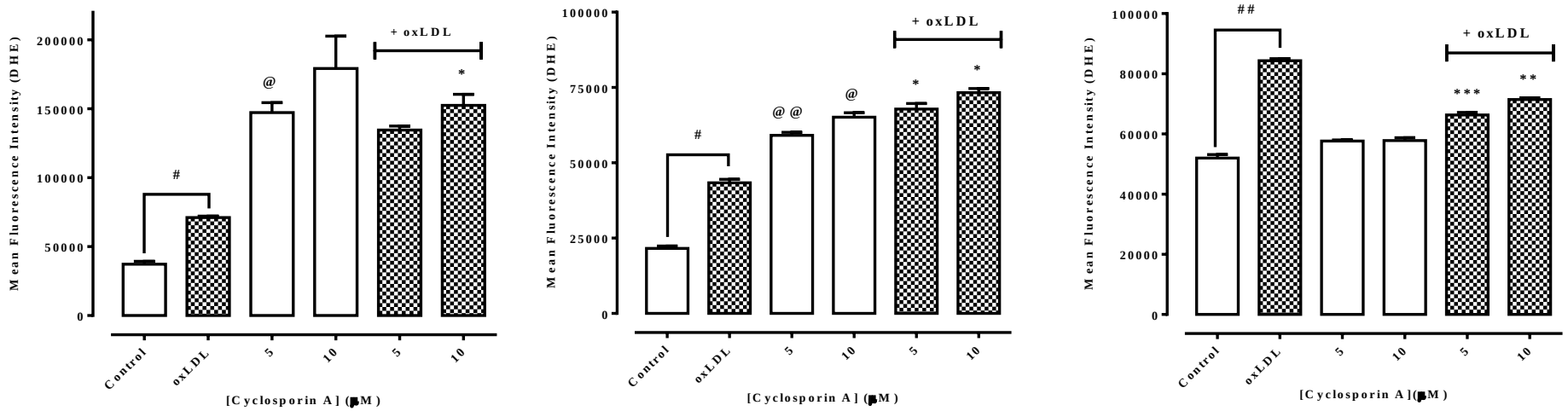

Figure 5.54: Effect of cyclosporin A (CsA) and oxLDL on intracellular ROS levels in U937, human monocytes and HMDM cells.

U937 cells (0.5×10^6 cells/mL), human monocytes (1×10^6 cells/mL) or HMDM cells (1×10^6 cells/mL) were incubated with 5 µM and 10 µM cyclosporin A for 30 minutes before incubation with LC_{50} concentration of oxLDL (0.5, 1 and 1.5 mg/mL for U937, human monocytes and HMDM cells) at 37°C in RPMI1640 no phenol red for 6 hours. A), B) and C) show the mean fluorescence intensity measured by flow cytometry in U937 cells, human monocytes and HMDM cells, respectively. 10,000 events were collected in the gated area for analysis. Results are displayed as mean fluorescence ± SEM of triplicates from a representative experiment. Significance (two-way ANOVA, Sidak's post test) is indicated from: cell only control vs oxLDL, #, $p<0.05$, ##, $p<0.01$; cell only control vs CsA, @, $p<0.05$, @@, $p<0.01$; oxLDL vs CsA + oxLDL, *, $p<0.05$, **, $p<0.01$, ***, $p<0.001$.

Effects of BrA and oxLDL on intracellular Ca^{2+} levels, ROS production and cell viability

Previous results in this chapter have clearly illustrated the ability of both calcium ionophore A23187 (BrA) and oxLDL to induce the increase in intracellular Ca^{2+}, ROS generation and subsequent cell death. Experiments were carried out to investigate these effects of both BrA and oxLDL on U937 cells, human monocytes and HMDM cells. A concentration of 5 µM BrA and LC_{50} concentration of oxLDL which have been observed to cause approximately 50% of cell viability loss in earlier experiments were used in the experiments.

Results showed that 5 µM BrA caused a large increase in intracellular Ca^{2+} compared to oxLDL in all cell types (**Figure 5.55 A, 5.56 A** and **5.57 A**). The rise in intracellular Ca^{2+} has also resulted in an elevated intracellular ROS production by both BrA and oxLDL but the increase caused by BrA was greater compared to oxLDL (**Figure 5.55 B, 5.56 B** and **5.57 B**). At the end of the experiments, cell viability data showed approximately similar percentage of cell viability loss (approximately 25 to 30% less than control – PI negative cells) incurred by both BrA and oxLDL in (**Figure 5.55 C, 5.56 C** and **5.57 C**). These results may indicate that increased levels of intracellular Ca^{2+} and ROS induced by oxLDL were sufficient to cause around 40% cell death. Additional increased in intracellular Ca^{2+} and ROS levels seen by BrA do not cause further cytotoxicity suggesting that results with BrA have reached a plateau.

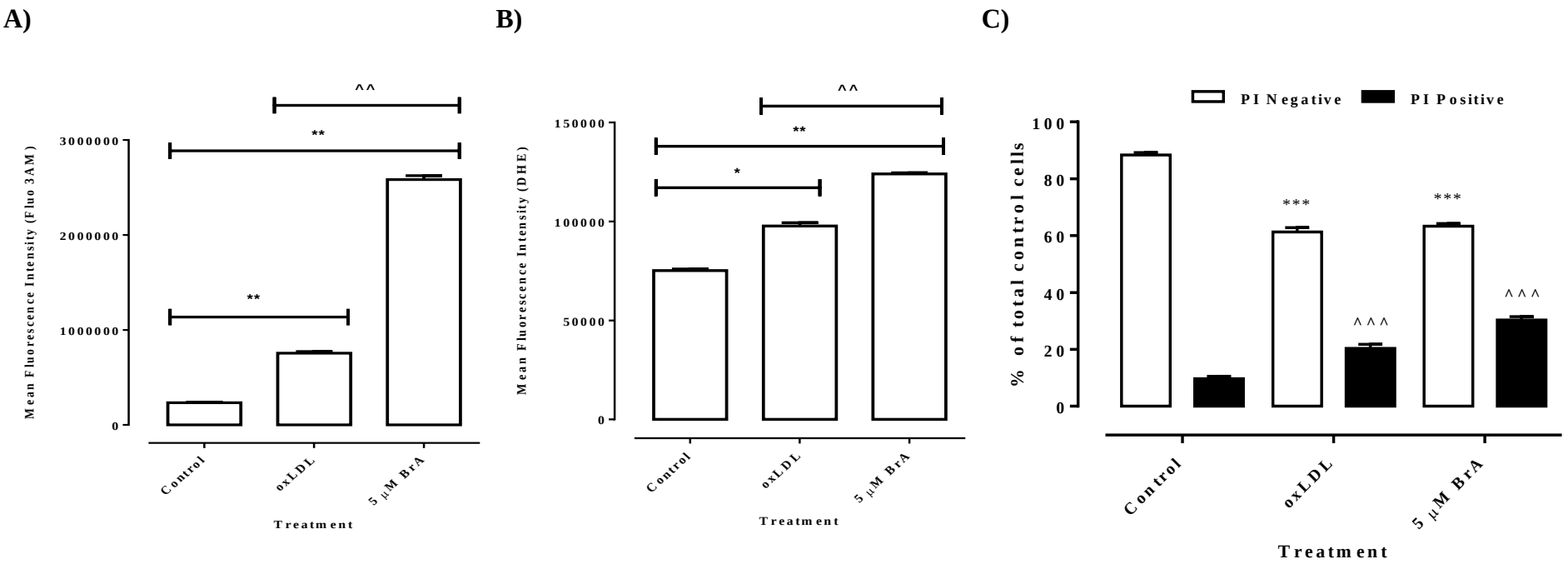

Figure 5.55: Effect of BrA and oxLDL on intracellular calcium levels, intracellular ROS levels and cell viability in U937 cells

U937 cells (0.5×10^6 cells/ml) were treated with the LC_{50} concentration (0.4 mg/mL) of oxLDL and 5 µM BrA followed by incubation at 37°C in non-phenol red RPMI-1640. A) Intracellular Ca^{2+} was measured using Fluo 3AM-flow cytometry assay after 1 hour. B) Intracellular ROS production was measured using DHE-flow cytometry assay after 3 hours. C) Cell viability was measured using the PI-flow cytometry assay after 12 hours. Results are displayed as mean ± SEM of triplicates from a representative experiment. Significance (two-way ANOVA, Sidak's multiple test) is indicated from: oxLDL vs BrA, ^^, $p<0.01$ (A & B); control vs oxLDL/BrA, ***, $p<0.001$ (PI negative cells), ^^^, $p<0.001$ (PI positive cells) (C).

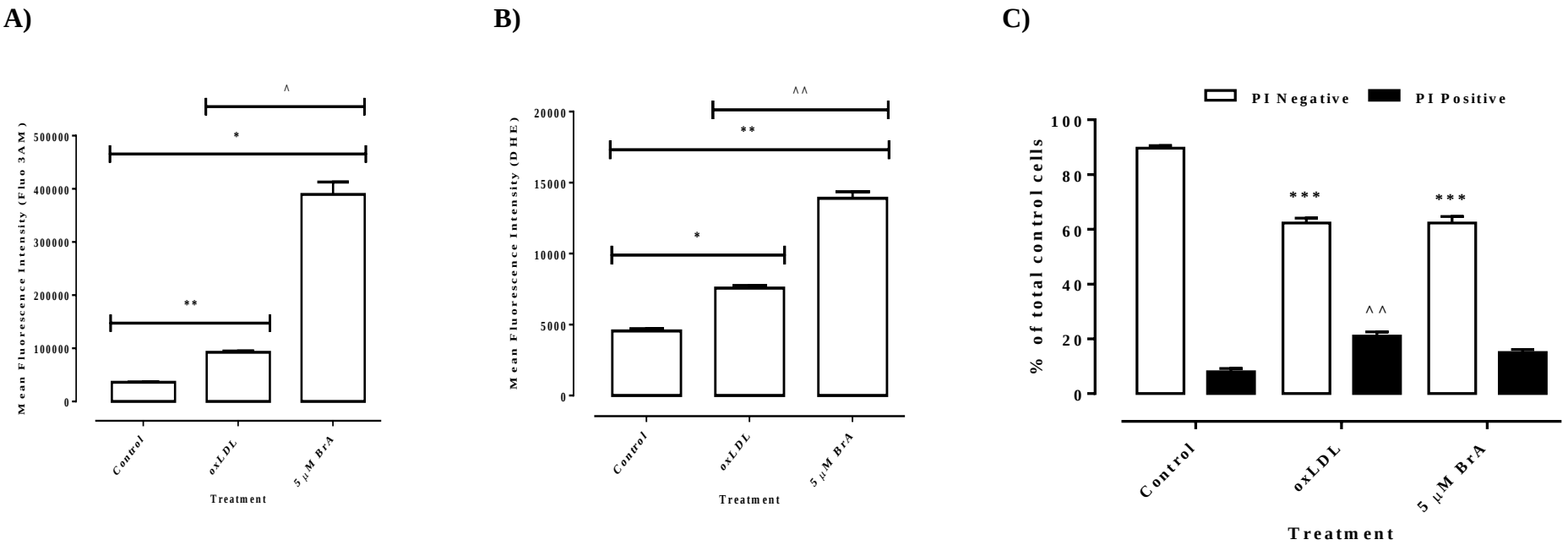

Figure 5.56: Effect of BrA and oxLDL on intracellular calcium levels, intracellular ROS levels and cell viability in human monocytes

Human monocytes (1×10^6 cells/ml) were treated with the LC_{50} concentration (0.8 mg/mL) of oxLDL and 5 µM BrA followed by incubation at 37°C in non-phenol red RPMI-1640. A) Intracellular Ca^{2+} was measured using Fluo 3AM-flow cytometry assay after 1 hour. B) Intracellular ROS production was measured using DHE-flow cytometry assay after 6 hours. C) Cell viability was measured using the PI-flow cytometry assay after 12 hours. Results are displayed as mean ± SEM of triplicates from a representative experiment. Significance (two-way ANOVA, Sidak's multiple test) is indicated from: oxLDL vs BrA, ^, $p<0.05$, ^^, $p<0.01$ (A & B); control vs oxLDL/BrA, ***, $p<0.001$ (PI negative cells), ^^, $p<0.01$ (PI positive cells) (C).

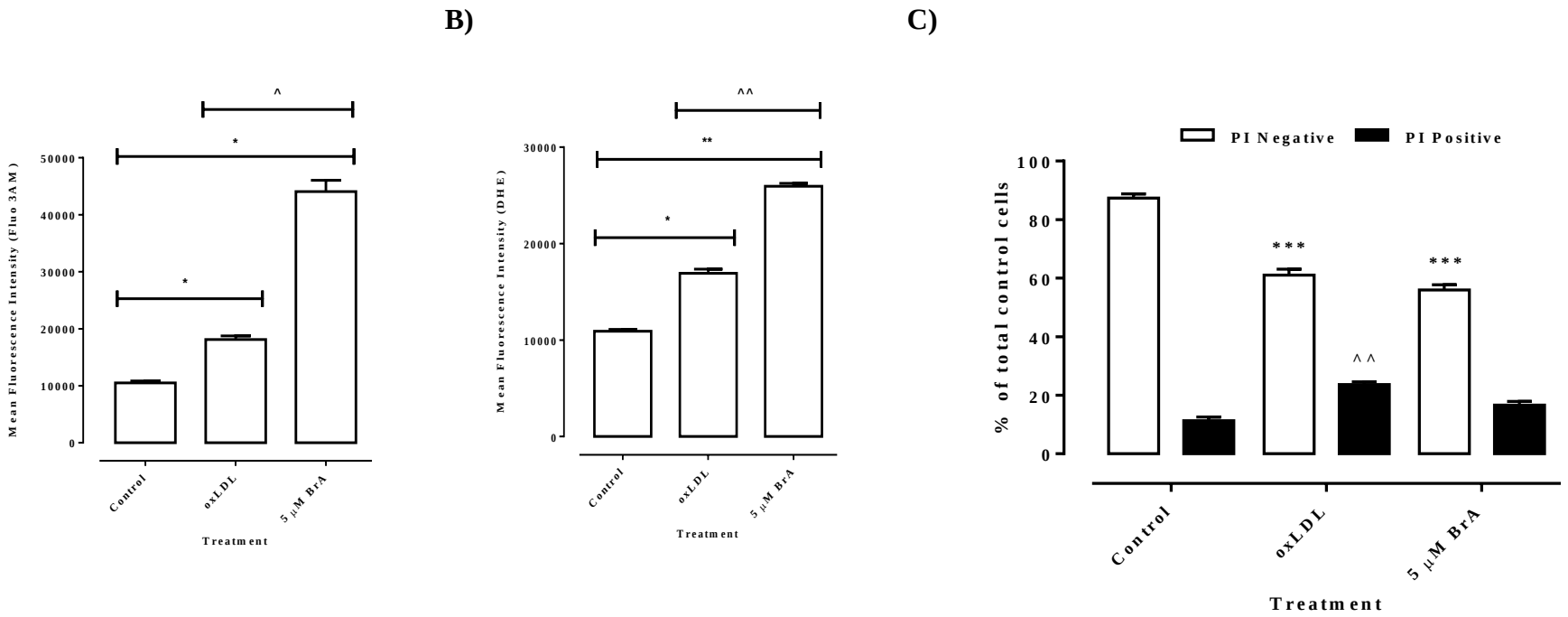

Figure 5.57: Effect of BrA and oxLDL on intracellular calcium levels, intracellular ROS levels and cell viability in HMDM cells.

HMDM cells (1×10^6 cells/ml) were treated with the LC_{50} concentration (1.25 mg/mL) of oxLDL and 5 µM BrA followed by incubation at 37°C in non-phenol red RPMI-1640. A) Intracellular Ca^{2+} was measured using Fluo 3AM-flow cytometry assay after 1 hour. B) Intracellular ROS production was measured using DHE-flow cytometry assay after 6 hours. C) Cell viability was measured using the PI-flow cytometry assay after 12 hours. Results are displayed as mean ± SEM of triplicates from a representative experiment. Significance (two-way ANOVA, Sidak's multiple test) is indicated from: oxLDL vs BrA, ^, $p<0.05$, ^^, $p<0.01$ (A & B); control vs oxLDL/BrA, ***, $p<0.001$ (PI negative cells), ^^, $p<0.01$ (PI positive cells) (C).

Effects of BrA and EGTA on intracellular ROS production and cell viability

Experiments were also carried out to assess the effect of BrA and EGTA on intracellular ROS generation and the subsequent effect on cell viability. In previous experiments, BrA has been shown to induce the increase in intracellular Ca^{2+}. Elevated level of intracellular Ca^{2+} caused by BrA has resulted in the rise of intracellular ROS generation which eventually ended in cell viability loss. On the other hand, EGTA has been shown to stop the rise of intracellular Ca^{2+} which in turn reduced intracellular ROS formation. Yet, oxLDL-induced cell viability loss was not recovered by EGTA despite its ability to stop intracellular Ca^{2+} rise and reduce intracellular ROS generation.

Results from the experiments showed that BrA-induced intracellular ROS level was reduced by EGTA in U937, human monocytes and HMDM cells (**Figure 5.58 A, 5.59 A** and **5.60 A**). In addition, BrA-induced cell viability loss was also recovered by EGTA. Cell viability loss (PI negative cells) in cells treated with BrA was between 25 to 45% compared to control cells. An average of 10 to 30% of cell viability loss was recovered by EGTA (cells treated with both BrA and EGTA) compared to cells treated with BrA only (**Figure 5.58 B, 5.59 B** and **5.60 B**).

DHE results in this section and in the previous experiments showed that EGTA was able to reduce intracellular ROS levels induced by BrA and oxLDL. However, BrA-induced cell viability loss and not oxLDL-induced cell death was recovered by EGTA. Taken together, this suggests that oxLDL may trigger a Ca^{2+}-independent reaction/mechanism that eventually activates the cell death cascade.

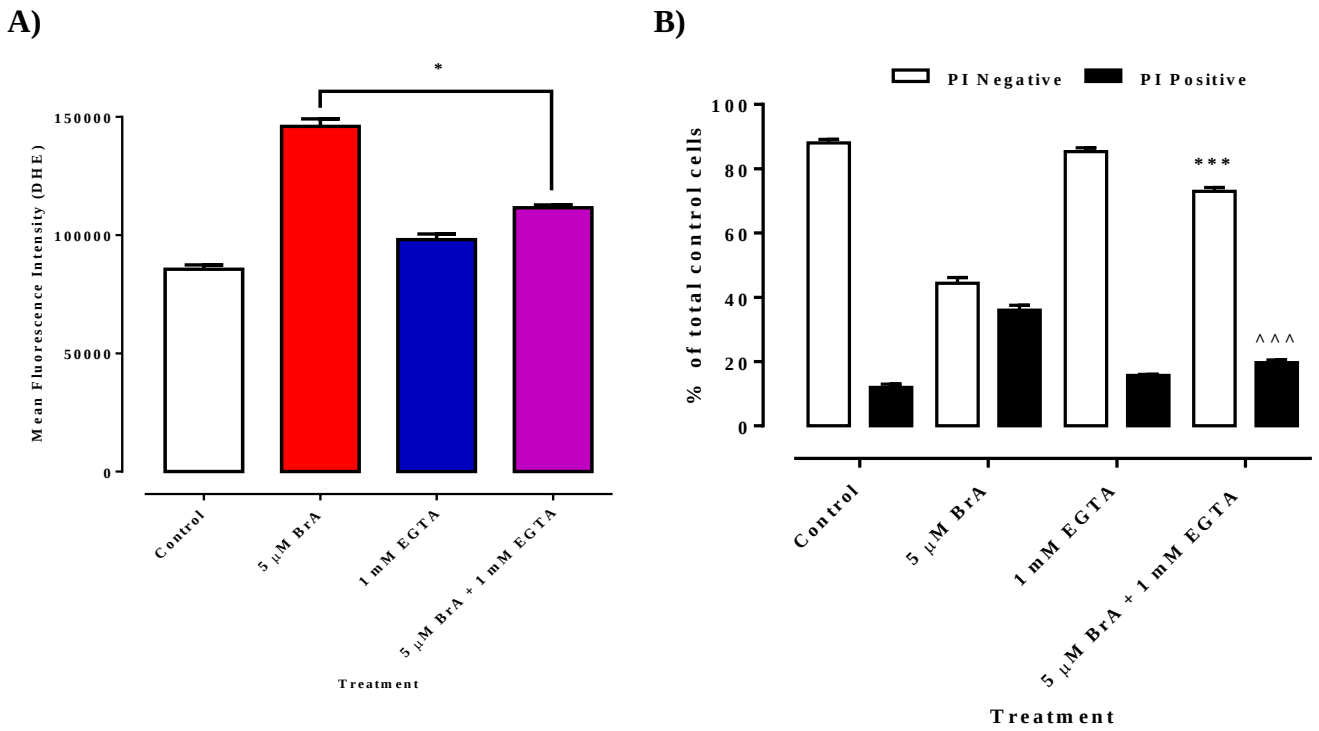

Figure 5.58: Effect of BrA and EGTA on intracellular ROS levels and cell viability in U937 cells

U937 cells (0.5×10^6 cells/ml) were treated with 5 µM BrA, 1 mM EGTA or combination of both followed by incubation at 37^{o}C in non-phenol red RPMI-1640. Intracellular ROS production was measured using DHE-flow cytometry assay after 3 hours and cell viability was measured using the PI-flow cytometry assay after 12 hours. A cell only control was included. A) shows the mean fluorescence intensity (MFI) of DHE measured by flow cytometry after 3 hours incubation. B) shows the percentage of cell viability measured using the PI-flow cytometry assay after 12 hours incubation. Results are displayed as mean ± SEM of triplicates from a representative experiment. Significance (two-way ANOVA, Sidak's multiple test) is indicated from: 5 µM BrA vs 5 µM BrA + 1 mM EGTA, *, $p<0.05$ (A); 5 µM BrA vs 5 µM BrA + 1 mM EGTA, ***, $p<0.001$ (PI negative cells), ^^^, $p<0.001$ (PI positive cells) (B).

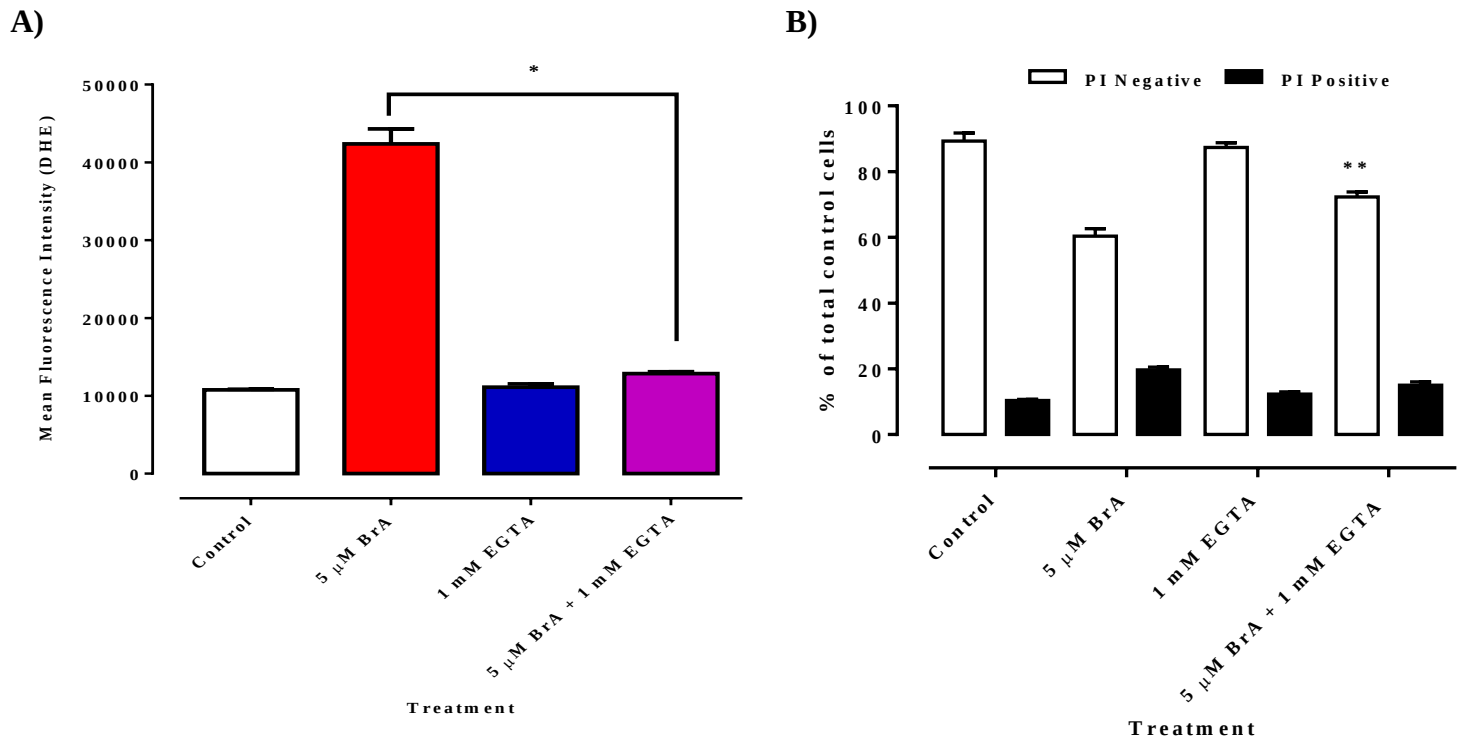

Figure 5.59: Effect of BrA and EGTA on intracellular ROS levels and cell viability in human monocytes

Human monocytes (1×10^6 cells/ml) were treated with 5 µM BrA, 1 mM EGTA or combination of both followed by incubation at 37^{o}C in non-phenol red RPMI-1640. Intracellular ROS production was measured using DHE-flow cytometry assay after 6 hours and cell viability was measured using the PI-flow cytometry assay after 12 hours. A cell only control was included. A) shows the mean fluorescence intensity (MFI) of DHE measured by flow cytometry after 6 hours incubation. B) shows the percentage of cell viability measured using the PI-flow cytometry assay after 12 hours incubation. Results are displayed as mean ± SEM of triplicates from a representative experiment. Significance (two-way ANOVA, Sidak's multiple test) is indicated from: 5 µM BrA vs 5 µM BrA + 1 mM EGTA, *, $p<0.05$ (A); 5 µM BrA vs 5 µM BrA + 1 mM EGTA, **, $p<0.01$ (PI negative cells) (B).

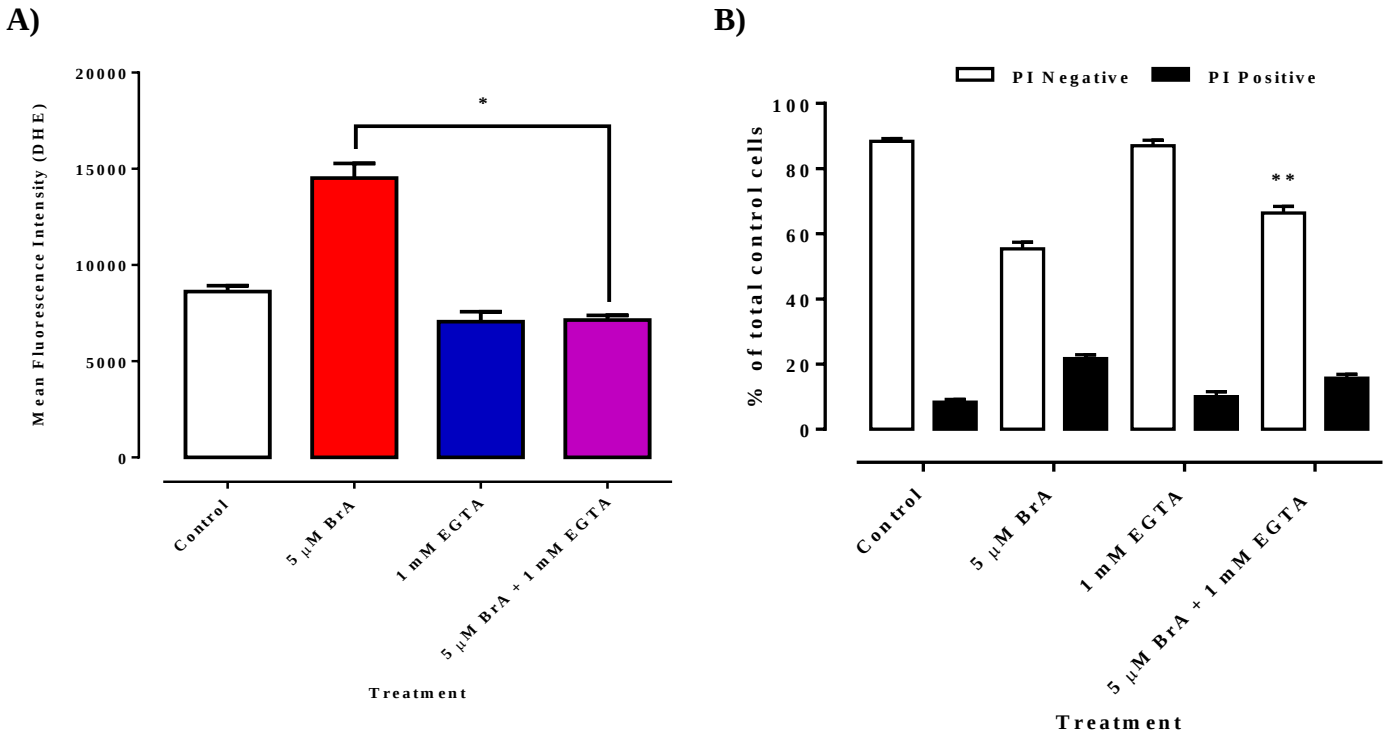

Figure 5.60: Effect of BrA and EGTA on intracellular ROS levels and cell viability in HMDM cells

HMDM cells (1×10^6 cells/ml) were treated with 5 µM BrA, 1 mM EGTA or combination of both followed by incubation at 37^{o}C in non-phenol red RPMI-1640. Intracellular ROS production was measured using DHE-flow cytometry assay after 6 hours and cell viability was measured using the PI-flow cytometry assay after 12 hours. A cell only control was included. A) shows the mean fluorescence intensity (MFI) of DHE measured by flow cytometry after 6 hours incubation. B) shows the percentage of cell viability measured using the PI-flow cytometry assay after 12 hours incubation. Results are displayed as mean ± SEM of triplicates from a representative experiment. Significance (two-way ANOVA, Sidak's multiple test) is indicated from: 5 µM BrA vs 5 µM BrA + 1 mM EGTA, *, $p<0.05$ (A); 5 µM BrA vs 5 µM BrA + 1 mM EGTA, **, $p<0.01$ (PI negative cells) (B).

Effects of BrA and 7,8-NP on intracellular ROS production and cell viability

In **Chapter Four**, 7,8-NP has been shown to reduce DHE levels as well as intracellular Ca^{2+} levels. Studies by previous researchers, particularly in this lab have revealed the ability of 7,8-NP to scavenge free radicals (Gieseg *et al.*, 1993) and protects cells from oxLDL-induced cell death (Baird, 2003). In this section, experiments were carried out to investigate and compare the effect of BrA and 7,8-NP on intracellular ROS generation and subsequent cell death.

Results from this section showed that BrA caused a great elevation in DHE fluorescence in all types of cells. In the earlier experiments of this chapter, BrA has been shown to have caused an increase in intracellular Ca^{2+} by increasing Ca^{2+} influx, thus the rise in intracellular Ca^{2+} could have contributed to the rise in intracellular ROS, reflected by the increase in DHE fluorescence levels. However, when the cells were incubated with a combination of BrA and 7,8-NP, the DHE fluorescence dropped significantly. As 7,8-NP has been demonstrated to reduce oxLDL-induced DHE level (**Chapter Four**), it may also act by scavenging the BrA-induced intracellular ROS caused by the increased in intracellular Ca^{2+} (**Figure 5.61 A, 5.62 A** and **5.63 A**). Consequently, cell viability (PI negative cells) has also increased in cells treated with BrA and 7,8-NP in combination compared to cells treated with BrA only (**Figure 5.61 B, 5.62 B** and **5.63 B**).

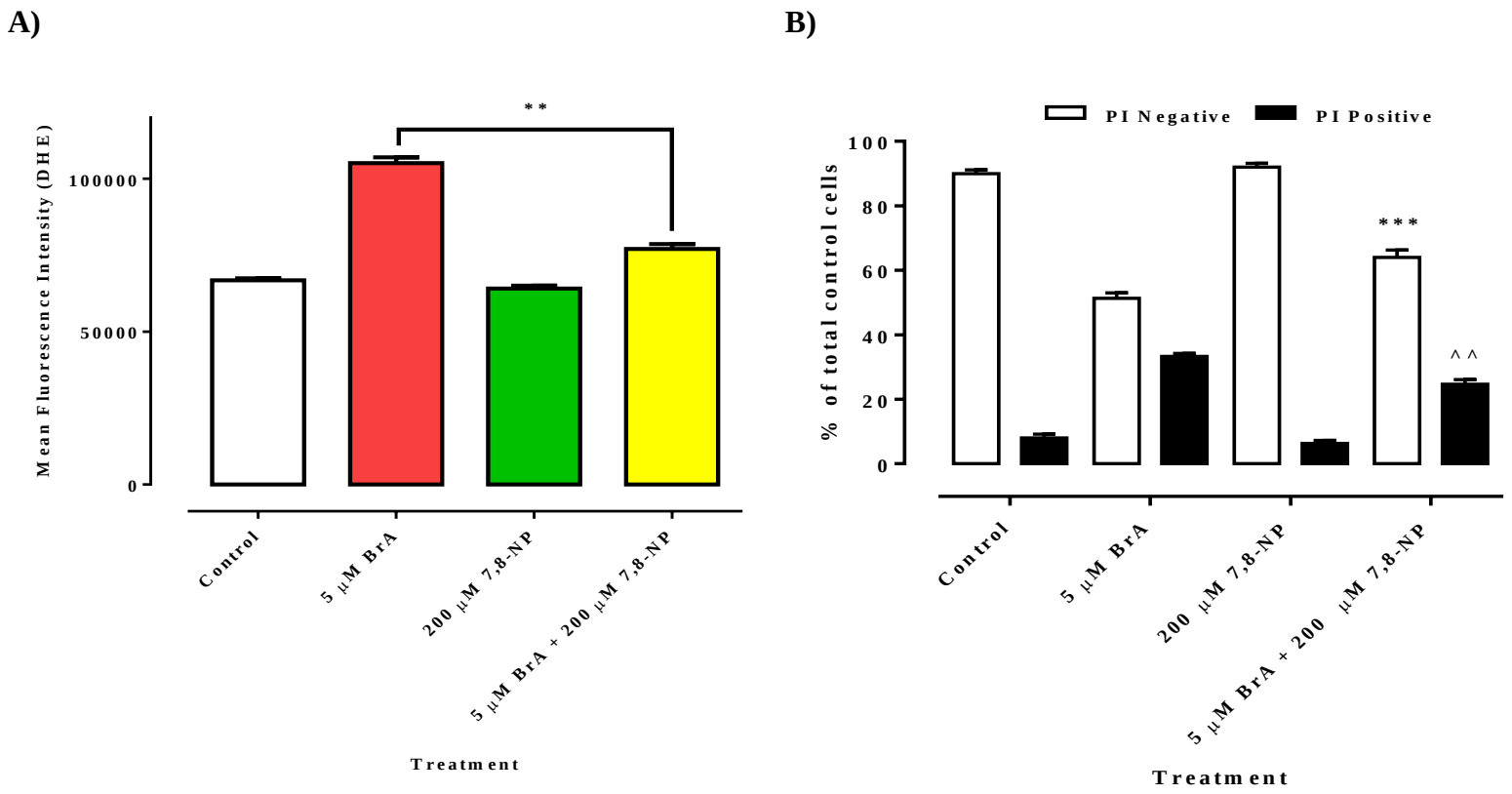

Figure 5.61: Effect of BrA and 7,8-NP on intracellular ROS levels and cell viability in U937 cells.

U937 cells (0.5×10^6 cells/mL) were treated with 5 µM BrA, 200 µM 7,8-NP or combination of both followed by incubation at 37^{o}C in non-phenol red RPMI-1640. Intracellular ROS production was measured using DHE-flow cytometry assay after 3 hours and cell viability was measured using the PI-flow cytometry assay after 12 hours. A cell only control was included. A) shows the mean fluorescence intensity (MFI) of DHE measured by flow cytometry after 3 hours incubation. B) shows the percentage of cell viability measured using the PI-flow cytometry assay after 12 hours incubation. Results are displayed as mean ± SEM of triplicates from a representative experiment. Significance (two-way ANOVA, Sidak's multiple test) is indicated from: 5 µM BrA vs 5 µM BrA + 200 µM 7,8-NP, **, $p<0.01$ (A); 5 µM BrA vs 5 µM BrA + 200 µM 7,8-NP, ***, $p<0.001$ (PI negative cells), ^^, $p<0.01$ (PI positive cells) (B).

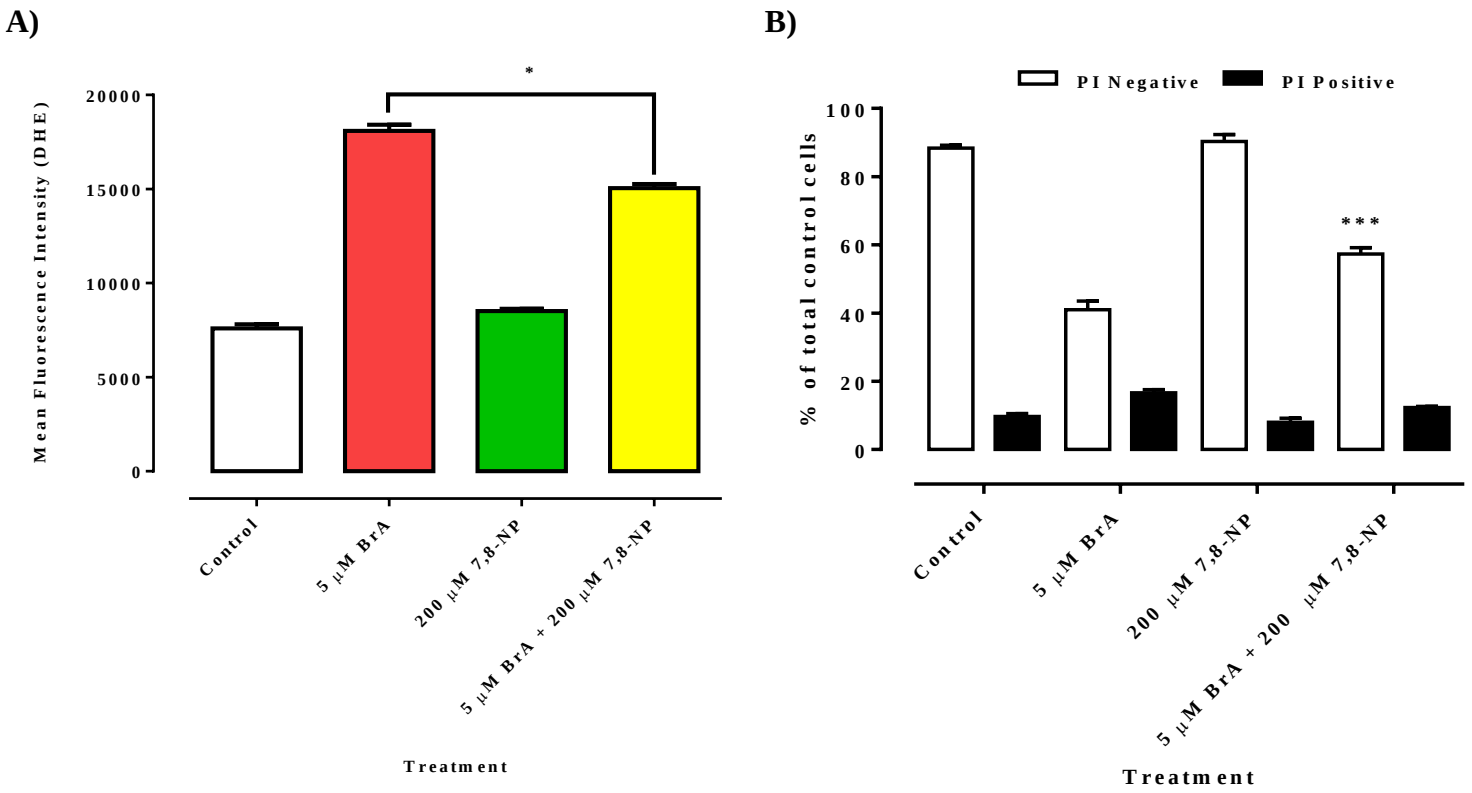

Figure 5.62: Effect of BrA and 7,8-NP on intracellular ROS levels and cell viability in human monocytes.

Human monocytes (1×10^6 cells/mL) were treated with 5 µM BrA, 200 µM 7,8-NP or combination of both followed by incubation at 37^{o}C in non-phenol red RPMI-1640. Intracellular ROS production was measured using DHE-flow cytometry assay after 3 hours and cell viability was measured using the PI-flow cytometry assay after 12 hours. A cell only control was included. A) shows the mean fluorescence intensity (MFI) of DHE measured by flow cytometry after 3 hours incubation. B) shows the percentage of cell viability measured using the PI-flow cytometry assay after 12 hours incubation. Results are displayed as mean ± SEM of triplicates from a representative experiment. Significance (two-way ANOVA, Sidak's multiple test) is indicated from: 5 µM BrA vs 5 µM BrA + 200 µM 7,8-NP, **, $p<0.01$ (A); 5 µM BrA vs 5 µM BrA + 200 µM 7,8-NP, ***, $p<0.001$ (PI negative cells) (B).

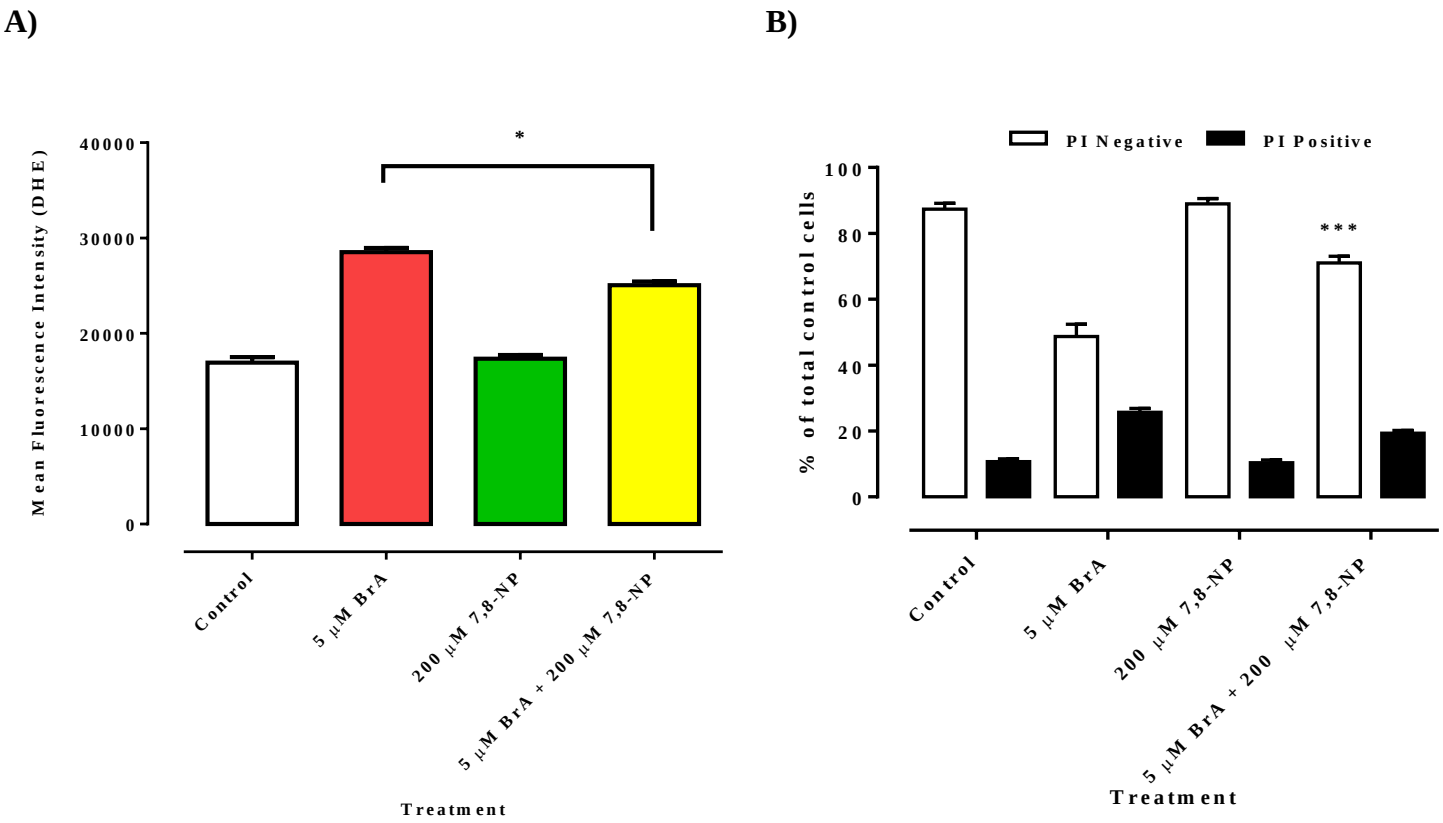

Figure 5.63: Effect of BrA and 7,8-NP on intracellular ROS levels and cell viability in HMDM cells.

HMDM cells (1×10^6 cells/mL) were treated with 5 µM BrA, 200 µM 7,8-NP or combination of both followed by incubation at 37^{o}C in non-phenol red RPMI-1640. Intracellular ROS production was measured using DHE-flow cytometry assay after 3 hours and cell viability was measured using the PI-flow cytometry assay after 12 hours. A cell only control was included. A) shows the mean fluorescence intensity (MFI) of DHE measured by flow cytometry after 3 hours incubation. B) shows the percentage of cell viability measured using the PI-flow cytometry assay after 12 hours incubation. Results are displayed as mean ± SEM of triplicates from a representative experiment. Significance (two-way ANOVA, Sidak's multiple test) is indicated from: 5 µM BrA vs 5 µM BrA + 200 µM 7,8-NP, *, $p<0.05$ (A); 5 µM BrA vs 5 µM BrA + 200 µM 7,8-NP, ***, $p<0.001$ (PI negative cells) (B).

Discussion

Effect of oxLDL on intracellular Ca^{2+} increase

The effect of oxLDL on cytosolic Ca^{2+} levels was studied using Fluo 3AM probe via flow cytometry. Results obtained showed a continuous rise in the intracellular Ca^{2+} levels within the 6 hours after oxLDL treatment (**Figure 5.2, 5.3** and **5.4**). It is clearly depicted by the results that intracellular Ca^{2+} level increase was the greatest within the first three hours of incubation with oxLDL whereby the major boost happened after 1 hour. Generally, the increase slowed down after the third hour but remained high. These results clearly illustrate that oxLDL induced a high and sustained rise in cytosolic Ca^{2+}.

This finding is supported by Maziere *et al.* (2005) who have demonstrated the increase in intracellular Ca^{2+} in Jurkat cells as early as 15 minutes after the addition of oxLDL. In addition, van Tits *et al.* (2000) have found that oxLDL evoked an early but sustained increase in intracellular Ca^{2+} but a delayed generation of superoxide. Morever, Deng *et al.* (2005) have also showed that intracellular Ca^{2+} level was increased in U937-derived macrophages following 20 minutes incubation with oxLDL of 100 µg/mL. Meanwhile, Matsumura *et al.* (1997) and Weisser *et al.* (1992) have shown that oxLDL induces Ca^{2+} mobilization in mouse peritoneal macrophages and smooth muscle cells cultured from rat aortas respectively. In another study by Yun *et al.* (2004), lysophosphatidylcholine (lysoPC) which is a phospholipid component of oxLDL has been shown to mobilised Ca^{2+} in U937 cells and the Ca^{2+} influx was from extracellular media. Moreover, they have demonstrated that G protein-coupled receptors in the plasma membrane (G2A and GPR4) were not present in U937 cells thus allowing influx of Ca^{2+} into the intracellular compartment of the cells.

This study has also demonstrated that intracellular Ca^{2+} increase induced by oxLDL is concentration-dependent (**Figure 5.5**) which has also been observed by Maziere *et al.* (2005). Therefore, cytosolic (intracellular) Ca^{2+} increase could be regarded as a secondary initiator of the subsequent oxidative damage in response to oxLDL. However, how oxLDL triggers Ca^{2+} influx is unclear and yet to be determined.

Ca^{2+} ionophore A23187 (BrA) is highly selective and enhances the ability of Ca^{2+} to cross the cell membrane and increases cytoplasmic Ca^{2+}. It was used in this study as a positive control to confirm that the increase in fluorescence resulted from Ca^{2+} reacting with Fluo 3AM dye

and not oxLDL reacting with the dye. BrA had caused a concentration-dependent increase in cytosolic Ca^{2+} levels after 3 hours incubation with the cells (**Figure 5.6**). This indicates that the observed increase in the fluorescence intensity in oxLDL-treated cells was most possibly due to the cytosolic Ca^{2+} reacting with the Fluo 3AM dye and not oxLDL reacting with the dye. Incubation with BrA after a period of time resulted in cell viability loss in all three types of cells (**Figure 5.7**). The degree of cell death correlated with the concentration of BrA which indicates increased cell death is associated with increased cytosolic Ca^{2+} accumulation (**Figure 5.8)**. Salvayre *et al.* (2002) has indicated that a sustained elevation in cytosolic Ca^{2+} is important in oxLDL-induced cell death (apoptosis and necrosis).

In this study, cells incubated in media without Ca^{2+} (EBSS-Ca^{2+}) still showed an increase in fluorescence level with the presence of oxLDL although it was not as high as in cells incubated with Ca^{2+} (EBSS+Ca^{2+} and RMPI1640). This indicates that, while the extracellular Ca^{2+} is mandatory for the rise in intracellular Ca^{2+}, the involvement of intracellular mechanisms that mediate the overall increase is still important.

Effects of different media on oxLDL-induced intracellular Ca^{2+} levels and subsequent removal of oxLDL on cell viability

Experiments performed in EBSS with Ca^{2+} (EBSS+Ca^{2+}) and EBSS without Ca^{2+} (EBSS-Ca^{2+}) have indicated the effect of extracellular Ca^{2+} influx on intracellular Ca^{2+} levels. OxLDL has been showed to induce Ca^{2+} flux not only from extracellular compartment but also from intracellular organelles as seen in **Figure 5.9 A, 5.10 A** and **5.11 A**. Cell viability results revealed that despite demonstrating a lower intracellular Ca^{2+} level in EBSS-Ca^{2+}, removal of oxLDL did not help in restoring cell viability (**Figure 5.9 B, 5.10 B** and **5.11 B**). This phenomenon indicates that the increase in intracellular Ca^{2+} might not be important in oxLDL-induced cell death. OxLDL might have triggered other cellular responses which could have initiated cell death mechanisms upstream to intracellular Ca^{2+} increase. Previous study in our lab by Shchepetkina (2013) showed that HMDM cells incubated for 6 hours in oxLDL lost almost 50% of intracellular GSH. When oxLDL was removed after 6 hours incubation with the cells, intracellular GSH was recovered but no recovery of cell viability was observed. This indicates that the cells were losing metabolic activity after 6 hours incubation with oxLDL. This effect was not reversible and could contribute to cell death.

Effects of Ca^{2+} channel blockers and Ca^{2+} chelators on intracellular Ca^{2+}, ROS production and cell viability

The intracellular Ca^{2+} homeostasis maintained low levels of Ca^{2+} (~100 nM) in resting cells by concerted operation of enzymes that translocate Ca^{2+} ions across the plasma membrane and intracellular store system (Carafoli, 1987; Hanson *et al.*, 2004). Therefore, disruption of this operation caused by agents like oxLDL could result in increased Ca^{2+} influx and release of Ca^{2+} from intracellular stores. This could lead to an uncontrolled and sustained elevation in intracellular Ca^{2+} level (Nicotera *et al.*, 1988). The increase in cytosolic Ca^{2+} could be caused by Ca^{2+} influx from the extracellular media and Ca^{2+} release from ER, which is the major intracellular Ca^{2+} store. Extracellular Ca^{2+} influx could occur via L- or T-type Ca^{2+} channels on plasma membrane while Ca^{2+} release from ER is through ryanodine receptors (RyRs) as well as inositol triphosphate receptors (IP3Rs) on SR/ER membrane (Deng *et al.*, 2005; Negre-Salvayre *et al.*, 1992; Yang, 2009; Yang *et al.*, 2012a).

Nifedipine was found to offer a limited protection in all types of cells against oxLDL-induced intracellular Ca^{2+} influx especially at lower concentration (5 µM) (**Figure 5.13**). Likewise, flunarizine and verapamil were found to inhibit intracellular Ca^{2+} rise caused by oxLDL in U937 cells and human monocytes and U937 cells only, respectively (**Figure 5.12** and **5.14**). However, intracellular DHE data revealed that there was no protection against oxLDL-induced intracellular ROS found with any of the Ca^{2+} channel blockers tested (**Figure 5.15, 5.16** and **5.17**). This phenomenon may indicate that oxLDL could have caused a Ca^{2+}-independent increase intracellular ROS or oxLDL may also trigger other mechanism of releasing ROS such as NOX on the plasma membrane. Consequently, none of the L- or T-type Ca^{2+} channel blockers was able to protect the cells against oxLDL-mediated cell viability loss (**Figure 5.18, 5.19, 5.20, 5.21, 5.22, 5.23, 5.24, 5.25** and **5.26**). Moreover, flunarizine alone at 50 µM was cytotoxic to U937 cells and it did not increase intracellular Ca^{2+} but caused a rise in intracellular ROS instead.

Earlier, it was reported by Negre-Salvayre and Salvayre (1992) that nifedipine (dihydropyridine) but not verapamil (phenylalkylamine) was protective against oxLDL-mediated cell death in cultured lymphoid cells. In our lab, Yang (2009) has demonstrated that flunarizine, nifedipine and verapamil were able to block intracellular Ca^{2+} rise in HMDM cells caused by HOCl insult, suggesting that extracellular Ca^{2+} entered HMDM cells upon HOCl treatment mainly through L- and T-type Ca^{2+} channels on HMDM plasma membrane.

However, the cytosolic Ca^{2+} increase was never completely prevented using those Ca^{2+} channel blockers, indicating that cytosolic Ca^{2+} accumulation might also occur through other pathways. Likewise, HOCl-induced cell viability loss was also inhibited by the above Ca^{2+} channel blockers but the inhibition was also not complete, suggesting that HOCl caused cell death by activating other pathways or Ca^{2+} released from intracellular stores could result in cell death.

The opening of Ca^{2+} channels on the plasma membrane could occur via plasma membrane depolarization. Maack and O'Rourke (2007) have previously suggested that plasma membrane depolarization in cardiac myocytes caused by voltage-gated Na^{+}-channel activation resulted in inward Na^{+}- current, facilitating L-type Ca^{2+}-channels on the plasma membrane. Since Ca^{2+} transport systems are susceptible to redox conditions (Camello-Almaraz *et al.*, 2006), it is highly possible that ROS produced by oxLDL regulates the plasma membrane Ca^{2+} channels through thiol modification within the protein complex (Inoue *et al.*, 2008). In addition, Campbell *et al.* (1996) have reported that the thiol oxidizing agent 5,5'-dithiobis (2-nitrobenzoic acid) (DTNB) upregulated L-type Ca^{2+} channels at the extracellular face of the cell membrane. They have also hypothesized that an allosteric thiol-containing 'redox switch' is present on the L-type Ca^{2+} channel subunit complex. Superoxide and other ROS could inhibit L-type Ca^{2+} channels by acting directly on voltage sensor domain of the channels (Kourie, 1998).

NADPH oxidase (NOX) on the plasma membrane could also be a possible regulator in the opening of the L- or T-type Ca^{2+}channels upon cells exposure to oxLDL. A study by Wang *et al.* (2010) have showed that inhibition of NOX by specific NOX inhibitors i.e. apocynin, DPI and gp91ds-tat suppressed the L-type Ca^{2+} channel expression and blocked the influx of extracellular Ca^{2+} . It has been shown in **Chapter Four** of this study that apocynin decreases intracellular Ca^{2+} levels in U937 cells but not in human monocytes and HMDM cells.

In this study, dantrolene (RyR inhibitor) provided limited protection against oxLDL-induced cytosolic Ca^{2+} increase only human monocytes but not U937 or HMDM cells (**Figure 5.27**). However, in the presence of oxLDL, intracellular ROS level was raised in cells treated with dantrolene (**Figure 5.29**) and cell viability loss caused by oxLDL was also not prevented (**Figure 5.31, 5.32** and **5.33**). This suggests that Ca^{2+} might also be released from ER

possibly via another channel i.e. IP3R whilst Ca^{2+} influx from extracellular source could caused a rise in intracellular Ca^{2+}.

It has been suggested that Ca^{2+} release from ER/SR could be a result from the influx of extracellular Ca^{2+} which triggers the opening of the RyRs on the ER/SR membrane (a process termed as Ca^{2+}-induced Ca^{2+} release) (Maack & O'Rourke, 2007). However, other studies have demonstrated that oxLDL induced a gradual rise in cytosolic Ca^{2+} with time in the absence of external Ca^{2+} source (Deng *et al.*, 2009; Deng *et al.*, 2005), implying that mobilization of Ca^{2+} from intracellular ER store occurred in the absence of external Ca^{2+} and the opening of RyR on the ER membrane did not have to be initiated by the extracellular Ca^{2+} influx. Therefore, it is likely that the critical thiol groups within the RyR protein are targeted by ROS in responses to oxLDL, leading to ER-Ca^{2+} release. Previous finding of HOCl interacting with the essential thiols leading to RyR activity suggests that RyR receptors on ER membrane could be activated via thiol oxidation by oxidants (Anzai *et al.*, 1998; Sun *et al.*, 2001).

It has also been implicated that ER is the major intracellular Ca^{2+} store and plays a dual role in Ca^{2+} regulation. Ca^{2+} can be released by the ER via IP3R and RyR to generate the Ca^{2+} signal during stimulation whereas Ca^{2+} accumulation can occur through sarco/endoplasmic reticulum Ca^{2+}-ATPase (SERCA) to buffer Ca^{2+} after stimulation, allowing cytosolic Ca^{2+} concentration to return to the resting state (Berridge *et al.*, 2003). Treatment of cells with thapsigargin (Tg) depleted Ca^{2+} store in ER causing ER stress. Our results showed an increase in intracellular Ca^{2+} in cells treated with Tg only and was further increased in the presence of oxLDL (**Figure 5.28**). Since Ca^{2+} was already depleted from the ER by Tg and accumulated in the cytosol, oxLDL further raised the cytosolic Ca^{2+} levels by probably increasing Ca^{2+} influx from the extracellular media. Likewise, intracellular ROS level was further enhanced by the presence of oxLDL (**Figure 5.30**). Eventually, this resulted in cell death whereby Tg alone was found to cause a drop in cell viability loss and it was further increased by oxLDL (**Figure 5.34, 5.35** and **5.36**). Depleting Ca^{2+} from the ER by Tg has caused stress to the ER, thus oxidative injury induced by oxLDL may potentiate the existing stress on the ER leading to increase in cell death.

Studies have also reported that oxidants could release Ca^{2+} from the ER (Ermak & Davies, 2001), most probably by inhibiting SERCA. ROS may also trigger ER stress through

generation and accumulation of oxidized protein. Additionally, ROS could directly damage proteins of the ER folding machinery such as the ER chaperones. This will then mediate the buildup of misfolded protein resulting in UPR activation (Dejeans *et al.*, 2010). Tg has been shown to induce an increase in intracellular Ca^{2+} and cell death in cultured porcine aortic SMC (Chin *et al.*, 2007). However, cell death mediated by Tg was not related to the increase in intracellular Ca^{2+} but was induced by targeting of the activated pro-apoptotic factor, Bax to the mitochondria and opening of the mitochondrial permeability transition pore (MPTP). The opening of MPTP then triggered several key events leading to cell death including $\Delta\Psi m$ loss, cytochrome c release and caspase-3 activation.

Next, when cells were treated with oxLDL in the presence of with calcium chelators (BAPTA AM and EGTA), intracellular Ca^{2+} influx was significantly blocked (**Figure 5.37** and **5.38**). In addition, intracellular ROS level was also reduced compared to oxLDL treated cells (**Figure 5.39**). However, cell viability loss was not prevented (**Figure 5.40, 5.41, 5.42, 5.43, 5.44** and **5.45**) which suggests that cytosolic Ca^{2+} increase was not important and was not the cause for cell viability loss mediated by oxLDL. Moreover, the rise in intracellular ROS level was not greatly reduced as compared to the blocking of intracellular Ca^{2+} level indicating that oxLDL might induce a Ca^{2+}-independent intracellular ROS which could then trigger a Ca^{2+}-independent cell death pathway. This finding is different from that found with HOCl in this lab, where cytosolic Ca^{2+} rise was responsible in HOCl-mediated cell death in HMDM cells (Yang, 2009).

However, cytosolic Ca^{2+} increase could also occur via other non-specific pathway (Deng *et al.*, 2005). This is supported by previous study by Yang (2009) in this laboratory that showed HOCl-induced intracellular Ca^{2+} increase was never completely prevented using any of the Ca^{2+} channel blockers or Ca^{2+} chelator. Much evidence have revealed that ROS can induce intracellular Ca^{2+} rise by releasing Ca^{2+} from internal stores as well as disturbing Ca^{2+} clearance systems. Indeed, elevated intracellular Ca^{2+} level is a constant feature associated with oxidative stress in pathological conditions (Camello-Almaraz *et al.*, 2006).

Effect of oxLDL-induce intracellular Ca^{2+} increase on mitochondria

Studies have suggested that the increase in cytosolic Ca^{2+} induced by oxLDL to be an important event triggering Ca^{2+}-dependent necrosis or apoptosis (Gieseg *et al.*, 2009b; Nicotera & Orrenius, 1998; Porn-Ares *et al.*, 1998; Salvayre *et al.*, 2002). Although oxLDL-

induced cytosolic Ca^{2+} increase is mainly caused by either extracellular Ca^{2+} influx or exhaustion of ER Ca^{2+}, not much information is available describing the exact mechanism whereby the increased intracellular Ca^{2+} are involved in the oxLDL-toxicity effect. One possibility is that cytosolic Ca^{2+} accumulation triggers mitochondrial dysfunction leading to cell death. A recent study by Deng *et al.* (2009) reported that a significant increase in mitochondrial Ca^{2+} correlated with the cytosolic Ca^{2+} influx mediated by oxLDL in PMA-stimulated U937 cells. This suggests that oxLDL-induced cytosolic Ca^{2+} rise triggered the Ca^{2+} mobilization from the cytosol into the mitochondria via Ca^{2+} uniporter on inner mitochondrial membrane (IMM), resulting in the MPTP opening and $\Delta\Psi m$ loss. Similar findings by Yang *et al.* (2012a) in our laboratory were also described in HOCl-treated HMDM cells.

Mitochondria have the ability to rapidly accumulate and to release large quantities of Ca^{2+} (Mattson & Chan, 2003). Excessive mitochondrial Ca^{2+} uptake makes up the essential steps in mitochondrial ROS production in Ca^{2+}-induced cytotoxicity yet mitochondrial Ca^{2+} overload is also vital in the mechanism of oxidative stress leading to oxidation injury (Peng & Jou, 2010). Thus, oxLDL-induced cytosolic Ca^{2+} overload may contribute to mitochondrial destabilization by inducing mitochondrial ROS production as a result of Ca^{2+} influx into the mitochondria. Grijalba *et al.* (1999) have demonstrated that Ca^{2+} modifies IMM lipid organization by interacting with the anionic head of cardiolipin molecules which suggests that increased Ca^{2+} levels may affect the mitochondrial respiratory chain function and favour superoxide radical production at intermediate steps of the respiratory chain. Moreover, mitochondrial ROS generation could serve as the oxidizing agent for MPT pore activation (Inoue *et al.,* 2008). The excess oxidants possibly involves in the oxidation of thiols on the MPTP complex in cooperation with Ca^{2+} (Petronilli *et al.,* 1994). The sensitivity of MPTP could also be increased by oxidation or cross-linking of critical dithiols in membrane proteins, thus promoting the subsequent MPTP opening (Chernyak *et al.,* 1995). Alternatively, Ca^{2+} could bind to the matrix side of IMM membrane and promotes extensive conformational changes of membrane proteins which caused the thiol groups to be more susceptible to oxidation (Kowaltowski *et al.,* 1997).

Mitochondrial Ca^{2+} may also induce MPTP opening by activating Ca^{2+}-dependent calpains (Gores *et al.,* 1998). Active calpain 10 has been demonstrated in the outer membrane, intermembrane and mostly matrix fractions of isolated mitochondria. Early study showed

mitochondrial matrix calpain 10 triggered MPTP and caused damage to mitochondrial Complex I (Arrington *et al.*, 2006). Therefore, it is likely that mitochondrial calpain activates MPTP opening by cleaving proteins to generate positively charged peptides which may allosterically alter pore opening by binding at a site that normally binds cations (Aguilar *et al.*, 1996). Mitochondrial Ca^{2+} released from MPTP could subsequently activate cytosolic calpain. The inhibition of mitochondrial calpain activation prevented cytosolic calpain activation in HOCl-treated HMDM cells which indicates that cytosolic calpain activation occurs after MPT pore opening (Yang, 2009). Activated calpains have been shown to cause bleb formation and necrotic cell death by proteolytically cleaving cytoskeletal proteins (Miyoshi *et al.*, 1996; Weber *et al.*, 2005). Calpain activation can also cause lysosomal destabilization and the release of cathepsin, a protease responsible for degradation of cellular components that leads to necrotic or apoptotic cell death (Yap *et al.*, 2006). Furthermore, there are also other apoptotic factors released from mitochondria through the activated MPTP such as cytochrome *c*, leading to caspase activation and subsequent apoptotic cell death (Nicotera & Orrenius, 1998).

In this study, ruthenium red has been found to protect cells from oxLDL-induced cell death (**Figure 5.47, 5.48** and **5.49**). Likewise, oxLDL-induced intracellular ROS levels were also suppressed by ruthenium red (**Figure 5.50**). This showed that, inhibiting Ca^{2+} uptake into the mitochondria by ruthenium red has resulted in a reduction in intracellular ROS (possibly including mitochondrial ROS) levels which in turn protected cells from oxLDL-induced cell death. Thus, it is likely that ruthenium red protected against MPT activation and prevented $\Delta\Psi m$ loss to a certain degree. However, cell viability loss was not completely prevented by ruthenium red, suggesting other mechanisms might be inducing MPT activation caused by oxLDL. An incomplete protection against HOCl-induced cell death was also observed by (Yang, 2009) in this laboratory although $\Delta\Psi m$ loss was protected by ruthenium red. Calpains are also found in the intermembrane space of the mitochondria (Tavares & Duque-Magalhaes, 1991). Thus, it is possible that Ca^{2+} diffused to the intermembrane space through VDAC, initiated the calpains and MPT was somehow activated. Additionally, Ca^{2+} binding to an extramitochondrial site might also activate MPT. In studies done by Kowaltowski *et al.* (1997), phenylarsine oxide-induced MMP was inhibited by EGTA but not by ruthenium red. This suggests that phenylarsine oxide induces MPT activation via a mechanism independent of matrix Ca^{2+} but dependent on Ca^{2+} binding to an extramitochondrial site. Further study

could be carried out to confirm and determine the effect of ruthenium red on oxLDL-induced ΔΨm loss.

The exact mechanism on how Ca^{2+} stimulates mitochondrial ROS production remains elusive although possible mechanisms have been proposed (Brookes *et al.*, 2004). Among others, the suggested mechanisms include Ca^{2+} stimulated increase of metabolic rate, Ca^{2+} induced nitric oxide and the effects exerted on respiratory complexes, Ca^{2+} triggered cytochrome *c* dissociation, Ca^{2+} induced cardiolipin peroxidation, Ca^{2+}-calmodulin dependent protein kinases activation as well as Ca^{2+} induced MPT pore opening that could results in the release of cytochrome *c* and GSH- and NADPH- dependent antioxidative enzymes (Peng & Jou, 2010). Additionally, different experimental conditions such as different types of mitochondrial preparations (intact or isolated mitochondria), mitochondria from different cells/tissues/animals species and combination of different pharmacological inhibitors used may affect and initiate different mechanism of ROS production by Ca^{2+} (Peng & Jou, 2010).

OxLDL-induced cellular oxidative stress involves in modulating the functions of a series of signalling pathways which include activating the cell death pathway, dysregulating mitochondria and ER as well as promoting inflammation (Chang *et al.*, 2014) whereby most of these pathways are potentially cytotoxic (Irani, 2000; Salvayre *et al.*, 2002; Steinberg, 1997).

Effects of oxLDL on MPT activation and mitochondrial membrane potential (ΔΨm)

Mitochondrial membrane potential (ΔΨm) is critical for maintaining the physiological function of the respiratory chain to generate ATP. Since mitochondria are the major machinery for ATP generation in cells, a significant loss of ΔΨm causes cells to be depleted of energy with subsequent death. In this study, results from preliminary experiments using TMRM showed that oxLDL caused a time-dependent decrease in ΔΨm in U937, human monocytes and HMDM cells (**Figure 5.46**). However, the common excitation wavelength of 488 nm measured using flow cytometry was not optimal compared to 548 nm (Plasek *et al.*, 2005; Russell *et al.*, 2002; Wlodkowic *et al.*, 2006). Thus, studies on oxLDL-induced ΔΨm loss are underway using JC-1 dye, which should be more specific for flow cytometry measurement. Nevertheless, preliminary results suggest that ΔΨm might contribute to the necrotic cell death in these cells. Moreover, previous studies by Katouah (2012) in this lab

have clearly showed that oxLDL has caused ATP depletion in U937 and HMDM cells. The decrease in ATP was significant as early as 3 hours after incubation with oxLDL and remained low until 12 hours. However, the exact timing of mitochondrial shutdown is not known because with increasing incubation time of oxLDL, the number of dead cells increases.

Tetramethylrhodamine methyl ester (TMRM) was the fluorescent dye used in this study and it has no effect on mitochondrial respiration at low concentrations (Scaduto & Grotyohann, 1999). In addition, TMRM does not accumulate in cell membrane or interact with membrane proteins. There are other fluorescence probes available for the determination of $\Delta\Psi m$ including rhodamine 123 and tetramethylrhodamine ethyl ester (TMRE) and these dyes were found to inhibit the respiratory processes in isolated mitochondria (Scaduto & Grotyohann, 1999).

Cyclosporin A (CsA) was demonstrated by this study to protect only HMDM cells against oxLDL-induced cell death but not U937 cells and human monocytes (**Figure 5.51, 5.52** and **5.53**). It was found that CsA alone had caused an increased in intracellular ROS levels in both U937 cells and human monocytes and intracellular ROS production sustained the in presence of oxLDL (**Figure 5.54 A** and **B**). The rise in intracellular ROS thus resulted in increased cell viability loss in U937 cells and human monocytes pre-treated with CsA. This finding is supported by de Hornedo *et al.* (2007) and O'Connell *et al.* (2012), who reported that CsA induced oxidative stress and mitochondrial dysfunction in renal tubular cells and human renal mesangial cells, respectively. Likewise, Diederich *et al.* (1994) found that endothelial dysfunction was caused by an increased in superoxide production by CsA whilst Wolf *et al.* (1997) demonstrated that CsA induced oxidative stress in rat hepatocytes.

Interestingly, CsA was not toxic to HMDM cells but offered protection against oxLDL-induced cell viability loss (**Figure 5.53**) and intracellular ROS production (**Figure 5.54 C**). CsA is potent immunosuppressive drug widely used in treating autoimmune disorders and in organ transplantation (Kahan, 1992). CsA has been shown to inhibit both apoptosis and necrosis in rat hepatocytes induced by Ca^{2+} ionophore (A23187) (Qian *et al.*, 1999). This drug is known to bind and block the peptidyl-prolyl *cis-trans* isomerase activity of matrix cyclophilin D (CyP-D) (Bernardi *et al.*, 2006), which is required to form an ANT/CyP-D protein complex for MPT pore opening (McStay *et al.*, 2002; Vieira *et al.*, 2000; Woodfield *et al.*, 1998). Previous work by Yang (2009) showed that MPT activation was involved in

MMP loss in HMDM cells. The protection against oxLDL-induced cell viability loss provided by CsA possibly suggests that oxLDL-mediated MPT activation triggered ΔΨm loss which then resulted in HMDM necrotic cell death. This is in agreement with Asmis and Begley (2003) who demonstrated that oxLDL-induced peroxyl radical production caused MMP loss and subsequent necrotic cell death in macrophages.

Mitochondrial permeability transition pore (MPTP) opening has been associated mostly with necrotic cell death but various stimulants such as BrA (Qian *et al.*, 1999) were also found to induce apoptosis through Ca^{2+}-dependent MPT activation (Zhivotovsky & Orrenius, 2011). Additionally, MPT activation has also been proposed to be a common pathway leading to both necrosis and apoptosis (Kim *et al.*, 2003a; Lemasters *et al.*, 2009). MPT activation is triggered by a high level of Ca^{2+} in the matrix and could be further stimulated by oxidative stress, pyridine nucleotide and thiol oxidation, alkalinisation and low transmembrane potential (Zhivotovsky & Orrenius, 2011). MPTP is in contact sites between the IMM and OMM and act as voltage-operated channel (Zhivotovsky & Orrenius, 2011) whereby MPT activation increases of the IMM permeability to low molecular weight ions and solutes (up to 1500 Da) (Bernardi, 1999; Crompton, 1999) to escape from the matrix into the cytosol. This will then leads to rapid depolarization and uncoupling of oxidative phosphorylation while influx of water and solutes from the cytosol causes mitochondrial swelling due to osmotic disequilibrium and eventually outer membrane rupture (Kim *et al.*, 2003b; Lemasters *et al.*, 2009). Consequently, this could either lead to the release of cytochrome *c*, activation of caspase cascades and apoptosis or severe loss of ATP through the disruption of the IMM and necrotic cell death. In their studies, Qian *et al.* (1999) have showed that MPT mediates both necrosis and apoptosis in BrA-induced mitochondrial Ca^{2+} increase in rat hepatocytes whereby necrotic and apoptotic cell death occurred in the absence of ATP and in the presence of glycolytic ATP, respectively. However, it might not be possible to clearly distinguish between the two types of death pathways (Jaeschke & Lemasters, 2003; Lemasters, 1999) and studies have suggested cross-talks between the different cell death mechanisms (Zhivotovsky & Orrenius, 2010). In this study, morphological characteristics of the cells treated with oxLDL resembled necrotic cells such cell swelling and disruption of cell membrane. Previous findings such as rapid loss of GSH and caspase-3 inactivation by other researchers in this group (Baird *et al.*, 2004; Chen, 2012; Katouah, 2012) on oxLDL-induced toxicity suggested that oxLDL-induced cell death was necrotic rather than apoptotic.

Results in **Chapter Four** showed that oxLDL caused a time-dependent increase in mitochondrial ROS (measured using MitoSOX) in HMDM cells (**Figure 4.7**) whereby studies have suggested that mitochondria-mediated ROS production, as a results of exposing cells to oxidative stress or apoptotic stimuli could initiate MPT activation (Kim *et al.*, 2003b; Kowaltowski *et al.*, 2001). Other studies however, indicated that the mitochondrial ETC components such as cytochrome *c*, could leaked out from the mitochondria through the activated MPTP. Subsequently, this lead to the escape of electrons from Complex III which could reduce oxygen molecules forming superoxide radicals (Luetjens *et al.*, 2000). Ca^{2+}, oxidative stress, reactive chemicals, Pi, $NAD(P)^{+}$ and high pH are among the factors that keep the MPTP opens whereas low pH (less than 7), high membrane potential, Mg^{2+}, ADP and NAD(P)H block the opening of MPTP (Hansson *et al.*, 2003; Lemasters *et al.*, 2009).

Effects of BrA on intracellular ROS and cell viability – in comparison with oxLDL, EGTA and 7,8-NP

Results from this study have showed that oxLDL triggered an increase in intracellular Ca^{2+} as well as intracellular ROS. However, the increase in both intracellular Ca^{2+} and ROS was not as great as that caused by Ca^{2+} ionophore, BrA although both agents caused death to the cells (**Figure 5.55, 5.56** and **5.57**). This suggests that oxLDL-induced intracellular Ca^{2+} alone is not sufficient to cause cell death. Jou *et al.* (2010) have found that BrA treatment resulted in mitochondrial ROS production which relates to Ca^{2+} overload caused by BrA while previous study by Yang (2009) in this lab showed BrA activated MPT, which could be the cause of cell death.

Further studies using BrA and EGTA revealed that intracellular ROS caused by BrA was significantly reduced by EGTA. Subsequently, cell viability loss was also protected (**Figure 5.58, 5.59** and **5.60**). This showed that Ca^{2+} chelation by EGTA has a positive effect in reducing intracellular ROS caused by BrA-induced Ca^{2+} influx which also protected the cells from death. However, earlier results showed that EGTA was not able to inhibit oxLDL-induced ROS production despite its ability to block intracellular Ca^{2+} increase. Taken together, this showed that oxLDL might be causing a Ca^{2+}-independent increased in intracellular ROS compared to BrA.

Results also showed the ability of 7,8-NP to reduce BrA-induced intracellular ROS level and provide protection against cell viability loss (**Figure 5.61, 5.62** and **5.63**). This suggests that

the mechanism of action of 7,8-NP is scavenging ROS induced by BrA. Results in **Chapter Four** and from previous work done by other researchers in this lab have clearly revealed that 7,8-NP works by scavenging oxidants induced by oxLDL, thus protecting cells from oxLDL insult. Taken together, this also suggests that 7,8-NP scavenges ROS/oxidants that might be generated by Ca^{2+} and non-Ca^{2+} sources.

Summary

Results from the experimental works done for this chapter clearly showed that oxLDL initiated a rapid Ca^{2+} influx and accumulation of Ca^{2+} in the cytosol. Most of the Ca^{2+} flux is from extracellular origin but Ca^{2+} mobilisation from intracellular stores does play a role.

Intracellular Ca^{2+} increase triggered by oxLDL correlated with the increase in intracellular ROS. However, blocking oxLDL-induced intracellular Ca^{2+} rise by Ca^{2+} chelator did not inhibit the increase in intracellular ROS. In contrast, blocking Ca^{2+} uptake by mitochondria had reduced intracellular ROS production and improved cell viability. This suggests that intracellular Ca^{2+} increased mediated by oxLDL is important in inducing mitochondrial ROS production and oxLDL may also trigger a Ca^{2+}-independent pathway of cell death.

Excess cytosolic Ca^{2+} can be taken up into the mitochondria and could caused mitochondrial Ca^{2+} overload. This could increase mitochondrial ROS generation and also trigger the opening of MPT pores, thus caused the collapse of MMP as a result of mitochondrial outer membrane rupture. These events will subsequently result in cell death. Results from this chapter clearly showed that blocking Ca^{2+} uptake into the mitochondria protected cells from oxLDL-induced cell death possibly by reducing ROS production and preventing MPT activation. Indeed, oxLDL insult to the mitochondria might play a vital role in oxLDL-mediated cell death and should be the future direction.

A diagram showing the proposed involvement of Ca^{2+} and ROS in oxLDL-mediated toxicity to the three types of cells studied in this research is shown by **Figure 5.64**.

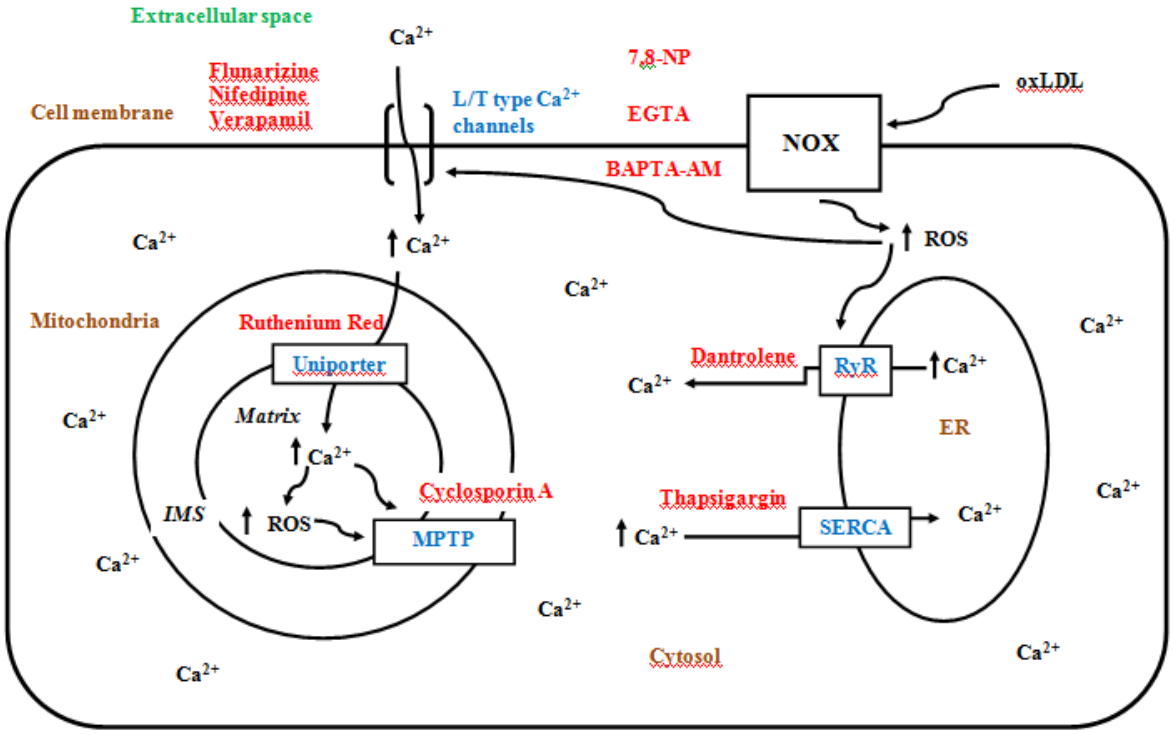

Figure 64: Proposed involvement of Ca^{2+} and ROS in oxLDL-mediated toxicity to U937 cells, human monocytes and HMDM cells.

OxLDL activates NADPH oxidase (NOX) on the plasma membrane. NOX-derived ROS triggers the voltage-dependent L- and T-type Ca^{2+} channels on cell membrane and ryanodine receptors (RyR) on endoplasmic reticulum (ER), resulting in the influx of extracellular Ca^{2+} and release of Ca^{2+} from ER stores to cytosol. Both events lead to cytosolic Ca^{2+} increase. Excess cytosolic Ca^{2+} can be taken up into mitochondria via Ca^{2+} uniporter on the inner mitochondrial membrane (IMS). Ca^{2+} accumulation in mitochondrial matrix increases mitochondrial ROS production, causing mitochondrial permeability transition pore (MPTP) to open. MPTP activation leads to mitochondrial membrane potential loss and will subsequently results in cell death. Ca^{2+} channel blockers (flunarizine, nifedipine, verapamil, dantrolene, thapsigargin, ruthenium red), Ca^{2+} chelators (EGTA and BAPTA-AM), cyclosporin A and 7,8-NP used in this study are shown in red at their respective target sites.

CHAPTER SIX

6. Hydrogen sulfide (H_2S) and oxLDL-mediated cell death

Introduction

This chapter aims to investigate the effects of different types of slow releasing H_2S donors on oxLDL-mediated cell death. This will include studying their effects on cell viability, intracellular Ca^{2+} and ROS productions in U937 cells, human monocytes and HMDM cells.

An increasing body of evidence has implicated the involvement of hydrogen sulfide (H_2S) in biological systems through a variety of interrelated mechanisms (Szabo, 2007). In the past decade, H_2S has emerged as an important mediator in various physiological and pathophysiological processes (Whiteman *et al.*, 2011a). Studies have shown that H_2S can either protect or damage cells and this depends on its concentration, type of cell and experimental conditions (Wagner *et al.*, 2009). High levels of H_2S are always accompanied by cytotoxic effects that could result from free radical generation and loss of GSH. Low levels of H_2S have been shown to be either cytoprotective or proapoptotic (Adhikari & Bhatia, 2008; Baskar *et al.*, 2007; Cao *et al.*, 2006). H_2S has been reported to cause apoptosis in aortic smooth muscle (Yang *et al.*, 2004; Yang *et al.*, 2006), lung fibroblasts (Baskar *et al.*, 2007) and pancreatic acinar cells (Adhikari & Bhatia, 2008) but it is protective in neural cells (Xiao *et al.*, 2012).

H_2S as ROS scavenger and inhibitor

H_2S is capable of scavenging free radicals by single electron or hydrogen atom transfer (Carballal *et al.*, 2011). H_2S has been reported to scavenge reactive oxygen and nitrogen species such superoxide (Yan *et al.*, 2006), hydrogen peroxide (Lu *et al.*, 2008), peroxynitrate (Whiteman *et al.*, 2004), hypochlorous acid (Whiteman *et al.*, 2005) and lipid hydroperoxides (Carballal *et al.*, 2011; Muellner *et al.*, 2009).

In human endothelial cells (Muzaffar *et al.*, 2008a) and vascular smooth muscle cells (Muzaffar *et al.*, 2008b), H_2S has been demonstrated to inhibit superoxide production by reducing NOX expression and activity. Samhan-Arias *et al.* (2009) have also showed that H_2S protects synaptic plasma membranes from oxidative stress by the inhibition of ROS production via NOX. Moreover, H_2S has been shown to increase GSH levels, thus protecting mitochondria from oxidative stress in neurons (Kimura *et al.*, 2010). **Figure 6.1** shows the suggested protective effects of H_2S against ROS in the vasculature.

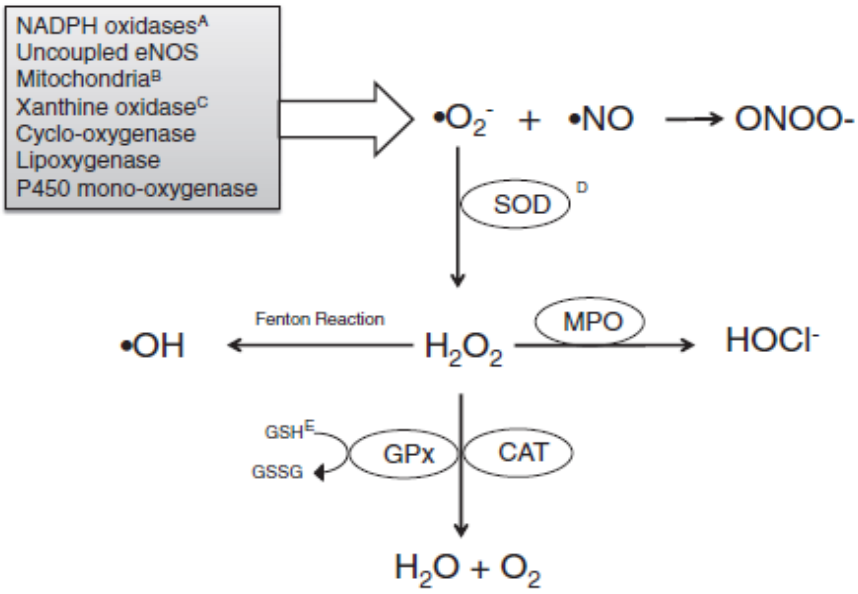

Figure 6.1: Potential protective effects of H_2S towards vascular ROS

H_2S has been shown to inhibit NADPH oxidase activity and expression (A); mitochondrial ROS production (B) and possibly xanthine oxidase activity (C). It has also been reported to scavenge ROS and promote the actions of SOD (D) and GSH (E) (Streeter *et al.*, 2013).

H_2S roles in mitochondria

Mitochondria play a vital role as the key source and target for detrimental intracellular oxidants generation (Murphy, 2009). Studies have implicated the importance of H_2S in regulating mitochondrial function (Modis *et al.*, 2013a) as well as reducing mitochondrial ROS generation (Sun *et al.*, 2012). Recent studies by Modis *et al.* (2013a) demonstrated that low levels of H_2S generated by mitochondrial enzyme, 3-MST, has donated electrons to the Krebs cycle, enhancing mitochondrial electron transport and bioenergetics (**Figure 6.2**). In hepatoma cells, this effect is suppressed during oxidative stress but reversed with administration of exogenous H_2S (Modis *et al.*, 2013b).

Translocation of CBS (cystathionine-β-synthase) (Fu *et al.*, 2012) and CSE (cystathionine-γ-lyase) (Modis *et al.*, 2013b; Szabo *et al.*, 2013) from the cytosol to the mitochondrial matrix in response to hypoxic and calcium stress have been observed. The resulting H_2S generation within the mitochondria might act as an electron acceptor in the mitochondrial respiratory chain which then increases cellular ATP production, thus preserving cell viability (Fu *et al.*, 2012; Modis *et al.*, 2013b; Szabo *et al.*, 2013; Teng *et al.*, 2013).

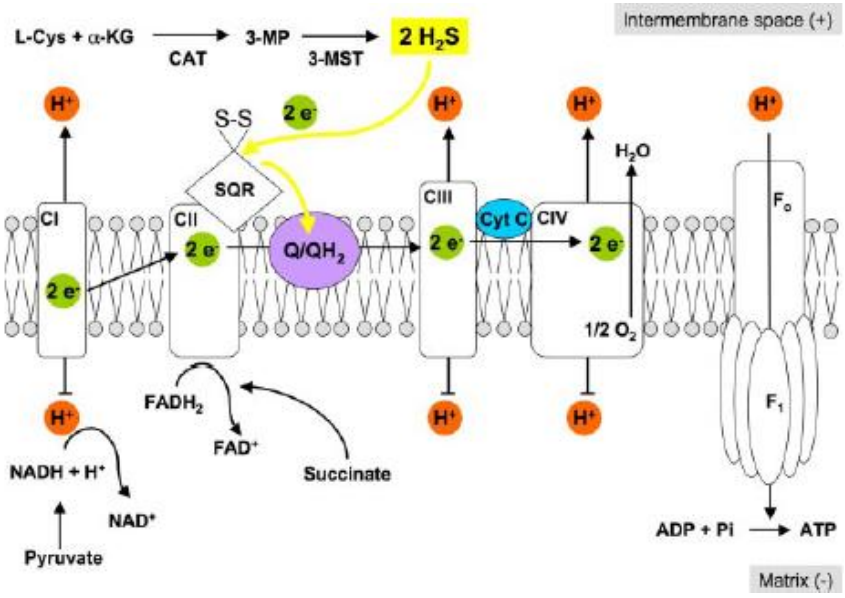

Figure 6.2: Role of endogenous H_2S in the mitochondrial electron transport

H_2S and Krebs-cycle-derived electron donors (NADH+H, $FADH_2$) donate electrons to complexes I and II respectively. Mitochondrial enzyme, 3-MST, converts 3-MP to H_2S, which then serve as an inorganic electron donor that stimulates mitochondrial electron transport. H_2S donates electrons into the mitochondrial electron transport chain via an enzyme linked to complex II, SQR (sulfide:quino-oxidoreductase) (Modis *et al.*, 2013a).

H_2S and intracellular calcium regulation

Calcium (Ca^{2+}) plays an important role as key signalling molecule in regulating a various biological processes. Cytoplasmic concentration of Ca^{2+} is being tightly regulated within nanomolar range, which is approximately ten thousand fold difference across plasma membrane (1.5 mM at extracellular and 0.1 µM in cytosol) (Montell, 2005). The mechanisms responsible for regulating the influx of external calcium are well established (Berridge, 1998). Extracellular Ca^{2+} can cross plasma membrane via two major pathways i.e. voltage-operated Ca^{2+} channels (VOCCs) and receptor operated Ca^{2+} channels (ROCCs) (Pinilla *et al.*, 2005). Studies have demonstrated that H_2S has the capability of either inhibiting or

activating Ca^{2+} entry and this depends on the molecular nature of the Ca^{2+} entry pathway [reviewed by Munaron *et al.* (2012)].

In exerting cardioprotective effect, it has been proposed that H_2S causes indirect inhibitory action on L-type calcium channels (VOCCs) besides directly inhibiting the β-adrenergic receptors (Mancardi *et al.*, 2009). Thus, Sun *et al.* (2008) have showed the ability of H_2S to inhibit L-type calcium channels in NaHS treated rat cardiomyocytes while (Maeda *et al.*, 2009) has reported that H_2S may facilitate membrane currents through T-type calcium channels. In studies done on endothelial cells, Bauer *et al.* (2010) concluded that H_2S can directly regulate Ca^{2+} homeostasis and signalling via multiple mechanisms.

H_2S roles in atherosclerosis

Atherosclerosis is characterised by multiple key events including endothelial dysfunction, infiltration of monocytes into the vascular wall and their differentiation into macrophages, uptake of oxLDL and conversion of lipid laden macrophages into foam cells and smooth muscle cell proliferation. Increasing evidence has implicated the significant involvement of H_2S in these biological processes and disruption of H_2S homeostasis may contribute to the pathogenesis of atherosclerosis (Lynn & Austin, 2011).

Recent studies have suggested that macrophages can produce H_2S endogenously (Zhu *et al.*, 2010). Zhu *et al.* (2010) has reported the presence of CSE as well as endogenous H_2S production in peritoneal and RAW 264.7 macrophages treated with L-cysteine and PLP. They have also showed that lipopolysaccharide (LPS) stimulated CSE but not CBS expression and H_2S generation in macrophages. Moreover, NaHS in a dose-dependent manner has been found to suppress oxLDL-induced foam cell formation in THP-1 derived macrophages (Wang *et al.*, 2009).

Laggner *et al.* (2007) demonstrated that H_2S counteracts LDL oxidation by HOCl, whereby 50 µM HOCl was completely scavenged in the presence of equimolar concentrations of NaHS for 30 min at 37^{o}C. In addition to its HOCl scavenging potential, the authors also found that H_2S inhibited myeloperoxidase (MPO) activity and scavenge H_2O_2. Studies done on HMDM cells by Zhao *et al.* (2011) revealed that NaHS treatment significantly suppressed macrophage derived foam cell formation by inhibiting oxLDL binding and uptake into macrophages. In addition, NaHS treatment significantly lowered the levels of CD36,

scavenger receptor A and acetyl co-enzyme A acyltransferase-1 (ACAT1) expressions which were up-regulated by oxLDL in HMDM cells via KATP/ERK1/2 pathway. **Figure 6.3** summarises the possible protective effects of H_2S in impeding atherogenesis at all stages of atherosclerosis development.

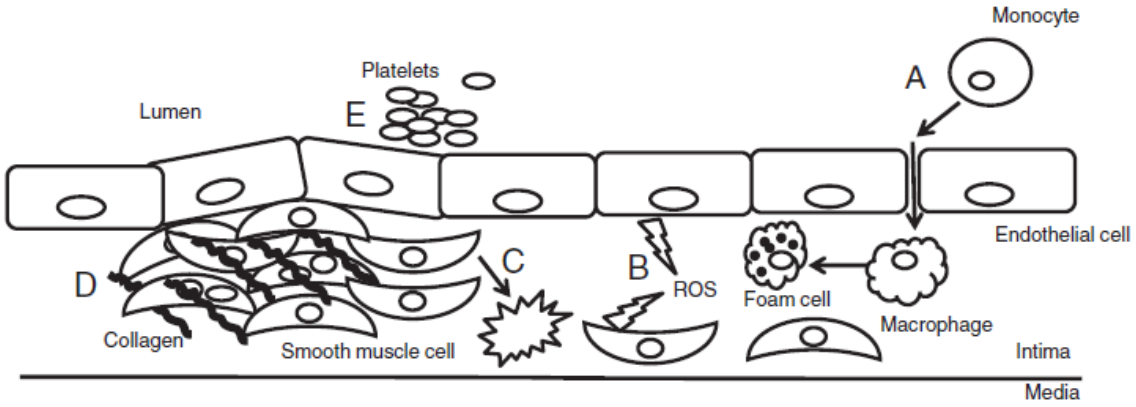

Figure 6.3: Potential protective effects of H_2S in the vasculature
H_2S has been shown to decrease adhesion and migration of leukocytes and their differentiation to foam cells (A); inhibits as well as scavenges the production of ROS (B); prevents proliferation and promotes apoptosis of vascular smooth muscle cells (C); prevents collagen deposition and neo-intima formation (D) and inhibits platelet adhesion (E) (Streeter *et al.*, 2013).

H_2S donors

Recently, several H_2S releasing molecules (termed as H_2S donors) have been developed to deliver a controlled and stable delivery of H_2S to cells and tissues. The development and characterisation of appropriate H_2S donors are vital for pharmacological use. H_2S donors should not be toxic, should be soluble in aqueous media, should not metabolise rapidly and should release H_2S *in vivo* slowly (Whiteman *et al.*, 2011a).

Although sulfide salts such as NaSH or Na_2S (Szabo, 2007) can be conveniently used to prepare standardised H_2S solution, they are not useful to study in H_2S physiology. This is because generation of both H_2S and Na^+ as an instantaneous release of bolus dissipates in a very short period of time (Li *et al.*, 2008; Whiteman *et al.*, 2010) rather than replicate the slow and sustained generation of H_2S from CSE, CBS or 3-MST enzymes in the tissues. Additionally, a huge and quick release of H_2S result in rapid fall of blood pressure which may have damaging effects in tissues or organs (Li *et al.*, 2008).

Thus, organic H_2S donors which generate H_2S in a physiologically-like manner were developed and synthesised (Whiteman *et al.*, 2011a) to avoid the use of sulfide salts. Existing non-steroidal anti-inflammatory drugs (NSAIDs) compounds such as indomethacin (ATB-343), diclofenac (ACS-15), naproxen (ATB-345) and mesalamine (ATB-429) (Whiteman & Winyard, 2011b) have been modified by adding ADT-OH [5-(4-hydroxyphenyl-3H-1,2-dithiole-3-thione] group. Studies have shown that these organic H_2S donors actively alleviate and limit the adverse effects and toxicity of NSAIDs and demonstrate promising outcomes in treating inflammatory bowel disease, oedema, acute inflammation and endotoxic shock. Even though the precise mechanism of how ADT-OH releases H_2S is unknown (Whiteman *et al.*, 2011a; Whiteman *et al.*, 2010), the potential therapeutic effects of ADT-OH derivatives in treating inflammatory and vascular disease as well as cancer is at least partly due to the release of H_2S (Whiteman *et al.*, 2011a).

The more recently synthesised and characterised H_2S donors do not consist of structurally modified established drug molecules such as GYY4137 (Whiteman *et al.*, 2011a). The novel H_2S donors used in this study were a gift from Professor Matthew Whiteman (University of Exeter Medical School, St. Luke's Campus, Exeter, England). These water-soluble novel H_2S donors provide as pharmacological tools which generate H_2S at different rates [AP67 (fastest) > AP72 > AP105 > AP106 >>> GYY4137 (slowest)]. Recently, AP39, which is a novel dithiolethione derivative containing a triphenylphosphonium moiety enabling specific delivery of sub-nanomolar concentrations of the compounds to mitochondria was also developed (Le Trionnaire *et al.*, 2014). The chemical structures and characteristics of these H_2S donors are shown in **Figure 6.4** and **Table 6.1**.

The aim of this chapter is to investigate the effects of individual H_2S donors on U937 cells, human monocytes and HMDM cells. Effects of these H_2S donors on cell viability, intracellular calcium level and ROS production were studied following incubation with these compounds and also with oxLDL. The results section will present the data obtained from the experiments according to the type of cells being studied i.e. U937 cells, human monocytes and HMDMs respectively.

GYY4137

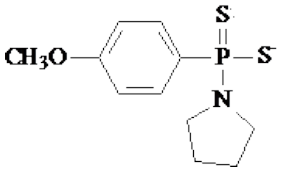

AP67

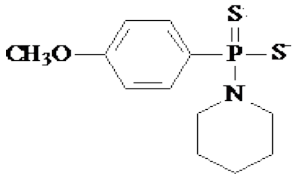

AP72

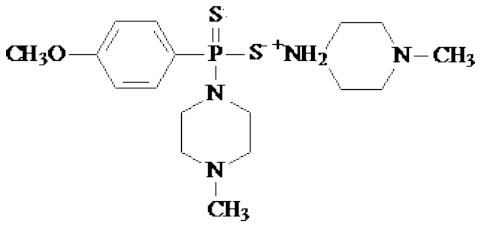

AP106

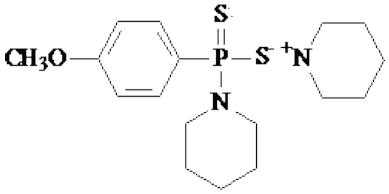

AP106

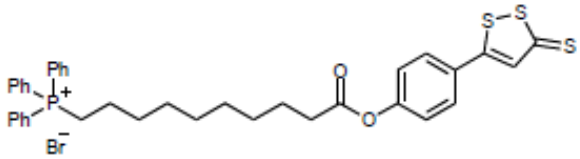

AP39

Figure 6.4: Chemical structures of H_2S donors

Table 6.1: Characteristics of H_2S donors

H_2S donors	Molecular weight (g/mol)	Physical appearance	Location of action	Final concentration used in this study
GYY4137	376.4	White powder	Cytoplasm	200 µM
AP39	721.7	Orange-brownish solid	Mitochondria	100 nM
AP67	273.3	Whitish powder	Cytoplasm	200 µM
AP72	287.3	Whitish powder	Cytoplasm	200 µM
AP105	372.5	Yellowish powder	Cytoplasm	200 µM
AP106	402.5	Yellowish powder	Cytoplasm	200 µM

Results

Effects of various H_2S donors on U937 cells, human monocytes and HMDM cells in the absence or presence of oxLDL: cell viability

This is the first time these H_2S donors are being used to examine their effects on oxLDL-mediated cell death. Initial experiments were carried out on U937 cells (**Figure 6.5** and **6.6)**, human monocytes (**Figure 6.7** and **6.8**) and HMDM cells (**Figure 6.9** and **6.10**) to assess their effects on the cells, with and without the presence of oxLDL. Cell viability results illustrated that all H_2S donors were not toxic to the three different types of cells. However, when oxLDL was added to the cells, these H_2S donors reacted differently that only certain H_2S donors were able to protect the cells from oxLDL-mediated cytotoxicity.

All of the H_2S donors were not toxic when incubated with U937 cells for 28 hours (**Figure 6.5**). However, in the presence of oxLDL, only GYY4137, AP67, AP72 and AP105 were found to be statistically significant in protecting the cells from oxLDL cytotoxicity i.e 15 to 20% of protection compared to oxLDL only treated cells (PI negative cells). Additionally, the percentage of PI positive cells was also significantly reduced in cells pre-treated with GYY4137, AP67 and AP72 compared to oxLDL only treated cells. Meanwhile, no protection from oxLDL-induced toxicity was observed in cells treated with AP106 and AP39 (**Figure 6.6**).

Incubation of H_2S donors only with human monocytes did not cause cell viability loss (**Figure 6.7**). Human monocytes treated with oxLDL had cell viability loss of approximately 40% (PI negative cells). Novel H_2S donors, AP67 and AP72 were found to be protecting human monocytes from oxLDL-mediated cell death (statistically significant) with approximately 15% more viable cells compared to oxLDL-only treated cells (PI negative cells) (**Figure 6.8**). Surprisingly, GYY4137 did not convey any protection to human monocytes against oxLDL insult as observed in U937 cells. Likewise, no protection against oxLDL-induced cell viability loss was seen in cells treated with AP105, AP106 and AP39. In fact, in the presence of oxLDL, cell viability loss was greater in AP105 pre-treated cells (lower percentage of PI negative cells and higher percentage of PI positive cells) compared to oxLDL treated cells.

Similarly, all H_2S donors used in this study were not toxic to HMDM cells (**Figure 6.9**). However, in the presence of oxLDL, only three of the H_2S donors were found to be protective to HMDM cells against oxLDL-induced toxicity. Cells treated with oxLDL had a reduction in cell viability by 40% (PI negative cells) whilst AP67, AP72 and AP39 had significantly decreased oxLDL-induced cell viability loss by 15 to 20% (increased in PI negative cells). Moreover, the percentage of PI positive cells were also significantly decreased in HMDM cells pre-treated with AP39 compared to oxLDL treated cells. Likewise, no protection against oxLDL-mediated cell viability loss was found in HMDM cells pre-treated with GYY4137, AP105 and AP106 (**Figure 6.10**).

A)

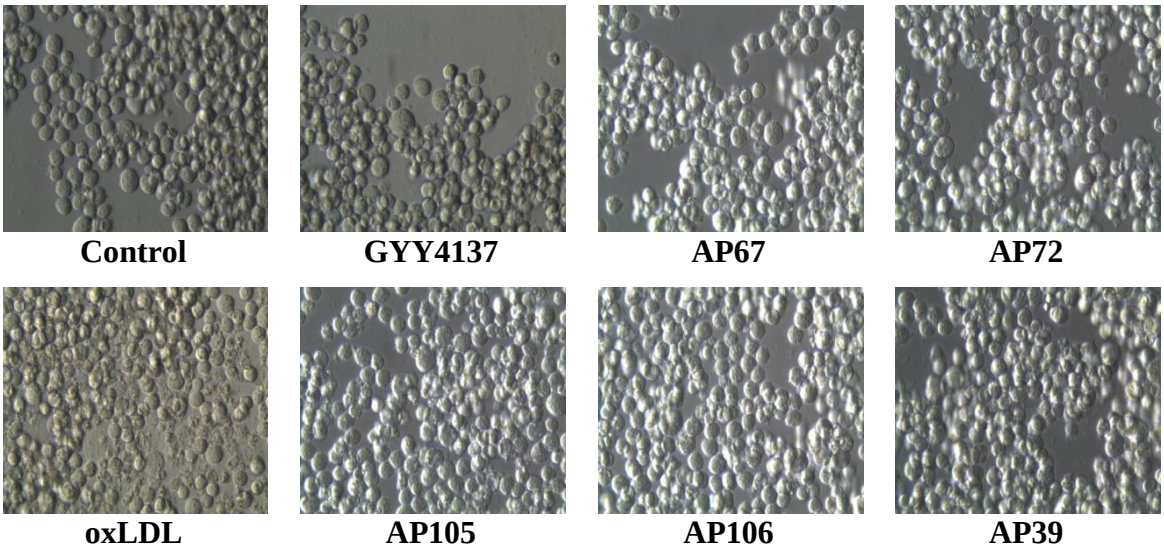

B)

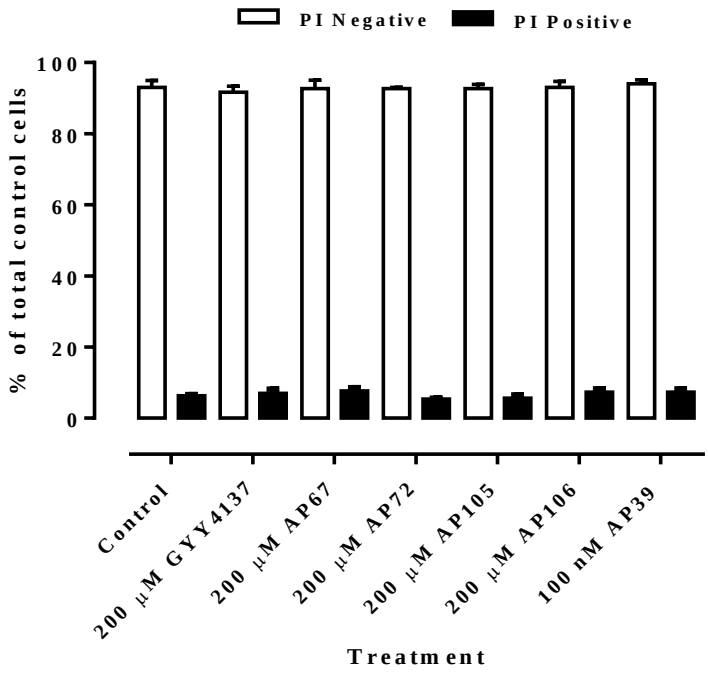

Figure 6.5: Effect of various H_2S donors on cell viability of U937 cells.

U937 cells (0.5×10^6 cells/mL) were incubated at 37°C in non-phenol red RPMI-1640 with various types of H_2S donors for 28 hours. A) Cells were viewed *in situ* in tissue culture wells using an inverted microscope (400x magnification) after 28 hour. Images were taken using a Leica C-Mount camera and processed using Leica Application Suite software. B) Cell viability was determined using PI-flow cytometry. A cell only treatment was included as control and data are expressed as percentage of the total number of cells in control samples. Results shown are mean ± SEM of triplicates from a representative experiment.

A)

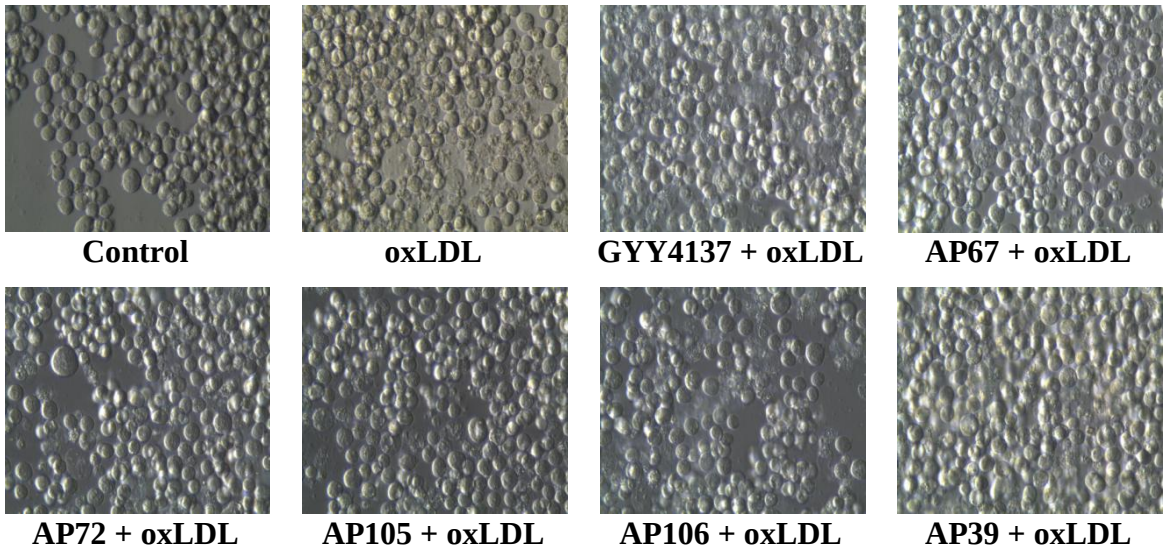

B)

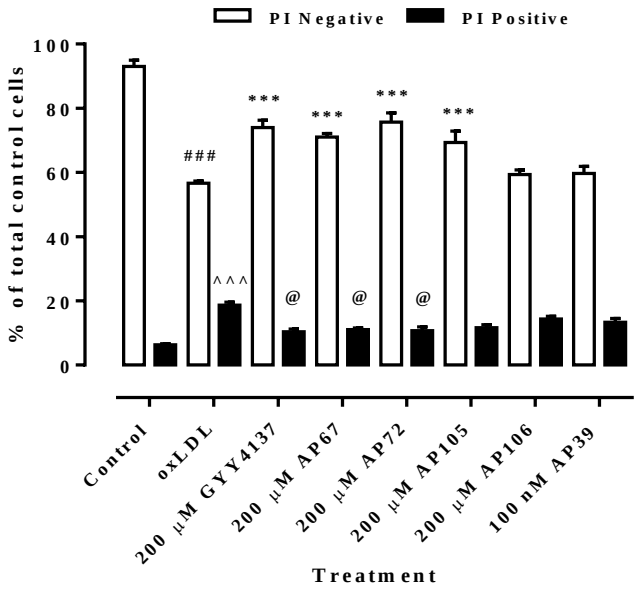

Figure 6.6: Effect of various H_2S donors and oxLDL on cell viability of U937 cells.

U937 cells (0.5×10^6 cells/mL) were incubated at 37°C in non-phenol red RPMI-1640 with various types of H_2S donors for 4 hours before the addition of the LC_{50} concentration (0.25 mg/mL) of oxLDL and incubated for another 24 hours. A) Cells were viewed *in situ* in tissue culture wells using an inverted microscope (400x magnification) after 24 hours incubation with oxLDL. Images were taken using a Leica C-Mount camera and processed using Leica Application Suite software. B) Cell viability was determined using PI- flow cytometry. A cell only treatment was included as control and data are expressed as percentage of the total number of cells in control samples. Results shown are mean ± SEM of triplicates from a representative experiment. Statistical significance (two-way ANOVA, Sidak's multiple comparison test) is indicated from: PI negative cells - control vs oxLDL, ###, $p<0.001$ and oxLDL vs H_2S donors + oxLDL, ***, $p<0.001$; PI positive cells – control vs oxLDL, ^^^, $p<0.001$ and oxLDL vs H_2S donors + oxLDL , @, $p<0.05$.

A)

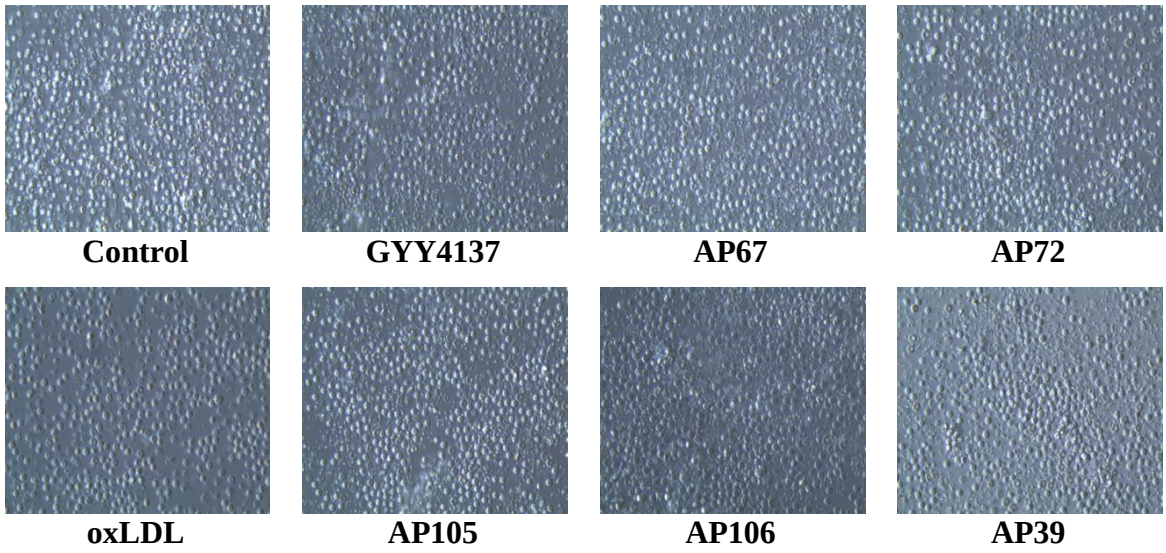

B)

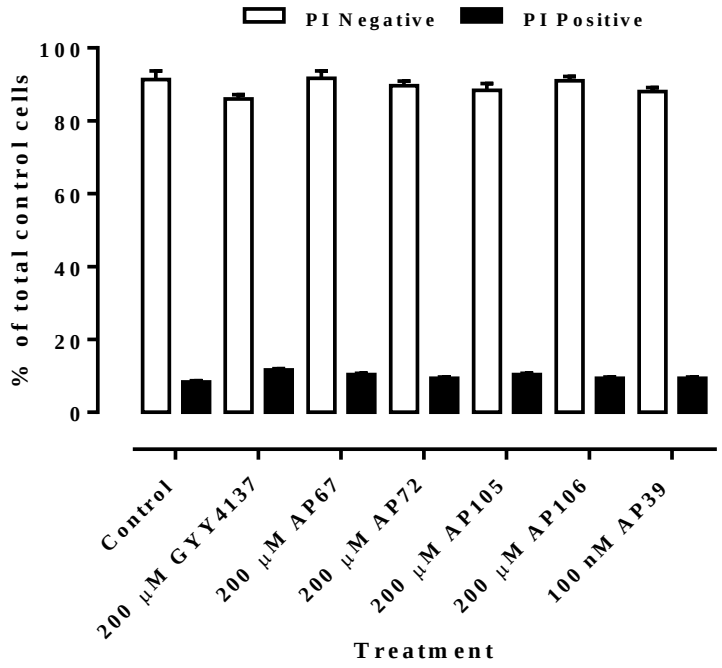

Figure 6.7: Effect of various H_2S donors on cell viability of human monocytes.

Human monocytes (1×10^6 cells/mL) were incubated at 37°C in non-phenol red RPMI-1640 with various types of H_2S donors for 28 hours. A) Cells were viewed *in situ* in tissue culture wells using an inverted microscope (400x magnification) after 28 hour. Images were taken using a Leica C-Mount camera and processed using Leica Application Suite software. B) Cell viability was determined using PI-flow cytometry. A cell only treatment was included as control and data are expressed as percentage of the total number of cells in control samples. Results shown are mean ± SEM of triplicates from a representative experiment.

A)

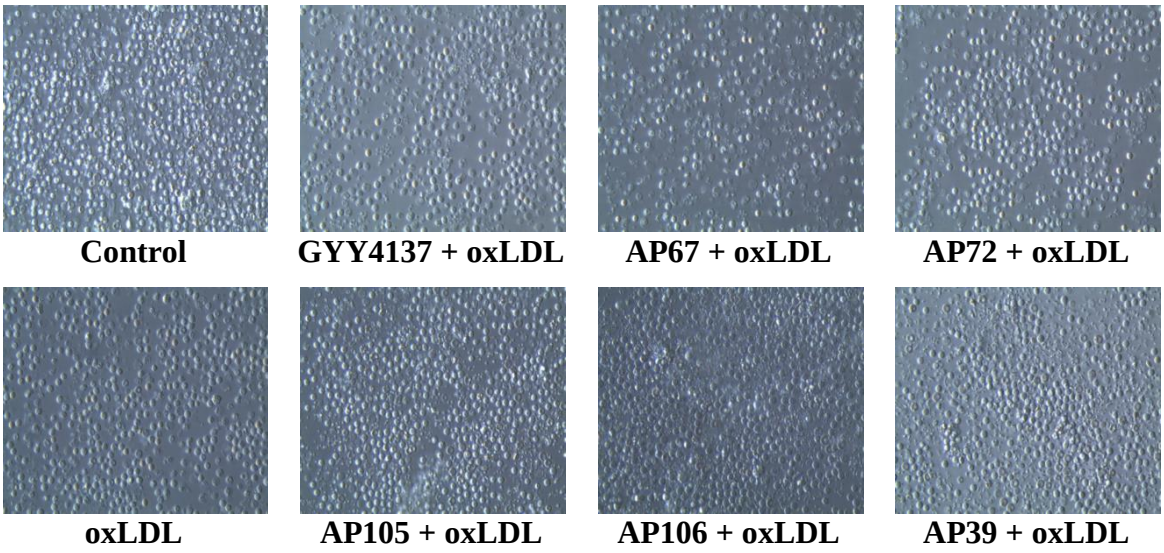

B)

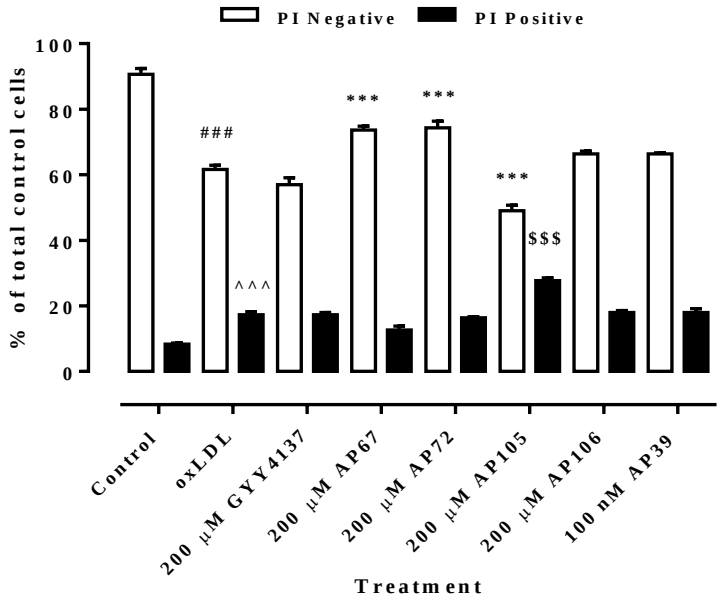

Figure 6.8: Effect of various H_2S donors and oxLDL on cell viability of human monocytes.

Human monocytes (1×10^6 cells/mL) were incubated at 37°C in non-phenol red RPMI-1640 with various types of H_2S donors for 4 hours before the addition of the LC_{50} concentration (0.75 mg/mL) of oxLDL and incubated for another 24 hours. A) Cells were viewed *in situ* in tissue culture plates using an inverted microscope (400x magnification) after 24 hours incubation with oxLDL. Images were taken using a Leica C-Mount camera and processed using Leica Application Suite software. B) Cell viability was determined using PI via flow cytometry. A cell only treatment was included as control and data are expressed as percentage of the total number of cells in control samples. Results shown are mean ± SEM of triplicates from a representative experiment. Statistical significance (two-way ANOVA, Sidak's multiple comparison test) is indicated from: PI negative cells - control vs oxLDL, ###, $p<0.001$ and oxLDL vs H_2S donors + oxLDL, ***, $p<0.001$; PI positive cells – control vs oxLDL, ^^^, $p<0.001$ and oxLDL vs H_2S donors + oxLDL , $$$, $p<0.001$.

A)

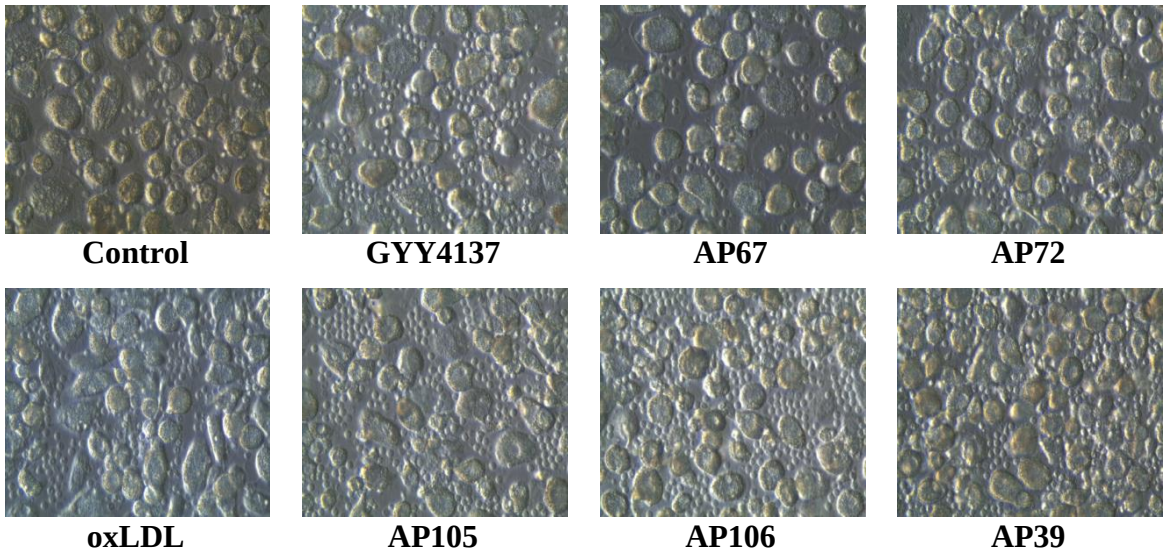

B)

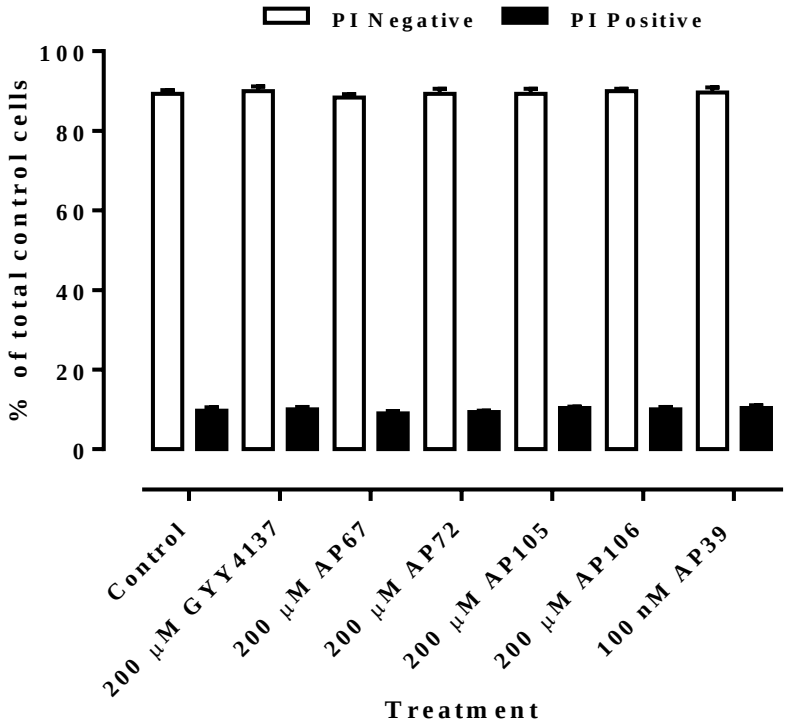

Figure 6.9: Effect of various H_2S donors on cell viability of HMDM cells.

HMDM cells (1×10^6 cells/mL) were incubated at 37°C in non-phenol red RPMI-1640 with various types of H_2S donors for 28 hours. A) Cells were viewed *in situ* in tissue culture wells using an inverted microscope (400x magnification) after 28 hour. Images were taken using a Leica C-Mount camera and processed using Leica Application Suite software. B) Cell viability was determined using PI-flow cytometry. A cell only treatment was included as control and data are expressed as percentage of the total number of cells in control samples. Results shown are mean ± SEM of triplicates from a representative experiment.

A)

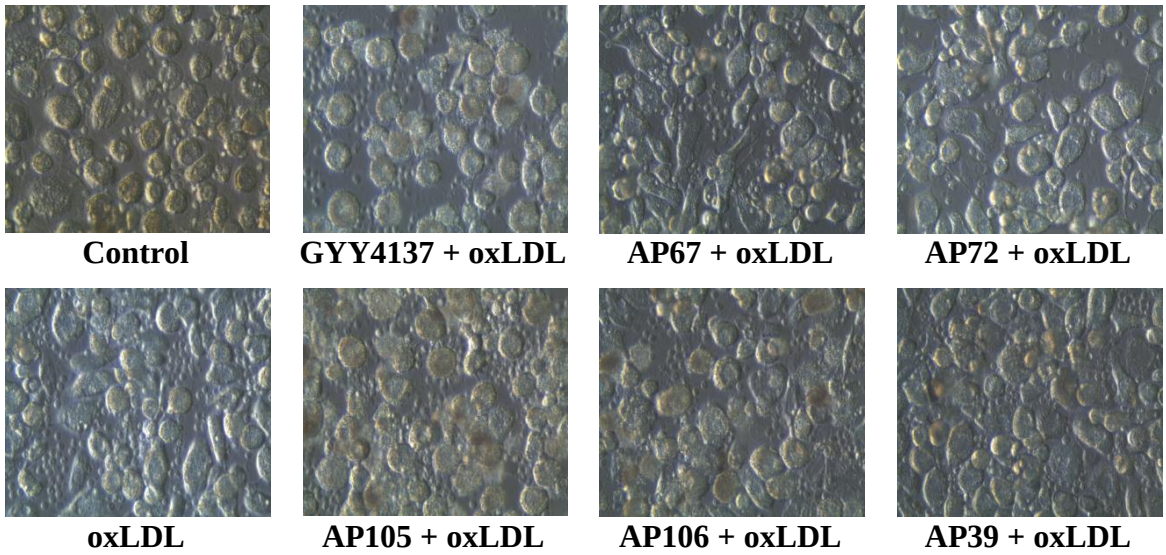

B)

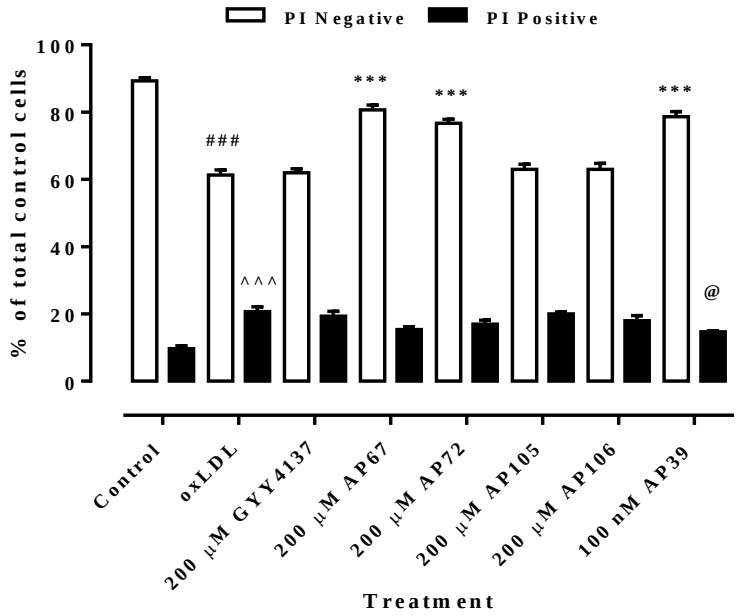

Figure 6.10: Effect of various H_2S donors with oxLDL on cell viability of HMDM cells.

HMDM cells (1×10^6 cells/mL) were incubated at 37°C in non-phenol red RPMI-1640 with various types of H_2S donors for 4 hours before the addition of the LC_{50} concentration of oxLDL (1.5 mg/mL) and incubated for another 24 hours. A) Cells were viewed *in situ* in tissue culture wells using an inverted microscope (400x magnification) after 24 hours incubation with oxLDL. Images were taken using a Leica C-Mount camera and processed using Leica Application Suite software. B) Cell viability was determined using PI via flow cytometry. A cell only treatment was included as control and data are expressed as percentage of the total number of cells in control samples. Results shown are mean ± SEM of triplicates from a representative experiment. Statistical significance (two-way ANOVA, Sidak's multiple comparison test) is indicated from: PI negative cells - control vs oxLDL, ###, $p<0.001$ and oxLDL vs H_2S donors + oxLDL, ***, $p<0.001$; PI positive cells – control vs oxLDL, ^^^, $p<0.001$ and oxLDL vs H_2S donors + oxLDL, @, $p<0.05$.

Effects of various H_2S donors on U937 cells, human monocytes and HMDM cells in the absence or presence of oxLDL: intracellular calcium levels

Results from the first part of this chapter showed that some of these novel H_2S donors were able to protect U937 cells, human monocytes and HMDM cells from oxLDL-induced cytotoxicity. Therefore, the next part of this study will investigate the mechanism of action of these novel H_2S donors in protecting those cells against oxLDL-mediated cell death.

A number of studies have found a role of H_2S in regulating ion channels in the cells including Ca^{2+} ion channels (Munaron *et al.*, 2012; Yong *et al.*, 2010). As being revealed in **Chapter Five**, oxLDL was able to cause a rapid increase in intracellular Ca^{2+} levels over time. The rise in intracellular Ca^{2+} was able to be blocked by certain Ca^{2+} channel blockers and Ca^{2+} chelators. Thus, experiments were performed to examine whether these H_2S donors can regulate intracellular Ca^{2+} caused by oxLDL in U937 cells, human monocytes and HMDM cells. Since oxLDL has been shown to cause a rapid rise in intracellular Ca^{2+}, changes in Ca^{2+} levels were measured after 1 hour of exposure to oxLDL.

There was no significant difference in intracellular Ca^{2+} level in U937 cells treated with H_2S donors compared to cell only control although GYY4137 and AP105 showed some increase (**Figure 6.11 B**). When oxLDL was added to the cells, significant decreased of intracellular Ca^{2+} level was observed in cells treated with AP67, AP72 and AP105 compared to oxLDL treated U937 cells (**Figure 6.11 C**).

A)

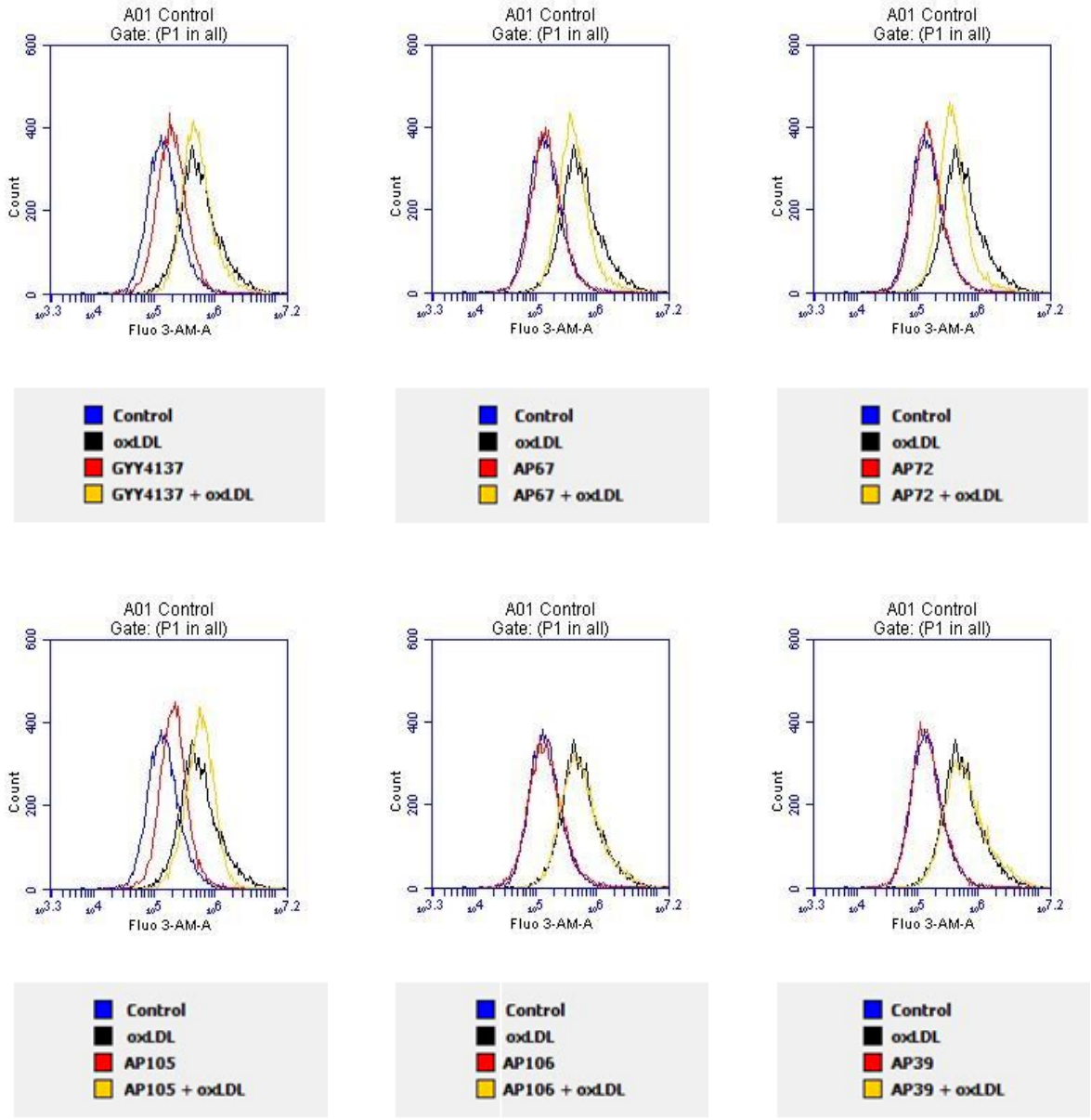
A01 Control
Gate: (P1 in all)
Count
Fluo 3-AM-A
Control
oxLDL
GYY4137
GYY4137 + oxLDL
A01 Control
Gate: (P1 in all)
Count
Fluo 3-AM-A
Control
oxLDL
AP67
AP67 + oxLDL
A01 Control
Gate: (P1 in all)
Count
Fluo 3-AM-A
Control
oxLDL
AP72
AP72 + oxLDL
A01 Control
Gate: (P1 in all)
Count
Fluo 3-AM-A
Control
oxLDL
AP105
AP105 + oxLDL
A01 Control
Gate: (P1 in all)
Count
Fluo 3-AM-A
Control
oxLDL
AP106
AP106 + oxLDL
A01 Control
Gate: (P1 in all)
Count
Fluo 3-AM-A
Control
oxLDL
AP39
AP39 + oxLDL

B)

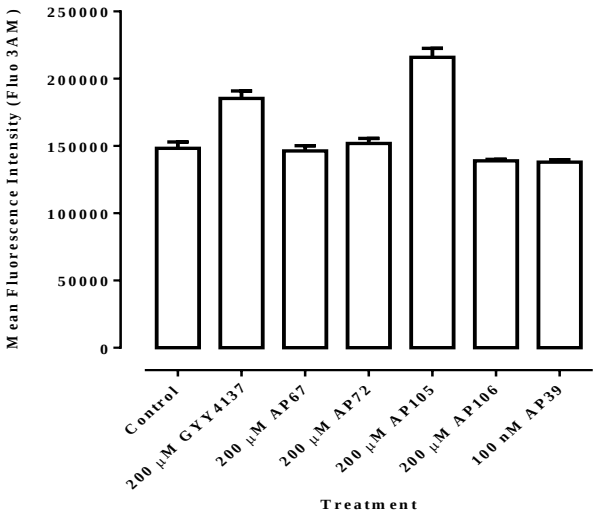

C)

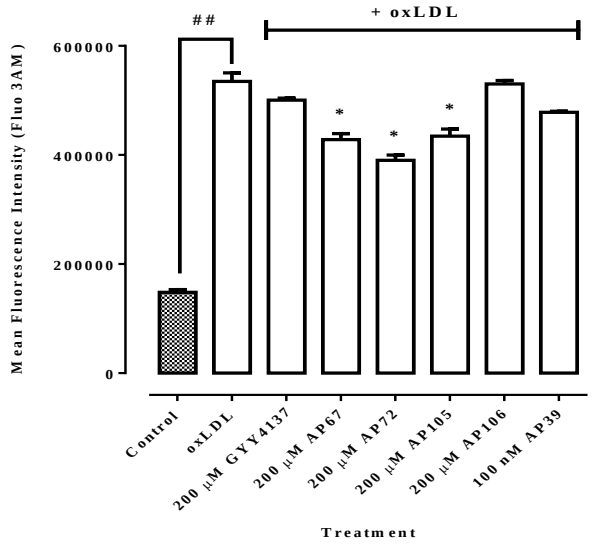

Figure 6.11: Effect of various H_2S donors with or without oxLDL on intracellular calcium levels of U937 cells.

U937 cells (0.5×10^6 cells/mL) were pre-incubated with 1.5 µM Fluo-3AM for 30 minutes at 37°C in non-phenol red RPMI-1640 followed by incubation with various types of H_2S donors for 4 hours before the addition of the LC_{50} concentration (0.25 mg/mL) of oxLDL and incubated for another hour before analysis by flow cytometry A) shows the representative flow cytometry histogram plot of cell counts against Fluo-3AM fluorescence. B) & C) shows mean fluorescence intensities measured by flow cytometry with and without oxLDL, respectively. Results shown are mean ± SEM of triplicates from a representative experiment. Statistical significance (two-way ANOVA, Sidak's multiple comparison) is indicated from: control vs oxLDL, ##, $p<0.01$; oxLDL vs H2S donors + oxLDL, *, $p<0.05$.

In human monocytes, AP67 and AP72 were found to be statistically significant in blocking oxLDL-induced intracellular Ca^{2+} increase compared to oxLDL treated cells while the effect of GYY4137 and AP105 were found to be of the opposite (**Figure 6.12 C**). There was no significant difference in intracellular Ca^{2+} levels in cells treated with H_2S donors only compared to cell only control (**Figure 6.12 B**).

A)

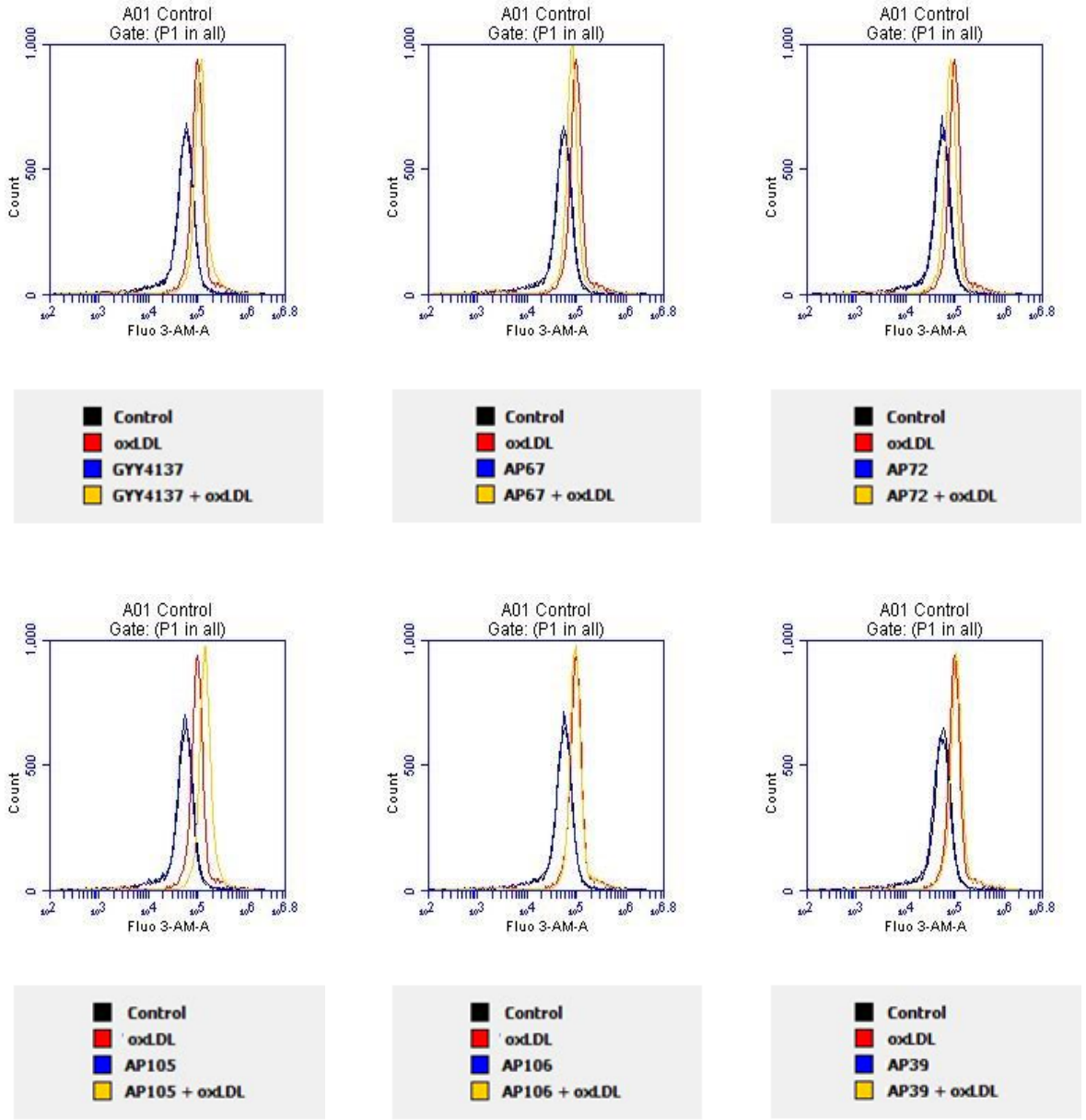

B)

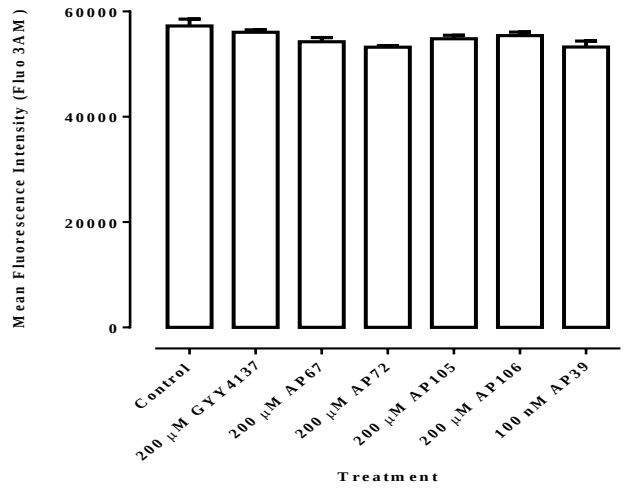

C)

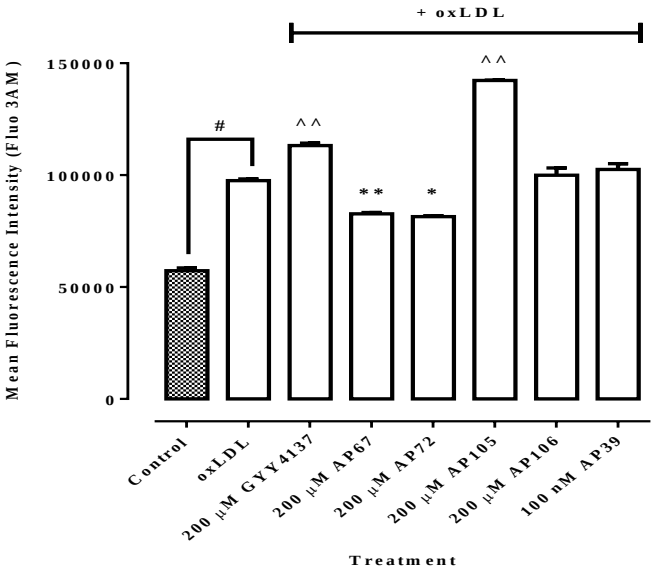

Figure 6.12: Effect of various H_2S donors with or without oxLDL on intracellular calcium levels of human monocytes.

Human monocytes (1×10^6 cells/mL) were pre-incubated with 1.5 µM Fluo-3AM for 30 minutes at 37^{o}C in non-phenol red RPMI-1640 followed by incubation with various types of H_2S donors for 4 hours before the addition of the LC_{50} concentration (0.75 mg/mL) of oxLDL and incubated for another hour before analysis by flow cytometry A) shows the representative flow cytometry histogram plot of cell counts against Fluo-3AM fluorescence. B) & C) shows mean fluorescence intensities measured by flow cytometry with and without oxLDL, respectively. Results shown are mean ± SEM of triplicates from a representative experiment. Statistical significance (two-way ANOVA, Sidak's multiple comparison) is indicated from: control vs oxLDL, #, $p<0.05$; oxLDL vs H_2S donors + oxLDL, *, $p<0.05$; **, $p<0.01$ (AP67, AP72), ^^, $p<0.01$ (GYY4137, AP105).

As for HMDM cells, the was no significant difference in intracellular Ca^{2+} levels in cells treated with various H_2S donors compared to cell only control even though some increase was observed with GYY4137, AP67 and AP105 (**Figure 6.13 B**). With the presence of oxLDL, AP67, AP72 and AP39 were able to block the rise of intracellular Ca^{2+} (statistically significant) caused by oxLDL as compared to oxLDL treated cells (**Figure 6.13 C**).

A)

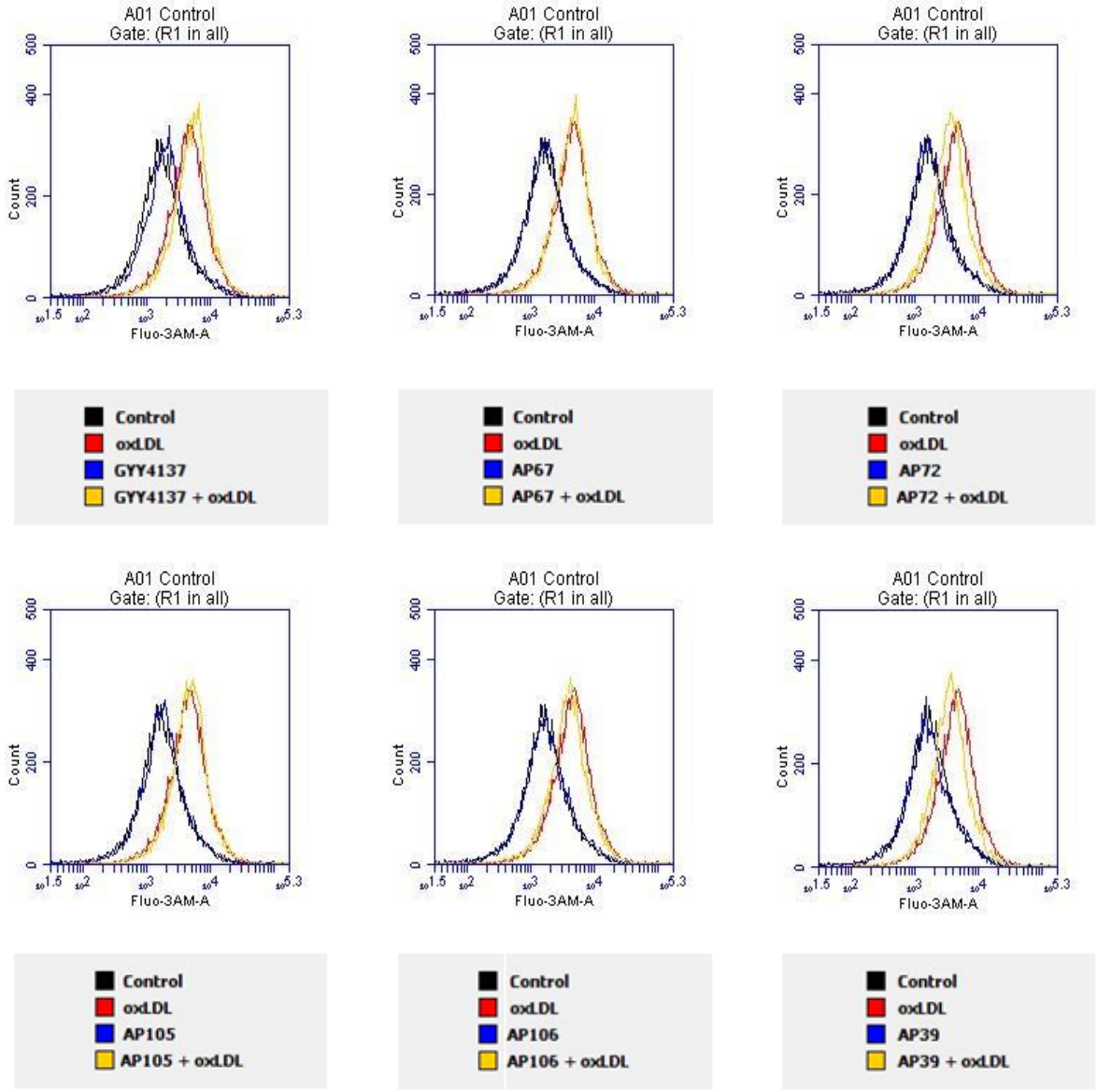

B)

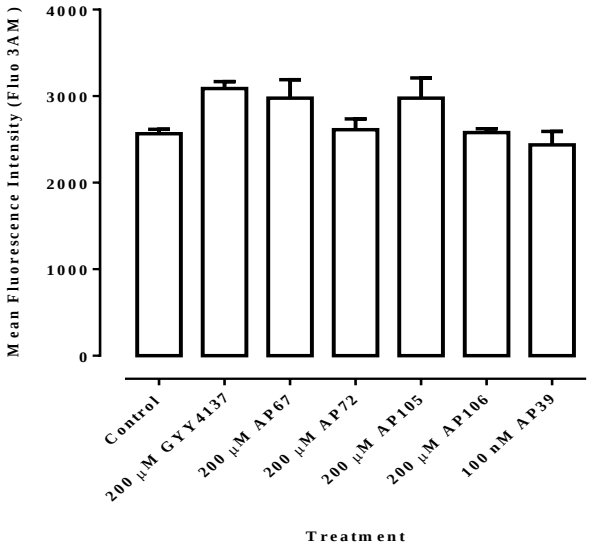

C)

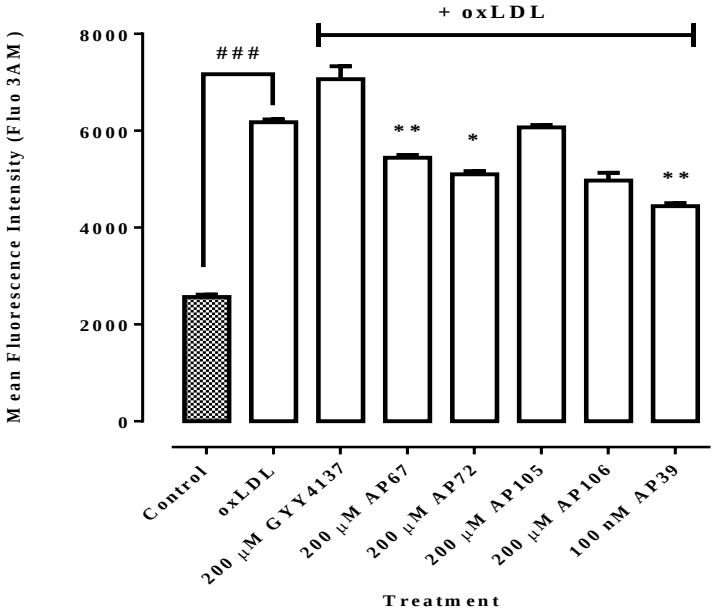

Figure 6.13: Effect of various H_2S donors with or without oxLDL on intracellular calcium levels of HMDM cells.

HMDM cells (1×10^6 cells/mL) were pre-incubated with 1.5 µM Fluo-3AM for 30 minutes at 37°C in non-phenol red RPMI-1640 followed by incubation with various types of H_2S donors for 4 hours before the addition of the LC_{50} concentration (1.5 mg/mL) of oxLDL and incubated for another hour before analysis by flow cytometry A) shows the representative flow cytometry histogram plot of cell counts against Fluo-3AM fluorescence. B) & C) shows mean fluorescence intensities measured by flow cytometry with and without oxLDL, respectively. Results shown are mean ± SEM of triplicates from a representative experiment. Statistical significance (two-way ANOVA, Sidak's multiple comparison) is indicated from: control vs oxLDL, ###, $p<0.001$; oxLDL vs H_2S donors + oxLDL, *, $p<0.05$; **, $p<0.01$.

Effects of various H_2S donors on U937 cells, human monocytes and HMDM cells in the absence or presence of oxLDL: intracellular ROS levels

It has been well known that oxidative stress and the increase of ROS play vital role in cell death mechanisms. **Chapter Four** of this thesis has clearly showed that oxLDL triggers an increased in intracellular ROS (superoxide) in a time dependent manner. Studies also showed the ability of H_2S to scavenge and inhibit ROS [reviewed in Streeter *et al.* (2013)]. Therefore, experiments were performed to examine the ability of these novel H_2S donors in inhibiting ROS formation or scavenging ROS. Cells were incubated with H_2S donors for 4 hours prior to addition of oxLDL. U937 cells were further incubated for 3 hours while human monocytes and HMDM cells were incubated for 6 hours before superoxide levels were measured via flow cytometry using DHE fluorescent probe to measure intracellular ROS (superoxide).

No significant difference in intracellular ROS level (DHE) was found in U937 cells treated with different H_2S donors compared to cell only control. Although AP105, AP106 and AP39 treated cells showed some increase in DHE levels, the increase was not significant (**Figure 6.14 B**). Only AP67 was found to be statistically significant in protecting U937 cells against oxLDL-induced superoxide increase compared to oxLDL treated cells. Higher DHE fluorescence levels were observed in cells treated with GYY4137 and AP 105 in the presence of oxLDL but is not statistically significant (**Figure 6.14 C**).

A)

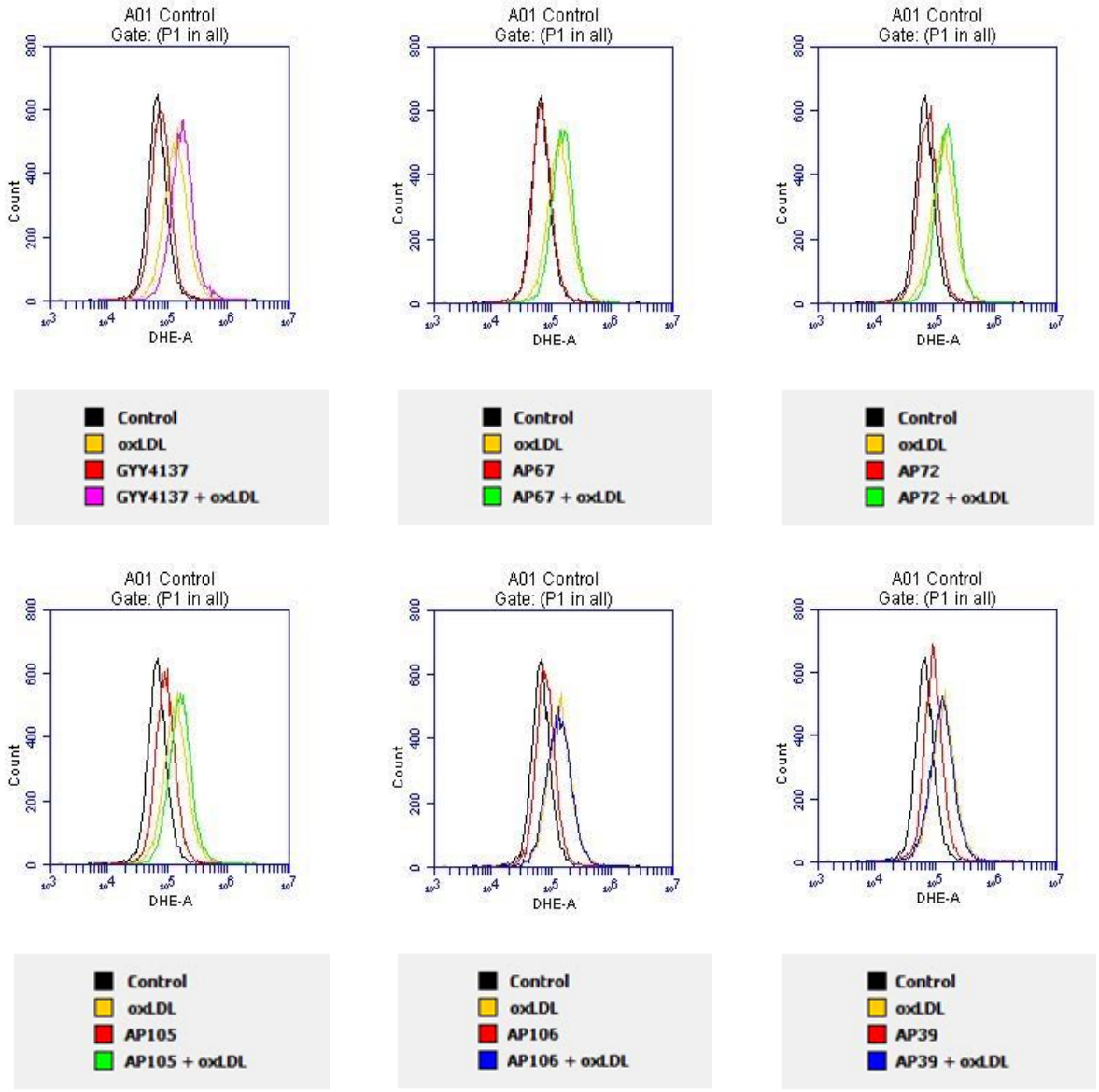
A01 Control
Gate: (P1 in all)
Count
DHE-A
Control
oxLDL
GYY4137
GYY4137 + oxLDL
A01 Control
Gate: (P1 in all)
Count
DHE-A
Control
oxLDL
AP67
AP67 + oxLDL
A01 Control
Gate: (P1 in all)
Count
DHE-A
Control
oxLDL
AP72
AP72 + oxLDL
A01 Control
Gate: (P1 in all)
Count
DHE-A
Control
oxLDL
AP105
AP105 + oxLDL
A01 Control
Gate: (P1 in all)
Count
DHE-A
Control
oxLDL
AP106
AP106 + oxLDL
A01 Control
Gate: (P1 in all)
Count
DHE-A
Control
oxLDL
AP39
AP39 + oxLDL

B)

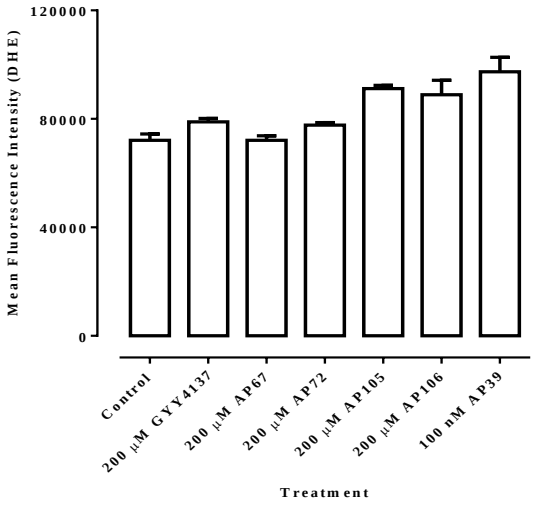

C)

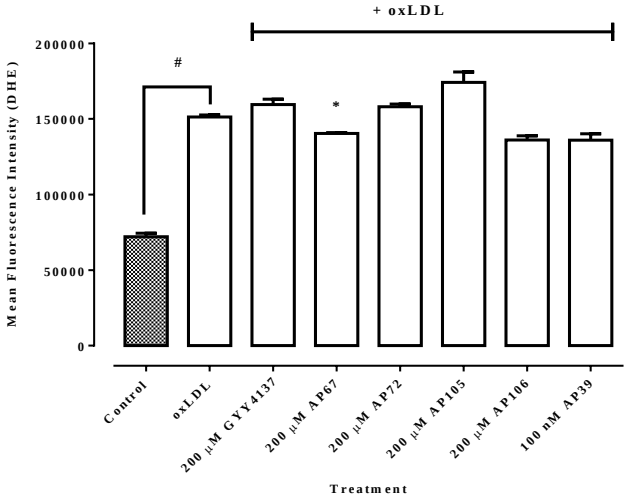

Figure 6.14: Effect of various H_2S donors with or without oxLDL on intracellular ROS levels of U937 cells.

U937 cells (0.5×10^6 cells/mL) were incubated with various types of H_2S donors for 4 hours at 37°C in non-phenol red RPMI-1640 followed by addition of the LC_{50} concentration (0.25 mg/mL) of oxLDL and incubated for another 3 hours. At the end of the treatment, cells were washed and probed with 10 μM DHE for 20 minutes in the dark before analysis by flow cytometry A) shows the representative flow cytometry histogram plot of cell counts against DHE fluorescence. B) B) & C) shows mean fluorescence intensities measured by flow cytometry with and without oxLDL, respectively. Results shown are mean ± SEM of triplicates from a representative experiment. Statistical significance (two-way ANOVA, Sidak's multiple comparison) is indicated from: control vs oxLDL, #, $p<0.05$; oxLDL vs H_2S donors + oxLDL, *, $p<0.05$.

In human monocytes, there was no significant difference observed for DHE levels between cells treated with H_2S donors and cell only control (**Figure 6.15 B**) indicating that H_2S donors did not trigger significant increase in intracellular ROS. However, when oxLDL was added, significant decrease in DHE levels were observed in cells treated with AP67 and AP72 compared to oxLDL treated cells (**Figure 6.15 C)**. In addition, oxLDL had caused an increase of DHE fluorescence levels in cells treated with GYY4137 and AP105 indicating higher levels of ROS compared to oxLDL only treated cells.

A)

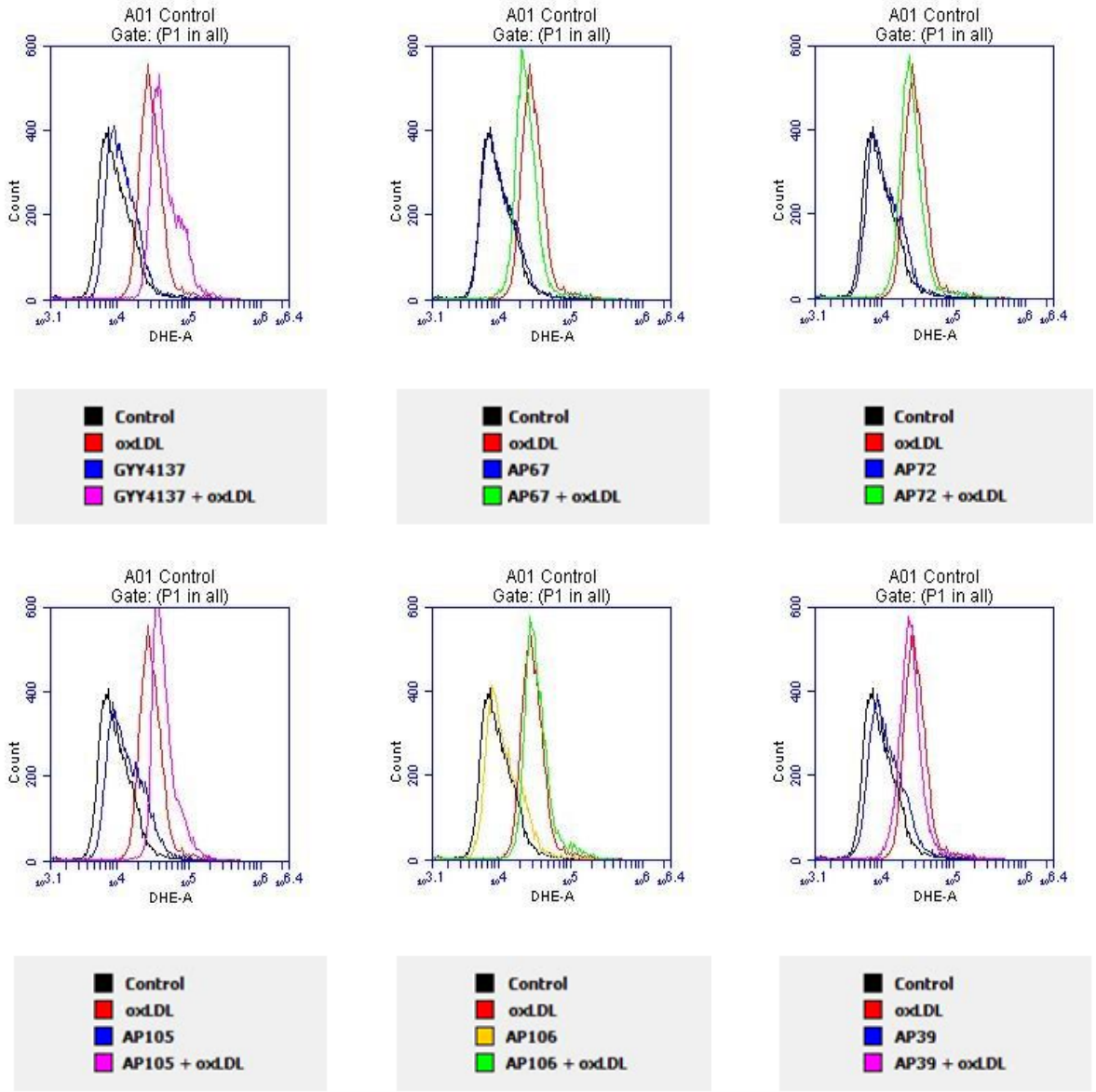

B)

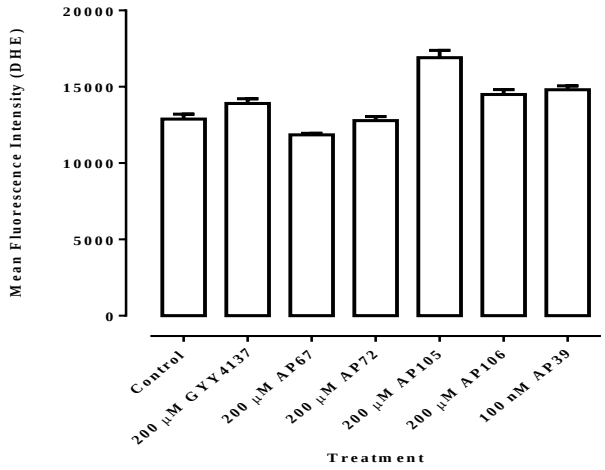

C)

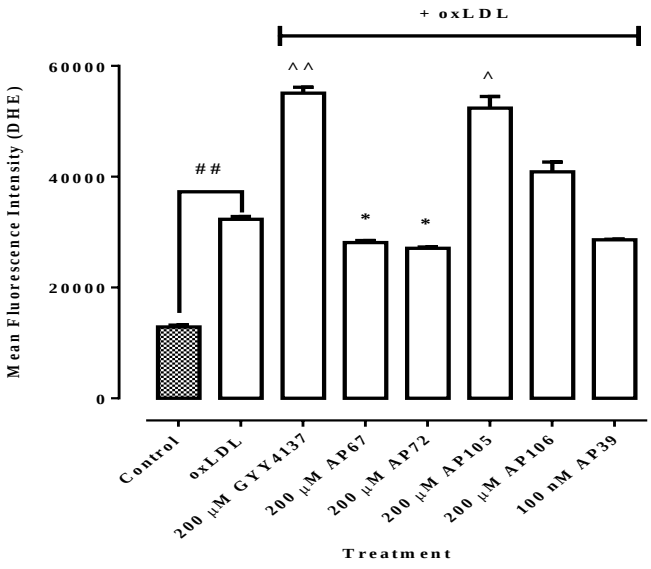

Figure 6.15: Effect of various H_2S donors with or without oxLDL on intracellular ROS levels of human monocytes.

Human monocytes (1×10^6 cells/mL) were incubated with various types of H_2S donors for 4 hours at 37°C in non-phenol red RPMI-1640 followed by addition of the LC_{50} concentration (0.75 mg/mL) of oxLDL and incubated for another 3 hours. At the end of the treatment, cells were washed and probed with 10 μM DHE for 20 minutes in the dark before analysis by flow cytometry A) shows the representative flow cytometry histogram plot of cell counts against DHE fluorescence. B) & C) shows mean fluorescence intensities measured by flow cytometry with and without oxLDL, respectively. Results shown are mean ± SEM of triplicates from a representative experiment. Statistical significance (two-way ANOVA, Sidak's multiple comparison) is indicated from: control vs oxLDL, ##, $p<0.01$; oxLDL vs H_2S donors + oxLDL, *, $p<0.05$ (AP67, AP72), ^, $p<0.05$, ^^, $p<0.001$ (GYY4137, AP105).

There was no difference in DHE levels in HMDM cells treated with H_2S donors compared to cell only control (**Figure 6.16 B**). In the presence of oxLDL, only cells treated with AP67, AP72 and AP39 have shown a decrease in DHE levels compared to oxLDL treated cells (**Figure 6.16**). In contrast, GYY4137, AP105 and AP106 were unable to inhibit or scavenge oxLDL-induced ROS that led to an increase in DHE levels.

A)

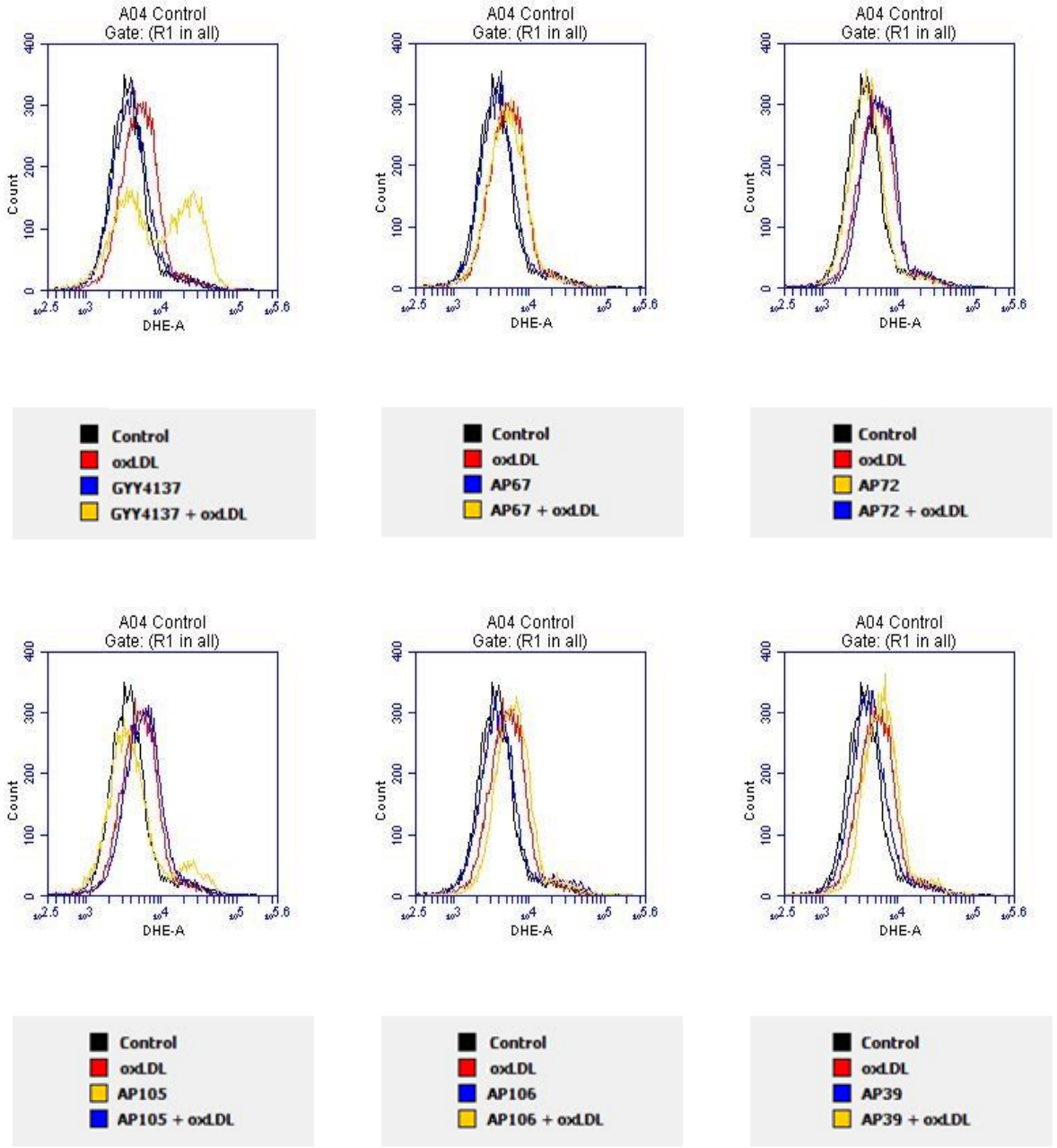

B)

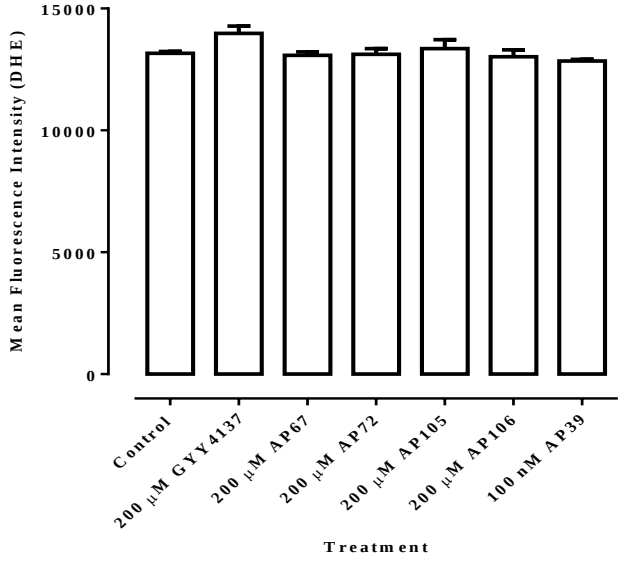

C)

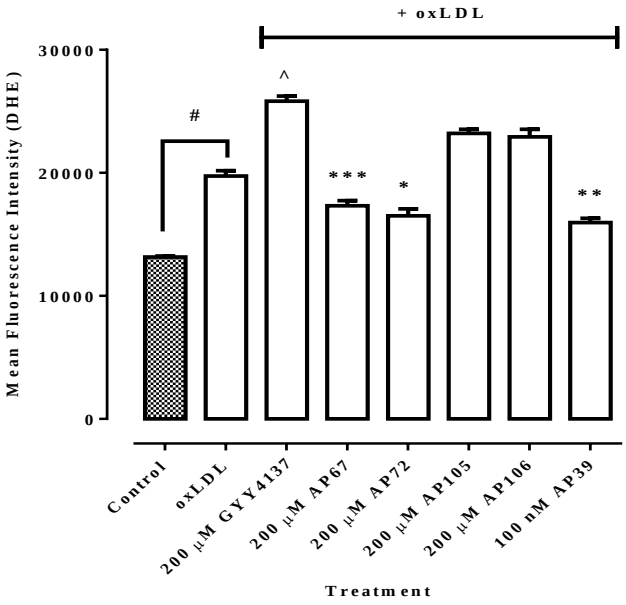

Figure 6.16: Effect of various H_2S donors with or without oxLDL on ROS levels of HMDM cells.

HMDM cells (1×10^6 cells/mL) were incubated with various types of H_2S donors for 4 hours at 37^oC in non-phenol red RPMI-1640 followed by addition of the LC_{50} concentration (1.5 mg/mL) of oxLDL and incubated for another 3 hours. At the end of the treatment, cells were washed and probed with 10 μM DHE for 20 minutes in the dark before analysis by flow cytometry A) shows the representative flow cytometry histogram plot of cell counts against DHE fluorescence. B) & C) shows mean fluorescence intensities measured by flow cytometry with and without oxLDL, respectively. Results shown are mean ± SEM of triplicates from a representative experiment. Statistical significance (two-way ANOVA, Sidak's multiple comparison) is indicated from: control vs oxLDL, #, $p<0.05$; oxLDL vs H_2S donors + oxLDL, *, $p<0.05$; **, $p<0.01$, ***, $p<0.001$ (AP67, AP72, AP39), ^, $p<0.05$ (GYY4137).

Discussion

Results achieved in this chapter clearly demonstrate varied responses of the different types of cell towards the novel H_2S donors (summarised in **Table 6.2**). It is likely that the cellular responsiveness to H_2S may be dependent upon the way in which cells are being exposed to these compounds (Li *et al.*, 2008). In general, these H_2S donors were not toxic to U937 cells, human monocytes and HMDM cells as there was no significant cell death observed in cells treated with H_2S donors only compared to cell only control. However, when oxLDL was added, the outcome of cell viability varied with each individual H_2S donor compounds.

In the current study, GYY4137, AP67, AP72 and AP105 were found to be significantly protective against oxLDL-induced cytotoxicity in U937 cells. As for human monocytes, significant protection from oxLDL-induced cell death was demonstrated only by AP67 and AP72. Three of the novel H_2S donors namely AP67, AP72 and AP39 were found to provide significant protection against oxLDL-induced cell death in HMDM cells. Among the factors that could have contributed to the findings are the rate of H_2S release from the donors as each of the donors has a different releasing rate and also different reactions by different types of cells (Wagner *et al.*, 2009) being used in this study. In addition, the protection from cell viability loss offered by these H_2S donors were around 15 to 20% from the percentage of cell death caused by oxLDL (PI negative cells).

GYY4137 which is the slowest releasing H_2S donor was only protective to U937 cells (**Figure 6.6**) but surprisingly not for human monocytes and HMDM cells. In this study, the mechanism of action by which GYY4137 protects U937 cells could not be explained since it neither block the rise of intracellular Ca^{2+} nor ROS formation at the time of measurement. In other studies, GYY4137 has been shown to inhibit inflammatory signalling in *in vivo* model of atherosclerosis (Liu *et al.*, 2013) as well as oxidative stress-mediated cytotoxicity and loss of mitochondrial function induced by oxidants such as H_2O_2 (Fox *et al.*, 2012a). However, since GYY4137 is highly water soluble (Li *et al.*, 2008), this will then limits its cellular permeability. Additionally, studies have shown that high concentrations (100 µM and above) of GYY4137 are needed to achieve anti-inflammatory, cytoprotective and mitochondrial protective effects which will then limits the therapeutic potential of this compound (Le Trionnaire *et al.*, 2014). GYY4137 has also been reported to have anti-hypertensive and anti-inflammatory action (Li *et al.*, 2009; Li *et al.*, 2008).

Among all of the H_2S donors, AP67 was the most potent in preventing cell death from oxLDL followed by AP72 and this finding is in line with the studies in endothelial cells done by Jeney *et al.* (2013). In this study, AP67 and AP72 were found to be protecting against oxLDL-induced cell viability loss in human monocytes and HMDM cells. Approximately, 20% recovery of cell loss has been observed with the two H_2S donors in human monocytes and HMDM cells (**Figure 6.7** and **6.9**). Experimental results showed that AP67 and AP72 were able to block intracellular Ca^{2+} rise (**Figure 6.11 B** and **6.12 B**) as well as scavenging ROS triggered by oxLDL (**Figure 6.14 B** and **6.15 B**). Therefore, this may suggest the mode of action by these H_2S donors.

This finding is in agreement with Le Trionnaire *et al.* (2012) whom showed that slow releasing H_2S donors, AP67 and AP72 significantly inhibited oxidative stress induced cell viability loss, ROS generation and $\Delta\Psi m$ loss in human microvascular endothelial cells (HMEC). Studies by Jeney *et al.* (2013) have showed the protective effects of H_2S donors including AP67 and AP72 against heme-mediated LDL oxidation and H_2O_2 oxidation. They have also found that these H_2S donors prevented lipid peroxidation of lipids taken from human soft plaques, this in turn reduced endothelial cytotoxicity by diminishing the accumulation of those peroxides. Moreover, AP67 was found to be the most potent in preventing haemoglobin oxidation (Jeney *et al.*, 2013).

In another study, Le Trionnaire *et al.* (2013) found that AP72 (100-500 µM) was able to inhibit the activation of caspase 3 and caspase 3/7 activity after treatment with staurosporine/etoposide in HMECs. Study in bovine retinal endothelial cells by Whatmore *et al.* (2013) has highlighted the therapeutic potential of AP67 in hyperglycaemic conditions. Other studies have showed that H_2S effects on oxidative stress may be by scavenging ROS and also up-regulating antioxidant defences (Lynn & Austin, 2011).

AP39 is the other H_2S donor found to offer protection against oxLDL-induced cytotoxicity in HMDM cells (**Figure 6.7**). AP39 has been shown to reduce oxLDL-induced intracellular Ca^{2+} level (**Figure 6.12 B**) and intracellular ROS generation (**Figure 6.15 B**). This relates to the experimental results in **Chapter Five** whereby blocking Ca^{2+} uptake into the mitochondria by ruthenium red decreases ROS production and improves cell vialbility. AP39 is the type of H_2S releasing molecule which targeted the mitochondria (Le Trionnaire *et al.*, 2014). In their studies, AP39 has been shown to preserve the mitochondria and inhibit

oxidative stress-induced cytotoxicity in HMECs although it was not possible to conclude whether the mitochondrial protection was the cause or consequence of cellular protection. Moreover, AP39 (<100 nM) has also been found to inhibit caspase 3/7 activity in HMEC (Le Trionnaire *et al.*, 2013). Le Trionnaire *et al.* (2014) have observed co-localisation of H_2S generation with mitochondria, preservation of ATP levels and $\Delta\Psi m$ as well as decreased mitochondrial oxidant production. This finding suggests that the endogenous enzymes responsible for H_2S production are either located within or being translocate to the mitochondria in response to cellular stress (Le Trionnaire *et al.*, 2014).

In the previous chapters in this thesis, oxLDL has been demonstrated to have caused a time-dependent intracellular Ca^{2+} increase which in turn caused an increase in intracellular ROS production. Taken together, such effects then initiated various intracellular events and pathways leading to the death of the cells.

Results in this chapter showed for the first time the effects of various slow release hydrogen sulfide donors on oxLDL-induced intracellular Ca^{2+} levels in U937 monocyte-like cells, human monocytes and HMDM cells. AP67, AP72 and AP39 (**Figure 6.11 B** & **6.12 B**) had shown promising effects in blocking cytoplasmic Ca^{2+} rise caused by oxLDL in human monocytes and HMDM cells although the exact mode of action of these donors could not be ascertain at this stage. Previous studies revealed that H_2S causes indirect inhibitory action on L-type calcium channels (Mancardi *et al.*, 2009; Sun *et al.*, 2008). Moccia *et al.* (2011) and Bauer *et al.* (2010) have showed that H_2S regulate store-operated calcium entry (SOCE) in rat aortic endothelium and human endothelial cells respectively. Moreover, H_2S may affect intracellular Ca^{2+} mobilisation by either inhibiting inositol triphosphate receptors (IP3Rs) or exciting ryanodine receptors (RyRs) (Hennig & Diener, 2009; Moccia *et al.*, 2011) considering that ORAI1, the crucial protein of SOCE, IP3Rs and RyRs are all prone to covalent modifications such as phosphorylation and nitrosilation. Munaron *et al.* (2012) recommended that future studies is needed to reveal the possible co-regulations of ion channels by H_2S and NO as some Ca^{2+} channels contain cysteine residues which may be the potential target through sulfhydration and nitrosilation.

On the other hand, Maeda *et al.* (2009) have reported that H_2S may facilitate membrane currents through T-type Ca^{2+} channels. Studies in neurons, astrocytes and microglia showed that prolonged treatment with H_2S may induce cell death via increasing cytosolic Ca^{2+} level

via L-type Ca^{2+} channels (Garcia-Bereguiain *et al.*, 2008; Lee *et al.*, 2006; Nagai *et al.*, 2004). It is noted that sulfide salt such as NaHS is normally used to examine H_2S roles in calcium signalling in variety of cell types. Thus, the effects of hydrogen sulfide from this type of donor might not be the same as the novel H_2S donors used in the current study due to different characteristics and nature of the molecules. The differences observed may be due to the rate of release, site of release and the generated local concentrations.

Other studies by Kimura and Kimura (2004) have showed that H_2S may protect neurons from oxidative stress by increasing GSH levels. H_2S has also been demonstrated to inhibited peroxynitrite ($ONOO^-$)-mediated cytotoxicity to a similar extent as GSH (Whiteman *et al.*, 2004). The potential antioxidant action of H_2S was attributed to the functional thiol group which can scavenge $ONOO^-$ (Halliwell *et al.*, 1999). It has also been demonstrated that H_2S possesses anti-neuroinflammatory, anti-oxidant and anti-apoptotic effects in neuron and glial cells (Hu *et al.*, 2009; Hu *et al.*, 2007; Lu *et al.*, 2008).

Table 6.2: Summary of H_2S donors effects on oxLDL-mediated cytotoxicity

H_2S donor	U937 cells			Human monocytes			HMDM cells		
	Cell viability	**Intracellular Ca^{2+}**	**Intracellular ROS**	**Cell viability**	**Intracellular Ca^{2+}**	**Intracellular ROS**	**Cell viability**	**Intracellular Ca^{2+}**	**Intracellular ROS**
GYY4137	Protective	Decrease (slight)	Increase (slight)	Non-protective	Increase (significant)	Increase (significant)	Non-protective	Increase	Increase (significant)
AP67	Protective	Decrease (significant)	Decrease (significant)	Protective	Decrease (significant)	Decrease (significant)	Protective	Decrease (significant)	Decrease (significant)
AP72	Protective	Decrease (significant)	No change	Protective	Decrease (significant)	Decrease (significant)	Protective	Decrease (significant)	Decrease (significant)
AP105	Protective	Decrease (significant)	Increase (slight)	Non-protective	Increase (significant)	Increase (significant)	Non-protective	No change	Increase
AP106	Non-protective	No change	Decrease (slight)	Non-protective	No change	Increase	Non-protective	Decrease	Increase
AP39	Non-protective	Decrease (slight)	Decrease (slight)	Non-protective	No change	Decrease	Protective	Decrease (significant)	Decrease (significant)

Summary

This chapter presented for the first time the results of the study done using six different types of slow releasing H_2S donors i.e. GYY4137, AP39, AP67, AP72, AP105 and AP106 on U937 cells, human monocytes and HMDM cells. These H_2S donors have diverse outcomes in different types of cell with results indicating that few of these donors might have some promising effects against oxLDL-mediated cell death particularly AP72, AP67 and AP39. Thus, the data highlight the potential therapeutic application of these compounds in the prevention and/or treatment of atherosclerosis and endothelial dysfunction.

Possible mechanisms of this protection are by inhibiting the increase in intracellular Ca^{2+} therefore preventing excessive ROS formation resulting in protection against oxLDL-mediated cytotoxicity as demonstrated by AP67, AP72 and AP39. Hence, the exact mechanisms of action by which these H_2S donors provide protection to the cells against oxLDL attack need to be explored further including their pharmacological properties to become therapeutic candidates for atherosclerosis.

CHAPTER SEVEN

7. General discussion, future work and conclusion

OxLDL toxicity and cell death mechanisms

This study began with investigating the effect of oxLDL on the monocytic lineage cells i.e. U937 cells, human monocytes and HMDM cells in order to confirm the previous findings by researchers from this lab (**Chapter Three**). OxLDL was found to be toxic and caused cell viability loss to all types of cells used in this study. The degree of toxicity was concentration- and time-dependent and in agreement with previous studies (Baird, 2003; Chen, 2012; Katouah, 2012; Shchepetkina, 2013). OxLDL caused rapid cell viability loss whereby approximately 40-50% cell death occurred within 12 hours of incubation with oxLDL. There was a lag time before cell viability loss could occur (after 3 hours) suggesting that oxLDL-induced cell death was not immediate. During this time of delay, oxLDL might trigger cellular events such as loss of glutathione (GSH), metabolic dysfunctions and oxidative stress that could lead to cell death.

Morphological examinations on the cells during incubation with oxLDL illustrated that oxLDL induced necrotic cell death. However, oxLDL has been shown to induce necrotic or apoptotic cell death depending on types of cells (Baird *et al.*, 2004; Gieseg *et al.*, 2009b). It has been shown by Baird *et al.* (2004) that oxLDL-induced oxidative stress was adequate to inhibit caspase-3 which blocks the apoptotic process, thus activates necrosis in U937 cells. In THP-1 cells, oxLDL caused apoptosis with characteristics of caspase-3 activation, cell shrinkage and a small reduction in cellular GSH level (Baird *et al.*, 2004). Furthermore, examination of atherosclerotic plaque also showed a significant amount of extracellular debris (Stocker & Keaney, 2004) suggesting that necrosis is major process occurring within the plaque.

In addition, studies have implicated the importance of endoplasmic reticulum (ER) stress in atherosclerosis and plaque rupture due to the presence of oxidised lipids, inflammation and

metabolic stress (Muller *et al.*, 2011a). Recently, Yao *et al.* (2013) have demonstrated that oxLDL was capable to induce ER stress. Since ER is the major site for intracellular Ca^{2+} storage and protein folding, ER stress could result in protein misfolding and activates unfolded protein response (UPR). If ER stress is sustained and unresolved, apoptosis could occur via the induction of the proapoptotic transcriptional factor C/EBP homologous protein (CHOP), activation of c-jun amino-terminal kinase (JNK) and Bcl-2 proteins (Muller *et al.*, 2011a). Moreover, studies have also shown that NOX is activated by ER stress and is involved in modulating ER stress signaling (Jiang *et al.*, 2011). Therefore, future studies could further investigate the role of oxLDL in ER stress that leads to the activation of cell death pathway.

This research has examined three types of cells of similar lineage, namely monocyte-like U937 cells, primary human monocytes and primary HMDM cells. U937 cell line has been an excellent cell model in various health and disease related studies. Primary human monocytes and primary HMDM cells are the best type of cells for *in vitro* study of atherosclerosis since both are involved in atherosclerotic plaque progression *in vivo*. Studying the three types of cells adds validity to the research data obtained whereby similar results or trends were found for most of the investigations done. This leads to a valid interpretation of the effect of oxLDL on these cell types in atherosclerosis development. However, there were cases where these cells responded differently to various types of treatments. It has been shown by numerous studies that different types of cells acted differently when treated with the same treatment or compound/molecule. In my opinion, this phenomenon could happen due to various factors such as differences in cell metabolism, cell size and uptake of compounds/molecules into the cell. As an example in this study, human monocytes might act differently compared to HMDM cells because HMDM cells have been stimulated using GM-CSF while in culture. This could introduce changes to the cells (e.g. number of receptors) that might influence these cells to react differently to the same treatment.

NADPH oxidase (NOX) as oxidants generator

In **Chapter Four**, it was shown that oxLDL induced rapid intracellular ROS generation (measured by DHE fluorescent probe). Additionally, it has also been demonstrated that oxLDL caused an increase in mitochondrial ROS (measured by MitoSOX). Furthermore, Western blot results demonstrated that oxLDL activated NOX. Thus, it is of high possibility

that NOX might be the key generator of intracellular ROS mediated by oxLDL. However, only limited protection was conveyed by apocynin against oxLDL-induced cell death on U937 cells and no cellular viability protection was seen in human monocytes and HMDM cells. Lack of protection suggests unspecific action of apocynin or the potential involvement of other sources of intracellular ROS that causes oxidative damage such as from the mitochondria. NOX activation by oxLDL indicates the involvement of NOX2 in oxLDL-induced ROS generation since NOX2 is dependent on $p47^{phox}$ activation. Therefore, a specific NOX2 inhibitor, gp91-ds-tat (NOX2-ds-tat) would be a potential candidate to further investigate the involvement of NOX2 in oxLDL-mediated ROS production.

gp91-ds-tat (gp91/NOX2 docking sequence-tat) (Rey *et al.*, 2001) is regarded as the most specific and efficacious NOX inhibitor available (Cifuentes-Pagano *et al.*, 2012). gp91ds-tat is a chimeric 18-amino acid peptide ([H]-R-K-K-R-R-Q-R-R-R-C-S-T-R-I-R-R-Q-L- [NH2]) that has been shown to inhibit *in vivo* and *in vitro* NOX activity (Rey *et al.*, 2001; Touyz, 2002). The gp91-ds portion of the peptide is a 9 amino acid sequence from the cytosolic B-loop of NOX2 (amino acids 86–94) designed to selectively inhibit the interaction between NOX2 and $p47^{phox}$ (Rey *et al.*, 2001), thus prevents the assembly of NOX. The tat portion of the peptide corresponds to a 9 amino acid sequence of the HIV-tat transport region that facilitates internalization by the cells (Fawell *et al.*, 1994). The viability of gp91-ds as an inhibitor was predicted by random-sequence peptide phage display library analysis of the human NOX2 and was shown to inhibit NOX activity in a neutrophil cell-free system (DeLeo *et al.*, 1995). Since HMDM cells are expressing mainly NOX2 isoform of NOX, therefore it could be beneficial to incorporate this compound into oxLDL-induced intracellular oxidants generation studies. This investigation is currently underway.

Lee *et al.* (2010) have demonstrated the existence of oxLDL-inducible NOX4 in human monocytes and macrophages. NOX4 have been shown to localise in intracellular organelles and colocalises with $p22^{phox}$ that formed a functional ROS-generating enzyme complex (Bedard & Krause, 2007). It has been suggested that NOX4 is present as NOX4/$p22^{phox}$ dimers and constitutively active in HMDM cells (Lee *et al.*, 2010). GKT137831 is another compound that has been investigated as a possible NOX inhibitor, particularly for NOX1 and NOX4. In their recent review, Altenhofer *et al.* (2014) have indicated GKT137831 as the first NOX inhibitor in clinical development that will soon provide information for the clinical

potential of NOX inhibition. Thus, GKT137831 would be another NOX inhibitor candidate worth pursuing.

Mitochondrial ROS generation could be the most possible source of intracellular ROS in HMDM cells. It has been shown in this study that oxLDL induced an increase in mitochondrial ROS level in HMDM and Complex III of the mitochondrial electron transport chain (mETC) was recognised as the source of superoxide in damaged cells (Turrens, 2003). Therefore, it would be beneficial to investigate the involvement of oxLDL-induced mitochondrial ROS by investigating the effect of mitochondrial inhibitors such as antimycin A (Complex III) and rotenone (Complex I).

OxLDL-induced Ca^{2+} increase and its effect on mitochondria

OxLDL induced a rapid and sustained cytosolic Ca^{2+} increase with extracellular Ca^{2+} as the main contributor. Excess accumulation of cytosolic Ca^{2+} could be taken up into the mitochondria and resulted in mitochondrial Ca^{2+} overload. This could then increase mitochondrial ROS production, triggers MPTP opening and subsequently ruptures the OMM which caused the collapse of mitochondrial membrane potential ($\Delta\Psi m$) whereby preliminary results from this study have showed that oxLDL caused $\Delta\Psi m$ loss. In **Chapter 5**, it has been shown that blocking Ca^{2+} uptake by ruthenium red (mitochondrial Ca^{2+} uniporter inhibitor) protected cells from oxLDL-induced cell death, possibly by reducing ROS generation and preventing MPT activation. Additionally, cyclosporin A (CsA) also prevented oxLDL-mediated cell viability loss in HMDM cells, possibly by preventing $\Delta\Psi m$ loss triggered by MPT activation. Thus, it will be worth investigating whether these agents protect cell viability loss by inhibiting MPT activation which in turn protects from oxLDL-induced $\Delta\Psi m$ loss.

Protective effect of H_2S donors on oxLDL-mediated cell death

Preliminary results from this study (**Chapter 6**) have showed the promising effect of selective, slow releasing, H_2S donors in protecting monocytic lineage cells from oxLDL toxicity. H_2S have been proposed to have multiple protective effects in the vasculature which include scavenging intracellular ROS production (reviewed in Streeter *et al.* (2013)). In this

study, the H_2S donors were able to reduce intracellular Ca^{2+} level as well as intracellular ROS generation induced by oxLDL, thus protects cells from death. Therefore, further investigations in the determining the specific mechanism of action of these H_2S donors will be worth pursuing. Moreover, one of the H_2S donors, AP39, is specific in targeting mitochondria and has been shown to protect HMDM cells against oxLDL insult. It would be beneficial to further investigate its effect such as on MPT activation and mitochondrial ROS generation.

Conclusion

This study has further characterised the cytotoxicity of oxLDL to various types of cells. Toxic concentration of oxLDL caused a rapid loss in cell viability which is time- and concentration-dependent, whereby almost half of the cell viability loss occurred during the first 12 hours of incubation with oxLDL. Morphological changes of the cells revealed that oxLDL caused necrotic cell death with the characteristics of cell swelling, disrupted cell membrane and loss of cellular contents. This research also detailed the procedures and served as a bench-mark study for flow cytometric approach in assessing cell viability using propidium iodide (PI) fluorescent probe.

OxLDL has been shown to induce intracellular oxidative stress including in the mitochondria whereby the increased in ROS production showed a time-dependent trend. NOX could be the key generator of intracellular ROS in oxLDL-induced cells. Immunoblotting results demonstrated that oxLDL activated NOX and increased the expression of $p47^{phox}$ of NOX protein subunit. The progression of NOX activation was strongly associated with oxLDL-induced ROS generation which suggests that NOX produces a burst of ROS in response to oxLDL, thus resulting in the increase of oxidative stress and cell viability loss. Since apocynin and VAS2870 were unable to inhibit NOX, this suggests that either these NOX inhibitors are unspecific for the targeted NOX or other sources of ROS might also exist and caused the increase in oxidative flux. Additionally, 7,8-NP has been shown to reduce oxidative stress and protected cells from oxLDL insult by scavenging intracellular ROS.

OxLDL is also capable in inducing a rapid and sustain increase in intracellular Ca^{2+}. Intracellular Ca^{2+} does play a role in Ca^{2+} flux but extracellular Ca^{2+} involvement is crucial. OxLDL-induced intracellular Ca^{2+} increase correlates with the increase in intracellular ROS.

Inhibiting intracellular Ca^{2+} rise did not inhibit the increase in intracellular ROS suggests that oxLDL may trigger a Ca^{2+}-independent cell death pathway and increase in Ca^{2+} level is not the cause of oxLDL-mediated cell death. Blocking mitochondria from Ca^{2+} overload protected cells from oxLDL-induced cell death possibly by reducing ROS generation and preventing $\Delta\Psi m$ loss.

Selective slow releasing H_2S donors are shown in this study to offer protection against oxLDL-induced cell death. Although the exact mechanism of action of the H_2S donors has yet to be determined, a select few of these H_2S donors (AP39, AP67 and AP72) have been shown to reduce the rise of oxLDL-induced intracellular ROS and Ca^{2+} levels, which in turn, reduced cell viability loss.

An overall diagram showing the pathways involved for oxLDL to exert its toxicity in the cells and the agents used to lessen oxLDL-mediated cell death in this study is illustrated by **Figure 7.1.**

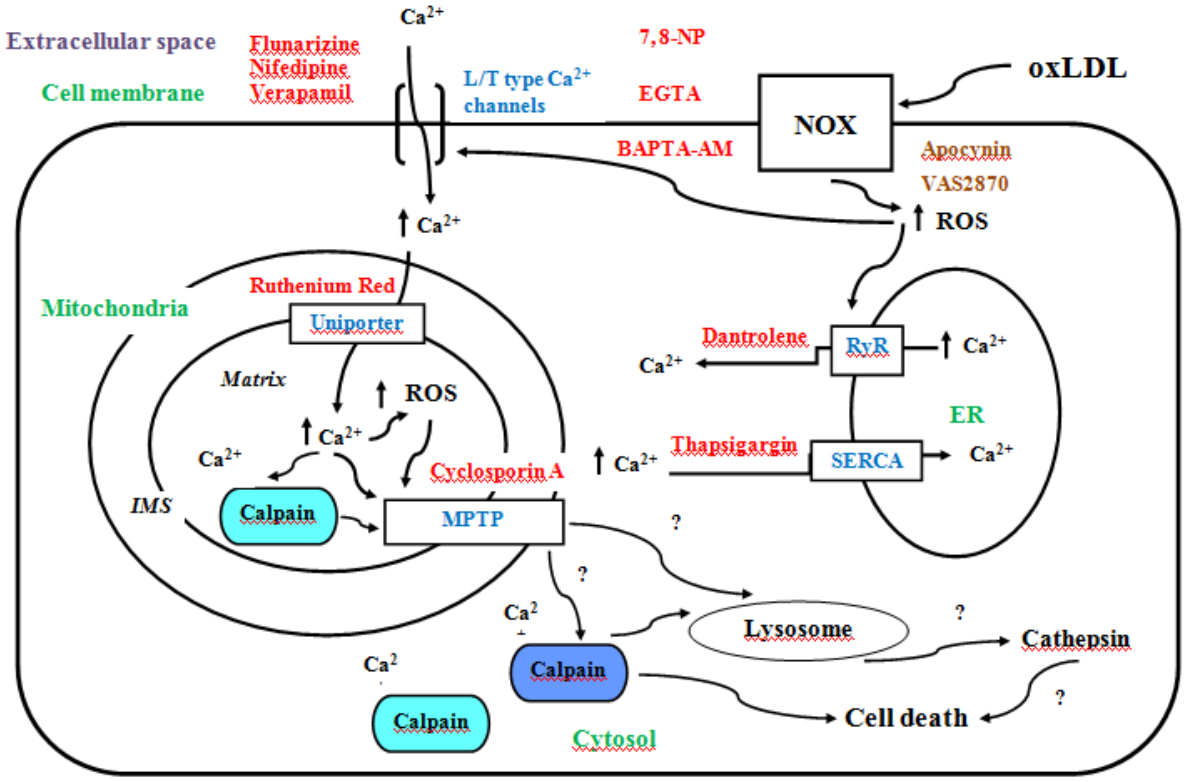

Figure 17 Overall diagram of proposed pathways for oxLDL toxicity and agents used to lessen oxLDL-mediated cell death

OxLDL activates NADPH oxidase (NOX) on the cell membrane to produce ROS. NOX-derived ROS stimulates L- and T-type Ca^{2+} channels on cell membrane and ryanodine receptors (RyR) on endoplasmic reticulum (ER), causing the influx of extracellular Ca^{2+} and the release of Ca^{2+} from ER stores into the cytosol which lead to cytosolic Ca^{2+} increase. Excess cytosolic Ca^{2+} can be taken up into the mitochondria via Ca^{2+} uniporter on the inner mitochondrial membrane (IMS). Ca^{2+} accumulation in mitochondrial matrix could possibly activates mitochondrial calpain (light blue), triggering the opening of mitochondrial permeability transition pore (MPTP). Ca^{2+} also causes the increase in mitochondrial ROS production, which also contributes to MPTP opening. MPTP activation leads to mitochondrial membrane potential (MMP) loss, along with the release of activated mitochondrial matrix calpain (light blue), Ca^{2+} and other factors, such as cytochrome c. The released Ca^{2+} also activates cytosolic calpain (dark blue). Together with the mitochondrial calpain, they may lead to necrotic cell death by degrading cytoskeletal proteins, leading to cell membrane blebbing and rupture. They can also destabilise lysosomes, resulting in the release of cathepsin protease that may degrade cellular components, causing cell death. Apocynin and VAS2870 were the two NOX inhibitors used in this research. Apocynin reduces ROS generation and provides partial protection against oxLDL-mediated cell death in U937 cells only. VAS2870 was not protecting against oxLDL-mediated ROS generation and cell death in all types of cells. Ruthenium red reduces ROS generation by blocking Ca^{2+} uptake into the mitochondria, thus protects against oxLDL-induced cell death in all types of cells. Cyclosporin A reduces oxLDL-induced ROS generation and cell death only in HMDM cells only, possibly by inhibiting MPTP activation. EGTA decreases intracellular Ca^{2+} level but not ROS in oxLDL-mediated cells. 7,8-NP was able to reduce intracellular Ca^{2+} and ROS levels as well as protecting cells against oxLDL-induced toxicity. The arrows with "?" indicate that the pathways are a hypothesis and are not investigated in this study.

References

Abe, K., & Kimura, H. (1996). The possible role of hydrogen sulfide as an endogenous neuromodulator. *The Journal of Neuroscience, 16*(3), 1066-1071.

Adhikari, S., & Bhatia, M. (2008). H2S-induced pancreatic acinar cell apoptosis is mediated via JNK and p38 MAP kinase. *J Cell Mol Med, 12*(4), 1374-1383.

Ago, T., Kitazono, T., Ooboshi, H., Iyama, T., Han, Y. H., Takada, J., Wakisaka, M., Ibayashi, S., Utsumi, H., & Iida, M. (2004). Nox4 as the major catalytic component of an endothelial NAD(P)H oxidase. *Circulation, 109*(2), 227-233.

Ago, T., Kuribayashi, F., Hiroaki, H., Takeya, R., Ito, T., Kohda, D., & Sumimoto, H. (2003). Phosphorylation of p47phox directs phox homology domain from SH3 domain toward phosphoinositides, leading to phagocyte NADPH oxidase activation. *Proceedings of the National Academy of Sciences USA, 100*(8), 4474-4479.

Aguilar, H. I., Botla, R., Arora, A. S., Bronk, S. F., & Gores, G. J. (1996). Induction of the mitochondrial permeability transition by protease activity in rats: A mechanism of hepatocyte necrosis. *Gastroenterology, 110*(2), 558-566.

Al Gadban, M. M., Smith, K. J., Soodavar, F., Piansay, C., Chassereau, C., Twal, W. O., Klein, R. L., Virella, G., Lopes-Virella, M. F., & Hammad, S. M. (2010). Differential trafficking of oxidized LDL and oxidized LDL immune complexes in macrophages: impact on oxidative stress. *PLoS One, 5*(9).

Al Ghouleh, I., Khoo, N. K., Knaus, U. G., Griendling, K. K., Touyz, R. M., Thannickal, V. J., Barchowsky, A., Nauseef, W. M., Kelley, E. E., Bauer, P. M., Darley-Usmar, V., Shiva, S., Cifuentes-Pagano, E., Freeman, B. A., Gladwin, M. T., & Pagano, P. J. (2011). Oxidases and peroxidases in cardiovascular and lung disease: new concepts in reactive oxygen species signaling. *Free Radic Biol Med, 51*(7), 1271-1288.

Alberdi, E., Sanchez-Gomez, M. V., & Matute, C. (2005). Calcium and glial cell death. *Cell Calcium, 38*(3-4), 417-425.

Alcouffe, J., Caspar-Bauguil, S., Garcia, V., Salvayre, R., Thomsen, M., & Benoist, H. (1999). Oxidized low density lipoproteins induce apoptosis in PHA-activated peripheral blood mononuclear cells and in the Jurkat T-cell line. *J Lipid Res, 40*(7), 1200-1210.

Aldieri, E., Riganti, C., Polimeni, M., Gazzano, E., Lussiana, C., Campia, I., & Ghigo, D. (2008). Classical inhibitors of NOX NAD(P)H oxidases are not specific. *Current Drug Metabolism, 9*(8), 686-696.

Alessio, M., De Monte, L., Scirea, A., Gruarin, P., Tandon, N. N., & Sitia, R. (1996). Synthesis, processing, and intracellular transport of CD36 during monocytic differentiation. *Journal of Biological Chemistry, 271*(3), 1770-1775.

Altenhofer, S., Kleikers, P. W., Radermacher, K. A., Scheurer, P., Rob Hermans, J. J., Schiffers, P., Ho, H., Wingler, K., & Schmidt, H. H. (2012). The NOX toolbox: validating the role of NADPH oxidases in physiology and disease. [Review]. *Cellular and Molecular Life Sciences, 69*(14), 2327-2343.

Altenhofer, S., Radermacher, K. A., Kleikers, P. W., Wingler, K., & Schmidt, H. H. (2014). Evolution of NADPH oxidase inhibitors: selectivity and mechanisms for target engagement. *Antioxidants & Redox Signalling, Feb 26*.

Amanso, A. M., & Griendling, K. K. (2012). Differential roles of NADPH oxidases in vascular physiology and pathophysiology. *Frontiers in Bioscience (Scholars Edition), 4*, 1044-1064.

Amit, Z. (2008). *A model of complex plaque formation: 7,8-dihydroneopterin protects human monocyte-derived macrophages from oxidised low density lipoprotein-induced death.* Ph.D., University of Canterbury, New Zealand.

Anderson, T. J. (1999). Assessment and treatment of endothelial dysfunction in humans. *J Am Coll Cardiol, 34*(3), 631-638.

Anzai, K., Ogawa, K., Kuniyasu, A., Ozawa, T., Yamamoto, H., & Nakayama, H. (1998). Effects of hydroxyl radical and sulfhydryl reagents on the open probability of the purified cardiac ryanodine receptor channel incorporated into planar lipid bilayers. *Biochem Biophys Res Commun, 249*(3), 938-942.

Arrington, D. D., Van Vleet, T. R., & Schnellmann, R. G. (2006). Calpain 10: A mitochondrial calpain and its role in calcium-induced mitochondrial dysfunction. *American Journal of Physiology - Cell Physiology, 291*(6), C1159-C1171.

Asmis, R., & Begley, J. G. (2003). Oxidized LDL promotes peroxide-mediated mitochondrial dysfunction and cell death in human macrophages: a caspase-3-independent pathway. *Circulation Research, 92*(1), e20-e29.

Asmis, R., & Wintergest, E. S. (1998). Dehydroascorbic acid prevents apoptosis induced by oxidized low-density lipoprotein in human monocyte-derived macrophages. *European Journal of Biochemistry, 255*, 147-155.

Auffray, C., Fogg, D., Garfa, M., Elain, G., Join-Lambert, O., Kayal, S., Sarnacki, S., Cumano, A., Lauvau, G., & Geissmann, F. (2007). Monitoring of blood vessels and tissues by a population of monocytes with patrolling behavior. *Science, 317*(5838), 666-670.

Augé, N., Fitoussi, G., Bascands, J. L., Pieraggi, M. T., Junquero, D., Valet, P., Girolami, J. P., Salvayre, R., & Nègre-Salvayre, A. (1996). Mildly oxidized LDL evokes a sustained Ca(2+)-dependent retraction of vascular smooth muscle cells. *Circulation Research, 79*(4), 871-880.

Aviram, M., Rosenblat, M., Etzioni, A., & Levy, R. (1996). Activation of NADPH oxidase required for macrophage-mediated oxidation of low-density lipoprotein. *Metabolism, 45*(9), 1069-1079.

Bahorun, T., Soobrattee, M. A., Luximon-Ramma, V., & Aruoma, O. I. (2006). Free radicals and antioxidants in cardiovascular health and disease. *Internet Journal of Medical Update, 1*(2).

Baird, S. (2003). *7,8-dihydroneopterin inhibition of oxidised low density lipoprotein-induced cellular death* Ph.D., University of Canterbury, New Zealand.

Baird, S. K., Hampton, M. B., & Gieseg, S. P. (2004). Oxidized LDL triggers phosphatidylserine exposure in human monocyte cell lines by both caspase-dependent and -independent mechanisms. *FEBS Lett, 578*, 169-174.

Baird, S. K., Reid, L., Hampton, M. B., & Gieseg, S. P. (2005). OxLDL induced cell death is inhibited by the macrophage synthesised pterin, 7,8-dihydroneopterin, in U937 cells but not THP-1 cells. *Biochim Biophys Acta, 1745*, 361-369.

Ball, R. Y., Stowers, E. C., Burton, J. H., Cary, N. R., Skepper, J. N., & Mitchinson, M. J. (1995). Evidence that the death of macrophage foam cells contributes to the lipid core of atheroma. *Atherosclerosis, 14*(1), 45-54.

Ballinger, S. W. (2005). Mitochondrial dysfunction in cardiovascular disease. *Free Radic Biol Med, 38*(10), 1278-1295.

Ballinger, S. W., Patterson, C., Yan, C. N., Doan, R., Burow, D. L., Young, C. G., Yakes, F. M., Van Houten, B., Ballinger, C. A., Freeman, B. A., & Runge, M. S. (2000). Hydrogen peroxide- and peroxynitrite-induced mitochondrial DNA damage and dysfunction in vascular endothelial and smooth muscle cells. *Circulation Research, 86*(9), 960-966.

Barbieri, S. S., Cavalca, V., Eligini, S., Brambilla, M., Caiani, A., Tremoli, E., & Colli, S. (2004). Apocynin prevents cyclooxygenase 2 expression in human monocytes through NADPH oxidase and glutathione redox-dependent mechanisms. *Free Radical Biology and Medicine, 37*(2), 156-165.

Barry-Lane, P. A., Patterson, C., van der Merwe, M., Hu, Z., Holland, S. M., Yeh, E. T. H., & Runge, M. S. (2001). p47phox is required for atherosclerotic lesion progression in ApoE–/– mice. *Journal of Clinical Investigation, 108*(10), 1513-1522.

Baskar, R., Li, L., & Moore, P. K. (2007). Hydrogen sulfide-induces DNA damage and changes in apoptotic gene expression in human lung fibroblast cells. *FASEB Journal, 21*(1), 247-255.

Basu, K., Dasgupta, B., Bhattacharya, S. K., & Debnath, P. K. (1971). Chemistry and pharmacology of apocynin, isolated from Picrorhiza kurroa Royle ex Benth. *Current Science, 40*(22), 603-604.

Bauer, C. C., Boyle, J. P., Porter, K. E., & Peers, C. (2010). Modulation of Ca2+ signalling in human vascular endothelial cells by hydrogen sulfide. *Atherosclerosis, 209*(2), 374-380.

Baysal, K., Jung, D. W., Gunter, K. K., Gunter, T. E., & Brierley, G. P. (1994). Na(+)-dependent Ca2+ efflux mechanism of heart mitochondria is not a passive Ca2+/2Na+ exchanger. *American Journal of Physiology, 266*(3 Pt 1), C800-C808.

Beauchamp, R. O. J., Bus, J. S., Popp, J. A., Boreiko, C. J., & Andjelkovich, D. A. (1984). A critical review of the literature on hydrogen sulfide toxicity. *Critical Reviews in Toxicology, 13*(1), 25-97.

Bedard, K., & Krause, K.-H. (2007). The NOX family of ROS-generating NADPH oxidases: physiology and pathophysiology. *Physiological Reviews, 87*, 245-313.

Berliner, J. A., & Heinecke, J. W. (1996). The role of oxidized lipoproteins in atherogenesis. *Free Radic Biol Med, 20*, 707-727.

Bernardi, P. (1999). Mitochondrial transport of cations: channels, exchangers, and permeability transition. *Physiological Reviews, 79*(4), 1127-1155.

Bernardi, P., Krauskopf, A., Basso, E., Petronilli, V., Blachly-Dyson, E., Di Lisa, F., & Forte, M. A. (2006). The mitochondrial permeability transition from in vitro artifact to disease target. *FEBS Journal, 273*(10), 2077-2099.

Berridge, M. J. (1998). Neuronal calcium signaling. *Neuron, 21*, 13-26.

Berridge, M. J., Bootman, M. D., & Roderick, H. L. (2003). Calcium signalling: dynamics, homeostasis and remodelling. *Nature Reviews Molecular Cell Biology, 4*(7), 517-529.

Berridge, M. J., & Irvine, R. F. (1989). Inositol phosphates and cell signalling. *Nature, 341*(6239), 197-205.

Berthier, A., Lemaire-Ewing, S., Prunet, C., Monier, S., Athias, A., Bessede, G., Pais de Barros, J. P., Laubriet, A., Gambert, P., Lizard, G., & Neel, D. (2004). Involvement of a calcium-dependent dephosphorylation of BAD associated with the localization of Trpc-1 within lipid rafts in 7-ketocholesterol-induced THP-1 cell apoptosis. *Cell Death Differ, 11*(8), 897-905.

Bertolino, M., & Llinas, R. R. (1992). The central role of voltage-activated and receptor-operated calcium channels in neuronal cells. *Annual Reviews of Pharmacology and Toxicology, 32*, 399-421.

Bertolotti, A., Zhang, Y., Hendershot, L. M., Harding, H. P., & Ron, D. (2000). Dynamic interaction of BiP and ER stress transducers in the unfolded-protein response. *Nat Cell Biol, 2*(6), 326-332.

Bhatia, M. (2012). Role of hydrogen sulfide in the pathology of inflammation. [Review]. *Scientifica (Cairo), 2012*.

Bhatia, M., Sidhapuriwala, J., Moochhala, S. M., & Moore, P. K. (2005b). Hydrogen sulphide is a mediator of carrageenan-induced hindpaw oedema in the rat. *Br J Pharmacol, 145*(2), 141-144.

Bhatia, M., Wong, F. L., Fu, D., Lau, H. Y., Moochhala, S. M., & Moore, P. K. (2005a). Role of hydrogen sulfide in acute pancreatitis and associated lung injury. *FASEB Journal, 19*(6), 623.

Bianchi, K., Rimessi, A., Prandini, A., Szabadkai, G., & Rizzuto, R. (2004). Calcium and mitochondria: mechanisms and functions of a troubled relationship. *Biochimica Biophysica Acta, 1742*(1-3), 119-131.

Brandes, R. P. (2005). Triggering mitochondrial radical release: a new function for NADPH oxidases. *Hypertension, 45*(5), 847-848.

Brandes, R. P., & Kreuzer, J. (2005). Vascular NADPH oxidases: molecular mechanisms of activation. *Cardiovasc Res, 65*(1), 16-27.

Brandes, R. P., Viedt, C., Nguyen, K., Beer, S., Kreuzer, J., Busse, R., & Gorlach, A. (2001). Thrombin-induced MP-1 expression involves activation of the p22phox-containing NADPH oxidase in human vascular smooth muscle cells *Thrombosis and Haemostasis, 85*(6), 1104-1110.

Brandes, R. P., Weissmann, N., & Schroder, K. (2010). NADPH oxidases in cardiovascular disease. *Free Radic Biol Med, 49*(5), 687-706.

Brookes, P. S., Yoon, Y., Robotham, J. L., Anders, M. W., & Sheu, S.-S. (2004). Calcium, ATP, and ROS: a mitochondrial love-hate triangle. *American Journal of Physiological Cell Physiology, 287*, C817-C833.

Cadenas, E., & Davies, K. J. A. (2000). Mitochondrial free radical generation, oxidative stress, and aging. *Free Radical Biology and Medicine, 29*(3/4), 222-230.

Calvert, J. W., Coetzee, W. A., & Lefer, D. J. (2010). Novel insights into hydrogen sulfide--mediated cytoprotection. *Antioxidants & Redox Signalling, 12*(10), 1203-1217.

Camello-Almaraz, C., Gomez-Pinilla, P. J., Pozo, M. J., & Camello, P. J. (2006). Mitochondrial reactive oxygen species and Ca(2+) signaling. *American Journal of Physiological Cell Physiology, 291*, C1082-C1088.

Campbell, D. L., Stamler, J. S., & Strauss, H. C. (1996). Redox modulation of L-type calcium channels in ferret ventricular myocytes: Dual mechanism regulation by nitric oxide and S-nitrosothiols. *Journal of General Physiology, 108*(4), 277-293.

Cao, Y., Adhikari, S., Ang, A. D., Moore, P. K., & Bhatia, M. (2006). Mechanism of induction of pancreatic acinar cell apoptosis by hydrogen sulfide. *American Journal of Physiological Cell Physiology, 291*, C503-C510.

Carafoli, E. (1987). Intracellular calcium homeostasis. *Annual Review of Biochemistry, 56*, 395-433.

Carafoli, E. (2010). The fateful encounter of mitochondria with calcium: how did it happen? *Biochim Biophys Acta, 1797*(6-7), 595-606. doi: 10.1016/j.bbabio.2010.03.024

Carballal, S., Trujillo, M., Cuevasanta, E., Bartesaghi, S., Moller, M. N., Folkes, L. K., Garcia-Bereguiain, M. A., Gutierrez-Merino, C., Wardman, P., Denicola, A., Radi, R., & Alvarez, B. (2011). Reactivity of hydrogen sulfide with peroxynitrite and other oxidants of biological interest. *Free Radical Biology and Medicine, 50*(1), 196-205.

Castor, L. R., Locatelli, K. A., & Ximenes, V. F. (2010). Pro-oxidant activity of apocynin radical. *Free Radical Biology and Medicine, 48*(12), 1636-1643.

Cathcart, M. K. (2004). Regulation of superoxide anion production by NADPH oxidase in monocytes/macrophages: contributions to atherosclerosis. [Review]. *Arteriosclerosis Thrombosis and Vascular Biology, 24*(1), 23-28.

Cathcart, M. K., McNally, A. K., & Chisolm, G. M. (1991). Lipoxygenase-mediated transformation of human low density lipoprotein to an oxidized and cytotoxic complex. *J Lipid Res, 32*, 63-70.

Cayatte, A. J., Rupin, A., Oliver-Krasinski, J., Maitland, K., Sansilvestri-Morel, P., Boussard, M. F., Wierzbicki, M., Verbeuren, T. J., & Cohen, R. A. (2001). S17834, a new inhibitor of cell adhesion and atherosclerosis that targets nadph oxidase. *Arteriosclerosis Thrombosis and Vascular Biology, 21*(10), 1577-1584.

Celsi, F., Pizzo, P., Brini, M., Leo, S., Fotino, C., Pinton, P., & Rizzuto, R. (2009). Mitochondria, calcium and cell death: a deadly triad in neurodegeneration. *Biochim Biophys Acta, 1787*(5), 335-344.

Chang, C. Y., Shen, C. Y., Kang, C. K., Sher, Y. P., Sheu, W. H., Chang, C. C., & Lee, T. H. (2014). Taurine protects HK-2 cells from oxidized LDL-induced cytotoxicity via the ROS-mediated mitochondrial and p53-related apoptotic pathways. *Toxicol Appl Pharmacol, 279*(3), 351-363.

Chapman, M. J., Guerin, M., & Bruckert, E. (1998). Atherogenic, dense low-density lipoproteins. Pathophysiology and new therapeutic approaches. *Eur Heart J, 19*(Supplement A), A24-A30.

Chen, Q., Camara, A. K., Stowe, D. F., Hoppel, C. L., & Lesnefsky, E. J. (2007). Modulation of electron transport protects cardiac mitochondria and decreases myocardial injury during ischemia and reperfusion. *American Journal of Physiological Cell Physiology, 292*(1), C137-C147.

Chen, Q., Moghaddas, S., Hoppel, C. L., & Lesnefsky, E. J. (2006). Reversible blockade of electron transport during ischemia protects mitochondria and decreases myocardial injury following reperfusion. *Journal of Pharmacology and Experimental Therapeutics, 319*(3), 1405-1412.

Chen, Y. A. (2012). *Role of intracellular oxidant release in oxidised low density lipoprotein-induced U937 cell death.* M.Sc., University of Canterbury, New Zealand.

Chernyak, B. V., Dedov, V. N., & Chernyak, V. Y. (1995). Ca2+-triggered membrane permeability transition in deenergized mitochondria from rat liver. *FEBS Lett, 365*(1), 75-78.

Chin, T.-Y., Lin, H.-C., Kuo, J.-P., & Chueh, S.-H. (2007). Dual effect of thapsigargin on cell death in porcine aortic smooth muscle cells. *American Journal of Physiological. Cell Physiology, 292*, C383-C395.

Chung, B. H., Wilkinson, T., Geer, J. C., & Segrest, J. P. (1980). Preparative and quantitative isolation of plasma lipoproteins: rapid, single discontinuous density gradient ultracentrifugation in a vertical rotor. *J Lipid Res, 21*(3), 284-291.

Cifuentes-Pagano, E., Csanyi, G., & Pagano, P. J. (2012). NADPH oxidase inhibitors: a decade of discovery from Nox2ds to HTS. [Review]. *Cellular and Molecular Life Sciences, 69*(14), 2315-2325.

Cifuentes, M. E., Rey, F. E., Carretero, O. A., & Pagano, P. J. (2000). Upregulation of p67(phox) and gp91(phox) in aortas from angiotensin II-infused mice. *American Journal of Physiology. Heart Circulation Physiology, 279*, H2234-H2240.

Clapham, D. E. (2007). Calcium signaling. [Review]. *Cell, 131*(6), 1047-1058.

Crompton, M. (1999). The mitochondrial permeability transition pore and its role in cell death. *Biochem J, 341*, 233-249.

Darley-Usmar, V. M., Severn, A., O'Leary, V. J., & Rogers, M. (1991). Treatment of macrophages with oxidized low-density lipoprotein increases their intracellular glutathione content. *Biochemical Journal, 278*, 429-434.

de Hornedo, J. P., de Arriba, G., Fernandez, M. C., Benito, S., & Cid, T. P. (2007). Cyclosporin A causes oxidative stress and mitochondrial dysfunction in tubular renal cells. *Nefrologia, 27*(5), 565-573.

Dejeans, N., Tajeddine, N., Beck, R., Verrax, J., Taper, H., Gailly, P., & Calderon, P. B. (2010). Endoplasmic reticulum calcium release potentiates the ER stress and cell death caused by an oxidative stress in MCF-7 cells. *Biochem Pharmacol, 79*(9), 1221-1230.

DeLeo, F. R., L., Y., Burritt, J. B., Loetterle, L. R., Bond, C. W., Jesaitis, A. J., & Quinn, M. T. (1995). Mapping sites of interaction of p47-phox and flavocytochrome b with random-sequence peptide phage display libraries. *Proceedings of the National Academy of Sciences USA, 92*(15), 7110-7114.

Deng, T., Zhang, L., Ge, Y., Lu, M., & Zheng, X. (2009). Redistribution of intracellular calcium and its effect on apoptosis in macrophages: induction by oxidized LDL. *Biomedicine & Pharmacotherapy, 63*(4), 267-274.

Deng, T. L., Yu, L., Ge, Y. K., Zhang, L., & Zheng, X. X. (2005). Intracellular-free calcium dynamics and F-actin alteration in the formation of macrophage foam cells. *Biochem Biophys Res Commun, 338*(2), 748-756.

Denizot, F., & Lang, R. (1986). Rapid colorimetric assay for cell growth and survival. Modifications to the tetrazolium dye procedure giving improved sensitivity and reliability. *Journal Immunological Methods, 83*, 271-277.

Dhalla, N. S., Temsah, R. M., & Netticadan, T. (2000). Role of oxidative stress in cardiovascular diseases. *Journal of Hypertension, 18*(6), 655-673.

di Masi, A., & Ascenzi, P. (2013). H_2S: a "double face" molecule in health and disease. *Biofactors, 39*(2), 186-196.

Diatchuk, V., Lotan, O., Koshkin, V., Wikstroem, P., & Pick, E. (1997). Inhibition of NADPH oxidase activation by 4-(2-aminoethyl)-benzenesulfonyl fluoride and related compounds. *Journal of Biological Chemistry, 271*(20), 13292-13301.

Diederich, D., Skopec, J., Diederich, A., & Dai, F. X. (1994). Cyclosporine produces endothelial dysfunction by increased production of superoxide. *Hypertension, 23*, 957-961.

Ding, Y., Chen, Z. J., Liu, S., Che, D., Vetter, M., & Chang, C. H. (2005). Inhibition of Nox-4 activity by plumbagin, a plant-derived bioactive naphthoquinone. *Journal of Pharmacy and Pharmacology, 57*(1), 111-116.

Doughan, A. K., Harrison, D. G., & Dikalov, S. I. (2008). Molecular mechanisms of angiotensin II-mediated mitochondrial dysfunction: linking mitochondrial oxidative damage and vascular endothelial dysfunction. *Circulation Research, 102*(4), 488-496.

Douglas, G., & Channon, K. M. (2010). The pathogenesis of atherosclerosis. *Medicine, 38*(8), 397-402.

Drake, T. A., Hannani, K., Fei, H., Lavi, S., & Berliner, J. A. (1991). Minimally oxidized low-density lipoprotein induces tissue factor expression in cultured human endothelial cells. *American Journal of Pathology, 138*(3), 601-607.

Duchen, M. R., Verkhratsky, A., & Muallem, S. (2008). Mitochondria and calcium in health and disease. [Review]. *Cell Calcium, 44*(1), 1-5.

Duggan, S., Rait, C., Gebicki, M., & Gieseg, S. P. (2001). Inhibition of protein oxidation by the macrophage-synthesised antioxidant 7,8-dihydroneopterin. *Redox Report, 6*(3), 188-190.

Duggan, S., Rait, C., Platt, A., & Gieseg, S. P. (2002). Protein and thiol oxidation in cells exposed to peroxyl radicals in inhibited by the macrophage synthesised pterin 7,8-dihydroneopterin. *Biochim Biophys Acta, 1591*, 139-145.

Duprez, L., Wirawan, E., Vanden Berghe, T., & Vandenabeele, P. (2009). Major cell death pathways at a glance. *Microbes and Infection, 11*(13), 1050-1062.

Dworakowski, R., Alom-Ruiz, S. P., & Shah, A. M. (2008). NADPH oxidase-derived reactive oxygen species in the regulation of endothelial phenotype. *Pharmacological Reports, 60*, 21-28.

Efimova, O., Szankasi, P., & Kelley, T. W. (2011). Ncf1 (p47phox) is essential for direct regulatory T cell mediated suppression of CD4+ effector T cells. *PLoS One, 6*(1), e16013.

Engels, F., Renirie, B. F., Hart, B. A., Labadie, R. P., & Nijkamp, F. P. (1992). Effects of apocynin, a drug isolated from the roots of Picrorhiza kurroa, on arachidonic acid metabolism. *FEBS Lett, 305*(3), 254-256.

Ermak, G., & Davies, K. J. A. (2001). Calcium and oxidative stress: from cell signalling to cell death. *Molecular Immunology, 38*, 713-721.

Ermak, N., Lacour, B., Goirand, F., Drueke, T. B., & Vicca, S. (2010). Differential apoptotic pathways activated in response to Cu-induced or HOCl-induced LDL oxidation in U937 monocytic cell line. *Biochem Biophys Res Commun, 393*(4), 783-787.

Escargueil-Blanc, I., Salvayre, R., & Negre-Salvayre, A. (1994). Necrosis and apoptosis induced by oxidized low density lipoproteins occur through two calcium-dependent pathways in lymphoblastoid cells. *FASEB, 8*, 1075-1080.

Fabiato, A. (1983). Calcium-induced release of calcium from the cardiac sarcoplasmic reticulum. *American Journal of Physiology, 245*(1).

Fawell, S., Seery, J., Y., D., Moore, C., Chen, L. L., Pepinsky, B., & Barsoum, J. (1994). Tat-mediated delivery of heterologous proteins into cells. *Proceedings of the National Academy of Sciences USA, 91*(2), 664-668.

Forbes, J. M., Coughlan, M. T., & Cooper, M. E. (2008). Oxidative stress as a major culprit in kidney disease in diabetes. *Diabetes, 57*(6), 1446-1454.

Fox, B., Schantz, J. T., Haigh, R., Wood, M. E., Moore, P. K., Viner, N., Spencer, J. P., Winyard, P. G., & Whiteman, M. (2012a). Inducible hydrogen sulfide synthesis in chondrocytes and mesenchymal progenitor cells: is H2S a novel cytoprotective mediator in the inflamed joint? *J Cell Mol Med, 16*(4), 896-910.

Frohlich, J., & Al-Sarraf, A. (2013). Cardiovascular risk and atherosclerosis prevention. [Review]. *Cardiovascular Pathology, 22*(1), 16-18.

Fu, M., Zhang, W., Wu, L., Yang, G., Li, H., & Wang, R. (2012). Hydrogen sulfide (H2S) metabolism in mitochondria and its regulatory role in energy production. *Proc Natl Acad Sci U S A, 109*(8), 2943-2948.

Galle, J., Hansen-Hagge, T., Wanner, C., & Seibold, S. (2006). Impact of oxidized low density lipoprotein on vascular cells. [Review]. *Atherosclerosis, 185*(2), 219-226.

Garcia-Bereguiain, M. A., Samhan-Arias, A. K., Martin-Romero, F. J., & Gutierrez-Merino, C. (2008). Hydrogen sulfide raises cytosolic calcium in neurons through activation of L-type Ca2+ channels. *Antioxidants & Redox Signalling, 10*(1), 31-42.

Geeraerts, M. D., Ronveaux-Dupal, M. F., Lemasters, J. J., & Herman, B. (1991). Cytosolic free Ca2+ and proteolysis in lethal oxidative injury in endothelial cells. *American Journal of Physiology, 261*, C889-C896.

Geng, B., Yang, J., Qi, Y., Zhao, J., Pang, Y., Du, J., & Tang, C. (2004). H2S generated by heart in rat and its effects on cardiac function. *Biochem Biophys Res Commun, 313*(2), 362-368.

Gerry, A. B., Satchell, L., & Leake, D. S. (2008). A novel method for production of lipid hydroperoxide- or oxysterol-rich low density lipoprotein. *Atherosclerosis, 197*, 579-587.

Gieseg, S. P., Amit, Z., Yang, Y.-T., Shchepetkina, A., & Katouah, H. (2010). Oxidant production, oxLDL uptake, and CD36 levels in human monocyte-derived macrophages are downregulated by the macrophage-generated antioxidant 7,8-dihydroneopterin. *Antioxid Redox Signal, 13*(10), 1525-1534.

Gieseg, S. P., Crone, E., & Amit, Z. (2009b). Oxidised low density lipoprotein cytotoxicity and vascular disease. In P. J. O'Brien & R. Bruce (Eds.), *Endogenous Toxins* (Vol. 2, pp. 619-645): Wiley-VCH Verlag GmbH & Co. KGaA.

Gieseg, S. P., Crone, E. M., Flavall, E. A., & Amit, Z. (2008). Potential to inhibit growth of atherosclerotic plaque development through modulation of macrophage neopterin/7,8-dihydroneopterin synthesis. *Br J Pharmacol, 153*(4), 627-635.

Gieseg, S. P., & Esterbauer, H. (1994). Low density lipoprotein is saturable by pro-oxidant copper. *FEBS Lett, 343*, 188-194.

Gieseg, S. P., G., M., & Glubb, D. (2000). Inhibition of haemolysis by the macrophage synthesized antioxidant, 7,8-dihydroneopterin. *Redox Report, 5*(2/3), 97-100.

Gieseg, S. P., Leake, D. S., Flavall, E. M., Amit, Z., Reid, L., & Yang, Y.-T. (2009a). Macrophages antioxidant protection within atherosclerotic plaque. *Frontiers in Bioscience, 14*, 1230-1246.

Gieseg, S. P., Maghzal, G., & Glubb, D. (2001a). Protection of erythrocytes by the macrophage synthesized antioxidant 7,8-dihydroneopterin. *Free Radic Res, 34*, 123-136.

Gieseg, S. P., Pearson, J., & Firth, C. A. (2003). Protein hydroperoxides are a major product of low density lipoprotein oxidation during copper, peroxyl radical and macrophage-mediated oxidation. *Free Radic Res, 37*(9), 983-991.

Gieseg, S. P., Reibnegger, G., Wachter, H., & Esterbauer, H. (1995). 7,8-dihydroneopterin inhibits low density lipoprotein oxidation in vitro. Evidence that this macrophage secreted pteridine is an anti-oxidant. *Free Radic Res, 23*(2), 123-136.

Gieseg, S. P., Simpson, J. A., Charlton, T. S., Duncan, M. W., & Dean, R. T. (1993). Protein-bound 3,4-dihydroxyphenylalanine is a major reductant formed during hydroxyl radical damage to proteins. *Biochemistry, 32*, 4780-4786.

Gieseg, S. P., Whybrow, J., Glubb, D., & Rait, C. (2001b). Protection of the U937 cells from free radical damage by the macrophage synthesized antioxidant 7,8-dihydroneopterin. *Free Radic Res, 35*, 313-318.

Giorgi, C., Baldassari, F., Bononi, A., Bonora, M., De Marchi, E., Marchi, S., Missiroli, S., Patergnani, S., Rimessi, A., Suski, J. M., Wieckowski, M. R., & Pinton, P. (2012). Mitochondrial Ca2+ and apoptosis. *Cell Calcium, 52*(1), 36-43.

Glass, C. K., & Witztum, J. L. (2001). Atherosclerosis: the road ahead. *Cell, 104*, 503-516.

Goldman, R., Moshonov, S., & Zor, U. (1998). Generation of reactive oxygen species in a human keratinocytes cell line: role of calcium. *Archives of Biochemistry and Biophysics, 350*(1), 10-18.

Goldstein, J. L., Ho, Y. K., Basu, S. K., & Brown, M. S. (1979). Binding site on macrophages that mediates uptake and degradation of acetylated low density lipoprotein, producing massive cholesterol deposition. *Proceedings of the National Academy of Sciences USA, 76*(1), 333-337.

Gonzalez, R. J., & Tarloff, J. B. (2001). Evaluation of hepatic subcellular fractions for Alamar blue and MTT reductase activity. *Toxicology in Vitro, 15*, 257-259.

Gores, G. J., Miyoshi, H., Botla, R., Aguilar, H. I., & Bronk, S. F. (1998). Induction of the mitochondrial permeability transition as a mechanism of liver injury during cholestasis: A potential role for mitochondrial proteases. *Biochimica et Biophysica Acta - Bioenergetics, 1366*(1-2), 167-175.

Gotoh, N., Graham, A., Nikl, E., & Darley-Usmar, V. M. (1993). Inhibition of glutathione synthesis increases the toxicity of oxidized low-density lipoprotein to human monocytes and macrophages. *Biochemical Journal, 296*, 151-154.

Griendling, K. K., Sorescu, D., & Ushio-Fukai, M. (2000). NAD(P)H Oxidase : Role in Cardiovascular Biology and Disease. *Circulation Research, 86*(5), 494-501.

Grijalba, M. T., Vercesi, A. E., & Schreier, S. (1999). Ca2+-induced increased lipid packing and domain formation in submitochondrial particles. A possible early step in the mechanism of Ca2+- stimulated generation of reactive oxygen species by the respiratory chain. *Biochemistry, 38*(40), 13279-13287.

Groemping, Y., Lapouge, K., Smerdon, S. J., & Rittinger, K. (2003). Molecular basis of phosphorylation-induced activation of the NADPH oxidase. *Cell, 113*(3), 343-355.

Groemping, Y., & Rittinger, K. (2005). Activation and assembly of the NADPH oxidase: a structural perspective *Biochemical Journal, 386*, 401-416.

Gunter, T. E., Buntinas, L., Sparagna, G., Eliseev, R., & Gunter, K. (2000). Mitochondrial calcium transport: mechanisms and functions. *Cell Calcium, 28*(5-6), 285-296.

Guyton, J. R., Lenz, M. L., Mathews, B., Hughes, H., Karsan, D., Selinger, E., & Smith, C. V. (1995). Toxicity of oxidized low density lipproteins for vascular smooth muscle cells and partial protection by antioxidants. *Atherosclerosis, 118*, 237-249.

Guzik, T. J., & Harrison, D. G. (2006). Vascular NADPH oxidases as drug targets for novel antioxidant strategies. [Review]. *Drug Discov Today, 11*(11-12), 524-533.

Halliwell, B. (2003). Oxidative stress in cell culture: an under-appreciated problem? *FEBS Lett, 540*(1-3), 3-6.

Halliwell, B., Evans, P., & Whiteman, M. (1999). Assessment of peroxynitrite scavengers in vitro. *Methods in Enzymology, 301*, 333-342.

Hampton, M. B., Kettle, A. J., & Winterbourn, C. C. (1998). Inside the neutrophil phagosome: oxidants, myeloperoxidase, and bacterial killing. *Blood, 91*(9), 3007-3017.

Han, C.-Y., & Pak, Y. K. (1999). Oxidation-dependent effects of oxidized LDL: proliferation or cell death. *Experimental and Molecular Medicine, 31*(4), 166-173.

Han, C. H., Freeman, J. L., Lee, T., Motalebi, S. A., & Lambeth, J. D. (1998). Regulation of the neutrophil respiratory burst oxidase. Identification of an activation domain in p67(phox). *Journal of Biological Chemistry, 273*(27), 16663-16668.

Han, D., Canali, R., Rettori, D., & Kaplowitz, N. (2003). Effect of glutathione depletion on sites and topology of superoxide and hydrogen peroxide production in mitochondria. *Mol Pharmacol, 64*(5), 1136-1144.

Hanson, C. J., Bootman, M. D., & Roderick, H. L. (2004). Cell signalling: IP3 receptors channel calcium into cell death. *Current Biology, 14*(21), R933-R935.

Hansson, M. J., Persson, T., Friberg, H., Keep, M. F., Rees, A., Wieloch, T., & Elmér, E. (2003). Powerful cyclosporin inhibition of calcium-induced permeability transition in brain mitochondria. *Brain Research*(960), 99-111.

Harding, H. P., Zhang, Y., & Ron, D. (1999). Protein translation and folding are coupled by an endoplasmic-reticulum-resident kinase. *Nature, 397*(6716), 271-274.

Hardwick, S. J., Hegyi, L., Clare, K., Law, N. S., Carpenter, K. L. H., Mitchinson, M. J., & Skepper, J. N. (1996). Apoptosis in human monocyte-macrophages exposed to oxidized low density lipoprotein. *Journal of Pathology, 179*, 294-302.

Harrison, D., Griendling, K. K., Landmesser, U., Hornig, B., & Drexler, H. (2003). Role of oxidative stress in atherosclerosis. *American Journal of Cardiology, 91*(3 SUPPL.), 7A-11A.

Haze, K., Yoshida, H., Yanagi, H., Yura, T., & Mori, K. (1999). Mammalian transcription factor ATF6 is synthesized as a transmembrane protein and activated by proteolysis in response to endoplasmic reticulum stress. *Mol Biol Cell, 10*(11), 3787-3799.

He, C., & Klionsky, D. J. (2009). Regulation mechanisms and signaling pathways of autophagy. *Annu Rev Genet, 43*, 67-93.

Heales, S. J. R., Blair, J. A., Meinschard, C., & Ziegler, I. (1988). Inhibition of monocyte luminol-dependent chemiluminescence by tetrahydrobiopterin and free radical oxidation of tetrahydrobiopterin, dihydrobiopterin and dihydroneopterin. *Cell Biochemistry and Function, 6*, 191-195.

Heath-Engel, H. M., Chang, N. C., & Shore, G. C. (2008). The endoplasmic reticulum in apoptosis and autophagy: role of the BCL-2 protein family. *Oncogene, 27*(50), 6419-6433.

Hegyi, L., Skepper, J. N., Cary, N. R., & Mitchinson, M. J. (1996). Foam cell apoptosis and the development of lipid core of human atherosclerosis. *Journal of Pathology, 180*(4), 423-429.

Hennig, B., & Diener, M. (2009). Actions of hydrogen sulphide on ion transport across rat distal colon. *Br J Pharmacol, 158*(5), 1263-1275.

Hessler, J. R., Robertson, A. L. J., & Chisolm, G. M. (1979). LDL-induced cytotoxicity and its inhibition by HDL in human vascular smooth muscle and endothelial cells in culture. *Atherosclerosis, 32*(3), 213-229.

Heumuller, S., Wind, S., Barbosa-Sicard, E., Schmidt, H. H., Busse, R., Schroder, K., & Brandes, R. P. (2008). Apocynin is not an inhibitor of vascular NADPH oxidases but an antioxidant. *Hypertension, 51*(2), 211-217.

Higashi, Y., Peng, T., Du, J., Sukhanov, S., Li, Y., Itabe, H., Parthasarathy, S., & Delafontaine, P. (2005). A redox-sensitive pathway mediates oxidized LDL-induced downregulation of insulin-like growth factor-1 receptor. *J Lipid Res, 46*(6), 1266-1277.

Holland, J. A., Meyer, J. W., Chang, M. M., O'Donnell, R. W., Johnson, D. K., & Ziegler, L. M. (1998). Thrombin stimulated reactive oxygen species production in cultured human endothelial cells. *Endothelium, 6*(2), 113-121.

Holland, J. A., Meyer, J. W., Schmitt, M. E., Sauro, M. D., Johnson, D. K., Abdul-Karim, R. W., Patel, V., Ziegler, L. M., Schillinger, K. J., Small, R. F., & Lemanski, L. F. (1997). Low-density lipoprotein stimulated peroxide production and endocytosis in cultured human endothelial cells: mechanisms of action. *Endothelium, 5*(3), 191-207.

Holvoet, P., De Keyzer, D., & Jacobs, D. R., Jr. (2008). Oxidized LDL and the metabolic syndrome. *Future Lipidol, 3*(6), 637-649.

Hsieh, C.-C., Yen, M.-H., Yen, C.-H., & Lau, Y.-T. (2001). Oxidized low density lipoprotein induces apoptosis via generation of reactive oxygen species in vascular smooth muscle cells. *Cardiovasc Res, 49*, 135-145.

Hu, L. F., Lu, M., Wu, Z. Y., Wong, P. T., & Bian, J. S. (2009). Hydrogen sulfide inhibits rotenone-induced apoptosis via preservation of mitochondrial function. *Mol Pharmacol, 75*(1), 27-34.

Hu, L. F., Wong, P. T., Moore, P. K., & Bian, J. S. (2007). Hydrogen sulfide attenuates lipopolysaccharide-induced inflammation by inhibition of p38 mitogen-activated protein kinase in microglia. *J Neurochem, 100*(4), 1121-1128.

Huang, J., & Kleinberg, M. E. (1999). Activation of the phagocyte NADPH oxidase protein p47(phox). Phosphorylation controls SH3 domain-dependent binding to p22(phox). *Journal of Biological Chemistry, 274*(28), 19731-19737.

Iino, M. (1999). Dynamic regulation of intracellular calcium signals through calcium release channels. *Mol Cell Biochem, 190*(1-2), 185-190.

Inoue, T., Suzuki, Y., Yoshimaru, T., & Ra, C. (2008). Reactive oxygen species produced up- or downstream of calcium influx regulate proinflammatory mediator release from mast cells: role of NADPH oxidase and mitochondria. *Biochim Biophys Acta, 1783*(5), 789-802.

Irani, K. (2000). Oxidant signaling in vascular cell growth, death, and survival : a review of the roles of reactive oxygen species in smooth muscle and endothelial cell mitogenic and apoptotic signaling. *Circulation Research, 87*(3), 179-183.

Ishii, H., Kizaki, K., Horie, S., & Kazama, M. (1996). Oxidized low density lipoprotein reduces thrombomodulin transcription in cultured human endothelial cells through degradation of the lipoprotein in lysosomes. *J Biol Chem, 271*(14), 8458-8465.

Itabe, H. (2003). Oxidized low-density lipoproteins: what is understood and what remains to be clarified. *Biological Pharmacology, 26*(1), 1-9.

Jaeschke, H., & Lemasters, J. J. (2003). Apoptosis versus oncotic necrosis in hepatic ischemia/reperfusion injury. *Gastroenterology, 125*, 1248-1257.

Janes, M. S., Hill, D. M., Cardon, C. M., Robinson, K. M., Walls, J. R., Leung, W. Y., Beckman, J. S., & Ignatius, M. J. (2004). Fluorogenic detection of mitochondrial superoxide in live cells. *The American Society for Cell Biology 44th Annual Meeting.* Washington DC, December 4-8.

Jeney, V., Potor, L., Whiteman, M., Wood, M. E., Balla, G., & Balla, J. (2013). Potential anti-atherogenic effects of hydrogen-sulfide releasing molecules. *Nitric Oxide, 31*, S11-S65.

Jiang, F., Zhang, Y., & Dusting, G. J. (2011). NADPH oxidase-mediated redox signaling: roles in cellular stress response, stress tolerance, and tissue repair. *Pharmacol Rev, 63*(1), 218-242.

Jimenez-Corona, A. E., Damian-Zamacona, S., Perez-Torres, A., Moreno, A., & Mas-Oliva, J. (2012). Osteopontin upregulation in atherogenesis is associated with cellular oxidative stress triggered by the activation of scavenger receptors. *Arch Med Res, 43*(2), 102-111.

Joshi, D. C., & Bakowska, J. C. (2011). Determination of mitochondrial membrane potential and reactive oxygen species in live rat cortical neurons. *Journal of Visualized Experiments, 51*.

Jou, M. J., Peng, T. I., Hsu, L. F., Jou, S. B., Reiter, R. J., Yang, C. M., Chiao, C. C., Lin, Y. F., & Chen, C. C. (2010). Visualization of melatonin's multiple mitochondrial levels of protection against mitochondrial Ca(2+)-mediated permeability transition and beyond in rat brain astrocytes. *Journal of Pineal Research, 48*(1), 20-38.

Kahan, B. D. (1992). Immunosuppressive therapy. *Current Opinion in Immunology, 4*(5), 553-560.

Kalyanaraman, B., Darley-Usmar, V., Davies, K. J., Dennery, P. A., Forman, H. J., Grisham, M. B., Mann, G. E., Moore, K., Roberts, L. J., 2nd, & Ischiropoulos, H. (2012). Measuring reactive oxygen and nitrogen species with fluorescent probes: challenges and limitations. [Review]. *Free Radic Biol Med, 52*(1), 1-6.

Katouah, H. A. (2012). *Inhibition of macrophage metabolism by oxLDL*. Ph.D., University of Canterbury, New Zealand.

Kawahara, T., Ritsick, D., Cheng, G., & Lambeth, J. D. (2005). Point mutations in the proline-rich region of p22phox are dominant inhibitors of Nox1- and Nox2-dependent reactive oxygen generation. *Journal of Biological Chemistry, 280*(36), 31859-31869.

Kerr, J. F. R., Wyllie, A. H., & Currie, A. R. (1972). Apoptosis: a basic biological phenomenon with wide-ranging implications in tissue kinetics. *British Journal of Cancer, 26*(4), 239-257.

Kim, J.-S., He, L., & Lemasters, J. J. (2003a). Mitochondrial permeability transition: a common pathway to necrosis and apoptosis. *Biochem Biophys Res Commun, 304*(3), 463-470.

Kim, J.-S., He, L., Qian, T., & Lemasters, J. J. (2003b). Role of the mitochondrial permeability transition in apoptotic and necrotic death after ischemia/reperfusion injury to hepatocytes. *Current Molecular Medicine, 3*(6), 527-235.

Kimura, H. (2000). Hydrogen sulfide induces cyclic AMP and modulates the NMDA receptor. *Biochem Biophys Res Commun, 267*(1), 129-133.

Kimura, Y., Goto, Y., & Kimura, H. (2010). Hydrogen sulfide increases glutathione production and suppresses oxidative stress in mitochondria. *Antioxidants & Redox Signalling, 12*(1), 1-13.

Kimura, Y., & Kimura, H. (2004). Hydrogen sulfide protects neurons from oxidative stress. *FASEB*.

Kinkade, K., Streeter, J., & Miller, F. J. (2013). Inhibition of NADPH oxidase by apocynin attenuates progression of atherosclerosis. *Int J Mol Sci, 14*(8), 17017-17028.

Kirichok, Y., Krapivinsky, G., & Clapham, D. E. (2004). The mitochondrial calcium uniporter is a highly selective ion channel. *Nature, 427*(6972), 360-364.

Klionsky, D. J., & Emr, S. D. (2000). Autophagy as a regulated pathway of cellular degradation. *Science, 290*(5497), 1717-1721.

Kojima, S., Nomura, T., Icho, T., Kajiwara, Y., Kitabake, K., & Kubota, K. (1993). Inhibitory effect of neopterin on NADPH-dependent superoxide-generating oxidase of rat peritoneal macrophages. *FEBS Lett, 329*(1-2), 125-128.

Kourie, J. I. (1998). Interaction of reactive oxygen species with ion transport mechanisms. *American Journal of Physiological Cell Physiology, 275*, C1-C24.

Kowaltowski, A. J., Castilho, R. F., & Vercesi, A. E. (2001). Mitochondrial permeability transition and oxidative stress. *FEBS Lett, 495*(1-2), 12-15.

Kowaltowski, A. J., Vercesi, A. E., & Castilho, R. F. (1997). Mitochondrial membrane protein thiol reactivity with N-ethylmaleimide or mersalyl is modified by Ca2+: Correlation with mitochondrial permeability transition. *Biochimica et Biophysica Acta - Bioenergetics, 1318*(3), 395-402.

Kroemer, G., L., G., & Brenner, C. (2007). Mitochondrial membrane permeabilization in cell death. *Physiological Reviews, 87*, 99-163.

Kugiyama, K., Ohgushi, M., Sugiyama, S., Murohara, T., Fukunaga, K., Miyamoto, E., & Yasue, H. (1992). Lysophosphatidylcholine inhibits surface receptor-mediated intracellular signals in endothelial cells by a pathway involving protein kinase C activation. *Circulation Research, 71*(6), 1422-1428.

Kume, N., & Gimbrone, M. A. J. (1994). Lysophosphatidylcholine transcriptionally induces growth factor gene expression in cultured human endothelial cells. *Journal of Clinical Investigation, 93*, 907-911.

Kundu, M., & Thompson, C. B. (2005). Macroautophagy versus mitochondrial autophagy: a question of fate? [Review]. *Cell Death Differ, 12* (Suppl 2), 1484-1489.

Kyaw, M., Yoshizumi, M., Tsuchiya, K., Izawa, Y., Kanematsu, Y., & Tamaki, T. (2004). Atheroprotective effects of antioxidants through inhibition of mitogen-activated protein kinases. *Acta Pharmacol Sin, 25*(8), 977-985.

Laggner, H., Muellner, M. K., Schreier, S., Sturm, B., Hermann, M., Exner, M., Gmeiner, B. M., & Kapiotis, S. (2007). Hydrogen sulphide: a novel physiological inhibitor of LDL atherogenic modification by HOCl. *Free Radic Res, 41*(7), 741-747.

Lange, S., Heger, J., Euler, G., Wartenberg, M., Piper, H. M., & Sauer, H. (2009). Platelet-derived growth factor BB stimulates vasculogenesis of embryonic stem cell-derived

endothelial cells by calcium-mediated generation of reactive oxygen species. *Cardiovasc Res, 81*(1), 159-168.

Lapperre, T. S., Jimenez, L. A., Antonicelli, F., Drost, E. M., Hiemstra, P. S., Stolk, J., W., M., & Rahman, I. (1999). Apocynin increases glutathione synthesis and activates AP-1 in alveolar epithelial cells. *FEBS Lett, 443*(2), 235-239.

Lassègue, B., & Clempus, R. E. (2003). Vascular NAD(P)H oxidases: specific features, expression, and regulation. *American Journal of Physiology. Regulatiory, Integrative and Comparative Physiology, 285*(2), R277-R297.

Lau, B. H. S. (2001). Suppression of LDL oxidation by garlic. *The Journal of Nutrition, 131*, 985S-988S.

Le Trionnaire, S., Perry, A., Szczesny, B., Csaba, S., Winyard, P., Whatmore, J., Wood, M. E., & Whiteman, M. (2014). The synthesis and functional evaluation of a mitochondria targeted hydrogen sulfide donor, 10-oxo-10-(4-(3-thioxo-3H-1,2-dithiol-5-yl) phenoxy decyl) triphenylphosphonium bromide (AP39). *Medicinal Chemistry Communications, 5*, 728-736.

Le Trionnaire, S., Perry, A., Whatmore, J. L., Wood, M. E., & Whiteman, M. (2013). Mitochondria-targeted hydrogen sulfide donors: a novel twist to an old "tail"? *Nitric Oxide, 31*, S11-S65.

Le Trionnaire, S., Whatmore, J., Perry, A., Wood, M. E., & Whiteman, M. (2012). Slow release H2S donors protect human microvascular endothelial cells from oxidative stress induced cell death: markedly increased potency by mitochondria-targeting. *Nitric Oxide, 27, Supplement 2*(0), S40-S41.

Lee, C. F., Qiao, M., Schroder, K., Zhao, Q., & Asmis, R. (2010). Nox4 is a novel inducible source of reactive oxygen species in monocytes and macrophages and mediates oxidized low density lipoprotein-induced macrophage death. *Circulation Research, 106*(9), 1489-1497.

Lee, S. W., Hu, Y. S., Hu, L. F., Lu, Q., Dawe, G. S., Moore, P. K., Wong, P. T., & Bian, J. S. (2006). Hydrogen sulphide regulates calcium homeostasis in microglial cells. *Glia, 54*(2).

Lemasters, J. J. (1999). V. Necrapoptosis and the mitochondrial permeability transition: shared pathways to necrosis and apoptosis. *American Journal of Physiology, 276*(1 Pt 1), G1-G6.

Lemasters, J. J., Theruvath, T. P., Zhong, Z., & Nieminen, A. L. (2009). Mitochondrial calcium and the permeability transition in cell death. *Biochimica Biophysica Acta, 1787*(11), 1395-1401.

Li, J.-M., Mullen, A. M., Yun, S., Wientjes, F., Brouns, G. Y., Thrasher, A. J., & Shah, A. M. (2002). Essential role of the NADPH oxidase subunit p47phox in endothelial cell superoxide production in response to phorbol ester and tumor necrosis factor-alpha. *Circulation Research, 90*(2), 143-150.

Li, J. M., & Shah, A. M. (2002). Intracellular localization and preassembly of the NADPH oxidase complex in cultured endothelial cells. *Journal of Biological Chemistry, 277*(22), 19952-19960.

Li, L., Bhatia, M., Zhu, Y. Z., Zhu, Y. C., Ramnath, R. D., Wang, Z. J., Anuar, F. B., Whiteman, M., Salto-Tellez, M., & Moore, P. K. (2005). Hydrogen sulfide is a novel mediator of lipopolysaccharide-induced inflammation in the mouse. *FASEB Journal, 19*(9), 1196-1198.

Li, L., Salto-Tellez, M., Tan, C.-H., Whiteman, M., & Moore, P. K. (2009). GYY4137, a novel hydrogen sulfide-releasing molecule, protects against endotoxic shock in the rat. *Free Radic Biol Med, 47*(1), 103-113.

Li, L., Whiteman, M., Guan, Y. Y., Neo, K. L., Cheng, Y., Lee, S. W., Zhao, Y., Baskar, R., Tan, C. H., & Moore, P. K. (2008). Characterization of a novel, water-soluble hydrogen sulfide-releasing molecule (GYY4137): new insights into the biology of hydrogen sulfide. *Circulation, 117*(18), 2351-2360.

Liao, T. T., Jia, R. W., Shi, Y. L., Jia, J. W., Wang, L., & Chua, H. (2011). Propidium iodide staining method for testing the cytotoxicity of 2,4,6-trichlorophenol and perfluorooctane sulfonate at low concentrations with Vero cells. *Journal of Environmental Science and Health. Part A: Toxic/Hazardous Substances and Environmental Engineering, 46*(14), 1769-1775.

Libby, P. (2002). Inflammation in atherosclerosis. *Nature, 420*(6917), 868-874.

Libby, P. (2006). Atherosclerosis: disease biology affecting the coronary vasculature. [Review]. *Am J Cardiol, 98*(12A), 3Q-9Q.

Libby, P., Okamoto, Y., Rocha, V. Z., & Folco, E. (2010). Inflammation in Atherosclerosis. *Circulation Journal, 74*(2), 213-220.

Liu, Y., Fiskum, G., & Schubert, D. (2002). Generation of reactive oxygen species by the mitochondrial electron transport chain. *J Neurochem, 80*(5), 780-787.

Liu, Y., Peterson, D. A., Kimura, H., & Schubert, D. (1997). Mechanism of cellular 3-(4,5-dimethylthiazol-2-yl)-2,5-diphenyltetrazolium bromide (MTT) reduction. *J Neurochem, 69*, 581-593.

Liu, Z., Han, Y., Li, L., Lu, H., Meng, G., Li, X., Shirhan, M., Peh, M. T., Xie, L., Zhou, S., Wang, X., Chen, Q., Dai, W., Tan, C. H., Pan, S., Moore, P. K., & Ji, Y. (2013). The hydrogen sulfide donor, GYY4137, exhibits anti-atherosclerotic activity in high fat fed apolipoprotein E(-/-) mice. *Br J Pharmacol, 169*(8), 1795-1809.

Lu, M., Hu, L. F., Hu, G., & Bian, J. S. (2008). Hydrogen sulfide protects astrocytes against H(2)O(2)-induced neural injury via enhancing glutamate uptake. *Free Radical Biology and Medicine, 45*(12), 1705-1713.

Luetjens, C. M., Bui, N. T., Sengpiel, B., Münstermann, G., Poppe, M., Krohn, A. J., Bauerbach, E., Krieglstein, J., & Prehn, J. H. (2000). Delayed mitochondrial dysfunction in excitotoxic neuron death: cytochrome c release and a secondary increase in superoxide production. *Journal of Neuroscience, 20*(15), 5715-5723.

Lusis, A. J. (2000). Atherosclerosis. *Nature, 407*(6801), 233-241.

Lyle, A.N., Deshpande, N. N., Taniyama, Y., Seidel-Rogol, B., Pounkova, L., Du, P., Papaharalambus, C., Lassegue, B., Griendling, K. K. (2009). Poldip2, a novel regulator of Nox4 and cytoskeletal integrity in vascular smooth muscle cells. *Circulation Research, 105*(3), 249-259.

Lynn, E. G., & Austin, R. C. (2011). Hydrogen sulfide in the pathogenesis of atherosclerosis and its therapeutic potential. *Expert Review of Clinical Pharmacology, 4*(1), 97-108.

Lytton, J., M., W., Burk, S. E., Shull, G. E., & MacLennan, D. H. (1992). Functional comparisons between isoforms of the sarcoplasmic or endoplasmic reticulum family of calcium pumps. *Journal of Biological Chemistry, 267*(20), 14483-14489.

Maack, C., & O'Rourke, B. (2007). Excitation-contraction coupling and mitochondrial energetics. *Basic Research in Cardiology, 102*(5), 369-392.

MacLennan, D. H., Rice, W. J., & Odermatt, A. (1997). Structure/function analysis of the Ca2+ binding and translocation domain of SERCA1 and the role in Brody disease of the ATP2A1 gene encoding SERCA1. *Annals New York Academy of Sciences, 834*, 175-185.

Madamanchi, N. R., & Runge, M. S. (2007). Mitochondrial dysfunction in atherosclerosis. *Circulation Research, 100*(4), 460-473.

Madamanchi, N. R., Vendrov, A., & Runge, M. S. (2005). Oxidative stress and vascular disease. [Review]. *Arteriosclerosis Thrombosis and Vascular Biology, 25*(1), 29-38.

Maeba, R., Maruyama, A., Tarutani, O., Ueta, N., & Shimasaki, H. (1995). Oxidized low-density lipoprotein induces the production of superoxide by neutrophils. *FEBS Lett, 377*, 309-312.

Maeda, Y., Aoki, Y., Sekiguchi, F., Matsunami, M., Takahashi, T., Nishikawa, H., & Kawabata, A. (2009). Hyperalgesia induced by spinal and peripheral hydrogen sulfide: evidence for involvement of Cav3.2 T-type calcium channels. *Pain, 142*(1-2), 127-132.

Maghzal, G. J., Krause, K. H., Stocker, R., & Jaquet, V. (2012). Detection of reactive oxygen species derived from the family of NOX NADPH oxidases. *Free Radical Biology and Medicine, 53*(10), 1903-1918.

Maiuri, M. C., Zalckvar, E., Kimchi, A., & Kroemer, G. (2007). Self-eating and self-killing: crosstalk between autophagy and apoptosis. *Nature Reviews Molecular Cell Biology, 8*(9), 741-752.

Majander, A., Finel, M., & Wikström, M. (1994). Diphenyleneiodonium inhibits reduction of iron-sulfur clusters in the mitochondrial NADH-ubiquinone oxidoreductase (Complex I). *Journal of Biological Chemistry, 269*(33), 21037-21042.

Mancardi, D., Penna, C., Merlino, A., Del Soldato, P., Wink, D. A., & Pagliaro, P. (2009). Physiological and pharmacological features of the novel gasotransmitter: hydrogen sulfide. *Biochim Biophys Acta, 1787*(7), 864-872.

Mani, S., Untereiner, A., Wu, L., & Wang, R. (2014). Hydrogen sulfide and the pathogenesis of atherosclerosis. *Antioxid Redox Signal, 20*(5), 805-817.

Marchant, C. E., Law, N. S., van der Veen, C., Hardwick, S. J., Carpenter, K. L. H., & Mitchinson, M. J. (1995). Oxidized low-density lipoprotein is cytotoxic to human monocyte-macrophages: protection with lipophilic antioxidants. *FEBS Lett, 358*, 175-178.

Martinez, F. O. (2009). The transcriptome of human subsets begins to emerge. *Journal of Biology, 8*, 99.

Maru, Y., Nishino, T., & Kakinuma, K. (2005). Expression of Nox genes in rat organs, mouse oocytes, and sea urchin eggs. *DNA Sequence, 16*(2), 83-88.

Massaeli, H., Hurtado, C., Austria, J. A., & Pierce, G. N. (2001). Increase in nuclear calcium in smooth muscle cells exposed to oxidized low density lipoprotein. *Free Radic Res, 34*(1), 9-16.

Matsumura, T., Sakai, M., Kobori, S., Biwa, T., Takemura, T., Matsuda, H., Hakamata, H., Horiuchi, S., & Shichiri, M. (1997). Two intracellular signaling pathways for activation of protein kinase C are involved in oxidized low-density lipoprotein–induced macrophage growth *Arteriosclerosis Thrombosis and Vascular Biology, 17*, 3013-3020.

Mattson, M. P., & Chan, S. L. (2003). Calcium orchestrates apoptosis. *Nat Cell Biol, 5*(12), 1041-1043.

Maziere, C., & Maziere, J. C. (2009). Activation of transcription factors and gene expression by oxidized low-density lipoprotein. [Review]. *Free Radic Biol Med, 46*(2), 127-137. doi: 10.1016/j.freeradbiomed.2008.10.024

Maziere, C., Morliere, P., Massy, Z., Kamel, S., Louandre, C., Conte, M. A., & Maziere, J.-C. (2005). Oxidized low-density lipoprotein elicits an intracellular calcium rise and increases the binding activity of the transcription factor NFAT. *Free Radic Biol Med, 38*(4), 472-480.

McFadzean, I., & Gibson, A. (2002). The developing relationship between receptor-operated and store-operated calcium channels in smooth muscle. *Br J Pharmacol, 135*, 1-13.

McStay, G. P., Clarke, S. J., & Halestrap, A. P. (2002). Role of critical thiol groups on the matrix surface of the adenine nucleotide translocase in the mechanism of the mitochondrial permeability transition pore. *Biochemical Journal, 367*(Pt 2), 541-548.

Mehta, S. L., & Li, P. A. (2009). Neuroprotective role of mitochondrial uncoupling protein 2 in cerebral stroke. *Journal of Cerebral Blood Flow & Metabolism, 29*(6), 1069-1078.

Meilhac, O., Escargueil-Blanc, I., Thiers, J. C., Salvayre, R., & Negre-Salvayre, A. (1999). Bcl-2 alters the balance between apoptosis and necrosis, but does not prevent cell death induced by oxidized low density lipoproteins. *FASEB, 13*, 485-494.

Meldolesi, J., & Pozzan, T. (1987). Pathways of Ca2+ influx at the plasma membrane: voltage-, receptor-, and second messenger-operated channels. *Exp Cell Res, 171*(2), 271-283.

Meyer, J. W., Holland, J. A., Ziegler, L. M., Chang, M. M., Beebe, G., & Schmitt, M. E. (1999). Identification of a functional leukocyte-type NADPH oxidase in human endothelial cells :a potential atherogenic source of reactive oxygen species. *Endothelium, 7*(1), 11-22.

Minta, A., Kao, J. P. Y., & Tsien, R. Y. (1989). Flourescent indicators for cytosolic calcium based on rhodamine and fluorescein chromophores. *J Biol Chem, 264*, 8171-8178.

Miyoshi, H., Umeshita, K., Sakon, M., Imajoh-Ohmi, S., Fujitani, K., Gotoh, M., Oiki, E., Kambayashi, J. I., & Monden, M. (1996). Calpain activation in plasma membrane bleb formation during tert-butyl hydroperoxide-induced rat hepatocyte injury. *Gastroenterology, 110*(6), 1897-1904.

Moccia, F., Bertoni, G., Pla, A., F., Dragoni, S., Pupo, E., A., M., Mancardi, D., Munaron, L., & Tanzi, F. (2011). Hydrogen sulfide regulates intracellular Ca2+ concentration in endothelial cells from excised rat aorta. *Current Pharmaceutical Biotechnology, 12*(9), 1416-1426.

Modis, K., Asimakopoulou, A., Coletta, C., Papapetropoulos, A., & Szabo, C. (2013b). Oxidative stress suppresses the cellular bioenergetic effect of the 3-mercaptopyruvate sulfurtransferase/hydrogen sulfide pathway. *Biochem Biophys Res Commun, 433*(4), 401-407.

Modis, K., Coletta, C., Erdelyi, K., Papapetropoulos, A., & Szabo, C. (2013a). Intramitochondrial hydrogen sulfide production by 3-mercaptopyruvate sulfurtransferase maintains mitochondrial electron flow and supports cellular bioenergetics. *FASEB Journal, 27*(2), 601-611.

Mogami, H., Tepikin, A. V., & Petersen, O. H. (1998). Termination of cytosolic Ca2+ signals: Ca2+ reuptake into intracellular stores is regulated by the free Ca2+ concentration in the store lumen. *The EMBO Journal, 17*(2), 435-442.

Mok, Y. Y., Atan, M. S., Cheong, Y. P., Wang, Z. J., Bhatia, M., Moochhala, S., & Moore, P. K. (2004). Role of hydrogen sulphide in haemorrhagic shock in the rat: protective effect of inhibitors of hydrogen sulphide biosynthesis. *Br J Pharmacol, 143*(7), 881-889.

Moller, W., Brown, D. M., Kreyling, W. G., & Stone, V. (2005). Ultrafine particles cause cytoskeletal dysfunctions in macrophages: role of intracellular calcium. *Part Fibre Toxicol, 2*, 7.

Montell, C. (2005). The latest waves in calcium signaling. *Cell, 122*(2), 157-163.

Mosmann, T. (1983). Rapid colorimetric assay for cellular growth and survival: Application to proliferation and cytotoxicity assays. *J Immunol Methods, 65*, 55-63.

Muellner, M. K., Schreier, S. M., Laggner, H., Hermann, M., Esterbauer, H., Exner, M., Gmeiner, B. M., & Kapiotis, S. (2009). Hydrogen sulfide destroys lipid hydroperoxides in oxidized LDL. *Biochemistry Journal, 420*(2), 277-281.

Mukhopadhyay, P., Rajesh, M., Yoshihiro, K., Hasko, G., & Pacher, P. (2007). Simple quantitative detection of mitochondrial superoxide production in live cells. *Biochem Biophys Res Commun, 358*(1), 203-208.

Muller, C., Salvayre, R., Negre-Salvayre, A., & Vindis, C. (2011a). Oxidized LDLs trigger endoplasmic reticulum stress and autophagy: prevention by HDLs. *Autophagy, 7*(5), 541-543.

Muller, C., Salvayre, R., Negre-Salvayre, A., & Vindis, C. (2011b). HDLs inhibit endoplasmic reticulum stress and autophagic response induced by oxidized LDLs. *Cell Death Differ, 18*(5), 817-828.

Munaron, L., Avanzato, D., Moccia, F., & Mancardi, D. (2013). Hydrogen sulfide as a regulator of calcium channels. *Cell Calcium, 53(2),*77-84.

Murphy, M. P. (2009). How mitochondria produce reactive oxygen species. *Biochem J, 417*(1), 1-13.

Mustafa, A. K., Sikka, G., Gazi, S. K., Steppan, J., Jung, S. M., Bhunia, A. K., Barodka, V. M., Gazi, F. K., Barrow, R. K., Wang, R., Amzel, L. M., Berkowitz, D. E., & Snyder, S. H. (2011). Hydrogen sulfide as endothelium-derived hyperpolarizing factor sulfhydrates potassium channels. *Circ Res, 109*(11), 1259-1268.

Muzaffar, S., Jeremy, J. Y., Sparatore, A., Del Soldato, P., Angelini, G. D., & Shukla, N. (2008a). H2S-donating sildenafil (ACS6) inhibits superoxide formation and gp91phox expression in arterial endothelial cells: role of protein kinases A and G. *Br J Pharmacol, 155*(7), 984-994.

Muzaffar, S., Shukla, N., Bond, M., Newby, A. C., Angelini, G. D., Sparatore, A., Del Soldato, P., & Jeremy, J. Y. (2008b). Exogenous hydrogen sulfide inhibits superoxide formation, NOX-1 expression and Rac1 activity in human vascular smooth muscle cells. *Journal of Vascular Research, 45*(6), 521-528.

Nagai, Y., Tsugane, M., Oka, J.-I., & Kimura, H. (2004). Hydrogen sulfide induces calcium waves in astrocytes. *FASEB Journal, 18*(3), 557-559.

Nakashima, Y., Wight, T. N., & Sueishi, K. (2008). Early atherosclerosis in humans: role of diffuse intimal thickening and extracellular matrix proteoglycans. *Cardiovasc Res, 79*(1), 14-23.

Negre-Salvayre, A., Fitoussi, G., Reaud, V., Pieraggi, M. T., Thiers, J. C., & Salvayre, R. (1992). A delayed and sustained rise of cytosolic calcium is elicited by oxidized LDL in cultured bovine aortic endothelial cells. *FEBS Lett, 299*(1), 60-65.

Negre-Salvayre, A., & Salvayre, R. (1992). Protection by Ca2+ channel blockers (nifedipine, diltiazem and verapamil) against the toxicity of oxidized low density lipoprotein to cultured lymphoid cells. *Br J Pharmacol, 107*, 738-744.

Nguyen-Khoa, T., Massy, Z. A., Witko-Sarsat, V., Canteloup, S., Kebede, M., Lacour, B., Drueke, T., & Descamps-Latscha, B. (1999). Oxidized low-density lipoprotein induces macrophage respiratory burst via its protein moiety: a novel pathway in atherogenesis. *Biochem Biophys Res Commun, 263*(804-809).

Nicotera, P., Bellomo, G., & Orrenius, S. (1992). Calcium-mediated mechanisms in chemically induced cell death. *Annual Review of Pharmacology and Toxicology, 32*, 449-470.

Nicotera, P., McConkey, D., Svensson, S. A., Bellomo, G., & Orrenius, S. (1988). Correlation between cytosolic Ca2+ concentration and cytotoxicity in hepatocytes exposed to oxidative stress. *Toxicology, 52*(1-2), 55-63.

Nicotera, P., & Orrenius, S. (1998). The role of calcium in apoptosis. *Cell Calcium, 23*(2-3), 173-180.

Niethammer, P., Grabher, C., Look, A. T., & Mitchison, T. J. (2009). A tissue-scale gradient of hydrogen peroxide mediates rapid wound detection in zebrafish. *Nature, 459*(7249), 996-999.

Nishida, S., Yoshida, L. S., Shimoyama, T., Nunoi, H., Kobayashi, T., & Tsunawaki, S. (2005). Fungal metabolite gliotoxin targets flavocytochrome b558 in the activation of the human neutrophil NADPH oxidase. *Infect Immun, 73*(1), 235-244.

Nishio, E., Arimura, S., & Watanabe, Y. (1996). Oxidized LDL induces apoptosis in cultured smooth muscle cells: a possible role for 7-ketocholesterol. *Biochem Biophys Res Commun, 223*, 413-418.

Novo, E., & Parola, M. (2008). Redox mechanisms in hepatic chronic wound healing and fibrogenesis. *Fibrogenesis Tissue Repair, 1*(1), 5.

O'Connell, S., Tuite, N., Slattery, C., Ryan, M. P., & McMorrow, T. (2012). Cyclosporine A--induced oxidative stress in human renal mesangial cells: a role for ERK 1/2 MAPK signaling. *Toxicological Sciences, 126*(1), 101-113.

Oettl, K., Dikalov, S., Freisleben, H. J., Mlekusch, W., & Reibnegger, G. (1997). Spin trapping study of antioxidant properties of neopterin and 7,8-dihydroneopterin. *Biochem Biophys Res Commun, 234*, 774-778.

Oettl, K., Greilberger, J., Dikalov, S., & Reibnegger, G. (2004). Interference of 7,8-dihydroneopterin with peroxynitrite-mediated reactions. *Biochem Biophys Res Commun, 321*(2), 379-385.

Oh, G. S., Pae, H. O., Lee, B. S., Kim, B. N., Kim, J. M., Kim, H. R., Jeon, S. B., Jeon, W. K., Chae, H. J., & Chung, H. T. (2006). Hydrogen sulfide inhibits nitric oxide production and nuclear factor-kappaB via heme oxygenase-1 expression in RAW264.7 macrophages stimulated with lipopolysaccharide. *Free Radic Biol Med, 41*(1), 106-119.

Ohgushi, M., Kugiyama, K., Fukunaga, K., Murohara, T., Sugiyama, S., Miyamoto, E., & Yasue, H. (1993). Protein kinase C inhibitors prevent impairment of endothelium-dependent relaxation by oxidatively modified LDL. *Arteriosclerosis Thrombosis and Vascular Biology, 13*(10), 1525-1532.

Orimo, H., & Ouchi, Y. (1990). The role of calcium and magnesium in the development of atherosclerosis. Experimental and clinical evidence. *Annals New York Academy of Sciences, 598*, 444-457.

Orrenius, S., Zhivotovsky, B., & Nicotera, P. (2003). Regulation of cell death: the calcium-apoptosis link. *Nature Reviews Molecular Cell Biology, 4*(7), 552-565.

Pagliara, P., Lanubile, R., Dwikat, M., Abbro, L., & Dini, L. (2005). Differentiation of monocytic U937 cells under static magnetic field exposure. *European Journal of Histochemistry, 49*(1), 75-86.

Palty, R., Silverman, W. F., Hershfinkel, M., Caporale, T., Sensi, S. L., Parnis, J., Nolte, C., Fishman, D., Shoshan-Barmatz, V., Herrmann, S., Khananshvili, D., & Sekler, I. (2010). NCLX is an essential component of mitochondrial Na+/Ca2+ exchange. *Proceedings of the National Academy of Sciences USA, 107*(1), 436-441.

Pan, L. L., Liu, X. H., Gong, Q. H., Wu, D., & Zhu, Y. Z. (2011). Hydrogen sulfide attenuated tumor necrosis factor-alpha-induced inflammatory signaling and dysfunction in vascular endothelial cells. *PLoS One, 6*(5), e19766.

Peiser, L., Mukhopadhyay, P., & Gordon, S. (2002). Scavenger receptors in innate immunity. *Current Opinion in Immunology, 14*, 123-128.

Peng, T. I., & Jou, M. J. (2010). Oxidative stress caused by mitochondrial calcium overload. [Review]. *Ann N Y Acad Sci, 1201*, 183-188.

Peterson, A., Castilho, R. F., Hansson, O., Wieloch, T., & Brundin, P. (2000). Oxidative stress, mitochondrial permeabilty transition and activation of caspases in calcium

ionophore A23187-induced death of cultured striatal neurons. *Brain Research, 857*, 20-29.

Petronilli, V., Costantini, P., Scorrano, L., Colonna, R., Passamonti, S., & Bernardi, P. (1994). The voltage sensor of the mitochondrial permeability transition pore is tuned by the oxidation-reduction state of vicinal thiols. Increase of the gating potential by oxidants and its reversal by reducing agents. *Journal of Biological Chemistry, 269*(24), 16638-16642.

Petronio, M. S., Zeraik, M. L., Fonseca, L. M., & Ximenes, V. F. (2013). Apocynin: chemical and biophysical properties of a NADPH oxidase inhibitor. *Molecules, 18*(3), 2821-2839.

Phair, R. D. (1988). Cellular calcium and atherosclerosis: a brief review. *Cell Calcium, 9*(5-6), 275-284.

Pinilla, P. J., Hernandez, A. T., Camello, M. C., Pozo, M. J., Toescu, E. C., & Camello, P. J. (2005). Non-stimulated Ca2+ leak pathway in cerebellar granule neurones. *Biochem Pharmacol, 70*(5), 786-793.

Plasek, J., Vojtiskova, A., & Houstek, J. (2005). Flow-cytometric monitoring of mitochondrial depolarisation: from fluorescence intensities to millivolts. *Journal of Photochemistry and Photobiology B, 78*(2), 99-108.

Porn-Ares, M. I., Ares, M. P. S., & Orrenius, S. (1998). Calcium signalling and the regulation of apoptosis. *Toxicology in Vitro, 12*(5), 539-543.

Porn-Ares, M. I., Saido, T. C., Andersson, T., & Ares, M. P. S. (2003). Oxidized low-density lipoprotein induces calpain-dependent cell death and ubiquitination of caspase 3 in HMEC-1 endothelial cells. *Biochem J, 374*, 403-411.

Przygodzki, T., Sokal, A., & Bryszewska, M. (2005). Calcium ionophore A23187 action on cardiac myocytes is accompanied by enhanced production of reactive oxygen species. *Biochim Biophys Acta, 1740*(3), 481-488.

Putney, J. W., Jr. (1997). Type 3 inositol 1,4,5-trisphosphate receptor and capacitative calcium entry. *Cell Calcium, 21*(3), 257-261.

Qian, T., Herman, B., & Lemasters, J. J. (1999). The mitochondrial permeability transition mediates both necrotic and apoptotic death of hepatocytes exposed to Br-A23187. *Toxicol Appl Pharmacol, 154*(2), 117-125.

Quinn, M. T., Parthasarathy, S., & Steinberg, D. (1985). Endothelial cell-derived chemotactic activity for mouse peritoneal macrophages and the effects of modified forms of low density lipoprotein. *Proceedings of the National Academy of Sciences USA, 82*, 5949-5953.

Rabelo, L. A., de Souza, V. N., da Fonseca, L. J. S., & Sampaio, W. O. (2010). Redox unbalance: NADPH oxidase as therapeutic target in blood pressure control. *Arquivos Brasileiros de Cardiologia, 94*(5), 643-651.

Rasola, A., & Bernardi, P. (2011). Mitochondrial permeability transition in Ca2+-dependent apoptosis and necrosis. *Cell Calcium, 50*(3), 222-233.

Ray, R., & Shah, A. M. (2005). NADPH oxidase and endothelial cell function. *Clinical Science, 109*(3), 217-226.

Rey, F. E., Cifuentes, M. E., Kiarash, A., Quinn, M. T., & Pagano, P. J. (2001). Novel competitive inhibitor of NAD(P)H oxidase assembly attenuates vascular O(2)(-) and systolic blood pressure in mice. *Circulation Research, 89*(5), 408-414.

Riganti, C., Costamagna, C., Bosia, A., & Ghigo, D. (2006). The NADPH oxidase inhibitor apocynin (acetovanillone) induces oxidative stress. *Toxicol Appl Pharmacol, 212*(3), 179-187.

Rizzuto, R., Bernardi, P., & Pozzan, T. (2000). Mitochondria as all-round players of the calcium game. *Journal of Physiology, 529*(1), 37-47.

Rizzuto, R., Pinton, P., Carrington, W., Fay, F. S., Fogarty, K. E., Lifshitz, L. M., Tuft, R. A., & Pozzan, T. (1998). Close contacts with the endoplasmic reticulum as determinants of mitochondrial Ca2+ responses. *Science, 280*(5370), 1763-1766.

Rizzuto, R., Simpson, A. W., Brini, M., & Pozzan, T. (1992). Rapid changes of mitochondrial Ca^{2+} revealed by specifically targeted recombinant aequorin. *Nature, 358*(6384), 325-327.

Robinson, K. M., Janes, M. S., Pehar, M., Monette, J. S., Ross, M. F., Hagen, T. M., Murphy, M. P., & Beckman, J. S. (2006). Selective fluorescent imaging of superoxide in vivo using ethidium-based probes. *Proceedings of the National Academy of Sciences USA, 103*(41), 15038-15043.

Rodrigues, B. P., Campagnaro, B. P., Balarini, C. M., Pereira, T. M. C., Meyrelle, S. S., & Vasquez, E. C. (2013). Sildenafil ameliorates biomarkers of genotoxicity in an experimental model of spontaneous atherosclerosis. *Lipids Health Dis, 12*, 128.

Rosenfeld, M. E., & Ross, R. (1990). Macrophage and smooth muscle cell proliferation in atherosclerotic lesions of WHHL and comparably hypercholesterolemic fat-fed rabbits. *Arteriosclerosis Thrombosis Vascular Biology, 10*(5), 680-687.

Ross, D. D., Joneckis, C. C., & Ordonez, J. V. (1989). Estimation of cell survival by flow cytometric quantification of fluorescein diacetate/propidium iodide viable cell number. *Cancer Research, 49*, 3776-3782.

Ross, R. (1986). The pathogenesis of atherosclerosis - an update. *New England Journal of Medicine, 314*, 488-500.

Ross, R. (1993). The pathogenesis of atherosclerosis: a perspective for the 1990s. *Nature, 362*, 801-809.

Ross, R. (1999). Atherosclerosis - an inflammatory disease. *The New England Journal of Medicine, 340*(2), 115-126.

Rothe, G., & Valet, G. (1990). Flow cytometric analysis of respiratory burst activity in phagocytes with hydroethidine and 2',7'-dichlorofluorescin. *J Leukoc Biol, 47*, 440-448.

Russell, J. W., Golovoy, D., Vincent, A. M., Mahendru, P., Olzmann, J. A., Mentzer, A., & Feldman, E. L. (2002). High glucose-induced oxidative stress and mitochondrial dysfunction in neurons. *FASEB Journal, 16*(13), 1738-1748.

Rutherford, L. D., & Gieseg, S. P. (2012). 7-Ketocholesterol is not cytotoxic to U937 cells when incorporated into acetylated low density lipoprotein. *Lipids, 47*, 239-247.

Sagara, Y., Fernandez-Belda, F., de Meis, L., & Inesi, G. (1992). Characterization of the inhibition of intracellular Ca2+ transport ATPases by thapsigargin. *Journal of Biological Chemistry, 267*(18), 12606-12613.

Salvayre, R., Auge, N., Benoist, H., & Negre-Salvayre, A. (2002). Oxidized low-density lipoprotein-induced apoptosis. *Biochim Biophys Acta, 1585*, 213-221.

Samhan-Arias, A. K., Garcia-Bereguiain, M. A., & Gutierrez-Merino, C. (2009). Hydrogen sulfide is a reversible inhibitor of the NADH oxidase activity of synaptic plasma membranes. *Biochem Biophys Res Commun, 388*(4), 718-722.

Sancho, P., & Fabregat, I. (2011). The NADPH oxidase inhibitor VAS2870 impairs cell growth and enhances TGF-beta-induced apoptosis of liver tumor cells. *Biochem Pharmacol, 81*(7), 917-924.

Scaduto, R. C. J., & Grotyohann, L. W. (1999). Measurement of mitochondrial membrane potential using fluorescent rhodamine derivatives. *Biophysical Journal, 76*, 469-477.

Schramm, A., Matusik, P., Osmenda, G., & Guzik, T. J. (2012). Targeting NADPH oxidases in vascular pharmacology. [Review]. *Vascul Pharmacol, 56*(5-6), 216-231.

Seimon, T., & Tabas, I. (2009). Mechanisms and consequences of macrophage apoptosis in atherosclerosis. *J Lipid Res, 50 Supplement*, S382-S387.

Sen, N., Paul, B. D., Gadalla, M. M., Mustafa, A. K., Sen, T., Xu, R., Kim, S., & Snyder, S. H. (2012). Hydrogen sulfide-linked sulfhydration of NF-kappaB mediates its antiapoptotic actions. *Mol Cell, 45*(1), 13-24.

Shaikh, S., Brittenden, J., Lahiri, R., Brown, P. A., Thies, F., & Wilson, H. M. (2012). Macrophage subtypes in symptomatic carotid artery and femoral artery plaques. *European Journal of Vascular and Endovascular Surgery, 44*(5), 491-497.

Shchepetkina, A. (2013). *Mechanisms of 7,8-dihydroneopterin protection of macrophages from cytotoxicity.* Ph.D, University of Canterbury, New Zealand.

Shen, R. (1994). Inhibition of luminol enhanced chemiluminescence by reduced pterins. *Archives of Biochemistry and Biophysics, 310*, 60-63.

Shen, X., Ellis, R. E., Lee, K., Liu, C. Y., Yang, K., Solomon, A., Yoshida, H., Morimoto, R., Kurnit, D. M., Mori, K., & Kaufman, R. J. (2001). Complementary signaling pathways regulate the unfolded protein response and are required for C. elegans development. *Cell, 107*, 893-903.

Shi, J., Ross, C. R., Leto, T. L., & Blecha, F. (1996). PR-39, a proline-rich antibacterial peptide that inhibits phagocyte NADPH oxidase activity by binding to Src homology 3 domains of p47 phox. *Proceedings of the National Academy of Sciences USA, 93*(12), 6014-6018.

Shibuya, N., Tanaka, M., Yoshida, M., Ogasawara, Y., Togawa, T., Ishii, K., & Kimura, H. (2009). 3-Mercaptopyruvate sulfurtransferase produces hydrogen sulfide and bound sulfane in the brain. *Antioxidants & Redox Signalling, 11*(4), 703-714.

Shiose, A., Kuroda, J., Tsuruya, K., Hirai, M., Hirakata, H., Naito, S., Hattori, M., Sakaki, Y., & Sumimoto, H. (2001). A novel superoxide-producing NAD(P)H oxidase in kidney. *Journal of Biological Chemistry, 276*(2), 1417-1423.

Simons, J. M., Hart, B. A., Ip Vai Ching, T. R., Van Dijk, H., & Labadie, R. P. (1990). Metabolic activation of natural phenols into selective oxidative burst agonists by activated human neutrophils. *Free Radical Biology and Medicine, 8*(3), 251-258.

Singh, U., & Jialal, I. (2006). Oxidative stress and atherosclerosis. *Pathophysiology, 13*(3), 129-142.

Smith, P. K., Krohn, R. I., Hermanson, G. T., Mallia, A. K., Gartner, F. H., Provenzano, M. D., Fujimoto, E. K., Goeke, N. M., Olson, B. J., & Klenk, D. C. (1985). Measurement of protein using bichinconinic acid. *Anal Biochem, 150*(1), 76-85.

Smith, R. A., Hartley, R. C., & Murphy, M. P. (2011). Mitochondria-targeted small molecule therapeutics and probes. *Antioxidants & Redox Signalling, 15*(12), 3021-3038.

Smith, R. P., & Gosselin, R. E. (1979). Hydrogen sulfide poisoning. *Journal of Occupational Medicine, 21*(2), 93-97.

Smook, M. L., van Leeuwen, M., Heeringa, P., Damoiseaux, J. G., Theunissen, R., Daemen, M. J., Lutgens, E., & Tervaert, J. W. (2008). Anti-oxLDL antibody isotype levels, as potential markers for progressive atherosclerosis in APOE and APOECD40L mice. *Clin Exp Immunol, 154*(2), 264-269.

Song, Z. J., Ng, M. Y., Lee, Z.-W., Dai, W., Hagen, T., Moore, P. K., Huang, D., Deng, L.-W., & Tan, C.-H. (2014). Hydrogen sulfide donors in research and drug development. *MedChemComm, 5*(5), 557.

Sorescu, D., Weiss, D., Lassegue, B., Clempus, R. E., Szocs, K., Sorescu, G. P., Valppu, L., Quinn, M. T., Lambeth, J. D., Vega, J. D., Taylor, W. R., & Griendling, K. K. (2002). Superoxide production and expression of Nox family proteins in human atherosclerosis. *Circulation, 105*(12), 1429-1435.

Steinberg, D. (1997). Low density lipoprotein oxidation and its pathobiological significance. *J Biol Chem, 272*(34), 20963-20966.

Steinberg, D. (2009). The LDL modification hypothesis of atherogenesis: an update. [Review]. *J Lipid Res, 50 Supplement*, S376-S381.

Steinberg, D., Parthasarathy, S., Carew, T. E., Khoo, J. C., & Witztum, J. L. (1989). Beyond cholesterol: Modifications of low-density lipoprotein that increase its atherogenicity. *New England Journal of Medicine, 320*(14), 915-924.

Steinbrecher, U. P., Parthasarathy, S., Leake, D. S., Witztum, J. L., & Steinberg, D. (1984). Modification of low density lipoprotein by endothelial cells involves lipid peroxidation and degradation of low density lipoprotein phospholipids. *Proceedings of the National Academy of Sciences USA, 81*, 3883-3887.

Stielow, C., Catar, R. A., Muller, G., Wingler, K., Scheurer, P., Schmidt, H. H., & Morawietz, H. (2006). Novel Nox inhibitor of oxLDL-induced reactive oxygen species formation in human endothelial cells. *Biochem Biophys Res Commun, 344*(1), 200-205.

Stocker, R., & Keaney, J. F. J. (2004). Role of oxidative modifications in atherosclerosis. *Physiological Reviews, 84*, 1381-1478.

Stolk, J., Hiltermann, T. J., Dijkman, J. H., & Verhoeven, A. J. (1994a). Characteristics of the inhibition of NADPH oxidase activation in neutrophils by apocynin, a methoxy-substituded cathecol. *American Journal of Respiratory Cell and Molecular Biology, 11*(1), 95-102.

Stolk, J., Rossie, W., & Dijkman, J. H. (1994b). Apocynin improves the efficacy of secretory leukocytes protease inhibitor in experimental emphysema. *American Journal of Respiratory and Critical Care Medicine, 150*(6), 1628-1631.

Streeter, E., Ng, H. H., & Hart, J. L. (2013). Hydrogen sulfide as a vasculoprotective factor. *Medical Gas Research, 3*(9), 1-7.

Strehler, E. E. (1990). Plasma membrane Ca2+ pumps and Na+/Ca2+ exchangers. *Seminars in Cell Biology, 1*(4), 283-295.

Sugiyama, S., Okada, Y., Sukhova, G. K., Virmani, R., Heinecke, J. W., & Libby, P. (2001). Macrophage myeloperoxidase regulation by granulocyte macrophage colony-stimulating factor in human atherosclerosis and implications in acute coronary syndromes. *American Journal of Pathology, 158*(3), 879-891.

Sukhanov, S., Higashi, Y., Shai, S. Y., Itabe, H., Ono, K., Parthasarathy, S., & Delafontaine, P. (2006). Novel effect of oxidized low-density lipoprotein: cellular ATP depletion via downregulation of glyceraldehyde-3-phosphate dehydrogenase. *Circulation Research, 99*(2), 191-200.

Sun, F. C., Shyu, H. Y., Lee, M. S., & Lai, Y. K. (2013). Involvement of calcium-mediated reactive oxygen species in inductive GRP78 expression by geldanamycin in 9L rat brain tumor cells. *Int J Mol Sci, 14*(9), 19169-19185.

Sun, J., Xu, L., Eu, J. P., Stamler, J. S., & Meissner, G. (2001). Classes of thiols that influence the activity of the skeletal muscle calcium release channel. *Journal of Biological Chemistry, 276*(19), 15625-15630.

Sun, W. H., Liu, F., Chen, Y., & Zhu, Y. C. (2012). Hydrogen sulfide decreases the levels of ROS by inhibiting mitochondrial complex IV and increasing SOD activities in cardiomyocytes under ischemia/reperfusion. *Biochem Biophys Res Commun, 421*(2), 164-169.

Sun, Y. G., Cao, Y. X., Wang, W. W., Ma, S. F., Yao, T., & Zhu, Y. C. (2008). Hydrogen sulphide is an inhibitor of L-type calcium channels and mechanical contraction in rat cardiomyocytes. *Cardiovasc Res, 79*(4), 632-641.

Sundstrom, C., & Nilsson, K. (1976). Establishment and characterization of a human histiocytic lymphoma cell line (U937). *International Journal of Cancer, 17*(5), 565-577.

Syntichaki, P., & Tavernarakis, N. (2003). The biochemistry of neuronal necrosis: rogue biology? *Nature Reviews Neuroscience, 4*(8), 672-684.

Szabo, C. (2007). Hydrogen sulphide and its therapeutic potential. *Nature Reviews Drug Discovery, 6*(11), 917-935.

Szabo, C., Coletta, C., Chao, C., Modis, K., Szczesny, B., Papapetropoulos, A., & Hellmich, M. R. (2013). Tumor-derived hydrogen sulfide, produced by cystathionine-β-synthase, stimulates bioenergetics, cell proliferation, and angiogenesis in colon cancer. *Proc Natl Acad Sci U S A, 110*(30), 12474-12479.

Tabas, I. (2005). Consequences and therapeutic implications of macrophage apoptosis in atherosclerosis: the importance of lesion stage and phagocytic efficiency. *Arteriosclerosis Thrombosis and Vascular Biology, 25*(11), 2255-2264.

Tan, G., Pan, S., Li, J., Dong, X., Kang, K., Zhao, M., Jiang, X., Kanwar, J. R., Qiao, H., Jiang, H., & Sun, X. (2011). Hydrogen sulfide attenuates carbon tetrachloride-induced hepatotoxicity, liver cirrhosis and portal hypertension in rats. *PLoS One, 6*(10), e25943.

Taniguchi, S., Kang, L., Kimura, T., & Niki, I. (2011). Hydrogen sulphide protects mouse pancreatic beta-cells from cell death induced by oxidative stress, but not by endoplasmic reticulum stress. *Br J Pharmacol, 162*(5), 1171-1178.

Tarpey, M. M., Wink, D. A., & Grisham, M. B. (2004). Methods for detection of reactive metabolites of oxygen and nitrogen: in vitro and in vivo considerations. *American Journal of Physiology. Regulatory Integrative and Comparative Physiology, 286*(3), R431-444.

Tavares, A., & Duque-Magalhaes, M. C. (1991). Demonstration of three calpains in the matrix of rat liver mitochondria. *Biomedica Biochima Acta, 50*(4-6), 523-529.

ten Freyhaus, H., Huntgeburth, M., Wingler, K., Schnitker, J., Baumer, A. T., Vantler, M., Bekhite, M. M., Wartenberg, M., Sauer, H., & Rosenkranz, S. (2006). Novel Nox inhibitor VAS2870 attenuates PDGF-dependent smooth muscle cell chemotaxis, but not proliferation. *Cardiovasc Res, 71*(2), 331-341.

Teng, H., Wu, B., Zhao, K., Yang, G., Wu, L., & Wang, R. (2013). Oxygen-sensitive mitochondrial accumulation of cystathionine beta-synthase mediated by Lon protease. *Proc Natl Acad Sci U S A, 110*(31), 12679-12684.

Tertov, V. V., Sobenin, I. A., Gabbasov, Z. A., Popov, E. G., & Orekhov, A. N. (1989). Lipoprotein aggregation as an essential condition of intracellular lipid accumulation caused by modified low density lipoproteins. *Biochem Biophys Res Commun, 163*(1), 489-494.

Touyz, R. M. (2002). Expression of a Functionally Active gp91phox-Containing Neutrophil-Type NAD(P)H Oxidase in Smooth Muscle Cells From Human Resistance Arteries: Regulation by Angiotensin II. *Circulation Research, 90*(11), 1205-1213.

Turrens, J. F. (2003). Mitochondrial formation of reactive oxygen species. [Review]. *Journal of Physiology, 552*(Pt 2), 335-344.

Valko, M., Leibfritz, D., Moncol, J., Cronin, M. T., Mazur, M., & Telser, J. (2007). Free radicals and antioxidants in normal physiological functions and human disease. *Int J Biochem Cell Biol, 39*(1), 44-84.

Van den Worm, E., Beukelman, C. J., Van den Berg, A. J., Kroes, B. H., Labadie, R. P., & Van Dijk, H. (2001). Effects of methoxylation of apocynin and analogs on the inhibition of reactive oxygen species production by stimulated human neutrophils. *Eur J Pharmacol, 433*(2-3), 225-230.

van Engeland, M., Nieland, L. J., Ramaekers, F. C., Schutte, B., & Reutelingsperger, C. P. (1998). Annexin V-affinity assay: a review on an apoptosis detection system based on phosphatidylserine exposure. *Cytometry, 31*(1), 1-9.

van Tits, L. J. H., Hak-Lemmers, H. L. M., Demacker, P. N. M., Stalenhoef, A. F., & Willems, P. H. G. M. (2000). Oxidized low-density lipoprotein induces calcium influx in polymorphonuclear leukocytes. *Free Radic Biol Med, 29*(8), 747-755.

Vandiver, M., & Snyder, S. H. (2012). Hydrogen sulfide: a gasotransmitter of clinical relevance. *Journal of Molecular Medicine (Berl), 90*(3), 255-263.

Vejrazka, M., Micek, R., & Stipek, S. (2005). Apocynin inhibits NADPH oxidase in phagocytes but stimulates ROS production in non-phagocytic cells. *Biochim Biophys Acta, 1722*(2), 143-147.

Vicca, S., Hennequin, C., Nguyen-Khoa, T., Massy, Z. A., Descamps-Latscha, B., Drueke, T. B., & Lacour, B. (2000). Caspase-dependent apoptosis in THP-1 cells exposed to oxidized low-density lipoproteins. *Biochem Biophys Res Commun, 273*(3), 948-954.

Vieira, H. L., Haouzi, D., El Hamel, C., Jacotot, E., Belzacq, A. S., Brenner, C., & Kroemer, G. (2000). Permeabilization of the mitochondrial inner membrane during apoptosis: impact of the adenine nucleotide translocator. *Cell Death Differ, 7*, 1146-1154.

Vignais, P. V. (2002). The superoxide-generating NADPH oxidase:structural aspects and activation mechanism. *Cellular and Molecular Life Sciences, 59*(9), 1428-1459.

Vindis, C., Elbaz, M., Escargueil-Blanc, I., Auge, N., Heniquez, A., Thiers, J. C., Negre-Salvayre, A., & Salvayre, R. (2005). Two distinct calcium-dependent mitochondrial pathways are involved in oxidized LDL-induced apoptosis. *Arteriosclerosis Thrombosis and Vascular Biology, 25*(3), 639-645.

Wagner, F., Asfar, P., Calzia, E., Radermacher, P., & Szabo, C. (2009). Bench-to-bedside review: hydrogen sulfide--the third gaseous transmitter: applications for critical care. [Review]. *Critical Care, 13*(3).

Wang, R. (2002). Two's company, threes's a crowd: can H2S be the third endogenous gaseous transmitter? *FASEB, 16*, 1792-1798.

Wang, R. (2003). The gasotransmitter role of hydrogen sulfide. *Antioxidants & Redox Signalling, 5*(4), 493-501.

Wang, W., Pang, L., & Palade, P. (2010). Angiotensin II upregulates CaV1.2 protein expression in cultured arteries via endothelial H2O2 production. *Journal of Vascular Research, 48*(1), 67-78.

Wang, Y.-Y., & Zheng, X.-X. (2002). A flow cytometry-based assay for quantitative analysis of cellular proliferation and cytotoxicity in vitro. *J Immunol Methods, 268*, 179-188.

Wang, Y., Qiao, M., Mieyal, J. J., Asmis, L. M., & Asmis, R. (2006). Molecular mechanism of glutathione-mediated protection from oxidized low-density lipoprotein-induced cell injury in human macrophages: role of glutathione reductase and glutaredoxin. *Free Radic Biol Med, 41*(5), 775-785.

Wang, Y., Zhao, X., Jin, H., Wei, H., Li, W., Bu, D., Tang, X., Ren, Y., Tang, C., & Du, J. (2009). Role of hydrogen sulfide in the development of atherosclerotic lesions in apolipoprotein E knockout mice. *Arteriosclerosis Thrombosis and Vascular Biology, 29*(2), 173-179.

Warnholtz, A., Nickenig, G., Schulz, E., Macharzina, R., Brasen, J. H., Skatchkov, M., Heitzer, T., Stasch, J. P., Griendling, K. K., Harrison, D. G., Bohm, M., Meinertz, T., & Munzel, T. (1999). Increased NADH-oxidase mediated superoxide production in the early stages of atherosclerosis: evidence for involvement of the renin-angiotensin system. *Circulation, 99*(15), 2027-2033.

Weber, H., Huhns, S., Luthen, F., Jonas, L., & Schuff-Werner, P. (2005). Calpain activation contributes to oxidative stress-induced pancreatic acinar cell injury. *Biochem Pharmacol, 70*(8), 1241-1252.

Weisser, B., Locher, R., Mengden, T., & Vetter, W. (1992). Oxidation of low density lipoprotein enhances its potential to increase intracellular free calcium concentration

in vascular smooth muscle cells. *Arteriosclerosis Thrombosis and Vascular Biology, 12*(2), 231-236.

Whatmore, J. L., Wolanska, K. I., Perry, A., Wood, M. E., & Whiteman, M. (2013). Slow release hydrogen sulfide (H2S) donors prevent hyperglycaemic-induced glycocalyx loss in retinal microvascular endothelial cells. *Nitric Oxide, 31*, S11-S65.

Whiteman, M., Armstrong, J. S., Cheung, N. S., Siau, J. L., Rose, P., Schantz, J. T., Jones, D. P., & Halliwell, B. (2004). Peroxynitrite mediates calcium-dependent mitochondrial dysfunction and cell death via activation of calpains. *FASEB Journal, 18*(12), 1395.

Whiteman, M., Armstrong, J. S., Chu, S. H., Jia-Ling, S., Wong, B. S., Cheung, N. S., Halliwell, B., & Moore, P. K. (2004). The novel neuromodulator hydrogen sulfide: an endogenous peroxynitrite 'scavenger'? *J Neurochem, 90*(3), 765-768.

Whiteman, M., Cheung, N. S., Zhu, Y. Z., Chu, S. H., Siau, J. L., Wong, B. S., Armstrong, J. S., & Moore, P. K. (2005). Hydrogen sulphide: a novel inhibitor of hypochlorous acid-mediated oxidative damage in the brain? *Biochem Biophys Res Commun, 326*, 794-798.

Whiteman, M., Le Trionnaire, S., Chopra, M., Fox, B., & Whatmore, J. (2011a). Emerging role of hydrogen sulfide in health and disease: critical appraisal of biomarkers and pharmacological tools. [Review]. *Clinical Science, 121*(11), 459-488.

Whiteman, M., Li, L., Rose, P., Tan, C.-H., Parkinson, D. B., & Moore, P. K. (2010). The effect of hydrogen sulfide donors on lipopolysaccharide-induced formation of inflammatory mediators in macrophages. *Antioxidants & Redox Signalling, 12*(10), 1147-1154.

Whiteman, M., & Winyard, P. G. (2011b). Hydrogen sulfide and inflammation: the good, the bad, the ugly and the promising. *Expert Reviews in Clinical Pharmacology, 4*(1), 13-32.

Wilkinson, B. L., & Landreth, G. E. (2006). The microglial NADPH oxidase complex as a source of oxidative stress in Alzheimer's disease. *J Neuroinflammation, 3*, 30.

Williams, H. C., & Griendling, K. K. (2007). NADPH oxidase inhibitors: New antihypertensive agents? *Journal of Cardiovascular Pharmacology, 50*(1), 9-16.

Williams, K. J., & Tabas, I. (1995). The response-to-retention hypothesis of early atherogenesis. *Arteriosclerosis Thrombosis and Vascular Biology, 15*(5), 551-561.

Wind, S., Beuerlein, K., Eucker, T., Muller, H., Scheurer, P., Armitage, M. E., Ho, H., Schmidt, H. H., & Wingler, K. (2010). Comparative pharmacology of chemically distinct NADPH oxidase inhibitors. *Br J Pharmacol, 161*(4), 885-898.

Wingler, K., Hermans, J. J. R., Schiffers, P., Moens, A. L., M., P., & Schmidt, H. H. H. W. (2011). NOX1, 2, 4, 5: counting out oxidative stress. *Br J Pharmacol, 164*(3), 866-883.

Wintergerst, E. S., Jelk, J., Rahner, C., & Asmis, R. (2000). Apoptosis induced by oxidized low density lipoprotein in human monocyte-derived macrophages involves CD36 and activation of caspase-3. *European Journal of Biochemistry, 267*, 6050-6058.

Witztum, J. L. (1994). The oxidation hypothesis of atherosclerosis. *Lancet, 344*(8925), 793-795.

Wlodkowic, D., Skommer, J., & Pelkonen, J. (2006). Multiparametric analysis of HA14-1-induced apoptosis in follicular lymphoma cells. *Leuk Res, 30*(9), 1187-1192.

Wolf, A., Trendelenburg, C. F., Diez-Fernandez, C., Prieto, P., Houy, S., Trommer, W. E., & Cordier, A. (1997). Cyclosporine A-induced oxidative stress in rat hepatocytes. *J Pharmacol Exp Ther, 280*(3), 1328-1334.

Woodfield, K., Rück, A., Brdiczka, D., & Halestrap, A. P. (1998). Direct demonstration of a specific interaction between cyclophilin-D and the adenine nucleotide translocase

confirms their role in the mitochondrial permeability transition. *Biochemical Journal, 336*(Pt 2), 287-290.

Xiao, L., Lan, A., Mo, L., Xu, W., Jiang, N., Hu, F., Feng, J., & Zhang, C. (2012). Hydrogen sulfide protects PC12 cells against reactive oxygen species and extracellular signal-regulated kinase 1/2-mediated downregulation of glutamate transporter-1 expression induced by chemical hypoxia. *Int J Mol Med, 30*(5), 1126-1132.

Ximenes, V. F., Kanegae, M. P., Rissato, S. R., & Galhiane, M. S. (2007). The oxidation of apocynin catalyzed by myeloperoxidase: proposal for NADPH oxidase inhibition. *Archives of Biochemistry and Biophysics, 457*(2), 134-141.

Yan, S. K., Chang, T., Wang, H., Wu, L., Wang, R., & Meng, Q. H. (2006). Effects of hydrogen sulfide on homocysteine-induced oxidative stress in vascular smooth muscle cells. *Biochem Biophys Res Commun, 351*(2), 485-491.

Yang, G., Sun, X., & Wang, R. (2004). Hydrogen sulfide-induced apoptosis of human aorta smooth muscle cells via the activation of mitogen-activated protein kinases and caspase-3. *FASEB Journal, 18*(14), 1782-1784.

Yang, G., Wu, L., Jiang, B., Yang, W., Qi, J., Cao, K., Meng, Q., Mustafa, A. K., Mu, W., Zhang, S., Snyder, S. H., & Wang, R. (2008). H2S as a physiologic vasorelaxant: hypertension in mice with deletion of cystathionine gamma-lyase. *Science, 322*(5901), 587-590.

Yang, G., Wu, L., & Wang, R. (2006). Pro-apoptotic effect of endogenous H_2S on human aorta smooth muscle. *FASEB Journal, 20*(3), 553-555.

Yang, Y.-T. T., Whiteman, M., & Gieseg, S. P. (2012a). HOCl causes necrotic cell death in human monocyte derived macrophages through calcium dependent calpain activation. *Biochim Biophys Acta, 1823*, 420-429.

Yang, Y.-T. T., Whiteman, M., & Gieseg, S. P. (2012b). Intracellular glutathione protects human monocyte-derived macrophages from hypochlorite damage. *Life Sciences, 90*, 682-688.

Yang, Y. T. (2009). *Mechanism and inhibition of hypochlorous acid-mediated cell death in human monocyte-derived macrophages.* Ph.D., University of Canterbury, New Zealand.

Yao, S., Zong, C., Zhang, Y., Sang, H., Yang, M., Jiao, P., Fang, Y., Yang, N., Song, G., & Qin, S. (2013). Activating transcription factor 6 mediates oxidized LDL-induced cholesterol accumulation and apoptosis in macrophages by up-regulating CHOP expression. *Journal of Atherosclerosis and Thrombosis, 20*(1), 94-107.

Yap, Y. W., Whiteman, M., Bay, B. H., Li, Y., Sheu, F. S., Qi, R. Z., Tan, C. H., & Cheung, N. S. (2006). Hypochlorous acid induces apoptosis of cultured cortical neurons through activation of calpains and rupture of lysosomes. *J Neurochem, 98*(5), 1597-1609.

Yla-Herttuala, S., Palinski, W., Rosenfeld, M. E., Parthasarathy, S., Carew, T. E., Butler, S., Witztum, J. L., & Steinberg, D. (1989). Evidence for the presence of oxidatively modified low density lipoprotein in atherosclerotic lesions of rabbit and man. *Journal of Clinical Investigation, 84*, 1086-1095.

Yong, Q. C., Choo, C. H., Tan, B. H., Low, C. M., & Bian, J. S. (2010). Effect of hydrogen sulfide on intracellular calcium homeostasis in neuronal cells. *Neurochem Int, 56*(3), 508-515.

Yuan, J., & Yankner, B. A. (2000). Apoptosis in the nervous system. *Nature, 407*(6805), 802-809.

Yun, M.-R., Okajima, F., & Im, D.-S. (2004). The action mode of lysophosphatidylcholine in human monocytes. *The Journal of Pharmacological Sciences, 94*, 45-50.

Zhang, M., Aguillera, D., Das, C., Vasquez, H., Zage, P., Gopalakrishnan, V., & Wolff, J. (2006). Measuring cytotoxicity: a new perspective on LC50. *Anticancer Research, 27*, 35-38.

Zhao, B., Ehringer, W. D., Dierichs, R., & Miller, F. N. (1997). Oxidized low-density lipoprotein increases endothelial intracellular calcium and alters cytoskeletal f-actin distribution. *European Journal of Clinical Investigation, 27*(1), 48-54.

Zhao, F., Li, P., Chen, S. R., Louis, C. F., & Fruen, B. R. (2001). Dantrolene inhibition of ryanodine receptor Ca2+ release channels. Molecular mechanism and isoform selectivity. *Journal of Biological Chemistry, 276*(17), 13810-13816.

Zhao, H., Joseph, J., Fales, H. M., Sokoloski, E. A., Levine, R. L., Vasquez-Vivar, J., & Kalyanaraman, B. (2005). Detection and characterization of the product of hydroethidine and intracellular superoxide by HPLC and limitations of fluorescence. *Proceedings of the National Academy of Sciences USA, 102*(16), 5727-5732.

Zhao, H., Kalivendi, S., Zhang, H., Joseph, J., Nithipatikom, K., Vásquez-Vivar, J., & Kalyanaraman, B. (2003). Superoxide reacts with hydroethidine but forms a fluorescent product that is distinctly different from ethidium: potential implications in intracellular fluorescence detection of superoxide. *Free Radic Biol Med, 34*(11), 1359-1368.

Zhao, W., Zhang, J., Lu, Y., & Wang, R. (2001). The vasorelaxant effect of H(2)S as a novel endogenous gaseous K(ATP) channel opener. *The EMBO Journal, 20*(21), 6008-6016.

Zhao, Z. Z., Wang, Z., Li, G. H., Wang, R., Tan, J. M., Cao, X., Suo, R., & Jiang, Z. S. (2011). Hydrogen sulfide inhibits macrophage-derived foam cell formation. *Experimental Biology and Medicine, 236*(2), 169-176.

Zhivotovsky, B., & Orrenius, S. (2010). Cell death mechanisms: cross-talk and role in disease. *Exp Cell Res, 316*(8), 1374-1383.

Zhivotovsky, B., & Orrenius, S. (2011). Calcium and cell death mechanisms: a perspective from the cell death community. *Cell Calcium, 50*(3), 211-221.

Zhu, X. Y., Liu, S. J., Liu, Y. J., Wang, S., & Ni, X. (2010). Glucocorticoids suppress cystathionine gamma-lyase expression and H2S production in lipopolysaccharide-treated macrophages. *Cellular and Molecular Life Sciences, 67*(7), 1119-1132.

Zmijewski, J. W., Moellering, D. R., Le Goffe, C., Landar, A., Ramachandran, A., & Darley-Usmar, V. M. (2005). Oxidized LDL induces mitochondrially associated reactive oxygen/nitrogen species formation in endothelial cells. *American Journal of Physiology-Heart and Circulatory Physiology, 289*(2), H852-H861.

Zucchi, R., & Ronca-Testoni, S. (1997). The sarcoplasmic reticulum Ca^{2+} channel/ryanodine receptor: modulation by endogenous effectors, drugs and disease states. *Pharmacol Rev, 49*(1), 1-51.